frontiers | Research Topics

Blue foods security and sustainability

Edited by
Ruijie Zhang, Jingzhen Wang, Tangtian He and Andrea Belgrano

Published in
Frontiers in Marine Science
Frontiers in Aquaculture

ISSN 1664-8714
ISBN 978-2-8325-5536-1
DOI 10.3389/978-2-8325-5536-1

About Frontiers

Frontiers is more than just an open access publisher of scholarly articles: it is a pioneering approach to the world of academia, radically improving the way scholarly research is managed. The grand vision of Frontiers is a world where all people have an equal opportunity to seek, share and generate knowledge. Frontiers provides immediate and permanent online open access to all its publications, but this alone is not enough to realize our grand goals.

Frontiers journal series

The Frontiers journal series is a multi-tier and interdisciplinary set of open-access, online journals, promising a paradigm shift from the current review, selection and dissemination processes in academic publishing. All Frontiers journals are driven by researchers for researchers; therefore, they constitute a service to the scholarly community. At the same time, the *Frontiers journal series* operates on a revolutionary invention, the tiered publishing system, initially addressing specific communities of scholars, and gradually climbing up to broader public understanding, thus serving the interests of the lay society, too.

Dedication to quality

Each Frontiers article is a landmark of the highest quality, thanks to genuinely collaborative interactions between authors and review editors, who include some of the world's best academicians. Research must be certified by peers before entering a stream of knowledge that may eventually reach the public - and shape society; therefore, Frontiers only applies the most rigorous and unbiased reviews. Frontiers revolutionizes research publishing by freely delivering the most outstanding research, evaluated with no bias from both the academic and social point of view. By applying the most advanced information technologies, Frontiers is catapulting scholarly publishing into a new generation.

What are Frontiers Research Topics?

Frontiers Research Topics are very popular trademarks of the *Frontiers journals series*: they are collections of at least ten articles, all centered on a particular subject. With their unique mix of varied contributions from Original Research to Review Articles, Frontiers Research Topics unify the most influential researchers, the latest key findings and historical advances in a hot research area.

Find out more on how to host your own Frontiers Research Topic or contribute to one as an author by contacting the Frontiers editorial office: frontiersin.org/about/contact

Blue foods security and sustainability

Topic editors

Ruijie Zhang — Guangxi University, China

Jingzhen Wang — Beibu Gulf University, China

Tangtian He — Hong Kong Polytechnic University, Hong Kong, SAR China

Andrea Belgrano — Swedish University of Agricultural Sciences, Sweden

Citation

Zhang, R., Wang, J., He, T., Belgrano, A., eds. (2024). *Blue foods security and sustainability*. Lausanne: Frontiers Media SA. doi: 10.3389/978-2-8325-5536-1

Table of contents

frontiers | Frontiers in Marine Science

TYPE Editorial
PUBLISHED 25 September 2024
DOI 10.3389/fmars.2024.1487645

OPEN ACCESS

EDITED AND REVIEWED BY
Stephen J. Newman,
Western Australian Fisheries and Marine Research Laboratories, Australia

*CORRESPONDENCE
Jingzhen Wang
wangjingzhen-1@163.com
Ruijie Zhang
rjzhang@gxu.edu.cn
Tangtian He
hetangtian@gmail.com
Andrea Belgrano
andrea.belgrano@slu.se

RECEIVED 28 August 2024
ACCEPTED 04 September 2024
PUBLISHED 25 September 2024

CITATION
Wang J, Zhang R, He T and Belgrano A (2024) Editorial: Blue foods security and sustainability.
Front. Mar. Sci. 11:1487645.
doi: 10.3389/fmars.2024.1487645

Editorial: Blue foods security and sustainability

Jingzhen Wang[1]*, Ruijie Zhang[2]*, Tangtian He[3]* and Andrea Belgrano[4,5]*

[1]Guangxi Key Laboratory of Marine Environmental Change and Disaster in Beibu Gulf, Beibu Gulf University, Qinzhou, China, [2]Guangxi Laboratory on the Study of Coral Reefs in the South China Sea, School of Marine Sciences, Guangxi University, Nanning, China, [3]Department of Civil and Environmental Engineering, The Hong Kong Polytechnic University, Hong Kong, Hong Kong SAR, China, [4]Institute of Marine Research, Department of Aquatic Resources, Swedish University of Agricultural Sciences, Lysekil, Sweden, [5]Swedish Institute for the Marine Environment (SIME), University of Gothenburg, Gothenburg, Sweden

KEYWORDS

blue food, aquaculture, mariculture, climate change, innovative practices, environmental resilience

Editorial on the Research Topic
Blue foods security and sustainability

Blue foods, encompassing aquatic foods sourced from marine and freshwater environments, serve as a cornerstone of global nutrition and food security. They offer an accessible and affordable supply of protein and essential micronutrients to over 3.2 billion people worldwide, while also sustaining the livelihoods of 600 million individuals and providing employment to 58.5 million workers (FAO, 2022). As such, blue foods are intrinsically linked to the achievement of several Sustainable Development Goals (SDGs), particularly those focused on ending hunger, ensuring healthy lives, and promoting sustainable economic growth. The remarkable surge in blue food production, from 19.9 million tons in 1950 to 214 million tons in 2020 (FAO, 2022), further underscores their growing significance within the global food landscape. Despite this growth, however, persistent hunger remains a significant global issue. Adding to the problem is the fact that 28.9 percent of the global population remained moderately or severely food insecure in 2023 (FAO et al., 2024), highlighting the need for continued expansion of blue food production to meet future demands.

The rapid expansion of aquaculture and fisheries, however, has introduced significant ecological and environmental challenges including biodiversity loss, pollution, and habitat degradation. These issues are compounded by the impacts of climate change, ocean acidification, and other environmental stressors, which threaten the sustainability of blue food systems. Despite these challenges, blue foods remain a critical component of sustainable food systems and offer a lower environmental footprint compared to terrestrial animal-sourced foods. Addressing the ecological and environmental impacts through innovative practices and sustainable management is essential to ensure that blue foods can continue to contribute to global food security and environmental resilience.

1 Current research landscape

The articles in this Research Topic explore various aspects of blue food security and sustainability, ranging from environmental impacts and climate change to innovative management strategies and technological advancements.

1.1 Impact on and by the environment and ecology

Several articles provide key data on how blue food production can both contribute to and be affected by ecological and environmental change. The study on atmospheric CO_2 emissions from bottom trawling (Atwood et al.) highlights the impact of fishing practices on carbon release and ocean acidification, emphasizing the need for sustainable management strategies. Another article (Bu et al.) examines the eutrophication effects of mariculture in Sansha Bay, demonstrating how nutrient management practices can influence ecosystem health. More importantly, a long-term observation on Fukushima-derived radiocesium (Lin et al.) provides critical insights into the persistence and distribution of radiocesium in marine ecosystems. It highlights the importance of ongoing monitoring to assess the impact of environmental contamination (especially nuclide content) on blue food safety.

1.2 Climate change and adaptation

Climate change poses a significant threat to blue food production. The impacts of climate events on fish life history parameters (Hong et al.) underscore the need for adaptive management strategies to ensure the resilience of fisheries. Similarly, the study on Pacific oyster mortality (Mackenzie et al.) explores nature-based solutions to enhance resilience to environmental stressors, offering insights into sustainable aquaculture practices. The research by Shang et al. also indicates that by simply modulating the temperature could help to optimize the utilization of diatoms as an aquatic feed source. The findings underscore the potential of diatoms as a high-quality aquafeed and lay the foundation for its success in ocean warming scenarios.

1.3 Technological innovations and sustainable practices

Technological advancements and innovative management practices are crucial for enhancing the sustainability of blue foods.

1.3.1 Breeding and hatchery technologies

The work on hatchery release frameworks (Zhang et al.), and mass production of mola seed (Rajts et al.) offers valuable insights into improving the sustainability and nutritional value of aquaculture systems. These studies suggest that enhancing broodstock management and developing standardized breeding techniques are essential for promoting sustainable aquaculture practices that can meet the growing demand for blue foods.

1.3.2 Genetic or molecular approaches

The development of a controllable fertility switch in zebrafish (Shi et al.) offers a promising tool for managing the genetic aspects of aquaculture, supporting both productivity and sustainability. Zheng et al. also identified numerous differentially expressed genes (DEGs) related to immune function that can serve as the basis for subsequent immune response analysis of allotransplantation and xenotransplantation. *In situ* labeling technology, such as calcein (Gao et al.), can act as a promising and low-hazard method to monitor the proliferation, release, and resource conservation of shellfish in tidal flats.

1.3.3 Integrate macro-scale monitoring and management approaches

The use of Geographic Information System (GIS) and remote sensing to evaluate aquaculture suitability (Li et al.) highlights the potential of technology integration in optimizing production and minimizing environmental impacts. Integrating large-scale monitoring techniques into the surveillance of field aquaculture activities has also helped to address the challenge of quantifying plastic loads in aquaculture (Tian et al., 2022).

1.3.4 Nature-based solutions

The development of nature-based solutions to enhance the resilience of aquaculture species is another key area of research. It has been highlighted in several studies, particularly in relation to population connectivity (Close et al.), mitigation of eutrophication (Bu et al.), natural aquafeed production, and intertidal farming (Mackenzie et al.). The connectivity study on scallops in the Irish Sea demonstrates how understanding larval dispersal and population dynamics can inform more effective fisheries management strategies. The research by Bu et al. on Sansha Bay shows how mariculture can exacerbate eutrophication, suggesting that integrated management approaches are necessary to balance production with environmental health. Mackenzie et al. demonstrates how intertidal farming can improve the resilience of Pacific oysters to summer mortality syndrome, suggesting that partial culture in the intertidal zone could be an effective strategy for mitigating the impacts of environmental stressors on aquaculture species.

1.4 Socioeconomic and policy dimensions

Ensuring that the benefits of blue food security are equitably distributed is another significant challenge. The research on shellfish mariculture in China (Gu et al.) and the suitability of oyster aquaculture (Li et al.) suggests that market demand and socio-economic factors play a crucial role in the sustainability of blue food systems. Policymakers must consider these factors when designing

and implementing regulations to support sustainable blue food production.

2 Challenges and opportunities

2.1 Balancing growth with environmental sustainability

The rapid expansion of blue food production presents challenges related to biodiversity loss, environmental pollution, and habitat degradation. Addressing these issues requires a comprehensive understanding of the interactions between blue food systems and their environments. Further research should focus on developing sustainable practices that balance production growth with environmental conservation.

2.2 Climate change adaptation and mitigation

The impacts of climate change on blue food systems necessitate adaptive management strategies to ensure resilience. This includes developing climate-resilient species and practices, as well as exploring the potential of blue foods in carbon reduction and sequestration. Collaborative efforts across disciplines are essential to address the complex challenges posed by climate change.

2.3 Technological advancements and innovations

Technological innovations offer significant opportunities to enhance blue food security and sustainability. Advances in breeding techniques, genetic manipulation, ecosystem modelling, and integrated resource management approaches can improve production efficiency and reduce environmental impacts. Continued investment in research and development is crucial to harness the potential of technology in blue food systems.

2.4 Policy and governance

Effective governance and policy frameworks are essential for promoting sustainable blue food systems. This includes implementing regulations that address overfishing, habitat protection, and pollution control. Collaborative governance models that involve stakeholders at all levels can foster sustainable practices and ensure equitable access to blue food resources.

3 Conclusion

The research on blue foods security and sustainability highlights the critical role of aquatic foods in addressing global food security challenges. The articles in this Research Topic provide valuable insights into the environmental, technological, and policy dimensions of blue food systems. By advancing our understanding of these issues, we can develop strategies that promote the sustainable growth of blue foods, to ensure their continued contribution to global food security and environmental sustainability.

Author contributions

JW: Writing – original draft. RZ: Writing – review & editing. TH: Writing – review & editing. AB: Writing – review & editing.

Funding

The author(s) declare financial support was received for the research, authorship, and/or publication of this article. The authors thank the fundings from National Natural Science Foundation of China (No. 41776174) and Guangxi Natural Science Foundation (2020GXNSFDA297005).

Acknowledgments

We extend our gratitude to the authors, reviewers, and editorial team for their contributions to this Research Topic. Their efforts have significantly advanced our understanding of blue foods and the role of blue foods in global food systems.

Conflict of interest

The authors declare that the research was conducted in the absence of any commercial or financial relationships that could be construed as a potential conflict of interest.

The author(s) declared that they were an editorial board member of Frontiers, at the time of submission. This had no impact on the peer review process and the final decision.

Publisher's note

References

FAO (2022). "The state of world fisheries and aquaculture 2022," in *Towards Blue Transformation* (Rome: FAO). doi: 10.4060/cc0461en

FAO, IFAD, UNICEF, WFP and WHO (2024). *The state of food security and nutrition in the world 2024: financing to end hunger, food insecurity and malnutrition in all its forms* (Rome: FAO). doi: 10.4060/cd1254en

Tian, Y., Yang, Z., Yu, X., Jia, Z., Rosso, M., Dedman, S., et al. (2022). Can we quantify the aquatic environmental plastic load from aquaculture? *Water Res.* 219, 118551. doi: 10.1016/j.watres.2022.118551

frontiers | Frontiers in Marine Science

TYPE Original Research
PUBLISHED 20 July 2023
DOI 10.3389/fmars.2023.1232211

OPEN ACCESS

EDITED BY
Jingzhen Wang,
Beibu Gulf University, China

REVIEWED BY
Xiujuan Shan,
Chinese Academy of Fishery Sciences (CAFS), China
Qutu Jiang,
The University of Hong Kong, Hong Kong SAR, China

*CORRESPONDENCE
Xuefeng Wang
xuefeng1999@126.com

RECEIVED 31 May 2023
ACCEPTED 04 July 2023
PUBLISHED 20 July 2023

CITATION
Gu Y, Wang L, Lyu S, Dong J, Liu B and Wang X (2023) Assessing potential driving factors of the ecosystem service value of mariculture shellfish in China using a structural equation modeling approach. *Front. Mar. Sci.* 10:1232211. doi: 10.3389/fmars.2023.1232211

Assessing potential driving factors of the ecosystem service value of mariculture shellfish in China using a structural equation modeling approach

Yixin Gu[1], Lifei Wang[2], Shaoliang Lyu[1], Jianyu Dong[1], Bilin Liu[3] and Xuefeng Wang[1]*

[1]Fisheries College, Guangdong Ocean University, Zhanjiang, Guangdong, China, [2]Department of Biological Sciences, University of Toronto Scarborough, Toronto, ON, Canada, [3]College of Marine Science, Shanghai Ocean University, Shanghai, China

China is one of the major mariculture countries for shellfish in the world and provides more than 70% of the total global shellfish production. However, there is limited knowledge of the potential driving factors of the ecosystem service value of mariculture shellfish in China. Understanding what factors and how they drive the ecosystem can provide reference for further improving the ecosystem service value of mariculture shellfish, which is both theoretically and practically important for promoting the development of marine fishery economy in China. In this study, data of six major mariculture shellfish species in nine coastal provinces of China from 2009 to 2020 were analyzed using a structural equation modeling approach to quantify the effects of resource distribution characteristics and market demand on the ecosystem service value of mariculture shellfish in China. The results indicated that both resource distribution characteristics and market demand are important driving factors of the ecosystem service value of mariculture shellfish in China. Specifically, from the perspective of path coefficient, market demand plays a more important role (0.58) than resource distribution characteristics (0.36) in influencing the ecosystem service value of mariculture shellfish in China. Therefore, the research results for shellfish marine culture can be summarized as: (1) to actively respond to changes in shellfish market demand, (2) to enhance development planning for coastal shellfish cultivation area, and (3) to strengthen systematic management of mariculture shellfish resources. Results of this study could provide theoretical support and serve as a basis for promoting sustainable development of shellfish culturing industry and fisheries economy in China.

KEYWORDS

China, ecosystem service value, mariculture shellfish, marine fisheries resources, structural equation modeling

1 Introduction

China is one of the major mariculture countries in the world, with more than 70% of the total global mariculture production (Dai et al., 2022). With the exploitation of marine biological resource, mariculture has become the core industry in the "Blue Granary" project (Zhao, 2021). Nowadays the promising development of mariculture is not only essential for improving residents' dietary structure, but also important for maintaining food security to humans (Liu et al., 2022). The Food and Agriculture Organization of the United Nations (FAO) predicted that mariculture products would become the main source of food worldwide in the next fifty years (The State of World Fisheries and Aquaculture 2022, 2022). Shellfish mariculture is playing an increasingly important role in relieving the pressure of food demand, compensating for global food shortages, and increasing the income of fishermen (Gomes et al., 2017). Meanwhile, the development of mariculture shellfish products has not only brought significant economic benefits to China, but also promoted the trade cooperation among China, *ASEAN*, and the coastal countries of "the Belt and Road" (Noman et al., 2018; Zhang and Li, 2022). The production and trade of mariculture shellfish products have been rapidly increasing in China (Zhang et al., 2021). As of 2020, China's mariculture shellfish production has reached 14.8 million tons, accounting for 83.67% of the total global production (The State of World Fisheries and Aquaculture 2022, 2022).

During the expansion process and intensification of shellfish mariculture practices in China, there is also an increase of stress level on the limited carrying capacity of coastal marine ecosystems to afford the increasing mariculture space or density and market demand (Liu et al., 2022; Yan et al., 2022). Identifying the constraints and key factors can provide clues for improving ecosystem service value of mariculture shellfish in China (Cao and Yang, 2022). In 2021, Chinese government proposed to develop marine economy as one of the goals for the "14th Five-Year Plan" and "2035 Long-Term Goal" (Liu and Li, 2023). The exploitation of marine resources has become a hotspot for economic development with the orientation from high-speed development to high- quality development (Wang et al., 2021). Therefore, enhancing the core competitiveness of the shellfish industry is of great importance for promoting high- quality development of the marine economy in China (Yang and Chen, 2022).

Core competitiveness is an important evaluation indicator for measuring the level of industrial development (Nguyen et al., 2022). Many studies have analyzed the competitiveness of Chinese fisheries by using relevant indicators such as resource distribution characteristics coefficient, international market share, and trade complementarity index (Feng, 2019). Based on Porter's diamond model, Zhao et al. suggested that the competitiveness of marine fisheries is mainly influenced by basic production, market demand, related enterprises, and social environment (Yang and Chen, 2022). Shan et al. examined the competitiveness of marine fisheries across countries, and measured the resource distribution characteristics coefficient and the dominant comparative advantage index of Chinese fisheries catch, and concluded that Chinese fisheries were facing challenges in the utilization of resource distribution characteristics and the implementation of marine environmental protection (Shan and Jiang, 2005). However, these studies mainly focused on the point-to-point direct relationships, but overlooked the relationships of dependent variables and lacked a comprehensive perspective (Zhang et al., 2019). Therefore, it is imperative to choose suitable statistical approaches to determine the potential driving factors of the ecosystem service value of mariculture shellfish in China. As a novel and promising modeling approach, structural equation model (SEM) integrates path analysis with multiple factor analysis (Yang et al., 2018; Lai et al., 2022a; Ou et al., 2022). Compared with traditional statistical methods, SEM can not only reveal the interrelationship and strength of individual influencing factors, but also fit and evaluate the overall model, thus providing a more comprehensive understanding of the underlying mechanisms that affect response variables (Cao et al., 2020). SEM has been applied in psychology, economic management, social behavior, and other fields (Du et al., 2015), but there is little research reported on fisheries management (Zhang et al., 2022).

The objective of this research is to quantify how the potential driving factors influence the ecosystem service value of mariculture shellfish in China. The SEM approach was used to analyze the influencing factors and construct a path map. Results of this study could provide theoretical support for improving the ecosystem service value of China's mariculture shellfish industry, and also serve as a basis for promoting the sustainable development of marine fisheries in China.

2 Materials and methods

2.1 Data sources

According to the current distribution of mariculture shellfish industry in China, six major mariculture shellfish species (oyster, ark clam, mussel, scallop, clam, and razor clam) in nine coastal provinces (Liaoning, Hebei, Shandong, Jiangsu, Zhejiang, Fujian, Guangdong, Guangxi, and Hainan) from 2009 to 2020 were analyzed. All the historical data were derived from China Fishery Statistical Yearbook (Fishery Bureau of Ministry of Agriculture and Rural Affairs of China (2010–2021)). The original data were transformed with log10 function before analysis, and the records with missing or invalid values were excluded. There 105 sets of valid data were finally pooled to the SEM analysis (S1).

2.2 Variable selection

The elements of marine production can be optimized in different proportions in spatial form in the market economy, and the optimizing process will update the layout of the whole marine industry (Wei et al., 2021). The mariculture shellfish industry in

China is mainly dependent on natural conditions (Zheng et al., 2020; Liu et al., 2022).The area suitable for cultivating shellfish and hatching with more fisheries practitioners are mainly distributed in coastal area (Liu and Li, 2023). The advantages of regional resource distribution characteristics underpin the spatial pattern of the mariculture shellfish industry in China (Zhang et al., 2004). The competitive advantage mostly depends on the market demand (Cao and Yang, 2022), the greater competitiveness indicating that more domestic and foreign market share, (Gao et al., 2018).

The ecosystem service value of mariculture shellfish (fishery output value herein) depends on factors as follow: resource distribution characteristics (shellfish mariculture production, shellfish mariculture area, shellfish seeding, fishery practitioners) and market demand (aquatic products import volume and export volume) (Chen et al., 2012; Miao et al., 2014).Therefore, this study is to build a model to assess the roles of factors affecting the ecosystem service value of mariculture shellfish (Jacobucci et al., 2016). Three latent variables were included: the ecosystem service value of mariculture shellfish, the resource distribution characteristics, and the market demand (Table 1). Two hypotheses have been proposed to explain which factor has a positive impact on the ecosystem service value of mariculture shellfish:

H1: Resource distribution characteristics.

H2: Market demand.

2.3 Model building

2.3.1 Data processing

Due to the different units of the variables in this study, the data were log10-transformed before conducting statistical analysis. Values of the indices were standardized to the same order of magnitude, and 105 sets of standardized data were obtained.

2.3.2 Model structure and configuration

In this study, structural equation modeling was used to determine the weight of factors influencing the ecosystem service value of mariculture shellfish in China (Yang et al., 2018). The principal goal of SEM is to develop models to evaluate and represent the underlying causal processes (Li et al., 2018; Ma et al., 2022). So, the measurement model and structural model can be constructed based on the relationships between variables (Fox, 2006; Zhao and Zhu, 2014; Wang et al., 2022).

$$\eta = B\eta + \Gamma\xi + \zeta \tag{1}$$

$$X = \wedge x\xi + \delta \tag{2}$$

$$Y = \wedge y\eta + \epsilon \tag{3}$$

Equation (1) is the structural model, in which η is the endogenous latent variable; ξ is the exogenous latent variable; B and Γ are coefficient matrices; and ζ is an error term. Equations (2)and (3) are both measurement models, in which Y represents the measurable variables for the endogenous latent variable; Λy is the correlation coefficient matrix between the endogenous latent variables and their measurable variables; ϵ represents measurement errors; X represents the measurable variables for the exogenous latent variables; Λx is the correlation coefficient matrix between the exogenous latent variable and its measurable variables; and δ represents measurement errors.

According to the above hypothesis, resource distribution characteristics, market demand and ecosystem service value of mariculture shellfish in China were regarded as the latent variables, which were described using 7 measured variables. In summary, the first endogenous latent variable (the ecosystem service value of mariculture shellfish in China) was described by one measured variable (fishery output value). The second exogenous latent variable (resource distribution characteristics) was described by four measured variables (shellfish production, Shellfish seeding, fishery practitioners, shellfish mariculture area). The third exogenous latent variable was market demand, expressing as the aquatic products export value and the aquatic products import value. The model was established by using the R "Lavaan" package, of which the maximum-likelihood estimation method was used (Fan et al., 2016; Kline, 2016; Li et al., 2022; Shi et al., 2022).

2.3.3 Model fitting and assessment

The model fit index is a statistical indicator that examines how well a theoretical structural model fits the data. The model fit indices of distinct categories can be measured for model complexity, sample size, relativity, and absoluteness. Therefore, the following seven commonly used indicators were selected (Yuan et al., 2017).

Chi square test (X^2), the model has a good fitting effect when P value > 0.05.

TABLE 1 The indicator variables in structural equation model.

Indicator Classification	Latent Variable	Observations Variable
Result Metrics	Ecosystem service value of mariculture shellfish	Fishery output value
Influencing Factor Measurements	Resource distribution characteristics	Shellfish mariculture production
		Shellfish mariculture area
		Shellfish seeding
		Fisheries practitioners
	Market demand	Aquatic products export volume
		Aquatic products import volume

Goodness of Fit Index (*GFI*). The more *GFI* approaches to 1, the better the model fits the data. *GFI* > 0.900 is usually used as the threshold.

Relative Fit Index (*RFI*). *RFI* > 0.90 is considered acceptable.

Comparative Fit Criterion (*CFI*) is between 0 and 1. *CFI* equals 1 if the model fits the data perfectly.

Standardized Root Mean Square Residual (*SRMR*) is like *RMSEA* and should be< 0.09 for a good model fit.

Tucher Lewis Index (*TLI*) is a non-normed fit index, *TLI* > 0.90 is considered acceptable.

Root Means Square Error of Approximation (*RMSEA*) can overcome the drawback of the overall different value influenced by the estimated parameters in model validation. *RMSEA* is less than 0.05 when the fitness of the model is good. *RMSEA* is higher than 0.1 when the fitness of the model is bad, and modification is needed. *RMSEA* between 0.050 and 0.100 means that the model is not much satisfied but acceptable.

3 Results

3.1 Spatiotemporal characteristics of mariculture shellfish

The distribution of mariculture shellfish along the coast of China showed an overall agglomeration trend (Figure 1) characterized with high at both ends and low in the middle. Provinces including Shandong, Fujian, Liaoning, and Guangdong were the main high-yield coastal provinces, accounting for 80% of the coastal provinces, with 44.08 million tons, 31.41 million tons, 26.31 million tons, and 22.51 million tons, respectively. The production of mariculture shellfish in Shandong Province accounts for over 25% of the total national.

The overall area of shellfish mariculture decreased significantly in 2016, with a slight downward trend thereafter. Since 2009, Liaoning Province and Shandong Province had consistently

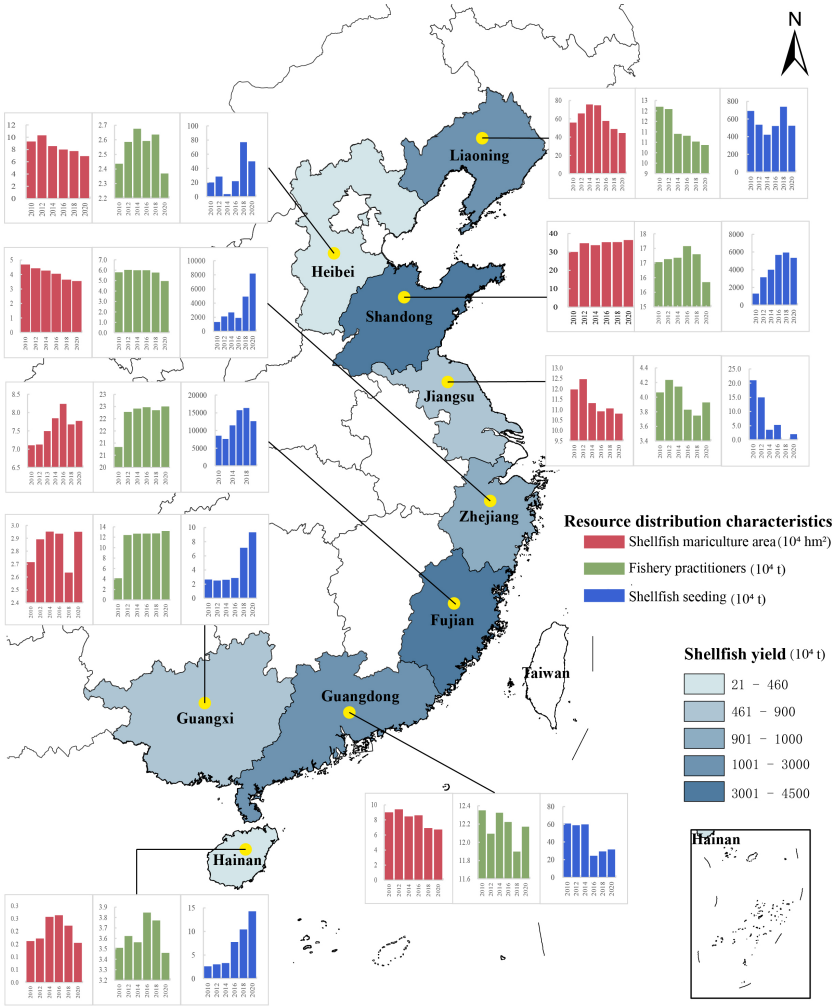

FIGURE 1
The indicators shellfish production, mariculture area, shellfish seeding, fishery practitioners of resource distribution characteristics of mariculture shellfish in China. The map color saturation represents the shellfish mariculture production, and the histogram color distinguishes different indicators.

ranked in the top two, while the mariculture area in Hainan province was relatively small. The top three provinces in terms of shellfish seeding were Fujian, Zhejiang, and Shandong Province, with input exceeding 25 million tons from 2009 to 2020. Since 2016, the number of shellfish seedings in Hainan Province had been increasing annually (with an increase rate of 17%), while the number of shellfish seedings in Guangdong Province had been decreasing, far below the average level. Although Fujian Province ranked first in the number of shellfish seedings, the mariculture area was comparatively small. As the primary industry, fisheries in Fujian, Shandong, and Liaoning provinces had attracted more fishery practitioners. In 2020, the number of fishery practitioners reached 490 000, accounting for 40% in coastal areas.

The overall shellfish mariculture had been in rapid developing nationally, which was shown in indices such as fishery output value, and the import and export volume of fishery products, with a decline in fishery output value only in 2011 (Figure 2). Both the volume of import and export of fishery products had declined since 2019, partly due to the Covid-19 pandemic.

The differences in fishery output value between provinces was shown in Figure 3. The highest fishery output value with a continuous upward trend in Shandong, Fujian, Guangdong, and Liaoning provinces contributed substantially to the northern and southern marine economic zones. The import and export volume of aquatic products had shown an growth trend in all though varied in some year. The top four provinces of export volume were Fujian, Shandong, Guangdong, and Liaoning, while the top four provinces of import volume are Shandong, Liaoning, Guangdong, and Fujian. In recent years, the development of fisheries in Fujian Province had been more and more prominent, and the gap between imports and exports after 2016 expanded, with a difference of 3.88 million dollars in imports and exports in 2020. The neighboring province Jiangsu was slower than Fujian, and the export volume in 2020 is less than 20% of Fujian Province.

3.2 Model validation

3.2.1 Multivariate cross correlation

Mariculture shellfish production showed high correlation (r=0.86) with the mariculture area (Figure 4). The correlations between the import and export volume of aquatic products and the production of mariculture shellfish, as well as the fishery practitioners, had reached over 0.65. Both the significant increase in the production of mariculture shellfish and the fishery practitioners had greatly promoted the development of the import and export scale of aquatic products.

3.2.2 Goodness-of-fit test

The SEM for the ecosystem service value of mariculture shellfish in nine coastal provinces of China were successfully built. The multiple parameter evaluations were conducted for the SEM, and all met the standards (Table 2): P = 0.104, GFI = 0.972, RFI = 0.958, CFI = 0.995, TLI = 0.981, $RMSEA$ = 0.085, $SRMR$ = 0.023. The minimum acceptance criteria for RMSEA< 0.90 and SRMR< 0.08, respectively, and all of this measurement model fitness met the critical value requirements. Therefore, the model fitting evaluation met the standards, indicating that the indicator system and logical relationship of the three latent variables were reasonable and reliable.

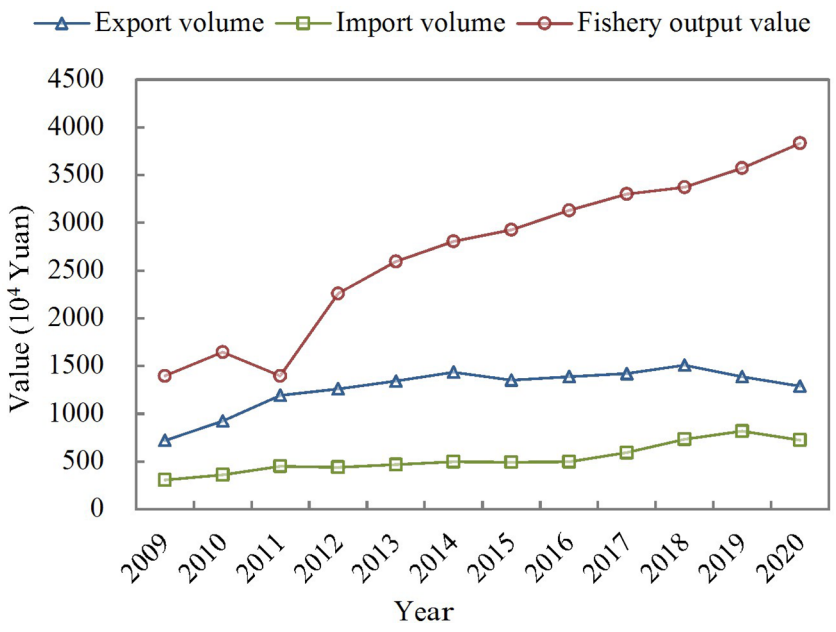

FIGURE 2
The trend of fishery output value, and the import and export volume of fishery products in China's coastal provinces from 2009 to 2020.

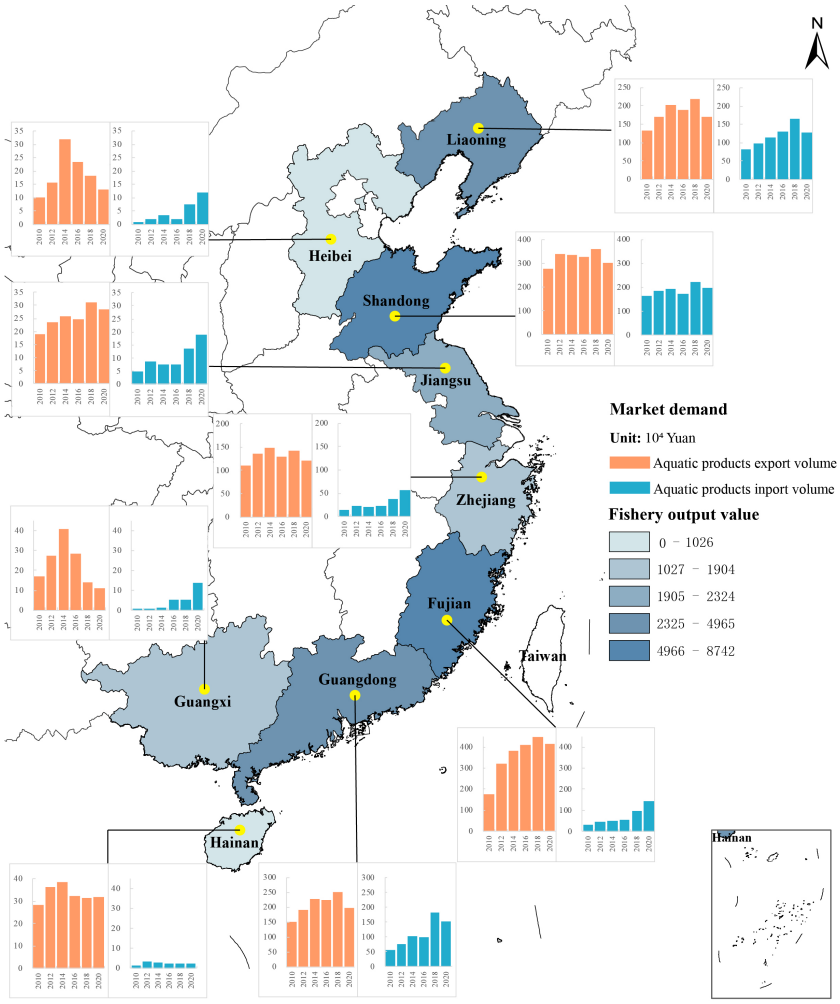

FIGURE 3
The indicators fishery output value, import volume, and export volume of market demand of mariculture shellfish in China. The map color saturation represents the fishery output value, and the histogram color distinguishes different indicators.

3.3 Path graph on SEM

As for the direct effects, the correlation coefficients between the ecosystem service value of Chinese mariculture shellfish and resource distribution characteristics, as well as market demand, were 0.36 and 0.58 respectively. It indicated that the impact of resource distribution characteristics and market demand on the ecosystem service value was significant. Among them, the competitive advantage of Chinese mariculture shellfish in terms of market demand was the most prominent (Figure 5).

The correlation coefficients between the latent variable resource endowment and the observed variables of shellfish yield, mariculture area, shellfish seeding, and fishery practitioners with were 0.87, 0.69, 0.73, and 0.86, respectively. The correlation coefficients between the latent variable market demand and the observed variables aquatic product export volume, import volume, were 0.90 and 0.99, respectively. The correlation coefficient between the observed variable total fishery output value and the ecosystem service value of Chinese mariculture shellfish was 1.00. Meanwhile, the correlation coefficients of mariculture area had a negative impact on the number of fishery practitioners and the export volume of aquatic products with correlation coefficients of -0.41 and -0.22, respectively. In summary, the seven observed variables had a positive and significant impact on the three latent variables.

4 Discussions

4.1 Resource distribution characteristics of mariculture shellfish in China

China holds the Yellow Sea, the Bohai Sea, the East China Sea and the South China Sea, which are rich in marine resources and large scale of mariculture (Lai et al., 2022b), which is the basis for the ecosystem service value of Chinese shellfish products (Niu, 2015). In terms of the scale of Chinese mariculture industry, shellfish is the most important sector in both mariculture area and the correlation coefficients between the observed variables of production. This study found that the total area of mariculture in China in 2020 was 1995.55 thousand hectares, of which 1197.41 thousand hectares were used for shellfish culturing,

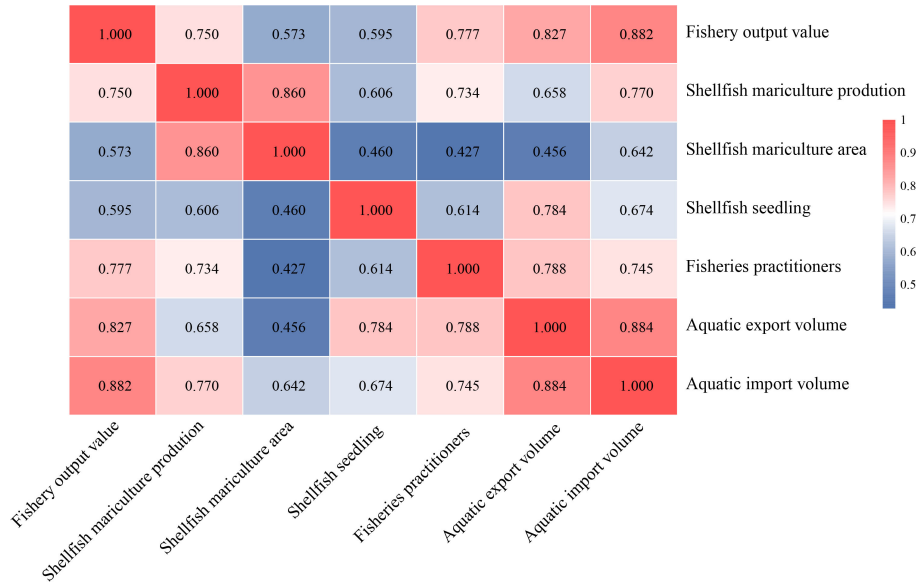

FIGURE 4
Pearson correlation heatmap among all indicators.

TABLE 2 The goodness-of-fit test results of structural equation model.

	P	GFI	RFI	CFI	RMSEA	SRMR	TLI
Model	0.104	0.972	0.958	0.995	0.085	0.023	0.981

accounting for approximately 60.01%. Owing to the increasing production capacity, the production of mariculture shellfish reached 14.8 million tons in 2020, accounting for 83.67% of the global total (Teng et al., 2021).

The shellfish seedlings/hatchery is vital for the development mariculture industry (Bai et al., 2022). Compared with the step-by-step growing trend of mariculture shellfish production, the quantity of shellfish seedings varied rather largely. At present, the specific

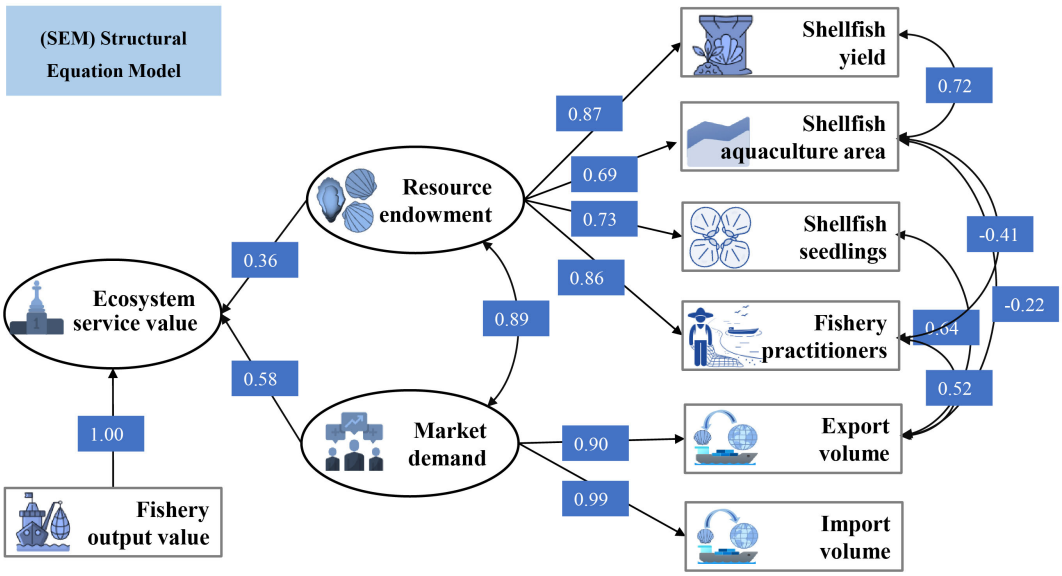

FIGURE 5
Path diagram based on structural equation model. The ellipses represent latent variables. The variables in the rectangle are observation variables. The value on the arrow line is the Pearson correlation coefficient.

shellfish breeding institutions and seed farms for advanced biological technical application are still insufficient in China, with only some such farms established in Zhejiang, Jiangxi, and Hunan provinces (Guan et al., 2022). The introduction of improved varieties can quickly form new industrial clusters and play a huge role in promoting industrial development (Tang et al., 2022). In addition, farmers will transfer the shells from the south to north, or from north to the south in coastal waters to provide more preferred habitats for shells rapid growth, intending to making more profit (Lai et al., 2022b). The transfer of shells during process of culturing possibly cause potential threats such as confusion in genetic background and a deficiency of high-quality large-sized seedlings (Lai et al., 2022b). In such situations, the quality of shell seeding are more dependent on local breeding selection or the introduction of foreign seed-parent (Liu et al., 2020). From the perspective of germplasm resources protection, both updating the cultivation technology and optimizing the infrastructure of shellfish seedling are fundamental to high-quality development of fishery (Wang and Han, 2017). For example, the NSSP of the United States has detailed research results in shellfish seedling planning and breeding, and has established a set of shellfish seedling quality control system (van Senten et al., 2020).

The mode of mariculture in coastal area of China is also in ungrading (Feng et al., 2004). The overcrowded shellfish mariculture in coastal waters have posed threats on wetlands and product quality/food safety (Jiang and Mu, 2022; Tian P. et al., 2022). In 2015, China endeavored to rectify the mariculture environment and cleared a large number of illegal mariculture area (Jiang et al., 2021). After 2017, the implementation of the "13th Five-Year Plan" and the rapid advancement of marine development activities (Liang et al., 2018). Due to the saturated/over saturated of the shellfish culturing capacity, and the area of shellfish mariculture is facing the trend of shrinkage (Gu et al., 2022). Therefore, countermeasures are imperative to improve the capacity of mariculture shellfish (Figure 6) (Liang et al., 2018). Marine ranching is potential and an effective means to alleviate the deterioration of the coastal environmental pollution and the decline of fishery resources (Suo et al., 2023). It's also important to fulfill the marine ecological civilization (Zhou et al., 2019). Additionally, the utilization of mudflat for shellfish culture is also promising (Meng and Feagin, 2019). Mendoza et al. assessed the coastal protection capacity of the mudflats and proposed the Coastal Resilience Index from Remote Sensors (CRIfRS) method to improve the coastal protection capacity of mudflats (Bian et al., 2020; Mendoza et al., 2022). The protection of coastal mudflats and wetlands is helpful to solve the "saturation" of coastal area, but also to develop a rising ecological industry (Cui L. et al., 2022).

In addition, the number of fisheries practitioners has been increasing accordingly with the expansion of mariculture. The experienced culturing personnel are irreplaceable in the development of the whole industry (Xu and Gao, 2022). Although the coastal governments provide financial support for mariculture research, the overall amount of investment is still insufficient (Miao et al., 2023). In recent years, the aquatic seed industry is causing wide concerns of fisheries management agencies, researchers and farmers (Zhang, 2016; Hu et al., 2020). The sustainable development of shellfish industry in China depends on the integration of scientific research, culturing technique and management strategies (Li, 2019; Chen, 2022). The EU Common Fisheries Policy established the scientific committee system for marine fisheries, offering scientific supports on fisheries development (Jensen et al., 2014).

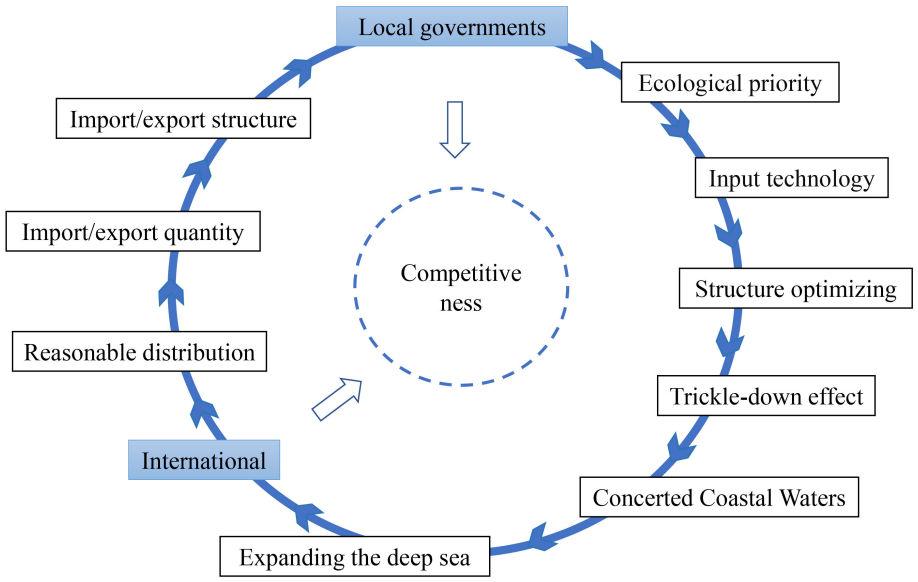

FIGURE 6
Framework proposed based on the research on the ecosystem service value of mariculture shellfish in China.

4.2 Market demand of mariculture shellfish in China

The growing demand for aquatic products in China significantly influenced the development of the global seafood market (Li et al., 2011; Peng et al., 2021). China's fishery economy reached as high as 400,482 billion dollars in 2020. This study showed that China's import and export of aquatic products amount to 34,606 billion dollars in 2020 (The State of World Fisheries and Aquaculture 2022, 2022).

The mariculture shellfish has strong international competitiveness in China (Zhang et al., 2004). In 2011, there were 158,500 tons of shellfish exported in China, accounting for 25.07% of the world's total shellfish exports, which made China the world's largest shellfish export country. The quality and added-value of shellfish products in China still needs to be improved (Feng, 2019). Tan et al. quantitatively analyzed the competitive advantages and market share of Chinese shellfish trade (Tan et al., 2020). Despite the huge scale of mariculture shellfish industry in China, the mariculture structure of shellfish "high at both ends and low in the middle" still has gaps in meeting the demands for consumers (Tan et al., 2020). The shellfish industry tends to be low-level and redundant, with making profit as the single target (Niu, 2015; Miao et al., 2021).

The results of the study showed that aquatic products trade contributed to the rapid development of marine economy in coastal area, though the culturing industry was scattered and unbalanced in terms of regional distribution (Xu and Yang, 2022). The characteristics of regional distribution implies that the development of shellfish industry in China should be market oriented, i.e. the quality/seafood security of shellfish quality is top important and the quantity is subsequent. So the utilization of culturing coastal waters and culturing technique, culturing species are fundamental to the supply of shellfish (Wang and Somogyi, 2019). Additionally, increasing the shares in the international market of shellfish products is also an essential part of competitive advantage (Figure 6) (Li, 2019; Wang and Somogyi, 2019).

Fisheries management strategies should be made according to the characteristics of shellfish industry. The first priority for regions with abundant shellfish should increase their shares in international market (Li et al., 2011), and for other regions should increase the sustainable utilization of culturing area (Ferreira et al., 2007; Meng and Feagin, 2019; Su et al., 2020; Lyu et al., 2022). Meanwhile, to alleviate the global risks such as COVID-19 on shellfish marine culture industry, the whole supply chains needs to be strengthened from shell seeds breeding to culturing technique and the products market (Zhang and Ma, 2022).

5 Conclusion

This study investigated the potential driving factors of the ecosystem service value of mariculture shellfish in China using data of six mariculture shellfish species in nine coastal provinces of China from 2009 to 2020. The SEM approach was used to quantify the impacts of resource distribution characteristics and market demand on the ecosystem service value of mariculture shellfish in China. The results indicated that both resource distribution characteristics and market demand are important driving factors of the ecosystem service value of mariculture shellfish in China. Specifically, from the perspective of path coefficient, market demand plays a more important role than resource distribution characteristics in influencing the ecosystem service value of mariculture shellfish in China. Future directions would be to incorporate the import and export volume of fisheries products as a response variable to market demand, although such import and export volume data are still limited. Results of this study could provide theoretical guidance for improving the competitiveness of China's mariculture shellfish industry, and serve as a basis for promoting the development of marine fisheries economy and supporting the sustainability of marine resources and coastal ecosystems in China.

Data availability statement

The original contributions presented in the study are included in the article/Supplementary Material. Further inquiries can be directed to the corresponding author.

Ethics statement

Ethical review and approval was not required for the animal study because this study did not involve animal tissue sampling, and studied aquaculture shellfish from a data and model perspective.

Author contributions

YG: methodology and initial draft preparation. LW: investigation and methodology. SL, BL and JD: revision and data collection. XW: experiment design, reviewing and editing, supervision, and funding acquisition. All authors contributed to the article and approved the submitted version.

Funding

This research was supported by special funds for the Sino-Indonesian Technical Cooperation in Coastal Marine Ranching (12500101200021002) and Guangdong Basic and Applied Basic Research Foundation (2022A1515110957).

Acknowledgments

We thank Dr. Ning Chen for her valuable comments and Dr. Benben Miao for assisting with figure drawing.

Conflict of interest

The authors declare that the research was conducted in the absence of any commercial or financial relationships that could be construed as a potential conflict of interest.

Publisher's note

All claims expressed in this article are solely those of the authors and do not necessarily represent those of their affiliated organizations, or those of the publisher, the editors and the reviewers. Any product that may be evaluated in this article, or claim that may be made by its manufacturer, is not guaranteed or endorsed by the publisher.

Supplementary material

The Supplementary Material for this article can be found online at: https://www.frontiersin.org/articles/10.3389/fmars.2023.1232211/full#supplementary-material

References

Bai, Z., Wen, P., Yuan, L., Wang, G., and Li, J. (2022). Germplasm resources situation and protection utilization of freshwater molluscs in China. *J. Fisheries China* 46, 149–157. doi: 10.11964/jfc.20210212638

Bian, H., Li, W., Li, Y., Ren, B., Niu, Y., and Zeng, Z. (2020). Driving forces of changes in china's wetland area from the firs-2001) to secon-2011) national inventory of wetland resources. *Glob. Ecol. Conserv.* 21, e00867. doi: 10.1016/j.gecco.2019.e00867

Cao, X., Li, J., Zhao, W., Wei, X., and Pang, Y. (2020). Effects of stand spatial structure on herbaceous species diversity in forests based on structural equation modeling. *Acta Ecologica Sin.* 40, 9164–9173. doi: 10.5846/stxb202001280179

Cao, L., and Yang, D. (2022). Construction and empirical analysis of evaluation index system of china's pelagic fishery competitiveness. *Mar. Economy* 12, 41–50. doi: 10.19426/j.cnki.cn12-1424/p.20220120.001

Chen, Q. (2022). Policy research on fishery resource management in China. *Ocean Dev. Manage.* 39, 65–72. doi: 10.20016/j.cnki.hykfygl.20220929.008

Chen, D., Li, S., and Wang, K. (2012). Enhancement and conservation of inland fisheries resources in China. *Environ. Biol. Fishes* 93, 531–545. doi: 10.1007/s10641-011-9948-2

Cui, L., Li, W., Dou, Z., Zhang, M., Wu, G., Hu, Z., Gao, Y., et al. (2022). Changes and driving forces of the tidal flat wetlands in coastal China during the past 30 years. *Acta Ecologica Sin.* 42, 7297–7307. doi: 10.5846/stxb202203080551

Dai, Y., Yuan, Y., Yuan, Y., Zhou, Z., and Zhang, H. (2022). Factors influencing Chinese consumer attitudes on the safety of aquatic products. *J. World Aquaculture Soc.* 53, 47–59. doi: 10.1111/jwas.12823

Du, X., Garcia-Berthou, E., Wang, Q., Liu, J., Zhang, T., Li, Z., et al. (2015). Analyzing the importance of top-down and bottom-up controls in food webs of Chinese lakes through structural equation modeling. *Aquat. Ecol.* 49, 199–210. doi: 10.1007/s10452-015-9518-3

Fan, Y., Chen, J., Shirkey, G., John, R., Wu, S. R., Park, H., et al. (2016). Applications of structural equation modeling (SEM) in ecological studies: an updated review. *Ecol. Processes* 5, 19. doi: 10.1186/s13717-016-0063-3

Feng, X. (2019). Research on the export international competitiveness of aquatic product in China. Master's Thesis. Zhanjiang: Shanghai Ocean University. doi: 10.27314/d.cnki.gsscu.2019.000393

Feng, Y. Y., Hou, L. C., Ping, N. X., Ling, T. D., and Kyo, C. I. (2004). Development of mariculture and its impacts in Chinese coastal waters. *Rev. Fish. Biol. Fish.* 14, 1–10. doi: 10.1007/s11160-004-3539-7

Ferreira, J. G., Hawkins, A. J. S., and Bricker, S. B. (2007). Management of productivity, environmental effects and profitability of shellfish aquaculture - the farm aquaculture resource management (FARM) model. *Aquaculture* 264, 160–174. doi: 10.1016/j.aquaculture.2006.12.017

Fishery Bureau of Ministry of Agriculture and Rural Affairs of China (2010–2021a). *China Fishery statistical yearbook* (Beijing: China Agriculture Press).

Fox, J. (2006). Structural equation modeling with the sem package in r. *Struct. Equ. Modeling* 13, 465–486. doi: 10.1207/s15328007sem1303_7

Gao, X., Gong, L., and Zhang, X. (2018). Influence factors of the international competition advantage of OceanFisheries in China from the perspective of the global value chain. *Mar. Economy* 8, 26–39. doi: 10.19426/j.cnki.cn12-1424/p.2018.06.004

Gomes, T., Albergamo, A., Costa, R., Mondello, L., and Dugo, G. (2017). Potential use of proteomics in shellfish aquaculture: from assessment of environmental toxicity to evaluation of seafood quality and safety. *Curr. Org. Chem.* 21, 402–425. doi: 10.2174/1385272820666161102121232

Gu, Y., Lyu, S., Wang, L., Chen, Z., and Wang, X. (2022). Assessing the carbon sink capacity of coastal mariculture shellfish resources in China from 1981-2020. *Front. Mar. Sci.* 9. doi: 10.3389/fmars.2022.981569

Guan, H., Sun, Z., and Zhao, A. (2022). Spatio-temporal evolution and influencing factors of net carbon sink in marine aquaculture in China. *Front. Environ. Sci.* 10. doi: 10.3389/fenvs.2022.978073

Hu, P., Yan, S., Shi, P., zheng, Z., and Lin, L. (2020). The situation and protection suggestions of MarineEcological environment in guangdong province. *Ocean Dev. Manage.* 37, 115–120. doi: 10.20016/j.cnki.hykfygl.2020.06.022

Jacobucci, R., Grimm, K. J., and McArdle, J. J. (2016). Regularized structural equation modeling. *Struct. Equ. Modeling* 23, 555–566. doi: 10.1080/10705511.2016.1154793

Jensen, F., Nielsen, M., and Nielsen, R. (2014). Increased competition for aquaculture from fisheries: does improved fisheries management limit aquaculture growth? *Fisheries Res.* 159, 25–33. doi: 10.1016/j.fishres.2014.05.004

Jiang, Q., Liu, C., and Qiu, K. (2021). Factor inputs, returns to scale and technical efficiency analysis ofChinese fisheries. *J. Fisheries China* 45, 785–797. doi: 10.11964fc.20200712331

Jiang, Y., and Mu, Y. (2022). Regional differences and causes of china's marine fishery economic development. *Regional Dif. causes China's* 40, 61–69.

Kline, R. B. (2016). *Principles and practice of structural equation modeling. 4th ed* (New York, NY, US: Guilford Press).

Lai, C.-H., Chen, Y.-K., Wang, Y., and Liao, H.-C. (2022a). The study of learning computer programming for students with medical fields of specification-an analysis via structural equation modeling. *Int. J. Environ. Res. Public Health* 19, 6005. doi: 10.3390/ijerph19106005

Lai, Q., Ma, J., He, F., Zhang, A., Pei, D., and Yu, M. (2022b). Current and future potential of shellfish and algae mariculture carbon sinks in China. *Int. J. Environ. Res. Public Health* 19, 8873. doi: 10.3390/ijerph19148873

Li, Y. (2019). Implementation views on accelerating the green development of aquaculture. *Ocean Fishery* 299, 12–13.

Li, S., Fan, M., and Wu, X. (2018). Effect of social capital between construction supervisors and workers on workers' safety behavior. *J. Constr. Eng. Manage.* 144, 04018014. doi: 10.1061/(ASCE)CO.1943-7862.0001467

Li, X., Li, J., Wang, Y., Fu, L., Fu, Y., Li, B., et al. (2011). Aquaculture industry in China: current state, challenges, and outlook. *Rev. Fish. Sci.* 19, 187–200. doi: 10.1080/10641262.2011.573597

Li, J., Miao, B., Wang, S., Dong, W., Xu, H., Si, C., et al. (2022). Hiplot: a comprehensive and easy-to-use web service for boosting publication-ready biomedical data visualization. *Briefings Bioinf.* 23, bbac261. doi: 10.1093/bib/bbac261

Liang, Y., Xianwei, C., Hui, Z., Shutes, B., Baixing, Y., Qingwei, Z., et al. (2018). Historical evolution of mariculture in China during past 40 years and its impacts on eco-environment. *Chin. Geogr. Sci.* 28, 363–373. doi: 10.1007/s11769-018-0940-z

Liu, Y., Jiang, Y., Pei, Z., Han, L., Shao, H., Jiang, Y., et al. (2022). Coordinated development of the marine environment and the marine fishery economy in China. *Fishes* 7, 391. doi: 10.3390/fishes7060391

Liu, Y., and Li, X. (2023). An empirical analysis of the relationship between china's marine economy and marine environment. *Appl. Nanosci.* 13, 2831–2836. doi: 10.1007/s13204-021-02131-9

Liu, Q., Zhang, M., Chen, L., Jia, Q., Kong, Y., and Hu, Z. (2020). Effects of algal species, shellfish body size and density on the feeding rates of anodonta woodiana and corbicula fluminea. *J. Of Shanghai Ocean Univ.* 29, 331–338. doi: 10.12024/jsou.20180402256

Lyu, S., Deng, S., Lin, K., Zeng, J., and Wang, X. (2022). Designing and the pilot trial of bivalve molluscan fishing quotas on maoming coastal waters of China, northern south China Sea. *Front. Mar. Sci.* 9. doi: 10.3389/fmars.2022.863376

Ma, J., Liu, J., Li, Y., and Hu, X. (2022). Comparison of wheat aphid population structural equation model considering climatic factors and simplified model. *J. Anshan Normal Univ.* 24, 1–5.

Mendoza, E. T., Torres-Freyermuth, A., Ojeda, E., Medellin, G., Rioja-Nieto, R., Salles, P., et al. (2022). Seasonal changes in beach resilience along an urbanized barrier island. *Front. Mar. Sci.* 9. doi: 10.3389/fmars.2022.889820

Meng, W., and Feagin, R. A. (2019). Mariculture is a double-edged sword in China. *Estuar. Coast. Shelf Sci.* 222, 147–150. doi: 10.1016/j.ecss.2019.04.018

Miao, M., Cai, H., and Ye, Y. (2023). Reflections on several issues in the construction and management ofmarine ranching in zhejiang province. *J. Fisheries Res.* 45, 88–95. doi: 10.14012/j.cnki.fjsc.2023.01.012

Miao, X., Li, J., and Zhu, X. (2014). International food consumption and its implicationson china's food gap: evidence from historical data. *Econ. Theory Business Manage.* 284, 103–112.

Miao, M., Liu, H., and Chen, J. (2021). Factors affecting fluctuations in china's aquatic product exports to Japan, the USA, south Korea, southeast Asia, and the EU. *Aquac. Int.* 29, 2507–2533. doi: 10.1007/s10499-021-00761-y

Nguyen, T. V., Simioni, M., Quyen, C. L., and Valtysson, H. P. (2022). Productivity, technical efficiency, and technological change in Vietnamese oceanic tuna fisheries. *Fish Res.* 248, 106202. doi: 10.1016/j.fishres.2021.106202

Niu, T. (2015). Trade situation of China shellfish products to the EU and analysis of international competitiveness. Master's Thesis. Shanghai: Shanghai Ocean University.

Noman, M., Mu, Y., Zhu, Y., Mohsin, M., Memon, A., and Shah, S. (2018). Maximum sustainable yield estimation of shellfish fishery in Chinese marine waters by using surplus production modelling approach. *Indian J. Geo-Marine Sci.* 47, 1774–1781.

Ou, Y., Zheng, J., and Nam, K.-M. (2022). Impacts of urban rail transit on on-road carbon emissions: a structural equation modeling approach. *Atmosphere* 13, 1783. doi: 10.3390/atmos13111783

Peng, D., Mu, Y., and Zhu, Y. (2021). Evaluating the level of coordinated development of fisheries economic growth and environmental quality in selected Chinese regions. *Environ. Impact Assess. Rev.* 89, 106605. doi: 10.1016/j.eiar.2021.106605

Shan, S., and Jiang, A. (2005). Analysis on the comparative advantage and export competity of china's aquatic products. *J. Int. Trade* 20–24. doi: 10.13510/j.cnki.jit.2005.05.005

Shi, Y., Shi, S., and Huang, X. (2022). The application of structural equation modeling in ecology based on r. *J. Ecol.* 41, 1015–1023. doi: 10.13292/j.1000-4890.202203.016

Su, S., Tang, Y., Chang, B., Zhu, W., and Chen, Y. (2020). Evolution of marine fisheries management in China from 1949 to 2019: how did China get here and where does China go next? *Fish. Fish.* 21, 435–452. doi: 10.1111/faf.12439

Suo, A., Zhou, W., and Ding, D. (2023). Suitability evaluation on marine ranching in guangdong, south China. *J. Oceanol. Limnol.* 41, 778–791. doi: 10.1007/s00343-022-1423-8

Tan, L., Wu, C., and Qu, Y. (2020). Measuring the international trade competitiveness of china's aquatic products from 2008–18. *J. Coast. Res.* 106, 157. doi: 10.2112/SI106-038.1

Tang, H., Dai, W., Liang, S., Liang, J., Guo, Y., and Bi, X. (2022). Development status, bottlenecks and countermeasures of marine shellfish aquaculture in circum-Yellow-Sea. *J. Tianjin Agric. Univ.* 29, 71–77. doi: 10.19640/j.cnki.jtau.2022.03.013

Teng, X., Zhao, Q., Zhang, P., Liu, L., Dong, Y., Hu, H., et al. (2021). Implementing marine functional zoning in China. *Mar. Policy* 132, 103484. doi: 10.1016/j.marpol.2019.02.055

The State of World Fisheries and Aquaculture 2022 (2022). doi: 10.4060/cc0461en

Tian, P., Li, J., Cao, L., Liu, Y., and Zhang, H. (2022). Evaluation of fishery economic efficiency anddevelopment trend forecast in China. *Chin. J. Agricultural Resour. Regional Plann.* 1–15.

Van Senten, J., Engle, C. R., Hudson, B., and Conte, F. S. (2020). Regulatory costs on pacific coast shellfish farms. *Aquaculture Economics Manage.* 24, 447–479. doi: 10.1080/13657305.2020.1781293

Wang, Q., Chen, B., Zhong, X., Zhou, H., Zhang, M., Mai, N., et al. (2022). Neuropsychiatric symptoms mediated the relationship between odor identification and cognition in alzheimer's disease spectrum: a structural equation model analysis. *Front. Aging Neurosci.* 13. doi: 10.3389/fnagi.2021.732840

Wang, B., and Han, L. (2017). A study on the basic situation and pattern of Shellfish breeding in China. *J. Ocean Univ. China* 153, 5–12. doi: 10.16497/j.cnki.1672-335x.2017.03.002

Wang, Q., Liu, Q., and Yang, L. (2021). Research on management countermeasures of high-level protection and efficient utilization of marine resources —a case study of guandong province. *Natural Resource Economics China* 34, 66–71+83. doi: 10.19676/j.cnki.1672-6995.000618

Wang, O., and Somogyi, S. (2019). Consumer adoption of sustainable shellfish in China: effects of psychological factors and segmentation. *J. Clean Prod.* 206, 966–975. doi: 10.1016/j.jclepro.2018.09.189

Wei, X., Hu, Q., Shen, W., and Ma, J. (2021). Influence of the evolution of marine industry structure on the green total factor productivity of marine economy. *Water* 13, 1108. doi: 10.3390/w13081108

Xu, S., and Gao, Y. (2022). Spatial-temporal differences of marine ranching DevelopmentPotential in China. *Mar. Economy* 12, 64–73. doi: 10.19426/j.cnki.cn12-1424/p.2022.06.008

Xu, X., and Yang, Z. (2022). Does aquatic products trade waste or save water resources? an analysis of virtual water trade. *Water Policy* 24, 305–323. doi: 10.2166/wp.2022.156

Yan, Y., Tian, P., and Li, J. (2022). Spatio-temporal evolution of high quality development level of china's fishery industry. *Chin. Fisheries Economics* 40, 36–46.

Yang, W., and Chen, D. (2022). Analysis of influencing factors and potential estimation of aquatic product imports in China:A case study of stochastic frontier gravity model. *Ocean Dev. Manage.* 39, 60–68. doi: 10.20016/j.cnki.hykfygl.2022.11.014

Yang, W., Li, X., Jin, Y., and Sun, T. (2018). The impact of multiple seashore reclamation activities on vegetation cover in the yellow river delta, China: implications based on structural equation modeling. *J. Coast. Conserv.* 22, 283–292. doi: 10.1007/s11852-017-0575-8

Yuan, Z., Zheng, X., Zhang, L., and Zhao, G. (2017). Urban competitiveness measurement of Chinese cities based on a structural equation model. *Sustainability* 9, 666. doi: 10.3390/su9040666

Zhang, L. (2016). The research on Guangdong marine fishery ecologicalcompensation mechanism. Master's Thesis. Zhanjiang: Guangdong Ocean University.

Zhang, Y., Dong, L., Yang, J., Wang, S., and Song, X. (2004). Sustainable development of marine economy in China. *Chin. Geogr. Sci.* 14, 308–313. doi: 10.1007/s11769-004-0033-z

Zhang, Y., Folarin, A. A., Sun, S., Cummins, N., Vairavan, S., Bendayan, R., et al. (2022). Longitudinal relationships between depressive symptom severity and phone-measured mobility: dynamic structural equation modeling study. *JMIR Ment. Health* 9, e34898. doi: 10.2196/34898

Zhang, Y., and Li, X. (2022). Factors influencing china's export of aquatic products. *Mar. Sci.* 46, 63–73. doi: 10.11759/hykx20220831003

Zhang, L., Lu, J., Wei, X., and Pan, J. (2019). Bayesian Structural equation modeling and its current researches. *Adv. psychol. Sci.* 27, 1812–1825. doi: 10.3724/SP.J.1042.2019.01812

Zhang, W., and Ma, X. (2022). Sustainable supply of aquatic food in China. *J. Shanghai Ocean Univ.* 31, 1304–1316. doi: 10. 12024 / jsou. 20220703927

Zhang, S., Mu, Y., and Sun, Y. (2021). Early impact of COVID-19 pandemic on the molluscan shellfish supply chain in China. *Ocean Coast. Manage.* 213, 105852. doi: 10.1016/j.ocecoaman.2021.105852

Zhao, Y. (2021). Analysis on the time sequence change and regional difference of china′s marine fishery competitiveness. *Mar. Economy* 11, 36–44. doi: 10.19426/j.cnki.cn12-1424/p.20201217.002

Zhao, B., and Zhu, Y. (2014). Formalizing and validating the web quality model for web source quality evaluation. *Expert Syst. Appl.* 41, 3306–3312. doi: 10.1016/j.eswa.2013.11.027

Zheng, D., Chen, D., and Lin, Q. (2020). Research on the influencing factors of the development level of marine economy in fujian province. *J. Coast. Res.* 115, 434–437. doi: 10.2112/JCR-SI115-122.1

Zhou, X., Zhao, X., Zhang, S., and Lin, J. (2019). Marine ranching construction and management in East China Sea: programs for sustainable fishery and aquaculture. *Water* 11, 1237. doi: 10.3390/w11061237

frontiers | Frontiers in Marine Science

TYPE Opinion
PUBLISHED 28 September 2023
DOI 10.3389/fmars.2023.1252589

OPEN ACCESS

EDITED BY
Jingzhen Wang,
Beibu Gulf University, China

REVIEWED BY
Carlos Rosas,
National Autonomous University of Mexico, Mexico
Eric Saillant,
University of Southern Mississippi, United States
Sharifah Rahmah,
University of Malaysia Terengganu, Malaysia

*CORRESPONDENCE
Zonghang Zhang
zhangzh@stu.edu.cn

RECEIVED 04 July 2023
ACCEPTED 18 September 2023
PUBLISHED 28 September 2023

CITATION
Zhang Z (2023) Problems and solutions for hatchery release: a framework.
Front. Mar. Sci. 10:1252589.
doi: 10.3389/fmars.2023.1252589

Problems and solutions for hatchery release: a framework

Zonghang Zhang [1,2]*

[1]Guangdong Provincial Key Laboratory of Marine Disaster Prediction and Prevention, Shantou University, Shantou, Guangdong, China, [2]Department of Biology, Shantou University, Shantou, Guangdong, China

KEYWORDS

stock enhancement, aquaculture, fisheries, behavioral adaptability, ecological fitness, environmental enrichment

1 Hatchery release

Hatchery release is a method of breeding fingerlings in artificial environments and then releasing them into natural water bodies (Kitada, 2018). Commonly, the application scenario of hatchery release is categorized into five types in a sequence ranging from the most production-centered to the most conservation-oriented aims: culture-based fisheries, stock enhancement, restocking, supplementation, and reintroduction (Lorenzen et al., 2021). Over the past century, hatchery release has been widely used as a tool to enhance, restore, and rebuild fishery resources (Blaxter, 2000; Svåsand et al., 2000). In their update to the responsible approach to marine stock enhancement, which integrated biological, economic, social, and governance aspects of captive propagation programs, Lorenzen et al. (2010) established the implementation framework of hatchery release (Lorenzen et al., 2010). However, the public and scientific community are still concerned about the effectiveness and sustainability of hatchery release initiatives, especially in light of assessments that suggested that many programs have not achieved the desired outcomes (Johnsson et al., 2014; Näslund, 2021). A contrasting perspective is that hatchery release is implemented at a large scale in several countries and these programs should not be cancelled lightly until other tools are demonstrated to be more effective in restoring fishery resources (Armstrong and Seddon, 2008; Taylor et al., 2017). To say the least, there is no necessity to abolish the activity that supports livelihood fisheries (especially in developing countries) and is endowed with a cultural or religious significance (e.g., the Buddhist practice of releasing fish) (Lorenzen et al., 2010). The alternative and maybe more sensible course of action is to identify potential problems existing in hatchery release and find effective approaches to solve them (Brown and Day, 2002).

2 Problems with hatchery release

From the perspective of biology, the main problems of hatchery release fall into the following categories. Firstly, the fitness of released fish is low. Regardless of the hatchery release application scenario, the primary objective is that the released fish can survive in the

wild (Wiley et al., 1993). If a released fish is not expected to survive in the wild, it undoubtedly undermines their most basic right to life and welfare (Brown and Day, 2002). The reasons for the low fitness of hatchery fish are mainly low behavioral adaptability and severe stress responses caused by release procedures (Näslund, 2021). Compared to wild fish, hatchery fish have poor predatory and anti-predatory abilities, tend to behave boldly and rigidly, are equipped with weak competitive ability in natural environments, and express low behavioral flexibility and diversity (Salvanes and Braithwaite, 2006). These differences between wild fish and hatchery fish originate from ontogenetic and genetic mechanisms (Olla et al., 1998). The ontogenetic deficiency is directly caused by the great differences in the structural, social, and sensory environment between the culture units and natural habitats, while the genetic discrepancy is mainly driven by deliberate or unintentional multi-generation artificial selection (Huntingford, 2004). Secondly, release may result in undesirable ecological and genetic interactions between wild and hatchery populations (Lorenzen et al., 2021). The ecological interaction is mainly mediated by a density-dependent mechanism, which is related to stocking number, release strategy (such as release time and location), wild population size, and environmental carrying capacity (Lorenzen et al., 2012). Genetic interaction can be direct (i.e., introgression due to reproductive activities) or indirect (e.g., reduction of wild population size through intraspecies competition) (Le Vay et al., 2007). Excessive gene flow may lead to changes in the genetic structure of the wild population, decrease in their genetic diversity, and thus weakening of their adaptive potential (Kitada, 2018). Thirdly, hatchery release may also promote interactions at higher ecological levels (Lorenzen et al., 2012). For example, released fish may compete for limited ecological niches, alter food web structure, influence energy flow through trophic relationships (i.e., eat and be eaten), and trigger cascade reactions (Lorenzen et al., 2021). Fish activities may also affect ecosystem function by modifying their habitats. Fourthly, releasing fish may cause disease transmission. It can be done either by introducing alien or evolved pathogens or by affecting the dynamics of established pathogens through changes in host population demography or immune status (Lorenzen et al., 2010). Fifthly, release procedures may also lead to technical interactions, such as the disturbance to the benthic ecosystem caused by broodstock capture and the changes in fishing pressure after the hatchery release activities (Lorenzen et al., 2010). In total, released fish have great ecological and genetic interactions with wild fish, and hatchery release may have technical and ethical interactions with ecosystems (including humans) (Le Vay et al., 2007). In the process of these interactions, the behavioral defects (and subsequent poor fitness) and decreased genetic diversity of released fish caused by limited sources of broodstock, captive environment, and release procedure are of great importance.

3 Finding solutions

Classical theories and practices offer several approaches to overcome the problems identified above. Genetic management is essential and needs to be addressed from the very beginning of a program because damage due to genetic impacts can be long-lasting and difficult to undo. Broodstock should be captured in the waters intended for release so as to avoid introducing non-native genotypes in the area and avoid disrupting the genetic background of the target wild population. Broodstock number should be as large as possible to minimize the risks of genetic diversity loss (Le Vay et al., 2007; Laikre et al., 2010). The first-generation fingerlings of native broodstock should be used to reduce the influence of artificial selection on the genome and epigenetics of hatchery fish and to avoid possible outbreeding depression (Johnsson et al., 2014). The second approach is to provide life skills training. It means that in the short term before release, hatchery fish undergo the key factors affecting their survival in the natural environment (such as predation, temperature change, etc.) so that they can acquire essential experience and adapt to the wild efficiently (Griffin et al., 2000; Brown and Day, 2002). As early as the beginning of this century, many related studies have been reported, and life skills training has been applied to the practice of hatchery release (Suboski and Templeton, 1989; Brown and Laland, 2001; Kelley and Magurran, 2003). Third, practitioners highlight the importance of optimizing release strategy. Various environmental factors should be considered to select the time and place suitable for individual species and specific developmental stages within a species (Lorenzen et al., 2010). At the same time, the beneficial effect of a larger size on fish survival, the detrimental effect of the captive environment on behavioral phenotype, and the economic cost involved in rearing fish to a large size in the hatchery prior to release should be comprehensively considered to select the appropriate fish size at release (Brown and Day, 2002). In addition, the soft release, which refers to the practice of providing an acclimatization period at the release site prior to actual release, is a promising method to help fish recover from various stresses involved in transportation, handling and change of environment (Tetzlaff et al., 2019).

How to optimize the hatchery environment to improve fish fitness has attracted wide attention in recent years (Ebbesson and Braithwaite, 2012; Johnsson et al., 2014). A basic principle is to introduce cues that fish receive in the wild to the captive environment to increase heterogeneity and complexity, in other words, simulate natural habitats (Johnsson et al., 2014). Projects based on this principle are often called environmental enrichment (Arechavala-Lopez et al., 2022). Most evidence shows that environmental enrichment can significantly improve the adaptive behaviors of hatchery fish by enhancing responses to behavioral and physiological stress as well as neural development and neurogenesis, although the mechanisms are not fully understood (Näslund and Johnsson, 2016; Zhang et al., 2022; Zhang et al., 2023a; Zhang et al., 2023b). More importantly, environmental enrichment can improve the learning ability of fish (Zhang et al., 2022). Considering that the nature of life skills training is associative learning behavior, it is expected that life skills training based on environmental enrichment will present an additive effect and equip hatchery fish with higher fitness (Brown and Laland, 2001; Kelley and Magurran, 2003). Interestingly, environmental enrichment can affect the level of DNA methylation in fish brains (Berbel-Filho et al., 2020). Although the ecological consequences of these modifications

remain unclear, these observations suggest that environmental optimization may be beneficial to the normal development of the epigenetic spectrum. A recent meta-analysis showed that introducing physical structures alone could not significantly improve fish survival rate, suggesting that the desired effect of environmental enrichment depends on whether the introduced cues match the target fish species, including the type, intensity, and duration of enrichment (Zhang et al., 2022). For examples, bottom-based structures (such as cobbles) are more suitable for demersal fish, longer duration of enrichment may be needed for species featuring greater longevity (such as Atlantic salmon vs. zebrafish), and fishes whose natural habitats have complex water flow fields (such as rocky fishes) may benefit from flow exercise (Arechavala-Lopez et al., 2022; Zhang et al., 2023a). In this case, a preference test is an appropriate candidate to determine these factors (Näslund and Johnsson, 2016; Zhang et al., 2023a). Generally, conditioning strategies are still evaluated primarily at the behavioral level, and there are few long-term *in-situ* monitoring studies on their effects on fitness. Furthermore, assessments of the effectiveness of conditioning on fish fitness are sharply contradictory among studies, and the causes of these discrepancies should be deeply investigated in the future.

Except for the considerations mentioned above, practitioners should particularly pay attention to the specificities of target environments where fish are to be released. A good example is provided by the constraints related to releases in marine versus freshwater environments. Freshwater ecosystems, generally, have higher habitat heterogeneity, more ecosystem-human interactions, but a lower spatial scale compared to marine ecosystems. These characteristics mean that the fish that will be released into freshwater may need to be equipped with higher cognitive abilities so they can cope with complicated physical and social situations. In contrast, released marine fish may need stronger swimming ability (but this does not mean that one does not need to train their cognitive abilities). However, information on these questions is very scarce to date.

4 Conclusions, suggestions and future directions

In conclusion, I summarize below a framework that emerged from this and other investigations on hatchery release. Stakeholders should consider the following aspects when designing and developing a hatchery release project. (1) Decision-makers should select species based on comprehensive considerations of ecological, economic, and social effects and then calculate the environmental capacity of the target water to determine the stocking number. (2) Practitioners should increase the number of broodstock as much as possible and release only first generation offspring. (3) Environmental enrichment during the captive period should be conducted to ensure hatchery fish develop phenotypic and epigenetic characteristics that will maximize their fitness in the wild environment. (4) Life skills of hatchery fish should be developed by training before release to provide them with essential experience that will improve their fitness. (5) Soft release should be implemented as much as possible, and the release area and time as well as fish size should be determined accounting for the specific context and objectives of a program.

Hatchery release is not an all-in-one solution to manage fishery resources, and past and on-going programs have illustrated shortfalls of this approach to population management and enhancement, such as high release mortality, genetic impacts, and low economic return relative to input. However, at present, hatchery release is still implemented in some programs in several countries, and the potential problems can be addressed through various ways. Overall, I believe that the integration of these environmental and genetic management tools can lead to success effectively restoring resources, boosting production, and reducing ecological and genetic risks of hatchery release. Hatchery release should be conducted in combination with other methods, such as habitat restoration, fisheries regulation, and establishment of marine protected areas, but this is another question beyond the scope of this paper. I encourage decision-makers and practitioners to comprehensively consider all available management tools, compare their specific strengths, and choose the most optimal strategy based on the trade-offs between biological, social, economic, and ethical effects.

This paper also aims to point to knowledge gaps and research needs. Since epigenetic modifications are an important mechanism by which fish adapt to their environment, it is urgent to explore the ecological consequences of these molecular changes induced by environmental enrichment. The impact of released fish on wild ecosystems at various levels and the effects of pre-release conditioning on these interactions should be studied more extensively. Finally, the rising number of studies on environmental conditioning could be exploited to assess the effectiveness of parameters of the conditioning process through a meta-analysis approach.

Author contributions

The author confirms being the sole contributor of this work and has approved it for publication.

Funding

This work was supported by the fund from the STU Scientific Research Initiation Grant (NTF22019) and the Program for University Innovation Team of Guangdong Province (2022KCXTD008).

Acknowledgments

ZZ thanks for the inspiration from Prof. Wenhua Liu (Shantou University, China), Prof. Xiumei Zhang (Zhejiang Ocean University, China), and Ms. Bingjie Chen (Shantou University, China), and ZZ

also thanks for the help with language editing from Dr. Hancheng Zhao (Shantou University, China).

Conflict of interest

The author declares that the research was conducted in the absence of any commercial or financial relationships that could be construed as a potential conflict of interest.

Publisher's note

References

Arechavala-Lopez, P., Cabrera-Álvarez, M. J., Maia, C. M., and Saraiva, J. L. (2022). Environmental enrichment in fish aquaculture: A review of fundamental and practical aspects. *Rev. Aquacult.* 14, 704–728. doi: 10.1111/raq.12620

Armstrong, D. P., and Seddon, P. J. (2008). Directions in reintroduction biology. *Trends Ecol. Evol.* 23, 20–25. doi: 10.1016/j.tree.2007.10.003

Berbel-Filho, W. M., Berry, N., Deiene, R. B., Sofia Rodrigues, T., Garcia De Leaniz, C., and Consuegra, S. (2020). Environmental enrichment induces intergenerational behavioural and epigenetic effects on fish. *Mol. Ecol.* 29, 2288–2299. doi: 10.1111/mec.15481

Blaxter, J. (2000). The enhancement of marine fish stocks. *Adv. Mar. Biol.* 38, 1–54. doi: 10.1016/S0065-2881(00)38002-6

Brown, C., and Day, R. L. (2002). The future of stock enhancements: lessons for hatchery practice from conservation biology. *Fish. Fish.* 3, 79–94. doi: 10.1046/j.1467-2979.2002.00077.x

Brown, C., and Laland, K. (2001). Social learning and life skills training for hatchery reared fish. *J. Fish Biol.* 59, 471–493. doi: 10.1111/j.1095-8649.2001.tb02354.x

Ebbesson, L., and Braithwaite, V. A. (2012). Environmental effects on fish neural plasticity and cognition. *J. Fish Biol.* 81, 2151–2174. doi: 10.1111/j.1095-8649.2012.03486.x

Griffin, A. S., Blumstein, D. T., and Evans, C. S. (2000). Training captive-bred or translocated animals to avoid predators. *Conserv. Biol.* 14, 1317–1326. doi: 10.1046/j.1523-1739.2000.99326.x

Huntingford, F. A. (2004). Implications of domestication and rearing conditions for the behaviour of cultivated fishes. *J. Fish Biol.* 65, 122–142. doi: 10.1111/j.0022-1112.2004.00562.x

Johnsson, J. I., Brockmark, S., and Näslund, J. (2014). Environmental effects on behavioural development consequences for fitness of captive-reared fishes in the wild. *J. Fish Biol.* 85, 1946–1971. doi: 10.1111/jfb.12547

Kelley, J. L., and Magurran, A. E. (2003). Learned predator recognition and antipredator responses in fishes. *Fish. Fish.* 4, 216–226. doi: 10.1046/j.1467-2979.2003.00126.x

Kitada, S. (2018). Economic, ecological and genetic impacts of marine stock enhancement and sea ranching: A systematic review. *Fish. Fish.* 19, 511–532. doi: 10.1111/faf.12271

Laikre, L., Schwartz, M. K., Waples, R. S., and Ryman, N. (2010). Compromising genetic diversity in the wild: unmonitored large-scale release of plants and animals. *Trends Ecol. Evol.* 25, 520–529. doi: 10.1016/j.tree.2010.06.013

Le Vay, L., Carvalho, G. R., Quinitio, E. T., Lebata, J. H., Ut, V. N., and Fushimi, H. (2007). Quality of hatchery-reared juveniles for marine fisheries stock enhancement. *Aquaculture* 268, 169–180. doi: 10.1016/j.aquaculture.2007.04.041

Lorenzen, K., Beveridge, M. C., and Mangel, M. (2012). Cultured fish: integrative biology and management of domestication and interactions with wild fish. *Biol. Rev.* 87, 639–660. doi: 10.1111/j.1469-185X.2011.00215.x

Lorenzen, K., Leber, K. M., and Blankenship, H. L. (2010). Responsible approach to marine stock enhancement: an update. *Rev. Fish. Sci.* 18, 189–210. doi: 10.1080/10641262.2010.491564

Lorenzen, K., Leber, K. M., Loneragan, N. R., Schloesser, R. W., and Taylor, M. D. (2021). Developing and integrating enhancement strategies to improve and restore fisheries. *B. Mar. Sci.* 97, 475–488. doi: 10.5343/bms.2021.0036

Näslund, J. (2021). Reared to become wild-like: addressing behavioral and cognitive deficits in cultured aquatic animals destined for stocking into natural environments—a critical review. *B. Mar. Sci.* 97, 489–538. doi: 10.5343/bms.2020.0039

Näslund, J., and Johnsson, J. I. (2016). Environmental enrichment for fish in captive environments: effects of physical structures and substrates. *Fish. Fish.* 17, 1–30. doi: 10.1111/faf.12088

Olla, B. L., Davis, M. W., and Ryer, C. H. (1998). Understanding how the hatchery environment represses or promotes the development of behavioral survival skills. *B. Mar. Sci.* 62, 531–550.

Salvanes, A. G. V., and Braithwaite, V. (2006). The need to understand the behaviour of fish reared for mariculture or restocking. *ICES J. Mar. Sci.* 63, 345–354. doi: 10.1016/j.icesjms.2005.11.010

Suboski, M. D., and Templeton, J. J. (1989). Life skills training for hatchery fish: social learning and survival. *Fish. Res.* 7, 343–352. doi: 10.1016/0165-7836(89)90066-0

Svåsand, T., Kristiansen, T. S., Pedersen, T., Salvanes, A. G. V., Engelsen, R., Nvdal, G., et al. (2000). The enhancement of cod stocks. *Fish. Fish.* 1, 173–205. doi: 10.1046/j.1467-2979.2000.00017.x

Taylor, G., Canessa, S., Clarke, R. H., Ingwersen, D., Armstrong, D. P., Seddon, P. J., et al. (2017). Is reintroduction biology an effective applied science? *Trends Ecol. Evol.* 32, 873–880. doi: 10.1016/j.tree.2017.08.002

Tetzlaff, S. J., Sperry, J. H., and DeGregorio, B. A. (2019). Effects of antipredator training, environmental enrichment, and soft release on wildlife translocations: A review and meta-analysis. *Biol. Conserv.* 236, 324–331. doi: 10.1016/j.biocon.2019.05.054

Wiley, R. W., Whaley, R. A., Satake, J. B., and Fowden, M. (1993). An evaluation of the potential for training trout in hatcheries to increase poststocking survival in streams. *N. Am. J. Fish. Manage.* 13, 171–177. doi: 10.1577/1548-8675(1993)013<0171:AEOTPF>2.3.CO;2

Zhang, Z., Chen, Q., Guan, X., Gong, M., Zhang, J., Cheng, F., et al. (2023b). Physical and social enrichment influences the adaptability-related behaviors of black rockfish *Sebastes schlegelii*: An effect mediated by social behaviors, HPI axis and neurogenesis. *Aquaculture* 564, 739056. doi: 10.1016/j.aquaculture.2022.739056

Zhang, Z., Gao, L., and Zhang, X. (2022). Environmental enrichment increases aquatic animal welfare: A systematic review and meta-analysis. *Rev. Aquacult.* 14, 1120–1135. doi: 10.1111/raq.12641

Zhang, Z., Lin, W., Li, Y., Yuan, X., He, X., Zhao, H., et al. (2023a). Physical enrichment for improving welfare in fish aquaculture and fitness of stocking fish: A review of fundamentals, mechanisms and applications. *Aquaculture* 574, 739651. doi: 10.1016/j.aquaculture.2023.739651

frontiers | Frontiers in Marine Science

TYPE Original Research
PUBLISHED 03 October 2023
DOI 10.3389/fmars.2023.1234772

OPEN ACCESS

EDITED BY
Jingzhen Wang,
Beibu Gulf University, China

REVIEWED BY
Xiujuan Shan,
Chinese Academy of Fishery Sciences (CAFS), China
Shuyang Ma,
Ocean University of China, China
Pablo Del Monte-Luna,
Centro Interdisciplinario de Ciencias Marinas (IPN), Mexico

*CORRESPONDENCE
Zuozhi Chen
chenzuozhi@scsfri.ac.cn

RECEIVED 05 June 2023
ACCEPTED 14 September 2023
PUBLISHED 03 October 2023

CITATION
Hong X, Zhang K, Li J, Xu Y, Sun M, Jiang J, Xu S, Cai Y, Qiu Y and Chen Z (2023) Impacts of climate events on life history parameters of major commercial fishes in the Beibu Gulf, South China Sea in the last 15 years. *Front. Mar. Sci.* 10:1234772. doi: 10.3389/fmars.2023.1234772

Impacts of climate events on life history parameters of major commercial fishes in the Beibu Gulf, South China Sea in the last 15 years

Xiaofan Hong[1,2,3], Kui Zhang[1,2], Jiajun Li[1,2], Youwei Xu[1,2], Mingshuai Sun[1,2], Jingyuan Jiang[4], Shannan Xu[1,2], Yancong Cai[1,2], Yongsong Qiu[1,2] and Zuozhi Chen[1,2]*

[1]South China Sea Fisheries Research Institute, Chinese Academy of Fishery Sciences, Guangzhou, China, [2]Key Laboratory for Sustainable Utilization of Open-sea Fishery, Ministry of Agriculture and Rural Affairs, Guangzhou, China, [3]College of Marine Sciences, Shanghai Ocean University, Shanghai, China, [4]Guangdong Provincial Academy of Environmental Science, Guangzhou, China

A detailed understanding of the impact of climate variability on fish life histories provides a fundamental basis for the ecosystem approach to fisheries management. In this study, we evaluated the relationship between fish life-history trait parameters and climate periods, using survey data from 2006–2020 for the Beibu Gulf of the northwestern South China Sea, a fishing ground with high commercial and ecological value. We show that climate events can significantly alter the structure of the life history for major commercial fishes, with more diverse life-history strategies during warm events and more concentrated mortality during cold events. Additionally, we detected special relationships between climate events and the life-history trait composite index (LTCI) in *Psenopsis anomala* and *Trichiurus lepturus*. It is possible that other indicators would be more appropriate than variability in Oceanic Niño Index (ONI), such as variation in fishing effort or the environmental resistance of fish. Anthropogenic disturbance and biological features may also help explain the magnitude of population variability. We found that changes in life-history traits of only a few commercial fishes (*Decapterus maruadsi*, *Pennahia macrocephalus*, and *Upeneus sulphureus*) were related to the shift in climate periods; these fishes were generally characterized by faster growth and higher mortality rates in the normal and El Niño periods, with the opposite trends in La Niña periods. However, the emergence of climate events has led to a clear complementarity of life-history strategies among some fish in the same ecological niche (same genus and/or feeding group), which may be explained by a balance between habitat conditions and fishing pressures. This study of fish life-history strategies under climate anomalies provides key insights into important attributes for managers to consider when implementing relevant measures to promote fisheries sustainability in the subtropical bay.

KEYWORDS

Beibu Gulf, major commercial fishes, ELEFAN, life-history trait parameters, El Niño-Southern Oscillation

1 Introduction

Climate anomalies, such as the El Niño–Southern Oscillation (ENSO), are one of the main drivers of marine ecosystem changes (Timmermann et al., 2018). Although the major signal of ENSO occurs in the equatorial Pacific with an intensity that can vary considerably from one event to another, it is unique among climate phenomena in its great influence on the patterns of weather variability worldwide (Lehodey et al., 2006; Mcphaden et al., 2006). The physical-biogeochemical changes in the marine ecosystem caused by ENSO affect the distribution and biomass of plankton, fish and invertebrates that depend on them (Gomez et al., 2019). The literature devoted to effects of climate variability on these components of the marine ecosystem is rapidly growing (Holbrook et al., 2020), as is also the case for the literature on freshwater and terrestrial ecosystems. However, there is growing evidence for interactions between climate change and ENSO dynamics and effects, complicating analyses of underlying mechanisms (Lehodey et al., 2020). A better understanding of these mechanisms will be useful for the exploration of relationship between climate anomalies and fishery resources, as well as formulate polices for fisheries management.

From the tropical Pacific open sea to the coasts of Asia and the Americas, ENSO affects the mortality, recruitment, and habitat distribution of commercially valuable fishes (Stenseth et al., 2002). ENSO events provide an excellent opportunity to observe and evaluate how changes in habitats influence the life-history traits, abundance, or distribution of fishes. Identifying changes in these population characteristics will increase understanding of the habitat requirements of important marine resources and will help local government departments and/or organizations better manage fisheries. Life-history traits and population dynamics of fish depend closely on environmental conditions (Chaparro-Pedraza and De Roos, 2019). Lots of studies have suggested that changes in meteorological variables and hydrographic, such as salinity, cloudiness, storminess, and temperature, will affect fish life histories (e.g., recruitment, mortality rates, migration patterns, growth, and spatial distributions) (Hunter et al., 2002; Hossain et al., 2012; Pécuchet et al., 2015; Chaparro-Pedraza and De Roos, 2019). These variables can therefore impact fish population dynamics substantially; for example, populations may exhibit oscillations in abundance and/or alternative pattern in distribution due to changes in the populations of prey (Blanchot et al., 1992) or predators (Sprogis et al., 2018). If these populations are commercially exploited, the oscillating trends in abundance and distribution will, in turn, guide the appropriate and efficient management of local fisheries (e.g., updating fisheries law, registering fishing vessels, and establishing closed fishing areas and seasons). Particular examples of populations that have undergone such fluctuations are the small pelagic fish populations in the northwestern offshore of Baja California in 1997–1998, these populations were concentrated in specific areas not influenced directly by ENSO events, and researchers suggested that it is necessary to regulate the fishing during climate anomalies (Rojas-Mendez and Mendoza, 2008).

Life history refers to the pattern of survival and reproduction events during the life of fish. Life-history traits include fecundity, age-at-maturity, maximum size, and longevity (Oli and Coulson, 2016; Brown and Choe, 2019). Life history theory holds that these traits have been shaped by natural selection to optimize trade-offs related to growth, reproduction, and survival (Petrik, 2019). Moreover, life-history traits are the underlying determinants for population responses to environmental forcing (King and Mcfarlane, 2003). There is no doubt that the diversity of life-history trait combinations is due to inherent trade-offs, as more energy allocated to reproduction reduces energy available for growth or maintenance and vice versa (Waples and Audzijonyte, 2016). Since the finite amount of energy cannot fully meet the demands of reproduction, growth, and maintenance, only certain combinations of life-history traits produce an organism with high fitness (Charnov, 1993). The particular life-history traits of any given fish can be shaped by the environment. For example, the impact of global warming will not only directly influence the duration of embryonic development, egg survival, size at hatching, developmental rate, pelagic larval duration, and survival but will also alter larval behavior and impair sensory capabilities through its companion effect (ocean acidification) (Pankhurst and Munday, 2011). The age-at-maturity and energy allocated to reproduction depend on growth conditions of the juvenile (Ward et al., 2017), and this will in turn impact population recruitment and connectivity patterns in marine fishes (Pankhurst and Munday, 2011). Life-history traits are the underlying determinants of population responses to environmental forcing. Accordingly, it is important to consider life-history strategies in fisheries management.

The Beibu Gulf is located in the northwestern South China Sea (17–22°N, 105–110°E) and covers a total area of 1.3×10^5 km^2 with an average depth of 50 m (Gao et al., 2017). As one of the four most prominent fishing grounds in China (Su et al., 2022), the vessel monitoring system shows that Beibu Gulf is one of the main areas where fishing vessels operate in the South China Sea (Qian et al., 2022), the rich fishery resources of this area are particularly important as a key contributor to ecosystem services. The Beibu Gulf serves as a spawning and feeding ground for many major commercial fish because of its unique geographic location and climatic conditions (Chen et al., 2009; Gao et al., 2017). In total, > 1000 fish species have been reported in the region to date, more than half of the fish species recorded in the northern South China Sea continental shelf (Liang, 2022), most of which are demersal (Khanh et al., 2013). However, the ecosystem structure has been altered considerably during the last decades of the 20th century, with overfishing leading to changes in species compositions and a decline in the biomass of most commercial species (Chen et al., 2011; Xu et al., 2011). The typical dominant species, including crimson snapper (*Lutjanus malabaricus*) and *Pomadasys hasta*, have been replaced by fishes of lower trophic levels, such as *Acropoma japonicum* and *Argyrosomus macrocephalus* (Qiu et al., 2010; Wang et al., 2013). Fortunately, the government of China has taken a series of strict management measures for the domestic fishery industry over the last 20 years, such as the implementation of a summer fishing moratorium (Shen and Heino, 2014) and the adjustment of fishery fuel subsidies for fishing vessels (Su M. et al., 2021). The mean trophic level of fish resources from bottom-trawl survey data in Beibu Gulf has slightly increased since 2000 (Su L. et al., 2021). However, increasing fishing pressure in the Beibu Gulf

by Vietnam fishery vessels appears to have made these measurements less effective, annual total catch in this region is decreasing (Huang and Huang, 2013; Tian et al., 2022). In addition, ENSO events can influence marine ecosystems via global atmospheric and oceanic processes. These effects could be particularly important in a subtropical gulf, such as the Beibu Gulf, where complex circulation and strong horizontal gradients in salinity, temperature, and oxygen concentrations control the reproduction and distribution of most species. Although most studies of fishery resources in the Beibu Gulf have focused on effects of anthropogenic activities and seasonality (Wang Y. et al., 2020; Su L. et al., 2021; Zhang et al., 2022), few published studies have considered the relationship between population status and climate variability. Therefore, this study aims to fill the gap in knowledge regarding the impact of climatic variability on fish populations in the subtropical semi-enclosed Beibu Gulf.

Here, we used the electronic length frequency analysis (ELEFAN) to estimate von Bertalanffy growth function (VBGF) parameters (Pauly, 1980) for major commercial fishes in the Beibu Gulf. Trends in life-history strategies (what kind of ways that organisms allocate limited resources to growth, health maintenance, and various life processes)(Wang et al., 2021) across climate periods were evaluated. Natural mortality and growth parameters were also examined for synchronicity across species to determine the potential for climate events to generate a synchronous trend in life-history strategies. Therefore, the relationships between the Oceanic Niño Index (ONI) and life-history traits of fishes were examined to analyze the potential impact of climate events.

2 Data and methods

2.1 Data sources

Fish sampling data were obtained from 34 otter trawl surveys at 52 stations (Figure 1) from 2006 to 2020. Apart from four survey cruises per year in January, April, July, and October in 2006 and 2007, surveys since 2008 were performed twice a year in January and July. Most survey cruises did not cover all 52 stations for a variety of reasons, but the samples were generally coherent in methodology. The surveys were undertaken by a commercial fishing vessel with a main engine of 600 HP. In every survey, each station was trawled once for 1 hour with a towing speed of 2.5~3.5 knots. The headrope length of the otter trawl net was 37.7 m and the cod-end mesh was 40 mm. Every trawl sample was sorted onboard and identified to the species level. Samples of each fish were counted, weighed, and recorded, and length and weight frequency data were also collected for major commercial fish. When fewer than 50 individuals were caught in a trap, all individuals were measured; otherwise, 50 individuals were randomly sampled for measurement. For each marine fish, total length (nearest cm) and body weight (nearest g) were measured. Based on the availability of data, we selected 13 species of major commercial fish (include 9 fish families, Table 1) with the highest frequencies of occurrence for analyses; according to data from the China Fishery Statistical Yearbook (2006-2020), these species account for about 45% of the total catch recorded in the Beibu Gulf.

To characterize ENSO events, data for the ONI in each month from 2006 to 2020 were obtained from products of the NOAA (National Oceanic and Atmospheric Administration) Climate Prediction Center (CPC; https://origin.cpc.ncep.noaa.gov/). The ONI is defined as 3-month running mean sea surface temperature (SST) departures in the Niño 3.4 region (5°N to 5°S, 120 to 170°W) and is a principal measure for monitoring, assessing, and predicting ENSO. Climate events are defined as five consecutive overlapping 3-month periods at or above a +0.5°C anomaly for warm (El Niño) events and at or below the −0.5°C anomaly for cold (La Niña) events. The threshold is further broken down into weak (with a 0.5–0.9°C SST anomaly), moderate (1.0–1.4°C), Strong (1.5–1.9°C), and very strong (≥2.0°C) events. The CPC considers that these anomalies must also be forecasted to persist for three consecutive months. In addition, the 1/4-resolution SST data were obtained

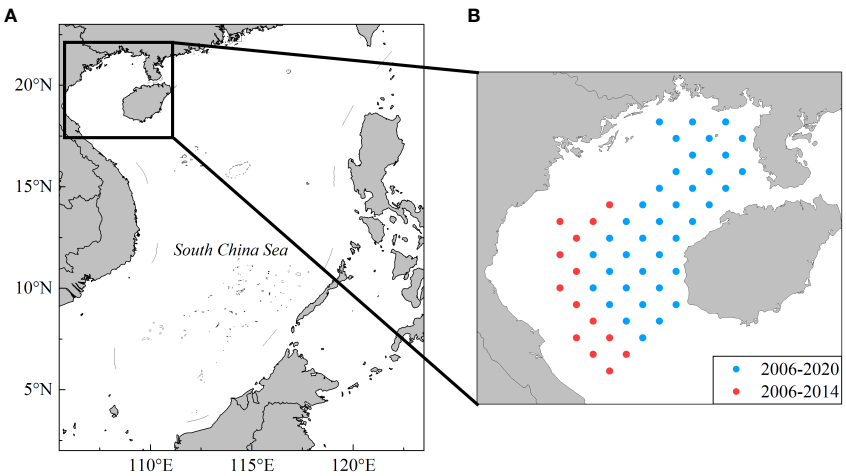

FIGURE 1
Map showing stations for otter trawl surveys in the Beibu Gulf during 2006–2020. **(A)** the location of the Beibu Gulf in the South China Sea; **(B)** the sampling station (dots) in the Beibu Gulf.

TABLE 1 The 13 major commercial fishes in the Beibu Gulf.

NO.	Scientific Name	Family	Common name	Habitat	Climate vulnerability	Catch rate
1	*Psenopsis anomala*	Centrolophidae	Pacific rudderfish	Benthopelagic	Moderate	3.08%
2	*Pennahia macrocephalus*	Sciaenidae	Big-head pennah croaker	Demersal	*	4.29%
3	*Trichiurus lepturus*	Trichiuridae	Largehead hairtail	Benthopelagic	High	1.21%
4	*Priacanthus macracanthus*	Priacanthidae	Red bigeye	Reef-associated	High	0.26%
5	*Saurida tumbil*	Synodontidae	Greater lizardfish	Reef-associated	High-Very high	1.98%
6	*Saurida undosquamis*	Synodontidae	Brushtooth lizardfish	Reef-associated	Low	0.96%
7	*Upeneus sulphureus*	Mullidae	Sulphur goatfish	Demersal	*	0.60%
8	*Upeneus japonicus*	Mullidae	Japanese goatfish	Demersal	*	0.15%
9	*Nemipterus virgatus*	Nemipteridae	Golden threadfin bream	Demersal	Moderate-High	0.43%
10	*Nemipterus bathybius*	Nemipteridae	Yellowbelly threadfin bream	Demersal	*	0.16%
11	*Decapterus maruadsi*	Carangidae	Japanese scad	Pelagic	Moderate	9.52%
12	*Trachurus japonicus*	Carangidae	Japanese jack mackerel	Pelagic	Low	15.67%
13	*Evynnis cardinalis*	Sparidae	Threadfin porgy	Reef-associated	*	6.78%

Except for the data of catch rate calculated from all surveys in this study, all the information on the major commercial species in the Beibu Gulf comes from www.fishbase.se; climate vulnerability represents the vulnerability of marine species to climate change based on the fuzzy logic framework (Jones and Cheung, 2018), * refers that the information is not available from the website.

from the OI SST V2 High Resolution Dataset provided by NOAA's Physical Science Laboratory, Boulder, Colorado, USA (https://psl.noaa.gov, accessed on 1 October 2022). Monthly mean SST data were collected at all survey stations to calculate the monthly mean SST in the Beibu Gulf from 2006 to 2020.

2.2 ELEFAN application

Length frequency data of major commercial fishes from 2006 to 2020 was pooled and converted to monthly catches with the assumption that the samples were representative of the total catch of the month (Zhang et al., 2023). We used ELEFAN in the R package "TropFishR (1.6.3)" (Mildenberger et al., 2017) to estimate the natural mortality, asymptotic length, and growth coefficient of major commercial fishes, and the optimization routine for the fitting of von Bertalanffy growth function (VBGF) parameters is the "ELEFAN_GA" function uses the Genetic Algorithm package "GA" (Scrucca, 2013; Scrucca, 2017). Growth parameters are described by the VBGF (Von Bertalanffy, 1938):

$$L_t = L_\infty\left(1 - e^{-k(t-t_0)}\right) \quad (1)$$

where L_t represents mean length (cm) at age t, L_∞ represents asymptotic length (cm), k represents growth coefficient, and t_0 is the theoretical age when $L_t = 0$.

To improve the precision of the growth parameters (L_∞ & k) estimation, the length frequency data of major commercial fishes was binned according to the maximum body length observed for the fish species (Wang K. et al., 2020), number indicating over how many length classes the moving average should be performed:

$$\text{Moving average (MA)} = 0.23L_{max}^{\ 0.6} \quad (2)$$

where L_{max} represents maximum body length (mm) of each fish being studied.

Natural mortality (M) was estimated by applied an updated version of the (Pauly, 1980) growth-based method (Then et al., 2015):

$$M = 4.118k^{0.73}L_\infty^{-0.33} \quad (3)$$

For optimum search and improvement in the accuracy of the output of ELEFAN_GA, we appropriately tuned key input settings (including Fix L_∞ (initial seed value of L_∞) and upper and lower limits of k) based on relevant literature (Taylor and Mildenberger, 2017; Mzingirwa et al., 2020; Wang K. et al., 2020) and used default TropFishR settings for all other parameters.

2.3 Life-history trait composite index

Based on the fundamental trade-offs between natural mortality (M) and parameters defining the maximum size and rate of growth in marine fish proposed by Gislason et al. (2010) and the empirical equation demonstrated by Charnov et al. (2013) (Equation (4), a life-history trait composite index (LTCI) was constructed to show the combinations of life-history traits, that is, life-history strategies. Given that for any combination of life-history traits, the points formed by the natural mortality (M) and growth state parameter $((L/L_\infty)^{-1.5}\bullet k$, a higher value indicates how fast the fish grows) of marine fishes on the coordinate axis are basically along the $y = x$ line (Charnov et al., 2013), the LTCI was calculated as the distance between the point

projected on the $y = x$ line of each point and the zero point (origin). The value of LTCI was calculated as shown in Equation (5):

$$M = \left(\frac{L}{L_\infty}\right)^{-1.5} \cdot k \tag{4}$$

$$LTCI = \pm\sqrt{\frac{(\ln(M))^2 + \left(\ln\left(\left(\frac{L}{L_\infty}\right)^{-1.5} \cdot k\right)\right)^2}{2}} \tag{5}$$

where L_∞ (cm) and k (year^{-1}) are the VBGF parameters and L (cm) is defined as the mean body length of the fish population. The value of LTCI will be positive if the projected point is on the right-hand side of the zero point, negative if it is on the left-hand side of the zero point, and 0 if it falls on the zero point (Figure 2).

2.4 Statistical analysis

Cross-correlation function (CCF) analysis was used to explore the hysteretic relationship between climate event intensity and SST in time series, for removing spurious correlations from the affected time series (Baumgartner et al., 2018), this study performed prewhitened CCF analysis using the "prewhiten" function from the R package "TSA". To investigate responses of fish populations to climate events, linear models were used to identify the relationships between the ONI and parameters of fish life-history traits. Spearman correlation coefficients were used to test the significance of these relationships ($p < 0.05$ was considered significant). Multivariate analysis of variance (MANOVA) and one-way analysis of variance (ANOVA) were employed to compare fish life-history trait parameters among climate periods. SPSS 27.0 (SPSS Inc.) was used to perform these statistical analyses.

Furthermore, the effects of climate events on the life history of the fish community were analyzed by using a hierarchical linear model and moderating effect estimation, and the R package "broom.mixed" and R package "bruceR" were used respectively. All R packages were operated in the R Environment (R Core Team, 2022).

3 Results

3.1 Climate periods

In 2006–2020, 11 climate periods were identified according to the afore-mentioned criteria for the classification of climate events,

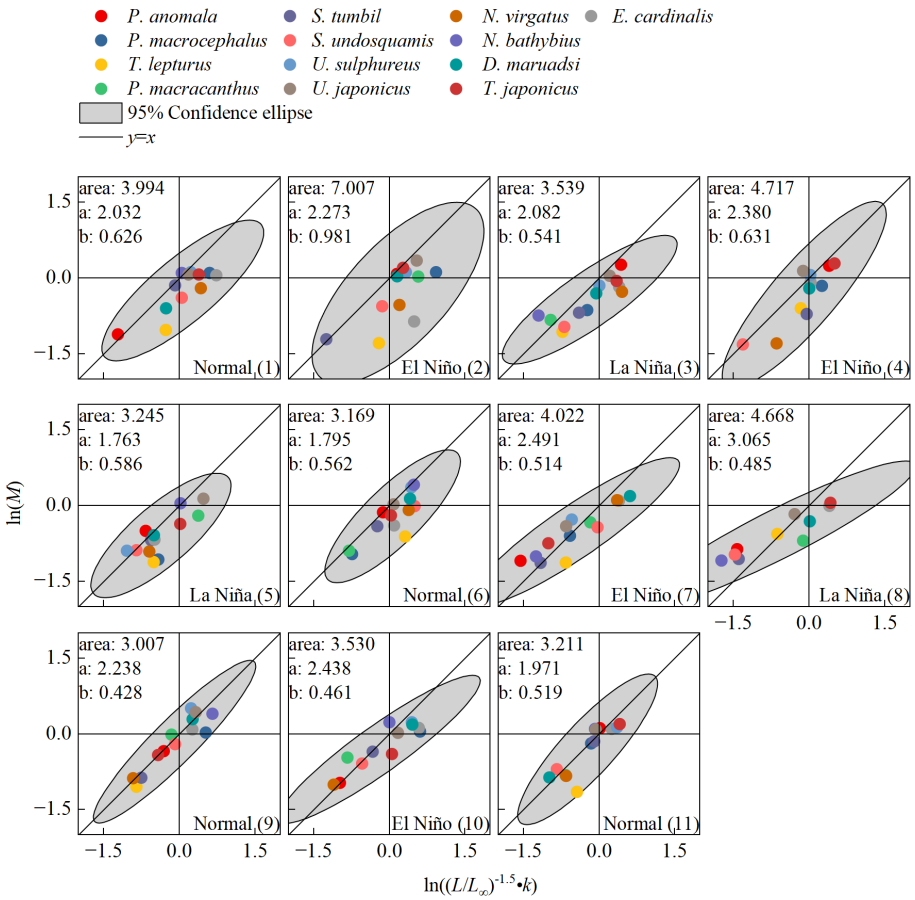

FIGURE 2
Log-log relationship between natural mortality (M) and growth parameters ($((L/L_\infty)^{-1.5} \cdot k)$) for fish community in the Beibu Gulf. The numbers represent the climate periods in the same order as Table 2, and the area (gray region) represents a 95% confidence ellipse, a and b refer to the major and minor axes of the 95% confidence ellipse, respectively.

of which four were normal climate periods, four were El Niño periods, and four were La Niña periods (Table 2).

3.2 Life-history traits of the fish community in the Beibu Gulf

The hierarchical linear model results indicated that the relationship between the growth status parameter ($\ln((L/L_\infty)^{-1.5} \bullet k)$) and natural mortality ($\ln(M)$) of fish community differ significantly by climate event type; the normal climate period regression slope (p_n = 0.772) was closest to 1.0, and it also was higher than the regression slopes of El Niño period (p_e=0.669) and La Niña period (p_l=0.593) (Figure 3A) The mean difference estimation also showed that climate events had an impact on LTCI in fish communities, and the mean diffidence of LTIC La Niña events also was the largest. In addition, regression analysis of the life history trait parameters of fish communities for each climate period was also shown the mean area of the 95% confidence ellipse (3.345 ± 0.382) was lowest in the normal period (Figure 2), followed by the La Niña period (3.817 ± 0.613), and was highest in the El Niño period (4.819 ± 1.332). The mean major axis of the ellipse (a) was also lowest in the normal period (2.009 ± 0.158) and larger in the La Niña (2.303 ± 0.554) and El Niño periods (2.396 ± 0.081), while the mean minor axes of the ellipse (b) in the normal (0.534 ± 0.072) and La Niña periods (0.537 ± 0.041) were similar, with the highest value in the El Niño period (0.647 ± 0.203). Overall, the results of MANOVA showed that the growth state parameter, natural mortality, and LTCI of fish in different climatic event periods showed significant differences ($p < 0.05$).

3.3 The variations of SST in the Beibu Gulf

The monthly mean SST in the Beibu Gulf (Figure 4A) presented significant and positive associations with ONI during 2006–2020 (r = 0.521). Considering the time with higher correlation values, there was a high correlation between the monthly mean SST in the Beibu Gulf and ONI without any lag (Figure 4B). In addition, although the effects of monthly mean SST on LTCI of fish communities were no significantly different in El Niño climate periods compared with normal and La Niña climate periods based on the results of moderate effect estimation ($p = 0.07$), the LTCI of fish communities strongly increased with monthly mean SST, while the LTCI of fish communities as a whole was lower than normal climate periods during La Niña climate periods (Figure 5).

3.4 Distribution of life history trait parameters of fishes

Except for *T. lepturus* and *E. cardinalis*, the natural mortality values and growth parameters of other fish showed a significant positive correlation (Figure 6). Some fish exhibited relatively stable life histories between climate periods; for example, the life-history trait parameters of *T. lepturus* clustered in the lower-left area of the coordinate plane. In addition, one-way ANOVA showed that these fish life-history trait parameters did not differ significantly among climate periods ($p > 0.05$), whereas life-history trait composite index (LTCI) of *P. macrocephalus* and *D. maruadsi* differed significantly during the transition of climate periods ($F = 38.986$ and $F = 14.921$, respectively, all $p < 0.05$). Except for *N. bathybius* and *P. anomala*, all fishes did not display any considerable oscillation in LTCI with the transformation of climate periods (Figure 7).

3.5 Relationship between LTCI and climate events

A Spearman correlation analysis indicated that the LTCI values for *D. maruadsi*, *P. macrocephalus*, and *U. sulphureus* were significantly correlated with ONI in 2006–2020 (r = 0.697, 0.762,

TABLE 2 Summary statistics of fish community in each climate period from 2006 to 2020.

NO.	Climate periods	Sampling time horizon	Mean ONI
1	Normal	2006.04~2006.07	0.020
2	El Niño	2006.10~2007.01	0.740
3	La Niña	2007.07~2009.01	-0.857
4	El Niño	2009.07~2010.01	1.033
5	La Niña	2010.07~2012.01	-0.982
6	Normal	2012.07~2014.07	-0.090
7	El Niño	2014.10~2015.04	1.467
8	La Niña	2016.07~2016.11	-0.620
9	Normal	2017.01~2017.05	0.000
10	El Niño	2018.09~2019.04	0.711
11	Normal	2019.08~2020.04	0.223

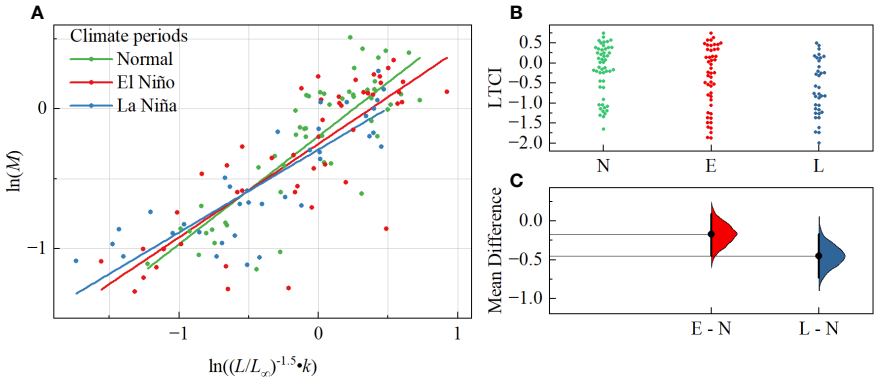

FIGURE 3
(A) Linear regressions of natural mortality and growth status parameter at the three climate periods since 2006-2020 within the Beibu Gulf; **(B, C)** Mean differences in LTCI of fish communities during climate event periods versus normal climate periods, N, E and L represent normal, El Niño and La Niña climate, respectively.

and 0.905, respectively, all $p < 0.05$). The most consistent changes in the LTCI of the three fish species occurred in 2006–2012, when transitions between warm and cold events was most frequent (Figure 8). Furthermore, in the latter six climate periods, there was a negative correlation between the LTCI of *T. japonicus* and *D. maruadsi*. While the relationships were not statistically significant, the LTCI of fishes belonging to the same genus showed the opposite trends in some climate periods, including *U. sulphureus* and *U. japonicus*, *S. tumbil* and *S. undosquamis*, and *N. virgatus* and *N. bathybius*.

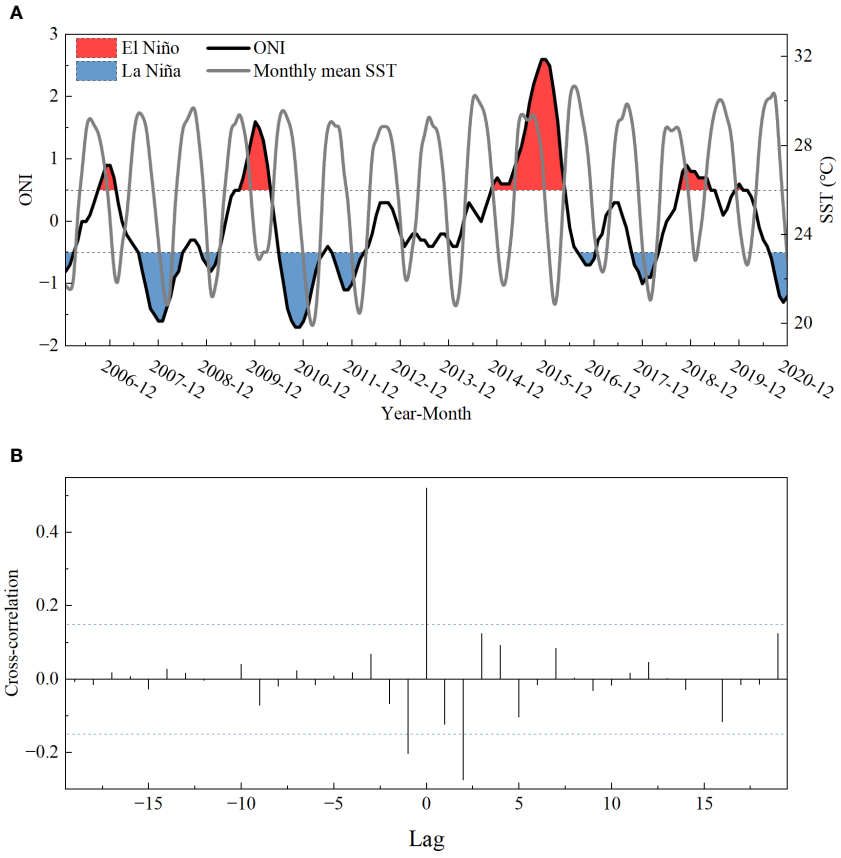

FIGURE 4
(A) Time-series of monthly mean SST and (ONI). **(B)** Cross- correlation functions (CCFs) between ONI and monthly mean SST; dashed lines indicate the significance threshold (α = 0.15).

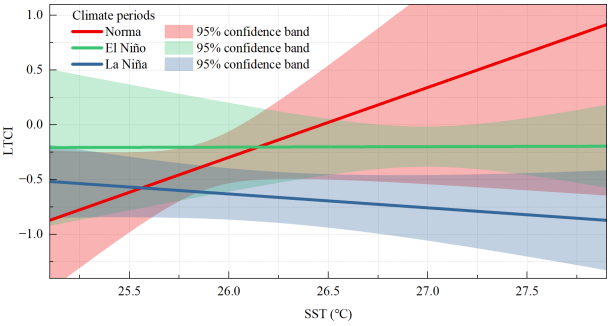

FIGURE 5
Linear regressions of LTCI and monthly mean SST at the three climate periods since 2006-2020 within the Beibu Gulf.

4 Discussion

According to Table 1, the vast majority of the 13 major commercial fishes in the Beibu Gulf that we selected were low vulnerable to fishing, but nearly half were recorded as having moderate to high vulnerability to climate. There is no doubt that it is interesting to analyze the correlation between the parameters of the life-history traits of these fishes and climatic events. By examining patterns of responses across 13 major commercial fishes in the Beibu Gulf, we found evidence that fluctuations in life-history traits and the abundance of some small fishes are best explained by changes in environmental variables caused by ENSO events. Frequent transformations of climate events were correlated with periodic fluctuation in LTCI, while the sensitivity of fishes to various environmental variables explained variation in abundance. However, our results also expand upon theoretical and regional results, highlighting the particularly high sensitivity of some fishes in the subtropical gulf to climate events.

4.1 Life-history traits of fish communities

Despite a large and growing body of evidence for the role of anthropogenic activities in the population dynamics of marine species (Pinsky and Palumbi, 2014; Sherman et al., 2017; García-March et al., 2020; Strøm et al., 2021), including dramatic fluctuations of pelagic and demersal fishes in the South China Sea over space and time scales (Masrikat, 2012; Yang et al., 2021; Zhang et al., 2022), our results suggest that the combination of life-history strategies for the Beibu Gulf fish community were most strongly

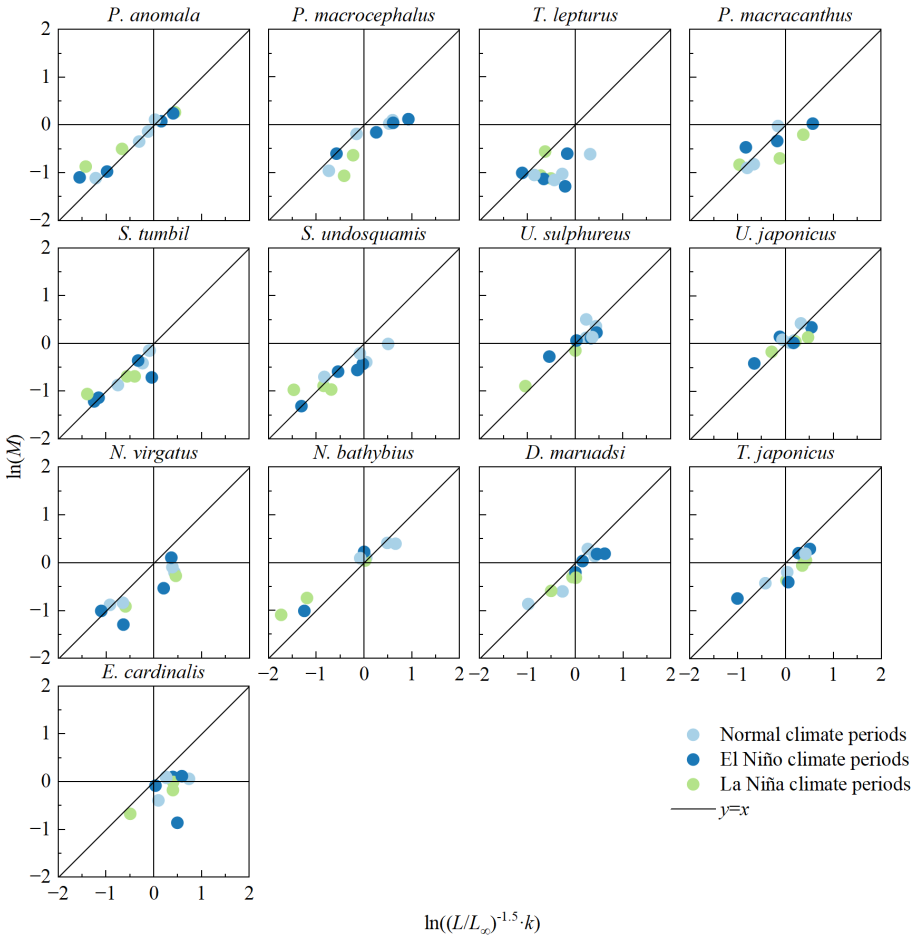

FIGURE 6
Log-log relationship between natural mortality (*M*) and growth parameters for 13 major commercial fishes in the Beibu Gulf.

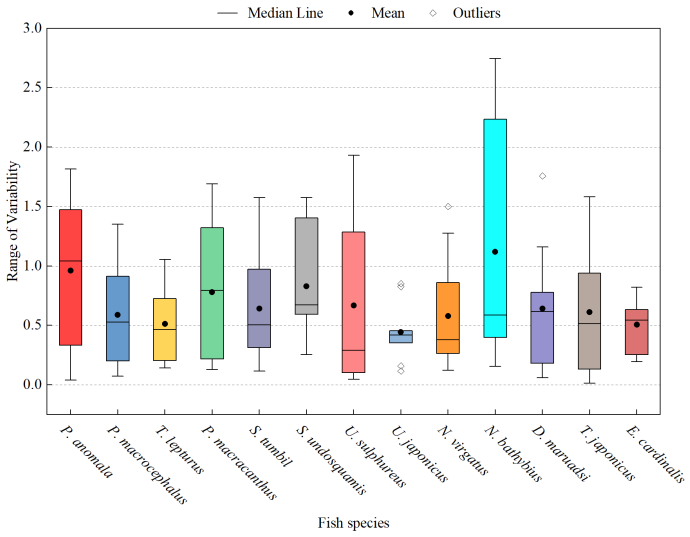

FIGURE 7
Boxplot of LTCI for 13 major commercial fishes. Each box represents fluctuation of LTCI of a fish between the climate periods; median value of LTCI is indicated by a filled point.

driven by climate events. Climate events significantly altered the slope of the regression of life-history trait parameters for fish communities, with slopes closest to 1.0 in the normal period (Figure 3). However, our results also revealed that both climate events would lead to a decrease in the mean correlation coefficient, especially La Niña periods, which can be explained by the fact that the combinations of life-history traits for most fish species fall in the lower-left quadrant (slower growth and lower *M*). Although the mean correlation coefficient of the El Niño period was between those for the normal and La Niña periods, the larger mean area of the confidence ellipse for the combinations of life-history traits in the El Niño period differed from those of other periods, and the former period tends to have a higher diversity of fish life-history strategies. While other studies have found that this climate variability may influence the biomass of certain fish species substantially via environmental variables (Yatsu et al., 2008; Yen and Lu, 2016), our results highlight the regular dynamics of life-history strategy selection in fish communities.

An important and relatively underappreciated mechanism underlying this dynamic may be related to ocean-atmosphere coupling. Temperature in all regions has pervasive effects on biological processes. Even though the mean SST in Beibu Gulf is on the rise under the background of global warming, this study found a positive correlation between the monthly mean SST in Beibu Gulf and ONI without any lag. This response to water temperature anomaly in the equatorial Pacific is bound to affect fish growth and development (Gillanders et al., 2012). In general, species characterized by fast growth and short generation times (high *M* values) would respond quickly to environmental changes (King and Mcfarlane, 2006), and the increase in seawater temperature caused by warm events may accelerate their growth and maturation. From the results of this study analysis, however, the relationship between LTCI of fish community and SST in the Beibu Gulf has a certain correlation with the type of climate events. On the one hand, since Beibu Gulf was a subtropical bay and its fishes were mainly warm-water species (Liang, 2022), temperate fishes tend to have smaller heating tolerances than tropical fishes (Payne et al., 2021). Therefore, an increase in environmental temperature would reduce the physiological function of fish and then affect the fish's life history (Dembski et al., 2006; Holt and Jorgensen, 2015), especially during the El Niño climate periods when the SST is significantly warmer, and this study observed a significant increase in LTCI in fish with increasing SST. On the other hand, fishes tend to choose more "conservative" life-history strategy (slower growth and lower *M*) selection because of the lack of suitable water temperature in the environment (Soyano and Mushirobira, 2018). This was also evident in the event of cold events, where significantly lower seawater temperatures undoubtedly result in a lower overall LTCI of fish communities compared to normal climate periods. Life-history traits of signal species evolve based on environmental conditions to maximize sustainable reproduction; however, changes in the life-history strategy of fast-growing species, as the most important component of the ecosystem (Waples and Audzijonyte, 2016), will inevitably affect their ecological functions. In addition, during El Niño periods, the South China Sea generally exhibits weakened circulatory gyres and warming of the SST, consistent with the weakening of East Asian winter monsoon (Qiu et al., 2015). Previous studies have suggested that warmer temperatures increase metabolic rates and therefore increase the energy demand of fishes, while simultaneously decreasing the quality and quantity of available prey (Overland et al., 2010). As a result, combinations of life-history traits of fish within communities have become more diverse, even if some combinations have deviated significantly from evolutionarily stable strategies. This mechanism may explain our finding that life-history strategies for the fish community in Beibu Gulf were sensitive to climate events. While marine species fluctuate strongly, even in the presence of

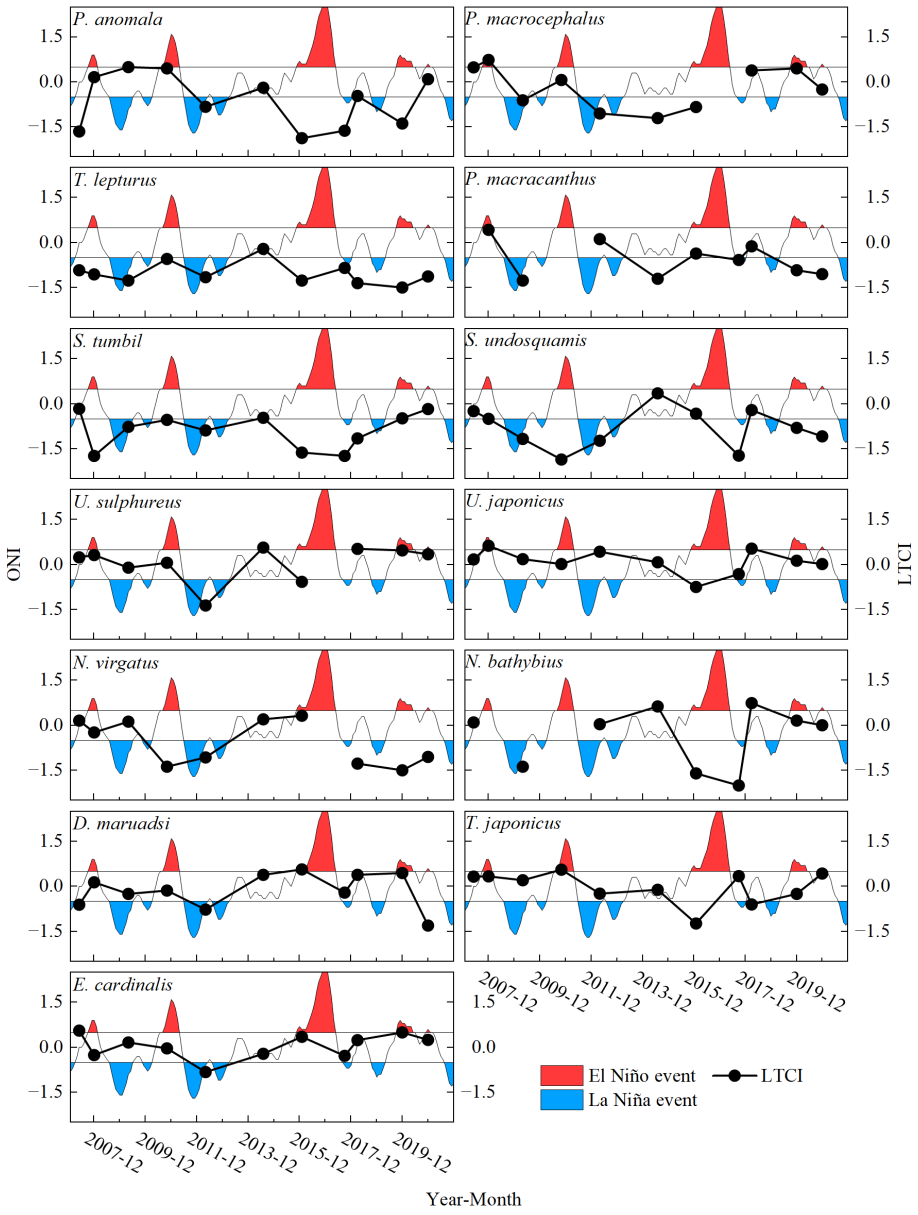

FIGURE 8
Relationship between the LTCI of major commercial fishes and climate events in the Beibu Gulf.

fishing (Adams, 1980; Hu et al., 2015), the strong interaction we found between climate events and life-history traits suggested that the composition and structure of the fish community in the subtropical semi-enclosed bay were also primarily caused by climate teleconnection.

4.2 Effects of climate events on fish life-history traits

The life-history traits of most fish species were optimized across all periods, i.e., variation in mortality coincided with variation in growth parameters; however, the variation in life-history traits of *T. lepturus* and *E. cardinalis* differed significantly from those of other species. Ribbonfish (*T. lepturus*) is a benthonic-pelagic species found worldwide in tropical and subtropical regions, mainly between 45°S and 60°N (Taghavi Motlagh et al., 2021). While *T. lepturus* is relatively short-lived and fast-growing (Clain et al., 2023) compared to larger fish in the marine ecosystem, they had the lowest mean mortality rate among the fish analyzed in this study and the distribution of *M* values was very similar at all periods, suggesting that their life-history traits could mainly be described as "longevity-slow." Although we were unable to find significant differences between growth parameters among climatic periods, relatively sharp variation in the growth of ribbonfish was clearly influenced by climatic events. Past research has suggested that *T. lepturus* possesses flexible reproduction strategies; in environments with marked temperature cycles or weak fishing pressure, populations are more likely to reach maturity after longer durations (Al-Nahdi

et al., 2009). However, in warmer and less productive environments, lower batch fecundity may be compensated for, in part, by a prolonged spawning period due to a smaller size (Martins and Haimovici, 2000). The increase in growth parameters in the case of relatively fixed mortality will promote a shift in the combination of life-history traits to the fourth quadrant. Therefore, *T. lepturus* would expend a great deal of energy to mature and begin reproduction early, retaining a small size and not capitalizing on the benefits of increased fecundity that come with a large size and long-life cycle (Waples and Audzijonyte, 2016). However, the reproduction strategy of a multiple batch spawner with a prolonged spawning period seems to allow for such a life-history strategy to exist.

We also observed that the life-history strategy of *E. cardinalis* was relatively constant in most climate periods. *E. cardinalis* is a small, warm-water, near-demersal fish with a fast rate of sexual maturity and a high reproductive rate (Zhang et al., 2020). The species exhibits significant periodic fluctuations in stock density (Sun and Lin, 2004) and can withstand a high fishing intensity (Chen, 2005). While *E. cardinalis* is one of the most economically important species in the northern South China Sea, the substantial increase in catch due to overfishing is a major threat (Zhang et al., 2020; Xu et al., 2021), and the species was even listed as endangered in a recent International Union for Conservation of Nature (IUCN) red list (Xu et al., 2022). Having a relatively unique niche in the ecosystem may be the main reason for the relatively stable life-history strategy selections of these fishes (Olden et al., 2006), with less interspecific competitive pressures making them more resistant to disturbances (Lewis, 2022). We also suggested that the relatively fixed combination of life-history traits may be a response of the population to overfishing; this stable life-history strategy would reduce the negative impacts of heavy exploitation on survival, and the effects of climate events may not be dominant.

Of note, *P. anomala* and *N. bathybius* showed substantial differences in LTCI among climate periods. Given that fishing may lead to populations with an elevated sensitivity to climate variability, interaction effects between fishing and climate cannot be ignored. Several recent studies have shown that the fishery resources in the Beibu Gulf have been overfished (Su L. et al., 2021; Zhang et al., 2021; Su et al., 2022), and loopholes in local management measures and the increased fishing pressure from Vietnam have resulted in the annual decreases of fishery resources in the region (Huang and Huang, 2013; Tian et al., 2022). This not only results in the replacement of dominant species with less valuable, small-sized, low trophic level species (Zhang et al., 2020) but also increases the magnitude of population fluctuations driven by environmental variability (Hsieh et al., 2006; Planque et al., 2010; Hidalgo et al., 2011; Rouyer et al., 2011; Shelton and Mangel, 2011). Therefore, synergistic interactions between climate anomalies and fishing are realistic (Waples and Audzijonyte, 2016). Fish whose life-history strategies are significantly affected by climate events are more frequent in overexploited areas.

4.3 Effects of climate events on fish LTCI

Among the commercially valuable fish species included in this study, only the LTCI values for *D. maruadsi*, *P. macrocephalus*, and *U. sulphureus* were significantly correlated with the fluctuations in ONI, which represents climate period transformations. Given the delayed response trait of the fish population to environmental changes, it is reasonable to estimate fish life-history traits separately by the types of climate periods over a longer time scale in this study. The life-history traits of these fishes are characterized by higher *M* and faster growth during the normal or El Niño periods. The LTCI for *D. maruadsi* generally decreased after the shift from El Niño to La Niña or normal conditions. Climate events will affect a range of abiotic factors that are tightly linked to the production and distribution of fish populations. Shallow areas will exhibit larger increases in sea temperatures than those in deeper waters. As warm-water fishes, *D. maruadsi*, *P. macrocephalus*, and *U. sulphureus* will grow faster with increased reproduction due to seawater warming, which expands aerobic scope initially (Holt and Jorgensen, 2015), and the increase in metabolic requirements intensify foraging and reduce survival. However, under higher or lower mortality, evolution toward a faster or slower growth, respectively, optimizes their combination of life-history traits to ensure the stability of population dynamics. High natural mortality is essential if fish growth is fast, as the stability of the ecosystem only limits population size within the carrying capacity. Furthermore, La Niña events also strongly affect the surface and subsurface patterns of the South China Sea through the anomalous cyclonic circulation in the low-level atmosphere (Kuo and Tseng, 2020). Like the west coast of the Atlantic (Mcphaden et al., 2006), tropical cyclones tend to be reduced in number and intensity during El Niño periods but stronger and more numerous during La Niña periods (Huang and Xu, 2010; Hsu et al., 2013; Chen and Duan, 2018). The frequent occurrence of weather phenomena reduces anthropogenic disturbances and the lower SST during La Niña periods (Qiu et al., 2015) results in a shift to increased growth over rapid reproduction.

We also found that changes in life-history strategies can differ among species within the same genus in response to climate events. In particular, for *U. sulphureus* and *U. japonicus*, *S. undosquamis* and *S. tumbil*, and *N. virgatus* and *N. bathybius*, the LTCI values of two species in the same genus were generally similar in normal periods, with divergence in opposite directions in response to climate events. These species of the same genus not only share very similar biological parameters but also have similar population characteristics, such as diet, habitat preference, and spawning period, suggesting that their ecological niche is basically the same (Lewis, 2022). However, the oceanographic features that change following ENSO events include surface seawater temperatures, the vertical and thermal structure of the ocean (especially in coastal regions) (Wu et al., 2014), and the coastal and upwelling currents (Chu et al., 2017; Dang et al., 2021). These effects will undoubtedly have a significant negative impact on the growth and fecundity of fish and consequently intensify competition for survival between species with similar ecological niches. Thus, species of the same genus, through the complementarity of life-history strategies, avoid intense competition for ecological niches during climate anomalies because the carrying capacity of the ecosystem can be increased by reducing the similarity in life stages.

Finally, *T. japonicus* and *D. maruadsi* are generally considered to belong to the same feeding group at the ecosystem level and are both

dominant species in offshore areas of China (Li et al., 2019; Su et al., 2022); accordingly, they have very similar ecological niches in long-term cohabitation. While the correlation was not statistically significant, we observed similar trends in LTCI for the two species over the first six climate periods in this study. Combined with the observation that there was a negative correlation between the LTCI value of *T. japonicus* and *D. maruadsi* in the latter six climate periods, we can conclude that the regularly alternating climate periods may explain the consistency of direction of change in life history strategies. The continued decline of fishery resources and increasing fishing pressure in the Beibu Gulf may also be responsible for the complementarity of life-history strategies between *D. maruadsi* and *T. japonicus* in the latter six climate periods. Overall, given the different relationships between life-history strategies and study periods, we emphasize the crucial importance of analyses of the effect of climate events on fish life history; overfishing weakens the resilience of fish populations to climate events, while interactions within communities also affect the response of fish life-history strategies to climate events.

There are some limitations in this study. The ELEFAN assumes that the body size composition of the survey data is representative of the exploited population major commercial fishes, and the study assumes that these survey data can be adequately analyzed in the corresponding climate event periods. However, the time span of each period of climate event is not uniform, and the composition of seasons varies from period to period. The energy storage of fish to adapt to seasonal environments is also reflected in changes in their life history (Giacomini and Shuter, 2013), which may affect our judgment of the influence of climate events on fish life-history trait parameters. For instance, although the effects of different types of climate events on the life history trait parameters of fish populations can be observed at the community level, these changes were relatively difficult to notice at the individual species level. Furthermore, the ONI has become the de-facto standard that NOAA uses for classifying warm and cool events in the eastern tropical Pacific. Although we have demonstrated a correlation between temperature changes in the Beibu Gulf and anomalies in the distant eastern equatorial Pacific, considering that ENSO's teleconnections to other regions have impacts beyond just affecting water temperature [e.g., rainfall, seawater salinity (Zhu et al., 2014; Ramos et al., 2019)], so we did not directly use the local sea surface temperature anomalies as a direct factor in this study. In conclusion, our research results have demonstrated a certain correlation between the changes in life-history traits of major commercial fishes in the Beibu Gulf and ENSO events, and identifying specific influencing environmental factors will be the focus of our further research. Therefore, in future studies on the relationship between climate change and fisheries in the Beibu Gulf, more factors will be taken into account when assessing the effects of climate events on the life-history trait parameters of fish, such as the temporal continuity of survey data.

Data availability statement

The original contributions presented in the study are included in the article/supplementary material. Further inquiries can be directed to the corresponding author.

Ethics statement

The requirement of ethical approval was waived by The Committee on Laboratory Animal Welfare and Ethics of South China Sea Fisheries Research Institute for the studies involving animals because the study area is in open water where is not a protected area and no endangered or protected marine species were involved. The studies were conducted in accordance with the local legislation and institutional requirements.

Author contributions

XH conceived the study and wrote the first manuscript. KZ, JL, YX, MS, and JJ performed the data analyses and prepared the graphs. SX, YC, YQ, and ZC provided the original length data and revised the manuscript. All the authors contributed to the article and approved the submitted version.

Funding

This work was supported by Key research and development project of Guangdong Province (2020B1111030001), the Central Public-interest Scientific Institution Basal Research Fund, Chinese Academy of Fishery Sciences (2023TD05), the Central Public-interest Scientific Institution Basal Research Fund, South China Sea Fisheries Research Institute, CAFS (2021SD01).

Acknowledgments

We thank all those involved in the marine surveys that collected the data used in this study. We appreciate the valuable comments made by reviewers, which significantly improved our manuscript. We thank Dr. Gang Zhang from MogoEdit (http://en.mogoedit.com/), for editing a draft of this manuscript.

Conflict of interest

The authors declare that the research was conducted in the absence of any commercial or financial relationships that could be construed as a potential conflict of interest.

Publisher's note

References

Adams, P. B. (1980). Life history patterns in marine fishes and their consequences for fisheries management. *Fishery Bull.* 78, 1–12.

Al-Nahdi, A., Al-Marzouqi, A., Al-Rasadi, E., and Groeneveld, J. (2009). The size composition, reproductive biology, age and growth of largehead cutlassfish Trichiurus lepturus Linnaeus from the Arabian Sea coast of Oman. *Indian J. Fisheries* 56, 73–79.

Baumgartner, M. T., De Oliveira, A. G., Agostinho, A. A., and Gomes, L. C. (2018). Fish functional diversity responses following flood pulses in the upper Paraná River floodplain. *Ecol. Freshw. Fish* 27, 910–919. (Amsterdam: Academic Press) doi: 10.1111/eff.12402

Blanchot, J., Rodier, M., and Le Bouteiller, A. (1992). Effect of El Niño Southern Oscillation events on the distribution and abundance of phytoplankton in the Western Pacific Tropical Ocean along 165°E. *J. Plankton Res.* 14, 137–156. doi: 10.1093/plankt/14.1.137

Brown, J. L., and Choe, J. C. (2019). "Behavioral ecology and sociobiology," in *Encyclopedia of animal behavior*, (Amsterdam: Academic Press)103–108.

Chaparro-Pedraza, P. C., and De Roos, A. M. (2019). Environmental change effects on life-history traits and population dynamics of anadromous fishes. *J. Anim. Ecol.* 88, 1178–1190. doi: 10.1111/1365-2656.13010

Charnov, E. L. (1993). *Life history invariants: some explorations of symmetry in evolutionary ecology*. (Oxford: Oxford University Press).

Charnov, E. L., Gislason, H., and Pope, J. G. (2013). Evolutionary assembly rules for fish life histories. *Fish Fisheries* 14, 213–224. doi: 10.1111/j.1467-2979.2012.00467.x

Chen, Z. (2005). Ecological distribution of Parargyrops edita Tanaka in the Beibu Gulf. *Mar. Fish. Res.* 26, 16–21.

Chen, Y., and Duan, Z. (2018). Impact of ENSO on typhoon wind hazard in the coast of southeast China. *Natural Hazards* 92, 1717–1731. doi: 10.1007/s11069-018-3283-2

Chen, Z., Qiu, Y., and Xu, S. (2011). Changes in trophic flows and ecosystem properties of the Beibu Gulf ecosystem before and after the collapse of fish stocks. *Ocean Coast. Manage.* 54, 601–611. doi: 10.1016/j.ocecoaman.2011.06.003

Chen, Z., Xu, S., Qiu, Y., Lin, Z., and Jia, X. (2009). Modeling the effects of fishery management and marine protected areas on the Beibu Gulf using spatial ecosystem simulation. *Fisheries Res.* 100, 222–229. doi: 10.1016/j.fishres.2009.08.001

Chu, X., Dong, C., and Qi, Y. (2017). The influence of ENSO on an oceanic eddy pair in the South China Sea. *J. Geophysical Research: Oceans* 122, 1643–1652. doi: 10.1002/2016JC012642

Clain, C., Stewart, J., Fowler, A., and Diamond, S. (2023). Reproductive biology of largehead hairtail (Trichiurus lepturus) in south-eastern Australia. *Aquaculture Fisheries* 8, 148–158. doi: 10.1016/j.aaf.2021.09.008

Dang, X., Bai, Y., Gong, F., Chen, X., Zhu, Q., Huang, H., et al. (2021). Different responses of phytoplankton to the ENSO in two upwelling systems of the South China Sea. *Estuaries Coasts* 45, 485–500. doi: 10.1007/s12237-021-00987-2

Dembski, S., Masson, G., Monnier, D., Wagner, P., and Pihan, J. C. (2006). Consequences of elevated temperatures on life-history traits of an introduced fish, pumpkinseed Lepomis gibbosus. *J. Fish Biol.* 69, 331–346. doi: 10.1111/j.1095-8649.2006.01087.x

Gao, J., Wu, G., and Ya, H. (2017). Review of the circulation in the beibu gulf, South China Sea. *Continental Shelf Res.* 138, 106–119. doi: 10.1016/j.csr.2017.02.009

García-March, J. R., Tena, J., Henandis, S., Vázquez-Luis, M., López, D., Téllez, C., et al. (2020). Can we save a marine species affected by a highly infective, highly lethal, waterborne disease from extinction? *Biol. Conserv.* 243, 108498. doi: 10.1016/j.biocon.2020.108498

Giacomini, H. C., and Shuter, B. J. (2013). Adaptive responses of energy storage and fish life histories to climatic gradients. *J. Theor. Biol.* 339, 100–111. doi: 10.1016/j.jtbi.2013.08.020

Gillanders, B. M., Black, B. A., Meekan, M. G., and Morrison, M. A. (2012). Climatic effects on the growth of a temperate reef fish from the Southern Hemisphere: a biochronological approach. *Mar. Biol.* 159, 1327–1333. doi: 10.1007/s00227-012-1913-x

Gislason, H., Daan, N., Rice, J. C., and Pope, J. G. (2010). Size, growth, temperature and the natural mortality of marine fish. *Fish Fisheries* 11, 149–158. doi: 10.1111/j.1467-2979.2009.00350.x

Gomez, F. A., Lee, S. K., Hernandez, F. J. Jr., Chiaverano, L. M., Muller-Karger, F. E., Liu, Y., et al. (2019). ENSO-induced co-variability of salinity, plankton biomass and coastal currents in the Northern Gulf of Mexico. *Sci. Rep.* 9, 178. doi: 10.1038/s41598-018-36655-y

Hidalgo, M., Rouyer, T., Molinero, J. C., Massutí, E., Moranta, J., Guijarro, B., et al. (2011). Synergistic effects of fishing-induced demographic changes and climate variation on fish population dynamics. *Mar. Ecol. Prog. Ser.* 426, 1–12. doi: 10.3354/meps09077

Holbrook, N. J., Claar, D. C., Hobday, A. J., Mcinnes, K. L., Oliver, E. C. J., Gupta, A. S., et al. (2020). "ENSO-driven ocean extremes and their ecosystem impacts," in *El Niño Southern oscillation in a changing climate*. (American Geophysical Union, Hoboken, NJ, Washington, D.C.: John Wiley & Sons, Inc.). 409–428.

Holt, R. E., and Jorgensen, C. (2015). Climate change in fish: effects of respiratory constraints on optimal life history and behaviour. *Biol. Lett.* 11, 20141032. doi: 10.1098/rsbl.2014.1032

Hossain, M. S., Gopal Das, N., Sarker, S., and Rahaman, M. Z. (2012). Fish diversity and habitat relationship with environmental variables at Meghna river estuary, Bangladesh. *Egyptian J. Aquat. Res.* 38, 213–226. doi: 10.1016/j.ejar.2012.12.006

Hsieh, C.-H., Reiss, C. S., Hunter, J. R., Beddington, J. R., May, R. M., and Sugihara, G. (2006). Fishing elevates variability in the abundance of exploited species. *Nature* 443, 859–862. doi: 10.1038/nature05232

Hsu, P.-C., Ho, C.-R., Liang, S.-J., and Kuo, N.-J. (2013). Impacts of two types of El Niño and La Niña events on typhoon activity. *Adv. Meteorology* 2013, 1–8. doi: 10.1155/2013/632470

Hu, W., Ye, G., Lu, Z., Du, J., Chen, M., Chou, L. M., et al. (2015). Study on fish life history traits and variation in the Taiwan Strait and its adjacent waters. *Acta Oceanologica Sin.* 34, 45–54. doi: 10.1007/s13131-015-0625-8

Huang, Y., and Huang, M. (2013). Implementation of the Sino-Vietnamese fishery agreement: mainly Chinese perspective. *Beijing Law Rev.* 04, 103–119. doi: 10.4236/blr.2013.43014

Huang, F., and Xu, S. (2010). Super typhoon activity over the western North Pacific and its relationship with ENSO. *J. Ocean Univ. China* 9, 123–128. doi: 10.1007/s11802-010-0123-8

Hunter, E., Aldridge, J. N., Metcalfe, J. D., and Arnold, G. P. (2002). Geolocation of free-ranging fish on the European continental shelf as determined from environmental variables. *Mar. Biol.* 142, 601–609. doi: 10.1007/s00227-002-0984-5

Jones, M. C., and Cheung, W. W. L. (2018). Using fuzzy logic to determine the vulnerability of marine species to climate change. *Glob Chang Biol.* 24, e719–e731. doi: 10.1111/gcb.13869

Khanh, N., Phu, T., Luong, N., and Opoku-Acheampong, A. (2013). Appropriate fishing depths for squid longline fishery in the Gulf of Tonkin, Vietnam. *Fish People* 11, 29–32.

King, J. R., and Mcfarlane, G. A. (2003). Marine fish life history strategies: applications to fishery management. *Fisheries Manage. Ecol.* 10, 249–264. doi: 10.1046/j.1365-2400.2003.00359.x

King, J. R., and Mcfarlane, G. A. (2006). A framework for incorporating climate regime shifts into the management of marine resources. *Fisheries Manage. Ecol.* 13, 93–102. doi: 10.1111/j.1365-2400.2006.00480.x

Kuo, Y. C., and Tseng, Y. H. (2020). Impact of enso on the south china sea during enso decaying winter–spring modeled by a regional coupled model (a new mesoscale perspective). *Ocean Modelling* 152, 101655.

Lehodey, P., Alheit, J., Barange, M., Baumgartner, T., Beaugrand, G., Drinkwater, K., et al. (2006). Climate variability, fish, and fisheries. *J. Climate* 19, 5009–5030. doi: 10.1175/JCLI3898.1

Lehodey, P., Bertrand, A., Hobday, A. J., Kiyofuji, H., Mcclatchie, S., Menkès, C. E., et al. (2020). "ENSO impact on marine fisheries and ecosystems," in *El Niño Southern oscillation in a changing climate*. (American Geophysical Union, Hoboken, NJ, Washington, D.C.: John Wiley & Sons, Inc.). 429–451.

Lewis, W. M. (2022). "The ecological niche in aquatic ecosystems," in *Encyclopedia of inland waters (Second edition)*. Eds. T. Mehner and K. Tockner (Oxford: Elsevier), 202–206.

Li, Y., Wang, C., Zou, X., Feng, Z., Yao, Y., Wang, T., et al. (2019). Occurrence of polycyclic aromatic hydrocarbons (PAHs) in coral reef fish from the South China Sea. *Mar. pollut. Bull.* 139, 339–345. doi: 10.1016/j.marpolbul.2019.01.001

Liang, Z. (2022). *Fish diversity and fauna characteristics in the northern South China Sea continental shelf* (Guandong Ocean University).

Martins, A. S., and Haimovici, M. (2000). Reprodution of the cutlassfish Trichiurus lepturus in the southern Brazil subtropical convergence ecosystem. 64.

Masrikat, J. A. (2012). Standing stock of demersal fish assessment in southern part of South China Sea. *J. Coast. Dev.* 15, 276–281.

Mcphaden, M. J., Zebiak, S. E., and Glantz, M. H. (2006). ENSO as an integrating concept in earth science. *Science* 314, 1740–1745. doi: 10.1126/science.1132588

Mildenberger, T. K., Taylor, M. H., Wolff, M., and Price, S. (2017). TropFishR: an R package for fisheries analysis with length-frequency data. *Methods Ecol. Evol.* 8, 1520–1527. doi: 10.1111/2041-210X.12791

Mzingirwa, F. A., Nyamora, J. M., Omukoto, J. O., and Tuda, P. (2020). Stock assessment of the Tigertooth croaker, Otolithes ruber (Bloch & Schneider 1801) from the commercial prawn trawl fishery by-catch in coastal Kenya. *Western Indian Ocean J. Mar. Sci.* 19, 149–165. doi: 10.4314/wiojms.v19i2.11

Olden, J. D., Poff, N. L., and Bestgen, K. R. (2006). LIFE-HISTORY STRATEGIES PREDICT FISH INVASIONS AND EXTIRPATIONS IN THE COLORADO RIVER BASIN. *Ecol. Monogr.* 76, 25–40. doi: 10.1890/05-0330

Oli, M. K., and Coulson, T. (2016). "Life history, what is?," in *Encyclopedia of evolutionary biology*. Ed. R. M. Kliman (Oxford: Academic Press), 394–399.

Overland, J. E., Alheit, J., Bakun, A., Hurrell, J. W., Mackas, D. L., and Miller, A. J. (2010). Climate controls on marine ecosystems and fish populations. *J. Mar. Syst.* 79, 305–315. doi: 10.1016/j.jmarsys.2008.12.009

Pankhurst, N. W., and Munday, P. L. (2011). Effects of climate change on fish reproduction and early life history stages. *Mar. Freshw. Res.* 62, 1015–1026. doi: 10.1071/MF10269

Pauly, D. (1980). On the interrelationships between natural mortality, growth parameters, and mean environmental temperature in 175 fish stocks. *ICES J. Mar. Sci.* 39, 175–192. doi: 10.1093/icesjms/39.2.175

Payne, N. L., Morley, S. A., Halsey, L. G., Smith, J. A., Stuart-Smith, R., Waldock, C., et al. (2021). Fish heating tolerance scales similarly across individual physiology and populations. *Commun. Biol.* 4, 264. doi: 10.1038/s42003-021-01773-3

Pécuchet, L., Nielsen, J. R., and Christensen, A. (2015). Impacts of the local environment on recruitment: a comparative study of North Sea and Baltic Sea fish stocks. *ICES J. Mar. Sci.* 72, 1323–1335. doi: 10.1093/icesjms/fsu220

Petrik, C. M. (2019). "Life history of marine fishes and their implications for the future oceans," in *Predicting future oceans*. (Amsterdam: Elsevier). 165–172.

Pinsky, M. L., and Palumbi, S. R. (2014). Meta-analysis reveals lower genetic diversity in overfished populations. *Mol. Ecol.* 23, 29–39. doi: 10.1111/mec.12509

Planque, B., Fromentin, J.-M., Cury, P., Drinkwater, K. F., Jennings, S., Perry, R. I., et al. (2010). How does fishing alter marine populations and ecosystems sensitivity to climate? *J. Mar. Syst.* 79, 403–417. doi: 10.1016/j.jmarsys.2008.12.018

Qian, J., Li, J., Zhang, K., Qiu, Y., Cai, Y., Wu, Q., et al. (2022). Spatial–temporal distribution of large-size light falling-net fisheries in the South China Sea. *Front. Mar. Sci.* 9. doi: 10.3389/fmars.2022.1075855

Qiu, Y., Lin, Z., and Wang, Y. (2010). Responses of fish production to fishing and climate variability in the northern South China Sea. *Prog. Oceanography* 85, 197–212. doi: 10.1016/j.pocean.2010.02.011

Qiu, F., Pan, A., Zhang, S., Cha, J., and Sun, H. (2015). Sea surface temperature anomalies in the South China Sea during mature phase of ENSO. *Chin. J. Oceanology Limnology* 34, 577–584. doi: 10.1007/s00343-016-4290-3

Ramos, R. D., Goodkin, N. F., Siringan, F. P., and Hughen, K. A. (2019). Coral records of temperature and salinity in the tropical Western Pacific reveal influence of the pacific decadal oscillation since the late nineteenth century. *Paleoceanography Paleoclimatology* 34, 1344–1358. doi: 10.1029/2019PA003684

R Core Team (2021). *R: A language and environment for statistical computing* (Vienna, Austria). Available at: https://www.R-project.org/.

Rojas-Mendez, J. A., and Mendoza, C. J. R. (2008). Effects of ENSO 1997?1998 on the distribution of small pelagic fish off the west coast of Baja California. *Int. J. Environ. Health* 2, 45–63. doi: 10.1504/IJENVH.2008.018672

Rouyer, T., Ottersen, G., Durant, J. M., Hidalgo, M., Hjermann, D.Ø., Persson, J., et al. (2011). Shifting dynamic forces in fish stock fluctuations triggered by age truncation? *Global Change Biol.* 17, 3046–3057. doi: 10.1111/j.1365-2486.2011.02443.x

Scrucca, L. (2013). GA: A package for genetic algorithms in R. *J. Stat. Software* 53, 1–37. doi: 10.18637/jss.v053.i04

Scrucca, L. (2017). On Some Extensions to GA Package: Hybrid Optimisation, Parallelisation and Islands Evolution On some extensions to GA package: hybrid optimisation, parallelisation and islands evolution. *R J.* 9, 187. doi: 10.32614/RJ-2017-008

Shelton, A. O., and Mangel, M. (2011). Fluctuations of fish populations and the magnifying effects of fishing. *Proc. Natl. Acad. Sci.* 108, 7075–7080. doi: 10.1073/pnas.1100334108

Shen, G., and Heino, M. (2014). An overview of marine fisheries management in China. *Mar. Policy* 44, 265–272. doi: 10.1016/j.marpol.2013.09.012

Sherman, K. D., King, R. A., Dahlgren, C. P., Simpson, S. D., Stevens, J. R., and Tyler, C. R. (2017). Historical Processes and Contemporary Anthropogenic Activities Influence Genetic Population Dynamics of Nassau Grouper (Epinephelus striatus) within The Bahamas. *Front. Mar. Sci.* 4. doi: 10.3389/fmars.2017.00393

Soyano, K., and Mushirobira, Y. (2018). The mechanism of low-temperature tolerance in fish. *Adv. Exp. Med. Biol.* 1081, 149–164. doi: 10.1007/978-981-13-1244-1_9

Sprogis, K. R., Christiansen, F., Wandres, M., and Bejder, L. (2018). El Nino Southern Oscillation influences the abundance and movements of a marine top predator in coastal waters. *Glob Chang Biol.* 24, 1085–1096. doi: 10.1111/gcb.13892

Stenseth, N. C., Mysterud, A., Ottersen, G., Hurrell, J. W., Chan, K.-S., and Lima, M. (2002). Ecological effects of climate fluctuations. *Science* 297, 1292–1296. doi: 10.1126/science.1071281

Strøm, H., Descamps, S., Ekker, M., Fauchald, P., and Moe, B. (2021). Tracking the movements of North Atlantic seabirds: steps towards a better understanding of population dynamics and marine ecosystem conservation. *Mar. Ecol. Prog. Ser.* 676, 97–116. doi: 10.3354/meps13801

Su, L., Chen, Z., Zhang, K., Xu, Y., Xu, S., and Wang, K. (2021). Decadal-scale variation in mean trophic level in Beibu gulf based on bottom-trawl survey data. *Mar. Coast. Fisheries* 13, 174–182. doi: 10.1002/mcf2.10144

Su, M., Wang, L., Xiang, J., and Ma, Y. (2021). Adjustment trend of China's marine fishery policy since 2011. *Mar. Policy* 124. doi: 10.1016/j.marpol.2020.104322

Su, L., Xu, Y., Qiu, Y., Sun, M., Zhang, K., and Chen, Z. (2022). Long-term change of a fish-based index of biotic integrity for a semi-enclosed bay in the Beibu gulf. *Fishes* 7 (3), 124. doi: 10.3390/fishes7030124

Sun, D., and Lin, Z. (2004). Variations of major commercial fish stocks and strategies for fishery management in Beibu Gulf. *J. Trop. Oceanography* 23, 62–68.

Taghavi Motlagh, S., Ghodrati Shojaei, M., and Vahabnezhad, A. (2021). Life history traits of ribbonfish Trichiurus lepturus (Linnaeus 1758) in the Persian Gulf and Oman Sea. *Iranian J. Fisheries Sci.* 20, 298–312.

Taylor, M. H., and Mildenberger, T. K. (2017). Extending electronic length frequency analysis in R. *Fisheries Manage. Ecol.* 24, 330–338. doi: 10.1111/fme.12232

Then, A. Y., Hoenig, J. M., Gedamke, T., and Ault, J. S. (2015). Comparison of two length-based estimators of total mortality: a simulation approach. *Trans. Am. Fisheries Soc.* 144, 1206–1219. doi: 10.1080/00028487.2015.1077158

Tian, H., Liu, Y., Tian, Y., Jing, Y., Liu, S., Liu, X., et al. (2022). Advances in the use of nighttime light data to monitor and assess coastal fisheries under the impacts of human activities and climate and environmental changes: A case study in the Beibu Gulf. *Mar. Policy* 144, 105227. doi: 10.1016/j.marpol.2022.105227

Timmermann, A., An, S.-I., Kug, J.-S., Jin, F.-F., Cai, W., Capotondi, A., et al. (2018). El Niño–southern oscillation complexity. *Nature* 559, 535–545. doi: 10.1038/s41586-018-0252-6

Von Bertalanffy, L. (1938). A QUANTITATIVE THEORY OF ORGANIC GROWTH (INQUIRIES ON GROWTH LAWS. II). *Hum. Biol.* 10, 181–213.

Wang, I. M., Michalak, N. M., and Ackerman, J. M. (2021). "Life history strategies," in *Encyclopedia of evolutionary psychological science*. Eds. T. K. Shackelford and V. A. Weekes-Shackelford (Cham: Springer International Publishing), 4560–4569.

Wang, X., Qiu, Y., Du, F., Lin, Z., Sun, D., and Huang, S. (2013). Spatio-temporal variability of fish diversity and dominant species in the Beibu Gulf. *J. Fishery Sci. China* 18, 427–436. doi: 10.3724/SP.J.1118.2011.00427

Wang, Y., Yao, L., Chen, P., Yu, J., and Wu, Q. E. (2020). Environmental influence on the spatiotemporal variability of fishing grounds in the Beibu Gulf, South China Sea. *J. Mar. Sci. Eng.* 8(12), 957. doi: 10.3390/jmse8120957

Wang, K., Zhang, C., Xu, B., Xue, Y., and Ren, Y. (2020). Selecting optimal bin size to account for growth variability in Electronic LEngth Frequency ANalysis (ELEFAN). *Fisheries Res.* 225, 105474. doi: 10.1016/j.fishres.2019.105474

Waples, R. S., and Audzijonyte, A. (2016). Fishery-induced evolution provides insights into adaptive responses of marine species to climate change. *Front. Ecol. Environ.* 14, 217–224. doi: 10.1002/fee.1264

Ward, H. G. M., Post, J. R., Lester, N. P., Askey, P. J., and Godin, T. (2017). Empirical evidence of plasticity in life-history characteristics across climatic and fish density gradients. *Can. J. Fisheries Aquat. Sci.* 74, 464–474. doi: 10.1139/cjfas-2016-0023

Wu, R., Chen, W., Wang, G., and Hu, K. (2014). Relative contribution of ENSO and East Asian winter monsoon to the South China Sea SST anomalies during ENSO decaying years. *J. Geophysical Research: Atmospheres* 119, 5046–5064. doi: 10.1002/2013JD021095

Xu, S., Chen, Z., Li, C., Huang, X., and Li, S. (2011). Assessing the carrying capacity of tilapia in an intertidal mangrove-based polyculture system of Pearl River Delta, China. *Ecol. Model.* 222, 846–856. doi: 10.1016/j.ecolmodel.2010.11.014

Xu, Y., Zhang, K., Sun, M., Su, L., and Chen, Z. (2022). Tempo-spatial distribution of an endangered fish species, threadfin porgy evynnis cardinalis (Lacepède 1802), in the northern South China Sea. *J. Mar. Sci. Eng.* 10(9), 1191.

Xu, S., Zhang, Z., Yu, K., Huang, X., Chen, H., Qin, Z., et al. (2021). Spatial variations in the trophic status of Favia Palauensis corals in the South China Sea: Insights into their different adaptabilities under contrasting environmental conditions. *Sci. China Earth Sci.* 64, 839–852. doi: 10.1007/s11430-020-9774-0

Yang, B., Herrmann, B., Yan, L., Li, J., and Wang, T. (2021). Size selectivity and catch efficiency of diamond-mesh codends in demersal trawl fishery for conger pike (Muraenesox cinereus) of the South China Sea. *Ocean Coast. Manage.* 211, 105777. doi: 10.1016/j.ocecoaman.2021.105777

Yatsu, A., Aydin, K. Y., King, J. R., Mcfarlane, G. A., Chiba, S., Tadokoro, K., et al. (2008). Elucidating dynamic responses of North Pacific fish populations to climatic forcing: Influence of life-history strategy. *Prog. Oceanography* 77, 252–268. doi: 10.1016/j.pocean.2008.03.009

Yen, K.-W., and Lu, H.-J. (2016). Spatial–temporal variations in primary productivity and population dynamics of skipjack tuna Katsuwonus pelamis in the western and central Pacific Ocean. *Fisheries Sci.* 82, 563–571. doi: 10.1007/s12562-016-0992-x

Zhang, K., Cai, Y., Liao, B., Jiang, Y., Sun, M., Su, L., et al. (2020). Population dynamics of threadfin porgy Evynnis cardinalis, an endangered species on the IUCN red list in the Beibu Gulf, South China Sea. *J. Fish Biol.* 97, 479–489. doi: 10.1111/jfb.14398

Zhang, K., Li, J., Hou, G., Huang, Z., Shi, D., Chen, Z., et al. (2021). Length-based assessment of fish stocks in a data-poor, jointly exploited (China and Vietnam) fishing ground, Northern South China Sea. *Front. Mar. Sci.* 8. doi: 10.3389/fmars.2021.718052

Zhang, K., Li, M., Li, J., Sun, M., Xu, Y., Cai, Y., et al. (2022). Climate-induced small pelagic fish blooms in an overexploited marine ecosystem of the South China Sea. *Ecol. Indic.* 145, 109598. doi: 10.1016/j.ecolind.2022.109598

Zhang, K., Zhang, J., Zhang, P., Su, L., Hong, X., Qiu, Y., et al. (2023). This is what we know: Assessing the stock status of the data-poor skipjack tuna (Katsuwonus pelamis) fishery in the South China Sea. *Front. Mar. Sci.* 10. doi: 10.3389/fmars.2023.1095411

Zhu, J., Huang, B., Zhang, R. H., Hu, Z. Z., Kumar, A., Balmaseda, M. A., et al. (2014). Salinity anomaly as a trigger for ENSO events. *Sci. Rep.* 4, 6821. doi: 10.1038/srep06821

frontiers | Frontiers in Aquaculture

TYPE Original Research
PUBLISHED 16 October 2023
DOI 10.3389/faquc.2023.1271715

OPEN ACCESS

EDITED BY
Jingzhen Wang,
Beibu Gulf University, China

REVIEWED BY
Vikash Kumar,
Central Inland Fisheries Research Institute (ICAR), India
Christopher Brown,
Pukyong National University, Republic of Korea
Yongkai Tang,
Chinese Academy of Fishery Sciences (CAFS), China

*CORRESPONDENCE
Sourabh Kumar Dubey
s.dubey@cgiar.org

†PRESENT ADDRESS
Ben Belton,
International Food Policy Research Institute, Dhaka, Bangladesh

RECEIVED 02 August 2023
ACCEPTED 15 September 2023
PUBLISHED 16 October 2023

CITATION
Rajts F, Dubey SK, Gogoi K, Das RR, Biswal SK, Padiyar AP, Rajendran S, Thilsted SH, Mohan CV and Belton B (2023) Cracking the code of hatchery-based mass production of mola (*Amblypharyngodon mola*) seed for nutrition-sensitive aquaculture. *Front. Aquac.* 2:1271715. doi: 10.3389/faquc.2023.1271715

Cracking the code of hatchery-based mass production of mola (*Amblypharyngodon mola*) seed for nutrition-sensitive aquaculture

Francois Rajts[1], Sourabh Kumar Dubey[2*], Kalpajit Gogoi[3], Rashmi Ranjan Das[2], Saurava Kumar Biswal[4], Arun Panemangalore Padiyar[2], Suresh Rajendran[3], Shakuntala Haraksingh Thilsted[1], Chadag Vishnumurthy Mohan[1] and Ben Belton[1,5†]

[1]WorldFish, Bayan Lepas, Penang, Malaysia, [2]WorldFish, Cuttack, Odisha, India, [3]WorldFish, Guwahati, Assam, India, [4]Biswal Aquatech, Jagatsinghpur, Odisha, India, [5]Department of Agricultural, Food, and Resource Economics, Michigan State University, East Lansing, MI, United States

Introduction: Small indigenous fish species (SIS) can be particularly rich in micronutrients and make a crucial contribution toward improving human nutrition. The introduction of mola (*Amblypharyngodon mola*), an SIS, which is particularly rich in vitamin A, into smallholder carp aquaculture systems has been widely promoted over the past decade as a promising nutrition-sensitive innovation. However, standardized techniques for the hatchery mass production of mola do not yet exist. We hypothesized that the lack of commercial hatchery mass-production techniques for mola seed is the key barrier limiting potential for widespread adoption of carp–SIS polyculture.

Methods: To address this gap, we conducted breeding trials at a private hatchery in Odisha, India, from July to September 2022, to identify standardized methods for the hatchery-based mass production of mola seed. Breeding was induced using a synthetic gonadotropin-releasing hormone analog (SGnRHa) at 0.5 mL and 0.25 mL per kg of body weight of female fish and male fish, respectively. Fish spawned in double hapas in breeding tanks.

Results: The average fertilization, spawning, and hatching rates over 10 breeding cycles were 81%, 82%, and 85%, respectively. A total of 8.5 million fertilized eggs and 6.4 million hatchlings were produced. The survival of fry during larval rearing trials at a stocking rate of 500 hatchlings/m2 was 58% after 22 days. The mola

hatchlings and fry were sold to 29 farmers at prices comparable to those of Indian major carp.

Discussion: This article makes a unique contribution to the literature by documenting the entire process of hatchery-based mass mola seed production, including broodfish collection and maintenance, hormone dose optimization, breeding arrangements, breeder characteristics, breeding behavior and performance fecundity, larval rearing, and seed sales to farmers. This information is intended to serve as a protocol to be followed by any individual or institution with an interest in mola breeding and represents an important contribution to the development of nutrition-sensitive aquaculture.

KEYWORDS

small indigenous fish species (SIS), mola (*Amblypharyngodon mola*), induced breeding, environmental manipulation, mass seed production, nutrition-sensitive aquaculture

1 Introduction

Fish is an irreplaceable source of micronutrients in diets in the Global South, where large numbers of vulnerable people belong to "fish-dependent" populations. Previous studies from South Asia have demonstrated that some small indigenous fish species—collectively called SIS[1]—can be particularly rich in micronutrients, including iron, calcium, zinc, and iodine, and vitamins A, B_{12}, and D, and make a crucial contribution toward human nutrition (Bogard et al., 2017).

Historically in South Asia, SIS sourced from inland capture fisheries were abundant and cheap, but the productivity of freshwater aquatic resources has declined sharply in recent decades in response to overexploitation and habitat degradation, making once plentiful and affordable SIS increasingly scarce and expensive (Toufique and Belton, 2014).

Carp[2] polyculture systems are the most widespread form of aquaculture throughout the Indian subcontinent. Introducing SIS into conventional carp polyculture has been promoted over the past decade as a promising nutrition-sensitive innovation, with the potential to substantially increase the micronutrient intakes of farming households, especially for women and children. Nutrition-sensitive aquaculture is defined as a food-based approach to aquaculture development that prioritizes the production of nutrient-dense SIS alongside conventional carp polyculture to support beneficial nutritional outcomes (Thilsted et al., 2016).

The promotion of nutrition-sensitive carp–SIS polyculture has centered around introducing mola carplet (*Amblypharyngodon mola*, hereafter referred to as "mola"), a small fish species which is particularly rich in vitamin A, into smallholder managed carp aquaculture systems in Bangladesh and India (Roos et al., 2002; Roos et al., 2007; Dubey et al., 2022). These efforts have been successful in producing significant quantities of mola in grow-out ponds with no additional inputs or management, and no reduction in carp yields (Wahab et al., 2003; Milstein et al., 2009). Subsequent studies have demonstrated that including mola in a carp polyculture system can increase the consumption of micronutrient-rich mola by women and children (Castine et al., 2017; Karim et al., 2017) and can be a cost-effective approach to reducing the burden of micronutrient malnutrition (Fiedler et al., 2016).

However, to date, efforts to promote nutrition-sensitive aquaculture have been dependent on the efforts of project or scheme extension workers to coordinate the harvesting of wild mola broodfish, maintain them in dedicated "brood ponds", and then distribute them to the ponds in target communities. The harvesting process for collecting mola broodfish from the wild also destroys small-sized mola and other SIS. The high costs, difficulties in sourcing and transporting wild mola broodfish, and the lack of incentives for adoption by the private sector associated with this approach make its long-term sustainability following the withdrawal of project support questionable.

In contrast, the development of most farmed aquatic species that are now cultured at scale in Asia (e.g., carps, tilapias, and catfishes) has followed a trajectory from reliance on the seed sourced from the wild, to the hatchery-based mass production of seed using wild broodfish and closure of the lifecycle, to the domestication of broodfish and the creation of seed multiplication and distribution networks by dynamic private-sector actors, including hatcheries, nurseries, and fish seed traders (Belton, 2012).

1 SIS are characterized by their diminutive size (they grow to a maximum length of approximately 25 cm) and largely inhabit freshwater habitats, such as floodplains, rivers, streams, canals, ponds, rice fields, and wetlands.

2 Carp species: Indian major carp (rohu, Labeo rohita; catla, Gibelion catla; mrigal, Cirrhinus mrigala), Indian minor carp (bata, Labeo bata, Labeo gonius; calbasu, Labeo calbasu), and exotic carp (grass carp, Ctenopharyngodon idella; silver carp, Hypophthalmichthys molitrix; common carp, Cyprinus carpio; bighead carp, Aristichthys nobilis; black carp, Mylopharyngodon piceus; silver barb, Barbonymus gonionotus).

Standardized hatchery techniques for the mass production of mola and other SIS seed do not yet exist. We hypothesized that a lack of commercial hatchery reproduction techniques for mola seed is a key bottleneck that limits the potential for widespread adoption of carp–SIS polyculture. The project reported on in this study was designed to overcome this key technical constraint to scaling up nutrition-sensitive aquaculture, by developing protocols for hatchery-based seed production of mola in Assam and Odisha, India.

This article reports the results of successful mola seed production trials, conducted in partnership with a private hatchery in Odisha, India, in 2022, which were designed to crack the code of mola seed mass production to facilitate the scaling up of nutrition-sensitive carp–SIS polyculture throughout South Asia. The article's methodology and results are intended to serve as a road map, to be replicated by any individual or institution with an interest in mola seed production, including hatchery design, induced breeding techniques, and larval rearing.

The article is organized into five sections. Section 1 contains the introduction and background. Section 2 contains a review of previous literature on the nutrient content, reproductive biology, and artificial reproduction of mola. Section 3 details the materials and methods used in the study, including those relating to broodfish collection and maintenance, hormone dose optimization, and breeding arrangements. Section 4 presents results relating to breeder characteristics, breeding behavior and performance, fecundity, larval rearing, and seed sales to farmers. Section 5 concludes by reviewing the implications of the results for the wider promotion of mola as a farmed species, and the potential for the mass production of other candidate SIS in hatcheries.

2 Nutrient content, reproductive biology, and reproduction of mola

Mola fish are distributed throughout Bangladesh, India, Myanmar, and Pakistan. It inhabits rivers, streams, lakes, ponds, ditches, and other stagnant waters (Froese and Pauly, 2022). Its maximum recorded length is 20 cm (Talwar and Jhingran, 1991), although Rahman (1989) reported its maximum length as only 15 cm. The average lifespan of male and female fish is 13 months and 15 months, respectively, as reported in the Payra River of Southern Bangladesh by Ahamed et al. (2017).

It was discovered decades ago that mola contains high contents of calcium, iron, vitamin A, and vitamin B_{12} (Zafri and Ahmad, 1981), and, therefore, has high nutritional value; since then, it has been one of the most studied SIS. Mola is particularly rich in vitamin A, with 2,503 μg of vitamin A present per a 100-g edible portion (Bogard et al., 2015). Mola also contains high levels of essential amino acids. Mustafa et al. (2015) found that the lipid content of mola is 4.5%, and that the percentage of omega-3 polyunsaturated fatty acids (PUFAs) in total fatty acids is 6.31% ± 1.4% in the head and 5.93% ± 0.75% in the body. Mola has a higher lipid content than and similar protein content to most carps (Bogard et al., 2015).

Mola has small gill rakers that are connected with a membrane to filter plankton, and is predominantly a phytoplankton feeder. Mola is herbivorous, and Chlorophyceae are its most preferred food source (Gupta and Banerjee, 2013).

Mola is a prolific breeder, with first maturity reported to occur at 3 months of age (Rajts et al., 1997). Mola is a fractional spawner (Gupta and Banerjee, 2013). The reproductive biology of mola varies with the climate, water quality, food availability, size, and habitat. The present state of knowledge on the reproductive biology of mola is summarized in Table 1.

TABLE 1 The reproductive biology of mola carplet (*Amblypharyngodon mola*) *.

Particulars	Value	Reference
Age of maturity (months)	3	Rajts et al. (1997)
Weight at maturity, female fish (g)	0.25–11.82	Rahman et al. (2018)
Weight at maturity, male fish (g)	0.39–6.86	Rahman et al. (2018)
Length at first maturity, female fish (cm)	3.57–9.94	Rahman et al. (2018)
Length at first maturity, male fish (cm)	3.69–8.88	Rahman et al. (2018)
Breeding habit	Batch spawner	Froese and Pauly (2022)
Parental care	None	Froese and Pauly (2022)
Breeding ground (preferable)	Freshly flooded dry land with plant substrate	Rajts et al. (1997)
Natural breeding events per year	2	Kohinoor et al. (2005)
Natural breeding events per year in Kaptai reservoir, Bangladesh	3	Azadi and Mamun (2004)
Seminatural breeding per year (induced by environmental manipulation)	5	Ghosh et al. (2018)
Gonadosomatic Index (GSI) female (January and June)	1.78 and 17.06	Kohinoor et al. (2005)
Eggs per female fish measuring 5 cm–5.5 cm and 8.1 cm–8.5 cm ♀	1,023 and 6,806	Hoque and Rahman (2008)
Relative fecundity per female fish measuring 5 cm–5.5 cm and 8.1 cm–8.5 cm ♀	200 and 850	Hoque and Rahman (2008)**
Relative fecundity of fish in Kaptai reservoir, Bangladesh	995/g	Azadi and Mamun (2004)
Diameter of vitellogenic oocyte (μm)	27–30	Hoque and Rahman (2008)

(Continued)

TABLE 1 Continued

Particulars	Value	Reference
Pituitary gland (PG) dose for induced breeding	2 mg/kg ♀ and 1 mg/kg ♂	S.I. Khondaker ±
PG dose for induced breeding	25 mg/kg ♀	Saha (2019)
Latency period for ovulation (hours at 27°C)	6–7	S.I. Khondaker ±
Time of egg development to hatching (hours at 27°C)	12	Saha (2019)
Larval development time to first feeding (hours at 27°C)	72	S.I. Khondaker ±
	48	Saha (2019)
Number of 4-day-old hatchlings per kg body weight	1.456 million	Saha (2019)
Size in nursery pond (at 34 days old)	5.15 cm; 1.54 g	Saha (2019)

*Source: Modified from Rajts and Shelley (2020).
**Calculated from data in Hoque and Rahman (2008).
The relative number increases with size.
± Personal communication, hatchery owner, Bangladesh.

Mola eggs are slightly adhesive, and an appropriate substrate on which broodfish lay eggs is needed for successful spawning. Mola breeding can be stimulated by introducing fresh water (particularly rainwater), increasing water levels, and the provision of previously dry but freshly inundated land with substrate for the slightly adhesive eggs. The substrate can be rice plants, remaining rice straw, or artificial grass.

During spawning, the rice straw can serve as a substrate for the eggs and helps to generate infusoria[3] and other zooplankton that provide a food source for young fry (Thilsted et al., 2016; Saha, 2019).

Kohinoor et al. (2005) studied the reproductive biology of mola for 1 year and found that the gonadosomatic index (GSI) values for female mola ranged from 1.78 ± 0.88 to 17.06 ± 2.66. The highest GSI values for female mola were observed in July. Monthly observation of the diameter of the ova indicated that the fish spawned at least two times per year, once between May and July, and again between September and October (Kohinoor et al., 2005).

The possibility of repeated induced breeding of mola has been demonstrated by several authors. Ghosh et al. (2018) carried out a successful breeding trial in West Bengal. They found that mola can be induced to breed five times in 1 year through environmental manipulation. They did so by flushing ponds with water of different origins. The spawning of mola was observed every time pond flushing occurred and also after heavy rain.

Mondal et al. (2020) maintained mola breeders in hapas in ponds throughout the year to study their breeding habits. Ripe ova were found for 9 months, that is, from April to December. The development of oocytes was identified at different stages in each batch, and natural breeding occurred several times during the culture period. This is consistent with the findings of Ghosh et al. (2018), which were that mola could be bred in captivity several times per year using environmental stimuli.

Saha (2019) reported success in hormonal-induced breeding with the use of carp pituitary gland (PG) extract. He reported that the best dose of PG extract for inducing mola to spawn in the hatchery was 25 mg per kg. The latency time was 6 h–8 h, and hatching occurred 17 h–18 h after fertilization, at a temperature of approximately 27°C. Saha estimated the average weight of 4-day-old hatchlings as 0.7 mg. The hatchlings were grown in a nursery pond and reached 5.14 cm± 0.42 cm in total length and 1.54 g± 0.33 g in weight in 34 days. Saha et al. (2014) also reported techniques for the successful transportation of live mola breeders, which are very sensitive to handling.

Despite a substantial body of work on the reproductive biology of mola, the efforts to conduct induced breeding have been largely *ad hoc* in nature. No comprehensive, standardized, easily replicable protocol for the mass breeding and larval rearing of mola under hatchery conditions has been published to date. In the rest of the article, we address this knowledge gap by reporting detailed results from our successful breeding and larval rearing trials of mola in Odisha, India, in 2022, which serve as a protocol for the future replication of mass mola seed production.

3 Materials and methods

3.1 Broodfish collection and maintenance

The induced breeding trial for the mass production of mola seed was conducted at the project partner hatchery complex located in Tulunga village (Biswal Aquatech; latitude 20°12′45.84'N/longitude 86°20′3.32'E), Jagatsighpur District, Odisha, India. A sample of wild mola weighing 40 kg was collected between March 2022 and April 2022 from three different sources—community water bodies, private ponds, and canals—to ensure high levels of genetic variation, and was transported to the partner hatchery in 10-L oxygenated plastic bags. On arrival, all live mola were treated with a 10 ppm potassium permanganate ($KMnO_4$) solution and were stocked in two separate broodfish ponds (area per pond: 400 m^2, depth: 1 m–1.5 m) at a density of 20 kg per pond (50 g/m^2), and maintained for 3 months.

The broodfish ponds were prepared in accordance with standard protocols (Horvath et al., 2002; Rajts et al., 2022). The ponds were semidried and, after cleaning, the wet bottom was treated with powdered hydrated lime [$Ca(OH)_2$], at the rate of 200 g/m^2. Basal organic fertilization was conducted using mustard oil cake (MOC) at a rate of 20 g/m^2, and water was gradually filled up to a depth of 1 m from a borewell. Following this, an initial application of the inorganic fertilizers urea and single superphosphate (SSP) was made at rates of 10 g/m^2 and 20 g/m^2, respectively, to augment pond productivity.

Mola broodfish were stocked when water transparency (Secchi disc reading) reached the optimum level of 25 cm–30 cm. The broodfish were fed to satiation twice daily with floating pelleted feed (Natpro feed; 1 mm in size; 42% protein). To maintain the healthy

3 Infusoria are live food organisms (mostly composed of microscopic protozoans) that are eaten by fish hatchlings.

growth of plankton in the ponds, weekly applications of urea and SSP were made at rates of 2 g/m^2 and 4 g/m^2, respectively.

The water quality of broodfish ponds was monitored periodically between 08:00 and 10:00 using a HANNA multiparameter kit. The average physicochemical parameters of the broodfish ponds were: temperature 30°C, pH 7.5, dissolved oxygen 6.2 mg L^{-1}, alkalinity 190 mg L^{-1}, hardness 85 mg L^{-1}, nitrite (NO_2-N) 0.0 mg L^{-1}, and ammonia (NH_4-N) 0.6 mg L^{-1}.

It is very difficult to distinguish between male and female mola during the early stages of maturity, but sex can be distinguished during the breeding season (Rajts and Shelley, 2020). When setting up the induced breeding, mature mola broodfish were identified based on their secondary sexual characteristics. Male fish are comparatively brighter than female fish, whereas female fish are larger in size and lighter in color than male fish. Mature female fish have smooth pelvic fins and a deeply forked caudal fin, and can be identified during the spawning season by their soft and conspicuously distended abdomen. Matured male fish have yellowish-colored caudal fins (Figure 1).

3.2 Induced breeding arrangements

The mature and healthy mola broodfish were collected from the broodfish ponds by repeated drag netting, followed by manual segregation by sex, and transferred to a concrete conditioning cum breeding tank (L × W × H: 3.9 m × 2.35 m × 1.10 m; capacity: 10 m^3) with a constant water showering for approximately 6 h–8 h, for acclimatization and stimulating spawning readiness. On average, a total of 3.36 kg of male and female mola broodfish were conditioned and injected together. The fish were not fed before the breeding commenced. A combination of hormone administration and environmental manipulation was used to increase seed production.

Two breeding tanks were prepared with double hapas. First, a 250-µm nylon mesh outer hapa was installed within the tank. Subsequently, with the aid of a galvanized iron frame, an inner hapa with a mesh size of 8 mm was installed inside the outer hapa. Throughout the trial, the breeding tank was exposed to a constant shower of oxygen-rich water from an overhead tank equipped with an aeration tower (Figure 2). A diagram illustrating the construction of an aeration tower is shown in Figure 3.

3.2.1 Preparation, dose optimization, and administration of inducing hormone

Synthetic gonadotropin-releasing hormone analog (SgnRHa with domperidone) (trade name—WOVA-FH™, manufactured by Biostadt India Limited, Mumbai, India) was used to induce spawning. To optimize the inducing hormone dose, we initially chose five different treatment doses, i.e., 0.1 mL to 0.5 mL per kg body weight of female fish (Table 2). Male fish were administered with half the dose given to female fish.

The hormone dose was diluted 15 times in 0.65% sterile sodium chloride (NaCl) solution. Dilution was necessary because of the high viscosity of the product and the very small dose required for SIS. The inducing solution was administered into the peritoneal cavity of mola broodfish using an insulin diabetic syringe of 1-mL capacity with 40 graduations. In brief, doses of 0.5 mL and 0.25 mL per kg body weight of female fish and male fish, respectively, yielded the highest hatchling production

FIGURE 1
Mature female (left) and male (right) mola.

FIGURE 2
Aeration tower installed in the overhead water reservoir tank.

among the five treatments, and these doses were selected for the mass production of mola seed.

The inducing solution was prepared and injected according to the individual body weight of the fish with an average 2: 1 male-to-female ratio. For female mola breeders weighing 1 kg, 8 mL of inducing solution (0.5 mL of hormone + 7.5 mL of water) was used. The following formula was used to determine the individual doses for breeders:

$$G = \left(\frac{H}{1,000} \times W\right) \times \frac{D}{V} \quad (1)$$

In which, G represents the number of graduations on the syringe, having the required volume of solution to be injected; H the desired dose of hormone to be applied (original hormone, mL kg^{-1}); W the weight of fish to be injected (g); D the dilution rate of hormone; and V the volume of the diluted solution in one unit of syringe graduation.

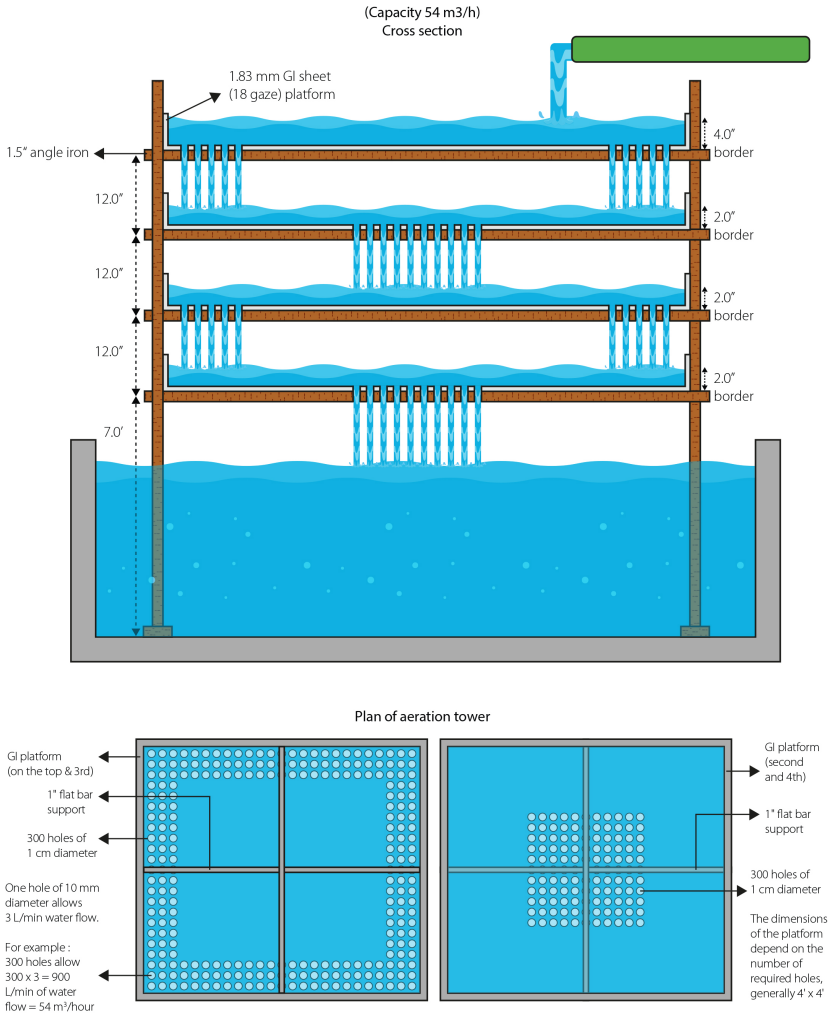

FIGURE 3
A diagram illustrating the construction of an aeration tower.

10.3389/faquc.2023.1271715

TABLE 2 Various doses of inducing agents (WOVA-FH) utilized for optimizing the best dose for mass seed production of mola (*Amblypharyngodon mola*).

Inducing agent dose (mL/kg^{-1} body weight of female fish)	Number of female broodfish	Number of male broodfish	Average weight of female fish (g)	Average weight of male (g)	Female fish that responded (%)	Number of eggs released	Fertilization rate (%)	Number of fertilized eggs	Hatching rate (%)	Number of hatchlings	Survival rate (%)	Number of hatchlings harvested
0.1	15	30	7.13	3.23	0	0	0	0	0	0	0	0
0.2	15	30	7.20	3.13	0	0	0	0	0	0	0	0
0.3	15	30	7.33	3.10	20	10,168	75	7,605	77	5,818	83	4,800
0.4	15	30	6.87	3.20	27	17,672	77	13,678	76	10,368	82	8,450
0.5	15	30	7.13	3.20	73	81,969	77	62,952	78	48,788	83	40,250

For instance, 0.04 mL (5 × 0.008) of inducing solution is required for a single female mola weighing 5 g. One graduation of insulin syringe contains 0.025 mL (1/40 mL). Therefore, for a 5-g female, the volume of solution contained in 1.6-graduations (0.04/0.025) needs to be injected. Immediately after administering the inducing solution, the broodfish were returned to the 10-mm mesh inner hapa, which was covered with nylon mosquito nets to prevent the fish from jumping out.

Table 3 details the characteristics of mola broodfish used over 10 production cycles. A sample of mola broodfish weighing 34 kg in total (female broodfish weighed 21 kg in total and male broodfish weighed 13 kg in total) was injected. Breeding took place over 16 h–22 h during the peak breeding season (i.e., June 2022–September 2022), with a natural photoperiod of 12 h light: 12 h dark. The water quality of the breeding tanks was monitored, and the average values for temperature, pH, and dissolved oxygen were 29.53°C ± 0.39°C, 8.03 ± 0.12, and 6.86 mg/L^{-1}± 0.31 mg/L^{-1}, respectively, over the 10 production cycles.

3.3 Evaluation of breeding performance

The breeding performance of hatchery-based mass production of mola was evaluated in terms of spawning rates (percentage of female fish that responded), fertilization rate (%), hatching rate (%), hatchling production, and survival (%). The numbers of eggs and hatchlings were calculated using the volumetric method and the following equations (Sarkar et al., 2005; Kumar et al., 2018; Kumar et al., 2021):

$$\text{Latency period (h)} = \text{duration from first injection to spawning} \quad (2)$$

$$\text{Spawning rate (\%)} = (\text{number of female fish that responded} / \text{total number of injected fish}) \times 100 \quad (3)$$

$$\text{Incubation period} = \text{duration from fertilization to hatching} \quad (4)$$

$$\text{Absolute fecundity} = \text{total number of eggs in the ovary of mature female fish} \quad (5)$$

$$\text{Relative fecundity (number of eggs spawned per g body weight of fish)} = \text{total number of eggs released/body weight of female fish} \quad (6)$$

$$\text{Fertilization rate (\%)} = (\text{number of fertilized eggs/total number of eggs counted}) \times 100 \quad (7)$$

TABLE 3 Morphometric characteristics and sex ratio of mola broodfish (*Amblypharyngodon mola*) used for mass seed production.

Breeding batch	Date	Number of female broodfish	Number of male broodfish	Total number of broodfish	M: F ratio	Total weight of female broodfish (g)	Total weight of male broodfish (g)	Total weight of all broodfish (g)	Average weight of female broodfish (g)	Average weight of male broodfish (g)	Average length of female broodfish (cm)	Average length of male broodfish (cm)
One	5/7/2022	264	418	682	1.6: 1	2,000	1,360	3,360	7.58	3.25	9.34	5.09
Two	14/7/2022	436	545	981	1.3: 1	3,150	1,650	4,800	7.22	3.03	9.06	5.07
Three	30/7/2022	515	795	1,310	1.5: 1	3,850	2,450	6,300	7.48	3.08	9.34	5.04
Four	31/7/2022	358	482	840	1.3: 1	2,450	1,250	3,700	6.84	2.59	8.75	4.64
Five	19/8/2022	381	482	863	1.3: 1	2,650	1,350	4,000	6.96	2.80	8.91	4.78
Six	21/8/2022	396	645	1,041	1.6: 1	2,600	1,720	4,320	6.57	2.67	8.55	4.58
Seven	20/9/2022	122	201	323	1.6: 1	793	574	1,367	6.50	2.86	8.46	4.81
Eight	21/9/2022	50	100	150	2.0: 1	318	288	605	6.35	2.88	8.21	4.83
Nine	26/9/2022	200	380	580	1.9: 1	1,300	995	2,295	6.50	2.62	8.49	4.75
10	27/9/2022	265	365	630	1.4: 1	1,850	997	2,847	6.98	2.73	8.98	4.84
Total	–	2,987	4,413	7,400	–	20,961	12,634	33,594	–	–	–	–
Mean	–	299	441	740	1.6: 1	2,096	1,263	3,359	6.79	2.82	8.72	4.83
SD	–	146	201	343	0.25	1,077	610	1,671	1.02	0.44	0.98	0.47
Minimum	–	50	100	150	1.3: 1	318	288	605	4.0	2.0	6.0	2.4
Maximum	–	515	795	1,310	2.0: 1	3,850	2,450	6,300	10.0	5.0	11.5	6.9

10.3389/faquc.2023.1271715

Hatching rate (%)

= (number of hatched eggs/total number of fertilized eggs) × 100 (8)

Hatchling survival (%)

= (number of live hatchlings harvested/total number of hatchlings hatched out) × 100 (9)

3.4 Nursery rearing of hatchery-produced mola

Three-day-old hatchlings were stocked from July 2022 to August 2022 in three different nursery ponds that were 400 m^2 in size (depth 1 m–1.5 m), at stocking densities of 500, 625, and 750 individuals per m^2, and reared for 21 days. The nursing ponds were located inside the partner hatchery complex, at a distance of approximately 200 m from the breeding tanks.

3.4.1 Nursery pond preparation

The nursery ponds were dewatered, and the pond bottom soil was kept moist until lime application. Hydrated lime in powder form was applied at a rate of 200 g/m^2 and left to dry on the pond bottom for a week. Mola hatchlings are sensitive to predation from copepods and some insects and insect larvae such as backswimmers and dragonfly larvae. Liming on wet soil followed by drying the pond bottom will eliminate most predators during pond preparation (Rajts et al., 2022).

Fermented MOC was sprayed on the pond bottom as organic fertilizer, after diluting in water at a rate of 20 g/m^2. The ponds were gradually filled from a borewell to a depth of 1 m 3–4 days before mola seed was stocked. The inorganic fertilizers urea and SSP were applied by dilution in pondwater at rates of 10 g/m^2 and 20 g/m^2, respectively, when water filling started. Fermented MOC was sprayed on the pond surface daily thereafter, mainly as an organic fertilizer, at a rate of 1.25 g/m^2.

During the initial days of rearing, hatchlings require plenty of small zooplankton because their mouths are small and they are unable to catch fast-moving prey (Rajts et al., 2022). This type of zooplankton consists of protozoans and rotifers. Dried grass was placed all-around the shallow areas of the pond to develop *Paramecium* and rotifer populations, which are the best source of food for the small mouths of hatchlings. The decomposing grass was removed after 7 days.

Before stocking mola hatchlings, the nursery ponds were netted several times with a mosquito net to remove other predatory insects such as backswimmers and their larvae. To repel predator copepods at the time of stocking, mola hatchlings were stocked within 3–4 days of filling with water. The stocking was conducted in the morning, with special attention paid to the gradual adjustment of the physicochemical characteristics of the carrying water and the pond water.

The hatchlings were fed with microencapsulated chicken eggs at a rate of five eggs per 100,000 hatchlings per day. This dose was divided across four separate feeding events per day. Feeding with the microencapsulated eggs was stopped after 5 days, but MOC application was continued. From day 6 onwards, commercial powdered feed (Natpro feed; 1 mm in size; 42% protein) was scattered on the water surface, *ad libitum*.

To enhance natural plankton productivity, urea and SSP were applied each week at rates of 2 g/m^2 and 4 g/m^2, respectively, depending on phytoplankton density (Secchi disc reading 25 cm–30 cm). Water quality deteriorates easily in nursery ponds when excess fertilizers are applied; therefore, 5 cm–6 cm of fresh water was added daily until the ponds were filled to a maximum depth of 1.5 m. After 3 weeks (i.e., on day 22), mola fry were harvested. Feeding was stopped 1 day prior to harvesting.

3.4.2 Survival and growth performance

To assess growth performance, weekly sampling was conducted to measure the length and weight of broodfish using ruler scales and a digital weighing balance (precision 1 mg; Saffron), respectively. Mortality and other behaviors were monitored daily. The growth performance was calculated using the following formulas:

Daily weight gain (mg) = final weight (mg)–initial weight (mg)/rearing duration. (10)

Specific growth rate (% day^{-1}) = [Ln (final weight (mg))–Ln (initial weight (mg))]/rearing duration × 100. (11)

Survival rate (%) = final number of fry/initial number of hatchlings × 100. (12)

3.4.3 Water quality

The water quality parameters of nursery ponds were monitored 3 days before stocking and subsequently at 3-day intervals using a HANNA multiparameter kit. The parameters measured were temperature (°C), pH, dissolved oxygen (mg/L^{-1}), ammonia-nitrogen (NH_3-N) (mg/L^{-1}), nitrite-nitrogen, (NO_2-N) (mg/L^{-1}), total alkalinity [as $CaCO_3$ (mg/L^{-1})], and total hardness [as $CaCO_3$) (mg/L^{-1})].

4 Results

4.1 Breeding behavior, latency, induced spawning, and egg production

Spawning was achieved within an average latency period of 6 h to 8 h after hormone administration and at an average water temperature of 29.5°C (range 28.5°C–30°C). The reproductive behavior of the mola fish was closely observed at regular intervals. Within 3 h–4 h after hormone administration, male mola initiated

courtship by exhibiting active movements around female mola, with occasional synchronized swimming alongside female mola, followed by frequent coordinated movements. We found that each female fish paired with a single male fish. After pairing, the male fish increased the intensity of their movements, and aggressively and repeatedly chased and contacted the female fish's abdominal area near the urogenital aperture. The frequency of coupling and twisting activity by male fish intensified during spawning.

Batch-specific information on average spawning and fertilization rates during mass production of mola seed is presented in Table 4. The spawning rate ranged from 74% to 87%, with a mean value of 82% ± 4.99%. The average absolute fecundity was recorded as 9,018 ± 3,120, with a range between 5,076 and 14,167, and the numbers of spawned eggs ranged between 515 and 778 eggs per g^{-1} female fish body weight, with a mean value of 609 ± 85 eggs per g^{-1} female fish body weight. Over the 10 production cycles, approximately 8.5 million fertilized eggs were produced. The fertilization rate ranged between 77% and 86%, with a mean value of 81% ± 2.39%, and the number of fertilized eggs per g body weight of female fish ranged between 415 and 618, with a mean value of 499 ± 73.

The fertilized eggs were light brown to yellowish in color, clear in appearance, demersal, and semi-adhesive (Figure 4). The eggs were found to be attached to the lower bottom part and lower lateral side of the 250-µm mesh outer hapa. The following morning, between 09:00 and 11:00, all breeders were removed from the inner hapa and relocated to a designated spent brood pond. The average numbers of dead male and female mola per spawning were 16.20 ± 10.24 and 9.90 ± 6.97, respectively, with mortality rates of between 5.54% ± 2.53% and 2.25% ± 1.07%, respectively.

4.2 Hatchling production and survival

Table 5 details information, by batch, on hatchling production during hatchery-based mass production of mola seed. Larvae were observed to hatch 12 h–14 h after fertilization, at a water temperature of 28.5°C–30°C. The hatching rate ranged from 76%–91%, with mean values of 85% ± 4.66%. Over the 10 production cycles, approximately 6.36 million hatchlings were harvested, with an average of 635,820 ± 335,171 hatchlings harvested per batch. The average number of hatchlings harvested per female fish ranged from 2,065 to 2,980, with a mean value of 2,580 ± 351. The total number of hatchlings produced per kg body weight of female fish ranged from 272,547 to 458,399, with a mean value of 375,979 ± 62,793.

The embryos began a twisting movement inside the egg capsule 5–7 times per minute before hatching. The twisting movement broke down the eggshell, and the embryo finally emerged tail first.

One-day-old hatchlings exhibit sluggish movement and tend to remain attached to the wall of the hapa (Figure 4). From the second day onwards, hatchlings move toward the water column and remain close to the side wall of the hapa while exhibiting resting swimming

TABLE 4 Information (by batch) on spawning fecundity and fertilization rate during hatchery-based mass seed production of mola (*Amblypharyngodon mola*).

Breeding batch	Number of eggs released by each female fish (spawning fecundity)	Spawning rate (% of female fish that responded)	Total eggs released	Number of eggs per g body weight of female fish	Number of fertilized eggs	Fertilization rate (%)	Number of fertilized eggs per g body weight of female fish
One	4,256	76	855,383	562	654,368	76.5	430
Two	4,101	87	1,550,234	568	1,263,441	81.5	463
Three	3,851	86	1,713,706	515	1,379,533	80.5	415
Four	3,632	86	1,122,318	531	903,466	80.5	427
Five	4,804	82	1,508,543	691	1,229,463	81.5	563
Six	5,106	83	1,679,733	778	1,335,388	79.5	618
Seven	4,257	80	417,188	655	356,696	85.5	560
Eight	3,400	74	125,813	535	102,538	81.5	436
Nine	4,333	75	649,915	667	542,679	83.5	557
10	4,437	77	900,705	636	743,081	82.5	524
Total	–	–	10,523,537	–	8,510,652	–	–
Mean	4,271	82.49	1,052,354	609	851,065	81	492
SD	512	4.99	555,532	85	444,719	2.39	73
Minimum	3,400	74	125,813	515	102,538	77	415
Maximum	5,106	87	1,713,706	778	1,379,533	86	618

FIGURE 4
Mola eggs attached to the outer hapa (left), and one-day-old hatchlings (right).

behavior. Beyond 48 h after hatching, hatchlings exhibit active swimming behavior, and the eyes and mouth become prominent. The yolk sac is completely absorbed within 72 h.

The newly hatched larvae are completely transparent, slender, and lack pigmentation. Rudimentary eye and otic vesicles are visible. A large yolk sac is present, which is bulbous in the anterior area and narrow in the posterior area.

From the third day onwards, the air bladder became pigmented black. The larva had three black spots when viewed from above; one of them was an air bladder, and the other two were eyeballs. Larval

TABLE 5 Information (by batch) on the production and survival rate of mola (*Amblypharyngodon mola*) hatchlings during hatchery-based mass seed production.

Breeding batch	Hatching rate (%)	Number of hatchlings hatched	Survival rate (%)	Total number of hatchlings harvested	Number of hatchlings harvested per female fish	Number of hatchlings harvested per kg body weight of female fish
One	75.5	494,048	84	415,000	2,065	272,537
Two	84	1,061,290	93	987,000	2,611	361,411
Three	86.5	1,193,296	89.5	1,068,000	2,400	321,039
Four	84.5	763,429	87.5	668,000	2,162	315,889
Five	80.5	989,718	88.5	875,900	2,789	401,055
Six	82.5	1,101,695	88.5	975,000	2,964	451,368
Seven	88.5	315,676	92.5	292,000	2,980	458,399
Eight	89.5	91,771	87.5	80,300	2,170	341,775
Nine	90.5	491,124	84.5	415,000	2,767	425,641
10	88.5	657,627	88.5	582,000	2,867	410,678
Total	–	7,159,674	–	6,358,200	–	–
Mean	85	715,967	89	635,820	2,580	375,979
SD	4.66	369,102	2.89	335,171	351	62793
Minimum	76	91,771	84	80,300	2,065	272,537
Maximum	91	1,193,296	93	1,068,000	2,980	458,399

TABLE 6 Survival and growth performance of mola (*Amblypharyngodon mola*) hatchling at different stocking densities after 21 days of nursery rearing.

Parameter	Stocking densities		
	500/m^2	625/m^2	750/m^2
Initial weight (mg)	0.002	0.002	0.002
Final weight (mg)	0.32	0.21	0.07
Daily weight gain (mg/day^{-1})	0.315	0.218	0.076
Specific growth rate (% per day^{-1})	30.71 ± 2.75	30.26 ± 2.70	29.21 ± 2.71
Survival (%)	58	53	48

movements became faster and more frequent, and the larvae were found to be swimming casually.

4.3 Larval rearing of hatchlings

The average growth performance during the 3-week larval rearing period in terms of daily weight gain (mg day^{-1}), specific growth rate (SGR; % day^{-1}), and survival are presented in Table 6. The highest growth and survival were recorded at the lowest stocking density. After 21 days of rearing, the mean SGRs were 30.71% ± 2.75%, 30.26% ± 2.70%, and 29.21% ± 2.71% at stocking densities of 500/m^2, 625/m^2, and 750/m^2, respectively. The respective survival values were 58%, 53%, and 48%, respectively.

The average water quality parameters of the three nursery ponds during the nursery rearing period are presented in Table 7. The temperature ranged between 29.70°C and 34.5°C, and the pH ranged between 7.60 and 8.90 throughout the study period. The level of dissolved oxygen varied from 5.21 mg/L to 8.95 mg/L, but the averages remained comparable in the three ponds. As expected, nitrite (NO_2-N) and ammonia (NH_3-N) were found to be highest in the pond with the highest stocking density.

TABLE 7 Different water quality parameters during nursery rearing of mola (*Amblypharyngodon mola*) hatchlings at different stocking densities.

Parameters	Stocking densities		
	500/m^2	625/m^2	750/m^2
Temperature (°C)	31.45 ± 1.42	30.90 ± 0.91	31.31 ± 1.24
pH	8.10 ± 0.37	8.57 ± 0.24	8.38 ± 0.36
Dissolved oxygen (mg/L^{-1})	7.26 ± 0.70	7.32 ± 1.14	7.25 ± 1.06
Nitrite (NO_2-N) (mg/L^{-1})	0.27 ± 0.14	0.30 ± 0.15	0.42 ± 0.24
Ammonia (NH_3-N) (mg/L^{-1})	0.75 ± 0.37	0.62 ± 0.23	1.12 ± 0.44
Alkalinity (mg/L^{-1})	134.25 ± 20.33	140.12 ± 19.55	128.00 ± 20.66
Hardness (mg/L^{-1})	134.50 ± 17.98	126.00 ± 16.27	126.62 ± 12.11
Transparency (cm)	29.16 ± 3.10	34.08 ± 2.60	34.33 ± 2.87

TABLE 8 Details of mola (*Amblypharyngodon mola*) seed sales from the partner hatchery of Odisha during 2022.

Item	Hatchlings	Fry
Number of farmers purchasing	9	20
Average quantity per purchase	236,667	3525
Total quantity sold (number)	2,130,000	70,500
Average sales value (INR)	1,043 per 100,000	0.28 per fry

4.4 Dissemination of mola seed

Mola hatchlings and fry were either sold or distributed on a complimentary basis to carp farmers at regular intervals who had come to purchase carp seed from the project partner hatchery. From July 2022 to October 2022, 29 farmers took mola seed from the hatchery, of which nine took 3-day-old hatchlings and 20 purchased mola fry that were 1–1.5 inches in size. These farmers came from five districts in Odisha (Jagatshingpur, Bhadrak, Jajpur, Cuttack, and Kendrapara). A summary of mola seed sales is given in Table 8.

Cumulatively, 2.13 million hatchlings were sold directly, with an average price of 1,043 INR per 100,000 fry, and 70,500 mola fry were sold at an average rate of 0.28 INR per 100 fry. Seed were sold in well-oxygenated plastic bags, filled with clean aerated groundwater. By October 2022, the partner hatchery had earned a total of 41,650 INR (around USD 510) by selling mola seed originating from the project.

The basic details of all the farmers who purchased mola seeds were recorded. Most of the farmers stocked mola seed into pond-based carp polyculture systems, which had an average pond area of 0.3 ha. The mola seed were also purchased by village committees to stock in two Gram Panchayat (GP) tanks[4], and by two private entrepreneurs for stocking biofloc aquaculture systems. Approximately 15,000 fry were distributed to women's self-help groups (WSHGs)[5] as part of promotional activities for stocking in GP tanks. The remaining

4 In Odisha, numerous earthen tanks or ponds have been excavated under government schemes and community programmes for water conservation through rainwater harvesting and multipurpose utilization. These tanks are managed by the decentralized governance system of Gram Panchayats under the Panchayati Raj and Drinking Water Department, the Government of Odisha. In Odisha there are approximately 62,000 multipurpose GP tanks, which have a total water area of 54,000 ha.

5 Women's self-help groups are informal community groups led by women that are often used as a means of reducing poverty and empowering women to undertake many livelihood-generating activities using credit facilities. Currently, the Government of Odisha nurtures approximately 600,000 WSHGs, which have approximately 7 million women in total who participate in village-level socioeconomic activities and promote women's empowerment.

unsold seed were stocked in carp polyculture ponds at the partner hatchery for grow-out and broodfish rearing.

5 Discussion

This article reports on the first systematic breeding methods aimed at developing a technical protocol for hatchery-based mass production of mola seed, a popular nutrient-rich SIS from South Asia. SIS are small and delicate to handle, making it difficult to produce seed from them in large quantities using conventional hatchery methods. Induced breeding, therefore, needs species-specific innovation and specially modified technology (Rajts et al., 2022).

In the present study, average absolute fecundity and spawning fecundity were found to be 9,018 and 4,271, respectively, which is comparable to the findings reported in the study by Saha (2019). Previous studies have also reported that mola is a highly fecund fish.

The average latency and incubation periods observed in the present study were 6 h–8 h and 12 h–14 h, respectively, which corresponds with the findings of Saha (2019). The latency period of mola is also similar to that of the endemic cyprinid fish *Dawkinsia rohani* (7 h–8 h at 22°C–25°C with 0.5 mL–0.7 mL of WOVA-FH per kg body weight of female fish and *Barilius barila* (6 h–7 h at 25° C–28°C with 0.5 mL of WOVA-FH per kg body weight of female fish) (Dey et al., 2016; Mariappan et al., 2021). However, the latency and incubation periods of mola are shorter than those of Indian major carps (Chattopadhyay, 2017).

In the present study, administering synthetic GnRH-based hormone through the peritoneal cavity at 0.5 mL kg^{-1} body weight of female mola resulted in a fertilization rate of 77%–86% (mean 81%), and hatching rate of 76%–91% (mean 85%). The number of hatchlings harvested per female fish ranged from 2,065 to 2,980 (mean: 2,580). This approach yielded better results than those previously reported by Saha (2019), which were observed in fish in their responses to PG hormone administration through the pectoral fin cavity [at 25 mg/kg^{-1} body weight of female mola (fertilization rate 84%, hatching rate 63%, and 678 hatchlings per female fish)].

This is supported by the fact that various cyprinids, such as Indian major carps, minor carps *Labeo bata*, and Pengba *Osteobrama belangeri*, performed better during breeding with synthetic hormone doses of 0.4 mL/kg^{-1} to 0.5 mL/kg^{-1} body weight for female fish and 2 kg^{-1} to 2.5 kg^{-1} body weight for male fish (Behera et al., 2007; Rath et al., 2007; Das et al., 2016). However, trials are required to explore the possibilities of higher doses of inducing agents for the mass seed production of SIS.

The efficacy of the synthetic GnRH-based hormones has been reported to be greater than that of PG hormone in cases of other cyprinid and carp species, as GnRHa works at a higher level of the brain–pituitary–gonadal axis, which can facilitate more balanced control of reproductive and physiological events for oocyte maturation and spawning (Rath et al., 2007; Das et al., 2016; Kumar et al., 2021). Commercial synthetic hormones are convenient for mass production of SIS seed because they are easily accessible in the market, in contrast to the time-consuming and labor-intensive process required to produce inducing solutions from carp pituitary extracts (hypophysation).

The present study was conducted with the intent of maintaining the sex ratio of male and female broodfish at 2: 1 (male > female), but in practice the ratio averaged 1.6: 1 over 10 production cycles. A male-biased sex ratio of two male fish to one female fish has been reported for many species to lead to a significantly higher fertilization rate, hatching rate, and larval survival (Mandal et al., 2016; Kumar et al., 2021).

With the same tanks set up for conditioning and spawning, the induced breeding protocol developed for the study eliminates the need for a separate breeding pool, hatching pool, tray, or incubator. Instead of a continuous flow of water, the current study used controlled showering, which also serves as a water-saving strategy. In addition, in contrast to Saha (2019), no substratum (grass, water, hyacinth, etc.) was used during the breeding trials; instead, eggs were attached to and gathered within the 250-µm outer hapa, which could be handled easily.

The hatchery setup included an aeration tower in the overhead water reservoir tank to maintain optimal levels of dissolved oxygen and degas groundwater during hatchery operations. The concept was first introduced in Bangladesh during the 1980s by Rajts (1986). Toxic gases are removed from the groundwater by the aeration tower as inflowing water pumped from the borewell passes through it on its way to the overhead tank. In addition, this process dissolves oxygen, ensuring that the water supply is almost completely saturated with oxygen, which increases larval survival Rajts (1986). By automatically aerating the water before it enters the overhead tank, this tool has the benefit of eliminating the need for additional aeration during breeding operation and is thus an energy-saving strategy. According to Avery and Steeby (2004), pretreating the water with degassing-aeration towers is a critical step in the enhancement of dissolved oxygen and the removal of unwanted gases, which are essential for effective hatching.

The spawning and hatching success of fish is influenced by factors that are related to water quality, especially water temperature. In our study, the water temperature in the breeding tanks was 29.53°C and the dissolved oxygen concentration was 6.86 mg/L^{-1}, both of which are favorable for breeding (Chattopadhyay, 2017). Although it has been reported that most small indigenous fish breed at a water temperature of 26.0°C–28.5°C under captivity (Das et al., 2016; Mariappan et al., 2021), in slightly higher water temperatures, the embryos hatch faster, and have a better survival rate (Olaniyi and Omitogun, 2013).

For SIS, such as mola, spontaneous spawning may also be achieved by manipulating water quality parameters, alone or in combination with hormone induction. This might be accomplished by maintaining a constant level of dissolved oxygen; implementing constant showering and flow from groundwater or pond water; adding soft water, such as rainwater; and adding substratum to mimic the situation in spawning ponds (Rajts et al., 2022). This approach might stimulate fish to spawn for an extended period, even outside of their typical spawning season. Therefore, rainwater storage and use could be a critical additional step to stimulate the

spontaneous spawning of SIS and extend the duration of spawning beyond the normal breeding season. In this regard, field trials are needed to better understand the interactions between environmental stimuli and reproductive parameters during the mola breeding cycle.

As mola is a prolific breeder, the sex-specific separation of mola broodfish should be maintained during both the off-season and breeding season to eliminate the possibility of auto-breeding. However, in the present study, sex-specific broodfish ponds were not maintained as it is very difficult to distinguish between male and female mola during the early-maturity stage, and sex can be determined only during the breeding season (Rajts and Shelley, 2020). It is also challenging to maintain the sex segregation of mola because of handling stress and injury to the fish during sorting.

During nursery rearing, the survival of mola fry depended on pond preparation, the presence of selectively cultured plankton in nursery ponds, and stocking density. For the first 3–4 days of nursery rearing, mola fry require that a sufficient number of rotifers (their food source) is present, but they are also at risk of being eaten by large copepod zooplankton. Therefore, management is necessary for the selective elimination of zooplankton, and also the selective development of protozoans and rotifers.

In the current study, ponds stocked with 500 individuals per m^2 yielded the highest survival and growth rates after 3 weeks of culture. However, from preliminary observations during the study, it appears advisable for farmers to stock mola hatchlings at a lower stocking density during nursery rearing, such as 200 individuals per m^2.

To prevent disease outbreaks and plankton shortages, fry should be harvested after 3 weeks of culture. They can then be stocked into a carp–mola polyculture grow-out pond at a rate of 5–10 individuals/m^2. Further focused study is required to optimize the stocking density of mola fry during nursery rearing, and also in grow-out ponds.

Stocking hatchery-produced mola seed offers several potential advantages over the previous practice of stocking broodfish harvested from natural water bodies. Stocking wild breeders in seasonal ponds where water is available for a short period only can be challenging because ponds may dry up before their progeny reach market size. Moreover, ponds stocked with wild breeders contain SIS populations comprising a mix of age groups, resulting in the production of fish of variable sizes, which are less marketable.

In contrast, hatchery-produced SIS seed are of uniform size and age, and can be stocked at the optimum time and density to maximize survival and growth. Moreover, hatchery-produced seed can be conditioned and packed in clean well-oxygenated water before it is delivered to farmers, which would reduce the number of mortalities during transport and stocking. Stocking hatchery-produced fry may also ensure a uniform size of SIS at harvest, making them more marketable and thus more likely to be sold at better prices. Hatchery-based seed production also offers the possibility of stimulating spawning much earlier than in the wild, giving farmers a head start over nature.

The project is monitoring sales of mola seed by the partner hatchery (WorldFish, 2022). The average selling price of mola hatchlings (INR 1,043 per 100,000 pieces) and fry (INR 0.28 per piece) was comparable to that of carp seed sold by the hatchery. For example, rohu hatchlings typically sell for INR 900 per 100,000 pieces, whereas mixed carp fry (rohu, mrigal, and catla) cost INR 0.20–0.25 per piece. Even so, further thorough economic analysis and modeling are crucial to determining the cost–benefit ratio and setting the mola seed price.

Micronutrient deficiencies are a major public health issue in the Global South. Therefore, it is crucial that forms of aquaculture that produce vital micronutrients without depleting underlying environmental resources are developed (Gephart et al., 2020). The higher levels of key micronutrients in mola than in carp, the compatibility of mola with carp polyculture systems, and the opportunity to obtain multiple harvests per year make mola an ideal species for nutrition-sensitive aquaculture.

We hope that this groundbreaking commercial mass mola seed production trial will facilitate the large-scale adoption of nutrition-sensitive carp–mola polyculture, which will boost farm incomes, increase the consumption of micronutrient-dense fish, and support the livelihoods and well-being of vulnerable populations who currently experience nutritional inadequacies in regions of India and South Asia.

6 Conclusion

To conclude, the mass seed production of the nutrient-dense SIS mola can be achieved through induced breeding using GnRH-based synthetic hormone (Wova-FH) at a dose of 0.5 mL and 0.25 mL per kg body weight of female and male fish, respectively, combined with environmental manipulation using oxygen-rich water. The breeding protocol is simple and can be adopted by small-scale hatchery operators.

Data availability statement

The original contributions presented in the study are included in the article/supplementary material. Further inquiries can be directed to the corresponding author.

Ethics statement

Ethical approval was not required for the study involving animals in accordance with the local legislation and institutional requirements because this project was considered to be a description of husbandry procedures and, thus, animal ethics approval was not required.

Author contributions

FR: Formal Analysis, Investigation, Methodology, Visualization, Writing – review & editing. SD: Formal Analysis, Investigation, Methodology, Project administration, Writing – original draft, Writing – review & editing. KG: Formal Analysis, Investigation,

Methodology, Writing – original draft. RD: Formal Analysis, Investigation, Writing – original draft. SB: Investigation, Resources, Writing – review & editing. AP: Supervision, Writing – review & editing. SR: Supervision, Writing – review & editing. ST: Funding acquisition, Writing – review & editing. CM: Supervision, Writing – review & editing. BB: Funding acquisition, Project administration, Supervision, Visualization, Writing – original draft, Writing – review & editing.

Funding

The author(s) declare financial support was received for the research, authorship, and/or publication of this article. This work received financial support from the German Federal Ministry for Economic Cooperation and Development (BMZ) commissioned by the Deutsche Gesellschaft für Internationale Zusammenarbeit (GIZ) through the Fund International Agricultural Research (FIA) (grant number: 81260866).

Acknowledgments

The authors are thankful to hatchery technician Mr. BB Das and other staff of hatchery and Seafood Solutions LLP, Andhra Pradesh for their support. The authors are also sincerely indebted to the Fisheries and Animal Resources Development Department, Government of Odisha, for its active support and collaboration. Sections of this study were presented at the World Aquaculture 2022 Singapore conference. Sections of this study have also been released in the form of a popular blog on the WorldFish website (WorldFish, 2022).

Conflict of interest

SB is employed by Biswal Auqatech.

The remaining authors declare that the project was conducted in the absence of any commercial or financial relationships that could be construed as a potential conflict of interest.

The author(s) BB, ST declared that they were editorial board members of Frontiers, at the time of submission. This had no impact on the peer review process and the final decision.

Publisher's note

References

Ahamed, F., Ahmed, Z. F., Hossain, M., and Ohtomi, J. (2017). Growth and longevity of the mola carplet *Amblypharyngodon mola* (Cyprinidae) in the Payra River, southern Bangladesh. *Egypt. J. Aquat. Res.* 43 (4), 291–295. doi: 10.1016/j.ejar.2017.11.002

Avery, J. L., and Steeby, J. A. (2004). "Hatchery management," in *Biology and culture of channel catfish. Developments in aquaculture and fisheries science-34*. Eds. C. S. Tucker and J. S. Hargreaves (Netherlands: Elsevier B.V.), 145–165. doi: 10.1016/s0167-9309(04)80009-7

Azadi, M. A., and Mamun, A. (2004). Reproductive biology of the cyprinid, *Amblypharyngodon mola* (Hamilton) from the Kaptai Reservoir, Bangladesh. *Pak. J. Biol. Sci.* 7, 1727–1729. doi: 10.3923/pjbs.2004.1727.1729

Behera, B. K., Das, P., Singh, N. S., and Sahu, A. K. (2007). Observation on the induced breeding of *Labeo bata* (Hamilton) with Ovaprim and Ovatide as inducing agents with a note to its development. *J. Aquac.* 15, 11–17.

Belton, B. (2012). Culture, social relations and private sector development in the Thai and Vietnamese fish hatchery sectors. *Asia Pac. Viewp.* 53 (2), 133–146. doi: 10.1111/j.1467-8373.2012.01487.x

Bogard, J. R., Farook, S., Marks, G. C., Waid, J., Belton, B., Ali, M., et al. (2017). Higher fish but lower micronutrient intakes: Temporal changes in fish consumption from capture fisheries and aquaculture in Bangladesh. *PloS One* 12 (4), e0175098. doi: 10.1371/journal.pone.0175098

Bogard, J. R., Thilsted, S. H., Marks, G. C., Wahab, M., Hossain, M. A. R., Jakobsen, J., et al. (2015). Nutrient composition of important fish species in Bangladesh and potential contribution to recommended nutrient intakes. *J. Food Compos. Anal.* 42, 120–133. doi: 10.1016/j.jfca.2015.03.002

Castine, S. A., Bogard, J. R., Barman, B. K., Karim, M., Hossain, M., Kunda, M., et al. (2017). Homestead pond polyculture can improve access to nutritious small fish. *Food Secur.* 9, 785–801. doi: 10.1007/s12571-017-0699-6

Chattopadhyay, N. R. (2017). *Induced fish breeding-A practical guide for hatcheries* (UK: Elesvier and Academic Press), 351.

Das, P., Behera, B. K., Meena, D. K., Singh, S. K., Mandal, S. C., Das, S. S., et al. (2016). Comparative efficacy of different inducing agents on breeding performance of a near threatened cyprinid *Osteobrama belangeri* in captivity. *Aquac. Rep.* 4, 178–182. doi: 10.1016/j.aqrep.2016.11.001

Dey, A., Nur, R., Sarkar, D., and Barat, S. (2016). Captive breeding through synthetic hormone induced breeding of an eastern Himalayan hill stream fish, *Barilius barila* (Hamilto). *Int. J. Fish. Aquat. Stud.* 4 (5), 354–358.

Dubey, S. K., Padiyar, A. P., Shenoy, N., Gaikawd, A., Mohanty, B., Baliarsingh, B. K., et al. (2022). "Climate-smart and nutrition sensitive aquaculture in Odisha, India: a new horizon in sustainability, adaptation, and mitigation," in *Handbook on climate change and disasters*. Ed. R. Shaw (UK: Edward Elgar Publishing Limited), 574–593. doi: 10.4337/9781800371613.00054

Fiedler, J. L., Lividini, K., Drummond, E., and Thilsted, S. H. (2016). Strengthening the contribution of aquaculture to food and nutrition security: The potential of a vitamin A-rich, small fish in Bangladesh. *Aquaculture* 452, 291–303. doi: 10.1016/j.aquaculture.2015.11.004

Froese, R., and Pauly, D. (2022). *FishBase* (World Wide Web electronic publication). Available at: www.fishbase.org.

Gephart, J. A., Golden, C. D., Asche, F., Belton, B., Brugere, C., Froehlich, H. E., et al. (2020). Scenarios for global aquaculture and its role in human nutrition. *Rev. Fish. Sci. Aquac.* 29 (1), 122–138. doi: 10.1080/23308249.2020.1782342

Ghosh, A. S., Ghosh, S. K., Ghosh, M., and Ali, A. (2018). Studies on biodiversity of selected indigenous fish species, in Beels and Baors of South Bengal and their breeding potential through habitat modification. *Int. J. Fish. Aquac. Stud.* 6 (4), 479–483.

Gupta, S., and Banerjee, S. (2013). Studies on some aspects of reproductive biology of *Amblypharyngodon mola* (Hamilton-Buchana). *Int. Res. J. Biol. Sci.* 2 (2), 69–77.

Hoque, A. S. M. M., and Rahman, M. R. (2008). Reproductive ecology of mola (*Amblypharyngodon mola*). *J. Agric. Rur. Dev.* 6 (1&2), 165–174.

Horvath, L., Tamás, G., and Seagrave, C. (2002). *Carp and pond fish culture* (London, UK: Fishing News Books, Blackwell Scientific Publications Ltd).

Karim, M., Ullah, H., Castine, S., Islam, M. M., Keus, H. J., Kunda, M., et al. (2017). Carp–mola productivity and fish consumption in small-scale homestead aquaculture in Bangladesh. *Aqua. Int.* 25, 867–879. doi: 10.1007/s10499-016-0078-x

Kohinoor, A. H. M., Islam, M. S., Thilsted, S. H., and Wahab, M. A. (2005). Reproductive biology of three important indigenous small fish viz., mola (*Amblypharyngodon mola*), Chela (*Chela cachius*) and punti (*Puntius sophore*). *Iran. J. Fish. Sci.* 5 (1), 29–48.

Kumar, P., Biswas, G., Ghoshal, T. K., Kailasam, M., and Vijayan, K. K. (2018). Embryonic and larval developments of brackish water catfish, *Mystus gulio* (Hamilton and Buchana) induced with human chorionic gonadotropin and consequent larval rearing. *Aqua. Res.* 49 (7), 2466–2476. doi: 10.1111/are.13706

Kumar, P., Kailasam, M., Biswas, G., Christina, L., and Ghoshal, T. K. (2021). Effect of different inducing hormones, sex ratio and oocyte diameter on breeding performance of brackish water catfish, *Mystus gulio*. *Aquaculture* 530, 735–821. doi: 10.1016/j.aquaculture.2020.735821

Mandal, B., Kumar, R., and Jayasankar, P. (2016). Efficacy of exogenous hormone (GnRHa) for induced breeding of climbing perch *Anabas testudineus* (Bloc) and influence of operational sex ratio on spawning success. *Anim. Reprod. Sci.* 171, 114–120. doi: 10.1016/j.anireprosci.2016.06.006

Mariappan, P., Antony, C., Subramaniam, B., Nagarahalli, M., and Bhosale, M. M. (2021). Successful breeding of the endemic cyprinid fish *Dawkinsia rohani* in controlled condition—First report. *Aqua. Res.* 52 (10), 4693–4700. doi: 10.1111/are.15303

Milstein, A., Wahab, M. A., Kadir, A., Sagor, M. F. H., and Islam, M. A. (2009). Effects of intervention in the water column and/or pond bottom through species composition on polyculture of large carps and small indigenous species. *Aquaculture* 286 (3–4), 246–253. doi: 10.1016/j.aquaculture.2008.09.036

Mondal, S., Wahab, A., Barman, B. K., and Abdulla, A. A. (2020). Breeding biology of Mola carplet, (*Amblypharyngodon mola*, Hamilton 1822) in semi-natural condition. *Asian J. Anim. Sci.* 14, 111–120. doi: 10.3923/ajas.2020.111.120

Mustafa, T., Naser, N., Murshed, S., Zeba, F., Akter, M., and Ali, L. (2015). Fatty acid composition of three small indigenous fishes of Bangladesh. *Bangladesh J. Zool.* 43 (1), 85–93. doi: 10.3329/bjz.v43i1.26141

Olaniyi, W. A., and Omitogun, O. G. (2013). Stages in the early and larval development of the African catfish *Clarias gariepinus* (Teleostei, Clariidae). *Zygote* 22, 314–330. doi: 10.1017/S0967199413000063

Rahman, A. K. A. (1989). *Freshwater fishes of Bangladesh*. 1st Edn. (Bangladesh: Zoological Society of Bangladesh, Department of Zoology, University of Dhaka).

Rahman, M., Hossain, M., Tumpa, A. S., Hossain, M., Billah, M., and Ohtomi, J. (2018). Size at sexual maturity and fecundity of the mola carplet *Amblypharyngodon mola* (Hamilton 1822) (Cyprinidae) in the Ganges River, Bangladesh. *Zool. Ecol.* 28 (4), 429–436. doi: 10.1080/21658005.2018.1537906

Rajts, F., Ahmed, K. K., Khan, A. M., and Kaiya, M. K. (1997). "Pond management and controlled breeding of *Amblypharyngodon mola* - a small indigenous fish species in Bangladesh," in *Proceedings of National Workshop on small indigenous fish culture in Bangladesh* (Dhaka, Bangladesh: Integrated food assisted development project SP-2 (IFADEP SP 2), 71–79.

Rajts, F., Belton, B., and Thilsted, S. H. (2022). *Guidelines for setting up breeding experiments for small indigenous species (SIS)*. (Penang, Malaysia: WorldFish). Program Report: 2022-03.

Rajts, F. (1986). *Summaries of inspection reports of fish farms and hatcheries of Bangladesh* Technical Report, (Rome, Italy: Food and Agriculture Organization). 371 pp.

Rajts, F., and Shelley, C. C. (2020). *Mola (Amblypharyngodon mola) aquaculture in Bangladesh: Status and future needs*. (Penang, Malaysia: WorldFish). Program Report: 2020–2045.

Rath, S. C., Sarkar, S. K., Gupta, S. D., and Sarangi, N. (2007). Comparative account of induced breeding of Indian major carps with Ovaprim, Ovatide, WOVA- FH and carp pituitary extract. *Indian J. Anim. Sci.* 77 (10), 1057–1060.

Roos, N., Leth, T., Jakobsen, J., and Thilsted, S. H. (2002). High vitamin A content in some small indigenous fish species in Bangladesh: perspectives food-based strategies to reduce vitamin A deficiency. *Int. J. Food Sci. Nutr.* 53 (5), 425–437. doi: 10.1080/0963748021000044778

Roos, N., Wahab, M. A., Hossain, M. A. R., and Thilsted, S. H. (2007). Linking human nutrition and fisheries: incorporating micronutrient-dense, small indigenous fish species in carp polyculture production in Bangladesh. *Food Nutr. Bull.* 28 (2 Suppl.), S280–S293. doi: 10.1177/15648265070282S207

Saha, M. K. (2019). *Studies on morphometry, breeding and larval development of Amblypharyngodon mola (Hamilto) from different regions of Bangladesh* (Mymensingh, Bangladesh: PhD thesis, Bangladesh Agricultural University).

Saha, M. K., Eunus, A. T. M., and Barman, B. K. (2014). "Transportation of mola (*Amblypharyngodon mola*) brood fish for stocking in the homestead ponds of Northwest Bangladesh," in *Advances in fisheries research in Bangladesh*. Eds. M. A. Wahab, S. M.S., M. A. R. Hossain, B. K. Barman and M. E. Hoq (Dhaka, Bangladesh: Bangladesh Fisheries Research Forum), 97–104.

Sarkar, U. K., Deepak, P. K., Kapoor, D., Negi, R. S., Paul, S. K., and Singh, S. (2005). Captive breeding of climbing perch *Anabas testudineus* (Bloc) with Wova-FH for conservation and aquaculture. *Aqua. Res.* 36 (10), 941–945. doi: 10.1111/j.1365-2109.2005.01281.x

Talwar, P. K., and Jhingran, A. G. (1991). *Inland fishes of India and adjacent countries* (New Delhi, India: Oxford-IBH Publishing Co. Pvt. Ltd.).

Thilsted, S. H., Thorne-Lyman, A., Webb, P., Bogard, J. R., Subasinghe, R., Phillips, M. J., et al. (2016). Sustaining healthy diets: The role of capture fisheries and aquaculture for improving nutrition in the post-2015 era. *Food Pol.* 61, 126–131. doi: 10.1016/j.foodpol.2016.02.005

Toufique, K. A., and Belton, B. (2014). Is aquaculture pro-poor? Empirical evidence impacts fish consumption Bangladesh. *World Dev.* 64, 609–620. doi: 10.1016/j.worlddev.2014.06.035

Wahab, M. A., Alim, M. A., and Milstein, A. (2003). Effects of adding the small fish punti (Puntius sophore Hamilton) and/or mola (*Amblypharyngodon mola* Hamilton) to a polyculture of large carp.2003. *Aqua. Res.* 24 (2), 149–163. doi: 10.1046/j.1365-2109.2003.00784.x

WorldFish (2022). *Cracking the code of mola mass production boosts nutrition-sensitive aquaculture in India*. (Penang, Malaysia: WorldFish).

Zafri, A., and Ahmad, K. (1981). Studies on the vitamin A content of fresh water fishes: content and distribution of vitamin A in mola (*Amblypharyagodon mola*) and dhela (*Rohte cotio*). *Bangladesh J. Biol. Sci.* 10, 47–53.6

frontiers | Frontiers in Marine Science

TYPE Original Research
PUBLISHED 03 January 2024
DOI 10.3389/fmars.2023.1274136

OPEN ACCESS

EDITED BY
Tangtian He,
Hong Kong Polytechnic University,
Hong Kong SAR, China

REVIEWED BY
Fabian J. Tapia,
University of Concepcion, Chile
David Stirling,
Scottish Government, United Kingdom

*CORRESPONDENCE
Hayden Close
hayden.close@cefas.gov.uk

RECEIVED 07 August 2023
ACCEPTED 28 November 2023
PUBLISHED 03 January 2024

CITATION
Close H, Lambert G, Robins P and Gimenez L (2024) Connectivity between populations of the scallop *Pecten maximus* in the Irish Sea and the implications for fisheries management. *Front. Mar. Sci.* 10:1274136. doi: 10.3389/fmars.2023.1274136

Connectivity between populations of the scallop *Pecten maximus* in the Irish Sea and the implications for fisheries management

Hayden Close[1]*, Gwladys Lambert[1], Peter Robins[2] and Luis Gimenez[2]

[1]Centre for Environment and Aquaculture Science (Cefas), Lowestoft, United Kingdom, [2]School of Ocean Sciences, Bangor University, Bangor, United Kingdom

Marine species with a pelagic larval phase have the potential to disperse hundreds of kilometres via ocean currents, thus connecting geographically distinct populations. Connectivity between populations therefore plays a central role in population dynamics, genetic diversity and resilience to exploitation or decline and can be an important vector in the management of fisheries. The scallop, *Pecten maximus*, is a valuable benthic bivalve with a variety of management measures at both regional and national scales. A bio-physical numerical model was developed to simulate and characterise the larval transport and population connectivity of scallops across commercial fishing grounds within the Irish and Celtic Seas. The model incorporated realistic oceanographic currents and known behavioural traits of *P. maximus* larvae including spawning times, pelagic larval duration, and vertical migration during the various developmental stages i.e., passive, active swimming, vertical migrations, since growth rates change with temperature, which varies spatially and temporally, it was used in the model to determine when an individual larva changed its behaviour. Simulations showed a high degree of connectivity between most populations, with multiple connections allowing for substantial exchanges of larvae. The exception was a population off North Cornwall that was entirely reliant on self-recruitment. A sensitivity analysis of the biological parameters suggested that ocean current patterns primarily controlled the connectivity network, but the strength of the connections was sensitive to spawning date and the specific features of diel vertical migrations. The model identified weakly connected populations that could be vulnerable to overfishing, and populations that are 'strong connectors' and a vital source of larvae to maintain the metapopulation. Our approach highlights the benefits of characterising population connectivity as part of an effective management strategy for sustainable fisheries.

KEYWORDS

scallop, fisheries, management, connectivity, retention, metapopulation, larvae

1 Introduction

Many marine benthic species have a pelagic larval stage whereby ocean currents can transport the larvae within the water column up to hundreds of kilometres over a few weeks (Shanks et al., 2003). For such species, they may exists as a metapopulation with spatially separated populations but with plentiful exchange of larvae between the geographically distant populations (Caley et al., 1996). This is important for gene flow and replenishment of natural populations and those which are commercial fishing grounds that become depleted e.g., through overfishing or disease (Malakoff, 1997). Some studies have suggested that over 60% of juvenile fish with a pelagic larval stage are returning to or being retained at their natal location (Swearer et al., 1999; Jones et al., 2009) – thereby posing the question as to the importance of connectivity networks within metapopulation dynamics.

Hydrodynamic models can simulate oceanographic circulation and variability that facilitate the transport of individual larvae and the dispersal of the spawned larval cohort. This provides the means to investigate the relative roles of different physical and bio-physical interactions; for example, inter-annual variability in heat- and wind-driven currents and seasonal spawning times (Robins et al., 2013). However, many models do not take account of the numerous behavioural characteristics with 56% of biophysical models published by 2019 assuming larvae are passive throughout development (Swearer et al., 2019). Nevertheless, many species of larvae go through various development stages such as being passive, actively swimming, performing diel vertical migrations, or delaying their settlement.

Spatial variability in scallop population sizes, commercial catch rates, biological characteristics, and oceanographic conditions pose difficulties for management. For example, assessing recruitment has been overlooked as a management tool but is now being considered (Nicolle et al., 2017; Handal et al., 2020; Hold et al., 2021). As a result, there may be little relationship between the spawning population and self-recruitment, which makes it difficult to use survey data, or commercial catch and effort data, to forecast the effects of management measures such as catch limitations, minimum landing sizes and effort restrictions. Predictions of connectivity and self-recruitment can help explain the species' genetic structure, population dynamics, and aid in the management of the ecosystem or resource (Crooks and Sanjayan, 2006; Botsford et al., 2009; Nicolle et al., 2013). Species that experience population decline from disease or exploitation can eventually recover via self-recruitment and/or larval flow from connecting populations, provided the connectivity network is sufficient (Grimm et al., 2003; Gimenez, 2019). Therefore, there is a strong incentive to characterise connectivity networks for a range of ecologically sensitive and commercially important marine species (Miller, 2007).

The King scallop *Pecten maximus* is a large benthic marine bivalve found in shallow depressions in the seabed down to a depth of approximately 100 m, preferring firm sand and fine gravel substrate but occasionally found on muddy sands. *P. maximus* can typically live up to 20 years and is a hermaphrodite, releasing both spermatozoa and oocytes (Beaumont and Budd, 1983); fertilization occurs in open water leading to a planktonic larva. The pelagic larval duration (PLD) of scallop larvae depends on larval growth, which is contingent on ambient water temperature and from laboratory experiments has been shown to range between 78 days at 9°C and to 24 days at 18°C (Beaumont and Barnes, 1992). Scallop larvae develop through seven stages, from gametes to pediveliger, until they settle as post larva. Juvenile scallops continue to grow and only begin to spawn when they deposit their second annual growth ring in their shell. Spawning generally takes place in spring (April – May) and again in early autumn (end of August and September), with reports of additional spawning throughout the summer (Kaartveldt et al., 1987; Raby et al., 1994; Gallager et al., 1996; Garland et al., 2002). Scallops have been consistently one of the most highly valuable commercial species with total landings in 2020 of 57,434 tonnes of which 48,122 were from ICES area VII (Irish Sea) (ICES, 2021). The majority of the fisheries are managed under national and local legislation with no quotas or catch limits. Currently, methods used to manage the fisheries vary depending on the locality with differing minimum landing sizes, seasonal closures and regulation of fishing effort such as dredge numbers (ICES, 2021). These measures are aimed at making the fishery sustainable but are currently not based on bio-physical interactions, ecology or the wider ecosystem function. In the past, poor management of scallop fisheries has caused numerous scallop populations to undergo boom and bust cycles caused by unsustainable exploitation and variable recruitment (Shumway, 1991; Beukers-Stewart et al., 2003; Bloor et al., 2021). This has resulted in populations relying heavily on recruitment every year, which is a high risk strategy both biologically and economically (Beukers-Stewart and Beukers-Stewart, 2009).

Previous work examining connectivity networks through modelling approaches in *P. maximus* populations have focused on using a fixed PLD (Nicolle et al., 2013; Le Goff et al., 2017; Nicolle et al., 2017; Hold et al., 2021). In this study, we developed a 3-dimensional ocean model coupled to a Lagrangian particle tracking model (PTM) that used the modelled water temperatures to determine the growth rate, thus the time taken to reach each larval stage; hence providing detailed representation of the biological phenomenon in the simulation of the behavioural characteristics. We quantified the larval transport and population connectivity of scallop larvae from delineated scallop beds under a range of oceanographic conditions within the Celtic and Irish Seas region. In addition, a sensitivity analysis was conducted to validate the outcomes of the model with regards to key biological parameters such as the spawning times, larval migration strategies and settlement criteria, to identify potential yearly recruitment variability from the environmental variables.

2 Methods

We used outputs of simulated velocities for the Irish and Celtic Seas obtained from a pre-existing and validated three-dimensional ocean model, developed by Robins et al. (2013). These velocity fields were used to drive the advection and diffusion (sub-grid-scale mixing) of virtual larvae, iteratively through space and time,

within a Lagrangian particle tracking model (PTM). The spatial domain of both models is shown in Figure 1.

2.1 Oceanographic model

The 3D Princeton Ocean Model is described in detail by Blumberg and Mellor (1987) and the Celtic/Irish Sea setup used for this study is detailed by Robins et al. (2013). In summary, the model is based upon a parallelised and sigma-coordinate (terrain-following vertical layers) representation of the primitive equations that describe the conservation of momentum, thermal energy and continuity. Variables within the model (e.g. velocity, elevation, turbulence and temperature) are solved using finite-difference discretisation on an orthogonal Arakawa-C grid in the horizontal plane, which provides an accurate representation of the velocity around complex coastlines such as within the Irish Sea, due to the staggered computation of elevation and velocity nodes.

The model domain is 280 km by 708 km, with a horizontal cell size of 1/30° (longitude) by 1/60° (latitude) resulting in a resolution of approximately 2 × 2 km. In the vertical plane, there are 20 equally segmented sigma layers, with an average and maximum distance between the surface layer and the next layer of 4.3 and 9.6 m respectively, these distances change spatially following the underwater terrain (Robins et al., 2013). Accurate simulations of the long-term circulation are a major challenge to ocean modellers and confidence in the predictions of the model can only be achieved through extensive validation of a range of variables (Robins et al., 2013). The year 1990 was chosen for validation based upon it being a mean representation of the long term (1989-1998) climate (Neill

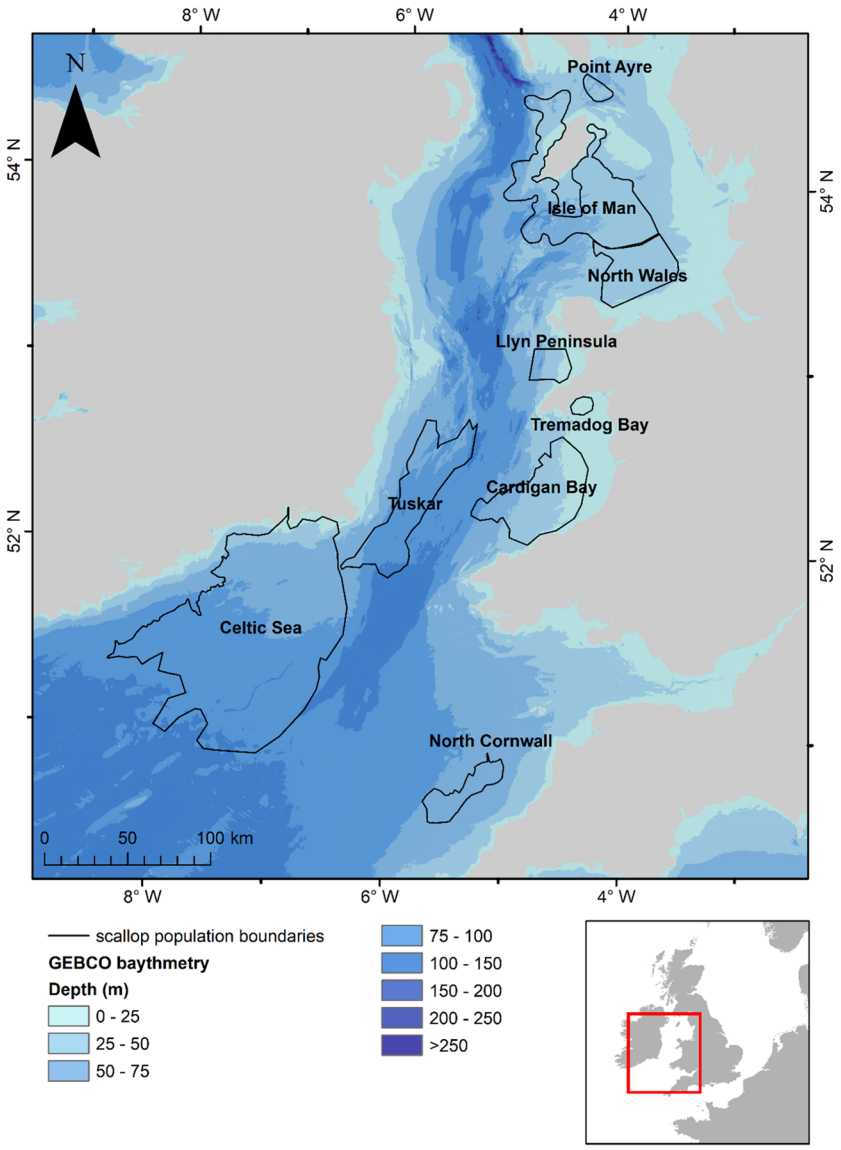

FIGURE 1
Map of the study area showing the identified scallop populations (ICES, 2021) that are modelled within the study along with sea surface temperatures for the 1st of September for 1990 predicted by the oceanographic model.

10.3389/fmars.2023.1274136

et al., 2010) and availability of temperature records to evaluate the models ability to simulate stratification that can be important for larval transport.

The simulation consisted of a six-month, three-dimensional, barotropic (tide-driven and wind-driven circulation) and baroclinic (density-driven circulation caused by surface solar heating) simulation for the period 1st April – 30th September 1990. The model was forced at the open ocean boundaries of the domain with six tidal constituents including the dominant lunar and solar cycles (Robins et al., 2013). These two constituents were validated by comparing the simulated amplitudes and phases of the lunar and solar elevations with records from 18 coastal stations with records of known values (Robins et al., 2013). Both baroclinic and barotropic components of circulation have the potential to play an important role in larval transport and as a result, the main oceanographic factors that transport larvae are the residual currents and tidal velocities. Oceanographic conditions such as, stratification, gyres, tidal range and depth-averaged residual currents for the period 1st April – 30th September 1990 are presented in Robins et al. (2013). Wind effects also contribute to the residuals, although due to the stochasticity of the wind over several weeks these are small compared to baroclinic components and are confined to the surface layer.

The ocean model simulated temperature change within the domain. The temperature data was outputted every two days; therefore, the temperature was interpolated between the two nearest recordings to the particle tracking model time step. The oceanographic model was run, and the outputs saved every 30 minutes to be used 'offline'; this meant that the model only had to be run once and allowed the computing time of the subsequent PTM to be drastically reduced.

2.2 Particle tracking model

A Langragian 3D PTM was developed in MATLAB to simulate the individual movement of particles spatially and temporally. These are based on advection (movement by simulated 3D currents from the ocean model), sub-grid-scale turbulent mixing, and the individual particle vertical migration parameterised on scallop behaviour. Turbulent mixing was simulated in the hydrodynamic model grid scale (i.e., >2 km). However, sub-2 km scale turbulence exists in reality and, so, was parameterised within the PTM (Robins et al., 2013). This was based upon random displacement models (random walks). For the random displacement, the longitudinal change in position ($\Delta\chi$, Equation 1a), the latitudinal change in position (Δy, Equation 1b) and the depth change (Δz, Equation 1c) over each time step (every save) of the hydrodynamic model of 1800 seconds (Δt, 30 minutes) can be expressed as:

$$\Delta x = \frac{R}{r} cos(2\pi R)(2Kx\Delta t)^{1/2} \quad (1a)$$

$$\Delta y = \frac{R}{r} sin(2\pi R)(2Ky\Delta t)^{1/2} \quad (1b)$$

$$\Delta z = K'_Z \Delta t + \frac{R}{r}(2K_Z\Delta t)^{1/2} \quad (1c)$$

Where R is a random number in the range of 0 – 1 and r is the standard deviation of $R\ cos(2\pi R)$. The horizontal diffusivities Kx and Ky ($m^2\ s^{-1}$) were set to $(u/100)^2$ and $(v/100)^2$, respectively.

Simulated larvae were released from locations that are known to have substantial populations of scallops identified from fishing data and stock assessment surveys (ICES, 2021); these were the waters surrounding the Isle of Man, a small population to the northeast of the Isle of Man (hereafter, referred to as Point of Ayre), North Wales, Llyn Peninsula, Tremadog Bay, Cardigan Bay, Tuskar, Celtic Sea and North Cornwall (Figure 1).

Within the model the initial egg size for each larva was randomly assigned within the range 64.2 to 72.2 µm with a mean of 68.8 µm, source: Iroise Sea, France, (Cochard and Devauchelle, 1993; Paulet et al., 1995) to allow for variability among individuals.

The PLD, identified from controlled laboratory experiments for *P. maximus* larvae from fertilisation to metamorphosis, can last 24 – 78 days depending on sea temperatures (Comely, 1972; Gruffydd and Beaumont, 1972; Beaumont and Barnes, 1992; Robert and Gérard, 1999). PLD is determined by temperature-dependent growth rates, with faster growth in warmer waters. However, within the domain where land meets the sea, and particularly in small embayment's, the temperature was overpredicted by the model, reaching in excess of 25°C. As a result, where the temperature exceeded 17°C, the maximum attainable temperature in the domain was limited to 17°C within the PTM as identified by the National Oceanography Centre (2022). The average sea surface temperature and bottom temperature is 8°C on the 1st April 1990 and is 15°C and 13.75°C on the 30th September respectively (Robins et al., 2013). To

TABLE 1 Mean growth rates between 9 – 18°C taken from **Beaumont and Barnes (1992)** who assumed growth was linear.

Temperature (°C)	Mean Growth Rate (mm d^{-1})	Temperature Range (°C)	Growth Rate Range (mm d^{-1})
9	1.61	9.5	1.36 – 1.86
10*	2.11*	[9.5 - 10.5]	1.86 – 2.36
11*	2.61*	[10.5 - 11.5]	2.36 – 2.87
12	3.13	[11.5 - 12.5]	2.87 – 3.29
13*	3.44*	[12.5 - 13.5]	3.29 – 3.60
14*	3.75*	[13.5 - 14.5]	3.60– 3.91
15	4.07	[14.5 - 15.5]	3.91 – 4.26
16*	4.45*	[15.5 - 16.5]	4.26 – 4.64
17*	4.83*	[16.5 - 17.5]	4.64 – 5.02
18	5.21	[17.5 – 18.5]	5.02 – 5.40

The growth rate range was calculated by using the mean value and difference between the upper and lower range. *indicates where interpolated values between actual values were used as no was data available. Note, no value for the temperature below 9°C or above 18°C so it was assumed the range was same for the temperatures either above or below.

simulate growth rates throughout the PLD, a novel approach was coded using growth rates (Table 1), taken from Beaumont and Barnes (1992), at a given temperature and combining it with known sizes of each development stages at 16°C to estimate the size of the larvae at each stage within the larval development (Table 2). This was important as the different larval stages (with different sizes) have a different behaviour in the water. Natural variability is expected in growth rates of individuals or from local food availability (Cochard and Gerard, 1987). Therefore, a random element was introduced to the growth rates (Equation 2a) as they were determined from laboratory studies and fed a stable diet. The larval length was calculated by adding the growth rate per iteration to the starting egg size (Equation 2b); this was calculated using the following equations:

$$\text{Growth Rate} = L + \frac{(R \star Ra)\Delta t}{(ts)} \quad (2a)$$

$$\text{Larval length} = \text{Previous length} + \text{Growth Rate} \quad (2b)$$

Where L is the lowest growth rate for a given temperature (Table 1), R is a random number in the range of 0 – 1 and Ra is the difference of the growth rate (Table 1) of the two temperature points either side of the given temperature and ts is the number of seconds in a 24 hour period (86400). The growth was assumed to be linear (Beaumont and Barnes, 1992).

In the model the larvae were grouped into five behavioural classes (Table 2) used to capture the development of behaviours in scallop larvae through their ontogeny. Vertical swimming behaviour was introduced into the model when the larvae became trochophores (77 µm) at a rate between 0.5 – 1.0 mm s^{-1} towards the surface (Cragg, 1980). Once the trochophores developed into veligers (82 µm), the swimming speed was assigned within the range of 1.0 – 1.5 mm s^{-1}. Diel vertical migrations (DVMs) were introduced at the same time, sinking during the day and rising to the surface during the night. The depth below the surface of the DVMs that the scallop migrate to was limited to 10 m, as identified by Kaartveldt et al. (1987); Tremblay and Sinclair (1990) and Raby et al. (1994). Once the larvae became eyed veligers (184 µm) they begin to sink and stay just above the substrate. Many authors have described that sinking rates are quicker than swimming rates, but the former have not been quantified (Cragg, 1980; Gallager et al., 1996; Garland et al., 2002). Therefore, it was assumed that sinking rates were the same as the swimming rates for the PTM. All swimming rates were randomly assigned a value within the ranges described (Table 2).

Estimates of the length at which larvae settle is described as between 225 – 258 µm (Gruffydd and Beaumont, 1972; Cochard and Devauchelle, 1993; Andersen et al., 2011). For the PTM the mean value of 241 µm was used as a settlement length threshold. Within the model the particles only settled when they entered the population area polygons delineated in Figure 1. It has been found that the scallop larvae can delay their settlement typically by two weeks (Robert and Gérard, 1999; Robert and Nicholas, 2000); therefore, particles >241 µm were allowed 14 days to disperse to one of the defined populations. If they encountered a population boundary within this time, then they settled and if they had not entered a boundary after the 14 extra days then the larvae were deemed unsuccessful.

TABLE 2 The size of larvae stages within their development.

Larval Stage/s	Size of Larva (µm)	References	Behaviour	References
1. Egg - Trochophore	64 - 76	Paulet et al. (1988) Cochard and Devauchelle (1993)	Close to substrate, unable to swim	Paulet et al. (1988) Cragg and Crisp, (1991) Comely, (1972)
2. Trochophore - Veliger	77 - 81	Comely, (1972) Gruffydd and Beaumont (1972) Comely, (1972) Robert and Gérard (1999)	Upwards swimming in range of 0.5 – 1 mm s^{-1}	Cragg (1980)
3. Veliger – Eyed Veliger	82 - 183	Beaumont and Budd (1983) Comely, (1972)	Vertical diel migrations with a swimming speed in the range of 1 – 1.5 mm s^{-1}	Kaartveldt et al. (1987); Tremblay and Sinclair (1990); Cragg (1980); Gallager et al. (1996)
4. Eyed Veliger - Pediveliger	184 - 214	Gruffydd and Beaumont (1972) Comely, (1972)	Downwards swimming in range of 1 – 1.5 mm s^{-1}	Comely, (1972)
5. Pediveliger - Settlement	215 - 240	Gruffydd and Beaumont (1972); Cragg (1980) Comely, (1972)	Downwards swimming in range of 1 – 1.5 mm s^{-1}	Comely, (1972)
6. Settlement	> 241	Cochard and Devauchelle (1993)	All movement stopped	

The size of the larva was estimated from a mean egg size of 68.2 µm with a mean growth rate of 4.45 µm d^{-1} at 16°C. Subsequently using the time taken from the literature on scallop development to reach each stage, the size of the larvae at each stage was predicted.

2.3 Boundary limits

The particles have the potential to leave the model domain at open sea boundaries in the southwest in the Celtic Sea and in the northwest where the Irish Sea meets the North Atlantic (Figure 1). As a result, larvae which encountered the domain boundaries were excluded from the analysis, this was limited to those released from the Celtic Sea and totalled 6.88% of particles released from this site. Larvae that reached a vertical boundary (sea surface or bed), were reflected back into the water column at their position on the previous iteration step. Similarly, larvae that encountered the coastline were reflected back to their previous position within the water column. This allowed for the maximum larval transport potential of each larval cohort to be investigated, following similar methods employed by North et al. (2006) and Robins et al. (2013).

2.4 Simulations

A minimum of 10,000 particles were released from each site, as Robins et al. (2013) identified that this was sufficient to satisfactorily simulate larval transport in this region (i.e. the transport pattern remains similar for larger numbers of particles). The larvae were randomly assigned to starting positions within the coordinates of each delineated population (Figure 1). Simulations were run for each site with all particles released on 1st April 1990 at once at 12:00, based on a spring spawning of *P. maximus* (Baird, 1966). At the end of each simulation the percentage of larvae settling within the natal population boundary (retention), settling within a different population boundary (connectivity) and those which did not settle with one of the delineated boundaries (unsuccessful) were calculated. A sensitivity analysis on the date of release and the biological parameters was also undertaken on Cardigan Bay, see Section 2.6.

2.5 Model description

Overall, the simulation of velocity and temperature fields from the oceanographic model were in good agreement with observational records and other models developed for this region (Xing and Davies, 2001; Horsburgh and Hill, 2003; Hartnett et al., 2007). A tidal analysis conducted by Robins et al. (2013) showed that the simulated circulation compared well with 18 coastal tide gauge stations, giving root-mean square errors of approximately 14 cm (M2) and 6 cm (S2) in elevation and 10° and 12° in phase. Comparisons of the simulated seasonal mean SST with satellite data (National Oceanography Centre 2022), showed that vertically mixed regions were 1-2°C cooler in the model than the satellite data. Despite this the Irish Sea front to the east of the Isle of Man and the Celtic Sea front across the St George's Channel were well simulated. It is important that these are accurately simulated within the model as they can act as barriers to larvae (Vera et al., 2022). In addition, the simulated temperatures compared well with observed monthly mean surface and bottom temperatures at Port Erin, Isle of Man (see Robins et al., 2013).

The depth profile of an individual particle parameterised on *P. maximus* larva, released from Cardigan Bay on the 1st of April 1990 (Figure 2), illustrates the simulated vertical swimming behaviour at different stages of the pelagic life, with migrations from the seabed to the surface once the larva developed into a trochophore after a PLD of 7 days (Figure 2, stage 2); exhibited DVM to 10 m when they became eyed-veligers at day 10 (Figure 2, stage 3) and at day 62 the pediveliger sank to the seafloor to just above the seabed (Figure 2, stage 4). The larvae are supposed to be next to the seabed surface, however, small differences of up to 10 m were seen for the larvae, most likely caused by the vertical velocities exceeding the directional swimming ability of the larvae, although the larvae only remained above the seabed for a short time. Despite their position above the

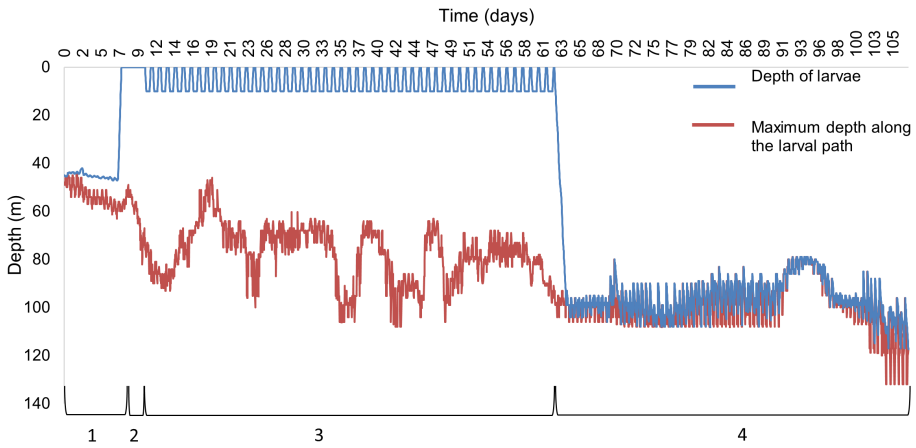

FIGURE 2
A depth profile of an individual *P. maximus* larva released from Cardigan Bay on 1st April 1990 showing the different swimming behaviours, (1) No swimming capacity, (2) swimming to the surface waters, (3) diel vertical migrations to 10 m, (4) swimming just above the seabed. The blue line indicates the vertical path of the larva and the red line indicates the maximum depth profile from the larval path.

seabed, the larvae were assumed to have settled, a common approach in larval modelling (Hartnett et al., 2007; Nicolle et al., 2013).

2.6 Sensitivity analysis

2.6.1 Sensitivity analysis on the biological parameters

A sensitivity analysis was conducted by varying the particle tracking model parameters for the Cardigan Bay population. The spawning times of adults are not clearly established on when larvae are released withing a tidal cycle (Mason, 1958; Comely, 1972; Bonardelli et al., 1996; Paugam et al., 2003); therefore, simulations were run with particles released on the 1st and 14th of every month from April to July to investigate the effect of the changing oceanographic parameters on a regular interval. All other simulations within Cardigan Bay were restricted to releases on 1st April. To test the sensitivity of the outputs to the growth rates, the values were restricted to the mean value identified by Beaumont and Barnes (1992), the mean ±1 and ±2 μm to allow for greater variability (Table 3). Scallop larvae have shown DVMs have generally only been observed in shallow depths (<15 m below surface) for scallop larvae from laboratory experiments (Kaartveldt et al., 1987; Raby et al., 1994; Gallager et al., 1996; Garland et al., 2002); therefore, to test the sensitivity of the model to the migration strategy, no migrations and migrations to a maximum of 5, 15, 20 and 25 m depth were modelled. As the settlement size can also vary, simulations on the settlement size were conducted using the minimum (225 μm) and maximum size defined (258 μm) (Gruffydd and Beaumont, 1972; Cochard and Devauchelle, 1993; Andersen et al., 2011). Larvae have been observed to delay their settlement by 2 – 3 weeks (Robert and Gérard, 1999; Robert and Nicholas, 2000) and it has been observed that bivalves can extend this by up to one month (Robert and Nicholas, 2000; Nicolas and Robert, 2001); therefore, this settlement delay was modelled using, 1 day, 1 week, 3 weeks, and 4 weeks.

Random numbers were incorporated into the model to randomise the particle starting positions, starting egg size, distances and angles of the horizontal turbulent movement (Equations 1a, 1b), growth rates (Equation 2a), and swimming speeds. A different random number was used for each application based on the same seed. To test sensitivity to the random numbers used, the experiments were repeated three times with different random numbers.

TABLE 3 Mean growth rates entered into the PTM for the temperatures between 9 and 18°C with growth rate range when ± 1 and ± 2 (μm d^{-1}).

Temperature (°C)	Mean (μm d^{-1})	Range (μm d^{-1})	
		± 1	± 2
9	1.61	0.61 – 2.61	0 – 3.61
10*	2.11	1.11 – 3.11	0.11 – 4.11
11*	2.61	1.61 – 3.61	0.61 – 4.61
12	3.13	2.13 – 4.13	1.13 – 5.13
13*	3.44	2.44 – 4.44	1.44 – 5.44
14*	3.75	2.75 – 4.75	1.75 – 5.75
15	4.07	3.07 – 5.07	2.07 – 6.07
16*	4.45	3.45 – 5.45	2.45 – 6.45
17*	4.83	3.83 – 5.83	2.83 – 6.83
18	5.21	4.21 – 6.21	3.21 – 7.21

2.6.2 Statistical analysis

The average effect of each biological factor on PLD and larval transport distance was determined using a General Linear Model (GLM) in R (R Core Team, 2022). This followed recommendations by White et al. (2014) that ecologists should focus on 'biological significance' such as effect sizes, since applying significance testing is not appropriate for modelling simulation outputs (Giménez et al., 2020). To determine which factors were the main drivers, the residuals from each simulation were compared for the PLD and population-averaged larval transport distance.

3 Results

3.1 Larval transport and settlement success

The mean PLD for all sites for the model was 95 days with the North Cornwall and the Llyn peninsula populations having the longest mean PLD at 109 and 107 days, respectively (Figure 3A). The smallest mean PLD was 83 days for North Wales. All sites except the Celtic Sea and Cornwall had larvae with PLDs across the range rather than aggregated around the mean. This is due to the larvae within the same location encountering areas of varying thermal properties that controls the growth rate. The mean larval transport distance of all sites combined (total distance travelled) was 2192 km with the longest mean transport distance of 3590 km for the Llyn Peninsula and the shortest for the Celtic Sea population, which is subject to low tidal velocities, at 1071 km (Figure 3B). In contrast, the pelagic larval distance for most of the populations tended to aggregate around the mean, with only a small number occasionally having a distance that was markedly different. However, larvae from within Cardigan Bay, Isle of Man and Tremadog Bay were subjected to varying tidal velocities such as strong tides around Anglesey, transporting them to the middle of the Irish Sea towards the Isle of Man. Interestingly, no relationship was observed between the PLD and distance travelled (Figure 3).

The regression analysis of connectivity and retention against the population-averaged larval transport distance, for all simulations conducted (n = 41), suggests that the shorter the distance travelled the greater number of larvae that are retained (Figure 4A, $r^2 = 0.30$). Conversely, no relationship between distance and connectivity was found (Figure 4B, $r^2 < 0.01$).

3.2 Larval connectivity and retention

The mean larval settlement success (connectivity and retention) from all populations was 41.3%; retention and total connectivity between populations accounted for 20.3% and 21.0%, respectively,

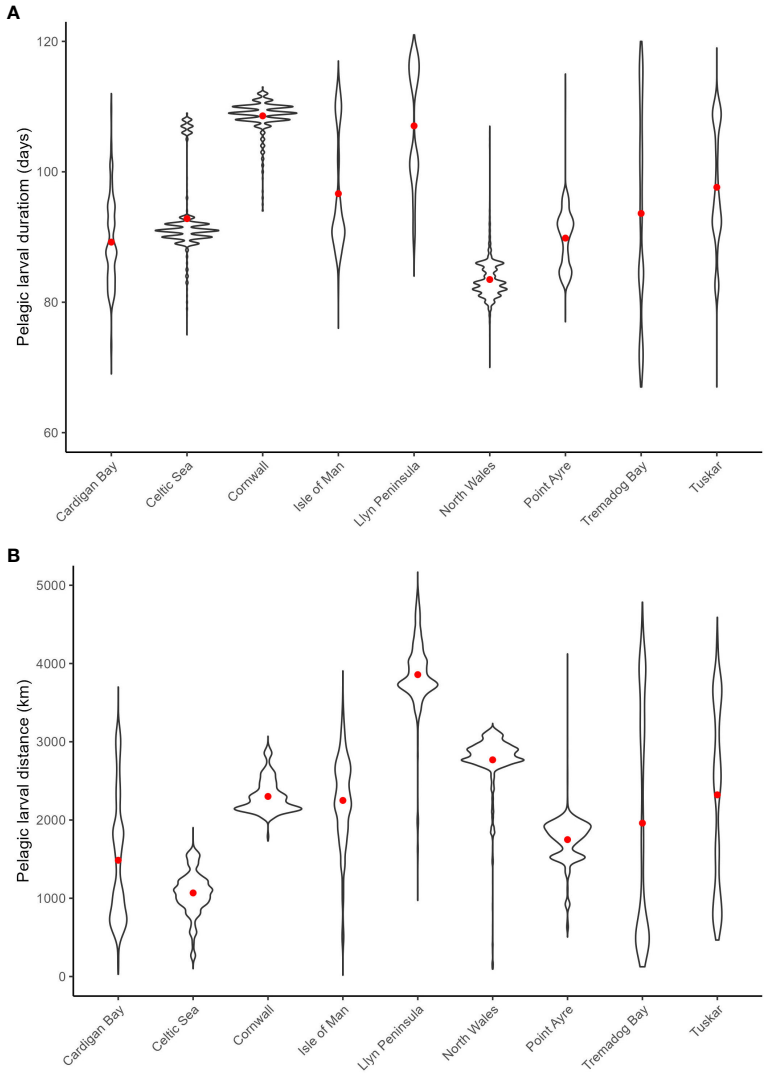

FIGURE 3
Violin plots for the pelagic larval duration **(A)** and larval transport distances (km) **(B)** with red dots denoting the mean values from spawning on the 1st April 1990 from all sites.

with connectivity occurring primarily between neighbouring populations. Hence, on average, 58.7% of larvae did not find a successful settlement site as delineated in this study. North Wales had the greatest larval settlement success of 89.1%, this was due to retention and primarily connecting to the adjacent Isle of Man population (Figure 5). Conversely, a high number of unsuccessful larvae were found from Point Ayre (99.5%) and North Cornwall populations (98.0%) (Figure 5). Greatest retention was found within the Celtic Sea and Isle of Man populations at 69.5% and 67.11%, respectively, whilst the least retention was found at in the Point Ayre and the Llyn Peninsula populations at < 0.1% and 0.9%, respectively (Figure 5). The number of populations that were connected varied; the Tremadog Bay population was the largest source of larvae, exporting to five different sites, whilst the Isle of Man population was the greatest sink for larvae with a total of four different sources (Figure 5). The Celtic Sea and North Cornwall populations did not connect to any other sites, but larvae had the potential to be retained (Figure 6). North Cornwall had a low retention of larvae (2.1%) and no external sources of larvae. Despite this, observations from Figure 6 demonstrate that North Cornwall had the potential for self-recruitment as most larvae were in close proximity to their release locations.

3.3 Sensitivity analysis on the biological parameters

The biological parameters included in the model explained 51% of variance in the PLD and 29% of the average larval transport distance from analysis on Cardigan Bay, with the remainder of the variation in these two metrics attributed to oceanographic conditions (Table 4). The release date contributed to 15% of the variation with a decrease in the PLD from 88.8 days when spawning was delayed from the 1st of April to 67.1 days for the 1st of June, due to increasing temperatures through the spring and summer. The exception from this trend was the simulation for the 1st of July

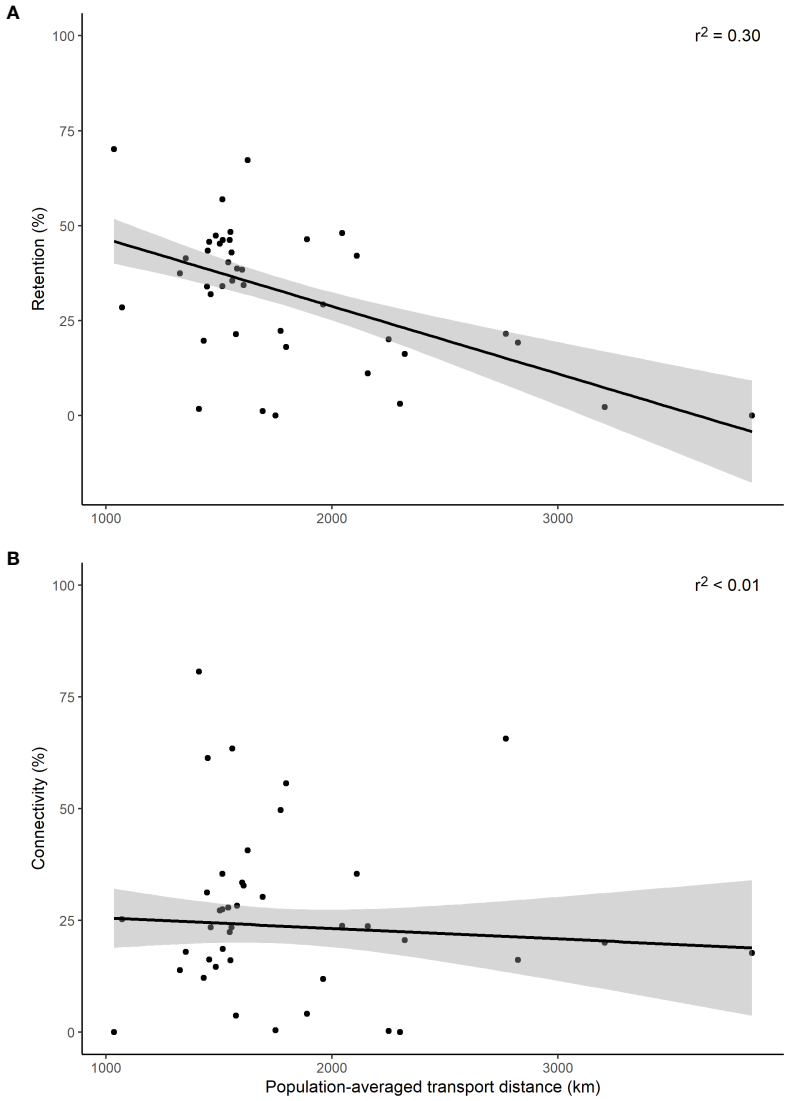

FIGURE 4
Retention **(A)** and connectivity **(B)** for the population-averaged larval transport distances (km). Black lines denote linear regression fit with the shaded area representing the 95% confidence intervals.

which had a slightly longer PLD (Figure 7). The population-averaged transport distances increased from 1072 km in April to 2158 km in July with the exception of 1st of April and the 14th of June 1990 (Figure 8). The change in the spawning date only contributed to 4% of the total variance within the model (Table 4).

The proportion of larvae being retained larvae stayed broadly the same until June (Figure 9A) for each release date. This is due to larvae being transported away from the Cardigan Bay coast towards the Irish coastline driven by a thermal front that develops across the middle of Cardigan Bay. The total proportion of larvae connecting to other populations, primarily Tuskar, the Celtic Sea and to a lesser extent Tremadog Bay, also tended to be broadly the same at between 20 and 30% except for the larvae released on the 14th of June (Figure 9A) which had 80% of the larvae connecting to other populations and 2% of larvae being retained in Cardigan Bay. In most instances where larvae were transported away from Cardigan Bay, no suitable settlement site was found. The change in the spawning date did not appear to drastically change distribution of the larvae, the larvae tended to stay within the area between south Wales and Ireland. The only exception to this occurred in the July simulation when large numbers of larvae were transported north towards the centre of the Irish Sea, with relatively few larvae traveling west towards the Tuskar site and then moving southwest towards the Celtic Sea site, along the thermal front as modelled in previous months leading up to July (see Supplementary Material for detailed distribution maps).

Of the variance presented in the larval transport distances, 22% can be explained by the DVM, which only explained 8% of the variance in the PLD (Table 4). When no migrations occur and migrations up to 5 m occurred, most larvae travelled north to their final destination. When the DVM was 10 m or greater, the larval transport distance was much lower (Figure 9B) and they generally

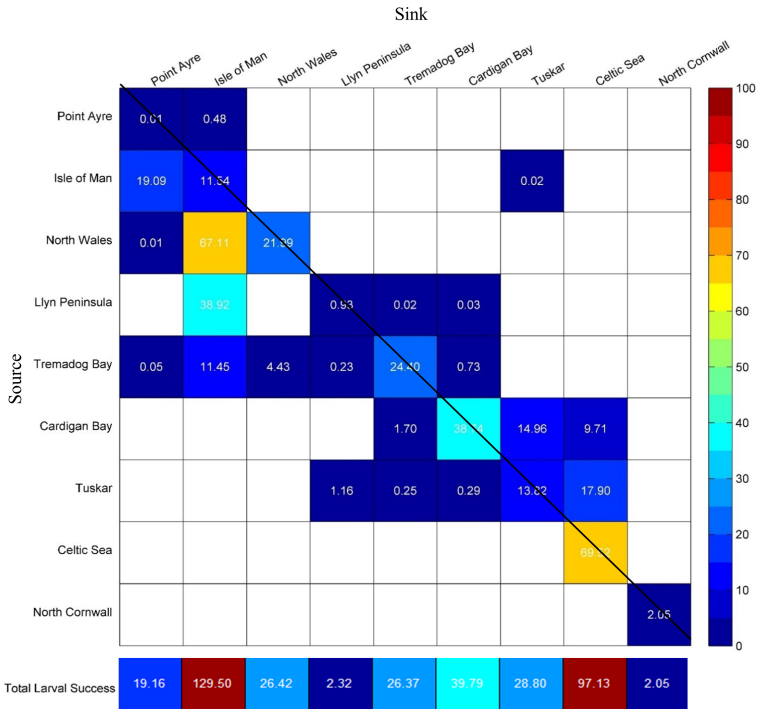

FIGURE 5
Connectivity matrix between larvae from a source (row) and sink (column). The colour scale represents the percentage (%) of larvae that are retained or connect to other populations; white cells indicate no connectivity. Retention within the same site is indicated by cells that cross the diagonal line. The total larval success indicating the retention and the larvae received from other populations (connectivity plus retention) for each site is shown below the matrix.

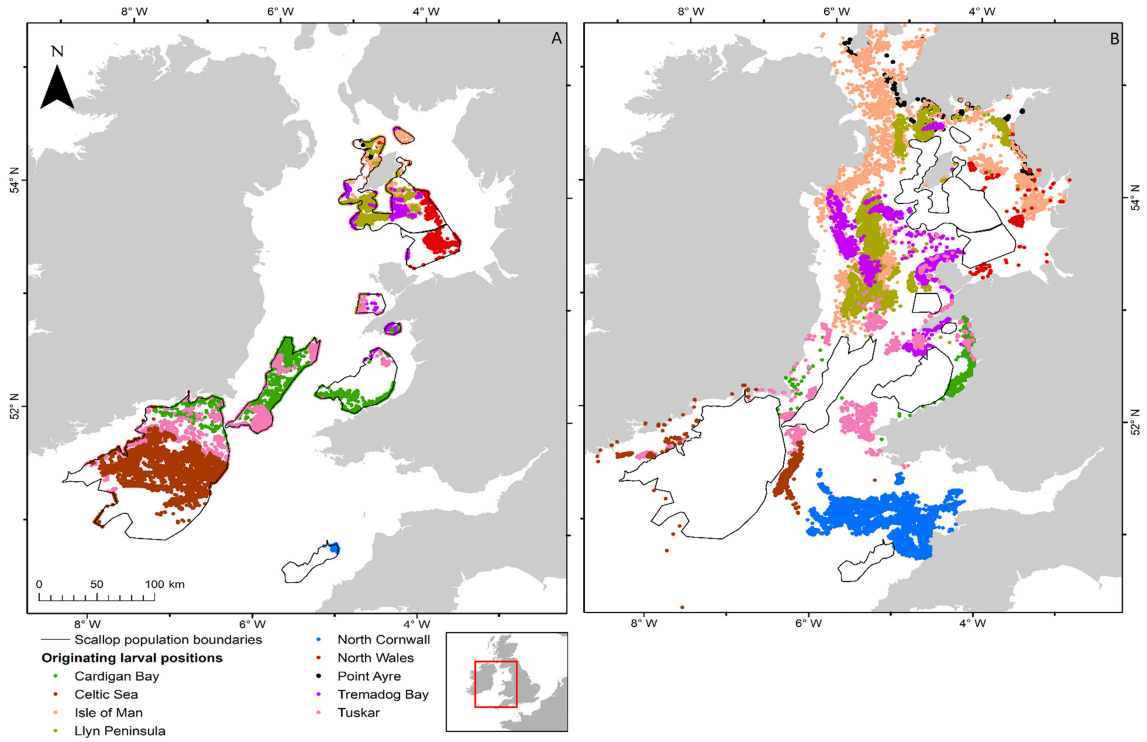

FIGURE 6
Distribution of larvae from spawning on the 1st April 1990 for *P. maximus* for all 9 populations within the Irish and Celtic Seas. **(A)** shows successful larvae and **(B)** shows unsuccessful larvae, the colour represents the site of release. The distribution of the larvae within the population is not representative of the distribution as larvae that are able to settle will do so at the edges of the sites, unless they are already within it.

10.3389/fmars.2023.1274136

TABLE 4 Contribution (%) of each variable to the total variance determined from a general linear model.

Variable	Contribution to the total variance (%)	
	PLD	Larval transport distance
Overall	51	29
Spawning date	15	4
Diel vertical migrations	8	23
Growth rate	<1	1
Settlement size	3	<1
Settlement delay	2	<1

travelled towards the west and southwest along the Irish coast. Connectivity also increased with the depth of the DVM from 20% with no DVM to over 50% for DVMs to 20 and 25 m (Figure 9B).

Changes to larval size at settlement and changes to the time spawning could be delayed by, explained very little variance in the model for PLD (3% and 2% respectively) and larval transport distance (both <1%). Despite limited influence upon the PLD and transport distance, the retention of larvae increased when the delay period was extended but decreased when the size of settlement increased (Figure 9D). Conversely, the connectivity increased slightly with increasing settlement size (Figure 9E). The variation in growth rate had little effect contributing to <1% of the variance with little change in percentage of the retention and connectivity of the larvae (Figure 9C).

3.4 Sensitivity analysis on the use of random numbers within the model

A random number was used within the model to simulate the natural variation in the environment. Observations from changing the random numbers in the parameters found differences in the distributions. Random numbers were used in assigning the individual larvae a starting position within a site, a starting egg size, the growth rate per iteration, the random walk and the swimming speed. However, the random number component explained <1% of the variance within the GLM.

4 Discussion

Our results are based on mesoscale (2-10 km) and interannual-mean perspectives of the Celtic and Irish Seas circulation. The simulated velocities from the ocean model were generally in good agreement with other similar scale models developed for this region (Xing and Davies, 2001; Horsburgh and Hill, 2003; Hartnett et al., 2007; Hold et al., 2021). We incorporated the general seasonal development of the hydrodynamics with some realistic natural variability; however, several dispersive processes have not been fully characterised, such as circulation patterns associated with different synoptic storm tracks (Bricheno et al., 2023) and fine-scale coastal circulation associated with

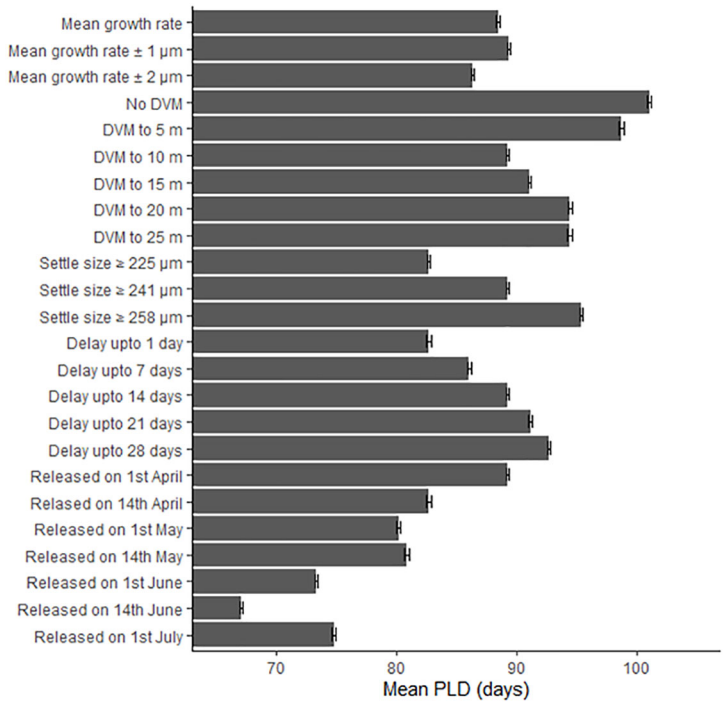

FIGURE 7
The effect of changing the growth rate, depth of the diel vertical migration (DVM), size at settlement, delay period and release date upon the pelagic larval duration (PLD) in days. Error bars represent the 95% confidence intervals.

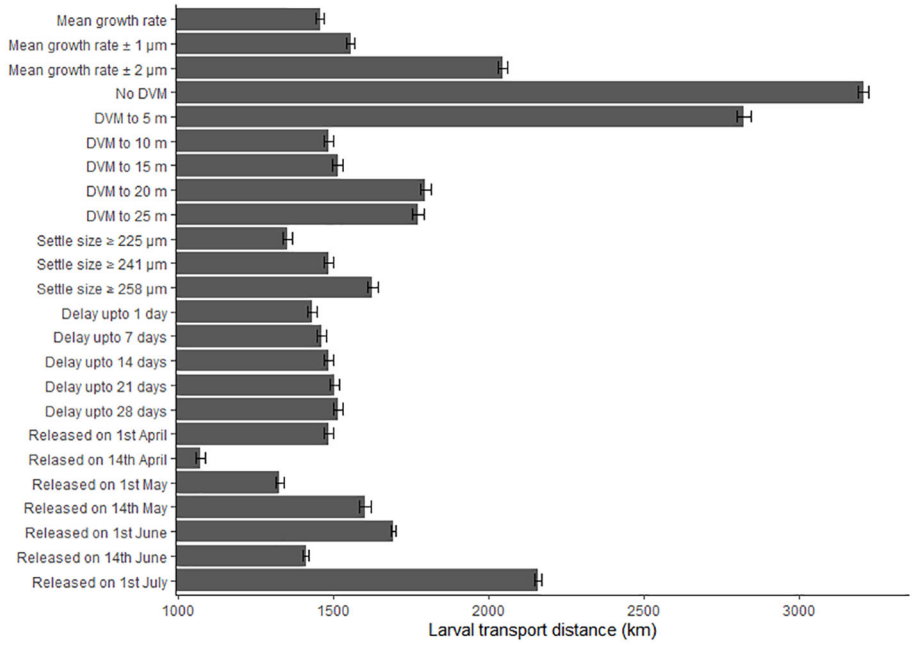

FIGURE 8
The effect of changing the growth rate, depth of the diel vertical migration (DVM), size at settlement, delay period and release date upon the larval transport distances (km). Error bars represent the 95% confidence intervals.

undulating topography (Ward et al., 2023) or estuaries (Robins et al., 2012). Extreme weather events may produce a connectivity network markedly different to the norm and could be an important vector in genetic structure over long-term cycles (Corte et al., 2018). Coastal and estuarine circulation will be an important driver of intertidal species such as mussels but arguably less important for scallops that inhabit deeper waters. However, simulations where large amounts of scallop larvae interacted with the coastline, such as larvae released from the Point Ayre population, may require a hydrodynamic model with a resolution higher than the 2 km used here for coastal modelling or unstructured grids which would allow high grid resolutions around the coast where it is needed, with coarser grids in more open water (Ward et al., 2023).

Many aspects of the behaviour and ecology of scallop larvae and juveniles are unknown and most investigations have been conducted in hatcheries under artificial conditions, which may have little relevance to the natural environment (Tian et al., 2009). In addition, some parameters are not well studied and/or have conflicting information available, for instance diel vertical migrations (Kaartveldt et al., 1987; Raby et al., 1994; Garland et al., 2002). The sensitivity analysis showed that, even if we varied the larval migration behaviour, similar connectivity networks prevailed as seen from similar results from modelling of scallop larvae by Hartnett et al. (2007) and Hold et al. (2020). However, the proportions of larvae that connected or were retained varied, which is key to understanding a population's resilience to fishing pressure. This variability in strength of connectivity was primarily caused by the larval length at settlement, DVM, and the potential to delay settlement, and should be investigated further in more detail.

The study was novel in that the modelled temperature, which varied spatially and temporally, was used to influence the larval growth rate; many previous studies used a fixed PLD to determine the connectivity of populations (Hartnett et al., 2007; Tian et al., 2009). However, an analysis by Nicolle et al. (2013) found that a 1°C change in temperature resulted in an error of 4 days for a pelagic larval duration (PLD) of 34 days. The PLD estimated during this study (mean 95 days) were greater than those determined from *in vitro* studies of 78 days at 9°C decreasing to 24 days at 18°C (Beaumont and Barnes, 1992). There was a degree of uncertainty regarding the modelled temperature particularly in coastal regions, such as the Bristol Channel and small inlets and bays, reaching in excess of 25°C in the summer within the model. Additionally, the model produced areas of cooler waters (11°C in September) found around Anglesey, North Wales and the Southwest coast of England, when sea surface temperature in these regions is typically 14 – 15°C (National Oceanography Centre, 2022) although September offshore temperatures have been shown to be below 12°C (Hartnett et al., 2007). Incongruity between the PLDs is likely due to variation in starting size of the larvae and the settlement size. However, the sensitivity analysis of the delay period revealed interesting results in that after seven days the retention of larvae did not increase, not even after 21 days were given to allow the larvae to find a suitable settlement site. This suggests that all larvae that could have been retained were retained. However, overestimation of the connectivity could be caused by an increased PLD by delaying the settlement up to 28 days. Further research is needed to clarify the starting and settling size along with the maximum length of time *P. maximus* larvae can delay their

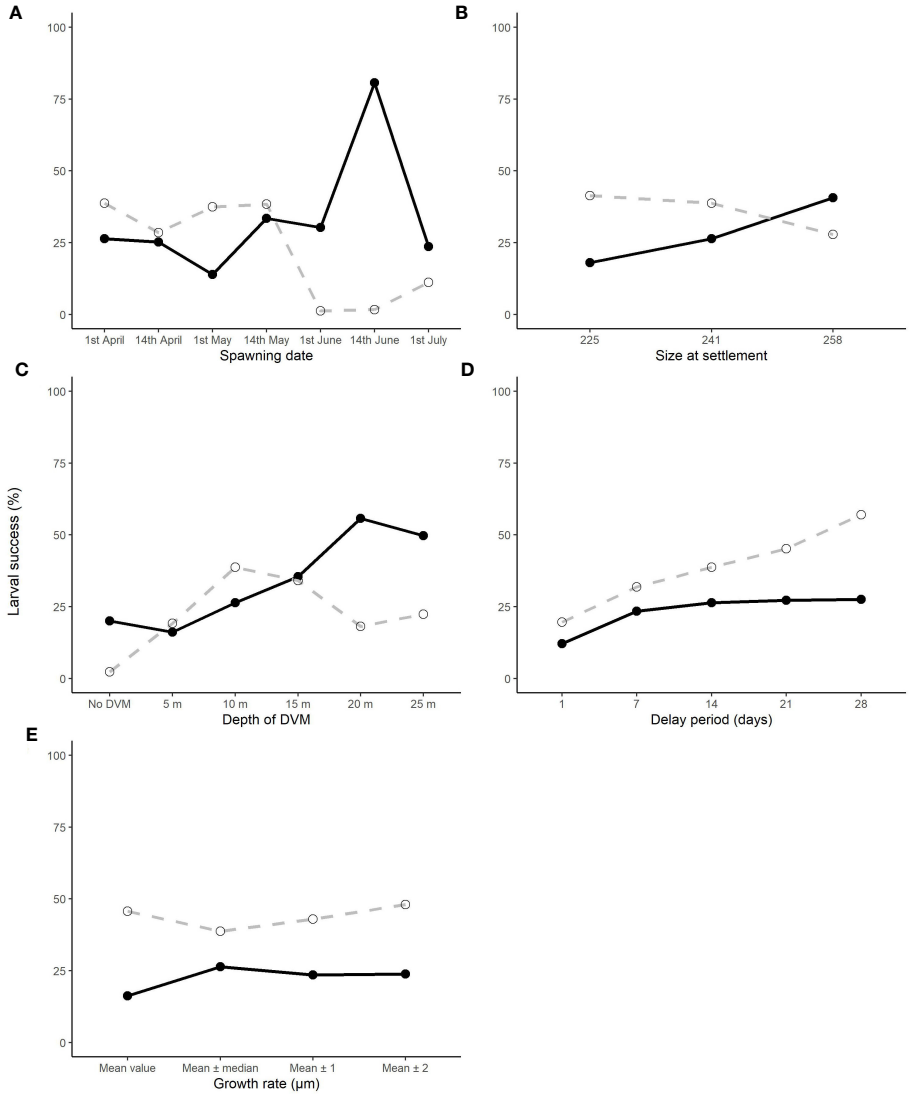

FIGURE 9
The effect of changing the spawning date **(A)**, depth of the diel vertical migration (DVM) **(B)**, growth rate **(C)**, delay period **(D)** and size at settlement **(E)** upon the larval success rate of those which connect (dashed line) and those that are retained (black line) in their natal population.

settlement, as this would prevent overestimation of the connectivity between populations.

Additionally, it was expected that the shorter the PLD, the smaller the distance the larvae would travel. However, the larval transport distance increased with the change of release date when growth rates would be larger and thus cause shorter PLD. This increase in distance was caused by mesoscale density-driven (baroclinic) flows that develop in stratified regions where surface heating had led to increased stratification along oceanographic fronts where well-mixed waters meet. During spring and summer months, these residual baroclinic currents are enhanced by the thermal fronts that contribute significantly to the circulation of the Irish Seas. Therefore, greater distances were covered despite a decrease of over 10 days in the PLD.

Spawning for *P. maximus* is thought to occur bi-annually; once in spring (April – May) and once in autumn (September) (Mason, 1958; Minchin, 1985). However, spawning has been reported throughout the year (Gruffydd and Beaumont, 1972). The simulations revealed that, as the spawning date was moved later in the year (April through to September), the PLD decreased due to warming seas and faster growth, but the larval transport distance increased. The increase in distance was caused by mesoscale density-driven (baroclinic) flows that develop in stratified regions where surface heating had led to increased stratification along oceanographic fronts where well-mixed waters meet. During spring and summer months, these residual baroclinic currents are enhanced by the thermal fronts that contribute significantly to the circulation of the Irish Seas. Therefore, greater distances were covered despite a decrease of over 10 days in the PLD. This is countering the expected reduced larval transport distance from the shorter PLD, as predicted in Gallager et al. (1996) and Duarte (2007). Additionally, the regression analysis of connectivity and retention against the population-averaged transport distance, for all simulations conducted, suggests that the shorter the distance

travelled the greater number of larvae that are retained. Conversely, no relationship between distance and connectivity was found. The results imply that retention may be increased for larvae developing in low energy environments such as the area around the Celtic Sea population. By contrast, decreased retention is expected in high-energy environments such as around Anglesey and the Llyn Peninsula where strong tidal (up to 3 m/s) and residual (up to 0.1 m/s) currents are found (Horrillo-Caraballo et al., 2021). Our simulations provide insights into larval transport from the early spawning in April/May, and for the potential of trickle spawning throughout the summer. Further studies could simulate the autumnal spawning, which may provide insightful results as the larvae become affected by the breakdown of the tidal mixing fronts and possibly increased storm activity.

The depth of the DVM has also been the subject of much discussion, with authors reporting shallow migrations between 5 – 15 m for *P. maximus* and *Placopecten magellanicus* (Kaartveldt et al., 1987; Tremblay and Sinclair, 1990; Raby et al., 1994; Gallager et al., 1996). When no migration occurred the larval transport distances were large and connectivity low, with retention particularly low, resulting in high proportions of larval wastage – a pattern that has been simulated in other models (Gilbert et al., 2010). Vertical migrations up to 5 m caused a 20% rise in the retention of larvae, demonstrating that the movement out of the immediate surface of the water can cause significant differences in the transport of larvae with DVMs after 20 m having a limited effect. This was because larvae may get entrained into different currents depending on the depth of the DVM and suggests that DVMs to 5 m or less are influenced by surface forcing rather than ocean currents. The retention of larvae when no DVM was used was 2% with surface forcing having a large role in the retention of larvae, particularly in the early stages when no migration behaviour has developed. Within the model, a fixed depth of the DVM was used but different stimuli such as light intensity (Kaartveldt et al., 1987), salinity discontinuation (Raby et al., 1994), increased pressure (Cragg, 1980) and stratification (Scrope-Howe and Jones, 1986; Tremblay and Sinclair, 1990; Raby et al., 1994) have been observed to modify the diel vertical migrations exhibited by veligers swimming behaviour. Therefore, local conditions might cause different depths of the DVM, thus causing differences in the temporal and spatial transport of the larvae.

Random elements introduced into the model to create variation such as small sub-scale turbulence (random walks), predator avoidance (swimming speed), food scarcity (growth rate) and release location had a minimal influence on the variance on the model. It may be that these small-scale effects do not have a large effect at the scale of the model but should be considered with higher resolution models.

4.1 Implications for management

Currently, scallop stocks are managed individually (ICES, 2021) with direct management in territorial waters (12 nautical miles) by regional bodies, and nationally for offshore waters within each country's exclusive economic zone. The retention and connectivity from this study are magnitudes higher than expectations as no mortality was introduced into the model. However, the general dispersal patterns suggest that there is a single metapopulation within the Celtic and Irish Seas, except for North Cornwall which was reliant on self-recruiting. However, other scallop modelling had identified metapopulations within the English Channel and along the French coast, not within the scope of this study, which have the potential to act as a source for North Cornwall and the Celtic Sea populations (Le Goff et al., 2017; Nicolle et al., 2017). The four populations between the west coast of Wales and Ireland (Llyn Peninsula, Tremadog Bay, Cardigan Bay and Tuskar) appeared to be key to the metapopulation, with a large interchange of larvae which is consistent with other larval models for the region (Hartnett et al., 2007; Coscia et al., 2013). In particular, the exchange of larvae between these three central populations (Cardigan Bay, Tuskar and Tremadog Bay) suggests that they may be resilient to over-fishing as external sources of larvae may be able to replenish the populations (Grimm et al., 2003). Additionally, they also provide larvae for each other and for populations in the south (the Celtic Sea) and north (Isle of Man, North Wales and Point Ayre). The northern area of the Celtic Sea population is reliant on the import of larvae and to maintain the population abundance, the Tuskar and Cardigan Bay populations will need strong management if they are to provide a continual source of larvae. In addition, the central populations appear to be a vital source of larvae for the Llyn Peninsula population which has a low retention rate (0.9%), which acts as a steppingstone connecting the central populations to the northerly populations; but modelling by Hartnett et al. (2007) found retention may occur in this region. The North Wales population is also a crucial population, appearing to be reliant on self-recruitment with low external recruitment of larvae but a large percentage of its larvae connected to the Isle of Man population, an important fishing ground (ICES, 2021). It should also be noted that not all scallop populations were simulated or represented in the model, with populations identified from extensive fishing pressure with defined boundaries used (ICES, 2021). Other populations of scallops are known to occur in waters surrounding Northern Ireland (AFBI, 2012), Scotland (Dobby et al., 2012) and France (Nicolle et al., 2013) with international cooperation needed to provide accurate data. Additionally, populations exist on smaller scales such as within Skomer Marine Nature Reserve, but the area of these populations could not be defined or were too small in scale to be accurately modelled.

The study does not consider that in the natural environment larvae may not settle and recruit into the established populations or the consideration of mortality; it only reflects the probability for a larva to complete its larval lifespan and find a settlement substrate in the defined populations. To simulate the larval transport and define the patterns of dispersal a year with average conditions was chosen. To achieve realistic predictions for a given year for management measures, validated hydrodynamic models should be used. Particularly as scallops take approximately two years from fertilisation to become reproductively active adults (Devauchelle and Mingant, 1991). Therefore, the fishery can benefit if accurate oceanographic models for this period can be created annually to predict patterns of recruitment. This could provide information about when recruitment may be high or low, which could be

proven by a coordinated stock assessment that would yield observed densities and distributions that would substantially improve the modelling. The implementation combined with microchemistry or genetic methods, could help validate patterns from mathematical models, particularly from external sources (Nicolle et al., 2013; Hold et al., 2021). For instance, in 1985 large numbers of larvae of *P. maximus* were trapped in an area with unsuitable settlement substrate by a whirlpool located in St. Brieuc Bay, France, which was caused by strong winds blowing in the opposite direction of the tidal currents. The poor recruitment of individuals from the larvae in 1985 was confirmed by a noticeable decline in the catch of adults three years later (Le Pennec et al., 2003). Therefore, understanding and predicting the larval transport can significantly improve fisheries management and conservation aims and objectives. Current management of scallops is conducted as though they are small unrelated stocks, but the results open up the possibility for the management of the fishery to be internationally integrated, so that the metapopulation can be maintained and to ensure resilience by recruitment from external sources.

4.2 Conclusion

The modelling conducted as part of this study provides the most detailed simulations of the connectivity of the well-known established *P. maximus* populations describing a large interconnected metapopulation in the Irish and Celtic Seas. The larval transport patterns, and hence connectivity networks, appeared to be driven by the hydrodynamics, but the proportion of larvae that were retained or dispersed to other populations appeared to be driven by the biological parameters. In particular, the sensitivity analysis demonstrated seasonal variability in spawning and the DVM may play an important role in the transport to geographically distinct areas. The PLD was overestimated in this study due to uncertainty in the starting larval size and final settlement size, and thus needs to be investigated further. However, a delay in settlement (longer PLD) had little effect on retention but suggest that modelled PLD that are longer than those that occur would overestimate the connectivity to other populations.

This study and others published in recent years (Tian et al., 2009; Nicolle et al., 2017; Hold et al., 2021) demonstrate that the current model of managing the fisheries is unsuitable, with populations reliant on retention and in some cases reliant on external recruitment. A strong effort should be made internationally to manage scallops based on their sensitivity to fishing pressure with key source populations given robust management measures.

Data availability statement

The raw data supporting the conclusions of this article will be made available by the authors, without undue reservation.

Author contributions

HC: Conceptualization, Formal analysis, Investigation, Methodology, Writing – original draft, Writing – review & editing. GL: Conceptualization, Methodology, Supervision, Writing – review & editing. PR: Methodology, Software, Supervision, Writing – review & editing. LG: Conceptualization, Formal analysis, Supervision, Writing – review & editing.

Funding

The author(s) declare financial support was received for the research, authorship, and/or publication of this article. This research was funded by the Bluefish Project (Grant Agreement No. 80991, part-funded by the European Regional Development Fund (ERDF) through the Ireland Wales Co-operation Programme), the European Fisheries Fund, and the European Maritime Fisheries Fund (Fisher-Scientist Project, 81920). The publication costs were funded by Cefas.

Acknowledgments

To Authors thank Tiago Silva for reviewing the manuscript and for the reviewers for their feedback and Cefas for supporting the write-up and funding the publication.

Conflict of interest

The authors declare that the research was conducted in the absence of any commercial or financial relationships that could be construed as a potential conflict of interest.

Publisher's note

Supplementary material

The Supplementary Material for this article can be found online at: https://www.frontiersin.org/articles/10.3389/fmars.2023.1274136/full#supplementary-material

References

AFBI (2012). *Dredge Fisheries in Northern Ireland* (Belfast).Sustainable Development Strategy for Northern Ireland's Inshore Fisheries (afbini.gov.uk).

Andersen, S., Christophersen, G., and Magnesen, T. (2011). Spat production of the great scallop (*Pecten maximus*): A roller coaster. *Can. J. Zoology* 89 (7), 579–598. doi: 10.1139/z11-035

Baird, R. H. (1966). Notes on an escallop (*Pecten maximus*) population in Holyhead harbour. *J. Mar. Biol. Assoc. United Kingdom* 46 (1), 33–47. doi: 10.1017/S0025315400017537

Beaumont, A. R., and Barnes, D. A. (1992). Aspects of veliger larval growth and byssus drifting of the spat of *Pecten maximus* and *Aequipecten (Chlamys) opercularis*. *ICES J. Mar. Sci.* 49 (4), 417–423. doi: 10.1093/icesjms/49.4.417

Beaumont, A. R., and Budd, M. D. (1983). Effects of self-fertilisation and other factors on the early development of the scallop *Pecten maximus*. *Mar. Biol.* 76, 285–289. doi: 10.1007/BF00393030

Beukers-Stewart, B. D., and Beukers-Stewart, J. S. (2009). *Principles for the management of inshore scallop fisheries around the United Kingdom* (York: University of York).

Beukers-Stewart, B. D., Mosley, M. W. J., and Brand, A. R. (2003). Population dynamics and predictions in the Isle of Man fishery for the great scallop *(Pecten maximus*, L.). *ICES J. Mar. Sci.* 60 (2), 224–242. doi: 10.1016/S1054-3139(03)00005-5

Bloor, I. S. M., Duncan, P. F., Dignan, S. P., Emmerson, J., Beard, D., Gell, F. R., et al. (2021). Boom not bust: Cooperative management as a mechanism for improving the commercial efficiency and environmental outcomes of regional scallop fisheries. *Mar. Policy* 132, 1–10. doi: 10.1016/j.marpol.2021.104649

Blumberg, A. F., and Mellor, G. L. (1987). "A description of a three-dimension coastal ocean circulation model," in *Three-dimensional coastal ocean models* (Washington DC: Coastal and Estuarine Sciences, American Geophysical Union), 1–16.

Bonardelli, J. C., Himmelman, J. H., and Drinkwater, K. (1996). Relation of spawning of the giant scallop, *Placopecten magellanicus*, to temperature fluctuations during downwelling events. *Mar. Biol.* 124, 637–649. doi: 10.1007/BF00351045

Botsford, L. W., Brumbaugh, D. R., Grimes, C., Kellner, J. B., Largier, J., O'Farrell, M.R., et al. (2009). Connectivity, sustainability, and yield: Bridging the gap between conventional fisheries management and marine protected areas. *Rev. Fish Biol. Fisheries* 19, 69–95. doi: 10.1007/s11160-008-9092-z

Bricheno, L., Amies, J. D., Chowdhury, P., Woolf, D., and Timmermans, B. (2023). Climate change impacts on storms and waves relevant to the UK and Ireland. *Mar. Climate Change Impacts Partnership Sci. Rev*, 1-22. doi: 10.14465/2023.reu09.str

Caley, M. J., Carr, M., Hixon, M., Hughes, T., Jones, G., and Menge, B. A.. (1996). Recruitment and the local dynamics of open marine populations. *Annu. Rev. Ecol. systematics* 27, 477–500. doi: 10.2307/4511867

Cochard, J. C., and Devauchelle, N. (1993). Spawning, fecundity and larval survival and growth in relation to controlled conditioning in native and transplanted populations of *Pecten maximus* (L.): evidence for the existence of separate stocks. *J. Exp. Mar. Biol. Ecol.* 169 (1), 41–56. doi: 10.1016/0022-0981(93)90042-M

Cochard, J.-C., and Gerard, A. (1987). "Artificial production of scallops spat *Pecten maximus* (L.): Analysis of factors affecting larval growth," in *Act Sixth International Pectinid Workshop*, Menai Bridge. 9–14.

Comely, C. A. (1972). Larval culture of the scallop *Pecten maximus* (L). *ICES J. Mar. Sci.* 34 (3), 365–378. doi: 10.1093/icesjms/34.3.365

Corte, G. N., Gonçalves-Souza, T., Checon, H. H., Siegle, E., Coleman, R. A., and Amaral, A. C.Z.. (2018). When time affects space: Dispersal ability and extreme weather events determine metacommunity organization in marine sediments. *Mar. Environ. Res.* 136, 139–152. doi: 10.1016/j.marenvres.2018.02.009

Coscia, I., Robins, P., Porter, J., Malham, S., and Ironside, J. (2013). Modelled larval dispersal and measured gene flow: Seascape genetics of the common cockle Cerastoderma edule in the southern Irish Sea. *Conserv. Genet.* 14 (2), 451–466. doi: 10.1007/s10592-012-0404-4

Cragg, S. M. (1980). Swimming behaviour of the larvae of *Pecten maximus* (L.) (Bivalvia). *J. Mar. Biol. Assoc. United Kingdom* 60 (3), 551–564. doi: 10.1017/S002531540004025X

Cragg, S. M., and Crisp, D. J. (1991). The biology of scallop larvae. *Biology Ecol. Aquaculture Scallops*, S. E. Shumway, Ed., Amsterdam: Elsevier, 75–132.

Crooks, K. R., and Sanjayan, M. A. (2006). *Connectivity conservation* (Cambridge: Cambridge University Press).

Devauchelle, N., and Mingant, C. (1991). Review of the reproductive physiology of the scallop, Pecten maximus , applicable to intensive aquaculture. *Aquat. Living Resour.* 4 (1), 41–51. doi: 10.1051/alr:1991004

Dobby, H., Millar, S., Blackadder, L., Turriff, J., and McLay, A. (2012). Scottish scallop stocks: Results of 2011 stock assessments. *Scottish Marine and Freshwater Science* 3 (10), 1-162.

Duarte, C. M. (2007). Marine ecology warms up to theory. *Trends Ecol. Evol.* 22 (7), 331–333. doi: 10.1016/j.tree.2007.04.001

Gallager, S. M., Manuel, J. L., Manning, D. A., and O'Dor, R. (1996). Ontogenetic changes in the vertical distribution of giant scallop larvae, *Placopecten magellanicus*, in 9-m deep mesocosms as a function of light, food, and temperature stratification. *Mar. Biol.* 124, 679–692. doi: 10.1007/bf00351049

Garland, E. D., Zimmer, C. A., and Lentz, S. J. (2002). Larval distributions in inner-shelf waters: The roles of wind-driven cross-shelf currents and diel vertical migrations. *Limnology Oceanography* 47 (3), 803–817. doi: 10.4319/lo.2002.47.3.0803

Gilbert, C. S., Gentleman, W. C., Johnson, C., DiBacco, C., Pringle, J., and Chen, C. (2010). Modelling dispersal of sea scallop (Placopecten magellanicus) larvae on Georges Bank: The influence of depth-distribution, planktonic duration and spawning seasonality. *Prog. Oceanography* 87 (1–4), 37-48. doi: 10.1016/j.pocean.2010.09.021

Gimenez, L. (2019). Incorporating the geometry of dispersal and migration to understand spatial patterns of species distributions. *Ecography* 42, 643–657. doi: 10.1111/ecog.03493

Giménez, L., Robins, P., and Jenkins, S. R. (2020). Role of trait combinations, habitat matrix, and network topology in metapopulation recovery from regional extinction. *Limnology Oceanography* 65 (4), 775–789. doi: 10.1002/lno.11347

Grimm, V., Reise, K., and Strasser, M. (2003). "Marine metapopulations: A useful concept?," in *Helgoland Marine Research* 56, 222–228. doi: 10.1007/s10152-002-0121-3

Gruffydd, L. D., and Beaumont, A. R. (1972). A method for rearing *Pecten maximus* larvae in the laboratory. *Mar. Biol.* 15 (4), 350–355. doi: 10.1007/BF00401395

Handal, W., Szostek, C., Hold, N., Andrello, M., Thiébaut, E., Ewan, H., et al. (2020). New insights on the population genetic structure of the great scallop (*Pecten maximus*) in the English Channel, coupling microsatellite data and demogenetic simulations. *Aquat. Conservation: Mar. Freshw. Ecosyst.* 30 (10), 1841–1853. doi: 10.1002/aqc.3316

Hartnett, M., Berry, A., Tully, O., and Dabrowski, T. (2007). Investigations into the transport and pathways of scallop larvae - The use of numerical models for managing fish stocks. *J. Environ. Monit.* 9 (5), 403–441. doi: 10.1039/b617035h

Hold, N., Robins, P., Szotek, C., Lambert, G., Lincoln, H., and Le Vay, L. (2021). Using biophysical modelling and population genetics for conservation and management of an exploited species, *Pecten maximus* L. *Fisheries Oceanography* 30 (6), 740–756. doi: 10.1111/fog.12556

Horrillo-Caraballo, J. M., Yin, Y., Fairley, I., Karunarathna, H., Masters, I., and Reeve, D. E. (2021). A comprehensive study of the tides around the Welsh coastal waters. *Estuarine Coast. Shelf Sci.* 254, 107326. doi: 10.1016/j.ecss.2021.107326

Horsburgh, K. J., and Hill, A. E. (2003). A three-dimensional model of density-driven circulation in the Irish Sea. *J. Phys. Oceanography* 33 (2), 343–365. doi: 10.1175/1520-0485(2003)033<0343:ATDMOD>2.0.CO;2

ICES (2021). The Scallop Assessment Working Group Report (WGSCALLOP). *ICES Scientific Reports* 3 (114), 106. doi: 10.17895/ices.pub.9561

Jones, G. P., Almany, G. R., Russ, G. R., Sale, P. F., Steneck, R. S., vanOppen, M. J.H., et al. (2009). Larval retention and connectivity among populations of corals and reef fishes: History, advances and challenges. *Coral Reefs* 28, 307–325. doi: 10.1007/s00338-009-0469-9

Kaartveldt, S., Aksnes, D. L., and Egge, J. K. (1987). Effect of light on the vertical distribution of *Pecten maximus* larvae. *Mar. Ecol. Prog. Ser.* 40, 195–197. doi: 10.3354/meps040195

Le Goff, C., Lavaud, R., Cugier, P., Jean, F., Flye-Sainte-Marie, J., Foucher, E., et al. (2017). A coupled biophysical model for the distribution of the great scallop Pecten maximus in the English Channel. *J. Mar. Syst.* 167, 55–67. doi: 10.1016/j.jmarsys.2016.10.013

Le Pennec, M., Paugam, A., and Le Pennec, G. (2003). The pelagic life of the pectinid *Pecten maximus* - A review. *ICES J. Mar. Sci.* 60, 211–233. doi: 10.1016/S1054-3139(02)00270-9

Malakoff, D. (1997). Extinction on the high seas. *Science* 277, 486–488. doi: 10.1126/science.277.5325.486

Mason, J. (1958). The breeding of the scallop, *Pecten maximus* (L.), in manx waters. *J. Mar. Biol. Assoc. United Kingdom* 37 (3), 653–671. doi: 10.1017/S0025315400005701

Miller, T. J. (2007). Contribution of individual-based coupled physical-biological models to understanding recruitment in marine fish populations. *Mar. Ecol. Prog. Ser.* 347, 127–138. doi: 10.3354/meps06973

Minchin, D. (1985). "Possible effects of an intense algal bloom of Gyrodinium aurelolum on a year class of scallops (*Pecten maximus*)," in *Fifth international Pectinid Workshop*(La Coruna, Spain).

National Oceanography Centre (2022). Available at: https://noc.ac.uk (Accessed June 20, 2022).

Neill, S. P., Scourse, J. D., and Uehara, K. (2010). Evolution of bed shear stress distribution over the northwest European shelf seas during the last 12,000 years. *Ocean Dynamics* 60, 1139–1156. doi: 10.1007/s10236-010-0313-3

Nicolas, L., and Robert, R. (2001). The effect of food supply on metamorphosis and post-larval development in hatchery-reared *Pecten maximus*. *Aquaculture* 192 (2–4), 347–359. doi: 10.1016/S0044-8486(00)00462-2

Nicolle, A., Dumas, F., Foveau, A., Foucher, E., and Thiébaut, E. (2013). Modelling larval dispersal of the king scallop (*Pecten maximus*) in the English Channel: Examples

from the bay of Saint-Brieuc and the bay of Seine. *Ocean Dynamics* 63, 661–678. doi: 10.1007/s10236-013-0617-1

Nicolle, A., Moitié, R., Ogor, J., Dumas Foveau, F. A., Foucher, A., and Thiébaut, E. (2017). Modelling larval dispersal of *Pecten maximus* in the English Channel: A tool for the spatial management of the stocks. *ICES J. Mar. Sci.* 74 (6), 1812-1825. doi: 10.1093/icesjms/fsw207

North, E. W., Hood, R. R., Chao, S. Y., and Sanford, L. P. (2006). Using a random displacement model to simulate turbulent particle motion in a baroclinic frontal zone: A new implementation scheme and model performance tests. *J. Mar. Syst.* 60 (3–4), 365–380. doi: 10.1016/j.jmarsys.2005.08.003

Paugam, A., Le Pennec, M., Marhic, A., and André-Fontaine, G. (2003). Immunological in *situ* determination of *Pecten maximus* larvae and their temporal distribution. *J. Mar. Biol. Assoc. United Kingdom* 83 (5), 1083–1093. doi: 10.1017/S0025315403008300h

Paulet, Y., Bekhadra, F., Devauchelle, N., Donval, N., and Dorange, G. (1995). Cycles saisonniers, reproduction et qualite des ovocytes chez Pecten maximus en rade de Brest. Programme rade : 3è rencontres scientifiques internationales: actes de colloque. *Brest les 14 - 15 16 mars 1995 au Quartz*. 2 (15), 1–13. Available at: https://archimer.ifremer.fr/doc/00044/15495/.

Paulet, Y. M., Lucas, A., and Gerard, A. (1988). Reproduction and larval development in two Pecten maximus (L.) populations from Brittany. *J. Exp. Mar. Biol. Ecol.* 119 (2), 145–156. doi: 10.1016/0022-0981(88)90229-8

Raby, D., Lagadeuc, Y., Dodson, J. J., and Mingelier, M. (1994). Relationship between feeding and vertical distribution of bivalve larvae in stratified and mixed waters. *Mar. Ecol. Prog. Ser.* 103, 275–284. doi: 10.3354/meps103275

R Core Team (2022). *R: A language and environment for statistical computing* (Vienna, Austria: R Foundation for Statistical Computing). Available at: https://www.r-project.org/.

Robert, R., and Gérard, A. (1999). Bivalve hatchery technology: The current situation for the Pacific oyster *Crassostrea gigas* and the scallop *Pecten maximus* in France. *Aquat. Living Resour.* 12 (2), 121–130. doi: 10.1016/S0990-7440(99)80021-7

Robert, R., and Nicholas, L. (2000). The effect of seawater flow and temperature on metamorphosis and post larval development in great scallop. *Aquaculture Int.* 8, 513–530. doi: 10.1023/A:1009274707986

Robins, P. E., Neill, S. P., Giménez, L., Jenkins., , , S. R., and Malham, S. (2013). Physical and biological controls on larval dispersal and connectivity in a highly energetic shelf sea. *Limnology Oceanography* 58 (2), 505–524. doi: 10.4319/lo.2013.58.2.0505

Robins, P. E., Neill, S. P., and Giménez, L. (2012). A numerical study of marine larval dispersal in the presence of an axial convergent front. *Estuarine Coast. Shelf Sci.* 100, 172–185. doi: 10.1016/j.ecss.2012.02.001

Scrope-Howe, S., and Jones, D. A. (1986). The vertical distribution of zooplankton in the western Irish Sea. *Estuarine Coast. Shelf Sci.* 22 (6), 785–802. doi: 10.1016/0272-7714(86)90099-5

Shanks, A. L., Grantham, B. A., and Carr, M. H. (2003). Propagule dispersal distance and the size and spacing of marine reserves. *Ecol. Appl.* 13 (1), 159–169. doi: 10.1890/1051-0761(2003)013[0159:pddats]2.0.co;2

Shumway, S. (1991). *Scallops: Biology, Ecology and Aquaculture*. Ed. S. Shumway (Amsterdam: Elsevier).

Swearer, S. E., Caselle, J. E., Lea, D. W., and Warner, R. R. (1999). Larval retention and recruitment in an island population of a coral-reef fish. *Nature* 402, 799–802. doi: 10.1038/45533

Swearer, S. E., Treml, E. A., and Shima, J. S. (2019). 'A review of biophysical models of marine larval dispersal'. *Oceanography Mar. Biol*, 1-32. doi: 10.1201/9780429026379-7

Tian, R. C., Chen, C., Stokesbury, K. D.E., Rothschild, B. J., Cowles, G. W., Xu, Q., et al. (2009). Modeling the connectivity between sea scallop populations in the Middle Atlantic Bight and over Georges Bank. *Mar. Ecol. Prog. Ser.* 380, 147–160. doi: 10.3354/meps07916

Tremblay, M., and Sinclair, M. (1990). Diel vertical migration of sea scallop larvae *Placopecten magellanicus* in a shallow embayment. *Mar. Ecol. Prog. Ser.* 67, 19–25. doi: 10.3354/meps067019

Vera, M., Maroso, F., Wilmes, S. B., Hermida, M., Blanco, A., Fernández, C., et al. (2022). Genomic survey of edible cockle (*Cerastoderma edule*) in the Northeast Atlantic: A baseline for sustainable management of its wild resources. *Evolutionary Appl.* 15 (2), 262–285. doi: 10.1111/eva.13340

Ward, S. L., Robins, P. E., Owen, A., Demmer, J., and Jenkins, S. R. (2023). The importance of resolving nearshore currents in coastal dispersal models. *Ocean Model.* 183, 102181. doi: 10.1016/j.ocemod.2023.102181

White, J. W., Rassweiler, A., Samhouri, J. F., Stier, A. C., and White, C. (2014). Ecologists should not use statistical significance tests to interpret simulation model results. *Oikos* 123 (4), 385–388. doi: 10.1111/j.1600-0706.2013.01073.x

Xing, J., and Davies, A. M. (2001). A three-dimensional baroclinic model of the Irish Sea: Formation of the thermal fronts and associated circulation. *J. Phys. Oceanography* 31 (1), 94–114. doi: 10.1175/1520-0485(2001)031<0094:ATDBMO>2.0.CO;2

frontiers | Frontiers in Marine Science

TYPE Original Research
PUBLISHED 18 January 2024
DOI 10.3389/fmars.2023.1125137

OPEN ACCESS

EDITED BY
Luisa Mangialajo,
Université Côte d'Azur,
France

REVIEWED BY
Maria Muñoz Muñoz,
University of Malaga, Spain
Simon Thrush,
The University of Auckland, New Zealand

*CORRESPONDENCE
Trisha B. Atwood
Trisha.atwood@usu.edu

RECEIVED 15 December 2022
ACCEPTED 01 December 2023
PUBLISHED 18 January 2024

CITATION
Atwood TB, Romanou A, DeVries T, Lerner PE, Mayorga JS, Bradley D, Cabral RB, Schmidt GA and Sala E (2024) Atmospheric CO_2 emissions and ocean acidification from bottom-trawling.
Front. Mar. Sci. 10:1125137.
doi: 10.3389/fmars.2023.1125137

Atmospheric CO_2 emissions and ocean acidification from bottom-trawling

Trisha B. Atwood[1*], Anastasia Romanou[2,3], Tim DeVries[4], Paul E. Lerner[2,3], Juan S. Mayorga[5,6], Darcy Bradley[6,7], Reniel B. Cabral[8], Gavin A. Schmidt[2] and Enric Sala[5]

[1]Department of Watershed Sciences and the Ecology Center, Utah State University, Logan, UT, United States, [2]NASA Goddard Institute for Space Studies, New York, NY, United States, [3]Department of Applied Physics and Applied Mathematics, Columbia University, New York, NY, United States, [4]Department of Geography and Earth Research Institute, University of California, Santa Barbara, Santa Barbara, CA, United States, [5]National Geographic Society, Washington, DC, United States, [6]Environmental Markets Lab, University of California, Santa Barbara, Santa Barbara, CA, United States, [7]Marine Science Institute, University of California, Santa Barbara, CA, United States, [8]College of Science and Engineering, James Cook University, Townsville, QLD, Australia

Trawling the seafloor can disturb carbon that took millennia to accumulate, but the fate of that carbon and its impact on climate and ecosystems remains unknown. Using satellite-inferred fishing events and carbon cycle models, we find that 55-60% of trawling-induced aqueous CO_2 is released to the atmosphere over 7-9 years. Using recent estimates of bottom trawling's impact on sedimentary carbon, we found that between 1996-2020 trawling could have released, at the global scale, up to 0.34-0.37 Pg CO_2 yr^{-1} to the atmosphere, and locally altered water pH in some semi-enclosed and heavy trawled seas. Our results suggest that the management of bottom-trawling efforts could be an important climate solution.

KEYWORDS

climate mitigation, natural climate solutions, fisheries management, ocean conservation, blue carbon

1 Introduction

Marine sediments are thought to be the ultimate long-term carbon store; once buried below the active layer, organic carbon can remain unmineralized for millennia to eons (Burdige, 2007; LaRowe et al., 2020). However, disturbances to the seabed by human activities threaten the permanency of this marine carbon (Levin et al., 2020; Paradis et al., 2021). In the case of bottom trawling, heavy fishing gear that is dragged across the seafloor mixes and resuspends sediments, exposing 0.16-0.40 Pg C yr^{-1} of previously buried organic carbon to potential microbial degradation (Sala et al., 2021). However, the ultimate fate of this disturbed organic carbon stock is as yet unquantified,

hampering our understanding of the effects that bottom trawling has on the global carbon cycle and the potential implications for climate policies.

The protection of organic carbon stored in marine sediments, plants, and animals has been identified as a powerful tool for tackling climate change (Hoegh-Guldberg et al., 2019). However, the uptake of ocean-based climate solutions has been slow due to prevailing climate policies and carbon markets that only recognize mitigation activities with measurable impacts on atmospheric emissions. The challenge with identifying ocean-based solutions under those current paradigms lies in the complexity of quantifying atmospheric emissions generated by anthropogenic activities that occur below the ocean's surface (Luisetti et al., 2020). Therefore, research addressing this challenge is crucial for discovering new opportunities that can harness the full potential of the ocean in contributing to mitigating climate change.

Here, we examined the fate of trawling-induced carbon released into the global ocean between 1996-2020 and under future scenarios, as well as estimated the fraction of CO_2 emitted to the atmosphere. To estimate trawling-induced CO_2 emissions, we used assumptions and data from Sala et al. (2021), the only study to date to estimate the global impact of trawling on CO_2 fluxes from marine sediments, and two classes of ocean circulation models: (I) the Ocean Circulation Inverse Model (OCIM; 2° resolution; Holzer et al., 2021) and (II) the NASA Goddard Institute for Space Studies (GISS) ModelE2.1 (1° x 1.25° ocean model resolution; Lerner et al., 2021). The latter was used in coupled climate simulations under two realizations: prescribed atmospheric CO_2 concentrations (GISScon) and prognostic atmospheric CO_2 based on anthropogenic emissions, the land and ocean sink, and benthic trawling (GISSemis; Ito et al., 2020). GISS and OCIM models are used to estimate air-sea fluxes and internal oceanic transport of CO_2 over time by simulating the complex interplay of atmospheric and oceanic processes. These models offer detailed spatial-temporal estimates of CO_2 exchange between the ocean and atmosphere by modeling the movement of CO_2 through currents, advection, vertical mixing, biological processes (GISS only), and surface gas exchange. Depending on the geographic location and water depth of bottom trawling, CO_2 is exposed to the sea surface within months to centuries (Siegel et al., 2021). GISS and OCIM models are systematically appraised against the latest observations, are internationally accepted, and are being used in the CMIP6 to represent ocean processes (e.g., air-sea fluxes) for the 6th Assessment report (IPCC, 2022) and in the Global Carbon Budget to estimate surface pCO_2 (Friedlingstein et al, 2020a).

2 Materials and methods

2.1 Trawling intensity and CO_2 remineralization

We estimate the aqueous CO_2 efflux that results from bottom trawling using the same approach as Sala et al. (2021). Data on bottom trawling activity was obtained from Global Fishing Watch (https://globalfishingwatch.org/) via Sala et al. (2021). The fraction of the total organic carbon in the first meter of marine sediments that is remineralized to aqueous CO_2 (f) in a given 1 km^2 pixel (i) is estimated as:

$$f_i = SVR_i \times p_l \times p_r \times (1 - e^{-k_i t})$$

Where SVR_i is the swept volume ratio and represents the fraction of the carbon in pixel i that is disturbed by bottom trawling, p_r is the proportion of organic carbon that resettles in pixel i after trawling, p_l is the fraction of organic carbon that is labile, k is the first-order degradation rate constant, and t represents time, which is set to one year. To accurately account for carbon impacts from trawling gear with various penetration depths and the resulting exposure of lower sediment layers due to a net annual loss in sediment from trawling activities, it was necessary to include organic carbon stocks down to one meter. However, the SVR_i term in our model constrains the impact of a trawling event to the proportion of carbon stored only up to the penetration depth of the specific trawling gear utilized in that pixel.

The swept volume ratio SVR_i is estimated as:

$$SVR_i = \sum_g (SAR_{i,g} \times pd_g)$$

where $SAR_{i,g}$ is the swept area ratio in pixel i by vessels using gear g, and pd_g is the average penetration depth of gear type g.

The swept area ratio (SAR) is estimated as:

$$SAR_{i,g} = \frac{\sum_V (TD_{i,v} \times W_v)}{A_i}$$

where $TD_{i,v}$ is the distance trawled by vessel v in pixel i, W_v is the width of the gear trawled by vessel v and A_i is the total area of pixel i. The distance trawled was estimated using fishing activity detected by automatic identification systems (AIS) data from Global Fishing Watch (globalfishingwatch.org) between 2016 and 2020. We used the vessel-size-footprint relationships reported by Eigaard et al. (2016) to calculate the width of the trawl gear for each vessel. Average penetration depths were as follows; otter trawls: 2.44 cm, beam trawls: 2.72 cm, towed dredges 5.47 cm, and hydraulic dredges: 16.11 cm (Hiddink et al., 2017). The fraction of organic carbon in each cell that resettles in that same cell after trawling (p_r) was assumed constant at 0.87 (Sala et al., 2021). The proportion of labile organic carbon (p_l) was assigned using sediment type with values from Sala et al. (2021); fine sediments: 0.7, coarse sediments: 0.286, and sandy sediments: 0.04 (Figure S1). First-order degradation rate constants k_i were also obtained from Sala et al. (2021) and assigned as follows for the different oceanic region: North Pacific = 1.67, South Pacific = 3.84, Atlantic = 1.00, Indian = 4.76, Mediterranean = 12.3, Arctic = 0.275, Gulf of Mexico and Caribbean = 16.8 (Sala et al., 2021).

Finally, the amount of organic carbon remineralized in pixel i, C_{ri}, is estimated as:

$$C_{ri} = C_{oi} \, x \, f_i \, x \, d_i$$

where C_{0i} is the amount of organic carbon stored in the first meter of marine sediments in pixel i (Atwood et al., 2020), f_i is the fraction of that organic carbon that is remineralized, and d_i corresponds to

an organic carbon depletion factor that accounts for the history of trawling in a given pixel *i*. Using the same approach as Sala et al. (2021) but with a more conservative annual organic carbon accumulation rate of 4.9 Mg C km^{-2} yr^{-1} that assumes that 75% of the annual carbon flux is naturally remineralizing regardless of trawling (Wilkinson et al., 2018), we estimate that the CO_2 efflux in a pixel that has been trawled for over a decade stabilizes at 27.2% of the year one flux (i.e., first year of trawling). As such, pixels that have been trawled for more than 10 years are assigned an organic carbon depletion factor (d_i) of 0.272. For pixels trawled less than 10 years, we assumed a depletion factor of 1. To estimate the number of years that trawling has taken place in each pixel we used spatial catch statistics from Watson (2017). Overall, 94% of trawled pixels between 1996-2000 have been trawled for > 10 years.

For hindcasting bottom trawling prior to 2016, we assume that the average intensity and extent of bottom trawling between 2018-2020 is representative of what it has been since 1996 (Watson, 2017; Amoroso et al., 2018). Bottom trawling locations appear to be consistent from year to year as illustrated by data from Watson (2017) and Amoroso et al. (2018). Our assumption of bottom trawling intensity is likely conservative given that bottom trawling catches peaked in several regions, including Europe and North America, in the 1980s and 1990s, and both the number of vessels and their installed capacity (kW) has been stable since the early 2000s (Watson et al., 2006; Rousseau et al., 2019; Pauly et al., 2020).

2.2 OCIM model simulations

OCIM is a data-assimilated model with a steady-state ocean circulation (Devries, 2014). The version used here is the OCIM2-48L used in a recent study of the ventilation of the deep Pacific Ocean (Holzer et al., 2021). An abiotic carbon cycle is implemented in this model using the formulation in DeVries (2014). The model is spun up to equilibrium using a pre-industrial atmospheric CO_2 concentration of 280 ppm. Then, a transient simulation is run using an interactive atmosphere (represented by a single well-mixed box) and carbon emissions into the atmosphere from the Global Carbon Budget 2020 (Friedlingstein et al., 2020a). Carbon emissions are the sum of carbon emissions from fossil fuel burning, cement manufacture, and land use change, minus the carbon absorbed by the terrestrial carbon sink (which is not represented in the model). The historical emissions data are used from 1780-2019, and after 2019 the emissions are held constant at 2019 levels.

Four different simulations are run to assess the impacts of trawling on the air-sea CO_2 flux. For the control simulation (A), there is no emission of dissolved inorganic carbon (DIC) from trawling activity. In simulation B, DIC emissions from trawling are applied for the years 1996-2020. In simulation C, trawling emissions occur from 1996-2030, and in simulation D, trawling emissions occur from 1996-2070. All model simulations are run to 2100.

Air-sea CO_2 fluxes, ocean DIC change, and pH changes (see methods below) due to trawling are assessed by subtracting these quantities in each simulation to that from simulation A (no trawling). Calculating CO_2 and pH in the model also requires temperature, salinity, alkalinity, and nutrient data. These are not tracked in the model, but are instead held fixed at their contemporary values from the World Ocean Atlas for temperature (Locarnini et al., 2019), salinity (Zweng et al., 2018), and nutrients (Garcia et al., 2019), and the Global Ocean Data Analysis Project phase 2 (GLODAPv2) for alkalinity (Olsen et al., 2016). CO_2 and pH are calculated using the CO2SYS calculator (van Heuven et al., 2011). Additional information about model development and parameters for the OCIM model can be found in Holzer et al. (2021).

2.3 GISS coupled model simulations

Simulations were also performed with the NASA Goddard Institute for Space Studies (GISS) E2.1-G coupled climate model that has 2x2.5° and 1x1.25° resolution in the atmosphere and the ocean respectively and is coupled to the NASA Ocean Biogeochemistry Module (NOBM) (Gregg and Casey, 2007; Romanou et al., 2013). CO_2 forcing for the period 1996-2014 comes from observed emissions of CO_2 while transient forcing for the period 2015-2100 follows SSP2-4.5, a mid-range shared socioeconomic pathway scenario, of the Coupled Model Intercomparison Project Phase 6 (CMIP6) (O'Neill et al., 2016; Meinshausen et al., 2020). Additional information about the development of the GISS models and their parameters can be found in Ito et al. (2020) and Lerner et al. (2021). All experiments for this study were branched off a long preindustrial simulation that ensured the ocean carbon flux at the air-sea interface was at equilibrium followed by a historical simulation with observed forcings for the period 1850-1995 (Miller et al., 2021). Two distinct realizations of this model were employed for the purposes of this study: a) a single run (GISScon) of the GISS-E2.1-G model (as in Lerner et al., 2021) where land and radiation only see prescribed observed atmospheric CO_2 concentrations. b) an ensemble of 15 runs with the Earth System Model GISS-E2.1-G-CC (GISSemis) that differs from GISS-E2.1-G only in that radiation responds to prognostic atmospheric CO_2 based on anthropogenic emissions, the land and the ocean sink (as in Ito et al., 2020) as well as trawling emissions. The impacts of trawling on the air-sea CO_2 flux in GISScon and GISSemis are assessed using simulations A-D as described in the previous section. The purpose of the GISSemis suite of simulations is to provide uncertainty envelopes of the response to trawling emissions which are related to the Earth system's intrinsic variability (e.g., natural cycles of tropical variability). More information is provided in the next section.

The pH and aragonite saturation state are computed following the carbonate chemistry routines described in Orr et al. (2017). These routines take as inputs DIC, alkalinity, phosphate, silicate, temperature, and salinity each of which is computed prognostically by the model. Since the model simulates nitrate instead of phosphate, dissolved phosphate is approximated by assuming a constant ratio of 1/16 (Redfield ratio) to nitrate. As surface ratios

can be highly variable, we examined the effect of NO_3^-:PO_4^{3-} ratios on delta pH and found little effect on model output (Supplementary Material Figure S2). Additionally, sources and sinks of alkalinity through carbonate production and dissolution are assumed to be proportional to net primary productivity locally, following OCMIP-2 protocols (Najjar and Orr, 1999).

2.4 Fraction of trawled CO_2 emitted to the atmosphere

The fraction of CO_2 from trawling activities emitted to the atmosphere (Figure 1) is calculated as:

$$fraction\ \ (t) = \frac{\sum_t \left(FCO_{2,trawl}(t) - \ FCO_{2,notrawl}(t)\right)}{\sum_t BFCO_2(t)}$$

where $FCO_{2,trawl}(t)$ is the globally-integrated atmosphere to ocean CO_2 flux in a simulation with trawling (positive into the ocean), $FCO_{2,notrawl}(t)$ is the globally-integrated atmosphere to ocean CO_2 flux in the simulation without trawling, and $BFCO_2(t)$ is the globally-integrated benthic emissions of CO_2 due to trawling. Note that $FCO_{2,notrawl}(t)$ only depends on the model used (GISSemis, GISScon, or OCIM), while $FCO_{2,trawl}(t)$ and $BFCO_2(t)$ also depends on the trawling scenario considered (historical, trawling ceases in 2030, or trawling ceases in 2070).

2.5 Historical and future changes in pH

To quantify historical changes in pH, we calculated a weighted average of pH in the upper 1000 m of a region. The weighted average is calculated as:

$$pH_{ave} = \frac{\sum_i (oarea_i pH_i)}{\sum_i oarea_i}$$

where i is an index for location of a model horizontal (lat/lon) grid cell, $oarea_i$ is the ocean area of that grid cell, and pH_i is the vertical average of pH in the upper 1000 m of that grid cell. Results for the East China/South China Sea reported in the manuscript are for the average change in pH due to trawling between 2000-2020. We take this as the averaging period to avoid the initial steep decline in pH at the beginning of the simulations, which is likely unrealistic given that trawling activities did exist prior to 1996.

It is important to note that while GISS and OCIM agree on the regions where pH changes are largest, they differ in the magnitude of these changes in some locations. Particularly for the East China/South China Sea, OCIM pH changes are larger than GISSemis changes. These differences likely reflect differences in how trawled carbon data is mapped onto model grids with different bathymetries, particularly as those differences become exaggerated near the coastlines where the majority of trawling is taking place. These differences therefore capture real uncertainty in the pH change in each region, as the models are an imperfect representation of reality. There are also differences in the pH between GISS and OCIM due to differences in their base state chemistry.

2.6 Uncertainty

2.6.1 Trawling intensity

Our estimate of trawling intensity uses a three-dimensional footprint that relies on estimation of both the total area trawled and the penetration depth of bottom trawling gear. We discuss sources of uncertainty relevant to each.

First, our estimate of the area impacted by bottom trawling has three potential sources of uncertainty: (1) uncertainty in the model prediction of active fishing from AIS derived location information, (2) uncertainty in coverage (i.e., what fraction of global trawling is observable via AIS data), and (3) uncertainty in estimated trawl width for each vessel. We have high confidence that bottom trawling fishing activity has been accurately estimated for vessels carrying AIS because Global Fishing Watch's neural net is notably good at detecting active fishing by trawlers (precision = 0.9, recall = 0.89, and f1-score = 0.89) (Taconet et al., 2019). However, AIS coverage on trawlers < 15 m in total length is low (Taconet et al., 2019); consequently, we underestimate the total footprint of bottom trawling globally because our estimate misses fishing activity from smaller fleets that are not equipped with AIS. Furthermore, the spatial distribution of known gaps in coverage is not uniform. While AIS provides accurate spatial patterns of fishing activity and intensity for some regions (e.g., FAO Area 21, Northwest Atlantic and FAO Area 27, Northeast Atlantic), important gaps in coverage have been identified in the Arctic Sea (FAO Area 18), Western Central Pacific (FAO Area 71), and the Eastern Indian Ocean (FAO Area 57) (Taconet et al., 2019). For example, AIS data are nearly absent from intensely fished regions in Southeast Asia and Indonesia. Additional uncertainty about the area trawled is introduced by our estimate of the width of the trawled gear, for which we use the vessel-size-footprint relationships reported by a study on bottom trawling on the European continental shelf (Eigaard et al., 2016). It is possible that the vessel-size-footprint relationship of the European fleet differs from other global fleets, but these data are not reported elsewhere.

Second, our gear-specific estimates of penetration depth are taken from Hiddink et al. (2017), who use a systematic literature review coupled with a nested linear model to predict the penetration depth for each gear component in each sediment type. Unfortunately, Hiddink et al. (2017) do not elaborate on error and uncertainty in their model for trawl penetration depth.

2.6.2 CO_2 remineralization

Sediment organic carbon stock estimates in the top 1 m horizon were obtained from Atwood et al. (2020), which represents the only study to date to quantify spatially-explicit stocks at a global scale down to 1 m in the sediment; such a depth is required for estimating multiyear impacts of trawling due to annual sedimentation deficits that ultimately require estimates of organic carbon stocks buried in

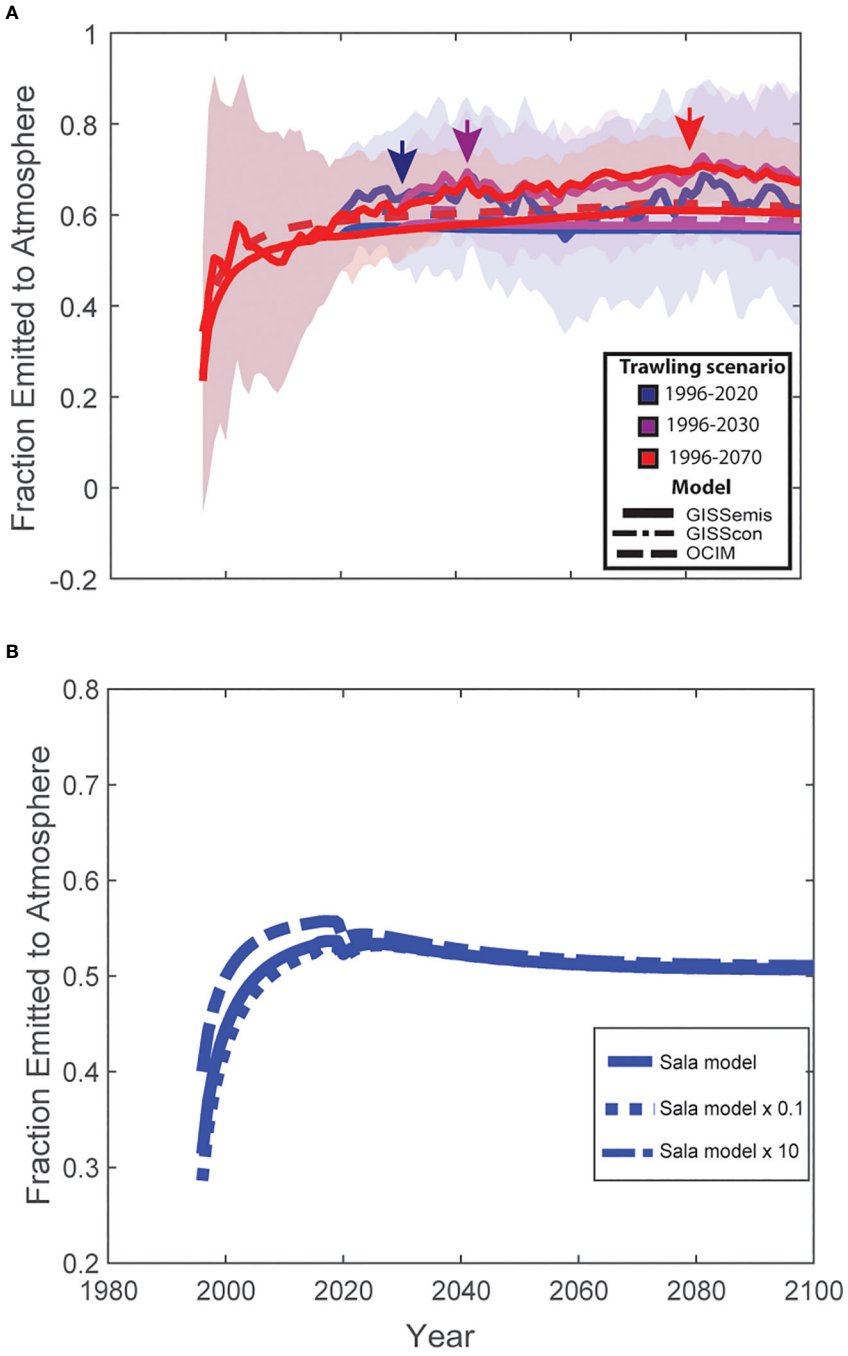

FIGURE 1
Fraction of trawled CO_2 emitted to the atmosphere. **(A)** The fraction of trawled CO_2 emitted to the atmosphere from historical trawling (1996-2020) and future projections. Colors represent different trawling scenarios, with blue denoting historical trawling from 1996-2020 and zero trawling thereafter, magenta denoting a future scenario where trawling stops in 2030, and red denoting a future scenario where global trawling ceases in 2070. Continuous lines are ensemble mean solutions from the GISSemis runs, dashed-dotted lines are from the GISScon runs (often not visible in the graph due to overlap with other data points), and dashed lines are from the OCIM simulations. Shading represents the internal variability in the ensemble simulations with the GISSemis model. Arrows indicate when ~99% of the total emissions are released to the atmosphere post-trawling for each of the three trawling scenarios. **(B)** Effect of the magnitude of CO_2 flux on the fraction of CO_2 emitted to the atmosphere. The solid data line represents the historical (1996-2020) trawling flux estimated using the Sala et al. (2021) carbon model, the dotted lines represent an arbitrarily increase (Sala model x 10) and decrease (Sala model x 0.1) of Sala et al. (2021) flux estimate by one-order of magnitude. Models represent OCIM simulations.

sediment layers that are deeper than the ones immediately impacted by the trawling gear. Atwood et al. (2020) model explained 76% of the variation in organic carbon stocks and had a root-mean-square error of 7306 Mg km^{-2}. An additional uncertainty in carbon stocks that is acknowledge, but not quantified by Atwood et al. (2020) is variation in carbon stocks with sediment depth. In many cases Atwood et al. (2020) had to extrapolate carbon stocks to 1 m using data from shallower samples.

The largest uncertainty in the CO_2 remineralization model is the estimates of first-order degradation rate constants (k-values). Field studies have shown that k-values can vary substantially both spatially and with depth in the sediment, and unfortunately, studies examining the effects of trawling on organic carbon activity and k-values are extremely limited. We used the k-values published in Sala et al. (2021), which used a literature review and independent validation sites to characterize and generalize region-specific k-values. Across their validation sites, their average model percent error for predicting sediment-water CO_2 fluxes ranged from -45% to +39% when accounting for annual organic carbon flux, with an average absolute error of 23% (Atwood et al., 2023).

It has been suggested by studies that organic carbon reactivity in subsurface sediments could be one to two-orders of magnitude lower than those used in Sala et al. (2021) (Epstein et al., 2022; Hiddink et al., 2023). As a result, we investigated how reductions of one- and two-orders of magnitude in Sala et al. (2021) first-order degradation rates would impact estimated atmospheric emissions. We found that Sala et al. (2021) emission estimates were relatively robust to changes in first-order degradation rates because in the multiyear trawling model, reductions in this parameter substantially reduced carbon depletion through time. Under Sala et al. (2021) original carbon model (global k = 2.6), GISS and OCIM models estimated that trawling emitted as much as ~0.34-0.37 Pg CO_2 yr^{-1} to the atmosphere. When first-order degradation rates were reduced by 1-order of magnitude (global average k = 0.28), resulting in only a ~6.8% remineralization efficiency of disturbed organic carbon, the magnitude of atmospheric emissions remained similar to Sala et al (2021) original model (0.19-0.21 Pg CO_2 yr^{-1}, Atwood et al., 2023). The magnitudes are comparable because in Sala et al, (2021) original model, organic carbon depletion after a decade of trawling results in emissions that are ~27.2% of the year one flux. Conversely, when degradation rates are reduced, more organic carbon stays in the system longer, and changes in trawling-induced fluxes across time stabilize quickly. However, a reduction of the first-order degradation rates by two orders of magnitude (global average k = 0.028; 1.2% remineralization efficiency) does result in a much larger decrease in atmospheric emissions, which are reduced to 0.02-0.03 Pg CO_2 yr^{-1} (Atwood et al., 2023), or ~1% of the global emissions from land-use change (Friedlingstein et al., 2020a).

Our models do not account for trawling-induced impacts on organic carbon remineralization due to changes in sediment biota (Epstein et al., 2022). Although the current paradigm in soil science is that microbial communities dominate benthic metabolism in marine sediments, a process that is accounted for in our models, animals undoubtedly play a key role in marine sediment carbon cycling (Snelgrove et al., 2018; LaRowe et al., 2020; Bianchi et al., 2021); yet aquatic and terrestrial animals are universally ignored in Earth Systems Models (Schmitz et al., 2018; Snelgrove et al., 2018; Bianchi et al., 2021). The absence of animals from Earth System Models stems from the lack of generalizable predictions about how animal community changes will likely affect carbon cycling (Schmitz et al., 2018; Schmitz et al., 2023). It can be argued that trawling can stimulate or retard organic carbon remineralization through its differing and often context-dependent effects on infauna communities (Epstein et al., 2022). Yet, the considerable particle mixing and sediment flushing that results from the movement of fishing gear across the seabed could offset some of the potential loss of processes like bioturbation and bioirrigation. Nevertheless, holistic models that include the indirect effects of trawling on organic carbon remineralization through changes in animal communities are needed to make more accurate predictions, especially at smaller spatial scales. However, to better characterize variability and uncertainty in model parameters, further large-scale empirical studies on the biotic and physical processes controlling carbon retention and remineralization in marine sediments, as well as how these processes are affected by trawling, are critical.

2.6.3 Atmospheric emissions

In terms of the response of the global air-sea CO_2 flux to a given trawling emissions pattern, the agreement of the two models suggests that atmospheric emission estimates are fairly robust and inter-model variation is low. Because of the coarse resolution of the models (OCIM: 2° resolution; GISS: 1° x 1.25° resolution), however, regional estimates will have more uncertainty. Thus, the greatest uncertainty in atmospheric emissions estimates comes from the quantification of CO_2 remineralization from trawling impacts on sedimentary carbon (see uncertainties above). Atmospheric emissions and the amount of trawling-induced CO_2 remineralized scale linearly because the air-sea partitioning depends on the circulation timescale and the gas exchange timescale, both of which are unaffected by the relatively small amount of CO_2 emitted by trawling compared to fossil fuel emissions. Therefore, any changes to the amount of trawling-induced CO_2 generated would result in a proportionally similar change in atmospheric CO_2 emissions.

Our models also do not account for the release of N or P from trawled sediments and the potential for those nutrients to stimulate pelagic primary productivity. Unfortunately, there are no global maps of N and P stocks in marine sediments and to our knowledge no empirical studies have explicitly tested this hypothesis. However, modeling studies and theory suggested that if impacts to light attenuation from suspended sediments is short-term, trawling could potentially stimulate primary productivity, and thus uptake of CO_2 (Dounas et al., 2007; Epstein et al., 2022).

2.6.4 Internal climate variability

The GISSemis suite of simulations aims to assess the relative importance of the response to the trawling emissions compared to the system's internal variability. The ensemble mean is very close to the GISScon and OCIM responses while the internal variability can produce a wide range of individual ensemble member responses that can be ±20% of the ensemble average for the atmospheric CO_2 change and ±40% of the ensemble average for the ocean carbon sink change (see Table S1). However, this uncertainty is model dependent and might be different for other climate models.

3 Results and discussion

Our retrospective and prospective analyses showed that 55-60% of the CO_2 released into the water column by bottom trawling

impacts on sediment carbon stocks is emitted to the atmosphere within ~9 years of the trawling event (Figure 1). Furthermore, we found that the fraction of CO_2 accumulating in the atmosphere remained at 55-60% until the end of our simulations at 2100, regardless of the magnitude of CO_2 predicted to be released into the water column by trawling (Figure 1). These results are significant in that they imply that the 55-60% fraction can be easily applied to estimate trawling-induced CO_2 emissions to the atmosphere under a variety of historical and future trawling scenarios.

Using Sala et al. (2021) estimates of sediment efflux, our models suggest that trawling could have emitted a cumulative 8.5-9.2 Pg CO_2 into the atmosphere between 1996 and 2020 (Table S1; Figure 2), contributing 0.97-1.14 ppm to atmospheric CO_2 concentrations (Figure 2). These emissions would equate to ~0.34-0.37 Pg CO_2 yr^{-1}, which is equivalent to ~9-11% of the global emissions from land-use change in 2020 (Friedlingstein et al., 2020b), or nearly double the estimated annual emissions from fuel combustion for the entire global fishing fleet (Parker et al., 2018). Trawling emissions of this magnitude suggest that the protection of seabed organic carbon from benthic trawling gear could prove to be an impactful climate solution. For example, if we continue to trawl at current intensities and spatial distributions, we estimate that bottom trawling could contribute an additional 0.2-0.5 ppm in atmospheric CO_2 concentrations by 2030 and 1.03-1.36 ppm by 2070 (Figure 2).

Whether or not reductions in trawling could be adapted as a climate solution not only depends on the magnitude of the emission reductions, but also the time frame over which those reductions can be achieved. We found that the release of trawling-induced CO_2 from the ocean to the atmosphere occurred rapidly, with ~99% of the total emissions occurring within 7-9 years post-bottom trawling (OCIM: 7 yrs; GISScon: 9 yrs; GISSemis: 9 yrs ± 5 yrs (standard deviation of ensemble members). When emissions were arbitrarily increased by one order of magnitude, it took slightly less time (OCIM:~5 yrs) for total emissions to be released into the atmosphere. The rapid release of CO_2 from the ocean to the atmosphere suggests that historical trawling has only short-term legacy effects on atmospheric emissions. Thus, policies that eliminate or significantly limit trawling impacts on sedimentary carbon stocks would quickly reduce this industry's contribution to rising atmospheric CO_2 concentrations with maximum benefits occurring 7-9 years after implementation.

In general, atmospheric CO_2 emission hotspots coincided with areas where trawling had the most significant impact on benthic carbon, mainly the East China Sea, the Baltic and the North Sea, and the Greenland Sea (Figure 3). However, horizontal advection can transport trawling-induced CO_2 and resuspended organic carbon to other locations, leading to cross-boundary effects of bottom trawling on local carbon cycles. This phenomenon likely explains why some areas such as the South China Sea, Norwegian Sea, and off the east

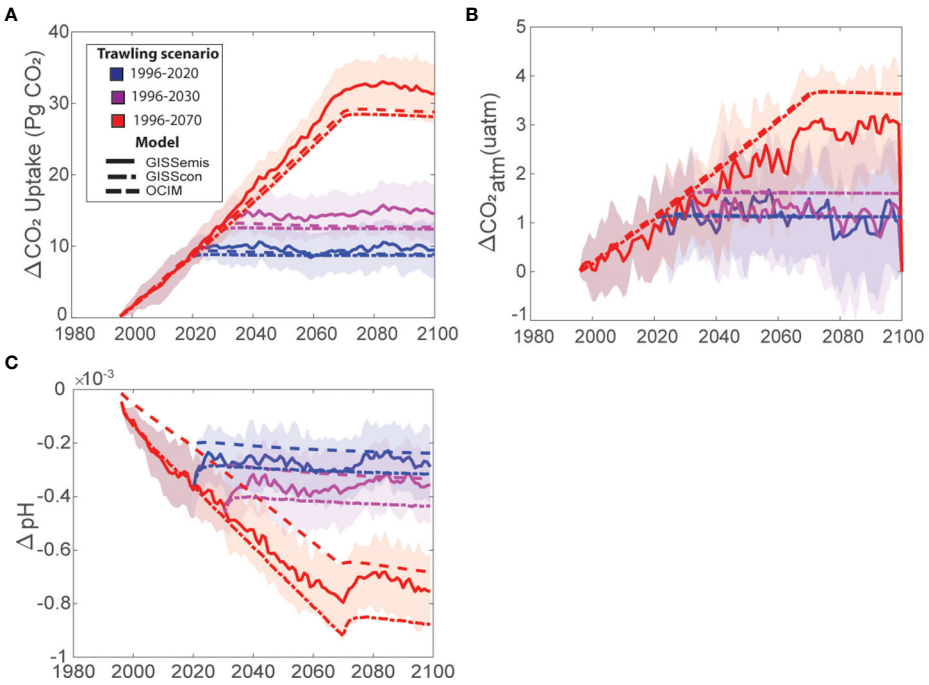

FIGURE 2
Effects of benthic trawling on CO_2 emissions and bottom water pH. Time series of the **(A)** change in cumulative carbon uptake by the ocean due to trawling, or equivalently a flux of CO_2 to the atmosphere, **(B)** change in atmospheric CO_2 concentrations due to trawling in the different model simulations (OCIM, GISScon, GISSemis), and **(C)** global ocean pH change due to trawling. Colors represent different trawling scenarios, with blue denoting historical trawling from 1996-2020 and zero trawling thereafter, magenta denoting a future scenario where trawling stops in 2030, and red denoting a future scenario where global trawling ceases in 2070. Continuous lines are ensemble mean solutions from the GISSemis runs, dashed-dotted lines are from the GISScon runs, and dashed lines are from the OCIM simulations. Shading represents the internal variability in the ensemble simulations with the GISSemis model.

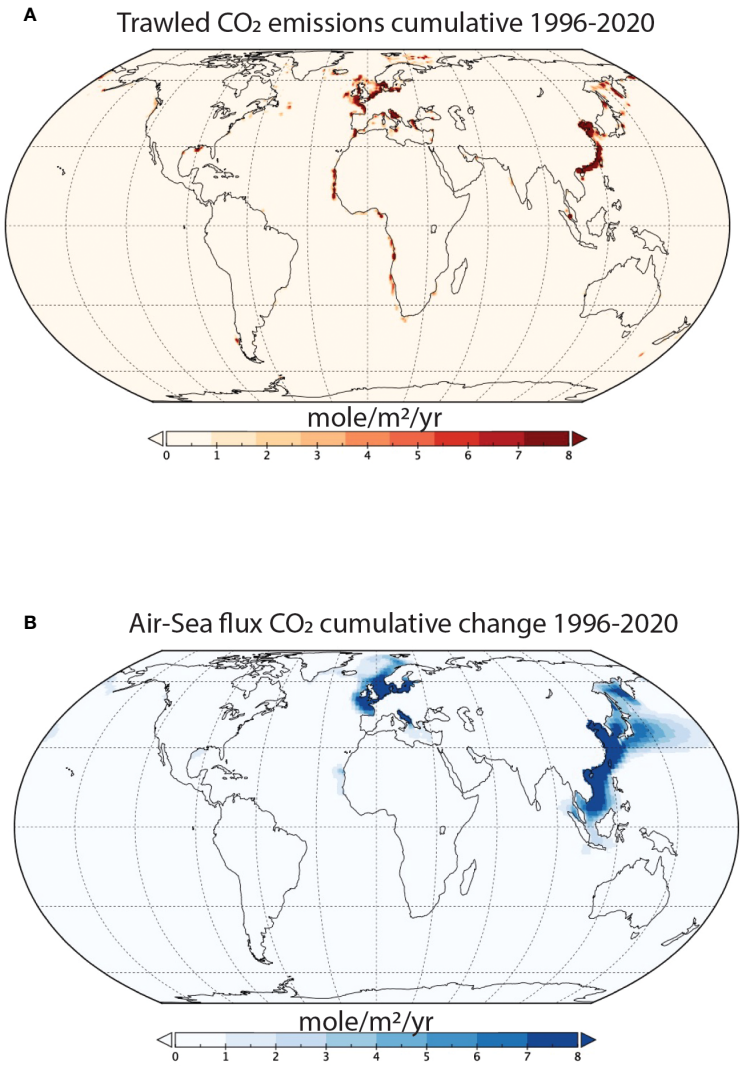

FIGURE 3
Spatial differences in the historical effects of benthic trawling on CO_2 emissions. **(A)** Cumulative emissions of trawled CO_2 between 1996-2020. **(B)** Cumulative changes in the air-sea CO_2 flux due to trawling between 1996-2020. It is important to note that significant knowledge gaps exist regarding trawling activity in the Arctic Sea (FAO Area 18), Western Central Pacific (FAO Area 71), and the Eastern Indian Ocean (FAO Area 57) (Taconet et al., 2019). Consequently, emissions attributed to trawling in these regions are likely underestimated.

coast of Japan in the Pacific Ocean had higher atmospheric emissions than expected based on the local rate of trawling emissions (Figure 3). As a result of these cross-boundary effects, we cannot assume that all the atmospheric emissions within a country's jurisdictional waters come from trawling activities within that zone.

Our ability to quantify the extent of the global bottom trawling fleet through time and space in this study was somewhat limited. Our estimates do not capture trawling activities before 1996, because the intensity and spatial distribution of bottom trawling before that time are unknown. Yet, large-scale bottom trawling began as early as 1950 and peaked in the 1980s and 1990s (Watson et al., 2006; Watson and Tidd, 2018). Furthermore, our model relies on the AIS vessel tracking database processed by Global Fishing Watch (https://globalfishingwatch.org/) to derive trawling events at the global level. Unfortunately, AIS coverage is poor in some fishing-intensive areas. Thus, we undoubtedly underestimate trawling activity in areas of Southeast Asia, the Bay of Bengal, the Arabian Sea, parts of Europe, and the Gulf of Mexico (Taconet et al., 2019).

There are additional uncertainties in the parameters used to estimate the amount of organic carbon remineralized after trawling due to a lack of rigorous field studies. Though our model is parameterized using the best available empirical data (Sala et al., 2021; Atwood et al., 2023), an alternative line of reasoning argues that first-order degradation rates could be one- to two orders of magnitude lower (Hiddink et al., 2023). Because we find that atmospheric emissions scale linearly with the amount of organic carbon remineralized to aqueous CO_2 by trawling, we can straightforwardly examine the sensitivity of our results to this alternative assumption. Leveraging Atwood et al. (2023) finding that reducing first-order degradation rates by one order of magnitude has a negligible effect on the estimated magnitude of organic carbon remineralized after 10 consecutive years of trawling,

we find that retaining this reduction to first-order degradation rates results in an estimated 0.19-0.21 Pg CO_2 yr^{-1} emitted to the atmosphere due to bottom trawling between 1996-2020. A two-orders of magnitude reduction to first-order degradation would result in 0.02-0.03 Pg CO_2 yr^{-1} emitted over the same time period – comparable to the mitigation potential for managing fires in temperate forests (Griscom et al., 2017).

Currently, climate actions aimed at reducing CO_2 emissions from anthropogenic practices (e.g., carbon markets, renewable energy standards, reforestation efforts, etc.) focus exclusively on atmospheric emissions. However, these frameworks overlook the total impact of ocean-use change activities on the carbon cycle, because they ignore the pool of DIC that remains sequestered by the ocean. In the case of trawling, we found that 40-45% of the cumulative trawling-induced CO_2 emissions remained dissolved in seawater, augmenting the acidification already occurring from the burning of fossil fuels. Using Sala et al. (2021) carbon model, we found that trawling increased the global DIC inventory by ~1.82-1.90 Pg C from 1996-2020 (Table S1). This additional dissolved inorganic carbon from trawling results in increased ocean acidification with a global reduction in pH of 3-5 $\times 10^{-4}$ by 2020 (Figure 2). At the global scale, a pH reduction of that magnitude by 2020 is not significant compared to the effect of anthropogenic emissions due to fossil fuels. However, our models suggest that some semi-enclosed seas could be highly sensitive to an injection of CO_2 from anthropogenic activities. In particular, our models showed that extensive trawling could lead to increased localized acidification in the East and South China Sea (Figure 4). The decrease in pH in this region due to trawling between 2000 and 2020 (GISSemis: -0.034+/-0.001; OCIM: -0.050) is comparable to that from rising atmospheric CO_2 due to the burning of fossil fuels over the same time period (GISSemis: -0.034+/-0.004; OCIM: -0.020). An important caveat to our pH findings is that our models are limited in resolving coastal processes both due to their coarse resolution and lack of biogeochemical complexity. Nevertheless, considering that

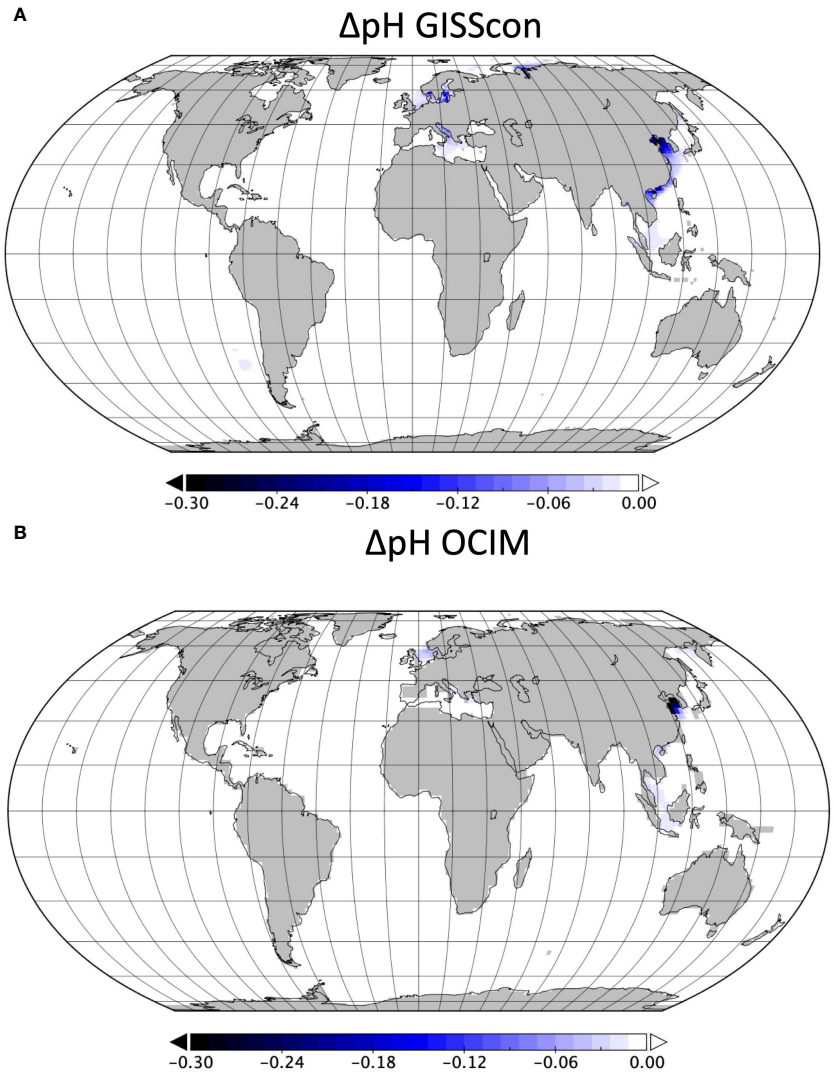

FIGURE 4
Spatial differences in the historical effects of benthic trawling on pH. Change in upper 1000-m average pH due to trawling in 2020 for **(A)** GISScon Model results and **(B)** OCIM Model results.

ocean chemistry can influence organismal development, physiology, and behavior (Baag and Mandal, 2022), and ultimately can affect a species' productivity and survival, future studies and policy should consider the potential impacts trawling can have on localized ocean acidification.

4 Conclusion

Ocean-based solutions offer promise in closing the emissions gap to limit global temperature increases to 1.5°C, while also supporting co-benefits like biodiversity preservation and food security (Hoegh-Guldberg et al., 2019; Sala et al., 2021). However, current climate policies and markets require estimates of avoided atmospheric emissions, posing challenges for identifying and implementing these solutions. Our study, which highlights that 55-60% of CO_2 produced from bottom trawling is released into the atmosphere within nine years, becomes a crucial tool for evaluating the reduction of bottom trawling effort as an effective ocean-based climate solution. To refine atmospheric emission estimates, it is essential for field studies to tackle uncertainties in our understanding of how bottom trawling influences the biological and physical processes that govern carbon remineralization and preservation. Furthermore, the incorporation of high-resolution regional models that resolve small-scale processes, such as local currents, will be pivotal in delivering more precise emission estimates at scales pertinent to local policy considerations. Lastly, our findings emphasize the need for policy to avoid exclusive focus on avoided atmospheric emissions, as our results show that trawling-induced increases in DIC in seawater could have severe implications for local or regional ocean acidification.

Data availability statement

The datasets presented in this study can be found in online repositories. The names of the repository/repositories and accession number(s) are as follows. Data on marine sedimentary carbon stocks is available at https://figshare.com/articles/dataset/marine_soil_carbon/9941816. Data on swept volume ratios and trawling activity are available by contacting Global Fishing research@globalfishingwatch.org. The code for GISS models is available at the TrawlingExpts2023 at http://simplex.giss.nasa.gov; for access to the simplex.giss.nasa.gov repository, email anastasia.romanou@nasa.gov. OCIM code is available upon email request to TD at tdevries@geog.ucsb.edu. All data used for this study and the figures can be found in the NASA Center for Climate Simulation portal: https://portal.nccs.nasa.gov/datashare/modelE_ocean/Atwood_etal2023_paper_data.

Author contributions

All authors contributed to the conceptualization and design of the study. AR, PL, TD, and JM ran data analyses. TA wrote the original draft of the manuscript and all authors contributed to reviewing and editing. All authors contributed to the article and approved the submitted version.

Funding

The author(s) declare financial support was received for the research, authorship, and/or publication of this article. TA, JM, DB, RC, and ES acknowledge funding from National Geographic Pristine Seas. TA was funded by an Early Career Research Fellowship from the Gulf Research Program of the National Academies of Sciences, Engineering, and Medicine (The content is solely the responsibility of the authors and does not necessarily represent the official views of the Gulf Research Program of the National Academies of Sciences, Engineering, and Medicine). TD was funded by the National Science Foundation under grant OCE-1948955. AR, PL, and GS were supported by the Modeling, Analysis and Prediction Program from NASA and by the High-End Computing Program through the NASA Center for Climate Simulation at Goddard Space Flight Center.

Acknowledgments

We thank Y. Rousseau for insights on temporal patterns in trawling.

Conflict of interest

The authors declare that the research was conducted in the absence of any commercial or financial relationships that could be construed as a potential conflict of interest.

Publisher's note

Supplementary material

The Supplementary Material for this article can be found online at: https://www.frontiersin.org/articles/10.3389/fmars.2023.1125137/full#supplementary-material

References

Amoroso, R. O., Pitcher, C. R., Rijnsdorp, A. D., McConnaughey, R. A., Parma, A. M., Suuronen, P., et al. (2018).). Bottom trawl fishing footprints on the world's continental shelves. *Proc. Natl. Acad. Sci.* 115, E10275–E10282. doi: 10.1073/pnas.1802379115

Atwood, T., Sala, E., Mayorga, J., Bradley, D., Cabral, R. B., Auber, A., et al. (2023). Response to comment on "Quantifying the carbon benefits of ending bottom trawling. *Nature* 617, E3–E5. doi: 10.1038/s41586-023-06015-6

Atwood, T. B., Witt, A., Mayorga, J., Hammill, E., and Sala, E. (2020). Global patterns in marine sediment carbon stocks. *Front. Mar. Sci.* 7. doi: 10.3389/fmars.2020.00165

Baag, S., and Mandal, S. (2022). Combined effects of ocean warming and acidification on marine fish and shellfish: A molecule to ecosystem perspective. *Sci. Total Environ.* 802. doi: 10.1016/j.scitotenv.2021.149807

Bianchi, T. S., Aller, R. C., Atwood, T. B., Brown, C. J., Buatois, L. A., Levin, L. A., et al. (2021). What global biogeochemical consequences will marine animal-sediment interactions have during climate change. *Elem. Sci. Anth.* 9, 1–25. doi: 10.1525/elementa.2020.00180

Burdige, D. J. (2007). Preservation of organic matter in marine sediments: Controls, mechanisms, and an imbalance in sediment organic carbon budgets? *Chem. Rev.* 107, 467–485. doi: 10.1021/cr050347q

DeVries, T. (2014). The oceanic anthropogenic CO2 sink: Storage, air-sea fluxes, and transports over the industrial era. *Global Biogeochem. Cycles* 28, 631–647. doi: 10.1002/2013GB004739

Dounas, C., Davies, I., Triantafyllou, G., Koulouri, P., Petihakis, G., Arvanitidis, C., et al. (2007). Large-scale impacts of bottom trawling on shelf primary productivity. *Cont. Shelf Res.* 27, 2198–2210. doi: 10.1016/j.csr.2007.05.006

Eigaard, O. R., Bastardie, F., Breen, M., Dinesen, G. E., Hintzen, N. T., Laffargue, P., et al. (2016). Estimating seabed pressure from demersal trawls, seines, and dredges based on gear design and dimensions. *ICES J. Mar. Sci.* 73, i27–i43. doi: 10.1093/icesjms/fsv099

Epstein, G., Middelburg, J. J., Hawkins, J. P., Norris, C. R., and Roberts, C. M. (2022). The impact of mobile demersal fishing on carbon storage in seabed sediments. *Glob. Change Biol.* 28, 2875–2894. doi: 10.1111/gcb.16105

Friedlingstein, P., O'Sullivan, M., Jones, M., Andrew, R., Hauck, J., Olsen, A., et al. (2020a). Global carbon budget 2021. *Preprint* 10.5194/es, 1–3. doi: 10.5194/essd-2020-286

Friedlingstein, P., O'Sullivan, M., Jones, M. W., Andrew, R. M., Hauck, J., Olsen, A., et al. (2020b). Global carbon budget 2020. *Earth Syst. Sci. Data* 12, 3269–3340. doi: 10.5194/essd-12-3269-2020

Garcia, H. E., Weathers, K. W., Paver, C. R., Smolyar, I. V., Boyer, T. P., Locarnini, R. A., et al. (2019). "Dissolved inorganic nutrients (phosphate, nitrate and nitrate + nitrite, silicate," in *World atlas 2018*. Ed. A. V. Mishonov (Silver Springs, MD: USA Department of Commerce), 35. NOAA Atlas NESDIS 84.

Gregg, W. W., and Casey, N. W. (2007). Modeling coccolithophores in the global oceans. *Deep. Res. Part II Top. Stud. Oceanogr.* 54, 447–477. doi: 10.1016/j.dsr2.2006.12.007

Griscom, B. W., Adams, J., Ellis, P. W., Houghton, R. A., Lomax, G., Miteva, D. A., et al. (2017). Natural climate solutions. *Proc. Natl. Acad. Sci.* 114, 11645–11650. doi: 10.1073/pnas.1710465114

Hiddink, J. G., Jennings, S., Sciberras, M., Szostek, C. L., Hughes, K. M., Ellis, N., et al. (2017). Global analysis of depletion and recovery of seabed biota after bottom trawling disturbance. *Proc. Natl. Acad. Sci. U.S.A.* 114, 8301–8306. doi: 10.1073/pnas.1618858114

Hiddink, J. G., van de Velde, S., McConnaughey, R. A., De Borger, E., O'Neill, F. G., Tiano, J., et al. (2023). Quantifying the carbon benefits of ending bottom trawling. *Nature* 617, E1–E2. doi: 10.1038/s41586-023-06014-7

Hoegh-Guldberg, O., Northrop, E., and Lubchenco, J. (2019). The ocean is key to achieving climate and societal goal. *Science* 365, 1372–1374. doi: 10.1126/science.aaz4390

Holzer, M., DeVries, T., and de Lavergne, C. (2021). Diffusion controls the ventilation of a Pacific Shadow Zone above abyssal overturning. *Nat. Commun.* 12, 1–13. doi: 10.1038/s41467-021-24648-x

IPCC (2022). Climate change 2022: impacts, adaptation, and vulnerability. contribution of working group ii to the sixth assessment report of the intergovernmental panel on climate change. H.-O. Pörtner, D. C. Roberts, M. Tignor, E. S. Poloczanska, K. Mintenbeck, A. Alegría, M. Craig, S. Langsdorf, S. Löschke, V. Möller, A. Okem and B. Rama (eds.). (Cambridge, UK and New York, NY, USA: Cambridge University Press), 3056 pp. doi: 10.1017/9781009325844

Ito, G., Romanou, A., Kiang, N. Y., Faluvegi, G., Aleinov, I., Ruedy, R., et al. (2020). Global carbon cycle and climate feedbacks in the NASA GISS ModelE2.1. *J. Adv. Model. Earth Syst.* 12, 1–44. doi: 10.1029/2019MS002030

LaRowe, D. E., Arndt, S., Bradley, J. A., Estes, E. R., Hoarfrost, A., Lang, S. Q., et al. (2020). The fate of organic carbon in marine sediments - New insights from recent data and analysis. *Earth-Science Rev.* 204, 103146. doi: 10.1016/j.earscirev.2020.103146

Lerner, P., Romanou, A., Kelley, M., Romanski, J., Ruedy, R., and Russell, G. (2021). Drivers of air-sea CO2 flux seasonality and its long-term changes in the NASA-GISS model CMIP6 submission. *J. Adv. Model. Earth Syst.* 13, 1–33. doi: 10.1029/2019MS002028

Levin, L. A., Wei, C. L., Dunn, D. C., Amon, D. J., Ashford, O. S., Cheung, W. W. L., et al. (2020). Climate change considerations are fundamental to management of deep-sea resource extraction. *Glob. Change Biol.* 26, 4664–4678. doi: 10.1111/gcb.15223

Locarnini, R. A., Mishonov, A. V., Baranova, O. K., Boyer, T. P., Zweng, M. M., Garcia, H. E., et al. (2019). *World ocean atlas 2018 , volume 1: temperature*Ed.A. Mishonov (Silver Springs, MD: USA Department of Commerce).

Luisetti, T., Ferrini, S., Grilli, G., Jickells, T. D., Kennedy, H., Kröger, S., et al. (2020). Climate action requires new accounting guidance and governance frameworks to manage carbon in shelf seas. *Nat. Commun.* 11, 1–10. doi: 10.1038/s41467-020-18242-w

Meinshausen, M., Nicholls, Z., Lewis, J., Gidden, M., Vogel, E., Freund, M., et al. (2020). The SSP greenhouse gas concentrations and their extensions to 2500. *Geosci. Model. Dev. Discuss.* 13, 3571–3605. doi: 10.5194/gmd-13-3571-2020

Miller, R. L., Schmidt, G. A., Nazarenko, L. S., Bauer, S. E., Kelley, M., Ruedy, R., et al. (2021). CMIP6 historical simulations, (1850–2014) with GISS-E2.1. *J. Adv. Model. Earth Syst.* 13, 1–35. doi: 10.1029/2019MS002034

Najjar, R., and Orr, J. (1999). "Design of ocmip-2 simulations of chlorofluorocarbons, the solubility pump and common biogeochemistry [OCMIP-2 Protocols]," in *OCMIP web applications*. (Silver Springs, MD: USA Department of Commerce). Available at: http://ocmip5.ipsl.fr/documentation/OCMIP/phase2/.

Olsen, A., Key, R. M., Van Heuven, S., Lauvset, S. K., Velo, A., Lin, X., et al. (2016). The global ocean data analysis project version 2 (GLODAPv2) - An internally consistent data product for the world ocean. *Earth Syst. Sci. Data* 8, 297–323. doi: 10.5194/essd-8-297-2016

O'Neill, B. C., Tebaldi, C., Van Vuuren, D. P., Eyring, V., Friedlingstein, P., Hurtt, G., et al. (2016). The scenario model intercomparison project (ScenarioMIP) for CMIP6. *Geosci. Model. Dev.* 9, 3461–3482. doi: 10.5194/gmd-9-3461-2016

Orr, J. C., Najjar, R. G., Aumont, O., Bopp, L., Bullister, J. L., Danabasoglu, G., et al. (2017). Biogeochemical protocols and diagnostics for the CMIP6 ocean model intercomparison project (OMIP). *J. Geophys. Res. Atmos.* 112, 2169–2199. doi: 10.1029/2007JD008643

Paradis, S., Goñi, M., Masqué, P., Durán, R., Arjona-Camas, M., Palanques, A., et al. (2021). Persistence of biogeochemical alterations of deep-sea sediments by bottom trawling. *Geophys. Res. Lett.* 48, 1–12. doi: 10.1029/2020gl091279

Parker, R. W. R., Blanchard, J. L., Gardner, C., Green, B. S., Hartmann, K., Tyedmers, P. H., et al. (2018). Fuel use and greenhouse gas emissions of world fisheries. *Nat. Clim. Change* 8, 333–337. doi: 10.1038/s41558-018-0117-x

Pauly, D., Zeller, D., and Palomares, M. L. D. (2020). *Sea around us concepts, design and data*. (Silver Springs, MD: USA Department of Commerce).

Romanou, A., Gregg, W. W., Romanski, J., Kelley, M., Bleck, R., Healy, R., et al. (2013). Natural air-sea flux of CO2 in simulations of the NASA-GISS climate model: Sensitivity to the physical ocean model formulation. *Ocean Model.* 66, 26–44. doi: 10.1016/j.ocemod.2013.01.008

Rousseau, Y., Watson, R. A., Blanchard, J. L., and Fulton, E. A. (2019). Evolution of global marine fishing fleets and the response of fished resources. *Proc. Natl. Acad. Sci. U.S.A.* 116, 12238–12243. doi: 10.1073/pnas.1820344116

Sala, E., Mayorga, J., Bradley, D., Cabral, R. B., Atwood, T. B., Auber, A., et al. (2021). Protecting the global ocean for biodiversity, food and climate. *Nature* 592, E25. doi: 10.1038/s41586-021-03496-1

Schmitz, O. J., Sylvén, M., Atwood, T. B., Bakker, E. S., Berzaghi, F., Brodie, J. F., et al. (2023). Trophic rewilding can expand natural climate solutions. *Nat. Clim. Chang.* 13, 324–333. doi: 10.1038/s41558-023-01631-6

Schmitz, O. J., Wilmers, C. C., Leroux, S. J., Doughty, C. E., Atwood, T. B., Galetti, M., et al. (2018). Animals and the zoogeochemistry of the carbon cycle. *Sci. (80-.).* 362, eaar3213. doi: 10.1126/science.aar3213

Siegel, D. A., Devries, T., Doney, S. C., and Bell, T. (2021). Assessing the sequestration time scales of some ocean-based carbon dioxide reduction strategies. *Environ. Res. Lett.* 16, 104003. doi: 10.1088/1748-9326/ac0be0

Snelgrove, P. V. R., Soetaert, K., Solan, M., Thrush, S., Wei, C. L., Danovaro, R., et al. (2018). Global carbon cycling on a heterogeneous seafloor. *Trends Ecol. Evol.* 33, 96–105. doi: 10.1016/j.tree.2017.11.004

Taconet, M., Kroodsma, D., and Fernandes, J. A. (2019). *Global atlas of AIS-based fishing activity-Challenges and opportunities* (FAO: Rome).

van Heuven, S., Pierrot, D., Rae, J. W. B., Lewis, E., and Walace, D. W. R. (2011). *CO2SYS v 1.1 : MATLAB program developed for CO2 system calculations. ORNL/CDIAC-105b*. (Silver Springs, MD: USA Department of Commerce). doi: 10.3334/CDIAC/otg.CO2SYS_MATLAB_v1.1

Watson, R. A. (2017). A database of global marine commercial, small-scale, illegal and unreported fisheries catch 1950-2014. *Sci. Data* 4, 1–9. doi: 10.1038/sdata.2017.39

Watson, R., Revenga, C., and Kura, Y. (2006). Fishing gear associated with global marine catches. II. Trends in trawling and dredging. *Fish. Res.* 79, 103–111. doi: 10.1016/j.fishres.2006.01.013

Watson, R. A., and Tidd, A. (2018). Mapping nearly a century and a half of global marine fishing: 1869–2015. *Mar. Policy* 93, 171–177. doi: 10.1016/j.marpol.2018.04.023

Wilkinson, G. M., Besterman, A., Buelo, C., Gephart, J., and Pace, M. L. (2018). A synthesis of modern organic carbon accumulation rates in coastal and aquatic inland ecosystems. *Sci. Rep.* 8, 1–9. doi: 10.1038/s41598-018-34126-y

Zweng, M. M., Reagan, J. R., Seidov, D., Boyer, T. P., Locarnini, R. A., Garcia, A. V., et al. (2018). *World ocean atlas 2018 volume 2 : salinity*Ed. A. Mishonov (Silver Springs, MD: USA Department of Commerce).

frontiers | Frontiers in Marine Science

TYPE Original Research
PUBLISHED 25 January 2024
DOI 10.3389/fmars.2024.1351657

OPEN ACCESS

EDITED BY
Ruijie Zhang,
Guangxi University, China

REVIEWED BY
Guo Wei,
East China University of Technology, China
Jiapeng Wu,
Guangzhou University, China

*CORRESPONDENCE
Yanpei Zhuang
zhuangyp@jmu.edu.cn
Di Qi
qidi@jmu.edu.cn

RECEIVED 12 December 2023
ACCEPTED 08 January 2024
PUBLISHED 25 January 2024

CITATION
Bu D, Zhu Q, Li J, Huang J, Zhuang Y, Yang W and Qi D (2024) Mariculture may intensify eutrophication but lower N/P ratios: a case study based on nutrients and dual nitrate isotope measurements in Sansha Bay, southeastern China.
Front. Mar. Sci. 11:1351657.
doi: 10.3389/fmars.2024.1351657

Mariculture may intensify eutrophication but lower N/P ratios: a case study based on nutrients and dual nitrate isotope measurements in Sansha Bay, southeastern China

Dezhi Bu[1], Qingmei Zhu[2], Jialin Li[1], Jiali Huang[1], Yanpei Zhuang[1,3]*, Wei Yang[1] and Di Qi[1]*

[1]Polar and Marine Research Institute, College of Harbour and Coastal Engineering, Jimei University, Xiamen, China, [2]College of Ocean and Meteorology, Guangdong Ocean University, Zhanjiang, China, [3]Southern Marine Science and Engineering Guangdong Laboratory (Zhuhai), Zhuhai, China

The mariculture industry has grown rapidly worldwide over the past few decades. The industry helps meet growing food demands and may provide an effective means of carbon sequestration; however, it may harm the marine ecological environment, and the extent of its impact depends on the type of mariculture. Here we focus on the impact of mariculture on the nutrient status and eutrophication in Sansha Bay, which is a typical aquaculture harbor in southeastern China that employs a combination of shellfish and seaweed farming. Nutrient concentrations and dual nitrate isotopes were measured in Sansha Bay during the winter of 2021. The average concentrations of nitrate and phosphate were 31.3 ± 10.5 and 2.26 ± 0.84 μM, respectively, indicating that the water was in a eutrophic state. However, the N/P ratios were relatively low (14.3 ± 2.2). Nitrate isotope measurements were 8.8‰–11.9‰ for δ^{15}N-NO_3^- and 2.2‰–6.0‰ for δ^{18}O-NO_3^-. Source analysis based on the nitrate isotope measurements indicates that nitrate in Sansha Bay is derived mainly from the excretion of organisms and sewage discharge from mariculture. The isotopic fractionation model of nitrate assimilation by organisms indicates that surface waters in Sansha Bay experience strong biological uptake of nitrate, which is likely related to seaweed farming in winter. The low N/P ratios may be attributed to excessive nitrogen uptake (relative to phosphorus) during shellfish and seaweed farming, as well as nitrogen removal through sediment denitrification, which is fueled by the sinking of particulate organic matter from mariculture. Overall, our study shows that mariculture activities dominated by shellfish and seaweed cultivation in Sansha Bay may exacerbate eutrophication but reduce N/P ratios in the water column in aquaculture areas.

KEYWORDS

marine aquaculture, nutrients, N/P ratio, nitrate isotopes, denitrification

1 Introduction

Under the combined influence of global warming and human activities, the open ocean regions of the world's oceans have become more nutrient-poor, whereas coastal areas have become more nutrient-rich (Cloern, 2001; Boyd et al., 2015; Zhuang et al., 2021a). Coastal eutrophication is primarily caused by excessive loading of nitrogen (N) and phosphorus (P). Over the past few decades, the influx of N and P into coastal waters has increased dramatically (Beusen et al., 2022), leading to dramatic ecological and environmental consequences such as the expansion of harmful algal blooms (Glibert et al., 2018) and hypoxia (Wang et al., 2017). In general, nutrients in coastal waters are derived mainly from river input, organic matter regeneration, atmospheric deposition, submarine groundwater discharge, and seasonal transport of water masses (Liu et al., 2012; Lao et al., 2022). Mariculture activities, dominated by the extractive culture of aquatic plants, filter-feeding bivalves, and fed-culture marine finfish and crustaceans, may also contribute to eutrophication in coastal zones (Gao et al., 2021; Beusen et al., 2022).

Owing to the growing global demand for seafood, the scale of mariculture has expanded rapidly in recent decades, and the Food and Agriculture Organization (FAO) predicts that this growth will continue (FAO, 2020). Studies have shown that mariculture may have significant environmental impacts that are closely related to the type of mariculture employed (Zhang et al., 2022; Xiong et al., 2023). Two generally accepted views are that fed culture (i.e., cages and ponds) releases N and P (Wang et al., 2012; Bannister et al., 2016; Carballeira et al., 2018), and photosynthetic seaweed may act as a nutrient sink (Xiao et al., 2017). The nitrogen discharged into the water as mariculture feed each year may reach levels as high as 2.1×10^6 tons, but most of the feed is not utilized by cultured organisms (Williams and Crutzen, 2010), thus promoting eutrophication in coastal waters. In contrast, mariculture systems involving seaweed cultivation can absorb nutrients through photosynthesis, converting nutrient-rich waters into beneficial resources and somewhat offsetting the environmental impact of heterotrophic fish and shrimp farming (Jiang et al., 2020). Furthermore, seaweed cultivation is widely recognized, not only for providing food and biofuels, but also for removing CO_2 from seawater, thus increasing the ocean's carbon absorption capacity and providing new potential means for carbon neutrality (Zhang et al., 2017; Gao et al., 2021). These studies emphasize the need to better understand the impact of mariculture systems involving seaweed cultivation on the nutrient dynamics of coastal waters in our quest to adopt sustainable and environmentally friendly mariculture models.

Sansha Bay is a semi-enclosed bay located in the coastal area of the East China Sea. It is known for its seaweed-based mariculture systems and is referred to as the "hometown of Chinese nori" and the "hometown of Chinese kelp" (Chen et al., 2013). The bay experiences minimal winter runoff, and its hydrography is primarily influenced by the China Coastal Current (CCC) in winter. The nutrient concentrations of the bay waters are more heavily affected by mariculture activities than other factors such as ocean currents owing to the narrow outlet connecting the bay to the open ocean (Han et al., 2021). *Larimichthys crocea* is the main species of fish cultured in the bay, and millions of tons of feed are required annually to maintain the fish culture (Xie et al., 2020). However, approximately 5%–10% of the feed decomposes in the water (Duan et al., 2001). Han et al. (2021) observed that the Sansha Bay water mass had relatively low salinity compared with the East China Sea Shelf Water and the CCC but much higher nutrient concentrations than other water masses in this coastal area, and they suggested this disparity may be due to the influence of intensive mariculture activities. These factors make Sansha Bay an ideal location for studying the environmental impact of mixed mariculture systems involving seaweed cultivation. The biogeochemical processes of nutrients in Sansha Bay are complicated; however, systematic biogeochemical studies are lacking.

The abundance of ^{15}N and ^{18}O in nitrates ($\delta^{15}N\text{-}NO_3^-$ and $\delta^{18}O\text{-}NO_3^-$) is useful for identifying the sources and biological transformations of N in coastal ecosystems (Wankel et al., 2009; Chen et al., 2022a; Tian et al., 2022). In this study, nutrients and dual nitrate isotopes ($\delta^{15}N\text{-}NO_3^-$, $\delta^{18}O\text{-}NO_3^-$) were measured in the waters of Sansha Bay during the winter of 2021. In addition, a Bayesian stable isotope mixing model was used to calculate the relative contributions from several nitrate sources. Our overall aims were to (1) determine the eutrophication status of the bay's winter seawater; (2) identify the ranges of dual nitrate isotope values and assess the main sources of nitrate in Sansha Bay; and (3) evaluate the impact of seaweed-based aquaculture on the nutrient dynamics of the bay waters.

2 Materials and methods

2.1 Study area

Sansha Bay (26°30′–26°58′E, 119°26′–120°10′N) is located on the northeast coast of Fujian Province, China (Figure 1). The surface current outside Sansha Bay is influenced by the CCC in winter and the South China Sea Warm Current (SCSWC) in summer. In late autumn and winter, seawater from the East China Sea or from farther north of China is transported along the coast under the influence of winter winds. In addition, observations based on radium isotopes (^{226}Ra and ^{228}Ra) have shown that groundwater input in Sansha Bay also affects the nutrient flux (Wang et al., 2018). Seasonal activities such as seeding, growing, and harvesting on the densely clustered floating mariculture mats in the bay also have a substantial effect on the spatial–temporal distribution of its hydrochemical parameters (Wang et al., 2018). In addition, driven by the Asian monsoon, the hydrographic characteristics of Sansha Bay were significantly influenced by the plume water of the Jiao River, which showed the highest freshwater discharge rate in warm months (from April to September) and the lowest in cold months (from October to April the following year). Han et al. (2021) observed a water mass with relatively lower salinity than CCC meandering in Sansha Bay and influenced by intensive mariculture activities, nutrient concentrations in this Bay were much higher than other water masses in this coastal area.

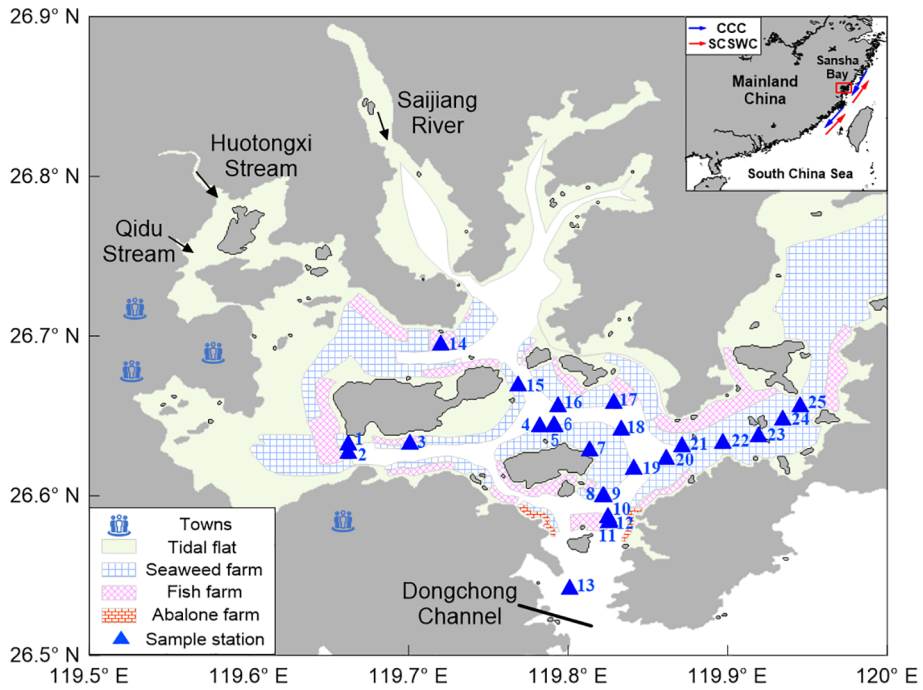

FIGURE 1
Location maps and sampling sites in Sansha Bay in December 2021. The top right inset shows a schematic trajectory of the surface current outside Sansha Bay, with the China Coastal Current (CCC, blue arrows) in winter and the South China Sea Warm Current (SCSWC, red arrows) in summer (Han et al., 2021). Sample stations are indicated by blue solid triangles. Light green areas represent tidal flats, and the various grids represent different types of mariculture.

2.2 Sampling strategy

A research cruise was carried out in Sansha Bay on 11–12 December, 2021 (Figure 1). Water samples were collected at 25 stations using a 5L Niskin bottle guided by a Conductivity–Temperature–Depth (CTD; Seabird® WQM 2019) recorder, which simultaneously measured sea surface temperature (SST) and salinity (SSS). Salinity in the water column samples was determined using a portable salinometer (Portasal 8410A, Guildline Co., Canada) and used to calibrate data from the CTD recorder. Water samples were obtained from two or three depth layers at each sampling site, depending on the overall water depth. "Surface waters" refer to waters 1 m below the surface, and "bottom waters" denote waters 1 m above the sediment bed.

2.3 Nutrient analysis

Nutrient samples were filtered using cellulose acetate membranes with a pore size of 0.45 μm that had been acid-cleaned. Two hundred and fifty mL of filtered seawater was frozen and stored at −20°C and used for routine spectrophotometric analysis of NO_3^-, NO_2^-, PO_4^{3-}, and $Si(OH)_4$ concentrations using the Technicon AA3 automatic analyzer (Bran-Lube, GmbH; Han et al., 2021). Concentrations of NO_3^- + NO_2^- were determined using a Cu–Cd column reduction method, and NO_2^- contents were determined using spectrophotometry with standard pink azo dye (Dai et al., 2008). Concentrations of PO_4^{3-} and $Si(OH)_4$ were measured using standard spectrophotometric methods (Knap et al., 1996). The detection limits for NO_3^- + NO_2^-, PO_4^{3-}, and $Si(OH)_4$ were 0.1, 0.08, and 0.08 μM, respectively. The relative standard deviations (RSD) of repeat measurements of selected samples were<5%.

2.4 Analysis of nitrate isotopes

Isotope analyses of NO_3^- were carried out according to the method of Sigman et al. (2001) and Casciotti et al. (2002) (Equations 1 and 2) using an isotope-ratio mass spectrometer (IRMS). The international nitrate reference materials NITS USGS34 ($\delta^{15}N$ = −1.8‰; $\delta^{18}O$ = −27.9‰) and NITS USGS35 ($\delta^{15}N$ = 2.7‰; $\delta^{18}O$ = 57.5‰) were used to correct for drift, oxygen isotopic exchange, and blanks. The average standard deviation was typically 0.2‰ for $\delta^{15}N$ and 0.5‰ for $\delta^{18}O$, which is applicable to samples with NO_3^- concentrations ≥ 1 μM. Isotope ratios are reported in delta (δ) notation in units of per mil (‰):

$$\delta^{15}N(‰) = \left[\frac{(15_N/14_N)_{sample}}{(15_N/14_N)_{reference}} - 1\right] \times 100 \quad (1)$$

$$\delta^{18}O(‰) = \left[\frac{(18_N/16_N)_{sample}}{(18_N/16_N)_{reference}} - 1\right] \times 1000 \quad (2)$$

where $(15_N/14_N)_{reference}$ denotes N_2 in air and $(18_N/16_N)_{reference}$ denotes Vienna Standard Mean Ocean Water (VSMOW).

2.5 Potential eutrophication

Phytoplankton absorbs nutrients from seawater according to the Redfield ratio (Redfield, 1963), leaving relative excess of nitrogen or phosphorus. Excess nitrogen or phosphorus do not have direct contribution to eutrophication but could be considered as a potential factor, known as potential eutrophication (Sun et al., 2006). In order to highlight the limiting characteristics of nutrient salts, dissolved inorganic nitrogen (DIN, including NO_3^-, NO_2^- and NH_4^+) and active phosphate (PO_4^{3-}), which play a bottleneck role in phytoplankton growth (Zhuang et al., 2021b), were selected as evaluation parameters. The potential eutrophication evaluation model (Table 1, Guo et al., 1998; Sun et al., 2016; Yang et al., 2020) was adopted for the evaluation of the nutrient condition in the study area.

2.6 Calculation of N*

To evaluate the nitrate deficit, we used the parameter N* proposed by Gruber and Sarmiento (1997), where $N^* = ([NO_3^-] - 16^*[PO_4^{3-}] + 2.9) \times 0.87$. In the equation, 16 is the Redfield ratio of 16:1, and 0.87 is a calculated factor based on the specific stoichiometric ratios in denitrification and remineralization processes. The constant (2.9) was introduced to set the mean N* to zero and is based on global measurements (Gruber and Sarmiento, 1997). The N* index reflects the net effect of N_2 fixation and denitrification, and negative N* values imply a nitrate deficit in the ocean (Deutsch and Weber, 2012).

2.7 Stable isotope analysis in R mixing model

SIAR (stable isotope analysis in R) is a software package that uses a Bayesian stable isotope mixing model, which is used to calculate the relative proportion of various nitrate sources. In the mixing model, the Bayesian framework is utilized to calculate the probability distribution amongst the different nitrate sources. The model framework is as follows:

$$X_{ij} = \sum_{k=1}^{k} P_k(S_{jk} + C_{jk}) + \epsilon_{ij} \quad (3)$$

$$S_{jk} \sim N(\mu_{jk}, \omega_{jk}^2)$$

$$C_{jk} \sim N(\lambda_{jk}, \tau_{jk}^2)$$

$$\epsilon_{jk} \sim N(0, \sigma_j^2)$$

where X_{ij} denotes the isotope values (j = 2, $\delta^{15}N\text{-}NO_3^-$, and $\delta^{18}O\text{-}NO_3^-$) of the sample i (i = 1, 2, 3, … N); S_{jk} is the isotope value j of the source k (k = 1, 2, 3, … K) and is normally distributed with an average μ_{jk} and standard deviation ω_{jk}; P_k is the proportion of source k, as calculated using the SIAR model; C_{jk} is the fractionation factor for j on source k and is normally distributed with an average λ_{jk} and standard deviation τ_{jk}; ϵ_{jk} is the residual error of the additional unquantified variations between individual samples and is normally distributed with an average 0 and standard deviation σ_j. The model uses CSV Microsoft Excel of $\delta^{15}N\text{-}NO_3^-$ and $\delta^{18}O\text{-}NO_3^-$, S_{jk}, and C_{jk} as inputs. It then outputs numerical and graphical depictions of the relative contributions of the potential sources (Zhang et al., 2018) (Equation 3). More detailed information of the Bayesian stable isotope mixing model has been provided by Moore and Semmens (2008); Xue et al. (2009), and Zhang et al. (2018).

3 Results

The water depth in Sansha Bay ranges from 8 to 50 meters (Figure 2A). During winter, water temperatures at the survey stations in Sansha Bay range from 17.8 to 18.6°C, with an average of 18.4 ± 0.1°C, and salinity ranges from 20.25 to 21.99, with an average of 21.45 ± 0.45 (Figures 2B, C; Supplementary Figure 1). There were only very small horizontal and vertical variations in temperature and salinity within the bay (Supplementary Figure 2), indicating a relatively homogeneous hydrographical property. The small amount of winter runoff from rivers into Sansha Bay

TABLE 1 The evaluation standards for potential eutrophication.

Grade	Nutrient level	DIN (μmol L^{-1})	DIP (μmol L^{-1})	DIN/DIP
I	Oligotrophic level	<14.28	<0.97	8-30
II	Moderate-level nutrient	14.28-21.41	0.97-1.45	8-30
III	Eutrophication	>21.41	>1.45	8-30
IV_p	Phosphate-limiting moderate-level nutrient	14.28-21.41	/	>30
V_p	Phosphate moderate limiting potential eutrophication	>21.41	/	30-60
VI_p	Phosphate-limiting potential eutrophication	>21.41	/	>60
IV_N	Nitrogen-limiting moderate-level nutrient	/	0.97-1.45	<8
V_N	Nitrogen moderate limiting potential eutrophication	/	>1.45	4-8
VI_N	Nitrogen-limiting potential eutrophication	/	>1.45	<4

(Supplementary Figure 3), the influence of riverine inputs on the physicochemical properties of the water is minimal, as reflected by the distribution patterns of temperature and salinity.

During the investigation, nitrate concentrations at the Sansha Bay survey stations ranged from 8.4 to 44.9 μM, with an average concentration of 31.3 ± 10.5 μM, phosphate concentrations ranged from 0.46 to 3.61 μM, with an average concentration of 2.26 ± 0.84 μM, and silicate concentrations ranged from 9.8 to 52.9 μM, with an average concentration of 32.8 ± 11.3 μM (Figures 2D–F; Supplementary Figure 1). The lowest nutrient concentrations in the surface and bottom waters were recorded at the mouth of Sansha Bay.

The NO_3^-/PO_4^{3-} ratios in the water at the survey stations ranged from 9.3 to 20.0, with an average value of 14.3 ± 2.2, which is lower than the Redfield ratio (16:1). The highest NO_3^-/PO_4^{3-} ratios in surface and bottom layers were observed at the mouth of Sansha Bay, corresponding to the lowest nutrient concentrations (Figure 2G; Supplementary Figure 1). The NO_3^-/PO_4^{3-} ratios in the bay were lower than those at the bay mouth, suggesting that biogeochemical processes modify the nutrient structure in the bay. During the investigation, the NO_3^-/DSi ratios in the water ranged from 0.6 to 1.1, with an average value of 0.96 ± 0.11, which is close to the Redfield ratio (1:1).

In winter, the $\delta^{15}N\text{-}NO_3^-$ values in Sansha Bay were 8.8‰–11.9‰, with an average value of 9.8‰ ± 0.6‰. $\delta^{18}O\text{-}NO_3^-$ values were 2.2‰–6.0‰, with an average value of 4.0‰ ± 0.8‰ (Figures 2H–I). There is a positive correlation between $\delta^{15}N\text{-}NO_3^-$ and $\delta^{18}O\text{-}NO_3^-$ in surface waters (using the equation $\delta^{18}O\text{-}NO_3^- = 0.70 \times \delta^{15}N\text{-}NO_3^- - 2.9$), indicating either a relatively uniform source of surface nitrate or that similar biogeochemical processes were active (Figure 3A). However, there is no significant correlation between $\delta^{15}N\text{-}NO_3^-$ and $\delta^{18}O\text{-}NO_3^-$ values in bottom waters (Figure 3B). As observed in the nutrient distribution pattern, $\delta^{15}N\text{-}NO_3^-$ and $\delta^{18}O\text{-}NO_3^-$ values were higher in the mariculture area within the bay and lower at the bay mouth.

4 Discussion

4.1 Nutrient status of Sansha Bay in winter

The winter waters in Sansha Bay, like most coastal harbors affected by the CCC in southeastern China, appear to be characterized by eutrophication (e.g., Cai et al., 2013; Yang et al., 2018). Approximately 81% of the data points (50/62) in this study exceeded the thresholds for eutrophication in harbor waters proposed by Guo et al. (Guo et al., 1998; NO_3^- >21.4 μM, PO_4^{3-}>1.45 μM), indicating that most of the winter water in Sansha Bay was eutrophic (Figure 4). The small amount of winter run off from rivers into Sansha Bay and another area of low surface nutrient concentrations was found at the mouth of the Sai River, suggesting that winter river input does not greatly influence nutrient levels in the bay. The lowest nutrient concentrations in the surface and bottom waters were recorded at the mouth of Sansha Bay., indicating that offshore water input may not be the main source of nutrients into the bay. Areas of high nutrient concentrations were observed mainly in mariculture areas, indicating that mariculture activities contribute to nutrient levels in the bay. The influence of the winter CCC extends from 26°N to 35°N along the southeastern coast (Wang et al., 2003).

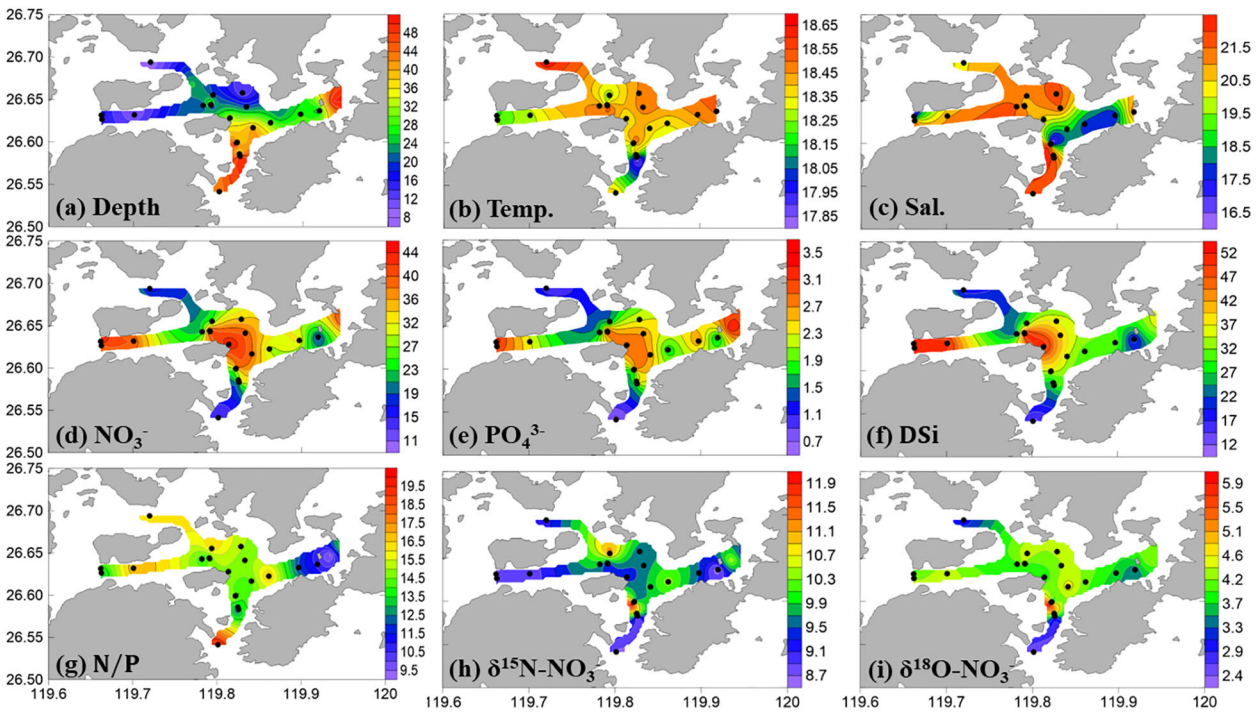

FIGURE 2
Surface distributions of **(A)** station depth (m), **(B)** temperature (°C), **(C)** salinity, **(D)** NO_3^- (μM), **(E)** PO_4^{3-} (μM), **(F)** Dsi (μM), **(G)** NO_3^-/PO_4^{3-}, **(H)** $\delta^{15}N\text{-}NO_3^-$, and **(I)** $\delta^{18}O\text{-}NO_3^-$ in Sansha Bay in winter 2021.

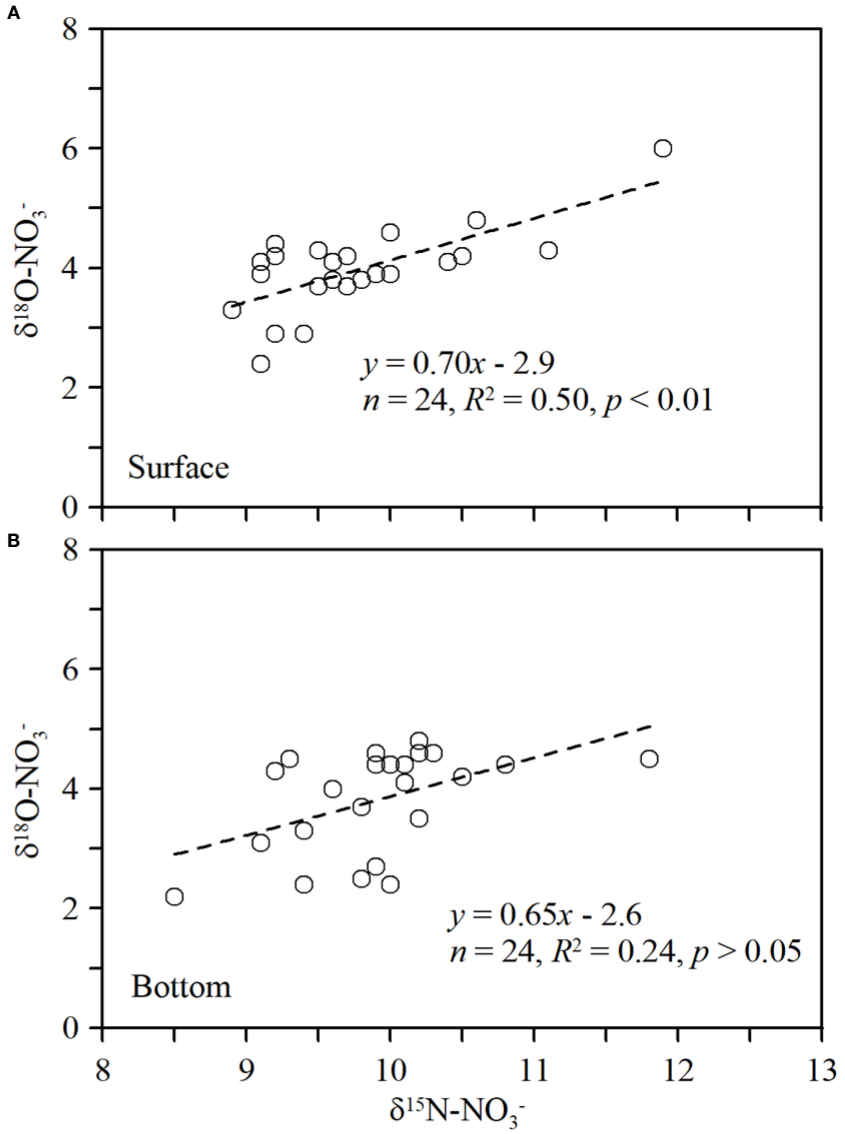

FIGURE 3
Relationship between δ^{15}N-NO_3^- and δ^{18}O-NO_3^- in surface **(A)** and bottom **(B)** waters in Sansha Bay in winter.

As shown in Figure 5, the NO_3^-/PO_4^{3-} ratios in CCC-influenced harbors along the southeastern coast of China generally decrease from north to south. Owing to the input of nutrients from the Yangtze River, NO_3^-/PO_4^{3-} ratios can exceed 80 in the winter waters of the Yangtze River estuary (Liu et al., 2009). The CCC carries signals from the land sources of the Yangtze River and a large volume of nutrients to the southeastern coastal harbors during winter, which is one of the main reasons for the high N/P ratios in these harbors (Yang et al., 2018). The NO_3^-/PO_4^{3-} ratios in Hangzhou Bay, Xiangshan Bay, and Sanmen Bay are relatively similar (Cai et al., 2013; Wu et al., 2020) and lower than those of the Yangtze River estuary, but they further decrease to 14.3 ± 2.2 in Sansha Bay (Figure 5; Supplementary Table 1).

The winter waters of Sansha Bay have lower NO_3^-/PO_4^{3-} and NO_3^-/DSi ratios than many other nearshore harbors influenced by the CCC (Supplementary Table 1). Correlation analysis showed significant positive relationships between concentrations of NO_3^- and both PO_4^{3-} and DSi (Figure 4). The relationship between NO_3^- and PO_4^{3-} concentrations was examined by linear regression and indicates that NO_3^- concentrations increased with increasing PO_4^{3-}; however, the slope was only 11.5, lower than the Redfield ratio (Figure 4A). Similarly, NO_3^- concentrations increased with increasing DSi, with a slope of 0.9 (Figure 4A). These results indicate that the winter waters of Sansha Bay are eutrophic but have relatively low N/P ratios.

The distribution of the N* index reflects the excess (positive values) or deficiency (negative values) of nitrate relative to phosphate (Deutsch and Weber, 2012). The N* values decrease gradually along the southeastern coast, with values approaching 0 in Sansha Bay, indicating that strong denitrification processes occur as the excess nitrate flows southward and enters coastal harbors.

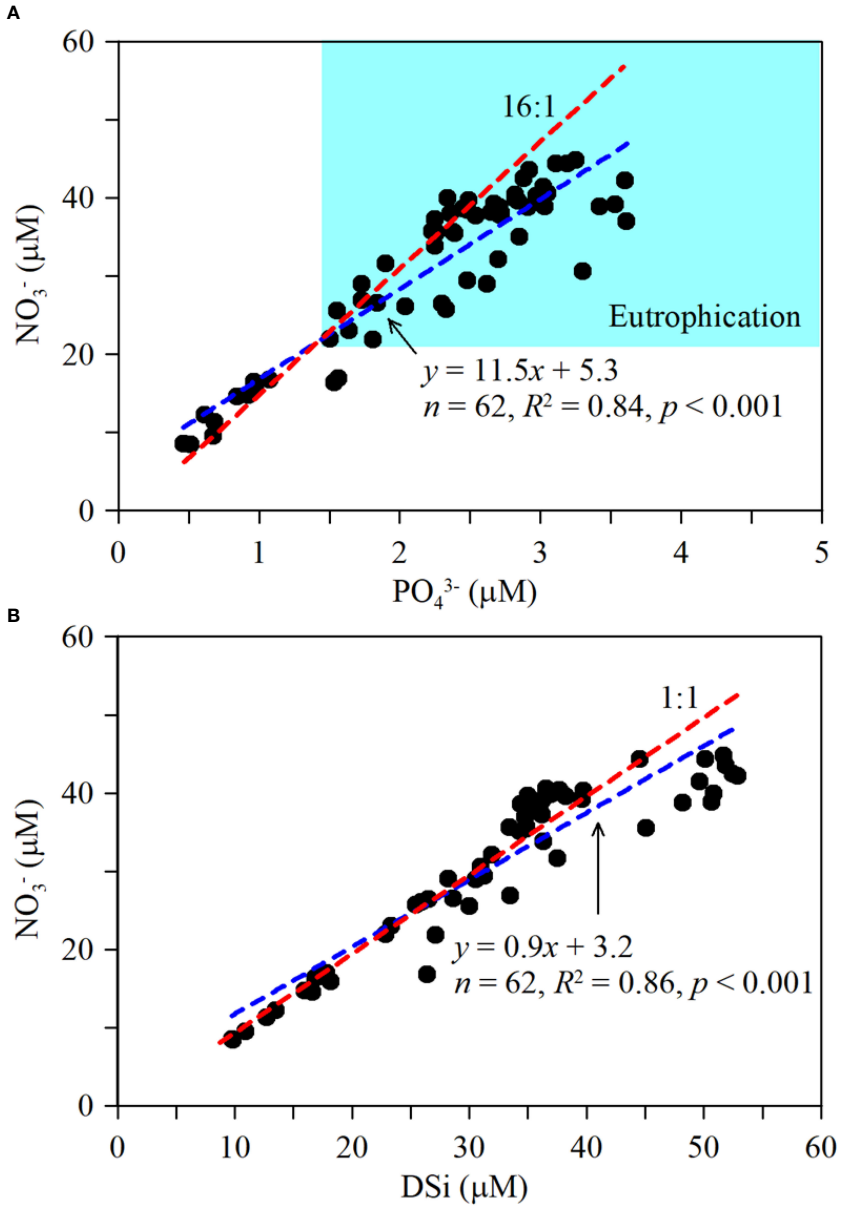

FIGURE 4
Relationship between **(A)** NO_3^- (μM) and PO_4^{3-} (μM), **(B)** NO_3^- and DSi (μM). Dashed red lines represent the Redfield ratios of NO_3^-/PO_4^{3-} = 16:1 and NO_3^-/DSi = 1:1. Dashed blue lines represent linear regression lines.

This may be related to intense nitrogen removal via sedimentary denitrification (Li et al., 2021). Indeed, observations show that denitrification at the mouth of the Yangtze River is the main pathway for the removal of excess nitrogen, with nitrogen removal rates reaching up to 28.49 ng N $g^{-1}{\cdot}h^{-1}$ (Li et al., 2021).

4.2 Sources and biochemical transformation of nitrate in Sansha Bay waters

Based on the dual isotope method for nitrate source identification (Kendall et al., 2007; Xue et al., 2009), the $\delta^{15}N\text{-}NO_3^-$ (8.8‰–11.9‰) and $\delta^{18}O\text{-}NO_3^-$ (2.2‰–6.0‰) values in Sansha Bay waters (Figure 6) suggest that the main sources of nitrate are manure and sewage, as evidenced by the more positive $\delta^{15}N\text{-}NO_3^-$ values. The $\delta^{15}N\text{-}NO_3^-$ values are lower at the mouths of the main rivers entering the bay (Figure 2) when the river input is low (Supplementary Figure 3), suggesting that the more positive anthropogenic signal may be introduced by mariculture activities within the bay. Previous studies have suggested that the main sources of nutrients in Sansha Bay during winter are the eutrophic coastal currents and mariculture inputs (Han et al., 2021); however, the extent of the latter depends heavily on the type of mariculture. Jiang et al. (2020) found that seaweed aquaculture in Xiangshan Bay absorbed nutrients and alleviated eutrophication. The type of mariculture may also affect

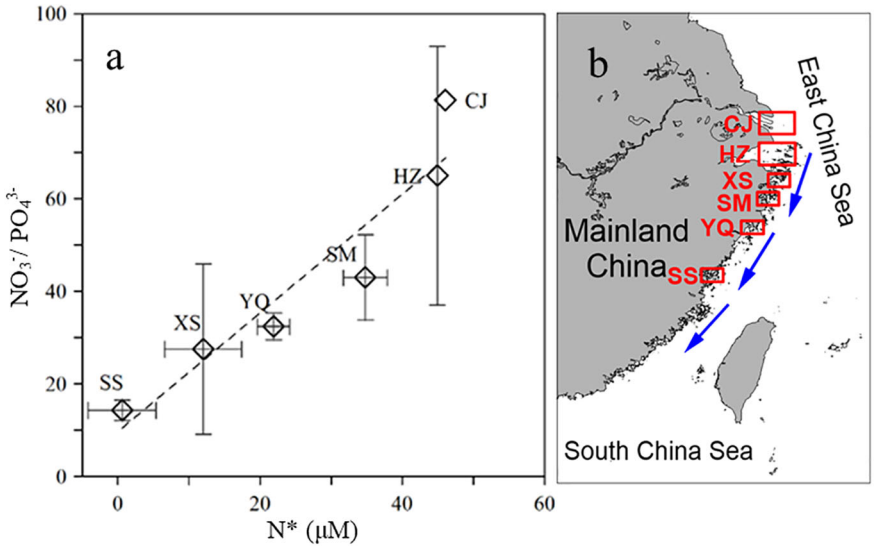

FIGURE 5
(A) North–south variations in NO_3^-/PO_4^{3-} and N* (μM), as measured in the coastal ports of Southeast China, which are under the influence of the CCC. **(B)** Geographical locations of the coastal harbors of Southeast China. Dashed lines represent linear regression lines. CJ: Changjiang estuary, HZ: Hangzhou Bay, XS: Xiangshan Bay, SM: Sanmen Bay; YQ: Yueqing Bay, SS: Sansha Bay.

the distribution of dual nitrate isotopes. In Xiangshan Bay, where seaweed aquaculture is dominant, $\delta^{15}N\text{-}NO_3^-$ and $\delta^{18}O\text{-}NO_3^-$ values range from 5.7‰ to 8.8‰ and from 1.8‰ to 6.8‰, respectively (Yang et al., 2018). In Laizhou Bay, where sea cucumber aquaculture is dominant, $\delta^{15}N\text{-}NO_3^-$ and $\delta^{18}O\text{-}NO_3^-$ values range from 2.0‰ to 11.8‰ and from −7.8‰ to 12.6‰, respectively (Kang and Xu, 2016).

The application of Bayesian mixing models reveals that the surface water in Sansha Bay has a mixture of sources (Supplementary Figure 4), which poses a challenge for nitrate source analysis. According to previous studies, the main nitrate sources in water are likely manure and sewage, reduced nitrogen fertilizer, nitrate derived from soil nitrogen, and atmospheric deposition (Dai et al., 2008; Ye et al., 2016). The relative contributions of these four potential nitrate sources have been calculated in many studies across a broad range of study areas (e.g., Moore and Semmens, 2008; Xue et al., 2012; Zhang et al., 2018; Lao et al., 2019). Therefore, we calculated the potential sources of nitrate using $\delta^{15}N\text{-}NO_3^-$ and $\delta^{18}O\text{-}NO_3^-$ values in a Bayesian isotope mixing model (Chen et al., 2022b). The uncertainty associated with these calculations is difficult to constrain with the present data because (a) the range of isotopic values from potential nitrate sources is relatively large (Supplementary Table 2), and (b) the end-members of the potential nitrate sources originate from the reference literature and not from the measurement of samples in Sansha Bay. Nevertheless, such an estimate can provide an insight into nitrate sources in Sansha Bay. The end-member values for the potential nitrate sources are presented in Supplementary Table 2, and the results are shown in Figure 6. The results suggest that manure and sewage were the predominant sources of nitrate in the surface waters of Sansha Bay (51%–75%, average 63%), followed by soil organic nitrogen (3%–45%, average 26%) and reduced nitrogen fertilizer (0%–24%, average 11%).

4.3 Impact of mariculture on nutrient loading and N/P ratios

Mariculture activities are commonplace in the harbors along the southeastern coast of China and include kelp farming in Xiangshan Bay (Yang et al., 2018), mixed crab and seaweed farming in Sanmen Bay (Cai et al., 2013), and mixed shellfish and seaweed farming in Sansha Bay (Han et al., 2021). Most mariculture activities increase nutrient loading in water owing to the excretion of farmed organisms and the addition of feed (Bouwman et al., 2013). In this study, the higher nutrient concentrations in Sansha Bay compared with the bay mouth suggest nutrient loading from mariculture. However, the low NO_3^-/PO_4^{3-} ratios in Sansha Bay compared with the bay mouth indicate the possibility of denitrification in the bay, which may be caused by the structural modification of nutrients, potentially owing to seaweed farming. Zhang et al. (2022) suggested that seaweed farming may increase N/P ratios, whereas bivalve farming may decrease N/P ratios. Overall, the N/P ratio of nutrients removed by mariculture is close to 18. In Sansha Bay, where mixed shellfish and seaweed farming occurs, excess nitrate (relative to phosphate) may be absorbed during mariculture activities under conditions of sufficient nitrogen, and excess nitrogen may be removed from the water during the harvest season (Han et al., 2021).

Previous studies have shown that when algae have high rates of nitrate assimilation, the $\delta^{15}N$ of the remaining nitrate will increase significantly owing to the preferential utilization of ^{14}N by the organism (Ahad et al., 2006; Chen et al., 2013). Average $\delta^{15}N\text{-}NO_3^-$ values in Sansha Bay during winter were as high as 9.8‰ ± 0.6‰, higher than the spring ratios measured in the Yangtze River Estuary (6.9‰, Chen et al., 2013) and the Pearl River Estuary (2.2‰–4.4‰, Chen et al., 2022b). These values are also higher than those measured in the upper bay area of Xiangshan Bay, where kelp

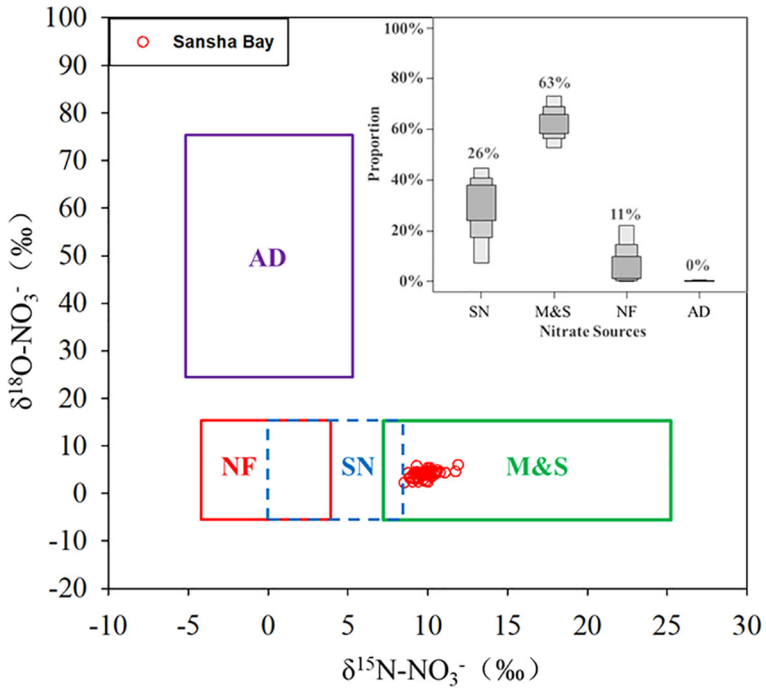

FIGURE 6
Cross plot of $\delta^{15}N\text{-}NO_3^-$ and $\delta^{18}O\text{-}NO_3^-$ values in the surface water samples of Sansha Bay (red dots) and the relative proportions of potential nitrate sources (atmospheric deposition, AD; manure and sewage, M&S; soil organic nitrogen, SN; and N fertilizer, NF), as calculated using the Bayesian isotopic mixing model. The isotopic compositions of the various sources are based on Kendall (1998) and Zhang et al. (2018).

farming is predominant (8.1‰ ± 0.5‰), and the lower bay area, which is significantly influenced by dilution via input from the Yangtze River (6.2‰ ± 0.3‰) (Yang et al., 2018). These results indicate that Sansha Bay experiences strong biological absorption and transformation of nitrate.

The intense biological production and deposition of organic debris in the surface layer during seaweed cultivation provides abundant organic matter to the sediment (Zhuang et al., 2022). The re-mineralization of this organic matter may enhance sedimentary denitrification (Wu et al., 2021), thus removing more nitrogen (while phosphates remain unaffected) and reducing N/P ratios. Denitrification enriches the residual nitrate, with $\delta^{15}N$ and $\delta^{18}O$ having a ratio close to 2:1 (Kendall, 1998; Mengis et al., 1999). The higher $\delta^{15}N\text{-}NO_3^-$ and $\delta^{18}O\text{-}NO_3^-$ values in the bottom waters of the mariculture area in Sansha Bay compared with the surface waters support the idea that denitrification processes are occurring in the sediment (Figure 3). These findings suggest that in areas where shellfish and seaweed are cultivated, the strong absorption of nitrate by organisms and enhanced sedimentary denitrification stimulated by the downward settling of organic matter result in the reduction of N/P ratios in the water.

5 Conclusion

The average concentrations of nitrate and phosphate in Sansha Bay during winter 2021 were 31.3 ± 10.5 and 2.26 ± 0.84 μM, respectively, indicating eutrophic conditions. However, N/P ratios were relatively low, with an average of only 14.3 ± 2.2. Nitrate isotope ratios in Sansha Bay were 8.8‰–11.9‰ for $\delta^{15}N\text{-}NO_3^-$ and 2.2‰–6.0‰ for $\delta^{18}O\text{-}NO_3^-$. Based on the nitrate isotopes, it is suggested that the main sources of nitrate in Sansha Bay are likely sewage discharge and biological excretion associated with mariculture activities. Therefore, mariculture has contributed to the eutrophication of the water. However, the isotopic fractionation model of nitrate assimilation by organisms indicates that strong biological uptake of nitrate is occurring in the surface waters of Sansha Bay, possibly owing to extensive algal cultivation during winter. The low N/P ratios of Sansha Bay may be attributed to excessive nitrogen uptake by shellfish and algae cultivation, as well as the introduction of organic matter from algal cultivation, which enhances denitrification and nitrogen removal in sediments. Therefore, aquaculture activities in Sansha Bay may exacerbate eutrophication while also altering nutrient compositions and reducing N/P ratios.

Data availability statement

The raw data supporting the conclusions of this article will be made available by the authors, without undue reservation.

Author contributions

DB: Writing – original draft. QZ: Writing – review & editing, Data curation, Methodology. JL: Writing – review & editing, Methodology. JH: Writing – review & editing, Data curation, Methodology. YZ: Writing – review & editing. WY: Writing – review & editing, Investigation. DQ: Writing – review & editing.

Funding

This study was funded by National Key Research and Development Program of China (2023YFC3108102), Fujian Provincial Science and Technology Plan & Natural Science Foundation of Fujian Province (2023J06036), and the Fujian Provincial Department of Education - Sea Economy government, industry, University and research alliance (FOCAL2023-0101) the Ocean Negative Carbon Emissions (ONCE) Program.

Conflict of interest

The authors declare that the research was conducted in the absence of any commercial or financial relationships that could be construed as a potential conflict of interest.

Publisher's note

Supplementary material

The Supplementary Material for this article can be found online at: https://www.frontiersin.org/articles/10.3389/fmars.2024.1351657/full#supplementary-material

References

Ahad, J. M. E., Ganeshram, R. S., Spencer, R. G. M., Uher, G., Upstill-Goddard, R. C., and Cowie, G. L. (2006). Evaluating the sources and fate of anthropogenic dissolved inorganic nitrogen (DIN) in two contrasting North Sea estuaries. *Sci. Total Environ.* 372, 317–333. doi: 10.1016/j.scitotenv.2006.09.018

Bannister, R. J., Johnsen, I. A., Hansen, P. K., Kutti, T., and Asplin, L. (2016). Near- and far-field dispersal modelling of organic waste from Atlantic salmon aquaculture in fjord systems. *ICES J. Mar. Sci.* 73, 2408–2419. doi: 10.1093/icesjms/fsw027

Beusen, A., Doelman, J., Van Beek, L., Van Puijenbroek, P., Mogollón, J., Van Grinsven, H., et al. (2022). Exploring river nitrogen and phosphorus loading and export to global coastal waters in the Shared Socio-economic pathways. *Global Environ. Change* 72, 102426. doi: 10.1016/j.gloenvcha.2021.102426

Bouwman, L., Beusen, A., Glibert, P. M., Overbeek, C., Pawlowski, M., Herrera, J., et al. (2013). Mariculture: significant and expanding cause of coastal nutrient enrichment. *Environ. Res. Lett.* 8, 044026. doi: 10.1088/1748-9326/8/4/044026

Boyd, P. W., Lennartz, S. T., Glover, D. M., and Doney, S. C. (2015). Biological ramifications of climate-change-mediated oceanic multi-stressors. *Nat. Climate Change* 5, 71–79. doi: 10.1038/nclimate2441

Cai, X., Pan, J., Yu, P., Liu, X., and Sun, W. (2013). The behavior of nutrients in different harbors in coastal waters of Zhejiang province. *Mar. Sci. Bull.* 32 (5), 488–493. doi: 10.11840/j.issn. 1001-6392.2003.05.002

Carballeira, C., Cebro, A., Villares, R., and Carballeira, A. (2018). Assessing changes in the toxicity of effluents from intensive marine fish farms over time by using a battery of bioassays. *Environ. Sci. Pollut. Res.* 25, 12739–12748. doi: 10.1007/s11356-018-1403-x

Casciotti, K. L., Sigman, D. M., Hastings, M. G., Böhlke, J., and Hilkert, A. (2002). Measurement of the oxygen isotopic composition of nitrate in seawater and freshwater using the denitrifier method. *Anal. Chem.* 74, 4905–4912. doi: 10.1021/ac020113w

Chen, C., Lao, Q., Shen, Y., Jin, G., Chen, F., Su, Q., et al. (2022a). Comparative study of nitrogen cycling between a bay with riverine input and a bay without riverine input, inferred from stable isotopes. *Front. Mar. Sci.* 9, 885037. doi: 10.3389/fmars.2022.885037

Chen, F., Chen, J., Jia, G., Jin, H., Xu, J., Yang, Z., et al. (2013). Nitrate δ 15 N and δ 18 O evidence for active biological transformation in the Changjiang Estuary and the adjacent East China Sea. *Acta Oceanol. Sin.* 32, 11–17. doi: 10.1007/s13131-013-0294-4

Chen, F., Deng, Z., Lao, Q., Bian, P., Jin, G., Zhu, Q., et al. (2022b). Nitrogen cycling across a salinity gradient from the pearl river estuary to offshore: Insight from nitrate dual isotopes. *J. Geophys. Res.: Biogeosci.* 127, e2022JG006862. doi: 10.1029/2022JG006862

Cloern, J. E. (2001). Our evolving conceptual model of the coastal eutrophication problem. *Mar. Ecol. Prog. Ser.* 210, 223–253. doi: 10.3354/meps210223

Dai, M., Wang, L., Guo, X., Zhai, W., Li, Q., He, B., et al. (2008). Nitrification and inorganic nitrogen distribution in a large perturbed river/estuarine system: the Pearl River Estuary, China. *Biogeosciences* 5, 1227–1244. doi: 10.5194/bg-5-1227-2008

Deutsch, C., and Weber, T. (2012). Nutrient ratios as a tracer and driver of ocean biogeochemistry. *Annu. Rev. Mar. Sci.* 4, 113–141. doi: 10.1146/annurev-marine-120709-142821

Duan, Q., Mai, K., Zhong, H., Si, L., and Wang, X. (2001). Studies on the nutrition of the large yellow croaker, Pseudosciaena crocea R. I: growth response to graded levels of dietary protein and lipid. *Aquacult. Res.* 32, 46–52. doi: 10.1046/j.1355-557x.2001.00048.x

FAO. (2020). *The State of World Fisheries and Aquaculture 2020. Sustainability in action* (Rome: Agriculture Organization of the United Nations. Fisheries Department). doi: 10.4060/ca9229en

Gao, G., Gao, L., Jiang, M., Jian, A., and He, L. (2021). The potential of seaweed cultivation to achieve carbon neutrality and mitigate deoxygenation and eutrophication. *Environ. Res. Lett.* 17, 014018. doi: 10.1088/1748-9326/ac3fd9

Glibert, P. M., Al-Azri, A., Icarus Allen, J., Bouwman, A. F., Beusen, A. H., Burford, M. A., et al. (2018). Key questions and recent research advances on harmful algal blooms in relation to nutrients and eutrophication. *Global Ecology and Oceanography of Harmful Algal Blooms, Ecological Studies* 232, 229–259. doi: 10.1007/978-3-319-70069-4_12

Gruber, N., and Sarmiento, J. L. (1997). Global patterns of marine nitrogen fixation and denitrification. *Global Biogeochem. cycles* 11, 235–266. doi: 10.1029/97GB00077

Guo, W., Zhang, X., Yang, Y., and Hu, M. (1998). Potential eutrophication assessment for Chinese coastal waters. *J. Oceanogr. Taiwan Strait/Taiwan Haixia* 17, 64–70.

Han, A., Kao, S. J., Lin, W., Lin, Q., Han, L., Zou, W., et al. (2021). Nutrient budget and biogeochemical dynamics in Sansha Bay, China: A coastal bay affected by intensive mariculture. *J. Geophys. Res.: Biogeosci.* 126, e2020JG006220. doi: 10.1029/2020JG006220

Jiang, Z., Liu, J., Li, S., Chen, Y., Du, P., Zhu, Y., et al. (2020). Kelp cultivation effectively improves water quality and regulates phytoplankton community in a turbid, highly eutrophic bay. *Sci. Total Environ.* 707, 135561. doi: 10.1016/j.scitotenv.2019.135561

Kang, P., and Xu, S. (2016). The impact of mariculture on nutrient dynamics and identification of the nitrate sources in coastal waters. *Environ. Sci. Pollut. Res.* 23, 1300–1311. doi: 10.1007/s11356-015-5363-0

Kendall, C. (1998). Tracing sources and cycling of nitrate in catchments. *Isotope Tracers Catchment Hydrol.* 839, 519–576. doi: 10.1016/B978-0-444-81546-0.50023-9

Kendall, C., Elliott, E. M., and Wankel, S. D. (2007). "Tracing anthropogenic inputs of nitrogen to ecosystems," in *Stable Isotopes in Ecology and Environmental Science, Second Edition*. (Wiley-Blackwell), 375–449. doi: 10.1002/9780470691854.ch12

Knap, A., Michaels, A., Close, A., Ducklow, H., and Dickson, A. (1996). Protocols for the joint global ocean flux study (JGOFS) core measurements. *JGOFS Reprint IOC Manuals Guides No. 29 UNESCO 1994* 19, 177.

Lao, Q., Chen, F., Liu, G., Chen, C., Jin, G., Zhu, Q., et al. (2019). Isotopic evidence for the shift of nitrate sources and active biological transformation on the western coast of Guangdong Province, South China. *Mar. Pollut. Bull.* 142, 603–612. doi: 10.1016/j.marpolbul.2019.04.026

Lao, Q., Zhang, S., Li, Z., Chen, F., Zhou, X., Jin, G., et al. (2022). Quantification of the seasonal intrusion of water masses and their impact on nutrients in the Beibu Gulf using dual water isotopes. *J. Geophys. Res.: Oceans* 127, e2021JC018065. doi: 10.1029/2021JC018065

Li, Y., Jin, H., Chen, J., Wang, D., Yang, Z., Wang, B., et al. (2021). Nitrogen removal through sediment denitrification in the Yangtze Estuary and its adjacent East China Sea: A nitrate limited process during summertime. *Sci. Total Environ.* 795, 148616. doi: 10.1016/j.scitotenv.2021.148616

Liu, S. M., Hong, G. H., Zhang, J., Ye, X. W., and Jiang, X. L. (2009). Nutrient budgets for large Chinese estuaries. *Biogeosciences* 6 (10), 2245–2263. doi: 10.5194/bg-6-2245-2009

Liu, S. M., Li, L. W., Zhang, G. L., Liu, Z., Yu, Z., and Ren, J. L. (2012). Impacts of human activities on nutrient transports in the Huanghe (Yellow River) estuary. *J. Hydrol.* 430, 103–110. doi: 10.1016/j.jhydrol.2012.02.005

Mengis, M., Schif, S., Harris, M., English, M., Aravena, R., Elgood, R., et al. (1999). Multiple geochemical and isotopic approaches for assessing ground water NO3– elimination in a riparian zone. *Groundwater* 37, 448–457. doi: 10.1111/j.1745-6584.1999.tb01124.x

Moore, J. W., and Semmens, B. X. (2008). Incorporating uncertainty and prior information into stable isotope mixing models. *Ecol. Lett.* 11, 470–480. doi: 10.1111/j.1461-0248.2008.01163.x

Redfield, A. C. (1963). "The Influence of Organisms on the Composition of Seawater," in *The Sea* (New York: Wiley Interscience), 26–77.

Sigman, D. M., Casciotti, K. L., Andreani, M., Barford, C., Galanter, M., and Böhlke, J. (2001). A bacterial method for the nitrogen isotopic analysis of nitrate in seawater and freshwater. *Anal. Chem.* 73, 4145–4153. doi: 10.1021/ac010088e

Sun, W., Tang, X. C., Xu, Y. D., Zhang, H. J., Wei, X., and Liu, Y. J. (2016). Characteristics of nutrients, restrictive analysis and eutrophication assessment in the Shuangdao Bay, Weihai. *Sci. Technol. Eng.* 16 (25), 168–172. doi: 10.3969/j.issn.1671-1815.2016.25.028

Sun, P. X., Wang, B., Zhang, Z. H., Wang, Z. L., and Xia, B. (2006). Relationship between nutrient distributions and eutrophication in seawater of the Laizhou Bay. *Adv. Mar. Sci.* 24 (3), 329–335. doi: 10.3969/j.issn.1671-6647.2006.03.009

Tian, S., Gaye, B., Tang, J., Luo, Y., Lahajnar, N., Daehnke, K., et al. (2022). Nitrate regeneration and loss in the Central Yellow Sea bottom water revealed by nitrogen isotopes. *Front. Mar. Sci.* 9, 834953. doi: 10.3389/fmars.2022.834953

Wang, B., Chen, J., Jin, H., Li, H., Huang, D., and Cai, W. J. (2017). Diatom bloom-derived bottom water hypoxia off the Changjiang estuary, with and without typhoon influence. *Limnol. Oceanogr.* 62, 1552–1569. doi: 10.1002/lno.10517

Wang, G., Han, A., Chen, L., Tan, E., and Lin, H. (2018). Fluxes of dissolved organic carbon and nutrients via submarine groundwater discharge into subtropical Sansha Bay, China. *Estuarine Coast. Shelf Sci.* 207, 269–282. doi: 10.1016/j.ecss.2018.04.018

Wang, X., Olsen, L. M., Reitan, K. I., and Olsen, Y. (2012). Discharge of nutrient wastes from salmon farms: environmental effects, and potential for integrated multi-trophic aquaculture. *Aquacult. Environ. Interact.* 2, 267–283. doi: 10.3354/aei00044

Wang, B., Wang, X., and Zhan, R. (2003). Nutrient conditions in the yellow sea and the east China sea. *Estuarine Coast. Shelf Sci.* 58, 127–136. doi: 10.1016/S0272-7714(03)00067-2

Wankel, S. D., Kendall, C., and Paytan, A. (2009). Using nitrate dual isotopic composition ($\delta^{15}N$ and $\delta^{18}O$) as a tool for exploring sources and cycling of nitrate in an estuarine system: Elkhorn Slough, California. *J. Geophys. Res.: Biogeosci.* 114, G01011. doi: 10.1029/2008J

Williams, J., and Crutzen, P. (2010). Nitrous oxide from aquaculture. *Nat. Geosci.* 3, 143–143. doi: 10.1038/ngeo804

Wu, J., Hong, Y., Liu, X., and Hu, Y. (2021). Variations in nitrogen removal rates and microbial communities over sediment depth in Daya Bay, China. *Environ. Pollut.* 286, 117267. doi: 10.1016/j.envpol.2021.117267

Wu, B., Jin, H., Gao, S., Xu, J., and Chen, J. (2020). Nutrient budgets and recent decadal variations in a highly eutrophic estuary: Hangzhou Bay, China. *J. Coast. Res.* 36, 63–71. doi: 10.2112/JCOASTRES-D-18-00071.1

Xiao, X., Agusti, S., Lin, F., Li, K., Pan, Y., Yu, Y., et al. (2017). Nutrient removal from Chinese coastal waters by large-scale seaweed aquaculture. *Sci. Rep.* 7, 46613. doi: 10.1038/srep46613

Xie, B., Huang, J., Huang, C., Wang, Y., Shi, S., and Huang, L. (2020). Stable isotopic signatures ($\delta^{13}C$ and $\delta^{15}N$) of suspended particulate organic matter as indicators for fish cage culture pollution in Sansha Bay, China. *Aquaculture* 522, 735081. doi: 10.1016/j.aquaculture.2020.735081

Xiong, Y., Gao, L., Qu, L., Xu, J., Ma, Z., and Gao, G. (2023). The contribution of fish and seaweed mariculture to the coastal fluxes of biogenic elements in two important aquaculture areas, China. *Sci. Total Environ.* 856, 159056. doi: 10.1016/j.scitotenv.2022.159056

Xue, D., Botte, J., De Baets, B., Accoe, F., Nestler, A., Taylor, P., et al. (2009). Present limitations and future prospects of stable isotope methods for nitrate source identification in surface-and groundwater. *Water Res.* 43, 1159–1170. doi: 10.1016/j.watres.2008.12.048

Xue, D., De Baets, B., Van Cleemput, O., Hennessy, C., Berglund, M., and Boeckx, P. (2012). Use of a Bayesian isotope mixing model to estimate proportional contributions of multiple nitrate sources in surface water. *Environ. Pollut.* 161, 43–49. doi: 10.1016/j.envpol.2011.09.033

Yang, Z., Chen, J., Li, H., Jin, H., Gao, S., Ji, Z., et al. (2018). Sources of nitrate in Xiangshan Bay (China), as identified using nitrogen and oxygen isotopes. *Estuarine Coast. Shelf Sci.* 207, 109–118. doi: 10.1016/j.ecss.2018.02.019

Yang, B., Gao, X., Zhao, J., Lu, Y., and Gao, T. (2020). Biogeochemistry of dissolved inorganic nutrients in an oligotrophic coastal mariculture region of the northern Shandong Peninsula, north Yellow Sea. *Mar. Pollut. Bull.* 150, 110693. doi: 10.1016/j.marpolbul.2019.110693

Ye, F., Jia, G., Xie, L., Wei, G., and Xu, J. (2016). Isotope constraints on seasonal dynamics of dissolved and particulate N in the P earl R iver E stuary, south C hina. *J. Geophys. Res.: Oceans* 121, 8689–8705. doi: 10.1002/2016JC012066

Zhang, J., Wu, W., Li, Y., Liu, Y., and Wang, X. (2022). Environmental effects of mariculture in China: An overall study of nitrogen and phosphorus loads. *Acta Oceanol. Sin.* 41, 4–11. doi: 10.1007/s13131-021-1909-9

Zhang, Y., Zhang, J., Liang, Y., Li, H., Li, G., Chen, X., et al. (2017). Carbon sequestration processes and mechanisms in coastal mariculture environments in China. *Sci. China Earth Sci.* 60, 2097–2107. doi: 10.1007/s11430-017-9148-7

Zhang, M., Zhi, Y., Shi, J., and Wu, L. (2018). Apportionment and uncertainty analysis of nitrate sources based on the dual isotope approach and a Bayesian isotope mixing model at the watershed scale. *Sci. Total Environ.* 639, 1175–1187. doi: 10.1016/j.scitotenv.2018.05.239

Zhuang, Y., Jin, H., Cai, W.-J., Li, H., Jin, M., Qi, D., et al. (2021a). Freshening leads to a three-decade trend of declining nutrients in the western Arctic Ocean. *Environ. Res. Lett.* 16, 054047. doi: 10.1088/1748-9326/abf58b

Zhuang, Y., Jin, H., Cai, W. J., Li, H., Qi, D., and Chen, J. (2022). Extreme nitrate deficits in the western Arctic ocean: Origin, decadal changes, and implications for denitrification on a polar marginal shelf. *Global Biogeochem. Cycles* 36, e2022GB007304. doi: 10.1029/2022GB007304

Zhuang, Y., Jin, H., Zhang, Y., Li, H., Zhang, T., Li, Y., et al. (2021b). Incursion of Alaska Coastal Water as a mechanism promoting small phytoplankton in the western Arctic Ocean. *Prog. Oceanogr.* 197, 102639. doi: 10.1016/j.pocean.2021.102639

frontiers | Frontiers in Marine Science

TYPE Original Research
PUBLISHED 11 March 2024
DOI 10.3389/fmars.2024.1381305

OPEN ACCESS

EDITED BY
Jingzhen Wang,
Beibu Gulf University, China

REVIEWED BY
Yong Zhu,
East Carolina University, United States
Yao Zheng,
Chinese Academy of Fishery Sciences (CAFS), China
Wensheng Li,
Sun Yat-sen University, China

*CORRESPONDENCE
Gang Zhai
zhaigang@ihb.ac.cn
Zhan Yin
zyin@ihb.ac.cn

†These authors have contributed equally to this work

RECEIVED 03 February 2024
ACCEPTED 26 February 2024
PUBLISHED 11 March 2024

CITATION
Shi S, Zhang Y, Huang J, Lou Q, Jin X, He J, Zhai G and Yin Z (2024) Effective "off-on" switch for fertility control in female zebrafish. *Front. Mar. Sci.* 11:1381305. doi: 10.3389/fmars.2024.1381305

Effective "off-on" switch for fertility control in female zebrafish

Shengchi Shi[1,2†], Yuqing Zhang[1,2†], Jianfei Huang[1,2], Qiyong Lou[1], Xia Jin[1], Jiangyan He[1], Gang Zhai[1,2,3*] and Zhan Yin[1,2,3,4*]

[1]State Key Laboratory of Freshwater Ecology and Biotechnology, Institute of Hydrobiology, Chinese Academy of Sciences, Wuhan, China, [2]College of Advanced Agricultural Sciences, University of Chinese Academy of Sciences, Beijing, China, [3]Hubei Hongshan Laboratory, Huazhong Agriculture University, Wuhan, China, [4]The Innovative Academy of Seed Design, Chinese Academy of Sciences, Wuhan, China

The implementation of a controllable sterility strategy is crucial for the commercialization of precise trait improvements in farmed fish using genome editing and sustainable development of fisheries. Our previous research has demonstrated that females deficient in pituitary gonadotropin *luteinizing hormone β-subunit* (*lhβ*) or gonadal steroidogenesis gene *steroidogenic acute regulatory protein* (*star*) exhibit sterility due to impaired oocyte maturation and ovulation. Nevertheless, the effective restoration of fertility in *lhβ*- or *star*-deficient females remains unsolved. This study has discovered that the administration of exogenous 17α,20β-dihydroxy-4-pregnen-3-one (DHP) at 100 and 300 μg/L for 6 h (from 02:00 to 08:00 a.m.) effectively restores the fertility of *lhβ*- or *star*-deficient females. Fertilized eggs from these mutant females can be raised without noticeable developmental defects for up to 3 weeks post-fertilization (wpf) compared to the wild-type (WT) control zebrafish. The increased expression levels of *adamts9* and *adam8b* in *lhβ*- or *star*-deficient zebrafish females treated with DHP demonstrate a positive correlation with oocyte maturation and ovulation restoration. In contrast, exogenous DHP administration did not rescue the sterility phenotype observed in *progesterone receptor* (*pgr*)-deficient females. Building on our recent success in generating an all-female carp population through *cytochrome P450, family 17, subfamily A, polypeptide 1* (*cyp17a1*)-depletion, our research presents a promising and effective strategy for an "off-on" switch for managing fertility in genome-edited cyprinids. The strategy would offer practical guidance and theoretical justification for developing "controllable fertility" in all-female fish, which would support the sustainable development of fisheries by promoting the use of novel biotechnologies in aquaculture in an eco-friendly manner.

KEYWORDS

gonadotropin, luteinizing hormone, DHP, controllable sterility, eco-friendly manner

Introduction

Advances in genome editing technologies, such as transcription activator-like effector nuclease (TALEN) and clustered regularly interspaced short palindromic repeats associated with Cas9 (CRISPR/Cas9), provide effective and precise tools for enhancing fish traits for aquaculture purposes. For example, improved growth and feed conversion efficiency have been observed in gibel carp (*Carassius gibelio*) and all-female common carp (*Cyprinus carpio*) populations by depleting the *phosphoinositide-3-kinase, regulatory subunit 1 (alpha)* (*pik3r1*), and *cytochrome P450, family 17, subfamily A, polypeptide 1* (*cyp17a1*) loci, respectively (Huang et al., 2021; Zhai et al., 2022a). However, potential spread of edited alleles into wild-type (WT) stocks limits use of genome-edited fish in aquaculture. To circumvent this, we have dedicated ourselves to developing a strategy by creating an all-female fish population (Zhai et al., 2022a) and its sterilization (Gratacap et al., 2019; Okoli et al., 2022). In this study, we establish a "off-on" switch for fertility control of female fish to breed and maintain desirable traits of sex-controlled breeding. Building on our recent success with the all-female carp population generated via the *cyp17a1*-depletion strategy, a practicable "off-on" technique for sterility in female cyprinids will be exhilarating particularly.

In vertebrates, pituitary gonadotropins are critical for ovarian development throughout the reproductive cycle, a multifaceted biological process (McGee and Hsueh, 2000). The pituitary gonadotropin, Lhβ, a member of the glycoprotein hormone family, binds to its receptor Lhcgr on the granulosa or theca cells to regulate of oocyte growth, development and maturation (Gharib et al., 1990). Mutation of *LH* or *Lhcgr* in both humans and mice can result in ovarian hypogonadism and infertility due to defective gonadal steroidogenesis (Lei et al., 2001; Zhang et al., 2001; Ma et al., 2004; Huhtaniemi and Themmen, 2005; Huhtaniemi, 2006; Li and Ge, 2020). Ovarian development in zebrafish can be categorized into five stages: primary oocyte growth (stage I), accumulation of cortical alveoli (stage II), vitellogenesis (stage III), and maturation (stages IV and V). Stage IV includes stage IVa (onset of oocyte maturation and 3 h before lights on), and stage IVb (oocytes mature but before ovulation, 1 h before lights on) (Liu et al., 2018). Stimulation from Luteinizing hormone-releasing hormone (LHRH) prompts Lh secretion from the pituitary gland, resuming the meiotic cell cycle and inducing germinal vesicle breakdown (GVBD), an indicator of oocyte maturation. In stage V, the completely developed eggs are released and prepared for spawning (Nagahama et al., 1995; Nagahama and Yamashita, 2008).

In zebrafish, the crucial regulatory roles of Lh in ovarian steroidogenesis have been documented. Briefly, LH activates the intracellular signaling pathway (cAMP/PKA/CREB), the production of maturation-induced hormone and 17α,20β-dihydroxy-4-pregnen-3-one (DHP), and oocyte maturation by binding to Lhcgr, which is located on the theca cells of the ovary (Ascoli et al., 2002; Nagahama and Yamashita, 2008; Levavi-Sivan et al., 2010). In theca cells, cholesterol undergoes conversion to 17α-hydroxy-progesterone and testosterone. These hormones are then respectively converted to DHP and estradiol in the granulosa cells (Clelland and Peng, 2009). Lh binds to Lhcgr to increase *insulin-like growth factor 3* (*igf3*) expression as well, which subsequently binds to the *insulin-like growth factor 1 receptor* (*igf1r*) and initiates oocyte maturation and ovulation (Li et al., 2018). Lh can also initiate follicle activation and promote follicle growth via the Fsh receptor (Fshr), which compensates for the absence of Fsh in folliculogenesis (Zhang et al., 2015). Steroidogenic acute regulatory protein (Star), an enzyme responsible for transporting cholesterol into the inner mitochondrial membrane for DHP production, has been identified as a downstream target of Lh for oocyte maturation in zebrafish (Shang et al., 2019) and some other teleost fishes (Nagahama and Yamashita, 2008). However, the specific functions and mechanisms of progestin signaling in initiating oocyte maturation and ovulation in zebrafish requires further elucidation.

Recently, we reported that the maturation-arrested oocyte phenotypes could be partially rescued by the administration of DHP precursors, pregnenolone or progesterone, including DHP itself, in *lhβ*- or *star*-deficient females (Shang et al., 2019). Progestin signals can be mediated through membrane progestin receptor α (mPRα) and nuclear progestin receptor (Pgr). Arrested oocyte maturation and mature oocytes trapped within the follicular cells were observed in *mPRs*-deficient and *npr*-deficient females, respectively (Zhu et al., 2015; Wu et al., 2020). These results indicate that the progestin signaling may be disrupted in *lhβ*- or *star*-deficient females due to impaired steroidogenesis in mutant fish. However, the exact pathological mechanisms responsible for impaired oocyte maturation and ovulation in *lhβ*- or *star*-deficient females remain elusive, hindering the development of effective restoration strategies for their fecundity.

A ovulation-impaired phenotype was also observed in the *pgr*-deficient females (Liu et al., 2018). In preovulatory follicular cells (stage IVb) of female zebrafish, the expression levels of four metalloproteinases, including *ADAM metallopeptidase with thrombospondin type 1 motif, 9* (*adamts9*), *ADAM metallopeptidase domain 8b* (*adam8b*), *ADAM metallopeptidase with thrombospondin type 1 motif, 1* (*adamts1*) and *matrix metallopeptidase 9* (*mmp9*), increased dramatically in WT females, but reduced in *pgr*-/- zebrafish (Liu et al., 2018). *In vitro* experiments conducted on pre-ovulatory follicles have demonstrated that DHP upregulates *adamts9* expression in a dose-, time-, and Pgr-indispensable manner (Liu et al., 2018). *adamts9* expression in pre-ovulatory follicular cells is also regulated by human chorionic gonadotropin (hCG, a LH analog), which has been demonstrated to be Lhcgr-dependent, but not Pgr-dependent (Liu et al., 2020). These findings suggest that the regulation of *adamts* expression in pre-ovulatory follicular cells may involve multiple contributing factors.

In this study, we examined the effects on oocyte maturation/ovulation caused by deficiencies in *lhβ* or *star* in female zebrafish. The strategy for restoring fecundity in these mutants has been continuously refined through synchronized assessments of the gonadal anatomy, fertility capacity, and the efficacy of each chosen steroid compound, along with its dosage and duration (Chen et al., 2013; Zhu et al., 2015; Lau et al., 2016; Tang et al., 2016; Lu et al., 2017; Yin et al., 2017; Crowder et al., 2018; Tang et al., 2018; Yu et al., 2018; Zhai et al., 2018; Li et al., 2020; Shu et al.,

2020). Our results indicate that treatment of exogenous DHP effectively restores the fecundity of *lhβ*- or *star*-deficient female zebrafish. The main findings of this study using genome editing models provide a valuable basis for developing an "off-on" switch to control female fertility in teleosts.

Materials and methods

Animals

Zebrafish were maintained under standard conditions at 28.5°C, in a circulated water system with a 14 h light and 10 h dark cycle as previously described (Westerfield, 2000). The *lhβ*, *star* and *pgr* heterozygous males and females were inbred to generate population that contained *lhβ*, *star* and *pgr* homozygotes, respectively (Tang et al., 2016; Shang et al., 2019). Mutant *lhβ* has an 8 bp deletion in the second exon, *star* has a 1 bp deletion in the second exon, and *pgr* has a deletion of the flanked genomic fragment (13.40 kb) between the first and the sixth exon.

Natural mating

Natural mating was conducted as previously described (Shu et al., 2020). Briefly, WT, *lhβ*- or *star*-deficient females were kept with WT males in a breeding tank with an insert and a divider in the middle. The divider was removed at 08:00 the following morning and the ratio of spawning, fertilization, and survival were recorded in every tank.

Administration with DHP

DHP (CAS No. 1662-06-2, P712080, Toronto Research Chemicals, Canada) was dissolved in Dimethylsulfoxide (DMSO), and the stock solutions of 10 g/L was sub-packed and stored in -80 ° C. The *lhβ*- and *star*-deficient females were subjected to immersion treatments with 100 and 300 μg/L DHP from 02:00 to 08:00, respectively.

hCG intraperitoneal injection and administration with DHP

The hCG (hor-250, PROSPEC, Israel) was dissolved in water at 25 IU/μL as stock solution and the working solution was diluted to 1/5 with normal saline. Intraperitoneal hCG injection was conducted as described in a previous study, with minor modifications (Kinkel et al., 2010). After anesthetization, *lhβ*- or *star*-deficient females were quickly placed on a piece of wet gauze and carefully injected with 10 μL of the working solution into the pelvic midline fins at 00:00 using a microsyringe. *lhβ*- and *star*-deficient females were subsequently administrated with the immersion treatments with 100 and 300 μg/L DHP from 02:00 to 08:00, respectively.

Collection of follicular cells from stage IV follicles

The ovaries were dissected, and follicular cells of preovulatory follicles at stage IV were collected approximately 1 h prior to ovulation with lights on. Follicular cells, collected from 100 follicles per fish were separated from stage IV follicles using precision tweezers, according to a previous study with minor modifications (Liu et al., 2018).

RNA extraction and quantitative real-time polymerase chain reaction (qPCR)

Total RNA was extracted from the follicular cells of *lhβ*- or *star*-deficient females with Trizol reagent (15596026, Ambion, TX, USA). 500 ng of the RNA template was used for reverse transcription and cDNA synthesis using the EasyScript One-Step gDNA Removal and cDNA Synthesis SuperMix Kit (AE311-03, Transgen, China). The qPCR was conducted using PerfectStartTM Green qPCR SuperMix (AQ601-02, Transgen, China) according to a previous study (Shi et al., 2022). qPCR was conducted using a Bio-Rad Real-Time System (Bio-Rad Systems, USA). All the mRNA levels were calculated as the fold change relative to *eukaryotic translation elongation factor 1 alpha 1* (*ef1a*). The primers of *adamts9*, *adam8b*, *adamts1*, and *mmp9* used for qPCR are listed in Table 1.

Histological analysis

Hematoxylin and eosin staining was performed as previously described (Zhai et al., 2022b). Briefly, fish were euthanized with MS-222 and the ovary was isolated for fixation in Bouin's solution. Fixed samples were dehydrated, infiltrated and embedded in paraffin for sectioning on a Leica microtome (RM2235, Leica Biosystems, German). Paraffin sections were stained with hematoxylin and eosin and examined microscopically using a Nikon Eclipse Ni-U microscope (Nikon, Tokyo, Japan). The scale bar is displayed in each image.

Statistical analysis

Detailed information regarding the number of zebrafish used per experiment is provided for each experiment and the corresponding figure. All analyses were conducted with the GraphPad Prism 6.0 software program and the differences were evaluated using the student's t-test. The results were expressed as the mean ± SD. For all statistical comparisons, a P value 0.05 was used to indicate a statistically significant difference.

Results

WT females could be induced to spawn after DHP administration

For the regular WT zebrafish natural mating group, one male and one female were placed overnight in a tank separated by a transparent divider. The following morning, the divider was removed for natural fish mating (Figure 1A). Ovulation of mating females was induced by overnight housing with the mating males (Figures 1B–I, Table 2). If a female was not primed by an overnight housing with a male before the mating (no priming group) (Figure 1J), this naïve single female would not naturally engage in ovulation and mating behavior with a male (Figures 1K–R, Table 2).

TABLE 1 Primers used in this study for qPCR.

Gene	Primer direction[a] and sequence (5′-3′)	Product size (bp[b])	References
adamts9	F: TCACCCAACCCCGATTTTCG	224	(Liu et al., 2018)
	R: CAAGAGCGCTGTTCAATGGG		
adam8b	F: CCTGGCATCCACAATTGCAC	254	(Liu et al., 2018)
	R: CATTACCACAGACAGGCCCA		
adamts1	F: ACACCGTGCACTCCAGATTC	247	(Liu et al., 2018)
	R: GGCTACGGCCTCCAAAAGAT		
mmp9	F: TCTGCCTTTGAGGACCACCT	260	(Liu et al., 2018)
	R: CCGAAAGCTGCATCAGTGAA		
ef1a	F: AAGATCGGCTACAACCCTGC	107	(Shang et al., 2019)
	R: TTCCATCCCTTGAACCAGCC		

[a]F, Forward; R, Reverse.
[b]base pair.

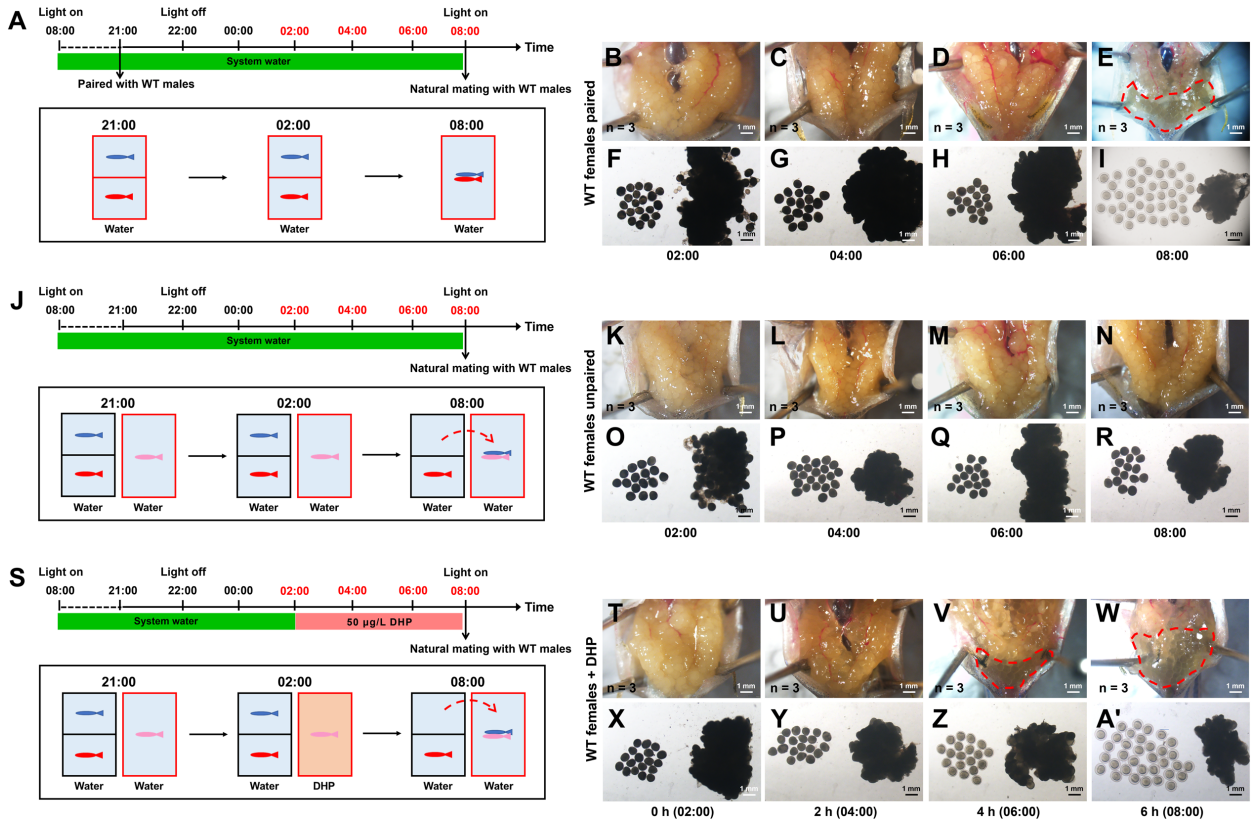

FIGURE 1
WT females could be induced to spawn after DHP administration. **(A)** Schematic illustration of the spawning test for paired WT females (depicted in red). One WT female (depicted in red) and one WT male (depicted in blue) are housed overnight in the tank, separated by a transparent divider. At 08:00 (light on), the divider is removed, then the spawning between the paired WT female and WT male succeeds. **(B–I)** The anatomical examination and microphotographs of follicles are sampled from paired WT females at 02:00, 04:00, 06:00, and 08:00 (n = 3 at each timepoint). **(J)** Schematic illustration of the spawning test for unpaired WT females (depicted in pink). WT females (depicted in red) are housed overnight in the tank with WT male (depicted in blue), then natural mating of the unpaired WT females (pink) with the paired males (blue) failed. **(K–R)** The anatomical examination and microphotographs of follicles sampled from unpaired WT females at 02:00, 04:00, 06:00, and 08:00 (n = 3 at each timepoint). **(S)** Schematic illustration of the spawning test for unpaired WT females (depicted in pink) treated with DHP (tank depicted in brown). WT females are exposed to 50 μg/L DHP from 2:00 to 8:00, then natural mating with males (depicted in blue) which are from another tank paired with WT females (depicted in red) overnight succeeds. **(T–A′)** The anatomical examination and microphotographs of follicles sampled from WT females treated with 50 μg/L DHP for 0 h (02:00), 2 h (04:00), 4 h (06:00), and 6 h (08:00) (n = 3 at each timepoint). The samples at the timepoints depicted in red are harvested for oocyte analysis. **(B, F, K, O, T, X)** 0 h **(C, G, L, P, U, Y)** 2 h **(D, H, M, Q, V, Z)** 4 h **(E, I, N, R, W, A′)** 6 h.

TABLE 2 Comparison of the fecundities of wild-type zebrafish female induced by overnight housing and DHP treatment.

Group	Ratio of spawning (%)	Number of spawning eggs	Ratio of fertilization (%)	Ratio of membrane break (%)	Ratio of survival at 3 wpf (%)	Fecundity index*	Relative fecundity ratio** (%)
WT + overnight housing of the mating partner	92.50 ± 8.29[a]	257.83 ± 100.94[a]	91.15 ± 6.09[a]	96.94 ± 2.24[a]	85.00 ± 7.83[a]	179.13	100.00
WT + DHP treatment	88.87 ± 7.87[a]	243.11 ± 55.60[a]	60.63 ± 9.39[b]	88.10 ± 7.56[b]	76.71 ± 8.50[a]	88.54	49.43

N = 6–10 for each group.
*Fecundity index = Ratio of spawning (%) × Number of spawning eggs × Ratio of fertilization (%) × Ratio of membrane break (%) × Ratio of survival at 3 wpf (%).
**Relative fecundity ratio = Fecundity index of the treated mutant group / Fecundity index of wild-type control fish group.
Different letters in the table represent significant differences compared with the control group ($P < 0.05$).

However, if the WT female was treated with 50 μg/L DHP for 6 h from 02:00 to 08:00, the effective ovulation could be seen in DHP treated female (Figures 1S-A'). When a pair of DHP-treated females and males was set up for mating after 6 h DHP treatment, the DHP treated WT females could naturally mate with the WT males and spawn (Table 2). Although the fertilization ratio of the offspring from DHP administrated WT females and WT males was significantly lower than that of the natural mating group, the ratios of membrane breakage and survival at 3 wpf were unaffected (Table 2). These results indicate that DHP treatment can effectively replace overnight housing with male fish to induce the ovulation and spawning in female fish. The viabilities of the naturally fertilized eggs from primed by overnight housing and DHP treatment were equivalent.

Anovulation defects in *lhβ*- or *star*-deficient females rescued with the DHP administration

Previously, the phenotypes of oocyte maturation and ovulation were observed in *lhβ*- or *star*-deficient females. We found that the follicles in the *lhβ* mutants did not enter stage V as it normally occurred in the WT control females between 06:30 and 07:30 when mated with WT males (Shang et al., 2019). We first examined the restorative effects of DHP on ovulation in these females. The *lhβ*- and *star*-deficient females were exposed to 100 and 300 μg/L DHP, respectively, from 02:00 to 08:00 (Figure 2A). At 02:00, the follicles from the dissected ovaries of *lhβ*-deficient females were non-transparent (Figures 2B, F); however, after 2 h DHP administration (at 04:00), the follicles became semi-transparent (Figures 2C, G), marking the beginning of oocyte maturation. More apparently, the anatomical examination of *lhβ*-deficient females exposed to 100 μg/L DHP for 4 h (at 06:00) was sufficient to induce maturation of oocytes, as evidenced by the microphotographs of follicles, which had become transparent embedded in the dissected ovaries and few eggs with egg membrane formed (characterized as stage V) (Figures 2D, H). At 08:00, when the *lhβ*-deficient females were exposed to DHP for 6 h, more eggs with membrane formed, suggesting that the follicles reached to stage V, and released into the vicinity of the genital pore in *lhβ*-deficient females (Figures 2E, I). The successful induction of follicles at different time points after DHP administration was also supported by the observed oocyte maturation and ovulation in *star*-deficient females (Figures 2J-Q). These results suggest that the arrested oocyte maturation and ovulation in *lhβ*- or *star*-deficient females *in vivo* could be effectively rescued by DHP administration.

Infertility of *lhβ*- or *star*-deficient females was rescued with DHP administration

Following the sketches depicted in Figure 2A, the rescue of the infertility phenotypes in *lhβ*- or *star*-deficient females administrated diverse combinations of the hormones, including DHP and hCG respectively, were evaluated with natural mating with WT males (Table 3). For comparison of the rescue efficiency, the "fecundity index" was adopted for representing the capacity of each experimental mating group to produce healthy offspring. The "relative fecundity" indicates the rescue efficiency of each treatment, represented by the fecundity index of the treated mutant group/fecundity index of WT control group (Table 3). After a 6 h treatment (from 02:00 to 08:00), the *lhβ*-deficient females were placed in a new breeding tank with an insert at the bottom and a divider in the middle. WT males, which had been kept with WT females in another breeding tank contained system water that night, were transferred into the tank with the DHP-treated *lhβ*-deficient females. Natural mating was observed between WT males and DHP-treated *lhβ*-deficient females. Compared with the hCG treatment, the administration of DHP effectively rescued the defects of oocyte maturation and ovulation of the *lhβ*-deficient females, as the spawned and fertilized eggs with the genotype of *lhβ*+/- were observed (76.00 ± 23.32% *lhβ*-deficient females spawned, 25.90 ± 12.28% alive eggs were fertilized, 68.11 ± 31.45% fertilized eggs broke the egg membrane, and 59.80 ± 39.56% fertilized eggs survived to juvenile stage) (Table 3).

Noteworthily, the administration of 100 μg/L DHP for 6 h, which was sufficient to rescue the defects of oocyte maturation and ovulation in the *lhβ*-deficient females, did not work well in the *star*-deficient females, as no spawned eggs were observed, even with artificial squeeze (Data not shown). The *star*-deficient females were subsequently exposed to 300 μg/L DHP from 02:00 to 08:00. Strikingly, 6 h DHP administration at 300 μg/L effectively rescued the defects of oocyte maturation and

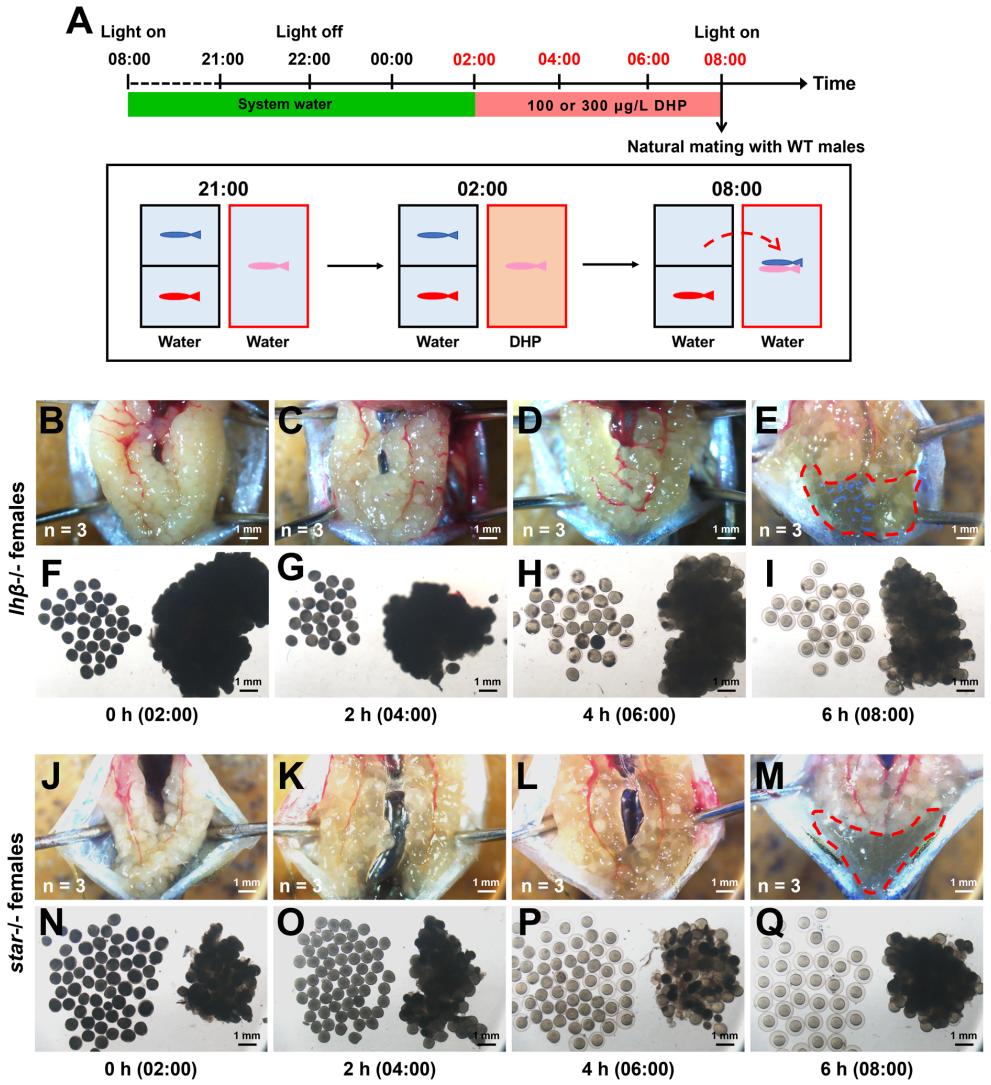

FIGURE 2
The arrested oocyte maturation of *lhβ*- or *star*-deficient females can be rescued by DHP administration. **(A)** Schematic illustration of the DHP administration for *lhβ*- or *star*-deficient females (depicted in pink) during the daily spawning cycle. *lhβ*- or *star*-deficient females are exposed to 100 or 300 µg/L DHP from 02:00 to 08:00, then natural mating with males (depicted in blue) which are from another tank and paired with WT females (depicted in red) overnight. **(B–I)** The anatomical examination and microphotographs of follicles sampled from *lhβ*-deficient females exposed to 100 µg/L DHP for 0 h (02:00), 2 h (04:00), 4 h (06:00), and 6 h (08:00) (n = 3 at each timepoint). **(J–Q)** The anatomical examination and microphotographs of follicles sampled from *star*-deficient females exposed to 300 µg/L DHP for 0 h, 2 h, 4 h, and 6 h (n = 3 at each timepoint). The samples at the timepoints depicted in red are harvested for oocyte analysis. **(B, F, J, N)** 0 h **(C, G, K, O)** 2 h **(D, H, L, P)** 4 h **(E, I, M, Q)** 6 h.

ovulation in the *star*-deficient females (Table 3), resulting in the observation of the spawned and fertilized eggs with the genotype of *star*+/- (51.90 ± 18.84% *star*-deficient females spawned, 72.87 ± 9.92% alive eggs were fertilized, 47.81 ± 26.25% fertilized eggs broke the egg membrane, and 66.04 ± 32.40% larvae of them survived to juvenile stage) (Table 3).

The developmental outcomes of the fish from the control females, the *lhβ*- or *star*-deficient females and WT males were also evaluated. The fertilized eggs at the early stage during embryonic development (12 h post-fertilization, hpf), larval stage (72 hpf and 5 days post-fertilization, dpf), and juvenile stage (3 weeks post-fertilization, wpf) from the control females and from the *lhβ*- or *star*-deficient females and WT males were comparable as evaluated by the gross appearance (Supplementary Figures 1A–L, Table 3). At 1-month post-fertilization (mpf), the body weight, body length and full length of the fish from control females were comparable with rescued fish from the *lhβ*- or *star*-deficient females mated with WT males (Supplementary Figures 1M–O). These results suggest that DHP at 100 or 300 µg/L from 02:00 to 08:00 is sufficient to rescue ovarian maturation and ovulation defects of *lhβ*- or *star*-deficient females as evaluated with natural mating with WT males, while the overall efficiency of *star*-

TABLE 3 Efficiencies of the fecundity rescue of *lhβ*- and *star*-deficient females with diverse steroids treatments.

Group	Ratio of spawning (%)	Number of spawning eggs	Ratio of fertilization (%)	Ratio of membrane break (%)	Ratio of survival at 3 wpf (%)	Fecundity index*	Relative fecundity ratio** (%)
WT Control	91.48 ± 9.02[a]	266.11 ± 83.96[a]	80.54 ± 22.35[a]	94.19 ± 6.62[a]	93.56 ± 8.97[a]	172.79	100.00
lhβ-/-	0	0	0	0	0	0	0
lhβ-/- + hCG	0	0	0	0	0	0	0
lhβ-/- + DHP	76.00 ± 23.32[a]	193.14 ± 81.39[a]	25.90 ± 12.28[b]	68.11 ± 31.45[b]	59.80 ± 39.56[b]	15.50	8.97
lhβ-/- + hCG + DHP	84.00 ± 14.97[a]	288.50 ± 136.70[a]	24.57 ± 12.95[b]	28.60 ± 21.78[c]	35.68 ± 21.62[b]	6.08	3.52
star-/-	0	0	0	0	0	0	0
star-/- + hCG	0	0	0	0	0	0	0
star-/- + DHP	51.90 ± 18.84[b]	251.75 ± 52.91[a]	72.87 ± 9.92[b]	47.81 ± 26.25[b]	66.04 ± 32.40[b]	30.06	17.40
star-/- + hCG + DHP	66.67 ± 9.43[b]	224.80 ± 91.63[a]	40.02 ± 19.05[c]	72.36 ± 25.63[b]	71.60 ± 22.32[b]	31.07	17.98

N = 6–10 for each group.
*Fecundity index = Ratio of spawning (%) × Number of spawning eggs × Ratio of fertilization (%) × Ratio of membrane break (%) × Ratio of survival at 3 wpf (%).
**Relative fecundity ratio = Fecundity index of the treated mutant group / Fecundity index of WT control fish group.
Different letters in the table represent significant differences compared with the control group ($P < 0.05$).

deficient females administrated with 300 μg/L DHP for 6 h is better than those of DHP-treated *lhβ*-deficient females.

DHP administration upregulated *adam8b* and *adamts9* expression in pre-ovulatory follicle cells of WT females mimicked the effect of natural mating with WT males

It is known that the metalloproteinases, including *adamts9* and *adam8b*, are required for zebrafish ovulation, and their expression significantly increased at 1 h prior to ovulation (Liu et al., 2018; Liu et al., 2020). Both metalloproteinases, *adamts9* and *adam8b*, but not *adamts1* and *mmp9* (Figures 3A–D, column 2 vs. 1), were significantly upregulated in the pre-ovulatory follicle cells of WT females paired with WT males 1 h before light on compared to those of unpaired WT females. Intriguingly, in the follicular cells of WT females exposed to DHP for 2 h (from 05:00 to 07:00) exhibited upregulated expression of *adamts9* and *adam8b* compared to the unpaired WT females, mimicking the effect of natural mating with WT males (Figure 3D, column 3 vs. 2).

DHP administration restores *adam8b* and *adamts9* expression in pre-ovulatory follicle cells of *lhβ*- or *star*-deficient females

Both metalloproteinases, *adamts9* and *adam8b* (Figures 4, 5A–E, column 2 vs. 1), but not *adamts1* and *mmp9* (Figures 4, 5F, G, column 2 vs. 1), were significantly upregulated in the pre-ovulatory follicle cells of control females paired with WT males 1 h before light on. Contrarily, the increased expression of *adamts9* and *adam8b* in follicular cells was not observed in *lhβ*- or *star*-deficient females paired with WT males 1 h before light on (Figures 4, 5D, E, column 4 vs. 3). We hypothesized that this may be one of the major reasons for arrested oocyte maturation and ovulation. Intriguingly, the follicular cells of *lhβ*- or *star*-deficient females exposed to DHP for 2 h (from 05:00 to 07:00) exhibited upregulated *adamts9* and *adam8b* expression, compared to the untreated fish (Figures 4, 5D, E, column 5 vs. 3). These results suggest that the upregulated *adamts9* and *adam8b* expression may be induced by DHP to restore the final maturation of oocyte and ovulation in *lhβ*- or *star*-deficient females.

Pgr signaling is indispensable for DHP-induced ovulation in zebrafish

Genomic progestin signaling and ovulation require the participation of Pgr, and *pgr* depletion is known to cause ovulation failure but does not affect oocyte maturation in zebrafish (Zhu et al., 2015). Our observations in the *pgr*-deficient female zebrafish replicated the manifestations of impaired ovulation reported in previous studies (Zhu et al., 2015). In control females paired with WT males, normal mature stage V oocytes that were released into the vicinity of the genital pores were observed at 08:00 (Figure 6A). However, anovulation with mature stage V oocytes trapped within the ovary was observed in *pgr*-deficient females (Figure 6B). The results of histological analysis demonstrated that the outer layer cells of the mature follicles failed to breakdown in the *pgr*-deficient fish (Figure 6C, D). Moreover, we found that the anovulation defects observed in *pgr*-deficient female zebrafish could not be rescued by DHP administration at a range of concentrations (Figure 6E-H). These results suggest that Pgr signaling is indispensable for DHP-mediated ovulation in zebrafish.

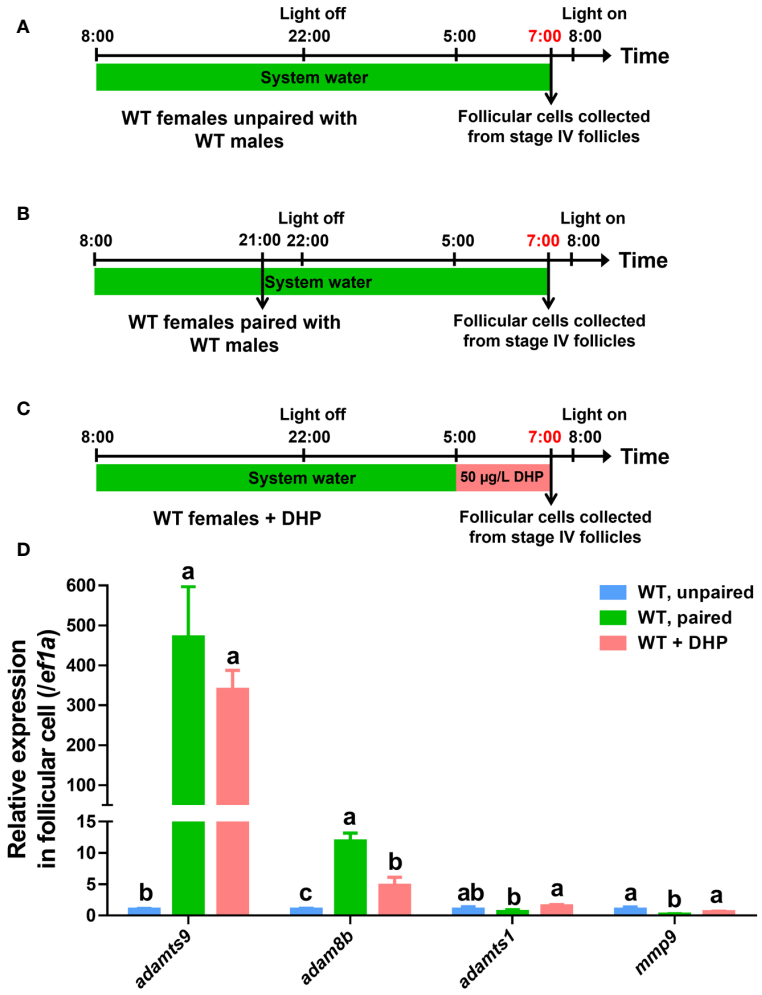

FIGURE 3
Expression of *adamts9* and *adam8b* is upregulated after DHP administration. **(A)** Schematic illustration of unpaired WT females. **(B)** Schematic illustration of paired WT females. **(C)** Schematic illustration of the DHP administration on WT females from 05:00 to 07:00. The samples at the timepoint depicted in red are harvested for analysis. **(D)** The expression of *adamts9*, *adam8b*, *adamts1*, and *mmp9* in pre-ovulatory follicular cells at 07:00 of paired WT females or WT females exposed to DHP are comparatively evaluated with that of control females unpaired with WT males. The letters in the bar charts represent significant differences.

Discussion

Although several studies have been conducted in zebrafish, the precise physiological processes and mechanisms involved in oocyte maturation and ovulation remain unclear. This study investigated the replacement of overnight mating partner housing with DHP treatment for oocyte maturation and ovulation induction in WT zebrafish. Based on these trails, DHP was selected to rescue sterility phenotype in *lhβ*- or *star*-deficient females. After multiple trials to determine the appropriate compound, dosage, and duration, it has been discovered that DHP and DHP + hCG administration can achieve consistently restore fertility in *lhβ*- or *star*-deficient females. The increased levels of *adamts9* and *adam8b* present in follicular cells of *lhβ*- or *star*-deficient females, as well as WT females exposed to overnight housing pairing or DHP treatment, demonstrated a positive relationship with the induction of oocyte maturation and ovulation induction. Since DHP administration failed to rescue the ovulation failure observed in *pgr*-deficient female zebrafish despite the presence of mature stage V oocytes (Zhu et al., 2015), we concluded that Pgr is imperative for DHP-mediated ovulation.

The process of oocyte maturation and ovulation lasts for a few hours in fish within the spawning cycle. In the preovulatory follicles of WT female zebrafish, the relative expression of *lhβ* began to increase from 03:30, and reached the peak at 05:30, the beginning of oocyte maturation (follicles started to become semi-transparent) (Shang et al., 2019). Similarly, the transcript and protein levels of Pgr begin to increase at 05:00 (prior to maturation) and peak level at 06:00–07:00 (in the middle of maturation) in female zebrafish (Liu et al., 2018). DHP is the major maturation-inducing hormone in zebrafish (Nagahama and Yamashita, 2008; Tokumoto et al., 2011; El Mohajer et al., 2022). Previously, we found that Lhβ regulates DHP synthesis in zebrafish by targeting *star*, the first step of gonad steroidogenesis from cholesterol (Shang et al., 2019). This is supported by the observations in *lhβ*-, or *star*-, or *mprs*-deficient females, wherein the oocyte maturation was impaired (Wu et al., 2020). These findings suggest that Lhβ/Star/Progestin signaling is

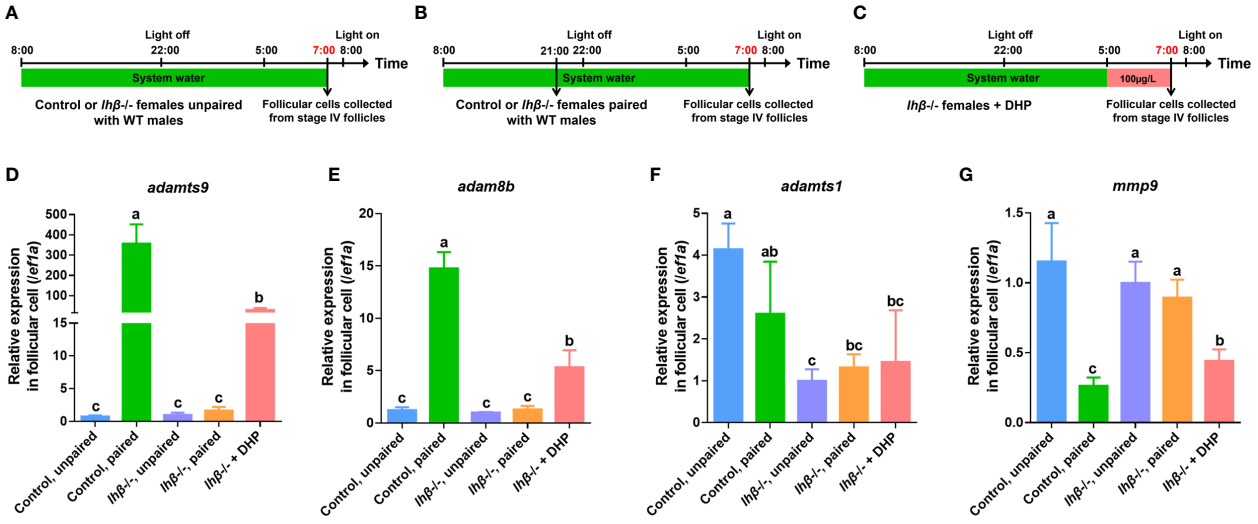

FIGURE 4
Expression of *adamts9* and *adam8b* in follicular cells of *lhβ*-deficient females after pairing with WT males or DHP administration. **(A)** Schematic illustration of unpaired control or *lhβ*-deficient females. **(B)** Schematic illustration of paired control or *lhβ*-deficient females. **(C)** Schematic illustration of the DHP administration on *lhβ*-deficient females from 05:00 to 07:00. The samples at the timepoint depicted in red are harvested for analysis. **(D–G)** The expression of *adamts9*, *adam8b*, *adamts1* and *mmp9* in preovulatory follicular cells at 07:00 of control females unpaired with WT males, control females paired with WT males, *lhβ*-deficient females unpaired with WT males, *lhβ*-deficient females paired with WT males, and *lhβ*-deficient females treated with DHP. The letters in the bar charts represent significant differences.

closely related to oocyte maturation. However, most of the conclusions that DHP promotes oocytes maturation were conducted on stage IV follicles *in vitro*. Here, the assessment of DHP in oocyte maturation and ovulation was firstly examined *in vivo* from 02:00 to 08:00 in *lhβ*- or *star*-deficient females with DHP administration at 100 and 300 μg/L, respectively. Oocytes become to be transparent following GVBD due to fusion of yolk proteins, allowing more lights to pass through. At 04:00, after 2 h DHP treatment, the follicles became semi-transparent, indicating the beginning of oocyte maturation. At 06:00, after 4 h DHP treatment, the follicles became transparent, and very few oocytes formed egg membranes, marking the completion of oocyte maturation (stage V) started. At 08:00, after 6 h DHP treatment, the transparent follicles were not trapped in the vicinity of the

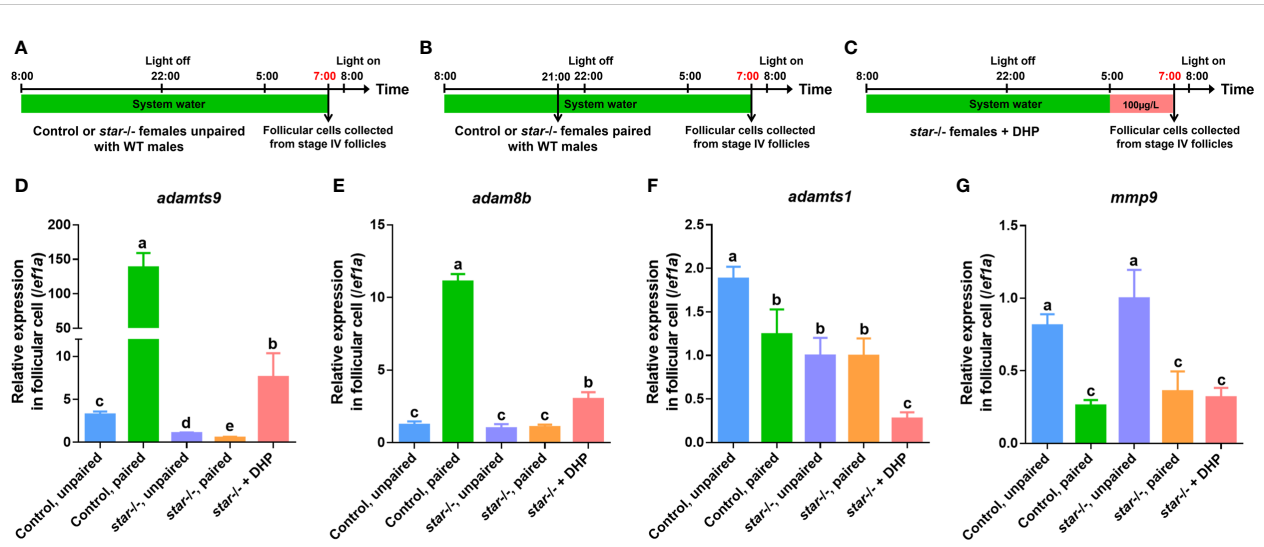

FIGURE 5
Expression of *adamts9* and *adam8b* in follicular cells of *star*-deficient females after paired WT males or DHP administration. **(A)** Schematic illustration of unpaired control or *star*-deficient females. **(B)** Schematic illustration of paired control or *star*-deficient females. **(C)** Schematic illustration of the DHP administration on *star*-deficient females from 05:00 to 07:00. The samples at the timepoint depicted in red are harvested for analysis. **(D–G)** The expression of *adamts9*, *adam8b*, *adamts1*, and *mmp9* in preovulatory follicular cells at 07:00 of control females unpaired with WT males, control females paired with WT males, *star*-deficient females unpaired with WT males, *star*-deficient females paired with WT males, and *star*-deficient females treated with DHP. The letters in the bar charts represent significant differences.

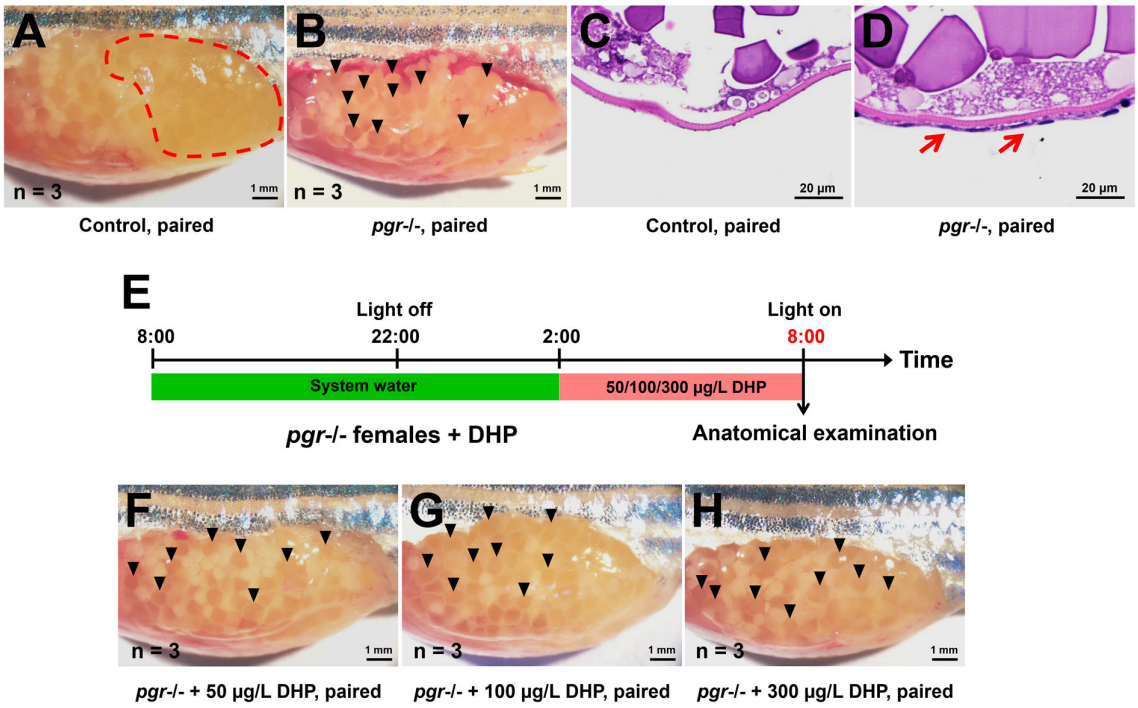

FIGURE 6
Comparison of ovaries from control and *pgr*-deficient female fish paired with WT males or treated with DHP after light onset. **(A, B)** Anatomical analysis of ovaries. Normal mature and ovulated oocytes were released into the vicinity of the genital pore in control females paired with WT males (**A**, dashed red circle), and anovulation with mature oocytes trapped within the ovary in *pgr*-deficient females paired with WT males (**B**, black arrow heads). **(C, D)** Histological analysis of mature follicles. Compared with control fish **(C)**, the outer layer cells of the mature follicles from the *pgr*-deficient female fish failed to breakdown (**D**, red arrows). **(E)** Schematic illustration of the DHP administration on *pgr*-deficient females from 02:00 to 08:00. The samples at the timepoint depicted in red are harvested for analysis. **(F–H)** The anovulation with mature oocytes trapped within the ovary in *pgr*-deficient females (black arrow heads) cannot be rescued by administration of 50, 100 and 300 μg/L DHP.

ejaculatory pore and were ready to spawn, forming egg membranes followed by dissection. These results provided direct *in vivo* evidence supporting that oocyte maturation and ovulation occurred effectively in *lhβ*- or *star*-deficient females after DHP administration.

The *lhβ*- or *star*-deficient females reared in control medium (1‰ DMSO system water) exhibited no egg-laying when naturally mated with WT males. Nevertheless, DHP treatment from 02:00 to 08:00 effectively rescued the defects in oocyte maturation and ovulation of *lhβ*- or *star*-deficient females when naturally mated with WT males, i.e. the restored spawned and fertilized eggs (Figure 2, Table 3). Noteworthily, the spawning ratio of the *lhβ*- or *star*-deficient females and the fertilization ratio of the offspring were decreased compared to the WT control group (Table 3). One possibility is that the spawned eggs may not be in their most appropriate status for fertilization with the above treatment method. Therefore, further efforts to optimize the process, including concentration of the chemical reagent, mode of the administration, or other factors, are needed to improve the quality of the eggs from the mutant females. This hypothesis could be partially supported by the observations that the ratio of membrane break and survival at 3 wpf of the offspring from the DHP + hCG treated *star*-deficient females mated with WT males were higher than with the females with DHP treatment only (Table 3). Intriguingly, the survived fish (*lhβ*+/- or *star*+/-) displayed normal growth performance (body weight, body length and full length) compared with the control fish (*lhβ*+/+ or *star*+/+) as observed at 1 mpf (Supplementary Figure 1).

Metalloproteinases are important for zebrafish ovulation. The relative expression of metalloproteinases, *adamts9*, *adam8b*, *mmp9*, and *adamts1*, was upregulated in the follicular cells of pre-ovulatory follicles at stage IV, approximately 1 h prior to ovulation and light on (Liu et al., 2018). Among the four metalloproteinases, *adamts9* and *adam8b*, were significantly upregulated in follicular cells of control females paired with WT males, and WT females, *lhβ*- or *star*-deficient females exposed to DHP for 2 h (from 05:00 to 07:00), but not in *lhβ*- or *star*-deficient females paired with WT males. Thereby, it is reasonable to speculate that dysregulated expressions of *adamts9* and *adam8b* in follicular cells of preovulatory follicles at stage IV of *lhβ*- or *star*-deficient females might be due to insufficient DHP synthesis. Thus the insufficient expressions of *adamts9* and *adam8b* may be the cause for the impaired oocyte maturation and ovulation, which is in agreement with a previous report on the reduced expression of *adam8b* and *adamts9* in the follicular cells of preovulatory follicles of *pgr*-/- females (Liu et al., 2018). We discovered that a concentration of 50 μg/L can induce oocyte maturation, ovulation, and spawning in WT females (Figure 1, Table 2). Upregulated *adamts9* and *adam8b* expression in the

follicular cells of the pre-ovulatory follicles of control females exposed to DHP from 05:00 to 07:00 mimicked the effect of natural mating with WT males (Figure 3D).

Anovulation, wherein mature oocytes were retained in the ovary, was observed in *pgr*-deficient females when mated with WT males. However, DHP administration was ineffective in restoring ovulation in *pgr*-deficient females when paired with WT males, indicating that the critical role of Pgr in ovulation. This is further demonstrated by the distinct phenotypes of *pgr*- and *lhβ*- or *star*-deficient females, which display impaired ovulation and oocyte maturation, respectively. Therefore, it is reasonable to hypothesize that Star plays a role in the downstream LH signaling pathway, leading to the direct synthesis of DHP to enhance oocyte maturation and ovulation, with ovulation being dependent on Pgr.

Previously, it has been reported that the intraperitoneally injection of hCG, DHP precursors (pregnenolone or progesterone), and DHP itself, partially rescued the maturation-arrested oocyte phenotypes in *lhβ*-deficient females (Shang et al., 2019; Chu et al., 2014). Among the chemicals, hCG administered via intraperitoneal injection successfully induced the maturation of a small number of follicles and ovulation in *lhβ*-deficient females. However, the report lacked clarity regarding the restorative effects of natural spawning and fertilization (Chu et al., 2014). Herein, we also evaluated the combined effect of hCG injection and DHP administration for 6 h (hCG injection at 00:00) and found no spawning and fertilized eggs from the hCG treated *lhβ*-deficient females mated with WT males. However, compared with the *star*-deficient females exposed to 300 μg/L DHP only, the improvement of the ratio of spawning, membrane broken and survival at 3 wpf were observed in *star*-deficient females with hCG injection and 300 μg/L DHP administration for 6 h (66.67 ± 9.43%, 72.36 ± 25.63%, and 71.60 ± 22.32%, respectively). The overall relative fecundity ratio, a novel concept evaluated in this study was that *star*-/- zebrafish treated with DHP and hCG exhibited a ratio at 17.98%. It is noteworthy that there was a limited improvement in these parameters in *lhβ*-deficient females after hCG injection and administration of 100 μg/L DHP for 6 h (Table 3). These observations suggest that although hCG is a LH analog, its function in regulating oocyte maturation and ovulation may differ in various animal species.

In channel catfish, sterilization was achieved through genetic editing of LH using a modified zinc finger nuclease technology with electroporation. This accomplishment not only enhances the comprehension of the roles of LH in farmed fish, but also represents progress towards fertility control in females of transgenic fish (Qin et al., 2016). CRISPR/Cas9 techniques have been suggested to improve economic traits. However, the application of sterilization technology can be utilized to establish fertility control strategies for genetically modified farm fish. Fertility-controlled fish, which are unable to breed naturally, offer natural biosecurity benefits by preventing escapee from mating with the WT stock and protecting intellectual property rights (Okoli et al., 2022). To the best of our knowledge, this study represents the first model with the manipulation of sex steroid-related genes, which opens up prospects for its application in the aquaculture industry, particularly in the genetic engineering of farmed fish with the aim of improving economic traits. Notably, our recent research involving zebrafish and common carp revealed that all homozygous *cyp17a1*-deficient fish gonads developed into testes with proper spermatogenesis; however, they lacked the typical male sexual characteristics and mating behaviors (Zhai et al., 2018; Zhai et al., 2022a). All offspring resulted from the artificial fertilization of the neomale common carp (*cyp17a1*-/-;XX genotype) sperm with the eggs from WT females (*cyp17a1*+/+;XX genotype) developed into all-female common carp. The genotype (*cyp17a1*+/-;XX genotype), all-ovarian differentiation (n>500) and significant growth advantage have been confirmed (Zhai et al., 2022a). The fertility of this genome-edited all-female population of common carp presents a potential eco-risk, thus hindering its application in aquaculture. This strategy offers the possibility of addressing the challenging situation. However, the "controllable fertility" strategy proposed in this study offers a solution by enabling the production and sterilization of the all-female population (*cyp17a1*+/-;*lhβ* (or *star*)-/-;XX). This can be achieved by crossing the *cyp17a1*-/-;*lhβ* (or *star*)-/-;XX males (neomales) with *cyp17a1*+/+;*lhβ* (or *star*)-/-;XX females, who are administered DHP. Fortunately, no obvious defect in fertility of *lhβ*-/- or *star*-/- male zebrafish was observed, suggesting that mutation of *lhβ* or *star* did not affect fertility in male fish (Shang et al., 2019). Based on the achieved relative fecundity ratio of *star*-/- zebrafish treated with the DHP and hCG procedure, a ratio of 17.98% was obtained (Table 3). This ratio suggests that more than 10,000 healthy fingerlings can be produced from each *star*-/- common carp with its egg-carrying capacity, providing an effective rescue strategy for farmed fish. However, further improvements will be required to enhance rescue efficiency. Overall, the genome-edited population of all-female carp rendered infertile via this procedure could impede the ecological risks by preventing the interbreeding of genome-edited escapees with WT carp stocks, as they are unable to reproduce naturally.

Data availability statement

The original contributions presented in the study are included in the article/Supplementary Material. Further inquiries can be directed to the corresponding author.

Ethics statement

The animal studies were approved by Guiding Principles for the Care and Use of Laboratory Animals, Institute of Hydrobiology, Chinese Academy of Sciences. The studies were conducted in accordance with the local legislation and institutional requirements. Written informed consent was obtained from the owners for the participation of their animals in this study.

Author contributions

SS: Data curation, Formal analysis, Investigation, Methodology, Writing – original draft. YZ: Data curation, Formal analysis,

Investigation, Methodology, Writing – review & editing. JH: Investigation, Validation, Visualization, Writing – review & editing. QL: Investigation, Resources, Validation, Writing – review & editing, Methodology. XJ: Resources, Supervision, Visualization, Writing – review & editing. JH: Resources, Software, Supervision, Writing – review & editing. GZ: Supervision, Writing – review & editing, Conceptualization, Funding acquisition, Project administration, Writing – original draft. ZY: Conceptualization, Funding acquisition, Project administration, Supervision, Writing – original draft, Writing – review & editing.

Funding

The author(s) declare that financial support was received for the research, authorship, and/or publication of this article. This work was supported by the National Key Research and Development Program, China (2022YFD2401800 to GZ and 2022YFF1000300 to ZY), the National Natural Science Foundation, China (32230108 to ZY and 31972779 to GZ), the Foundation of Hubei Hongshan Laboratory (2021hszd021 to ZY and 2021hskf013 to GZ), the Major Science and Technology Program of Wuhan City (2022021302024854 to ZY), the Youth Innovation Promotion Association of CAS (2020336 to GZ), and the State Key Laboratory of Freshwater Ecology and Biotechnology (2016FBZ05 to ZY).

Acknowledgments

We are grateful to Professor Xiaochun Liu of Sun Yat-Sen University for the generous gift of the *pgr*-deficient zebrafish line. We thank Mr. Wenyou Chen of the Institute of Hydrobiology, Chinese Academy of Sciences, for handling the zebrafish stocks. We would also like to thank Ms. Guangxin Wang from the Analysis and Testing Center of Institute of Hydrobiology, Chinese Academy of Sciences for assistance with confocal microscopy.

Conflict of interest

The authors declare that the research was conducted in the absence of any commercial or financial relationships that could be construed as a potential conflict of interest.

The author(s) declared that they were an editorial board member of Frontiers, at the time of submission. This had no impact on the peer review process and the final decision.

Publisher's note

Supplementary material

The Supplementary Material for this article can be found online at: https://www.frontiersin.org/articles/10.3389/fmars.2024.1381305/full#supplementary-material

SUPPLEMENTARY FIGURE 1
The gross appearance of offspring at diverse stages from control females, DHP-administrated *lhβ*- or *star*-deficient females naturally mated with WT males. **(A–C)** Representative image of the gross appearance of embryos at 12 hpf. **(D–F)** Representative image of the gross appearance of larvae at 72 hpf. **(G–I)** Representative image of the gross appearance of larvae at 5 dpf. **(J–L)** Representative image of the gross appearance of fish at 21 dpf. **(A, D, G, J)** Offspring from control females naturally mated with WT males. **(B, E, H, K)** offspring from *lhβ*-deficient females exposed to 100 μg/L DHP for 6 h and naturally mated with WT males. **(C, F, I, L)** Offspring from *star*-deficient females exposed to 300 μg/L DHP for 6 h and naturally mated with WT males. **(M)** The bar chart represents body weight of the fish at 1 mpf. **(N)** The bar chart represents body length of the fish at 1 mpf. **(O)** The bar chart represents full-length of fish at 1 mpf. The letter a in the bar charts indicates no significant difference.

References

Ascoli, M., Fanelli, F., and Segaloff, D. L. (2002). The lutropin/choriogonadotropin receptor, a 2002 perspective. *Endocr. Rev.* 23, 141–174. doi: 10.1210/edrv.23.2.0462

Chen, S. X., Bogerd, J., Schoonen, N. E., Martijn, J., de Waal, P. P., and Schulz, R. W. (2013). A progestin (17alpha,20beta-dihydroxy-4-pregnen-3-one) stimulates early stages of spermatogenesis in zebrafish. *Gen. Comp. Endocrinol.* 185, 1–9. doi: 10.1016/j.ygcen.2013.01.005

Chu, L. H., Li, J. Z., Liu, Y., Hu, W., and Cheng, C. H. K. (2014). Targeted gene disruption in zebrafish reveals noncanonical functions of lh signaling in reproduction. *Mol. Endocrinol.* 28, 1785–1795. doi: 10.1210/me.2014-1061

Clelland, E., and Peng, C. (2009). Endocrine/paracrine control of zebrafish ovarian development. *Mol. Cell Endocrinol.* 312, 42–52. doi: 10.1016/j.mce.2009.04.009

Crowder, C. M., Lassiter, C. S., and Gorelick, D. A. (2018). Nuclear androgen receptor regulates testes organization and oocyte maturation in zebrafish. *Endocrinology* 159, 980–993. doi: 10.1210/en.2017-00617

El Mohajer, L., Bulteau, R., Fontaine, P., and Milla, S. (2022). Maturation inducing hormones in teleosts: Are progestogens always the first to be nominated? *Aquaculture* 546, 737315. doi: 10.1016/j.aquaculture.2021.737315

Gharib, S. D., Wierman, M. E., Shupnik, M. A., and Chin, W. W. (1990). Molecular-biology of the pituitary gonadotropins. *Endocr. Rev.* 11, 177–199. doi: 10.1210/edrv-11-1-177

Gratacap, R. L., Wargelius, A., Edvardsen, R. B., and Houston, R. D. (2019). Potential of genome editing to improve aquaculture breeding and production. *Trends Genet.* 35, 672–684. doi: 10.1016/j.tig.2019.06.006

Huang, J. F., Shi, C., Gao, Y. P., Su, J. Z., Shu, Y. Q., Zeng, N. M., et al. (2021). Heterozygous depletion of improves growth and feed conversion efficiency in gibel carp. *Aquaculture* 545, 737207. doi: 10.1016/j.aquaculture.2021.737207

Huhtaniemi, I. (2006). Mutations along the pituitary-gonadal axis affecting sexual maturation: Novel information from transgenic and knockout mice. *Mol. Cell Endocrinol.* 254-255, 84–90. doi: 10.1016/j.mce.2006.04.015

Huhtaniemi, I. T., and Themmen, A. P. (2005). Mutations in human gonadotropin and gonadotropin-receptor genes. *Endocrine* 26, 207–217. doi: 10.1385/ENDO:26:3:207

Kinkel, M. D., Eames, S. C., Philipson, L. H., and Prince, V. E. (2010). Intraperitoneal injection into adult zebrafish. *J. Vis. Exp.* 42). doi: 10.3791/2126

Lau, E. S., Zhang, Z. W., Qin, M. M., and Ge, W. (2016). Knockout of zebrafish ovarian aromatase gene (cyp19a1a) by talen and crispr/cas9 leads to all-male offspring due to failed ovarian differentiation. *Sci. Rep.* 6, 37357. doi: 10.1038/srep37357

Lei, Z. M., Mishra, S., Zou, W., Xu, B., Foltz, M., Li, X., et al. (2001). Targeted disruption of luteinizing hormone/human chorionic gonadotropin receptor gene. *Mol. Endocrinol.* 15, 184–200. doi: 10.1210/mend.15.1.0586

Levavi-Sivan, B., Bogerd, J., Mananos, E. L., Gomez, A., and Lareyre, J. J. (2010). Perspectives on fish gonadotropins and their receptors. *Gen. Comp. Endocrinol.* 165, 412–437. doi: 10.1016/j.ygcen.2009.07.019

Li, J. Z., and Ge, W. (2020). Zebrafish as a model for studying ovarian development: Recent advances from targeted gene knockout studies. *Mol. Cell Endocrinol.* 507, 110778. doi: 10.1016/j.mce.2020.110778

Li, J. Z., Niu, C. Y., and Cheng, C. H. K. (2018). Igf3 serves as a mediator of luteinizing hormone in zebrafish ovulation. *Biol. Reprod.* 99, 1235–1243. doi: 10.1093/biolre/ioy143

Li, N., Oakes, J. A., Storbeck, K. H., Cunliffe, V. T., and Krone, N. P. (2020). The p450 side-chain cleavage enzyme cyp11a2 facilitates steroidogenesis in zebrafish. *J. Endocrinol.* 244, 309–321. doi: 10.1530/JOE-19-0384

Liu, D. T., Carter, N. J., Wu, X. J., Hong, W. S., Chen, S. X., and Zhu, Y. (2018). Progestin and nuclear progestin receptor are essential for upregulation of metalloproteinase in zebrafish preovulatory follicles. *Front. Endocrinol. (Lausanne).* 9. doi: 10.3389/fendo.2018.00517

Liu, D. T., Hong, W. S., Chen, S. X., and Zhu, Y. (2020). Upregulation of adamts9 by gonadotropin in preovulatory follicles of zebrafish. *Mol. Cell Endocrinol.* 499, 110608. doi: 10.1016/j.mce.2019.110608

Lu, H. J., Cui, Y., Jiang, L. W., and Ge, W. (2017). Functional analysis of nuclear estrogen receptors in zebrafish reproduction by genome editing approach. *Endocrinology* 158, 2292–2308. doi: 10.1210/en.2017-00215

Ma, X. P., Dong, Y. L., Matzuk, M. M., and Kumar, T. R. (2004). Targeted disruption of luteinizing hormone beta-subunit leads to hypogonadism, defects in gonadal steroidogenesis, and infertility. *Proc. Natl. Acad. Sci. U S A.* 101, 17294–17299. doi: 10.1073/pnas.0404743101

McGee, E. A., and Hsueh, A. J. (2000). Initial and cyclic recruitment of ovarian follicles. *Endocr. Rev.* 21, 200–214. doi: 10.1210/edrv.21.2.0394

Nagahama, Y., and Yamashita, M. (2008). Regulation of oocyte maturation in fish. *Dev. Growth Differ.* 50 Suppl 1, S195–S219. doi: 10.1111/j.1440-169X.2008.01019.x

Nagahama, Y., Yoshikuni, M., Yamashita, M., Tokumoto, T., and Katsu, Y. (1995). Regulation of oocyte growth and maturation in fish. *Curr. topics Dev. Biol.* 30, 103–145. doi: 10.1016/S0070-2153(08)60565-7

Okoli, A. S., Blix, T., Myhr, A. I., Xu, W. T., and Xu, X. D. (2022). Sustainable use of crispr/cas in fish aquaculture: The biosafety perspective. *Transgenic Res.* 31, 1–21. doi: 10.1007/s11248-021-00274-7

Qin, Z. K., Li, Y., Su, B. F., Cheng, Q., Ye, Z., Perera, D. A., et al. (2016). Editing of the luteinizing hormone gene to sterilize channel catfish, ictalurus punctatus, using a modified zinc finger nuclease technology with electroporation. *Mar. Biotechnol. (NY).* 18, 255–263. doi: 10.1007/s10126-016-9687-7

Shang, G. H., Peng, X. Y., Ji, C., Zhai, G., Ruan, Y. L., Lou, Q. Y., et al. (2019). Steroidogenic acute regulatory protein and luteinizing hormone are required for normal ovarian steroidogenesis and oocyte maturation in zebrafishdagger. *Biol. Reprod.* 101, 760–770. doi: 10.1093/biolre/ioz132

Shi, S. C., Shu, T. T., Li, X., Lou, Q. Y., Jin, X., He, J. Y., et al. (2022). Characterization of the interrenal gland and sexual traits development in cyp17a2-deficient zebrafish. *Front. Endocrinol. (Lausanne).* 13. doi: 10.3389/fendo.2022.910639

Shu, T. T., Zhai, G., Pradhan, A., Olsson, P. E., and Yin, Z. (2020). Zebrafish cyp17a1 knockout reveals that androgen-mediated signaling is important for male brain sex differentiation. *Gen. Comp. Endocrinol.* 295, 113490. doi: 10.1016/j.ygcen.2020.113490

Tang, H. P., Chen, Y., Wang, L., Yin, Y. K., Li, G. F., Guo, Y., et al. (2018). Fertility impairment with defective spermatogenesis and steroidogenesis in male zebrafish lacking androgen receptor. *Biol. Reprod.* 98, 227–238. doi: 10.1093/biolre/iox165

Tang, H. P., Liu, Y., Li, J. Z., Yin, Y. K., Li, G. F., Chen, Y., et al. (2016). Gene knockout of nuclear progesterone receptor provides insights into the regulation of ovulation by lh signaling in zebrafish. *Sci. Rep.* 6, 28545. doi: 10.1038/srep28545

Tokumoto, T., Yamaguchi, T., Ii, S., and Tokumoto, M. (2011). *In vivo* induction of oocyte maturation and ovulation in zebrafish. *PloS One* 6, e25206. doi: 10.1371/journal.pone.0025206

Westerfield, M. (2000). *The zebrafish book, a guide for the laboratory use of zebrafish (danio rerio). 4th ed* (Eugene, OR: University of Oregon Press).

Wu, X. J., Liu, D. T., Chen, S. X., Hong, W. S., and Zhu, Y. (2020). Impaired oocyte maturation and ovulation in membrane progestin receptor (mpr) knockouts in zebrafish. *Mol. Cell Endocrinol.* 511, 110856. doi: 10.1016/j.mce.2020.110856

Yin, Y. K., Tang, H. P., Liu, Y., Chen, Y., Li, G. F., Liu, X. C., et al. (2017). Targeted disruption of aromatase reveals dual functions of cyp19a1a during sex differentiation in zebrafish. *Endocrinology* 158, 3030–3041. doi: 10.1210/en.2016-1865

Yu, G. Q., Zhang, D. W., Liu, W., Wang, J., Liu, X., Zhou, C., et al. (2018). Zebrafish androgen receptor is required for spermatogenesis and maintenance of ovarian function. *Oncotarget* 9, 24320–24334. doi: 10.18632/oncotarget.v9i36

Zhai, G., Shu, T. T., Chen, K. X., Lou, Q. Y., Jia, J. Y., Huang, J. F., et al. (2022a). Successful production of an all-female common carp (cyprinus carpio l.) population using cyp17a1-deficient neomale carp. *Engineering-Prc* 8, 181–189. doi: 10.1016/j.eng.2021.03.026

Zhai, G., Shu, T. T., Xia, Y. G., Lu, Y., Shang, G. H., Jin, X., et al. (2018). Characterization of sexual trait development in cyp17a1-deficient zebrafish. *Endocrinology* 159, 3549–3562. doi: 10.1210/en.2018-00551

Zhai, G., Shu, T., Yu, G., Tang, H., Shi, C., Jia, J., et al. (2022b). Augmentation of progestin signaling rescues testis organization and spermatogenesis in zebrafish with the depletion of androgen signaling. *Elife* 11, 66118. doi: 10.7554/eLife.66118

Zhang, F. P., Poutanen, M., Wilbertz, J., and Huhtaniemi, I. (2001). Normal prenatal but arrested postnatal sexual development of luteinizing hormone receptor knockout (lurko) mice. *Mol. Endocrinol.* 15, 172–183. doi: 10.1210/mend.15.1.0582

Zhang, Z. W., Zhu, B., and Ge, W. (2015). Genetic analysis of zebrafish gonadotropin (fsh and lh) functions by talen-mediated gene disruption. *Mol. Endocrinol.* 29, 76–98. doi: 10.1210/me.2014-1256

Zhu, Y., Liu, D. T., Shaner, Z. C., Chen, S. X., Hong, W. S., and Stellwag, E. J. (2015). Nuclear progestin receptor (pgr) knockouts in zebrafish demonstrate role for pgr in ovulation but not in rapid non-genomic steroid mediated meiosis resumption. *Front. Endocrinol. (Lausanne).* 6. doi: 10.3389/fendo.2015.00037

frontiers | Frontiers in Marine Science

TYPE Original Research
PUBLISHED 12 March 2024
DOI 10.3389/fmars.2024.1345493

OPEN ACCESS

EDITED BY
Tangtian He,
Hong Kong Polytechnic University, Hong Kong SAR, China

REVIEWED BY
Liqiang Zhao,
Guangdong Ocean University, China
Zhe Zheng,
Guangdong Ocean University, China

*CORRESPONDENCE
Clara L. Mackenzie
Clara.Mackenzie@dfo-mpo.gc.ca

RECEIVED 27 November 2023
ACCEPTED 19 February 2024
PUBLISHED 12 March 2024

CITATION
Mackenzie CL, Raap MR, Leduc S, Walker CYV, Green TJ, Kim E, Montgomery EM, Gray SLM, Long A and Pearce CM (2024) Development of a nature-based solution for mitigation of Pacific oyster summer mortality: use of the intertidal zone to improve resilience to environmental stressors.
Front. Mar. Sci. 11:1345493.
doi: 10.3389/fmars.2024.1345493

Development of a nature-based solution for mitigation of Pacific oyster summer mortality: use of the intertidal zone to improve resilience to environmental stressors

Clara L. Mackenzie[1]*, Monique R. Raap[1], Sarah Leduc[2], Chen Yin V. Walker[1], Timothy J. Green[2], Eliah Kim[1], Emaline M. Montgomery[1], Sierra L. M. Gray[1], Amy Long[1] and Christopher M. Pearce[1]

[1]Pacific Biological Station, Fisheries and Oceans Canada, Nanaimo, BC, Canada, [2]Centre for Shellfish Research, Vancouver Island University, Nanaimo, BC, Canada

In recent years, Pacific oyster growers in British Columbia (BC), Canada have experienced devastating losses due to summer mortality syndrome. While anecdotal evidence suggests that intertidally-grown oysters may fare better during mass mortality events than deep-water counterparts, there remains a lack of research examining how different culture conditions may influence severity. To address this, we compared growth, condition, histopathology, reproductive status, and survival between intertidally- and deep-water-cultured oysters over 2 years at three oyster farms in Baynes Sound (BC). A reciprocal transplant was carried out after 1 year to test the use of the intertidal as a mechanism for promotion of physiological resilience prior to deep-water deployment. Field trial results showed significantly higher final survival in oysters transferred from the intertidal to deep water (83.5%) compared to those maintained in deep water (63.6%), but only at one farm, likely as a consequence of varying physical and/or biological characteristics associated with particular farm locations. Histopathology showed little role of disease with regards to varying survival among treatments, though higher occurrence of Viral Gametocytic Hypertrophy was observed in Year 1 oysters under deep-water (62.2%) versus intertidal (37.8%) conditions. Additionally, after 2 years, there was no significant difference in oyster size nor condition index between oysters transplanted from the intertidal to deep water and those solely cultured in deep water. A laboratory-challenge experiment determined significantly different survival curves of Year 1 intertidally- and deep-water-cultured oysters under immersion/emersion and warming conditions, with final survival of 88% and 64%, respectively, under conditions of high temperature (25°C) and immersion. Likewise, Year 2 (i.e. post-transfer) intertidally- and deep-water-cultured oysters showed significantly different survival curves

under laboratory-based *Vibrio* challenge conditions (16°C) with final survival of 63% and 34%, respectively. Results suggest that partial culture in the intertidal at some farms may be an effective method for conferring resilience to summer mortality in Pacific oysters.

KEYWORDS

food security, heatwaves, mitigation, Pacific oyster (*Crassostrea gigas*), shellfish aquaculture, summer mortality syndrome

1 Introduction

Pacific oyster (*Crassostrea gigas*) growers across the globe continue to contend with mass mortality events during summer months. In recent years, this widespread and recurrent phenomenon has caused increasing annual losses (20–100%) at farms spanning North America, Europe, Asia, and Australia (Malham et al., 2009; Cotter et al., 2010; Dégremont et al., 2010; Green et al., 2019; King et al., 2019; Lafont et al., 2019; Ashton et al., 2020; Yang et al., 2021). The shellfish aquaculture industry is a large global employer and provides an increasingly important dietary protein source for human populations (FAO, 2022). Likewise, the industry contributes greatly to international markets, global exports of bivalve mollusks being worth approximately USD 4.3 billion in 2020 (FAO, 2022). Accordingly, there is a critical need for the development of practical mitigation methods to reduce summer mortality in order to support regional economies and safeguard global food security.

Summer mortality of Pacific oysters is associated with a complex set of interrelated and interactive physical and biological factors. While events are primarily driven by high seawater temperatures (i.e. >19–20°C) (Green et al., 2019; Petton et al., 2021), there is a range of additional key contributory factors including reproductive status, genetics, growth and condition, and viral/bacterial pathogenic infection (Li et al., 2009; Barbosa Solomieu et al., 2015; Petton et al., 2021; Cowan et al., 2023). Other environmental factors, including low salinity events (Brown and Hartwick, 1988) and harmful algal blooms (Cassis et al., 2011), have also been associated with increased levels of mortality during the summer.

The Pacific oyster has broad environmental tolerance limits and consequently is successfully cultured under a wide range of growing conditions. Culture environments extend from the intertidal zone, where diurnal tidal emersion events generate large and regular environmental fluctuations, to deep-water (i.e. suspended culture) conditions where animals experience constant immersion and relatively stable growing conditions. The distinctive exposures associated with intertidal and deep-water culture environments drive contrasting magnitudes and frequencies of related stress responses with direct repercussions for growth/condition, reproduction, and survival (Cotter et al., 2010; Pernet et al., 2012, 2014; Petton et al., 2021; Cowan et al., 2023).

Species inhabiting the intertidal zone contend with daily fluctuations in physical (e.g. temperature, dissolved oxygen, pH) and biological (e.g. feed availability, predators) parameters. This is particularly relevant for oysters and clams, which, as non-motile thermo-conformers, cannot directly avoid such conditions. To combat this, intertidal bivalves have evolved a number of adaptative mechanisms that allow them to tolerate diurnal and seasonal variations in physical conditions (e.g. wide thermal fluctuations) and to survive short-term stressor events (e.g. hypoxia/anoxia, osmotic stress, heat stress) (Clark et al., 2018; Masanja et al., 2023). These include a well-developed antioxidant defense system, the ability to enter a metabolically-depressed state (including shifting to anaerobic glycolysis metabolism), mitochondrial adjustments, episodic shell gaping to access atmospheric oxygen, protective burrowing behaviors, and changes in shell morphology (Somero, 2002; Abele et al., 2009; Tagliarolo et al., 2012; Li et al., 2013; Zhang et al., 2016; Meng et al., 2018; Lafont et al., 2020; Amorim et al., 2021). Additionally, gene expression profiles of individuals from intertidal populations tend to be markedly different in comparison to those from subtidal ones, the former's characterized by an upregulation in genes involved in respiration, antioxidant production, protein degradation, DNA repair, and cytoskeleton pathways, reflecting the stressor conditions associated with the intertidal environment (Li et al., 2018; Clark et al., 2019). While animals in the intertidal face regular stress events (e.g. high atmospheric temperature, increased oxidative stress) (Pörtner, 2012; Zhang et al., 2016), deep-water counterparts largely experience less challenging physical conditions whilst also benefiting from increased availability of feed and reduced predation pressure.

Gene-environment interactions represent a major shaping force of the intertidal zone and lead to considerable intra-specific variation in the evolved responses of marine invertebrates across the intertidal environmental gradient. The interplay between genetics and the surrounding environment dictates phenotypic plasticity, which serves as an important mechanism by which intertidal species may respond to changing environmental conditions (Li et al., 2018; Clark et al., 2019). Indeed, phenotypic plasticity has been observed in an extensive range of bivalve traits including metabolism and shell structure (Tagliarolo et al., 2012; Clark et al., 2018), gene expression (Hamdoun et al., 2003; Clark

et al., 2018), energy allocation (Ernande et al., 2004), and feeding behavior (Bayne, 2004), with responses encompassing whole-organism to tissue-, cellular-, and molecular-level systems (Somero, 2002). A number of recent investigations have also demonstrated that phenotypic plasticity may be adaptively-favored by intertidal organisms (Clark et al., 2018; Li et al., 2018; Wang et al., 2021, 2023).

Anecdotal evidence from oyster growers (British Columbia Shellfish Growers Association, pers. comm.) and previous research (Peeler et al., 2012; Pernet et al., 2019) suggest that intertidally-grown oysters may fare more favorably during mass mortality events compared to counterparts in deep-water culture conditions. The higher mortality rates observed at deep-water sites compared to intertidal sites may be due to several factors. Firstly, as previously discussed, deep-water cultured oysters lack the exposure to short-term stress events regularly experienced by animals in the intertidal, which could serve as important physiological triggers for the development of resilience to more extreme stressor events (Wang et al., 2012; Zhang et al., 2016; Meng et al., 2018). Secondly, shore-based culture may promote an oyster microbiome that is better suited to contend with various pathogens (e.g. *Vibrio*) (King et al., 2019; Offret et al., 2020). As well, the reduced feeding duration of intertidal animals may result in lowered reproductive condition and reduced spawning, thus decreasing the stress associated with the latter (Cotter et al., 2010; Huvet et al., 2010; Cowan et al., 2023). In contrast, deep-water cultured animals may have to contend with an extended presence of seasonally-unfavorable seawater conditions that may be the result of environmental variations (e.g. high seasonal water temperatures, harmful algal blooms) (Evans et al., 2019) or due to high-density culture within oyster trays/stacks (e.g. reduced flow rates, low dissolved oxygen concentration, high dissolved waste concentration) (Campbell and Hall, 2019). Additionally, intertidal and deep-water culture conditions may vary in terms of altered host–pathogen interactions as intertidal host species spend less time underwater so benefit from reduced exposure to seawater pathogens (Pernet et al., 2012, 2014). The proliferation of pathogens in host oysters is also likely to vary according to site-driven differences in metabolism and growth (Pernet et al., 2014).

There remains a lack of research examining how the varying physical conditions and oyster physiologies associated with deep-water and intertidal culture sites may promote or reduce the severity of summer mortality events. To address this, the present study compared growth, condition, histopathology, reproductive status, and survival between intertidally- and deep-water-cultured oysters over one full growth cycle (i.e. 2 years, initial deployment to harvest). Additionally, we tested the use of the intertidal zone as a mechanism for promotion of physiological resilience prior to deep-water deployment via a reciprocal transplant between intertidal and deep-water sites after the first year. We also examined site-based responses to specific summer mortality stressors via controlled temperature and pathogen challenge experiments within a laboratory setting. Results will contribute to the collective understanding of drivers of Pacific oyster summer mortality and advance the development of practical mitigation strategies in order to promote the sustainability of this important global food resource.

2 Methodology

2.1 Field experiment

In March 2021, juvenile (~8 months old, mean shell height (± SD): 26.22 ± 3.30 mm, N = 30) Pacific oysters were placed in "surface" float bags (black Vexar® 9-mm mesh bags, L x W x H = ~100 x 50 x 15 cm). Approximately 500 individuals were placed in every bag (N = 180), representing commercial stocking densities, prior to deployment at an intertidal site and a deep-water site at each of three commercial farms: Deep Bay (DB), Denman Island (DN), and Fanny Bay (FB), located within Baynes Sound, British Columbia (BC), Canada (Figure 1). Baynes Sound represents the most intensely farmed shellfish area in BC (BCMSRM, 2002) and farms across the region have experienced considerable summer mortality events in recent years (Cowan, 2020; Cowan et al., 2023). Stocking of float bags with oysters and deployment of bags were carried out by an industry partner (Taylor Shellfish Canada) according to industry protocols. Two lines of 30 float bags (~15 cm between bags) were positioned near a main oyster growing area within each farm with one line positioned in a subtidal area and the other established in the intertidal zone. In the subtidal sites (hereafter referred to as deep-water sites), float bags remained floating in surface seawater (~50 cm depth) for the duration of the field trial, thus providing continuous immersion, irrespective of tidal phase. At the intertidal sites, float bags were positioned along the 6-foot tidal mark as per industry protocol, thus providing regular (i.e. diurnal) periods of emersion/immersion according to tidal phases. The distance between intertidal and deep-water sites was <300 m at all three farms. In August 2021, the density in all bags was reduced by 50% to approximately 250 animals per bag to ensure optimal growing densities, as per industry protocol. Bags were then left over the autumn and winter months (i.e. October through April) with periodic visits made to check the integrity of the float bags and the general condition of animals.

In May 2022, a reciprocal transplant of 15 bags from the deep-water site and 15 bags from the intertidal site was carried out at each farm. Alternating bags from each line were transferred and re-attached to the corresponding deep-water/intertidal line. This resulted in four experimental treatment groups: (1) animals solely cultured in deep-water (*Deep*), (2) animals initially cultured in deep water and then transplanted to the intertidal (*Deep→Intertidal*), (3) animals solely cultured in the intertidal (*Intertidal*), and (4) animals initially cultured in the intertidal and then transplanted to deep water (*Intertidal→Deep*). In early June 2022, all bag densities were reduced by 50% to approximately 100 animals per bag to ensure optimal growing densities, as per industry protocol.

2.2 Survival assessment

Survival assessments were carried out across all three farms on a bi-weekly (i.e. every 2 weeks) basis from May 2021 to September 2021 (Year 1: T01–T08). From April 2022 to September 2022 (Year 2: T09–T16), bi-weekly assessment was limited to two farms (DB, DN) due to winter damage occurring at the FB farm. In Year 1, survival was assessed in six bags per line (n = 6, N = 12 counts per

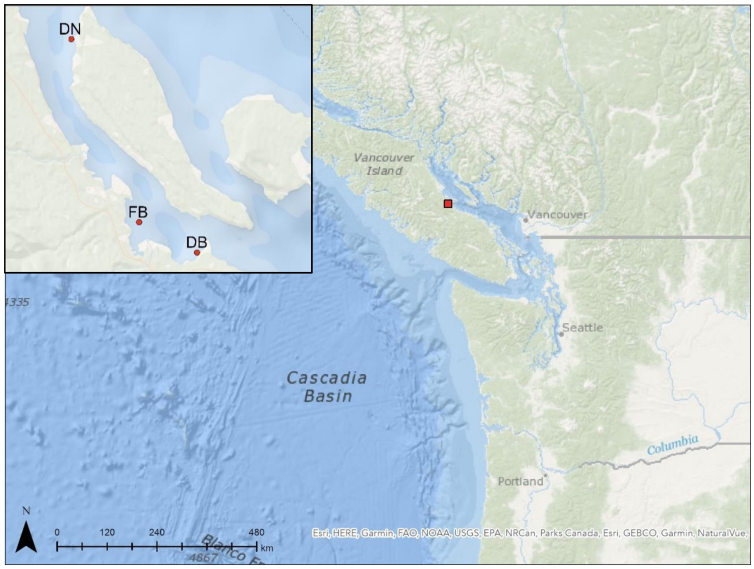

FIGURE 1
Maps of study location. Main map shows location of Baynes Sound (red square) in British Columbia, Canada. Inset map shows location of the three farms (red dots) where the experiment took place: Deep Bay (DB), Denman Island (DN), and Fanny Bay (FB). At each farm, oysters were deployed at an intertidal site and a deep-water suspended site in close proximity to one another. Maps produced using Canada Marine Planning Atlas interactive mapping tool and contain information licensed under the Open Government Licence - Canada.

farm) at each time point as the percent of the 500 (or 250, after thinning) original animals that were alive, as the shells of dead oysters were easily broken down/lost between sampling events due to the small size of animals. Counts were conducted according to a blocked design along the line (i.e. one bag counted per block of five bags). In Year 2, survival percent was assessed via live and dead counts on a sub-set of five bags from each treatment group (n = 5, N = 20 counts per farm). As in Year 1, counts were conducted according to a blocked design along the line (i.e. one bag of each treatment counted per block of six bags). Dead or moribund (determined as those displaying continuous gape) animals and any empty shells were recorded as "dead". Following counts, all live and dead animals and empty shells were replaced in the bags to mimic normal farm growing conditions.

2.3 Sampling

During survival assessment, animals were sampled for analyses of condition index, growth, reproductive status, and histopathology. In Year 1, a single animal was haphazardly sampled from every bag (N = 30) and a randomly chosen sub-set was then used for condition index (18) and histology (12). Due to sampling constraints in Year 2, the routine was reduced to haphazardly sampling five animals from bags that were used for survival assessment (N = 5). A randomly chosen sub-set was then used for condition index (3) and histopathological analyses (2). Sampled animals were placed into labelled bags and stored in cool insulated boxes for transport. Histology sections (one per sampled animal) were taken and fixed in Davidson's solution within 24 hours of collection (see details below). Animals to be used for measurement of condition index were frozen and stored at -80°C until subsequent processing.

2.4 Seawater monitoring

Sea surface temperatures (SST) at intertidal and deep-water sites, and air temperature during tidal emersion at intertidal sites, were tracked over the two summer periods (June–August) of the project. HOBO pendant loggers (ONSET, Bourne, MA, USA) were added to bags situated within each site (N = 3 per line) at each farm, with readings taken at 30-minute intervals. SST and salinity were also monitored via a ProQuatro hand-held multiparameter probe (YSI Incorporated, Yellow Springs, OH, USA) during sampling events at deep-water sites only. Triplicate readings were taken along each line of float bags (at end-points and mid-point) within the top 30 cm of surface waters. In addition, in Year 2, dissolved oxygen was monitored between May and August at DB and DN deep-water sites. U26-001 dissolved oxygen loggers (ONSET, Bourne, MA, USA) were positioned at two points across each line with readings taken at 15-minute intervals.

2.5 Reproductive status and histopathology

Tissue cross sections were processed using routine histological techniques (Marty et al., 2006). In brief, 5-µm-thick tissue sections were cut from paraffin-embedded samples, stained with Harris's modified hematoxylin and eosin (H&E), and then examined under light microscopy for assessment of reproductive stage (i.e. gonad maturity) and histopathology. Assessment was restricted to summer

months (June – August) in both years of the project. Reproductive stage was determined following a qualitative classification (six stages: 0 to 5; Supplementary Table 1), based on Mann (1979), Normand et al. (2008), and Steele and Mulcahy (1999). Sex ratio was determined as the ratio of females to males (F:M) excluding hermaphrodites and undifferentiated oysters. Histopathology included screening for Diffuse Haemocyte Infiltration (DHI), Focalized Haemocyte Infiltration (FHI), Rickettsia-like inclusion (RLP-like), Metaplasia of Digestive Gland Tubules (MDGT), and Viral Gametocytic Hypertrophy (VGH).

2.6 Condition index and growth

Condition index (CI) was determined according to Rainer and Mann (1992): CI = (P1 × 100)/P2, where P1 equals the dry weight (g) of soft tissues and P2 equals the dry weight (g) of the shell. Shell length, width, and height were taken with Vernier digital calipers to 0.01 mm. Wet and dry weights (DW) of tissues and shells were measured to 0.001 g (Pioneer PX, Ohaus, Parsippany, NJ, USA). DWs were taken after a 7-day drying period at 60°C, ensuring drying to constant weight. Mean growth values were determined as final shell height and tissue DW at the end of each growing season (T08, T15). At deployment, mean (± SD) CI, shell height, and tissue DW were 9.1 ± 2.1, 26.22 ± 3.30 mm, and 0.09 ± 0.03 g, respectively (N = 30).

2.7 Laboratory-challenge experiments

Challenge experiments were carried out to compare the survival of deep-water- and intertidally-cultured oysters under separate and/or coinciding high-temperature and *Vibrio aestuarianus* stress conditions. Juvenile oysters for the experiment were taken from treatment groups at the DB farm and were collected when bag densities were reduced in Year 1 (using excess individuals) and at the end of Year 2. Animals were then used in laboratory-challenge experiments carried out at Vancouver Island University's Centre for Shellfish Research (CSR).

2.7.1 Heatwave challenge (year 1)

In Year 1, following 8 months of culture under deep-water or intertidal conditions at DB, approximately 300 animals from each of the two treatment groups (*Deep, Intertidal*) were collected for use in a laboratory-challenge experiment comparing survival under high-temperature stress conditions. Ten haphazardly-selected animals from each treatment group were placed in each of fifteen 20-L glass tanks with 5 L of 80 µM-filtered seawater and held at 15, 20, or 25°C (n = 5 tanks per treatment level, N = 10 tanks per temperature level) via temperature-controlled rooms. Temperatures were chosen to reflect average summer temperatures (15–16°C, Cowan et al., 2023) and natural warming events (~25°C, present study) for the region, and the approximate temperature associated with the onset of summer mortality (19–20°C, Go et al., 2017). Salinity was approximately 30 ppt and a constant air supply was provided to each tank via an air stone. Oysters were acclimated to temperatures over a 24-hour period. No feed was administered over the experiment in order to prevent altered algal concentrations across temperature treatments and to avoid issues with bacterial growth. An additional emersion challenge (i.e. dry conditions) at the same temperatures was carried out in parallel (n = 5 per treatment, 10 animals per replicate) along bench tops in the temperature-controlled rooms. Animals were left under constant emersion conditions with no recovery period (i.e. immersion in seawater) over the entire exposure period. The authors emphasize that the emersion challenge was not carried out to simulate natural conditions but strictly posed as a fitness test for intertidally- versus deep-water-cultured oysters. Mortality in all treatments was assessed on a daily basis over a 10-day exposure period. Moribund animals and/or those displaying a lack of response to stimulus (i.e. continuous gape) were reported as "dead" and removed from the tanks/bench tops.

2.7.2 Heatwave and *Vibrio* challenge (year 2)

In Year 2, 5 months after the reciprocal transfer, approximately 250 animals from each of the deep-water treatment groups (*Deep*, *Intertidal→Deep*) at the DB farm were collected for use in a second laboratory-challenge experiment comparing survival rates under separate and/or coinciding high-temperature and *V. aestuarianus* stress conditions. The specific farm and treatment groups were selected for the challenge due to pre-observed differences in survival during the field trial, and as part of a continued investigation of whether time in the intertidal zone confers increased resilience to summer mortality stressors post-transfer to deep-water conditions, respectively. *Vibrio aestuarianus* was used for the pathogen challenge as has been previously isolated from moribund oysters displaying signs of summer mortality syndrome (Labreuche et al., 2006; Cowan et al., 2023). Prior to the challenge, all animals were notched on the distal portion of the shell (adjacent to the adductor muscle) for later inoculation. Following, 11 haphazardly-selected animals from each treatment group were placed in each of twenty 20-L glass tanks (N = 40) with 5 L of 80 µM-filtered seawater (i.e. static) and held overnight at 16°C. Salinity was approximately 30 ppt and a constant air supply was provided to each tank via an air stone. The following day, a 2x2 fully factorial design (high/low temperature x *Vibrio*/no *Vibrio*) was applied with animals from both treatment groups (*Deep*, *Intertidal→Deep*) (n = 5 tanks per treatment level, N = 20 tanks per temperature level). All *Vibrio* treatment oysters were inoculated with 50 µL of *V. aestuarianus* solution via injection into the adductor muscle as per Mackenzie et al. (2022). *Vibrio aestuarianus* was grown overnight with constant agitation at 21°C in tryptic soy broth containing 2% NaCl (TSB + 2% NaCl) with inocula taken from frozen glycerol stocks and tested for purity prior to use. Following, cells were washed and re-suspended to OD_{600} = 1.9 with concentration based on pilot studies carried out using subsets of individuals from each treatment group. The relationship between OD and colony-forming units (CFUs) was determined by serial dilution plating (OD_{600} = 2.50 per 50-µL dose; CFUs = 5.09 x 10^8 ml^{-1}). All pathogen control (i.e. no exposure to *Vibrio*) animals were injected with 50 µL of autoclaved seawater and placed in separate tanks from *Vibrio* treatment animals.

Seawater temperature was then maintained at 16°C (temperature control) or raised to 24°C. Temperature conditions were maintained via temperature-controlled rooms. As in Year 1, no feed was administered in order to prevent altered algal concentrations across temperature treatments and to avoid issues with bacterial growth. Mortality was assessed on a daily basis over a 2-week exposure period according to the same criteria as previously described. After 8 days, the high temperature (24°C) challenge was ended due to ≥50% mortality across all treatment groups. The control temperature (16°C) challenge continued for an additional week until ≥50% mortality was observed in the *Vibrio* treatment groups.

2.8 Data analyses

Three-way ANOVAs were applied to examine the effect of culture site/treatment, farm, timepoint, and all interactions on survival, condition index, and oyster size (shell height and tissue DW). Percent survival data were logit-transformed prior to ANOVA. Where significant differences were detected, Tukey's HSD method for multiple comparisons was applied. Additionally, one-way and two-way ANOVAs with *post-hoc* testing were carried out to compare treatment groups at a particular farm across time or at specific timepoints across farms. All data were tested to ensure assumptions of normality (Kolmogorov-Smirnov, $p < 0.05$) and homogeneity of variances (Levene's Test, $p < 0.05$) were met prior to analyses. All ANOVAs were carried out in RStudio (v4.2.2; R Core Team, 2022). Means ± SDs are presented.

Kaplan-Meier survival curves of treatment groups under laboratory-based heatwave and/or *Vibrio* challenges were generated in RStudio and compared via log-rank testing. Cox proportionate hazards analyses were carried out to investigate associations between survival time and predictor variables.

3 Results

3.1 Seawater monitoring

In April to August of Year 1 (2021), SST ranged between 7.5 and 30.8°C (DB), 7.6 and 26.8°C (DN), and 6.0 and 28.1°C (FB) at deep-water sites, and between 8.9 and 37.5°C (DB), 6.6 and 37.7°C (DN), and 6.4 and 44.8°C (FB) at intertidal sites (Figure 2). Mean salinities over sampling events for DB, DN, and FB over the same period ranged from 24.5 to 28.1 ppt, 24.5 to 27.7 ppt, and 23.8 to 25.2 ppt, respectively. Mean monthly SSTs, salinities, and DO levels measured during sampling events are provided in Supplementary Table 2. Of note, an acute warming event took place in late June 2021 lasting for

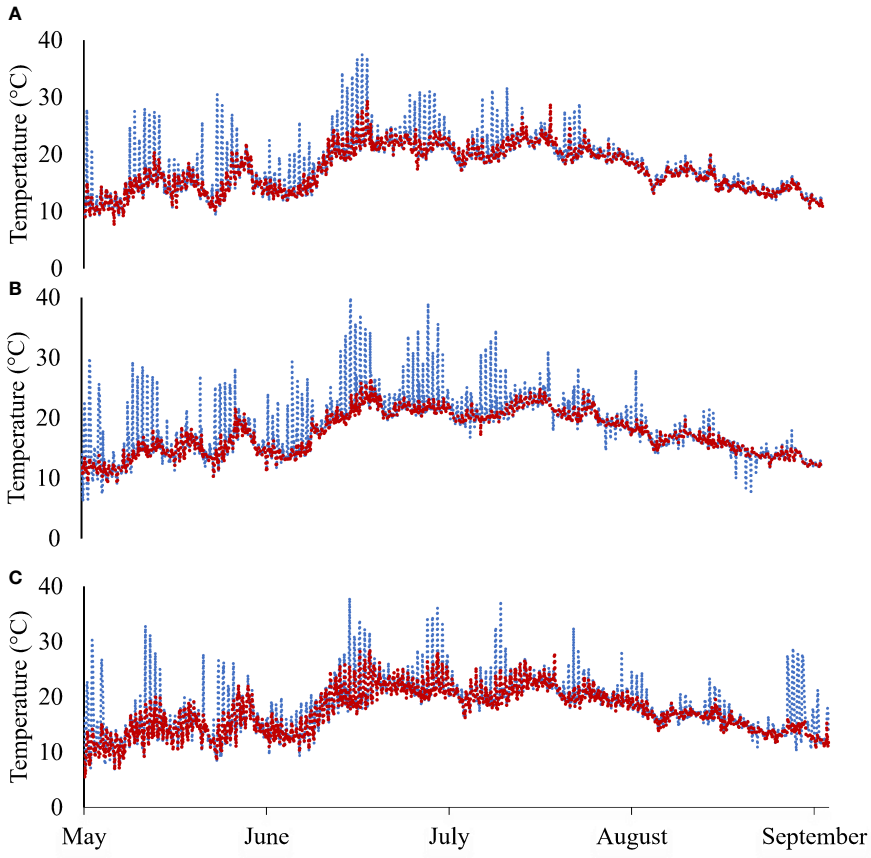

FIGURE 2
Continuous temperature data for deep-water sites (red-dashed line) and intertidal sites (blue-dashed line) at **(A)** Deep Bay, **(B)** Denman Island, and **(C)** Fanny Bay farms in Year 1 (May–September 2021).

approximately 1 week, during which average SSTs were 22.0 ± 2.4°C (DB), 21.5 ± 2.0°C (DN), and 21.2 ± 2.6°C (FB) at deep-water sites, and 23.3 ± 4.3°C (DB), 22.0 ± 4.1°C (DN), and 22.5 ± 4.6°C (FB) at intertidal sites (Figure 2). Mean SSTs at DB and DN from September 2021 through April 2022 were 8.2 ± 3.6°C and 8.4 ± 3.2°C, respectively.

In May to August of Year 2 (2022), SST ranged between 6.3 and 25.0°C (DB) and 7.9 and 27.5°C (DN) at deep-water sites, and between 9.2 and 35.0°C (DB) and 9.6 and 34.3°C (DN) at intertidal sites. Mean salinities at DB and DN over the same period were 24.4 ± 1.6 ppt and 23.9 ± 1.5 ppt, respectively. Of note, an acute warming event took place in late July 2022 lasting for approximately 1 week, during which average SSTs were 21.9 ± 1.1°C (DB) and 22.2 ± 1.2°C (DN) at deep-water sites, and 22.8 ± 2.5°C (DB) and 22.9 ± 2.6°C (DN) at intertidal sites. Maximum SSTs during this event were 25.0°C (DB) and 25.7°C (DN) at deep-water sites, and 32.9°C (DB) and 34.3°C (DN) at intertidal sites. In May to August of Year 2, DO levels at DB and DN showed a gradual decline over time with increasing daily temperature, and a clear increase in DO fluctuations (between hypoxia and normoxia) was observed following the warming event at the end of July 2021, with daily DO ranging from approximately 2 to 15 mg L^{-1} (Figure 3).

3.2 Survival

In Year 1, mean percent survivals in August (T07) for *Deep* and *Intertidal* treatment groups at DB, DN, and FB were 86.4 ± 6.1%, 91.7 ± 2.8%, and 96.6 ± 5.0% (*Deep*), and 89.5 ± 14.1%, 84.4 ± 9.8%, and 96.1 ± 4.3% (*Intertidal*), respectively (Figure 4). Collectively across all farms and sites, a 3-way ANOVA detected a significant difference in percent survival among sampling times ($F_{(6,245)}$ = 10.14, p = 0.003), but no significant effect of farm nor site, or any interaction between/among factors. For the time factor, only one pairwise comparison was significant, early May (T01) having significantly higher percent survival than early August (T07).

In Year 2, mean percent survivals in September in the four treatments at DB and DN farms were: 63.6 ± 10.2% and 70.6 ± 10.1% (*Deep*), 68.9 ± 14.4% and 65.4 ± 11.6% (*Deep→Intertidal*), 86.6 ± 10.7% and 61.2 ± 15.7% (*Intertidal*), and 83.5 ± 11.0% and 70.6 ± 13.1% (*Intertidal→Deep*), respectively (Figure 5). A three-way ANOVA showed a significant effect of time ($F_{(7,273)}$ = 8.51, p < 0.001) and treatment ($F_{(3,276)}$ = 13.15, p < 0.001), but no significant effect of farm ($F_{(1,278)}$ = 1.67, p = 0.197). There were, however, significant interactions between time and farm ($F_{(7,217)}$ = 3.76, p < 0.001) and treatment and farm ($F_{(3,217)}$ = 22.39, p < 0.001). A one-way ANOVA examining final percent survival at DB showed a significant treatment effect ($F_{(3,16)}$ = 11.56, p < 0.001). *Post-hoc* testing revealed the following: (*Intertidal* = *Intertidal→Deep*) > (*Deep→Intertidal* = *Deep*), demonstrating that oysters spending their first year in the intertidal zone had significantly increased percent survival in comparison to those spending Year 1 in deep water, regardless of Year 2 culture conditions. In contrast, a one-way ANOVA examining final percent survival at DN showed no significant treatment effect.

3.3 Reproductive status

In Year 1, the highest proportion of females for a given timepoint, irrespective of farm/site, occurred in early August

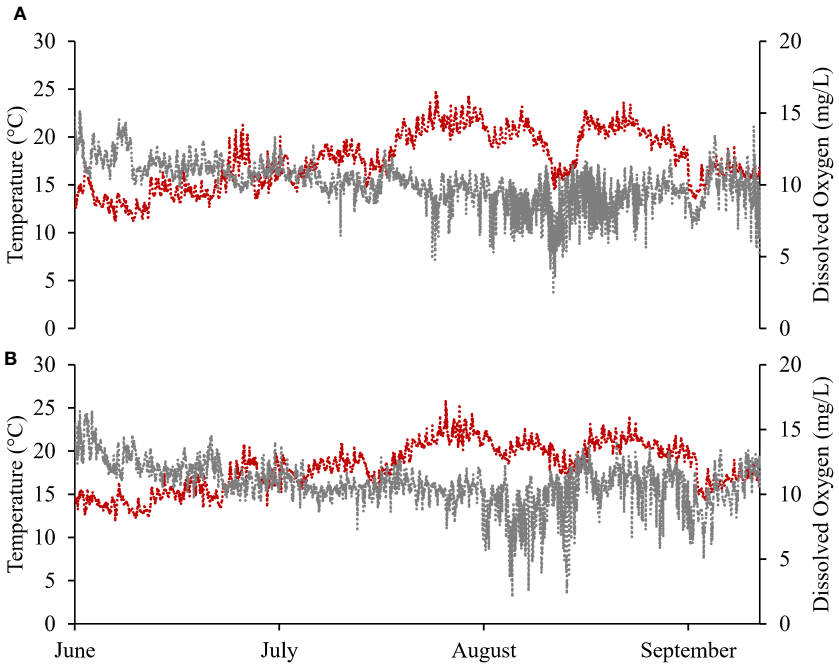

FIGURE 3
Continuous temperature (red-dashed line) and dissolved oxygen (grey-dashed line) data for deep-water sites at **(A)** Deep Bay and **(B)** Denman Island farms in Year 2 (June–September 2022).

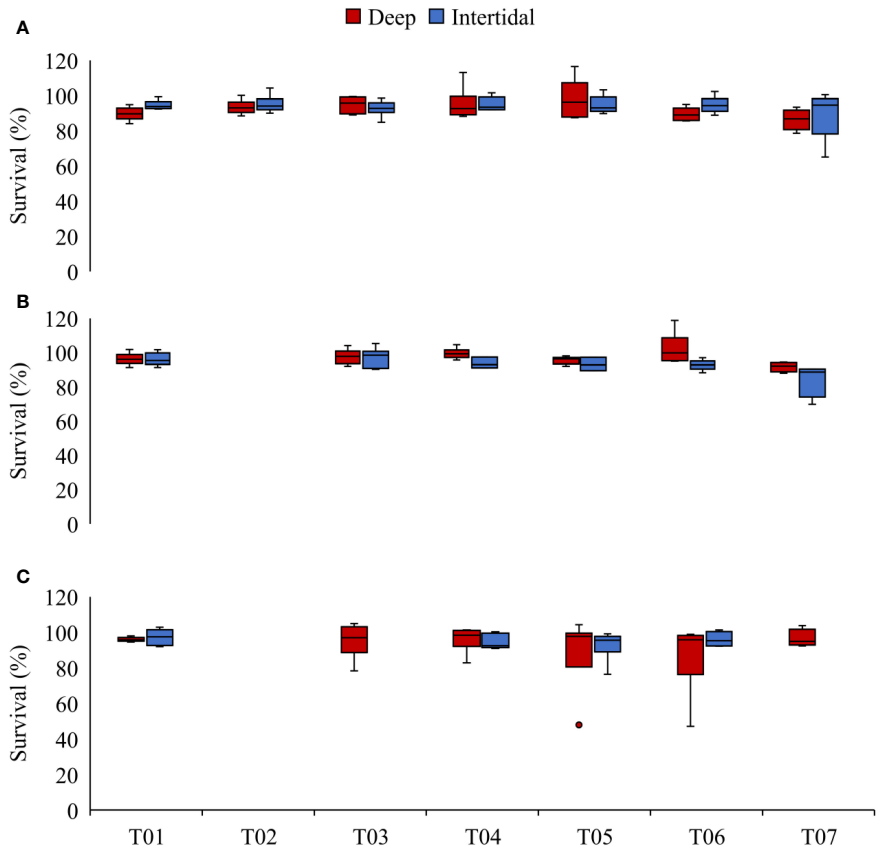

FIGURE 4
Box plots of survival (%) in *Deep* and *Intertidal* (blue) sites at **(A)** Deep Bay, **(B)** Denman Island, and **(C)** Fanny Bay farms in Year 1 (T01–T07). T01 = early May, T02 = late May, T03 = early June, T04 = late June, T05 = early July, T06 = late July, and T07 = early August. Due to inclement sea conditions, sampling could not take place at T02 at Denman Island (*Deep* and *Intertidal* sites) and Fanny Bay (*Deep* and *Intertidal* sites) nor at T07 at Fanny Bay (*Intertidal* site). T08 is not included as bag splitting (number of oysters per bag reduced from 500 to 250) occurred at this timepoint.

(T07) (83.3%, F:M = 6.1). When farms and sites were considered separately, the highest proportion of females occurring in *Deep* and *Intertidal* groups within each farm also occurred at T07. At DB, a higher proportion of females was reported in the *Deep* group (91.6%; F:M = 11.0) compared to the *Intertidal* group (83.3%, F:M = 10.0) at T07. In contrast, at DN and FB farms, higher proportions of females were reported in *Intertidal* groups (DN: 100%, F:M = n/a; FB: 83.5%, F:M = 5) than in *Deep* groups (DN: 75%, F:M = 3; FB: 66.7%, F:M = 2.7) at T07. Across all farms and sites, the majority of males and females were classed as Stage 3 maturity (Mature/Ripe) from mid-June through August.

In Year 2, the highest proportion of females for a given timepoint, irrespective of farm/treatment, occurred in late August (T14) (90.3%, F:M = 9.3). When farms and treatments were considered separately, the highest proportion of females occurred in late July (T12) at both DB and DN, but under varying treatments. At DB, the highest proportion of females occurred in late July at the *Intertidal* site (100%, F:M = n/a), followed by *Deep→Intertidal* (90.0%, F:M = 9.0), *Intertidal→Deep* (88.9%, F:M = 8.0), and *Deep* (70.0%, F:M = 7.0). By late August (T14), this pattern had generally reversed with the *Deep* treatment having the highest proportion of females (80.0%, F:M = 4.0). The majority of DB males and females, irrespective of treatment group, were classed at Stage 3 (Mature/Ripe) or Stage 4 (Partially Spawned) from late June (T10) through to late July (T12), thereafter largely shifting to Stage 4 through to late August.

At DN, the highest proportion of females in Year 2 also occurred in late July (T12) in the following treatment order: *Deep→Intertidal* (90%, F:M = 9), *Intertidal→Deep* (66.7%, F:M = 2), *Intertidal* (66.7%, F:M = 2), and *Deep* (62.5%, F:M = 1.7). Of note, there was also an elevated preponderance of females in the *Deep* treatment in late June (T10) (80%), which dropped to 62.4% by late July (T12) before steadily increasing again. The majority of males and females in the *Deep* and *Intertidal→Deep* treatments were classed at Stage 3–4 in late June (T10), shifting to mostly Stage 4 by early July (T11) and throughout August. The DN *Intertidal* and *Deep→Intertidal* treatments were largely classed at Stage 4 in late June (T10), shifting to Stages 4–5 by early July (T11), suggesting an earlier/faster maturation status at the intertidal site in comparison to deep water. By late July (T12), the DN intertidal treatment groups were generally classified as

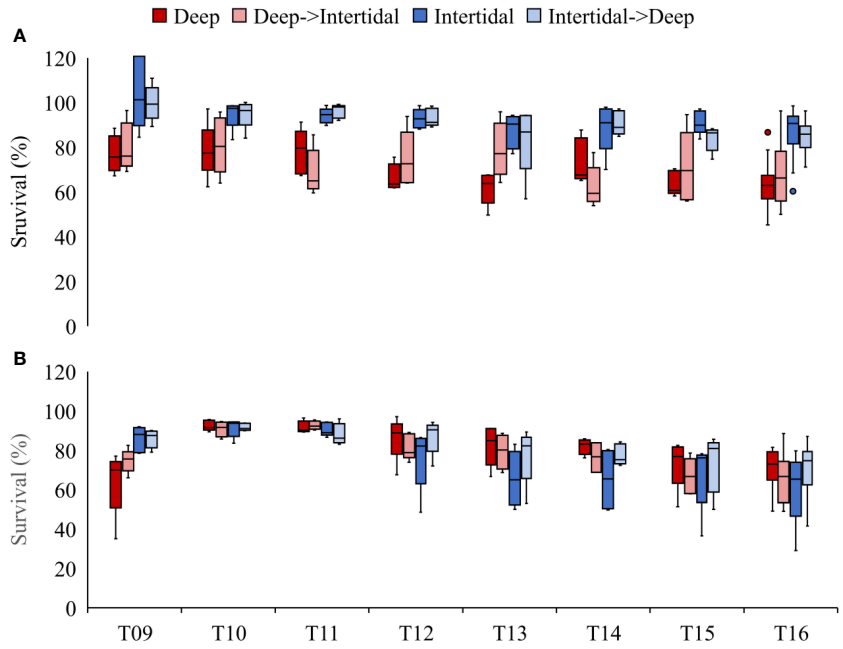

FIGURE 5
Box plots of survival (%) in *Deep* (dark red), *Deep→Intertidal* (light red), *Intertidal* (dark blue), and *Intertidal→Deep* (light blue) treatments at **(A)** Deep Bay and **(B)** Denman Island farms in Year 2 (T09–T16). T09 = late May, T10 = late June, T11 = early July, T12 = late July, T13 = early August, T14 = late August, T15 = mid-September, and T16 = late September. Bag splitting (number of oysters per bag reduced from 250 to 100) occurred between T09 and T10.

Stage 3 or 4, shifting to Stage 4 with some Stage 5 by late August (T14), suggesting that the DN intertidal treatment groups may have had multiple spawning events.

3.4 Histopathology

In general, there were minimal histopathological conditions observed in Year 1 samples. However, of note, VGH was observed in 37/330 (11.2%) of screened animals with more cases observed in oysters from deep-water (23/37, 62.2%) than intertidal sites (14/37, 37.8%). The highest proportion of infected individuals for a given timepoint, irrespective of farm or site, occurred in mid-August (T08) (9/37, 24.3%). Comparison of infection incidence across farms, irrespective of sites and timepoints, showed slightly higher incidence at FB (13/37, 35.1%) and DN (13/37, 35.1%) than at DB (11/37, 29.7%). In contrast, in Year 2, VGH was observed in only 13/358 (2.3%) of screened animals with slightly higher proportion of infected individuals in *Deep* (4/13, 30.8%) and *Deep→Intertidal* treatments (4/13, 30.8%) compared to *Intertidal* (3/13, 23.1%) and *Intertidal→Deep* (2/13, 15.4%) treatments. The highest proportion of infected individuals for a given timepoint, irrespective of farm or treatment, occurred in early August (T13) (6/13, 46.2%). The majority of infected animals were observed at the DB farm (7/13, 53.8%). A number of other histopathological conditions were reported in Year 2 samples including localized FHI and DHI (in various tissues), MDGT, and ciliate infection, but generally conditions were reported as minor or light infections with no associated pathogens. It should be noted that due to poor fixation, the histopathology of a large number of samples from late July (T12) and early August (T13) of Year 2 (2022) sampling periods could not be properly assessed.

3.5 Condition index and growth

3.5.1 Condition index

In Year 1, mean CIs at DB, DN, and FB were 11.9 ± 3.9, 12.8 ± 4.4, and 9.6 ± 2.0, respectively (Figure 6). Maximum CI in *Deep* and *Intertidal* sites at each farm occurred at T03 and T03 (DB), T03 and T04 (DN), and T08 and T06 (FB), respectively. Mean CIs at the end of Year 1 in *Deep* and *Intertidal* sites at each farm were 11.1 ± 3.1 and 10.9 ± 2.7 (DB), 10.7 ± 2.2 and 9.3 ± 2.1 (DN), and 10.3 ± 1.6 and 9.0 ± 1.8 (FB), respectively.

In Year 2, mean CIs at DB and DN were 9.7 ± 2.1 and 12.3 ± 3.0, respectively (Figure 7). Maximum CI in *Deep*, *Deep→Intertidal*, *Intertidal*, and *Intertidal→Deep* treatment groups at each farm occurred at: T09 and T14, T14, T13, and T15 (DB), and T10, T09, T09, and T10 (DN), respectively. Mean CIs at the end of the field trial in *Deep*, *Deep→Intertidal*, *Intertidal*, and *Intertidal→Deep* treatment groups at each farm were 11.1 ± 1.2, 7.3 ± 1.9, 7.4 ± 3.0, and 10.9 ± 3.1 (DB), and 11.5 ± 2.3, 9.1 ± 3.2, 10.4 ± 2.3, and 12.1 ± 2.3 (DN), respectively.

Two-way ANOVAs looking at the effect of site/treatment and farm on CI at the end of each growing season [i.e. late August 2020 (T08), mid-September 2021 (T15)] showed an influence of site ($F_{(1,102)} = 4.69$, $p < 0.05$) and farm ($F_{(2,102)} = 3.39$, $p < 0.05$) on CI at the end of Year 1 (T08), and an effect of treatment only ($F_{(3,32)} = 4.56$, $p < 0.01$) on CI in

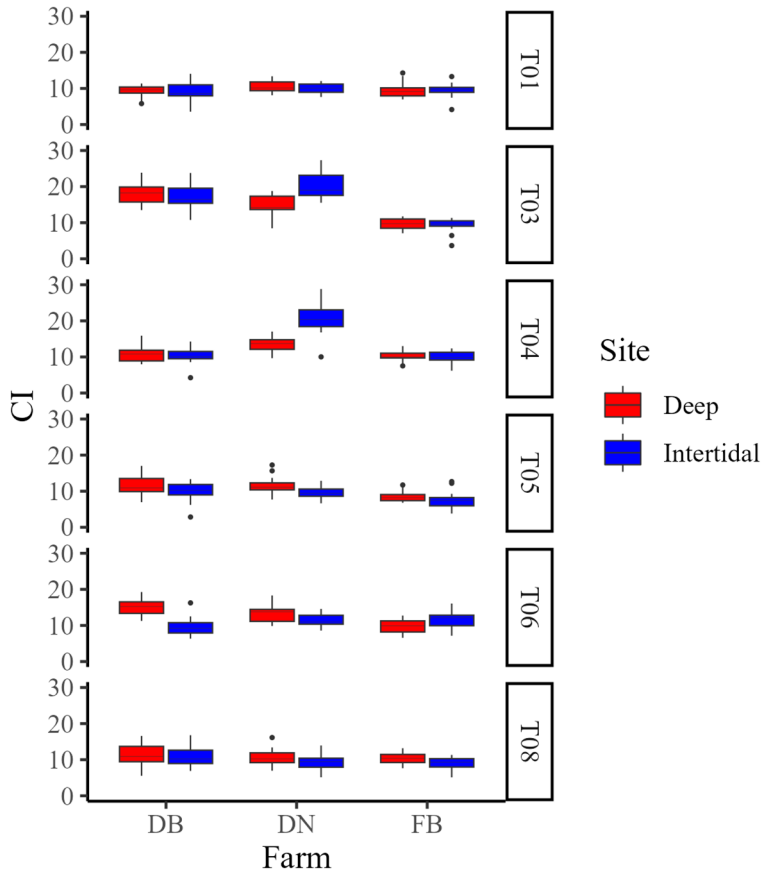

FIGURE 6
Box plots of condition index (CI) at *Deep* (red) and *Intertidal* (blue) sites at Deep Bay (DB), Denman Island (DN), and Fanny Bay (FB) farms in Year 1 (T01–T08). T01 = early May, T03 = early June, T04 = late June, T05 = early July, T06 = late July, and T08 = late August. T02 and T07 are not shown as no samples were collected due to logistical constraints.

Year 2 (T15), with no significant interactions between factors at either timepoint. One-way ANOVAs of CI between sites/treatments within each farm at the end of each growing season showed an effect of site ($F_{(1,34)} = 5.18$, $p < 0.05$) at the end of Year 1 (T08) at FB only, with *Deep* oysters having a significantly greater CI than *Intertidal* oysters, and a significant effect of treatment ($F_{(3,16)} = 3.77$, $p < 0.05$) on CI at the end of Year 2 (T15) at DB only. However, *post-hoc* testing detected no significant differences in CI between any treatment groups at the end of Year 2 at DB.

3.5.2 Growth

In Year 1, mean shell heights by late August (T08) at *Deep* and *Intertidal* sites at each farm were 78.10 ± 7.19 mm and 74.35 ± 4.73 mm (DB), 73.69 ± 4.78 mm and 64.68 ± 4.95 mm (DN), and 70.06 ± 6.32 mm and 72.07 ± 7.43 mm (FB), respectively (Figure 8A). Mean tissue DWs for the same timepoint (T08) at *Deep* and *Intertidal* sites at each farm were 1.64 ± 0.58 g and 1.55 ± 0.54 g (DB), 1.36 ± 0.45 g and 1.07 ± 0.29 g (DN), and 1.47 ± 0.41 g and 1.49 ± 0.39 g (FB), respectively (Figure 8B).

In Year 2, mean shell heights at the end of the field trial (T15) in *Deep*, *Deep→Intertidal*, *Intertidal*, and *Intertidal→Deep* treatment groups at each farm were 90.34 ± 6.88 mm, 94.66 ± 5.76 mm, 86.68 ± 3.03 mm, and 94.60 ± 9.28 mm (DB), and 95.00 ± 8.73 mm, 93.38 ± 2.43 mm, 93.02 ± 5.67 mm, and 87.20 ± 4.77 mm (DN), respectively (Figure 9A). Mean tissue DWs for the same timepoint (T15) in *Deep*, *Deep→Intertidal*, *Intertidal*, and *Intertidal→Deep* treatment groups at each farm were 4.52 ± 1.07 g, 3.37 ± 1.45 g, 2.43 ± 1.01 g, and 4.75 ± 1.46 g (DB), and 6.18 ± 2.28 g, 5.06 ± 1.88 g, 5.44 ± 1.74 g, and 6.16 ± 1.73 g (DN), respectively (Figure 9B).

Two-way ANOVAs looking at the effect of site/treatment and farm on shell height at the end of each growing season [i.e. late August 2020 (T08), mid-September 2021 (T15)] showed a significant influence of site ($F_{(1,102)} = 9.60$, $p < 0.01$) and farm ($F_{(2,102)} = 13.24$, $p < 0.001$), and an interaction effect ($F_{(2,204)} = 7.59$, $p < 0.001$) at the end of Year 1 (T08), but no significant effect of treatment or farm, nor interaction, at the end of Year 2 (T15). One-way ANOVAs of shell height between sites within each farm at the end of each growing season showed a significant effect of site ($F_{(1,34)} = 30.9$, $p < 0.001$) at the end of Year 1 (T08) at DN only, with *Deep* oysters having a significantly greater shell height than *Intertidal* oysters, but no significant effect of treatment at the end of Year 2 (T15) at either farm.

Two-way ANOVAs looking at the effect of site/treatment and farm on tissue DW at the end of each growing season [i.e. late August 2020 (T08), mid-September 2021 (T15)] showed a significant influence of farm ($F_{(2,102)} = 6.72$, $p < 0.01$) at the end

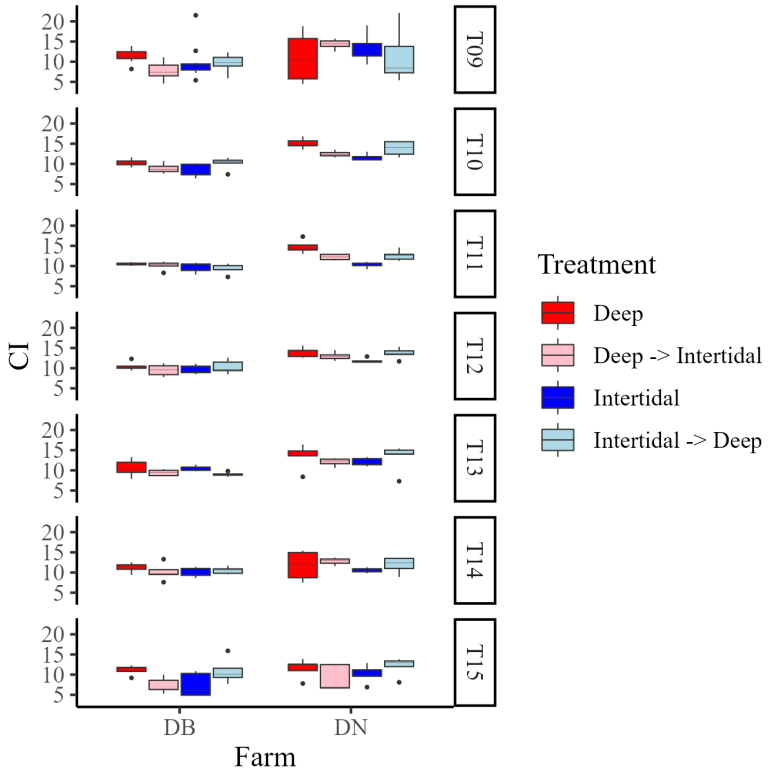

FIGURE 7
Box plots of condition index (CI) at *Deep* (dark red), *Deep→Intertidal* (light red), *Intertidal* (dark blue), and *Intertidal→Deep* (light blue) treatments at Deep Bay (DB) and Denman Island (DN) farms in Year 2 (T09–T15). T09 = late May, T10 = late June, T11 = early July, T12 = late July, T13 = early August, T14 = late August, and T15 = mid-September.

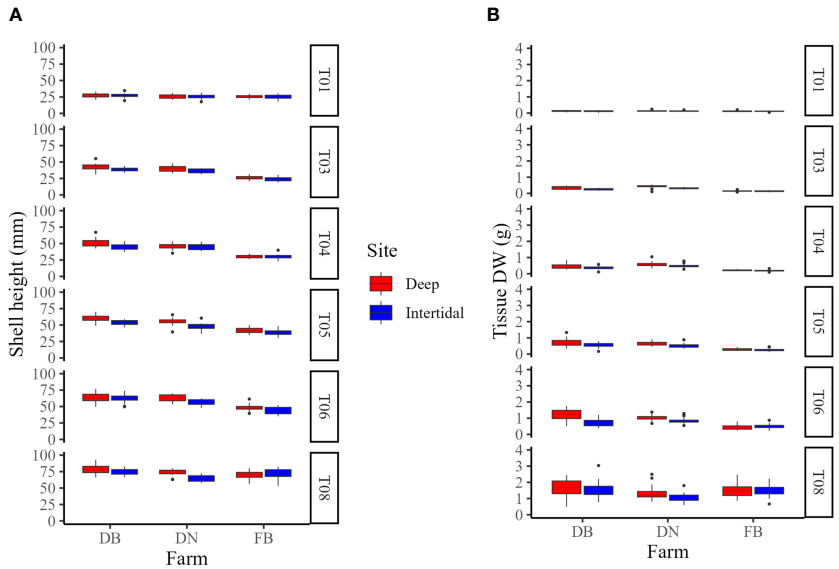

FIGURE 8
Box plots of **(A)** shell height and **(B)** tissue dry weight (DW) at *Deep* (red) and *Intertidal* (blue) sites at Deep Bay (DB), Denman Island (DN), and Fanny Bay (FB) farms in Year 1 (T01–T08). T01 = early May, T03 = early June, T04 = late June, T05 = early July, T06 = late July, and T08 = late August. T02 and T07 are not shown as no samples were collected due to logistical constraints.

10.3389/fmars.2024.1345493

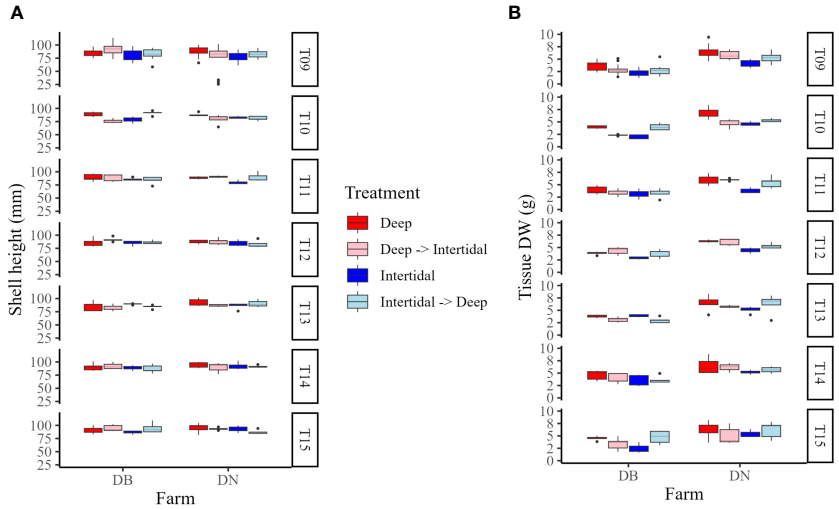

FIGURE 9
Box plots of **(A)** shell height and **(B)** tissue dry weight (DW) in *Deep* (dark red), *Deep→Intertidal* (light red), *Intertidal* (dark blue), and *Intertidal→Deep* (light blue) treatment groups at DB and DN farms in Year 2 (T09–T15). T09 = late May, T10 = late June, T11 = early July, T12 = late July, T13 = early August, T14 = late August, and, T15 = mid-September.

of Year 1 (T08), and significant effects of treatment ($F_{(3,32)} = 3.63$, $p < 0.05$) and farm ($F_{(1,32)} = 22.69$, $p < 0.001$) at the end of Year 2 (T15), with no significant interactions between factors at either timepoint. One-way ANOVAs of tissue DW between sites/treatments within each farm at the end of each growing season showed a significant effect of site ($F_{(1,34)} = 5.42$, $p < 0.05$) at the end of Year 1 (T08) at DN only, with *Deep* oysters having significantly greater tissue DW than the *Intertidal* oysters, and a significant effect of treatment ($F_{(3,16)} = 5.57$, $p < 0.01$) at the end of Year 2 (T15) at DB only, with *Deep* and *Deep→Intertidal* oysters having a significantly greater tissue DW than *Intertidal* oysters. Of note, there were no significant differences in the tissue DW of *Intertidal→Deep* and *Deep* treatments at either farm at the end of the field trial (T15).

3.6 Laboratory-challenge experiments

3.6.1 Heatwave challenge (year 1)

Under an immersion challenge at 15°C, final percent survivals were 100% and 98% in oysters from *Intertidal* and *Deep* sites, respectively, while under emersion at 15°C, final percent survivals were only 30% and 10%, respectively (Figure 10A). Under emersion conditions, log-rank testing showed a significant difference ($\chi^2 = 8.4$, df = 1, $p = 0.004$) in survival curves of oysters from *Intertidal* and *Deep* sites, and hazards analyses determined a significantly decreased hazard (HR = 0.53, 95% CI = 0.34–0.83, $p = 0.006$) in oysters from the *Intertidal* site in comparison to those from the *Deep* site (Figure 10A).

Under an immersion challenge at 20°C, final percent survivals were 100% and 88% in oysters from *Intertidal* and *Deep* sites, respectively (Figure 10B). Log-rank testing showed a significant difference ($\chi^2 = 6.3$, df=1, $p = 0.010$) in survival curves. Hazards analyses could not be carried out for this comparison due to total survival of oysters in the *Intertidal* treatment group. Under an emersion challenge at 20°C, final percent survivals were 4% and 2% in oysters from the *Intertidal* and *Deep* sites, respectively. Log-rank testing of oysters emersed at 20°C showed a significant difference ($\chi^2 = 19.2$, df = 1, $p < 0.001$) in survival curves of oysters from *Deep* and *Intertidal* sites, and hazards analyses determined a significantly decreased hazard (HR = 0.43, 95% CI = 0.28–0.64, $p < 0.001$) in oysters from the *Intertidal* site in comparison to those from the *Deep* site (Figure 10B).

Under an immersion challenge at 25°C, final percent survivals were 88% and 64% in oysters from *Intertidal* and *Deep* sites, respectively (Figure 10C). Log-rank testing showed a significant difference ($\chi^2 = 8.5$, df=1, $p = 0.004$) in survival curves of oysters from *Deep* and *Intertidal* sites, and hazards analyses determined a significantly decreased hazard (HR = 0.28, 95% CI = 0.11–0.70, $p = 0.007$) in oysters from the *Intertidal* site in comparison to those from the *Deep* site (Figure 10C). Under an emersion challenge at 25°C, the majority of animals from both sites spawned within 48 hours so the challenge was ended.

Under all temperature and immersion/emersion conditions, *Deep* oysters experienced earlier and greater mortality than their *Intertidal* counterparts. This was most obvious at 20 and 25°C under emersion challenge, where *Deep* oysters experienced some morality at 2 days (at both 20 and 25°C) compared with *Intertidal* counterparts that showed zero mortality (at 20°C) or delayed mortality until 6 days (at 25°C).

3.6.2 Heatwave and *Vibrio* challenge (year 2)

Under 16°C and control (no *Vibrio*) conditions, final percent survivals were 100% for oysters from both *Intertidal→Deep* and *Deep* treatments (Figure 11A). Under 16°C and a *Vibrio* challenge, final percent survivals were 63% and 34% for oysters from *Intertidal→Deep* and *Deep* treatments, respectively. Log-rank testing showed a significant difference ($\chi^2 = 4.4$, df = 1, $p = 0.040$) in survival curves and hazards analyses determined a

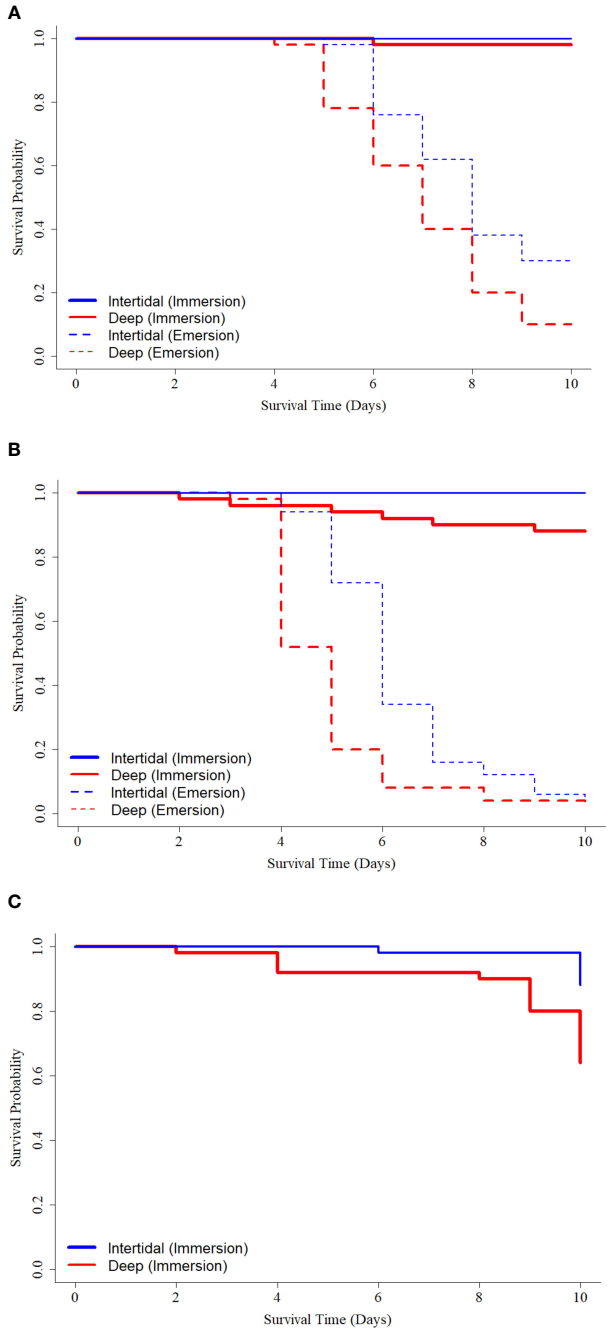

FIGURE 10
Kaplan-Meier survival curves of oysters from *Deep* (red lines) and *Intertidal* (blue lines) sites under immersion (solid lines) or emersion (dashed lines) exposures at **(A)** control (15°C) or **(B, C)** simulated heatwave (20 and 25°C, respectively) conditions.

significantly decreased hazard (HR = 0.49, 95% CI = 0.25–0.97, p = 0.041) for oysters from the *Intertidal→Deep* treatment in reference to those from the *Deep* treatment (Figure 11A).

Under 24°C and control (no *Vibrio*) conditions, final percent survivals were 54% and 37% for oysters from *Deep* and *Intertidal→Deep* treatments, respectively (Figure 11B). However, log-rank testing showed no significant difference (χ^2 = 0.8, df = 1, p = 0.400) in survival curves and hazards analyses showed an insignificant decrease in hazard (HR = 1.40, 95% CI = 0.71–2.60, p = 0.348) for oysters from the *Intertidal→Deep* treatment in reference to those from the *Deep* treatment (Figure 11B).

Under 24°C and *Vibrio* challenge, final percent survivals were 14% and 6% for oysters from *Intertidal→Deep* and *Deep* treatments, respectively (Figure 11B). Log-rank testing showed no significant difference (χ^2 = 0.2, df = 1, p = 0.600) in survival curves and hazards analyses showed an insignificant decrease in hazard (HR = 0.88, 95% CI = 0.54–1.50, p = 0.626) for oysters from the *Intertidal→Deep* treatment in reference to those from the *Deep* treatment (Figure 11B).

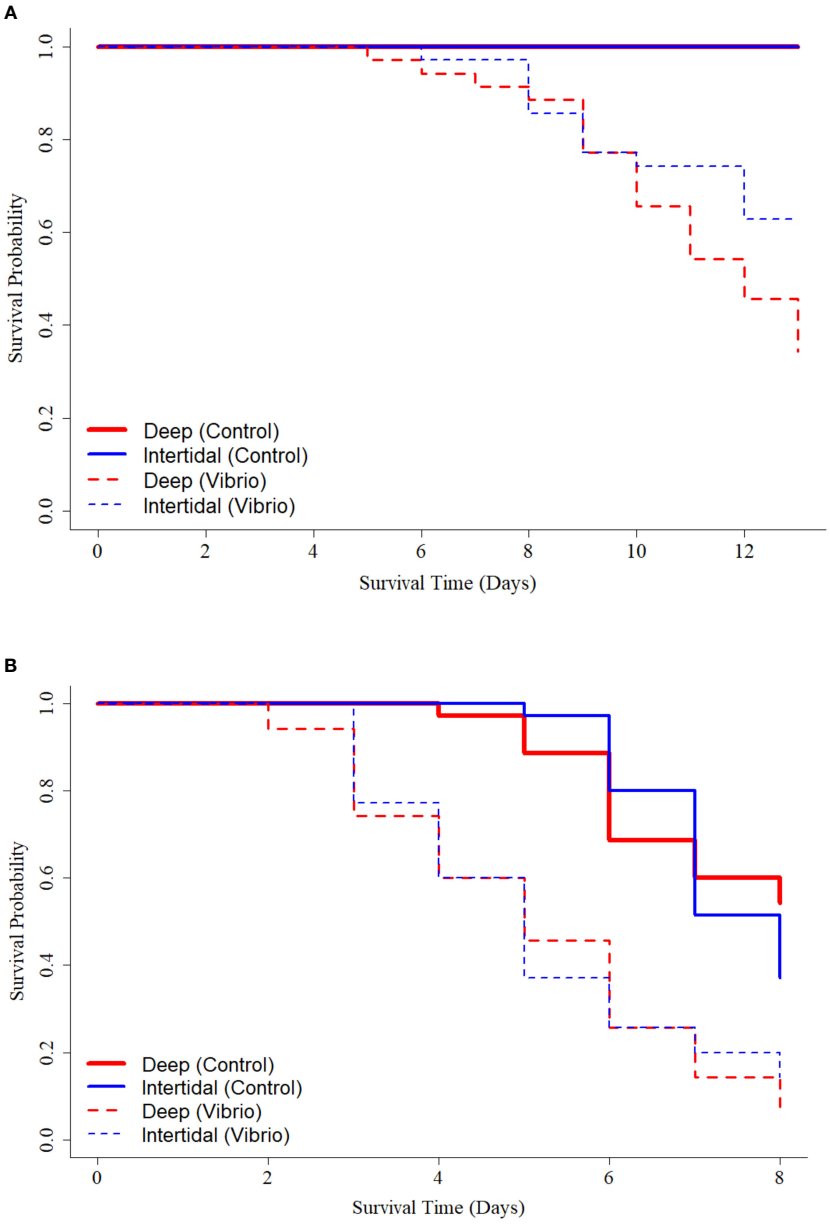

FIGURE 11
Kaplan-Meier survival curves for oysters from *Intertidal→Deep* (blue lines) and *Deep* (red lines) treatments under *Vibrio* (dashed lines) and control (solid lines) exposures at **(A)** control (16°C) or **(B)** simulated heatwave (24°C) conditions.

As observed in the Year 1 challenge experiment, *Deep* treatment oysters experienced earlier mortality than their *Intertidal→Deep* treatment counterparts. Under *Vibrio* conditions at both 16 and 24°C, and under 24°C (no *Vibrio*) conditions, *Deep* treatment oysters experienced mortality 1 day earlier than *Intertidal→Deep* treatment oysters.

4 Discussion

Results suggest that partial or full culture of oysters in the intertidal zone over a 2-year growth period does confer some resilience to summer mortality stressor conditions at some locations and should be considered as one tool under a collective approach for mitigation of Pacific oyster summer mortality. However, given that oyster summer mortality is a multi-faceted phenomenon (Dégremont et al., 2010; Barbosa Solomieu et al., 2015; Cowan et al., 2023), it is acknowledged that the specific physical and biological factors associated with any given farm will play contributory roles. Here we discuss how the intertidal zone may improve oyster resilience to summer mortality stressors and consider how farm-specific factors in the present study may have shaped responses.

We propose that the high level of phenotypic plasticity associated with intertidal oysters confers to them an increased level of resilience to summer mortality in comparison to deep-

water counterparts. In the present study, laboratory-challenge experiments demonstrated increased survival time and reduced mortality in intertidally-cultured oysters (Year 1: *Intertidal*, Year 2: *Intertidal→Deep*) as compared to deep-water-cultured oysters, which was paralleled under field settings at one farm site (DB). Corporeau et al. (2022) also reported a substantial (>1 week) delay in mortality in intertidal Pacific oysters compared with subtidal counterparts during a summer mortality event. Likewise, intertidal Pacific oysters have shown improved survival over subtidal equivalents during emersion stress (Meng et al., 2018).

Pre-exposure of oysters to stressor conditions may lead to improved resilience that is also maintained after introduction to a less dynamic/stressful environment. In the present study, the benefits conferred by time in the intertidal appeared to be maintained several months after transplantation to the subtidal environment, as evidenced by the increased survival of oysters from *Intertidal* and *Intertidal→Deep* treatments in the field (at the DB site only) and of those from the *Intertidal→Deep* treatment during the laboratory temperature/*Vibrio* challenge. We suggest that the persistence of phenotypic plasticity associated with intertidal conditions may account for improved survival after transplant. The extension of mechanisms of resilience from dynamic to more stable environments may be facilitated by epigenetic processes such as DNA acetylation and methylation, histone modifications, and non-coding RNAs (Hofmann, 2017; Li et al., 2018), which collectively allow phenotypes that confer resilience in one environment to be transferred to novel settings and/or later life stages (Jablonka and Lamb, 2002). Indeed, a number of prior studies have demonstrated that intertidal populations of bivalve species (including Pacific oysters) show increased genome methylation and acetylation compared to subtidal counterparts during exposure to novel conditions (Clark et al., 2018; Li et al., 2018). Wang et al. (2021) also reported a greater proportion of differentially-expressed genes and significantly greater methylation variation in intertidal Pacific oysters in comparison to subtidal equivalents under a high temperature challenge. Similarly, continued upregulation of genes involved in antioxidation processes was observed in intertidal populations of Antarctic limpets (*Nacella concinna*) after transplant to the subtidal zone (Clark et al., 2018).

Adult bivalves may also maintain some degree of resilience to environmental stressors when there is a history of parental or early-life-stage stress exposure (Reid et al., 2019; Dang et al., 2023). For example, F_2 generation intertidal Pacific oysters were shown to maintain differentially-methylated genes associated with the thermal responses of the F_0 generation (Wang et al., 2023). Similarly, adult Hong Kong oysters (*C. hongkongensis*) exposed to ocean acidification as larvae demonstrated a beneficial carry-over effect associated with the methylation of metabolic and endocytic genes under novel stressor conditions (Dang et al., 2023). In the same way, epigenetic mechanisms could account for the maintained resilience of intertidally-cultured oysters after transplant to the subtidal environment, as observed in the present study.

Other environmentally-driven physiological differences between intertidal and subtidal groups could also account for differences in survival. For example, intertidally-cultured animals have been observed to develop thicker shells and larger adductor muscles than their subtidal counterparts (Lewis and Seed, 1969; Hickman and Illlingworth, 1980; Tagliarolo et al., 2012), which may support improved resilience to temperature and pathogen stressors. Likewise, the intertidal environment may modify host-pathogen interactions via promotion of microbiomes, metabolism, inflammation, and innate immunity that collectively grant improved resistance to pathogen infections (King et al., 2019; Offret et al., 2020; Corporeau et al., 2022). Intertidal oysters may also fare better under stressor conditions due to an improved ability to enact larger energy metabolism depressions and earlier anaerobic glycolysis responses (Meng et al., 2018).

In the present study, while time in the intertidal was associated with improved survival (at the DB site) and largely equivalent condition across treatment groups, intertidal treatment groups did show decreases in growth metrics. Specifically, in Year 1, intertidal oysters were significantly smaller in shell height and tissue DW than deep-water cultured individuals within the same farm at a number of timepoints. The observed reductions in growth were likely a result of reduced feeding opportunities in the intertidal zone, but, importantly, could support higher survival during summer months as a result of associated delays in reproductive development and/or reduced spawning (Cotter et al., 2010; Huvet et al., 2010; Cowan et al., 2023). Moreover, it has been suggested that individuals demonstrating plasticity in order to tolerate a range of environmental conditions at the expense of normal physiological function and energetics, may show a rebound in growth and survival when under more optimal conditions (Barbosa et al., 2022). This could be the case in the present study, as growth discrepancies were no longer apparent by the end of Year 2 (i.e. at harvest), shell height, tissue DW, and CI being generally comparable across *Deep* and *Intertidal→Deep* treatments.

Site-related differences may have also had a significant effect on the subsequent performance of oysters in terms of growth and maturity, and could account for the differing patterns of survival observed among farm sites in the present study. Differing levels of nutrients and phytoplankton across the study's spatial extent, for example, could result in varying growth rates, reproductive development, and overall condition (Malham et al., 2009; Cotter et al., 2010), all of which represent key factors that shape susceptibility to summer mortality. While we did not observe obvious differences in physical parameters (temperature, salinity, and dissolved oxygen) among farm sites, variation in patterns of reproductive development, CI, and growth across the farms/sites does suggest temporal and spatial variations in levels of feed and nutrient availability.

Results of histopathological screening in the present study suggested a minimal role of disease in driving observed differences in survival between treatments. However, of note, there was a greater incidence of VGH observed in deep-water oysters compared to intertidal counterparts in Year 1, suggesting that oysters under suspended culture conditions have increased exposure risk and/or susceptibility to VGH infection. It is also of interest that increased VGH incidence was detected in August of both years, suggesting a link with increased temperatures, as has been previously observed (Choi et al., 2004). Historically, VGH infections have occurred at low frequency and intensity and lack correlation with increased mortality rates, cumulatively suggesting that the VGH virus poses little overall threat to oysters. However, in

recent years, a number of oyster-producing regions across the globe have reported an increasing prevalence of the virus, including higher infection rates within populations and a wider distribution range (Garcia et al., 2006). Results here could also suggest that VGH poses an increased threat under future climate change conditions, but further investigation is warranted.

We propose the use of intertidal culture in Year 1 as part of a practical mitigative approach in order to combat summer mortality in Pacific oysters and improve resilience to climate change stressors. Partial culture in the intertidal conferred improved resilience to summer mortality stressor conditions both in the field (at one farm) and under laboratory conditions, with no obvious detriment to harvest size or condition. These findings may inform industry practice under the context of a changing climate, though additional examination is needed. Future work should include re-testing the intertidal culture approach across an increased number of farms, incorporating other mitigative approaches (e.g. selective breeding programs), examining multiple grow-out gear types, and conducting comprehensive physical and biological monitoring at farm sites.

Summer mortality events and climate change are long-term and accelerating challenges that pose serious threats to the shellfish aquaculture sector. An improved understanding of impacts and a sustained focus on developing practical methods that promote resilience in oysters are critical for safe-guarding this important global resource.

Data availability statement

The raw data supporting the conclusions of this article will be made available by the authors, without undue reservation.

Ethics statement

The animal study was approved by the Pacific Region Animal Care Committee of Fisheries and Oceans Canada. The study was conducted in accordance with the local legislation and institutional requirements.

Author contributions

CM: Conceptualization, Formal analysis, Funding acquisition, Investigation, Methodology, Project administration, Supervision, Visualization, Writing – original draft. MR: Formal analysis, Investigation, Project administration, Supervision, Visualization, Writing – original draft. SL: Investigation, Project administration, Writing – review & editing. CW: Investigation, Writing – review & editing. TG: Investigation, Project administration, Resources, Supervision, Writing – review & editing. EK: Investigation, Writing – review & editing. EM: Investigation, Writing – review & editing. SG: Investigation, Writing – review & editing. AL: Project administration, Resources, Supervision, Writing – review & editing. CP: Conceptualization, Funding acquisition, Methodology, Project administration, Resources, Supervision, Writing – review & editing.

Funding

The author(s) declare financial support was received for the research, authorship, and/or publication of this article. Funding for this work was provided by Fisheries and Oceans Canada's Aquaculture Collaborative Research and Development Program (ACRDP 21-P-02) and Taylor Shellfish Canada ULC.

Acknowledgments

The authors gratefully acknowledge the contributions of Alex Munro (Taylor Shellfish Canada ULC) and the staff, students, and volunteers of the Deep Bay Marine Field Station (Vancouver Island University).

Conflict of interest

The authors declare that the research was conducted in the absence of any commercial or financial relationships that could be construed as a potential conflict of interest.

This project was carried out under Fisheries and Oceans Canada's Aquaculture Collaborative Research and Development Program with Taylor Shellfish Canada ULC as the industry partner. Taylor Shellfish Canada ULC provided project funds and in-kind contributions in support of the project. Two of the three field sites included in the study (DN, FB) are commercial farms of Taylor Shellfish Canada ULC.

Publisher's note

Supplementary material

The Supplementary Material for this article can be found online at: https://www.frontiersin.org/articles/10.3389/fmars.2024.1345493/full#supplementary-material

References

Abele, D., Brey, T., and Philipp, E. (2009). Bivalve models of aging and the determination of molluscan lifespans. *Exp. Gerontol.* 44, 307. doi: 10.1016/j.exger.2009.02.012

Amorim, K., Piontkivska, H., Zettler, M. L., Sokolov, E., Hinzke, T., Nair, A. M., et al. (2021). Transcriptional response of key metabolic and stress response genes of a nuculanid bivalve, *Lembulus bicuspidatus* from an oxygen minimum zone exposed to hypoxia-reoxygenation. *Comp. Biochem. Physiol. Part B: Biochem. Mol. Biol.* 256, 110617. doi: 10.1016/j.cbpb.2021.110617

Ashton, E. C., Guist, S., Roberts, D., and Sigwart, J. D. (2020). Effects of environmental factors and husbandry practices on summer mortality events in the cultivated Pacific oyster *Crassostrea gigas* in the North of Ireland. *J. Shellfish Res.* 39, 13–20. doi: 10.2983/035.039.0102

Barbosa, M., Schwaner, C., Pales Espinosa, E., and Allam, B. (2022). A transcriptomic analysis of phenotypic plasticity in *Crassostrea virginica* larvae under experimental acidification. *Genes* 13, 1529. doi: 10.3390/genes13091529

Barbosa Solomieu, V., Renault, T., and Travers, M. A. (2015). Mass mortality in bivalves and the intricate case of the Pacific oyster, *Crassostrea gigas*. *J. Invertebrate Pathol.* 131, 2–10. doi: 10.1016/j.jip.2015.07.011

Bayne, B. L. (2004). Phenotypic flexibility and physiological tradeoffs in the feeding and growth of marine bivalve molluscs. *Integr. Comp. Biol.* 44, 425–432. doi: 10.1093/icb/44.6.425

BCMSRM (2002). *The Baynes Sound coastal plan for shellfish aquaculture* (Victoria, BC, Canada: British Columbia Ministry of Sustainable Resource Management, Coast & Marine Planning Branch).

Brown, J. R., and Hartwick, E. B. (1988). Influences of temperature, salinity and available food upon suspended culture of the Pacific oyster, *Crassostrea gigas*. I. Absolute and allometric growth. *Aquaculture* 70, 231–251. doi: 10.1016/0044-8486(88)90099-3

Campbell, M. D., and Hall, S. G. (2019). Hydrodynamic effects on oyster aquaculture systems: a review. *Rev. Aquac.* 11, 896–906. doi: 10.1111/raq.12271

Cassis, D., Pearce, C. M., and Maldonado, M. T. (2011). Effects of the environment and culture depth on growth and mortality in juvenile Pacific oysters in the Strait of Georgia, British Columbia. *Aquac. Environ. Interact.* 1, 259–274. doi: 10.3354/aei00025

Choi, D. L., Lee, N. S., Choi, H. J., Park, M. A., McGladdery, S. E., and Mi, S. P. (2004). Viral gametocytic hypertrophy caused by a papova-like virus infection in the Pacific oyster *Crassostrea gigas* in Korea. *Dis. Aquat. Organ.* 59, 205–209. doi: 10.3354/dao059205

Clark, M. S., Suckling, C. C., Cavallo, A., Mackenzie, C. L., Thorne, M. A. S., Davies, A. J., et al. (2019). Molecular mechanisms underpinning transgenerational plasticity in the green sea urchin *Psammechinus miliaris*. *Sci. Rep.* 9 (1), 952. doi: 10.1038/s41598-018-37255-6

Clark, M. S., Thorne, M. A. S., King, M., Hipperson, H., Hoffman, J. I., and Peck, L. S. (2018). Life in the intertidal: cellular responses, methylation and epigenetics. *Funct. Ecol.* 32, 1982–1994. doi: 10.1111/1365-2435.13077/SUPPINFO

Corporeau, C., Petton, S., Vilaça, R., Delisle, L., Quéré, C., Le Roy, V., et al. (2022). Harsh intertidal environment enhances metabolism and immunity in oyster (*Crassostrea gigas*) spat. *Mar. Environ. Res.* 180, 105709. doi: 10.1016/j.marenvres.2022.105709

Cotter, E., Malham, S. K., O'Keeffe, S., Lynch, S. A., Latchford, J. W., King, J. W., et al. (2010). Summer mortality of the Pacific oyster, *Crassostrea gigas*, in the Irish Sea: the influence of growth, biochemistry and gametogenesis. *Aquaculture* 303, 8–21. doi: 10.1016/j.aquaculture.2010.02.030

Cowan, M. (2020). Exploring the mechanisms of Pacific oyster summer mortality in Baynes Sound aquaculture. MSc Thesis. Victoria, Canada: University of Victoria.

Cowan, M. W., Pearce, C. M., Finston, T., Meyer, G. R., Marshall, R., Evans, W., et al. (2023). Role of the *Vibrio* community, reproductive effort, and environmental parameters in intertidal Pacific oyster summer mortality in British Columbia, Canada. *Aquaculture* 565, 739094. doi: 10.1016/j.aquaculture.2022.739094

Dang, X., Lim, Y. K., Li, Y., Roberts, S. B., Li, L., and Thiyagarajan, V. (2023). Epigenetic-associated phenotypic plasticity of the ocean acidification-acclimated edible oyster in the mariculture environment. *Mol. Ecol.* 32, 412–427. doi: 10.1111/mec.16751

Dégremont, L., Bédier, E., and Boudry, P. (2010). Summer mortality of hatchery-produced Pacific oyster spat (*Crassostrea gigas*). II. Response to selection for survival and its influence on growth and yield. *Aquaculture* 299, 21–29. doi: 10.1016/j.aquaculture.2009.11.017

Ernande, B., Boudry, P., Clobert, J., and Haure, J. (2004). Plasticity in resource allocation based life history traits in the Pacific oyster, *Crassostrea gigas*. I. Spatial variation in food abundance. *J. Evol. Biol.* 17, 342–356. doi: 10.1046/j.1420-9101.2003.00674.x

Evans, O., Kan, J. Z. F., Pathirana, E., Whittington, R. J., Dhand, N., and Hick, P. (2019). Effect of emersion on the mortality of Pacific oysters (*Crassostrea gigas*) infected with *Ostreid herpesvirus*-1 (OsHV-1). *Aquaculture* 505, 157–166. doi: 10.1016/j.aquaculture.2019.02.041

FAO (2022). *The State of World Fisheries and Aquaculture 2022. Towards Blue Transformation* (Rome: FAO). doi: 10.4060/cc0463en

Garcia, C., Robert, M., Arzul, I., Chollet, B., Joly, J. P., Miossec, L., et al. (2006). Viral gametocytic hypertrophy of *Crassostrea gigas* in France: from occasional records to disease emergence? *Dis. Aquat. Organ.* 70, 193–199. doi: 10.3354/dao070193

Go, J., Deutscher, A. T., Spiers, Z. B., Dahle, K., Kirkland, P. D., and Jenkins, C. (2017). Mass mortalities of unknown aetiology in Pacific oysters Crassostrea gigas in Port Stephens, New South Wales, Australia. *Dis. Aquat. Org.* 125 (3), 227–242. doi: 10.3354/dao03146

Green, T. J., Siboni, N., King, W. L., Labbate, M., Seymour, J. R., and Raftos, D. (2019). Simulated marine heat wave alters abundance and structure of *Vibrio* populations associated with the Pacific oyster resulting in a mass mortality event. *Microb. Ecol.* 77, 736–747. doi: 10.1007/s00248-018-1242-9

Hamdoun, A. M., Cheney, D. P., and Cherr, G. N. (2003). Phenotypic plasticity of HSP70 and HSP70 gene expression in the Pacific oyster (*Crassostrea gigas*): implications for thermal limits and induction of thermal tolerance. *Biol. Bull.* 205, 160–169. doi: 10.2307/1543236

Hickman, R. W., and Illlingworth, J. (1980). Condition cycle of the green-lipped mussel *Perna canaliculus* in New Zealand. *Mar. Biol.* 60, 27–38. doi: 10.1007/BF00395603

Hofmann, G. E. (2017). Ecological epigenetics in marine metazoans. *Front. Mar. Sci.* 4. doi: 10.3389/fmars.2017.00004

Huvet, A., Normand, J., Fleury, E., Quillien, V., Fabioux, C., and Boudry, P. (2010). Reproductive effort of Pacific oysters: a trait associated with susceptibility to summer mortality. *Aquaculture* 304, 95–99. doi: 10.1016/j.aquaculture.2010.03.022

Jablonka, E., and Lamb, M. J. (2002). The changing concept of epigenetics. *Ann. N.Y. Acad. Sci.* 981, 82–96. doi: 10.1111/j.1749-6632.2002.tb04913.x

King, W. L., Jenkins, C., Go, J., Siboni, N., Seymour, J. R., and Labbate, M. (2019). Characterisation of the Pacific oyster microbiome during a summer mortality event. *Microb. Ecol.* 77, 502–512. doi: 10.1007/s00248-018-1226-9

Labreuche, Y., Lambert, C., Soudant, P., Boulo, V., Huvet, A., and Nicolas, J. L. (2006). Cellular and molecular hemocyte responses of the Pacific oyster, *Crassostrea gigas*, following bacterial infection with *Vibrio aestuarianus* strain 01/32. *Microbes Infect.* 8, 2715–2724. doi: 10.1016/j.micinf.2006.07.020

Lafont, M., Goncalves, P., Guo, X., Montagnani, C., Raftos, D., and Green, T. (2019). Transgenerational plasticity and antiviral immunity in the Pacific oyster (*Crassostrea gigas*) against Ostreid herpesvirus 1 (OsHV-1). *Dev. Comp. Immunol.* 91, 17–25. doi: 10.1016/j.dci.2018.09.022

Lafont, M., Vergnes, A., Vidal-Dupiol, J., De Lorgeril, J., Gueguen, Y., Haffner, P., et al. (2020). A sustained immune response supports long-term antiviral immune priming in the Pacific oyster *Crassostrea gigas*. *mBio* 11 (2), 10–1128. doi: 10.1128/mBio.02777-19

Lewis, J., and Seed, R. (1969). Morphological variations in *Mytilus* from south-west England in relation to the occurrence of *M. galloprovincialis* Lamarck. *Cahiers Biologie Mar.* 10, 231–253.

Li, L., Li, A., Song, K., Meng, J., Guo, X., Li, S., et al. (2018). Divergence and plasticity shape adaptive potential of the Pacific oyster. *Nat. Ecol. Evol.* 2, 1751–1760. doi: 10.1038/s41559-018-0668-2

Li, Y., Qin, J. G., Li, X., and Benkendorff, K. (2009). Monthly variation of condition index, energy reserves and antibacterial activity in Pacific oysters, *Crassostrea gigas*, in Stansbury (South Australia). *Aquaculture* 286, 64–71. doi: 10.1016/j.aquaculture.2008.09.004

Li, Q., Zhao, X., Kong, L., and Yu, H. (2013). Transcriptomic response to stress in marine bivalves. *Invertebrate Survival J.* 10, 84–93.

Mackenzie, C. L., Pearce, C. M., Leduc, S., Roth, D., Kellogg, C. T. E., Clemente-Carvalho, R. B. G., et al. (2022). Impacts of seawater pH buffering on the larval microbiome and carry-over effects on later-life disease susceptibility in Pacific oysters. *Appl. Environ. Microbiol.* 88 (22), e01654-22. doi: 10.1128/aem.01654-22

Malham, S. K., Cotter, E., O'Keeffe, S., Lynch, S., Culloty, S. C., King, J. W., et al. (2009). Summer mortality of the Pacific oyster, *Crassostrea gigas*, in the Irish Sea: the influence of temperature and nutrients on health and survival. *Aquaculture* 287, 128–138. doi: 10.1016/j.aquaculture.2008.10.006

Mann, R. (1979). Some biochemical and physiological aspects of growth and gametogenesis in *Crassostrea gigas* and *Ostrea edulis* grown at sustained elevated temperatures. *J. Mar. Biol. Assoc. United Kingdom* 59, 95–110. doi: 10.1017/S0025315400046208

Marty, G. D., Bower, S. M., Clarke, K. R., Meyer, G., Lowe, G., Osborn, A. L., et al. (2006). Histopathology and a real-time PCR assay for detection of *Bonamia ostreae* in *Ostrea edulis* cultured in western Canada. *Aquaculture* 261, 33–42. doi: 10.1016/j.aquaculture.2006.07.024

Masanja, F., Yang, K., Xu, Y., He, G., Liu, X., Xu, X., et al. (2023). Impacts of marine heat extremes on bivalves. *Front. Mar. Sci.* 10, 1159261. doi: 10.3389/fmars.2023.1159261

Meng, J., Wang, T., Li, L., and Zhang, G. (2018). Inducible variation in anaerobic energy metabolism reflects hypoxia tolerance across the intertidal and subtidal distribution of the Pacific oyster (*Crassostrea gigas*). *Mar. Environ. Res.* 138, 135–143. doi: 10.1016/j.marenvres.2018.04.002

Normand, J., Le Pennec, M., and Boudry, P. (2008). Comparative histological study of gametogenesis in diploid and triploid Pacific oysters (*Crassostrea gigas*) reared in an estuarine farming site in France during the 2003 heatwave. *Aquaculture* 282, 124–129. doi: 10.1016/j.aquaculture.2008.06.026

Offret, C., Paulino, S., Gauthier, O., Chateau, K., Bidault, A., Corporeau, C., et al. (2020). The marine intertidal zone shapes oyster and clam digestive bacterial microbiota. *FEMS Microbiol. Ecol.* 96, 78. doi: 10.1093/femsec/fiaa078

Peeler, E. J., Reese, R. A., Cheslett, D. L., Geoghegan, F., Power, A., and Thrush, M. A. (2012). Investigation of mortality in Pacific oysters associated with *Ostreid herpesvirus-1* µVar in the Republic of Ireland in 2009. *Prev. Vet. Med.* 105, 136–143. doi: 10.1016/j.prevetmed.2012.02.001

Pernet, F., Barret, J., Le Gall, P., Corporeau, C., Dégremont, L., Lagarde, F., et al. (2012). Mass mortalities of Pacific oysters *Crassostrea gigas* reflect infectious diseases and vary with farming practices in the Mediterranean Thau lagoon, France. *Aquac. Environ. Interact.* 2, 215–237. doi: 10.3354/aei00041

Pernet, F., Gachelin, S., Stanisiere, J.-Y., Petton, B., Fleury, E., and Mazurié, J. (2019). Farmer monitoring reveals the effect of tidal height on mortality risk of oysters during a herpesvirus outbreak. *ICES J. Mar. Sci.* 76, 1816–1824. doi: 10.1093/icesjms/fsz074

Pernet, F., Lagarde, F., Le Gall, P., and D'Orbcastel, E. R. (2014). Associations between farming practices and disease mortality of Pacific oyster *Crassostrea gigas* in a Mediterranean lagoon. *Aquac. Environ. Interact.* 5, 99–106. doi: 10.3354/aei00096

Petton, B., Destoumieux-Garzón, D., Pernet, F., Toulza, E., de Lorgeril, J., Degremont, L., et al. (2021). The Pacific oyster mortality syndrome, a polymicrobial and multifactorial disease: state of knowledge and future directions. *Front. Immunol.* 12, 630343. doi: 10.3389/fimmu.2021.630343

Pörtner, H. O. (2012). Integrating climate-related stressor effects on marine organisms: unifying principles linking molecule to ecosystem-level changes. *Mar. Ecol. Prog. Ser.* 470, 273–290. doi: 10.3354/meps10123

Rainer, J. S., and Mann, R. (1992). A comparison of methods for calculating condition index in Eastern oysters, *Crassostrea virginica* (Gmelin 1791). *J. Shellfish Res.* 11, 55–58.

R Core Team (2022). *R: A language and environment for statistical computing* (Vienna, Austria: R Foundation for Statistical Computing).

Reid, G. K., Gurney-Smith, H. J., Flaherty, M., Garber, A. F., Forster, I., Brewer-Dalton, K., et al. (2019). Climate change and aquaculture: considering adaptation potential. *Aquac. Environ. Interact.* 11, 603–624. doi: 10.3354/aei00333

Somero, G. N. (2002). Thermal physiology and vertical zonation of intertidal animals: optima, limits, and costs of living. *Integr. Comp. Biol.* 42, 780–789. doi: 10.1093/icb/42.4.780

Steele, S., and Mulcahy, M. F. (1999). Gametogenesis of the oyster *Crassostrea gigas* in southern Ireland. *J. Mar. Biol. Assoc. United Kingdom* 79, 673–686. doi: 10.1017/S0025315498000836

Tagliarolo, M., Clavier, J., Chauvaud, L., Koken, M., and Grall, J. (2012). Metabolism in blue mussel: intertidal and subtidal beds compared. *Aquat. Biol.* 17, 167–180. doi: 10.3354/ab00464

Wang, X., Cong, R., Li, A., Wang, W., Zhang, G., and Li, L. (2023). Transgenerational effects of intertidal environment on physiological phenotypes and DNA methylation in Pacific oysters. *Sci. Total Environ.* 871, 162112. doi: 10.1016/j.scitotenv.2023.162112

Wang, X., Li, A., Wang, W., Que, H., Zhang, G., and Li, L. (2021). DNA methylation mediates differentiation in thermal responses of Pacific oyster (*Crassostrea gigas*) derived from different tidal levels. *Heredity* 126, 10–22. doi: 10.1038/s41437-020-0351-7

Wang, J., Zhang, G., Fang, X., Guo, X., Li, L., Luo, R., et al. (2012). The oyster genome reveals stress adaptation and complexity of shell formation. *Nature* 490, 49–54. doi: 10.1038/nature11413

Yang, B., Zhai, S., Li, X., Tian, J., Li, Q., Shan, H., et al. (2021). Identification of *Vibrio alginolyticus* as a causative pathogen associated with mass summer mortality of the Pacific oyster (Crassostrea gigas) in China. *Aquaculture* 535, 736363. doi: 10.1016/j.aquaculture.2021.736363

Zhang, G., Li, L., Meng, J., Qi, H., Qu, T., Xu, F., et al. (2016). Molecular basis for adaptation of oysters to stressful marine intertidal environments. *Annu. Rev. Anim. Biosci.* 4, 357–381. doi: 10.1146/annurev-animal-022114-110903

frontiers | Frontiers in Marine Science

TYPE Original Research
PUBLISHED 17 April 2024
DOI 10.3389/fmars.2024.1362078

OPEN ACCESS

EDITED BY
Tangtian He,
Hong Kong Polytechnic University,
Hong Kong SAR, China

REVIEWED BY
Michio Suzuki,
The University of Tokyo, Japan
Qiang Fu,
Qingdao Agricultural University, China
Yu Shi,
Chinese Academy of Sciences (CAS), China

*CORRESPONDENCE
Sen Zhao
zhaosen@bbgu.edu.cn
Dahui Yu
pearlydh@163.com

†These authors have contributed equally to this work

RECEIVED 27 December 2023
ACCEPTED 02 April 2024
PUBLISHED 17 April 2024

CITATION
Zheng Y, Wang P, Guo Y, Bai L, Yu D and Zhao S (2024) Comparative transcriptome analysis reveals immune-related genes involved in allograft and xenograft transplantation in *Pinctada fucata*. *Front. Mar. Sci.* 11:1362078. doi: 10.3389/fmars.2024.1362078

Comparative transcriptome analysis reveals immune-related genes involved in allograft and xenograft transplantation in *Pinctada fucata*

Yusi Zheng[1†], Pei Wang[1,2†], Ying Guo[1,2], Lirong Bai[1], Dahui Yu[1*] and Sen Zhao[1*]

[1]Guangxi Key Laboratory of Beibu Gulf Marine Biodiversity Conservation, Beibu Gulf University, Qinzhou, China, [2]College of Life Science and Technology, Guangxi University, Nanning, China

Background: The marine pearl culture industry is a key industry in the Beibu Gulf of China that achieves large-scale pearl production by artificial nucleus insertion in pearls. High-quality pearls can produced by xenotransplantation, but allotransplantation or xenotransplantation can lead to various immune responses, resulting in nucleus rejection or even the recipient shell death and thereby causing significant losses in pearl production.

Methods: Few studies have investigated the immune defenses of oysters related to allografts and xenografts. In this study, transcriptomic comparisons of allograft and xenograft Pinctada fucata haemocytes were conducted to identify genes associated with immune responses.

Results: A total of 33.11 Gbp of clean reads were generated from five P. fucata haemocytes. De-novo assembly of quality-filtered reads generated a total of 26,526 unigenes, with 22,002 known genes and 4,524 predicted novel genes. In addition, 34,904 novel transcripts were detected, with 15,620 novel alternative splicing isoforms of known protein coding genes and 4,605 belonging to novel protein coding genes, with the remaining 14,679 comprising long non-coding RNA transcripts. Functional enrichment analysis of immune-related differentially expressed genes (DEGs) using the Gene Ontology (GO) and Kyoto Encyclopedia of Genes and Genomes (KEGG) databases revealed 36–44 significantly enriched GO terms and 34 significantly enriched KEGG pathways. Ten DEGs were subjected to validation of expression levels using RT-q PCR analysis, revealing generally consistent values as the high-throughput sequencing data.

Conclusion: Oyster haemocytes were comprehensively evaluated in this study using transcriptomic comparisons and with a focus on immune-related functional genes and pathways. The results revealed numerous DEGs related to immune function that can serve as the basis for subsequent immune response analysis of allotransplantation and xenotransplantation.

KEYWORDS

***Pinctada fucata*, transcriptome, allograft, xenograft, immunological response**

1 Introduction

The pearl oyster *Pinctada fucata martensii* is an economically important bivalve that is farmed for marine pearl production globally, with most Chinese marine pearls produced from this species (Zhang et al., 2022). The production of seawater pearls in China is primarily based on artificial cultivation. Specifically, nucleus transplantation is conducted with a mantle graft originating from a donor oyster, along with a shell bead nucleus, into the "pearl sac" of a recipient oyster. The quality of artificial beads consequently depends on the state of the recipient oyster and the choice of mantle graft. To achieve optimal results and produce smooth and round pearls after artificial nucleus insertion, the metabolism of the recipient oyster must remain in a low state, and the gonad must be generated without gametes (Arnaud-Haond et al., 2007; Fang et al., 2008; Inoue et al., 2010; Southgate and Lucas, 2011; Wei et al., 2017; Wang et al., 2024). Moreover, the small mantle graft of the recipient oyster is the primary factor that determines the formation of the pearl sac (Wei et al., 2017), with some studies detecting DNA from the donor oyster mantle in the pearl sac (Wang et al., 2024). Transplantation can either include allogeneic or xenogeneic insertions. Allogenic insertions are primarily conducted in China and produces small pearls with poor coloration, and average economic value. Previous studies demonstrated that xenografts did not significantly affect the formation of pearl sacs and subsequent nucleus retention but did influence pearl color, complexion, shape, nacre deposition, and nacre weight (McGinty et al., 2010). Consequently, xenografts hold potential in enhancing pearl quality attributes such as size, underscoring the importance of donor oysters in achieving desirable pearl growth, color, and surface characteristics (Fukushima et al., 2014). Thus, the study demonstrated the potential for xenografts to improve pearl quality characteristics like pearl size, while emphasizing a role of donor oysters in achieving ideal pearl growth, color, and surface complexion. However, the low output from such methods requires further optimization and improvement.

Allograft and xenograft transplantation have been evaluated in China in recent years. For example, transcriptomic sequencing has been used to evaluate immune system response mechanisms after xenotransplantation and allotransplantation (Wei et al., 2017). These methods have also been applied to investigations of freshwater pearl oysters (Zhang et al., 2016). RNA-seq based transcriptomic analysis is a highly effective approach for investigating the immune responses at the genomic and transcriptomic levels. Such analyses have been widely used in shellfish life science research, including in the investigation of *Perumytilus purpuratus* (Briones et al., 2018), *Patinopecten yessoensis* (Zhou et al., 2019), *Hyriopsis cumingii* (Zhang et al., 2016), *P. fucata* (Lu et al., 2022), *Mytilus galloprovincialis* (Dong et al., 2022), and *Argopecten irradians* (Dong et al., 2022). Numerous immune-related genes have been discovered and intensively studied in bivalves, including the toll-like receptor (Wei et al., 2017), C type lectin (He et al., 2020), HSP70 (Wei et al., 2017), and Interleukin (IL)-17 (Zhang et al., 2016).

Here, a transcriptomic analysis of *P. fucata* haemocytes after transplantation was conducted to better understand the molecular mechanisms related to *P. fucata* immune responses after allotransplantation and xenotransplantation. The resulting analyses providing insights into the immune defense mechanisms associated with recipient oyster transplants, help promote the mitigation of host oyster immune rejection of grafts, and inform the improved efficiency of pearl production.

2 Materials and methods

2.1 Oyster and mantle grafting

Healthy 1.5-year-old *P. fucata* (shell lengths: 4.5-5.5 cm, weights: 42-58 g) were obtained from the pearl oyster culture station of the South China Sea Fisheries Research Institute in Xincun Village, Hainan Province, China. Donor *P. maxima* (shell lengths: 8-15 cm, weights: 100-200 g) and *Pteria penguin* (shell lengths: 10-15 cm, weights: 200-300 g) were selected from wild populations in Hainan. Oysters were cultured in oxygenated seawater at 25°C and were fed *Chlorella vulgaris*. After temporary breeding for a week, professional technicians performed nucleus transplantation. The donors (*P. fucata, P. maxima, and P. penguin*) were first sacrificed and strips of mantle tissue were excised from the midventral regions of the mantle and then thoroughly cleaned in sterile seawater. Samples were then sectioned into small grafts (about 3×3 mm) and inserted into pearl sacs. Transplanted host oysters were placed in temporary culture ponds to breed, with four experimental groups and one control group established for analyses. The experimental groups were respectively implanted with *P. fucata*, *P. maxima*, and *P. penguin* mantle slices in the *P. fucata* group with nucleus insertion. Another group was implanted with *P. fucata* mantle slices without nucleus insertion. A control group was established comprising *P. fucata* without any implants. Host oysters were referred to as Pf_Pf, Pf_Pm, and Pf_Pp, respectively, after mantle allograft and xenograft surgery. The shellfish group that had only undergone surgical treatment without nucleus insertion was referred to as Mock, while the untreated control group was referred to as CK.

2.2 Hemocyte collection

At 192 hours post-transplantation, whole hemolymph samples were collected from the adductor muscles using 1 mL syringes (1 mL withdrawn per oyster and samples from 10 oysters were pooled together). Hemocytes were then harvested via centrifugation at 4,000 g for 10 minutes, the supernatant was discarded and 1 mL of Trizol (TransGen Biotech, China) was added, followed by mixing with the hemocytes. The samples were then immediately frozen in liquid nitrogen and stored at -70°C.

2.3 RNA extraction, library construction, and sequencing

Total RNA was extracted from the experimental and control group samples following the manufacturer's instructions. RNA concentration and integrity of the RNA were determined using a Lunatic high-throughput microfluidic spectrophotometer

(Unchained Labs, USA). cDNA libraries were then sequenced using the BGISEQ-500RS RNA-Seq platform.

2.4 RNA-seq data assembly and functional annotation

Library construction and RNA-Seq were conducted at BGI Genomics (Shenzhen, China) following typical protocols. To ensure the reliability of the analyses, the resulting raw data were filtered using the SOAPnuke software (Chen et al., 2018) program to remove data containing adaptors, poly-N's, and reads of low quality. The resulting clean reads were used in the subsequent analyses. After comparing the transcriptomic data against the reference genome, transcribed regions not originally annotated were observed to identify potentially novel genes for the species. The new genes were then compared against several databases, with the confidence in annotations following order of: Nt <KOG <Pfam <Swiss Prot <KO <GO <Nr (Ai et al., 2016).

2.5 Analysis of differentially expressed unigenes and GO/KEGG enrichment analysis

To determine physiological differences of *P. fucata* with different mantle inserts, the gene expression levels of each sample were calculated using the RSEM (Reads Per Kilobase Million) and FPKM (Fragments Per Kilobase Million) methods, followed by correction for sequencing depth. Unigenes meeting the criteria of $p < 0.005$ and $|\log2(\text{fold change})| > 2$ were considered differentially expressed genes (DEGs). DEGs were selected for further analyzed using the hypergeometric distribution principle and subjected to GO and KEGG enrichment analysis. GO enrichment was used to primarily analyze the functional classification of major biological features related to DEGs. In addition, KEGG pathway enrichment was performed to identify the primary biochemical metabolic and signal transduction pathways that DEGs were involved in. The statistical threshold for GO or KEGG enrichment was set at $p < 0.05$.

2.6 Real-time quantitative PCR analysis

To evaluate the accuracy of the transcriptomic analyses, 10 DEGs were selected for real-time quantitative PCR (RT-qPCR) analysis. The sequences of the10 genes were used for primer design (Table 1) using 18S rRNA genes as internal reference genes. The RNA samples used for RT-qPCR amplifications were the same as those used for constructing the RNA-Seq libraries described above. Total RNA was reverse transcribed using the EasyScript® All-in-One First-Strand cDNA Synthesis SuperMix for qPCR (TransGen Biotech China). Each reaction contained 1 µL reverse and forward primers each, 10 µL of SYBR Green Mix (TransGen, Beijing, China), and 2 µL of 1:8 diluted cDNA, with RNase-free water added to achieve a final reaction volume of 20 µL. The qPCR cycling program including 1 cycle of 10 min at 95°C, followed by 40 cycles of 10 s at 95°C, 15 s at 55°C, and 15 s at 72°C. The mRNA relative expression levels were calculated using the $2^{\wedge-\Delta\Delta Ct}$ method, and each experiment was performed in triplicate. Data were analyzed using the Least Significant Difference (LSD) method in the SPSS software program (version 22), with statistically significant differences identified at $p < 0.05$.

TABLE 1 RT-qPCR primer sequence information.

Gene name	Transcript ID	Primer Sequence ((5'→3')
N16 gene for matrix protein	BGI_novel_T000084	Forward CCTAGTATGTGTAAAGCCT Reverse CAACACTAGTTCTTCGGAT
TSSK	Pma_99.293	Forward ATTTCTCAGAAGAACACGCTA Reverse TTGGAAACCGACTGTACCAC
CROCC	Pma_75.463	Forward AACGAGGATCTGAGAAACACA Reverse GACATTGGCCTTTTGCTCT
Ryanodine receptor 1	Pma_530.903	Forward AACTTACCTAGGCTTTAGCTG Reverse TGATTCTGAAGATGCTCCA
Histone deacetylase complex subunit SAP18	Pma_399.417	Forward AGGTTAATCCAGATGCCAGACA Reverse TCCTGAGCAAGTAGTACCGAT
Cytochrome P450 family 2 subfamily K	Pma_368.87	Forward ATCCTTATCTAAAACCCGCAGT Reverse GTTTAGAATCGCCATCCCTGT
Mucin-2	Pma_253.267	Forward ACAAACTCGGACAAGACATGC Reverse GTTGACATAGAACTCACGACCA
TRIM2	Pma_192.483	Forward AAGGCAACATATGCTTCTCA Reverse CGCCAGATTTTGTAGATGACT
Transcription factor Sp4	Pma_145.1326	Forward AACAACAGAATCTGCTGCAA Reverse TGTACACTAACGTTGGCAT
SLC8A	BGI_novel_T013769	Forward CCATTACTTTGATGTCTGGC Reverse GTCTGATATCTTCCCCACC

3 Results

3.1 Transcriptomic sequence assembly and annotation

The transcriptomes from four experimental and control samples yielded a total of 33.11 Gbp of clean data (Table 2).

10.3389/fmars.2024.1362078

TABLE 2 Transcriptomic sequencing data statistics.

Sample	Total reads (M)	Total Clean Bases (Gbp)	GC content (%)	Clean Reads Q30 (%)	Total Mapping (%)	Uniquely Mapping (%)
CK	44.42	6.66	39.43	89.71	64.03	38.09
Mock	44.60	6.69	39.40	90.07	64.89	39.06
Pf_Pf	44.03	6.6	39.61	88.76	65.06	37.88
Pf_Pm	43.59	6.54	39.54	88.48	64.28	37.16
Pf_Pp	44.11	6.62	39.88	89.14	66.09	39.6

The clean reads data can be downloaded from NCBI under accession code PRJNA1068836. Over 88% of each sample exhibited >Q30 quality scores. The GC contents for the CK, Mock, Pf_Pf, Pf_Pm, and Pf_Pp libraries ranged from 39.43% to 39.88%. In addition, between 64.03 to 66.09% of the clean reads from each group aligned to the *P. fucata* genome (Table 2). Further, between 37.16% and 39.6% of the reads for the four experimental and control samples uniquely mapped to the genome (Table 2).

In addition, A total of 26,526 unigenes were identified among the expressed genes, with 22,002 known unigenes and 4,524 predicted novel genes. A total of 34,904 novel transcripts were also detected, of which 15,620 belonged to novel alternative splicing isoforms of known protein coding genes and 4,605 belonged to novel protein coding genes, with the remaining 14,679 comprising long non-coding RNA transcripts.

3.2 Functional annotation of DEGs

The CK vs Pf_Pm comparison comprised the largest number of differential genes, with 2,786 DEGs, of which 886 were up-regulated and 1,900 were down-regulated (Figure 1, Table 3). The DEGs were annotation based on GO classifications, revealing functions primarily related to biological processes, cellular components, and molecular functions, with each group comprising 36 to 44 sub-categories (Figure 2).

Considering the DEGs annotated within the biological processes group, the sub-categories of "cell movement process," "metabolic process," and "biological regulation" were the most abundant. Within the cellular component group, most differential genes were annotated to the "membrane" and "membrane part" sub-categories. Lastly, the "binding" and "catalytic activity" sub-categories were particularly prominent among the molecular function group.

DEGs classified to KEGG pathways related to signal transduction pathways comprised 398, 213, 427, 341, 268, 293, 269, 290, 188, and 253 pathways in the CK-vs-Mock, CK-vs-Pf_Pf, CK-vs-Pf_Pm, CK-vs-Pf_Pp, Mock-vs-Pf_Pf, Mock-vs-Pf_Pm, Mock-vs-Pf_Pp, Pf_Pf-vs-Pf_Pm, Pf_Pf-vs-Pf_Pp, and Pf_Pm-vs-Pf_Pp group comparisons. A total of 26 KEGG pathways were enriched among the DEGs (Figure 3), including the NOD-like receptor signaling pathway, the cytosolic DNA-sensing pathway, the Toll and Imd signaling pathway, the C-type lectin receptor signaling pathway, and the chemokine signaling pathway. Notably, the cytosolic DNA-sensing pathway had the highest enrichment of DEGs in the CK-vs-Mock group.

3.3 Enrichment of DEGs related to immune functioning

DEGs among all samples were compared, revealing 19,012 DEGs common to all samples, with the other different modules comprising

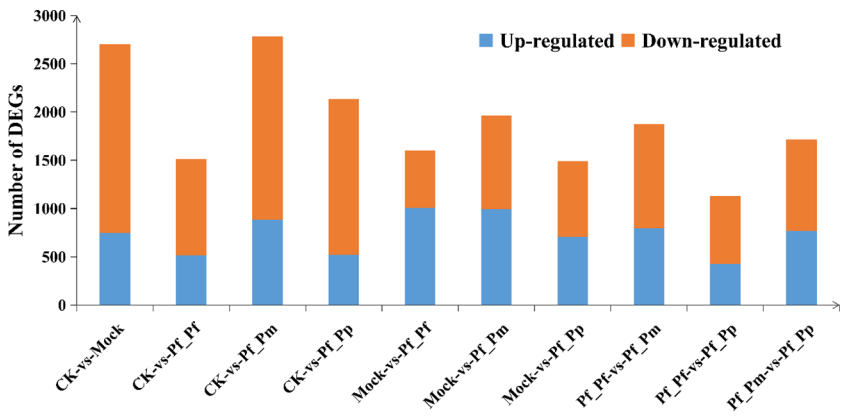

FIGURE 1
Up- and down-regulated DEGs of *P. fucata* in comparisons between post-transgraft groups.

10.3389/fmars.2024.1362078

TABLE 3 Comparison of the number of DEGs in the serum between the control group.

Group	Upregulated protein	Downregulated protein	Total DEGs
CK-vs-Mock	747	1957	2704
CK-vs-Pf_Pf	517	994	1511
CK-vs-Pf_Pm	886	1900	2786
CK-vs-Pf_Pp	519	1614	2133
Mock-vs-Pf_Pf	1007	594	1601
Mock-vs-Pf_Pm	996	967	1963
Mock-vs-Pf_Pp	705	784	1489
Pf_Pf-vs-Pf_Pm	794	1079	1873
Pf_Pf-vs-Pf_Pp	427	705	1132
Pf_Pm-vs-Pf_Pp	769	945	1714

(CK, Mock) and the xenograft group/allograft group (Pf_Pp, Pf_Pm, Pf_Pf).

unique genes for each sample (Figure 4). KEGG enrichment analysis revealed that the enriched pathways ($p < 0.05$) including a cytosolute DNA sensing pathway, in addition to pathways related to long-term inhibition, cholesterol metabolism, the PPAR signaling pathway, apoptosis, and terpenoid skeleton biosynthesis. Notably, long-term inhibition was represented in each differential comparison and comprised genes encoding cGMP-dependent protein kinase 1 (PRKG1), ryanodine receptor 1 (RYR1), cytosolic phospholipase A2 (PLA2), and phosphatidylinositol phospholipase C and beta (PLCB). In addition, other DEGs were identified, such as those encoding chitinase, perilipin-2 (PLIN2), calpain-5, neurexin, very low-density lipoprotein receptor, microphthalmia-associated transcription factor, and Man 1. The above genes exhibited higher expression in the recipient shellfish but lower expression in the control group. In addition, the mucin-2 and tubulin beta genes were highly expressed in the control group but lowly expressed in the surgical group.

3.4 Validation using quantitative real-time RT-PCR

To further validate the gene expression of DEGs, 10 immune-related DEGs were randomly selected for RT-qPCR validation (Figure 5), followed by comparison of fold-changes detected by qRT-PCR to the RNA-Seq expression levels. Most of the RT-qPCR results were

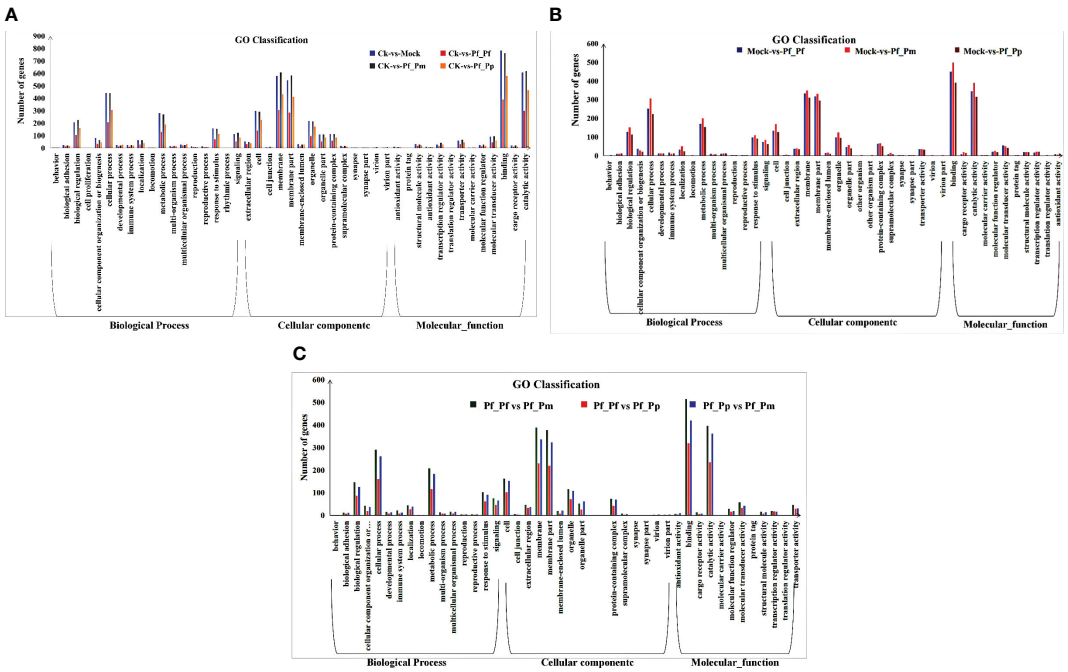

FIGURE 2
Functional classification of DEGs. **(A)** GO enrichment analysis of DEGs between the control and nucleus insertion groups. **(B)** GO Enrichment analysis of DEGs between the non-inserted and different insertion group. **(C)** GO enrichment analysis of DEGs between the allograft and xenograft groups.

10.3389/fmars.2024.1362078

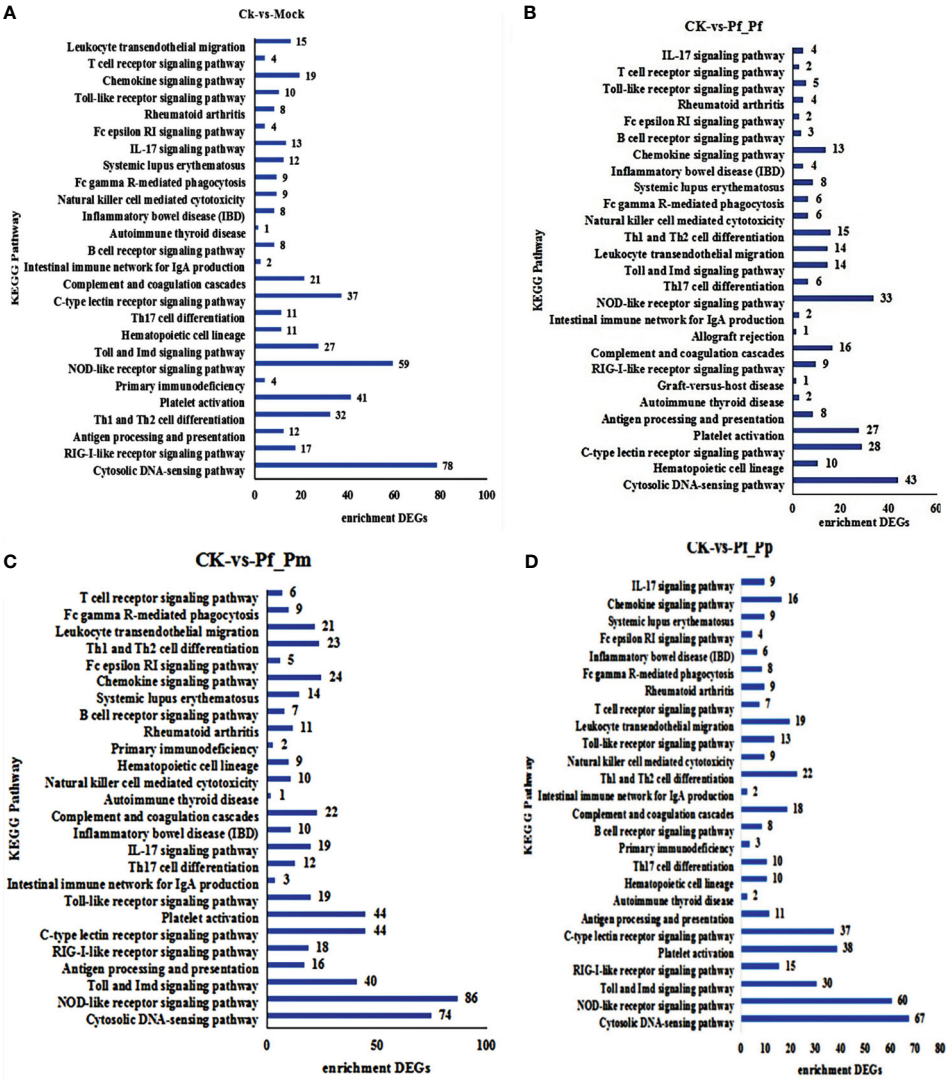

FIGURE 3
The KEGG pathways enriched among DEGs. **(A)** Ck-vs-Mock, **(B)** CK-vs-Pf_Pf, **(C)** CK-vs-Pf_Pm, and **(D)** CK-vs-Pf_Pp comparisons. The number inside represents the number of DEGs enriched.

consistent with the high-throughput sequencing data. Thus, the RNA-Seq data were appropriate for inference of differential gene expression.

4 Discussion

Mantle allograft surgery in pearl aquaculture has been successfully employed without immunosuppressants throughout the last century (Zhang et al., 2016). However, little is known of the immune responses generated after mantle tissue transplantation. The seventh day after mantle tissue implantation comprises the pearl sac formation period and an inflammatory milieu has been suggested in donor mantle tissues during this time. The inflammatory microenvironment leads to allograft rejection and also induces allograft tolerance in invertebrates (Land, 2012). Transcriptomic analyses of haemocytes at 192 h were consequently conducted in this study after allograft and xenograft transplantation to identify genes and important pathways involved in development and gametogenesis, along with evaluation of their differential expression between experimental and control groups. These findings provide a basis for the subsequent immune responses analysis of allotransplantation and xenotransplantation.

4.1 Enriched immune-related pathways

NOD-like receptors (NLRs) comprise a subgroup of cytosolic pattern recognition receptors (PRRs) that have recently been suggested to play new roles in antiviral innate immune signaling pathways (Zheng, 2021). The NLR protein family comprises 22 members that contain a common structural of an N-terminal effector domain, a central NACHT domain, and a C-terminal leucine-rich repeat sequence (LRR) (Zheng, 2021). The N-terminal effector domain participates in signal transduction,

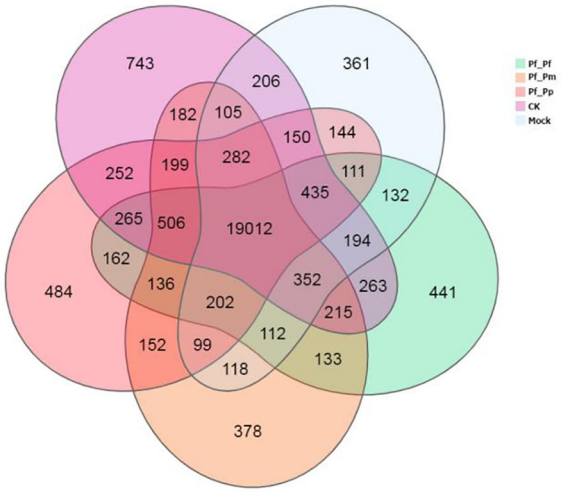

FIGURE 4
Venn diagram showing overlap in DEGs among treatment groups.

while the NACHT domain interacts with ATP/GTPase-specific P-rings, Mg^{2+} binding sites, and five other motifs to perform nucleotide binding functions based on self-oligomerization and ATPase activity (Koonin and Aravind, 2000). In addition, LRRs are responsible for pathogen-associated molecular patterns (PAMPs) recognition (Kanneganti et al., 2007). In this study, 86 DEGs were enriched in NOD-like receptors in the CK-vs-Pf-Pm comparison, followed by 67 DEGs in the CK-vs-Pf-Pp comparison, and relatively fewer in the CK-vs-Mock comparison. We speculate that these trends may be related to the degree of immune response produced by allotransplantation and xenotransplantation.

The cytosolic DNA-sensing pathway is primarily responsible for detecting foreign DNA derived from invading microorganisms or host cells and generating an innate immune response. The first identified cytosolic DNA sensor is DAI that activates the IRF and NF-kappaB transcription factors, to produce type I interferons and other cytokines. The second cytoplasmic DNA sensor is AIM2. After sensing DNA, AIM2 interacts with the assembly of the inflammasome, eventually leading to interleukin maturation (Yanai et al., 2009; Huijser et al., 2022). In the control and surgical groups comparison, a higher expression of cGAMP synthase (MB21D1) was detected in the control group and less expressed in the recipient shell. The cGAMP synthetase gene acts as an intracellular pattern recognition receptor (PRR) that senses cytosolic pathogen DNA and subsequently produces the second messenger cGAMP to initiate the TMEM173/STING pathway to produce interferon (IFN) that causes the overall immune response (Liang et al., 2014). Transcriptomic analyses revealed that its expression was down-regulation in the recipient shell, indicating a immune rejection effect. However, this hypothesis requires additional confirmation, including via the role of MB21D1 in the body during immune rejection reaction.

Type C lectin receptors (CLRs) contain one or more type C lectin-like domains (CTLDs) (Viswambari et al., 2010) and are involved in immune recognition reactions of some cells as pattern recognition receptors for pathogen-derived ligands. Dectin-1 is a CLR example that can recognize the fungal-derived ligandsβ-Glucan and high-mannose carbohydrates (Kato et al., 2006). After ligand binding, C-type lectins stimulate intracellular signaling cascades, include the production of various factors, and trigger immune responses against pathogens (Mentrup et al., 2022). The C-type lectin receptor signaling pathways appeared in each group of comparison between allogeneic and xenogeneic transplantation in this study, indicating that the C-type lectin receptor signaling pathway is an important pathway in the immune response of interspecific transplantation, with the abundant immune genes identified in the study deserving further investigation.

4.2 Differentially expressed immune genes

Immune genes all exhibited different expression patterns in individual fractions, suggesting that these genes may play important roles in immune processes. N16 is an active protein in *P. fucata* and can be inhibited to prevent the occurrence of osteoclasts (Lin et al., 2020). N16 may also be a membrane protein-like component of the nacre layer that involved in both crystal formation and the formation of Water Insoluble Organic Matrix (WISM) as a microfibrillar matrix, similar to the role of High Glycine/Tyrosine Proteins (FGTPs), and implicating the specificity of N16 in pearl formation and specific expression only in the mantle (Samata et al., 1999). N16 was distributed in almost every component, relative to that above the control group, consistent with the results of the study.

TSSK proteins establish relationships with two T6SS subcomplexes through direct interactions with TssL, Hcp, and TssC (Zoued et al., 2013). Interestingly, TSSK exhibited down-regulation relative to the control group. However, the roles of TSSK molecules remain unclear and further studies are needed. In addition, Ryanodinereceptor 1 (RYR1) is a skeletal muscle sarcoplasmic reticulum (SR), required for excitation-contraction coupling (EC coupling) of Ca^{2+} release channels in the sarcoplasmic terminal pool (O'connor et al., 2023). In this study, RYR1 was up-regulation in the CK-vs-Mock comparison, while the Pf_Pf, Pf_Pm, and Pf_Pp comparisons exhibited lower expression of RYR1 than in Mock. RYR1 may be consequently related to pearl sac formation from mantle fragments.

SAP18 was originally identified by immunopurification of sin3-related proteins and is a component of the Sin3-HDAC complex that can enhances sin3-mediated transcriptional inhibition. Specifically, SAP18 is a protein-protein adapter linking the transcription factor Gli, which is a transcriptional repressor fused to [Su (fu)] and the Sin3-HDAC complex (Cheng and Bishop, 2002). Overall, these proteins were down-regulation among the treatment groups, indicating that SAP18 may be involved in immune transplantation, although its mechanistic role remains unclear. CROCC plays important roles in tumors and the involvement of cytokine and cancer-related gene expression (Xu et al., 2019). CROCC was down-regulated as SAP18. A previous study (Xu et al., 2019) observed the up-regulation of miR-33 that could potentially suppress cell proliferation, migration, invasion, and epithelial–mesenchymal transition (EMT) in Gallbladder

10.3389/fmars.2024.1362078

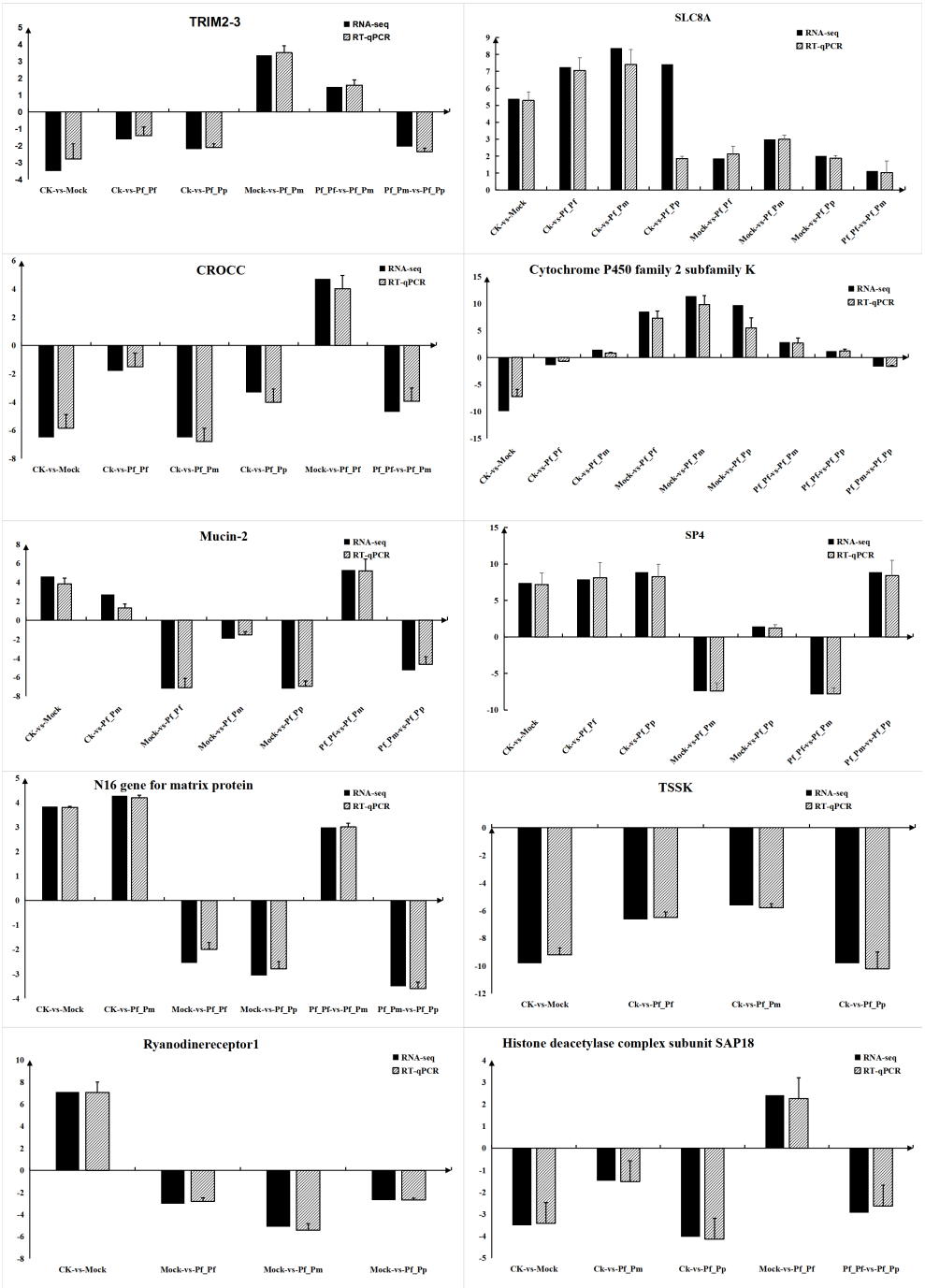

FIGURE 5
RT-qPCR validation of the expression levels for 10 DEGs. RNA-seq represents the increase or decrease multiple of the gene in the transcriptome data relative to a control group.RT-qPCR means using RT-qPCR technology to verify the quantitative test of the experimental group and the control group, and then calculating the multiple of the increase or decrease of the gene in the experimental group relative to the control group.

cancer (GBC) through down-regulation of CROCC. These results suggest that CROCC may modulate immune mechanisms by down-regulation after transplantation.

Cytochrome P450 isoenzymes (CYPs) are a hemoglobin superfamily and terminal oxidases of mixed functional oxidase systems on endoplasmic reticulum membranes. CYPs play critical roles in metabolism of many harmful substances (Muntane et al., 1995; Nelson, 2009), and modulation of CYP pathways can ultimately trigger immunosuppression of immune cells. In this study, CYPs were down-regulated in the Pf_Pf, Pf_Pm, and Pf_Pp groups relative to the control group. Consequently, the involvement of CYPs in the immune response mechanisms of organisms may indicate the generation of immune refection. MUC2 is one the most abundant gastrointestinal gel-forming

mucins and exhibits constitutive expression throughout the gastrointestinal tract (Yamashita and Melo, 2018). The MUC2 mucus barrier acts as the first defense against direct contact between intestinal bacteria and colon epithelial cells (Yao et al., 2021). During the development of ulcerative colitis (UC), bacterial factors associated with the MUC2 mucus barrier play important roles in responses to altered dietary patterns, dysfunction of the MUC2 mucus barrier, stimulation of contact with colon epithelial cells, and responses to mucosal and submucosal inflammation (Yao et al., 2021).

Sp4 is a member of the Sp1-like transcription factor family and is primarily expressed in neurons, where it is associated with various neuronal processes, including signal transduction and energy production, and conditions like bipolar disorder (Sheehan et al., 2019). Current research of SP4 focuses on controlling various neuronal processes (Sheehan et al., 2019; Zhang H. et al., 2020), with few studies investigating the direction of immune rejection. Thus, further studies in this area may help clarify its mechanism of action.

Transcripts encoding tripartite motif containing 23 (TRIM23) is an ubiquitin ligase belonging to the tripartite motif (TRIM) family (Bu et al., 2020). TRIM proteins with E3 ubiquitin ligase activity play important roles in virus infection in vertebrates and invertebrates (Zhang R. et al., 2020). Current understanding of TRIM23 primarily focuses on its antiviral immune defense mechanisms, although its precise role in the immune mechanisms remains unclear and requires further study.

The sodium/calcium exchanger or NCX (SLC8A) family is primarily expressed in excitable tissues including muscle and heart tissue, because their rapid and massive transport of Ca^{2+} is important in muscle and heart contractions (Brini and Carafoli, 2011). All the components of this family were up-regulated, with little observed differences in each group. SLC8A is primarily expressed in tissues like the heart, with the blood cells in the samples we collected primarily coming from hearts. These reasons might consequently explain their consistent up-regulation.

5 Conclusions

Here, a transcriptomic analysis was conducted to identify host defense gene activities against allograft and xenograft transplantation in *P.fucata* during pearl cultivation. Specifically, immune-related pathways and genes were identified and discussed. These results provide a theoretical basis and framework to further understand the role of *P.fucata* in immune defense systems, thereby helping to reduce host immunological rejection to transplantation.

Data availability statement

Raw sequence reads generated during the current study were deposited in the Sequence Read Archive of the National Center for Biotechnology Information (NCBI), accession number: PRJNA1068836.

Ethics statement

This study adhered to the guidelines set forth by the Ministry of Science and Technology of the People's Republic of China in their "Guidelines for the Care and Use of Experimental Animals" (approval number: 2006-398) and received approval from the Animal Research and Ethics Committee of Beibu gulf University for all experimental animal manipulations.

Author contributions

YZ: Investigation, Writing – original draft. PW: Writing – review & editing. YG: Writing – review & editing. LB: Writing – review & editing. DY: Supervision, Writing – review & editing. SZ: Funding acquisition, Supervision, Writing – review & editing.

Funding

The author(s) declare financial support was received for the research, authorship, and/or publication of this article. This work was supported by the Natural Science Foundation of Guangxi Zhuang Autonomous Region of China (Grant No. 2021GXNSFAA220031 and 2021GXNSFAA075008) and the Natural Science Foundation of China (Grant No. 31860734).

Acknowledgments

We thank LetPub (www.letpub.com) for linguistic assistance and pre-submission expert review.

Conflict of interest

The authors declare that the research was conducted in the absence of any commercial or financial relationships that could be construed as a potential conflict of interest.

Publisher's note

Supplementary material

The Supplementary Material for this article can be found online at: https://www.frontiersin.org/articles/10.3389/fmars.2024.1362078/full#supplementary-material

References

Ai, Y., Zhang, Q., Wang, W., Zhang, C., Cao, Z., Bao, M., et al. (2016). Transcriptomic analysis of differentially expressed genes during flower organ development in genetic male sterile and male fertile *Tagetes erecta* by digital gene-expression profiling. *PloS One* 11, e0150892. doi: 10.1371/journal.pone.0150892

Arnaud-Haond, S., Goyard, E., Vonau, V., Herbaut, C., Prou, J., and Saulnier, D. (2007). Pearl formation: persistence of the graft during the entire process of biomineralization. *Mar. Biotechnol.* 9, 113–116. doi: 10.1007/s10126-006-6033-5

Brini, M., and Carafoli, E. (2011). The plasma membrane Ca^{2+} ATPase and the plasma membrane sodium calcium exchanger cooperate in the regulation of cell calcium. *Cold Spring Harbor Perspect. Biol.* 3, a004168. doi: 10.1101/cshperspect.a004168

Briones, C., Nuñez, J. J., Pére, Z. M., Espinoza-Rojas, D., Molina-Quiroz, C., and Guiñez, R. (2018). *De novo* male gonad transcriptome draft for the marine mussel *Perumytilus purpuratus* with a focus on its reproductive-related proteins. *J. Genomics* 6, 127. doi: 10.7150/jgen.27864

Bu, N., Dong, Z., Zhang, L., Zhu, W., and Zheng, S. (2020). CircPVT1 regulates cell proliferation, apoptosis, and glycolysis in hepatocellular carcinoma *via* miR-377/TRIM23 axis. *Cancer Manage. Res.* 12, 12945–12956. doi: 10.2147/CMAR.S280478

Chen, Y., Chen, Y., Shi, C., Huang, Z., Zhang, Y., Li, S., et al. (2018). SOAPnuke: a MapReduce acceleration-supported software for integrated quality control and preprocessing of high-throughput sequencing data. *Gigascience* 7, 1–6. doi: 10.1093/gigascience/gix120

Cheng, S. Y., and Bishop, J. M. (2002). Suppressor of Fused represses Gli-mediated transcription by recruiting the SAP18-mSin3 corepressor complex. *Proc. Natl. Acad. Sci. United States America* 99, 5442–5447. doi: 10.1073/pnas.082096999

Dong, C., Wu, H., Zheng, G., Peng, J., Guo, M., and Tan, Z. (2022). Transcriptome analysis reveals MAPK/AMPK as a key regulator of the inflammatory response in PST detoxification in *Mytilus galloprovincialis* and Argopecten irradians. *Toxins* 14, 516. doi: 10.3390/toxins14080516

Fang, Z., Feng, Q. L., Chi, Y. Z., Xie, L., and Zhang, R. (2008). Investigation of cell proliferation and differentiation in the mantle of *Pinctada fucata* (bivalve, Mollusca). *Mar. Biol.* 153, 745–754. doi: 10.1007/s00227-007-0851-5

Fukushima, E., Iwai, T., Miura, C., Celino, F. T., Urasaki, S., and Miura, T. (2014). A xenograft mantle transplantation technique for producing a novel pearl in an akoya oyster host. *Mar. Biotechnol.* 16, 10–16. doi: 10.1007/s10126-013-9525-0

He, J., Shen, C., Liang, H., Fang, X., and Lu, J. (2020). Antimicrobial properties and immune-related gene expression of a C-type lectin isolated from Pinctada fucata martensii. *Fish Shellfish Immunol.* 105, 330–340. doi: 10.1016/j.fsi.2020.07.017

Huijser, E., Bodewes, I. L., Lourens, M. S., Van, H. C. G., Van, d. B. T. P. P., Grashof, D. G. B., et al. (2022). Hyperresponsive cytosolic DNA-sensing pathway in monocytes from primary Sjgren's syndrome. *Rheumatology* 61, 3491–3496. doi: 10.1093/rheumatology/keac016

Inoue, N., Ishibashi, R., Ishikawa, T., Atsumi, T., Aoki, H., and Komaru, A. (2010). Gene expression patterns and pearl formation in the Japanese pearl oyster (*Pinctada fucata*): comparison of gene expression patterns between the pear sac and mantle tissues. *Aquaculture* 308, 68–74. doi: 10.1016/j.aquaculture.2010.06.036

Kanneganti, T. D., LamkanfiM,, and Núñez, G. (2007). Intracellular NOD-like receptors in host defense and disease. *Immunity* 27, 549–559. doi: 10.1016/j.immuni.2007.10.002

Kato, Y., Adachi, Y., and Ohno, N. (2006). Contribution of N-linked oligosaccharides to the expression and functions of β-glucan receptor, Dectin-1. *Biol. Pharm. Bull.* 29, 1580–1586. doi: 10.1248/bpb.29.1580

Koonin, E. V., and Aravind, L. (2000). The NACHT family–a new group of predicted NTPases implicated in apoptosis and MHC transcription activation. *Trends Biochem. Sci.* 25, 223–224. doi: 10.1016/S0968-0004(00)01577-2

Land, W. G. (2012). Emerging role of innate immunity in organ transplantation part III: the quest for transplant tolerance *via* prevention of oxidative allograft injury and its consequences. *Transplant. Rev.* 26, 88–102. doi: 10.1016/j.trre.2011.07.001

Liang, Q., Seo, G. J., Choi, Y. J., Ge, J., Rodgers, M. A., Shi, M., et al. (2014). Autophagy side of MB21D1/cGAS DNA sensor. *Autophagy* 10, 1146–1147. doi: 10.4161/auto.28769

Lin, J. B., Wu, H., Liu, Y. L., Shaw, P. C., and Li, P. B. (2020). N16 suppresses RANKL-mediated osteoclatogenesis by down-regulating RANK expression. *Int. J. Biol. Macromolecules* 151, 1154–1162. doi: 10.1016/j.ijbiomac.2019.10.159

Lu, X., Zhang, M., Yang, S., Deng, Y., and Jiao, Y. (2022). Transcriptome analysis reveals the diverse response of pearl oyster *Pinctada fucata martensii* after different PAMP stimulation. *Fish Shellfish Immunol.* 131, 881–890. doi: 10.1016/j.fsi.2022.10.058

McGinty, E. L., Evans, B. S., Taylor, J. U. U., and Jerry, D. R. (2010). Xenografts and pearl production in two pearl oyster species, P. maxima and *P. margaritifera*: Effect on pearl quality and a key to understanding genetic contribution. *Aquaculture* 302, 175–181. doi: 10.1016/j.aquaculture.2010.02.023

Mentrup, T., Stumpff-niggemann, A. Y., Leinung, N., Schlosser, C., Schubert, K., Wehner, R., et al. (2022). Phagosomal signalling of the C-type lectin receptor Dectin-1 is terminated by intramembrane proteolysis. *Nat. Commun.* 13, 1880. doi: 10.1038/s41467-022-29474-3

Muntane, J., Ourlin, J. C., Domergue, J., and Maurel, P. (1995). Differential effects of cytokines on the inducible expression of CYP1A1, CYP1A2, and CYP3A4 in human hepatocytes in primary culture. *Hepatology* 22, 1143–1153. doi: 10.1002/hep.1840220420

Nelson, D. R. (2009). The cytochrome p450 homepage. *Hum. Genomics* 4, 1–7. doi: 10.1186/1479-7364-4-1-59

O'connor, T. N., Van Den Bersselaar, L. R., Chen, Y. S., Nicolau, S., Simon, B., Huseth, A., et al (2023). RYR-1-related diseases international research workshop: From mechanisms to treatments Pittsburgh, PA, USA, 21-22 July 2022. *J. Neuromuscular Dis.* 10, 135–154. doi: 10.3233/JND-221609

Samata, T., Hayashi, N., Kono, M., Hasegawa, K., Horita, C., and Akera, S. (1999). A new matrix protein family related to the nacreous layer formation of Pinctada fucata. *FEBS Lett.* 462, 225–229. doi: 10.1016/S0014-5793(99)01387-3

Sheehan, K., Lee, J., Chong, J., Zavala, K., Sharma, M., Philipsen, S., et al. (2019). Transcription factor Sp4 is required for hyperalgesic state persistence. *PloS One* 14, 1–24. doi: 10.1371/journal.pone.0211349

Southgate, P. C., and Lucas, J. S. (2011). *The Pearl Oyster* (Elsevier), 231–302.

Viswambari, D. R., Basilrose, M. R., and Mercy, P. D. (2010). Prospect for lectins in arthropods. *Ital. J. Zoology* 77, 254–260. doi: 10.1080/11250003.2010.492794

Wang, P., Guo, Y., Li, S., Zheng, Y., Li, T., Zhao, S., et al. (2024). Comparative proteomics reveal the humoral immune rejection of pearl oyster Pinctada fucata to xenograft from *Pinctada maxima*. *Aquaculture* 582, 740515. doi: 10.1016/j.aquaculture.2023.740515

Wei, J., Liu, B., Fan, S., et al. (2017). Differentially expressed immune-related genes in hemocytes of the pearl oyster *Pinctada fucata* against allograft identified by transcriptome analysis. *Fish Shellfish Immunol.* 62, 247–256. doi: 10.1016/j.fsi.2017.01.025

Xu, G., Wei, X., Tu, Q., and Zhou, C. (2019). Up-regulated microRNA-33b inhibits epithelial-mesenchymal transition in gallbladder cancer through downregulating CROCC. *Bioscience Rep.* 40, BSR20190108. doi: 10.1042/BSR20190108

Yamashita, M. S. A., and Melo, E. O. (2018). Mucin 2 (MUC2) promoter characterization: an overview. *Cell Tissue Res.* 374, 455–463. doi: 10.1007/s00441-018-2916-9

Yanai, H., Savitsky, D., Tamura, T., and Taniguchi, T. (2009). Regulation of the cytosolic DNA-sensing system in innate immunity: a current view. *Curr. Opin. Immunol.* 21, 17–22. doi: 10.1016/j.coi.2009.01.005

Yao, D., Dai, W., Dong, M., Dai, C., and Wu, S. (2021). MUC2 and related bacterial factors: therapeutic targets for ulcerative colitis. *Ebio Med.* 74, 103751. doi: 10.1016/j.ebiom.2021.103751

Zhang, H., Lu, J., and Wu, S. (2020). Sp4 controls constitutive expression of neuronal serine racemase and NF-E2-related factor-2 mediates its induction by valproic acid. *Biochim. Biophys. Acta (BBA)-Gene Regul. Mech.* 1863, 194597. doi: 10.1016/j.bbagrm.2020.194597

Zhang, M., Lu, J., Liang, H., Zhang, B., Liang, B., and Zou, H. (2022). The succinylome of *Pinctada fucata martensii* implicates lysine succinylation in the allograft-induced stress response. *Fish Shellfish Immunol.* 127, 585–593. doi: 10.1016/j.fsi.2022.07.009

Zhang, R., Dai, X., Cao, X., Zhang, C., Wang, K., Huang, X., et al. (2020). Trim23 promotes WSSV replication though negative regulation of antimicrobial peptides expression in Macrobrachium nipponense. *Mol. Immunol.* 124, 172–179. doi: 10.1016/j.molimm.2020.06.007

Zhang, R., Wang, M., Xia, N., Yu, S., Chen, Y., and Wang, N. (2016). Cloning and analysis of gene expression of interleukin-17 homolog in triangle-shell pearl mussel, *Hyriopsis cumingii*, during pearl sac formation. *Fish Shellfish Immunol.* 52, 151–156. doi: 10.1016/j.fsi.2016.03.027

Zheng, C. F. (2021). The emerging roles of NOD-like receptors in antiviral innate immune signaling pathways. *Int. J. Biol. Macromolecules* 169, 407–413. doi: 10.1016/j.ijbiomac.2020.12.127

Zhou, L., Liu, Z., Dong, Y., Sun, X., Wu, B., Yu, T., et al. (2019). Transcriptomics analysis revealing candidate genes and networks for sex differentiation of yesso scallop (*Patinopecten yessoensis*). *BMC Genomics* 20, 1–15. doi: 10.1186/s12864-019-6021-6

Zoued, A., Durand, E., Bebeacua, C., Brunet, Y. R., Douzi, B., Cambillau, C., et al. (2013). TssK is a trimeric cytoplasmic protein interacting with components of both phage-like and membrane anchoring complexes of the type VI secretion system. *J. Biol. Chem.* 288, 27031–27041. doi: 10.1074/jbc.M113.499772

frontiers | Frontiers in Marine Science

TYPE Original Research
PUBLISHED 03 May 2024
DOI 10.3389/fmars.2024.1382229

OPEN ACCESS

EDITED BY
Ruijie Zhang,
Guangxi University, China

REVIEWED BY
Neven Cukrov,
Ruđer Bošković Institute, Croatia
Wu Men,
Nanjing University of Information Science and Technology, China

*CORRESPONDENCE
Wuhui Lin
linwuhui8@163.com

RECEIVED 05 February 2024
ACCEPTED 02 April 2024
PUBLISHED 03 May 2024

CITATION
Lin W, Zhang Y, Du J, Xuan J and Tuo F (2024) Deciphering decadal observation of Fukushima-derived radiocesium in the most polluted port near the Fukushima Daiichi Nuclear Power Plant: from seawater to marine fish. *Front. Mar. Sci.* 11:1382229. doi: 10.3389/fmars.2024.1382229

Deciphering decadal observation of Fukushima-derived radiocesium in the most polluted port near the Fukushima Daiichi Nuclear Power Plant: from seawater to marine fish

Wuhui Lin[1,2]*, Yibang Zhang[3], Jinqiu Du[3], Jiliang Xuan[2] and Fei Tuo[4]

[1]Polar and Marine Research Institute, College of Harbour and Coastal Engineering, Jimei University, Xiamen, China, [2]State Key Laboratory of Satellite Ocean Environment Dynamics, Second Institute of Oceanography, Ministry of Natural Resources (MNR), Hangzhou, China, [3]National Marine Environmental Monitoring Center, Dalian, China, [4]National Institute for Radiological Protection, Chinese Center for Disease Control and Prevention, Beijing, China

The biological concentration effect of radionuclides in marine fish has exacerbated public anxiety about seafood security in the context of Fukushima nuclear-contaminated water discharged into the ocean. However, the most polluted port near the Fukushima Daiichi Nuclear Power Plant (FDNPP) has seldom been investigated, especially for radioactivity in marine fish. In this study, decadal observations of radiocesium in marine fish and seawater from the most polluted port were simultaneously established after the Fukushima Nuclear Accident. We found a generally decreasing trend of historical ^{137}Cs activity in seawater, with seasonal variations modulated by precipitation. Seasonal variations were elucidated with finer detail and divided into exponential decline in the dry season and steady variation in the wet season. A novel method was proposed to estimate the continuing source term of ^{137}Cs derived from the FDNPP, which was 3.9 PBq in 2011 and 19.3 TBq between 2012 and 2022 on the basis of historical ^{137}Cs. The biological concentration effect of marine fish is quantitatively emphasized according to the higher ratio of over-standards for radiocesium in marine fish relative to that in seawater. Long-term observation and analysis of radiocesium in marine fish and seawater from the most polluted port would provide insights into the scientific evaluation of the effectiveness of the decommissioning of the FDNPP in the past and share lessons on the fate of Fukushima-derived radionuclides in the future.

KEYWORDS

marine fish, ^{137}Cs, Fukushima, contaminated water, nuclear pollution

1 Introduction

Large amounts of artificial radionuclides have been released into the atmosphere (e.g., ~160 PBq of ^{131}I, 15 PBq of ^{137}Cs, and 14,000 PBq of ^{133}Xe) and the marine environment (e.g., 11 PBq of ^{131}I and 4 PBq of ^{137}Cs) since the Fukushima Nuclear Accident (FNA) on 11 March 2011 (Lin et al., 2016; Povinec et al., 2021). It has been estimated that 74% of Fukushima-derived artificial radionuclides released into the atmosphere were deposited in the North Pacific Ocean (Povinec et al., 2021), probably contributing to the FNA being the most serious nuclear accident that directly pollutes the marine environment with radioactive material (Lin et al., 2016). Artificial radionuclides are continuously discharged from the most polluted port (Figure 1) near the Fukushima Daiichi Nuclear Power Plant (FDNPP) (Machida et al., 2023). Subsequently, Fukushima-derived radionuclides have been widely elevated from the coastal sea to the open ocean (Povinec et al., 2021).

The most polluted port near the FDNPP serves as windows to reflect the progress and effectiveness of decommissioning of the FDNPP, which is inaccessible to the public and to many other counties around the world. Recently, extremely high $^{134+137}$Cs activity of 1.8×10^4 Bq/kg in marine fish from the most polluted port was reported to be 180 times higher than the Japanese regulatory limit (100 Bq/kg-wet) on 18 May 2023 (Tokyo-Electric-Power-Company, 2023a). Despite the continuous discharge of artificial radionuclides and frequent reports of abnormally high levels of radiocesium in marine fish, the most polluted port with the highest radioactivity near the FDNPP has seldom been investigated (Kanda, 2013; Machida et al., 2020, 2023), especially with regard to radioactivity in marine fish.

The biological concentration effect of radionuclides in marine fish has exacerbated public anxiety in the context of nuclear-contaminated water with 64 radionuclides discharged into the ocean (Buesseler, 2020; Lin et al., 2021; Liu et al., 2022). In this study, we primarily focus on the long-term observation of radiocesium in marine fish because seafood consumption is the dominant pathway of ionizing radiation to humans and is a primary concern of the public and countries around the Pacific Ocean after the FNA. Additionally, historical levels of radiocesium in seawater are simultaneously discussed to reveal its effect on marine fish. We also attempted to determine the mechanisms of seasonal fluctuation of ^{137}Cs in seawater in order to identify potential leak events, estimate the continuing source terms of ^{137}Cs discharged from the port, and verify the effectiveness of multiple countermeasures in the most polluted port near the FDNPP.

2 Materials and methods

2.1 ^{134}Cs and ^{137}Cs in seawater from the port

The most polluted port (Figure 1) near the FDNPP is inaccessible to the public and many other countries around the world. The availability and transparency of historical radioactivity in the most polluted port near the FDNPP played a key role in verifying the progress after the decommissioning of the FDNPP. We downloaded 1,196 daily reports of radiocesium in seawater provided by the Tokyo Electric Power Company (TEPCO) from 2 April 2011 to 30 June 2014 and 114 monthly reports of radiocesium in seawater released by the Ministry of Economy, Trade and Industry (METI) from July 2013 to April 2023 (Tokyo-Electric-Power-Company, 2011; Ministry-of-Economy-Trade-and-Industry, 2023b, 2018). The TEPCO's daily reports from 2 April 2011 to 30 June 2014 included 3–14 monitoring stations in the port, while the METI's monthly reports from July 2013 to April 2023 encompassed 9–14 monitoring stations in the port. In order to conservatively evaluate the radioactive level in seawater from the port, we chose and compiled the highest values of ^{134}Cs and ^{137}Cs activities among 3–14 stations in the port from the above-mentioned daily/monthly reports. If the data in the daily/monthly reports were lower than the minimum detection activity (MDA), the MDA was utilized for discussion. The highest value of ^{134}Cs and ^{137}Cs activity in a typical report is selected and shown in Figure 2.

2.2 ^{134}Cs and ^{137}Cs in marine fish from the port

Radiocesium levels in marine fish were compiled from 130 monthly reports provided by TEPCO from December 2012 to May 2023 (Tokyo-Electric-Power-Company, 2018, 2023b). There were seven fishing areas in the port (Figure 3) (Tokyo-Electric-Power-

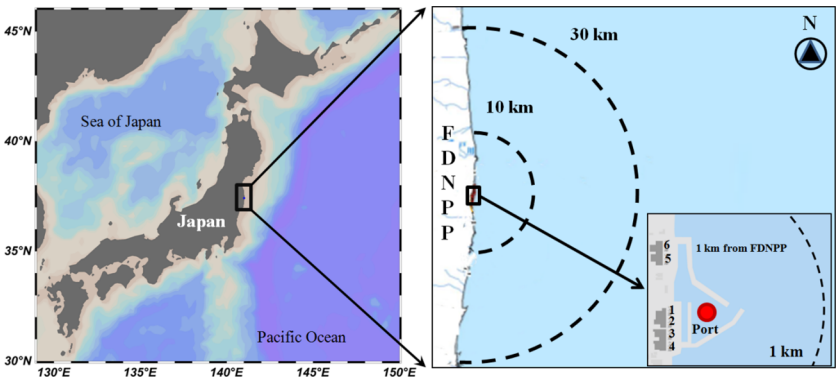

FIGURE 1
Map of the most polluted port near the FDNPP.

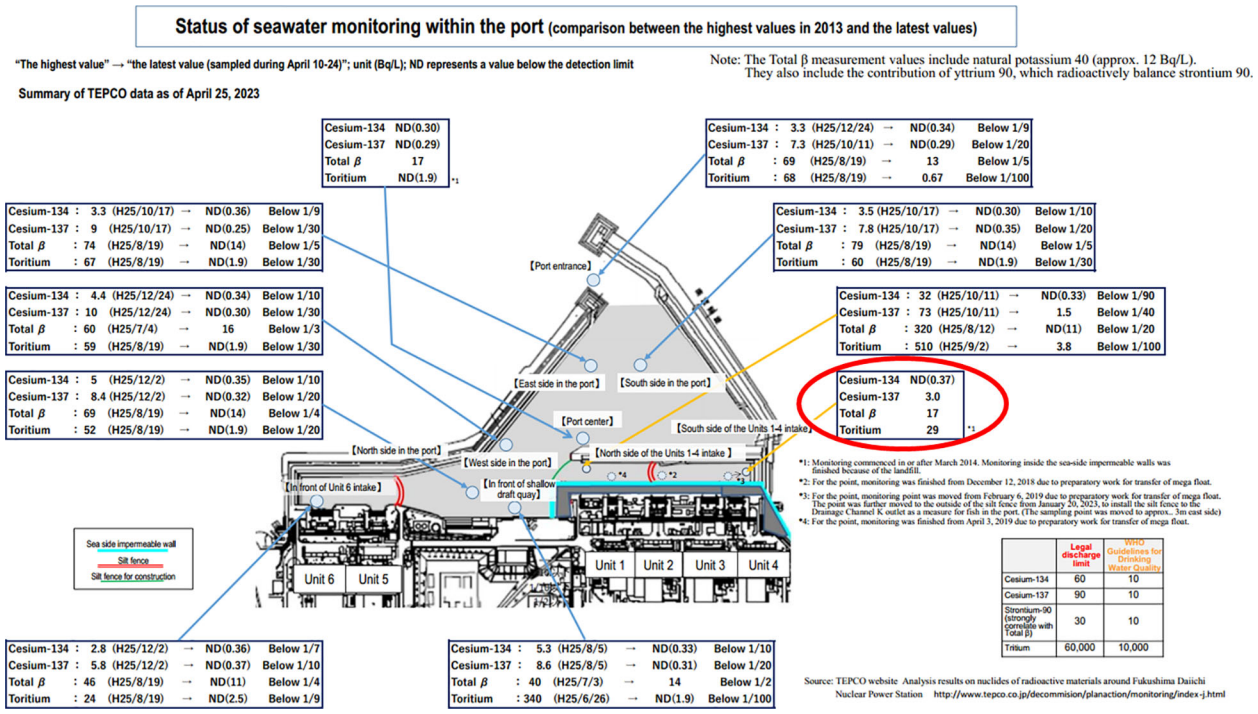

FIGURE 2
The red ellipse indicates the highest value of ^{134}Cs (MDA, 370 Bq/m^3) and ^{137}Cs (3,000 Bq/m^3) activities in seawater from the port in April 2023 (Ministry-of-Economy-Trade-and-Industry, 2023a).

Company, 2013). The typical species of marine fish from the port included *Conger myriaster*, *Hexagrammos otakii*, *Microstomus achne*, *Paralichthys olivaceus*, *Pleuronectes yokohama*, and *Sebastes cheni* (Tokyo Electric Power Company, 2023b). Detailed information on the size, diet, and habitat of marine fish was not provided in the monthly reports, probably because of the large number of fish and the temporal variations of fish species in the port. We conservatively selected and compiled the highest value of ^{134}Cs and ^{137}Cs activities in the muscle of marine fish caught from seven fishing areas in the port to conservatively evaluate the radiological impact. The value of MDA was utilized in the condition of the activity of radiocesium below the MDA. Only the maximum activity in marine fish was selected in order to discuss the relationship between radiocesium in seawater and marine fish; it was consistent with the highest value in seawater.

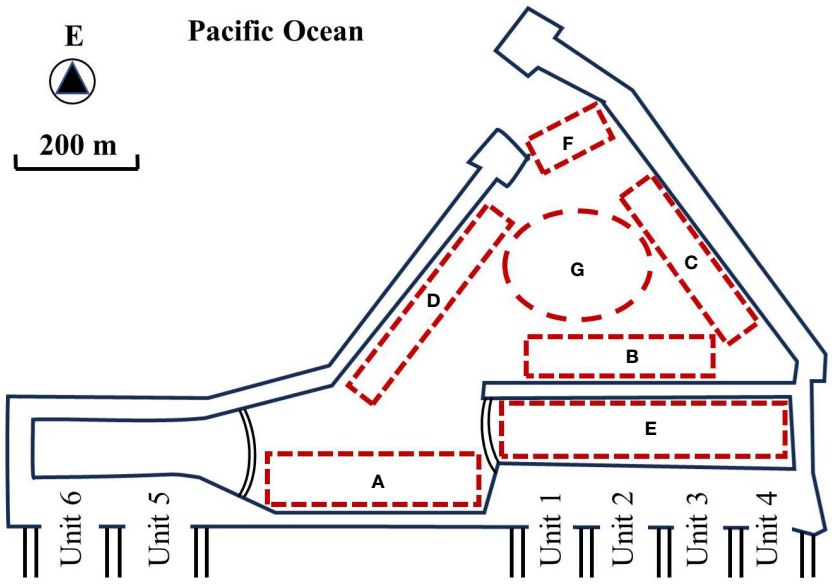

FIGURE 3
Fishing areas from "A" to "G" in the port.

2.3 Data on precipitation in Fukushima Prefecture

In order to investigate the mechanism of seasonal variation of ^{137}Cs in the port, we downloaded 145 monthly precipitation reports in Naniue and Tomioka near the FDNPP released by the Japan Meteorological Agency (JMA) from May 2011 to May 2023 (Japan-Meteorological-Agency, 2023). We calculated and compiled the mean value of monthly precipitation in Naniue and Tomioka because the FDNPP is located between them (Figure 4). The average monthly precipitation (119.8 mm) from May 2011 to May 2023 was calculated to define the wet season and the dry season in Fukushima Prefecture.

3 Results and discussion

3.1 Historical observation of ^{137}Cs activity in seawater from the port

Historical ^{137}Cs activity in seawater (Figure 5) from the most polluted port was systematically compiled from April 2011 to April 2023 based on 1,310 documents that were officially released by TEPCO and METI. Although the historical ^{137}Cs activity in seawater generally decreased due to the continuing decommissioning work at the FDNPP, the most recent monthly ^{137}Cs activity in seawater (3×10^3 Bq/m^3 in April 2023) was still over 1,000 times higher than the background value (1–2 Bq/m^3) of ^{137}Cs before the FNA (Povinec et al., 2021). In this study, the historical ^{137}Cs activity in seawater was divided into three periods: April 2011 to June 2011 (purple area in region I), July 2011 to January 2016 (brown area in region II), and February 2016 to April 2023 (green area in region III).

Region I from April 2011 to June 2011 was recognized as the initial stage of FNA and was characterized by the direct discharge of contaminated water into the coastal sea. Two peaks of ^{137}Cs—1.9×10^{12} Bq/m^3 on 2 April 2021 and 1.2×10^9 Bq/m^3 on 12 May 2021—were clearly recorded, corresponding to two leak events officially confirmed by TEPCO in 1–6 April and 10–11 May (Kanda, 2013). A sudden decline in ^{137}Cs activity was subsequently observed after TEPCO's operation to stop the leak in front of Unit 2 on 4 April 2016 (Kanda, 2013). The most significant phenomenon in region I was the appearance of an extremely high ^{137}Cs value, followed by a rapid exponential decline.

"Region II from July 2011 to January 2016 was defined because of the completed construction of the seaside impermeable walls in February 2016 after carefully comparing the progress after the decommissioning in the monthly reports from METI in January and February 2016. The ^{137}Cs activity gradually decreased in region II due to the continuing decommissioning work, such as the relocation of the drainage channels from June 2014 to April 2015, the seabed covering of the port in April 2015, the removal of highly contaminated retained water in December 2015, the filling of tunnels and towers in December 2015, and the completed construction of seaside impermeable walls in February 2016 (Machida et al., 2020, 2023). Seasonal fluctuation of ^{137}Cs activity was also observed, in addition to a decreasing trend at a slower rate in region II relative to a rapidly decreasing rate in region I. It was obvious that the average ^{137}Cs activity (7.0×10^3 Bq/m^3) in region III from February 2016 to April 2023 was approximately 40 times lower than that (2.7×10^5Bq/m^3) in region II after the completed construction of seaside impermeable walls. However, a seasonal variation of ^{137}Cs without a significant decreasing trend is shown in region III.

3.2 Estimation of continuing source terms of ^{137}Cs based on the wet–dry season model

Although the key feature of the seasonal variation of ^{137}Cs has been observed after the initial stage of FNA, the factors influencing the seasonal variation of ^{137}Cs have not been discussed in detail (Machida et al., 2020). To determine the seasonal variations of ^{137}Cs activity in seawater from July 2011 to April 2023 in detail, ^{137}Cs activity and monthly precipitation were simultaneously displayed to

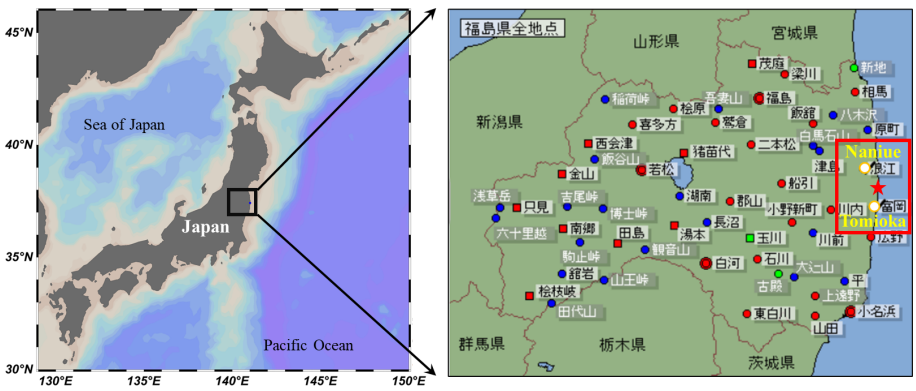

FIGURE 4
Map of Naniue and Tomioka. The star in the red rectangle represents the location of the FDNPP (Japan-Meteorological-Agency, 2023).

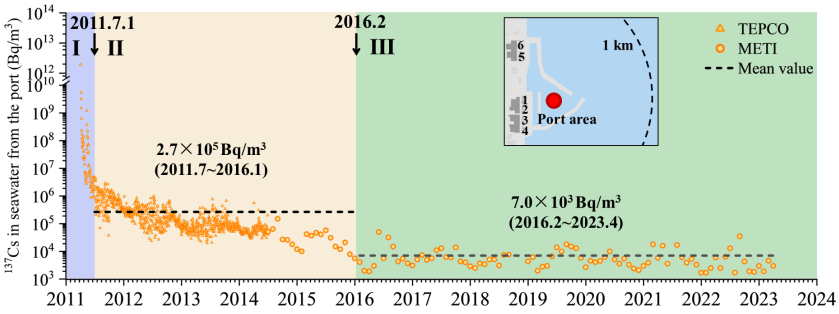

FIGURE 5
Historical ^{137}Cs activity in seawater from the most polluted port near the FDNPP from April 2011 to April 2023.

reveal the contrasting patterns of the exponential decrease of ^{137}Cs in the dry season (light blue in Figure 6) and the steady variation of ^{137}Cs in the wet season (yellow in Figure 6).

It was reasonable to expect the exponential decline in ^{137}Cs activity from the port, analogous to previous studies on the exponential decrease of ^{137}Cs activity in river water, seawater, sediment, and marine biotas because of the decommissioning work and stabilization at the FDNPP (Povinec et al., 2021). The exponential decline in ^{137}Cs activity in the dry season is well-fitted and quantitatively depicted with effective half-lives (EHLs) in different time intervals in Figure 6 and Table 1. Two groups of EHLs have been quantified: 0.14 ± 0.03 a (seven time intervals fitted with red lines) and 0.41 ± 0.26 a (six time intervals fitted with green lines). The EHLs of ^{137}Cs in region II and region III were much longer than those in region I (1.58 d) at the initial stage of the FNA (Kanda, 2013), implying multiple continuing source terms of ^{137}Cs to lengthen EHLs and slow down the decreasing trend in the port after the initial stage of the FNA. The apparent decreasing rate (k_2) in the dry season is calculated in Table 1. Combined with the exchange rate (k_1 = 0.44 d^{-1}) and seawater volume (2.78×10^5 m^3) in the port from Kanda (2013), the source terms of ^{137}Cs in the dry season could be quantified according to Equations 3, 4.

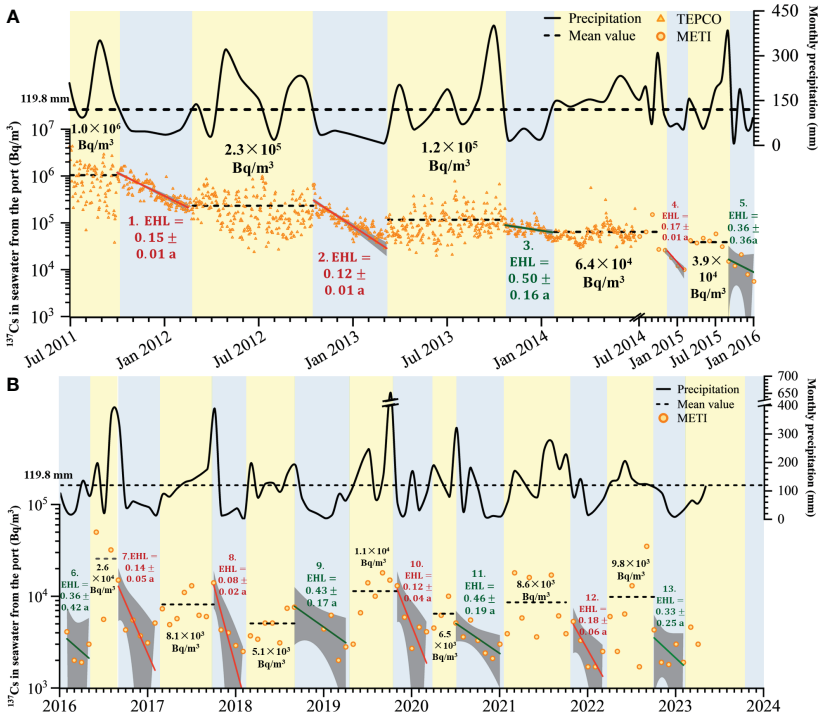

FIGURE 6
Seasonal variations of ^{137}Cs in seawater from the port and monthly precipitation in Fukushima Prefecture from July 2011 to January 2016 **(A)** and February 2016 to April 2023 **(B)**. The average monthly precipitation is presented with a dotted line to distinguish the wet season (yellow) from the dry season (light blue). Effective half-lives (EHLs) and average ^{137}Cs activity are quantitatively displayed for the dry season and wet season, respectively.

TABLE 1 Exponential fitting, EHLs, and apparent decreasing rate (k_2) of time intervals in dry seasons.

Group	Time	Exponential fitting	r	p	EHL (a)	k_2 (a^{-1})	Mean value of EHL	Mean value of k_2
1	20111002–20120225	$A = 1.2\times10^{6}\times e^{-}$ $^{4.6\times(T-2011.10.2)}$	0.80	6.2×10^{-27}	0.15 ± 0.01	4.56 ± 0.34	0.14 ± 0.03 a	4.95 ± 1.06a^{-1}
	20121016–20130307	$A = 3.1\times10^{5}\times e^{-}$ $^{6.0\times(T-2012.10.16)}$	0.75	5.9×10^{-23}	0.11 ± 0.01	6.08 ± 0.51		
	201411–201502	$A = 2.5\times10^{4}\times e^{-4.2\times}$ $^{(T-2014.11)}$	0.99	6.4×10^{-3}	0.17 ± 0.01	4.18 ± 0.34		
	201609–201702	$A = 1.2\times10^{4}\times e^{-5.1\times}$ $^{(T-2016.9)}$	0.80	0.06	0.14 ± 0.05	5.06 ± 1.99		
	201710–201802	$A = 1.3\times10^{4}\times e^{-8.2\times}$ $^{(T-2017.10)}$	0.94	0.04	0.08 ± 0.02	8.18 ± 2.25		
	201911–202003	$A = 1.1\times10^{4}\times e^{-5.6\times}$ $^{(T-2019.11)}$	0.87	0.06	0.12 ± 0.04	5.57 ± 1.95		
	202110–202203	$A = 5.0\times10^{3}\times e^{-3.9\times}$ $^{(T-2021.10)}$	0.86	0.06	0.18 ± 0.06	3.90 ± 1.36		
2	20131021–20140122	$A = 8.6\times10^{4}\times e^{-}$ $^{1.4\times(T-2013.10.17)}$	0.32	2.2×10^{-3}	0.50 ± 0.16	1.40 ± 0.44	0.41 ± 0.26 a	1.69 ± 1.07a^{-1}
	201509–201601	$A = 1.7\times10^{4}\times e^{-1.9\times}$ $^{(T-2015.9)}$	0.55	0.38	0.36 ± 0.36	1.90 ± 1.87		
	201602–201605	$A = 3.4\times10^{3}\times e^{-1.9\times}$ $^{(T-2016.2)}$	0.49	0.47	0.36 ± 0.42	1.94 ± 2.21		
	201809–201904	$A = 7.6\times10^{3}\times e^{-1.6\times}$ $^{(T-2018.9)}$	0.82	0.09	0.43 ± 0.17	1.57 ± 0.63		
	202007–202012	$A = 5.2\times10^{3}\times e^{-1.5\times}$ $^{(T-2020.7)}$	0.75	0.06	0.46 ± 0.19	1.51 ± 0.62		
	202210–202302	$A = 3.5\times10^{3}\times e^{-2.1\times}$ $^{(T-2022.10)}$	0.59	0.28	0.33 ± 0.25	2.06 ± 1.60		
Kanda, 2013	20110406–20110419						1.58 d	0.44 d^{-1}

$$V\frac{dA_{137Cs}}{dt} = S_{dry} - k_1 A_{137Cs} V = -k_2 A_{137Cs} V \quad (1)$$

$$S_{dry} = (k_1 - k_2) A_{137Cs} V \quad (2)$$

where A_{137Cs} refers to the ^{137}Cs activity in seawater. V and S_{dry} are the mean volume of seawater and the source terms of ^{137}Cs in the port during the dry season, respectively. k_1 and k_2 are the exchange rate of the port with outer seawater and the apparent decreasing rate of ^{137}Cs in the port, respectively (see values in Table 1).

By contrast, the steady variation of ^{137}Cs without the decreasing trend in the wet season is illustrated in Figure 6. We found that the average ^{137}Cs activities in wet seasons from July 2011 to January 2016 also gradually decreased from 1.0×10^{6} Bq/m^3 to 3.9×10^{4} Bq/m^3 in Figure 6A. The average ^{137}Cs activities in wet seasons from February 2016 to April 2023 varied from 5.1×10^{3} Bq/m^3 to 2.6×10^{4} Bq/m^3 without a decreasing trend in Figure 6B. Previous studies have pointed out that the ^{137}Cs activity in the river and coastal sea has been significantly elevated during the flood season, especially with the additional influences of typhoons and storms (Tanaka et al., 2022; Uchiyama et al., 2022). The positive relationship between ^{137}Cs activity and monthly precipitation (r = 0.44, p< 0.0001) from February 2016 to April 2023 is also shown in Figure 7. Precipitation probably contributed to the additional input of ^{137}Cs into the port via leaching and erosion of ^{137}Cs from a terrestrial environment in the wet season, resulting in the steady variation of ^{137}Cs activity in the wet season in contrast to a decreasing trend of ^{137}Cs in the dry season. The source terms of ^{137}Cs in the wet season could be quantified according to Equation 3, Equation 4.

$$V\frac{dA_{137Cs}}{dt} = S_{wet} - k_1 A_{137Cs} V = 0 \quad (3)$$

$$S_{wet} = k_1 A_{137Cs} V \quad (4)$$

where S_{wet} refers to the source terms of ^{137}Cs in the wet season. Other parameters are the same as in Equations 1, 2.

Therefore, historical ^{137}Cs activity and its associated mechanisms are suggested to be delicately classified into the wet

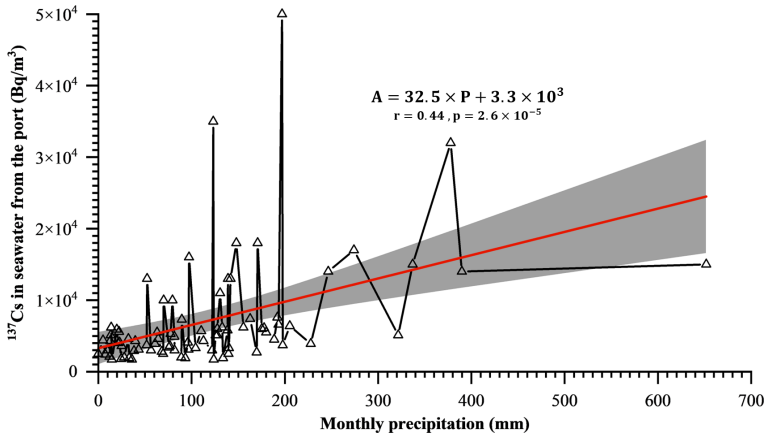

FIGURE 7
Positive relationship between ^{137}Cs activity from the port and monthly precipitation from February 2016 to April 2023.

season and the dry season for quantitative discussion. Our study also implied that the source terms of radionuclides derived from the FDNPP to the Pacific Ocean should be different between the wet season (Equation 2) and the dry season (Equation 4) rather than a simple assumption of steady state in previous studies (Kanda, 2013; Machida et al., 2020, 2023). The annual flux of ^{137}Cs discharged from the port to outer seawater was 3.9 PBq in 2011 and 19.3 TBq from 2012 to 2022, which is generally consistent with previous studies, as shown in Table 2 and Figure 8 (Machida et al., 2020).

3.3 Delayed increase of $^{134 + 137}$Cs in marine fish following the $^{134 + 137}$Cs peak in seawater from the port

The long-term monthly $^{134 + 137}$Cs activity in marine fish and the corresponding value in seawater from the most polluted port are simultaneously shown in Figure 9 from December 2012 to May 2023. A clear decline in $^{134 + 137}$Cs activity in marine fish was observed before February 2016, consistent with the decreasing trend

TABLE 2 Comparison of the annual flux of the ^{137}Cs discharged from the port.

Year	Annual flux of ^{137}Cs (Bq/a)					
	Tsumune et al (Tsumune et al., 2020)	Machida-V method (Machida et al., 2020)		Machida-K method (Machida et al., 2020)		This study
		Min	Max	Min	Max	
2011	3.55×10^{15}	1.9×10^{15}	1.9×10^{15}	2.3×10^{15}	2.3×10^{15}	3.9×10^{15}
2012	1.63×10^{13}	2.1×10^{12}	2.2×10^{12}	2.9×10^{12}	2.9×10^{12}	9.9×10^{12}
2013	7.81×10^{12}	7.0×10^{11}	8.1×10^{11}	1.4×10^{12}	1.4×10^{12}	4.5×10^{12}
2014	3.76×10^{12}	3.0×10^{11}	4.5×10^{11}	7.1×10^{11}	7.4×10^{11}	1.5×10^{12}
2015	1.81×10^{12}	2.4×10^{11}	4.1×10^{11}	3.2×10^{11}	6.4×10^{11}	1.2×10^{12}
2016	8.75×10^{11}	2.0×10^{11}	2.5×10^{11}	2.4×10^{11}	2.8×10^{11}	4.8×10^{11}
2017		1.3×10^{11}	1.6×10^{11}	1.9×10^{11}	2.4×10^{11}	3.1×10^{11}
2018		4.4×10^{10}	6.4×10^{10}	9.2×10^{10}	1.2×10^{11}	2.1×10^{11}
2019						3.7×10^{11}
2020						2.0×10^{11}
2021						3.5×10^{11}
2022						2.9×10^{11}

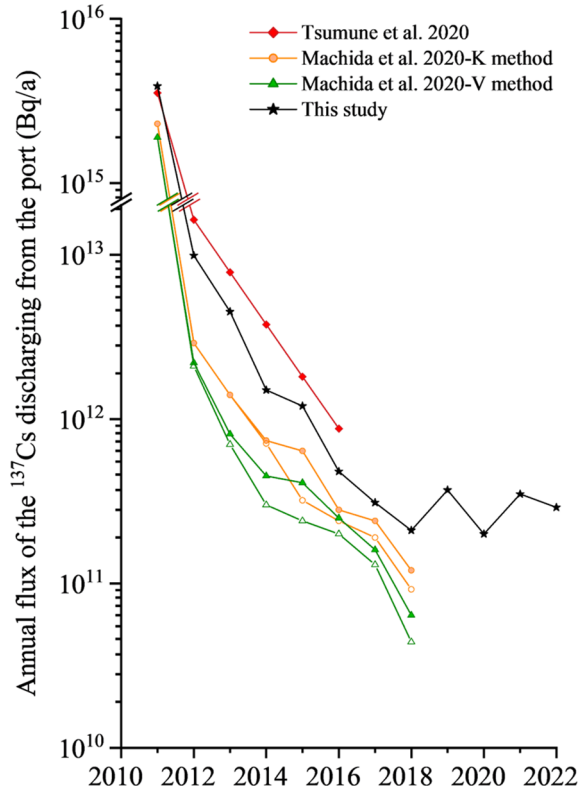

FIGURE 8
Comparison of the annual flux of the ^{137}Cs discharged from the port from 2011 to 2022.

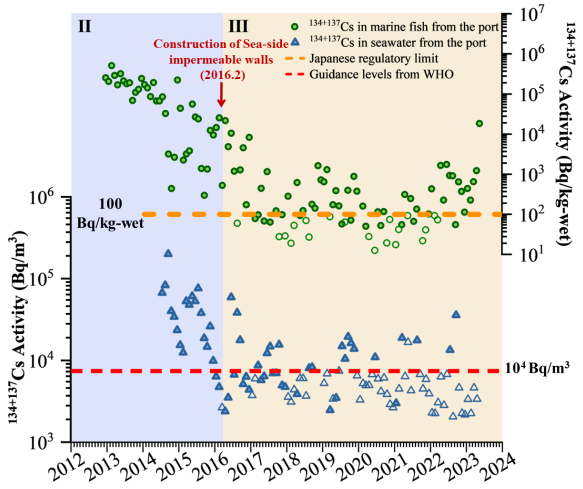

FIGURE 9
Simultaneous analysis of $^{134 + 137}$Cs in marine fish (green circle) from December 2012 to May 2023 and seawater (blue triangle) from July 2014 to April 2023. The solid symbols mean the sum of detectable ^{134}Cs and measurable ^{137}Cs, while the open symbols refer to the sum of measurable ^{137}Cs and the MDA of ^{134}Cs. The brown and red dotted lines refer to the Japanese regulatory limit for marine fish (100 Bq/kg-wet) and the WHO guidance levels for drinking water (10^4 Bq/m^3) for $^{134 + 137}$Cs.

of $^{134 + 137}$Cs activity in seawater (Figures 9, 10A). In contrast, periodic increases in $^{134 + 137}$Cs activity without a decreasing trend in marine fish and seawater were observed after February 2016 (Figure 10B). The Japanese regulatory limit for marine fish (100 Bq/kg-wet) and the WHO guidance levels for drinking water (10,000 Bq/m^3) for $^{134 + 137}$Cs were adopted to evaluate the radioactive level. We found that the ratio of over-standard for $^{134 + 137}$Cs in marine fish (>100 Bq/kg-wet) was 100% from December 2012 to January 2016 and 59% from February 2016 to May 2023. Meanwhile, the ratio of over-standard for $^{134 + 137}$Cs in seawater (>10,000 Bq/m^3) was 89.5% from July 2014 to January 2016 and 20.5% from February 2016 to April 2023. Obviously, the ratio of over-standard for $^{134 + 137}$Cs in marine fish was higher than that in seawater, probably attributed to the biological concentration effect of marine fish.

Additionally, the delayed increase in $^{134 + 137}$Cs activity in marine fish following the $^{134 + 137}$Cs peak in seawater is also depicted by the orange shadow in Figures 10A, B. The positive relationship of peak $^{134 + 137}$Cs activity between marine fish and seawater is well-fitted in Figure 11 ($r = 0.99$, $p < 0.0001$) on the basis of the corresponding peaks of $^{134 + 137}$Cs activity in marine fish and seawater. The concentration factors of $^{134 + 137}$Cs in marine fish ranged from 29 L/kg to 514 L/kg, with an average value of 136 L/kg from February 2016 to May 2023. The average value of 136 L/kg in marine fish was consistent with the recommended value of 100 L/kg provided by the IAEA (2004), confirming the corresponding relationship of $^{134 + 137}$Cs peaks between marine fish and seawater.

It was noted that radiocesium in sediment also contributed to the elevated activity of radiocesium in marine fish (Wang et al., 2018; Song et al., 2020). Unfortunately, radiocesium in the sediment from the most polluted port was not available from TEPCO and METI, limiting our discussion of the pathway of sediment ingestion by marine fish. However, the continuing source of radiocesium derived from the FDNPP should increase radiocesium levels in seawater followed by those in sediment and marine fish. The corresponding peaks of radiocesium between seawater and marine fish should be logically correlated. Even so, radiocesium in the sediment from the most polluted port should be measured for a better understanding of frequent reports of extremely high radiocesium levels in marine fish from the port in the future.

4 Conclusion

Overall, we revealed the distinct seasonal patterns of an exponential decline in the dry season and steady variation in the wet season in detail based on the historical ^{137}Cs activity in seawater and proposed a novel method to quantify the continuing source terms of ^{137}Cs derived from the FDNPP (3.9 PBq in 2011 and 19.3 TBq from 2012 to 2022). Moreover, the biological concentration effect of marine fish was quantitatively emphasized on the basis of the higher ratio of excess $^{134 + 137}$Cs in marine fish compared to seawater. Long-term observation and analysis of radiocesium in marine fish and seawater from the most polluted port would benefit

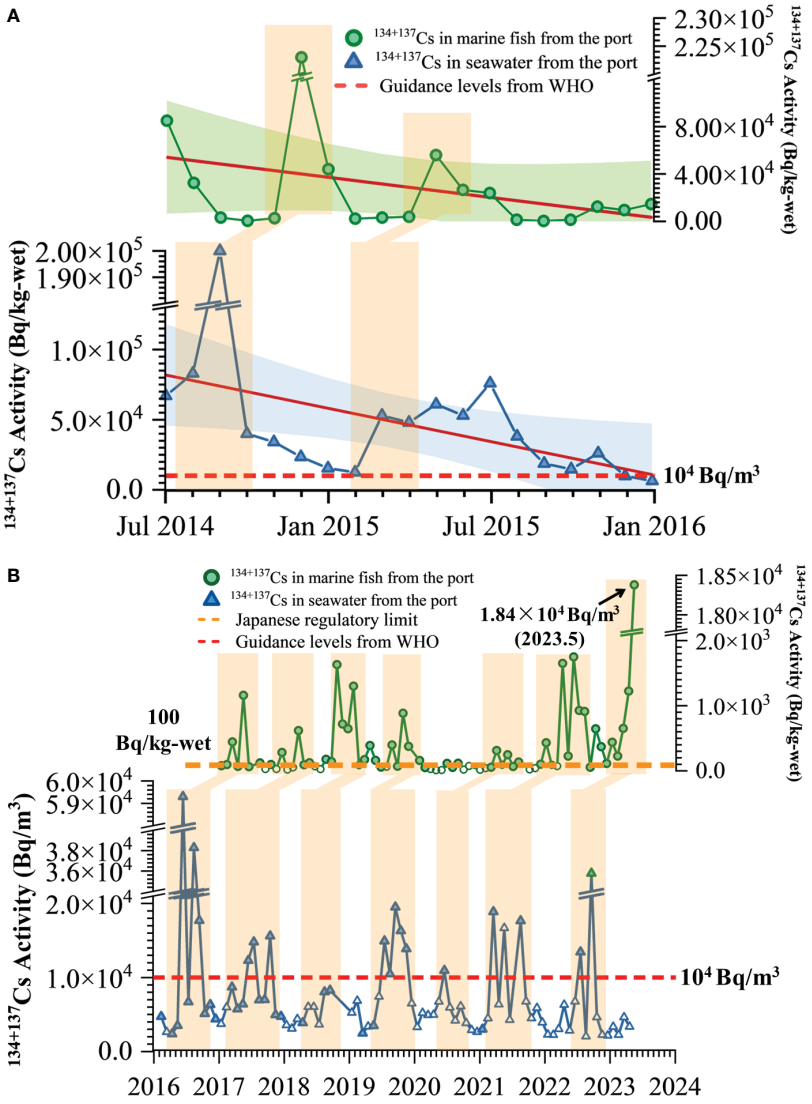

FIGURE 10
Delayed increase of $^{134+137}$Cs in marine fish following the $^{134+137}$Cs peak in seawater from July 2014 to January 2016 **(A)** and February 2016 to May 2023 **(B)**. The orange rectangles indicate the corresponding $^{134+137}$Cs peak in marine fish and seawater.

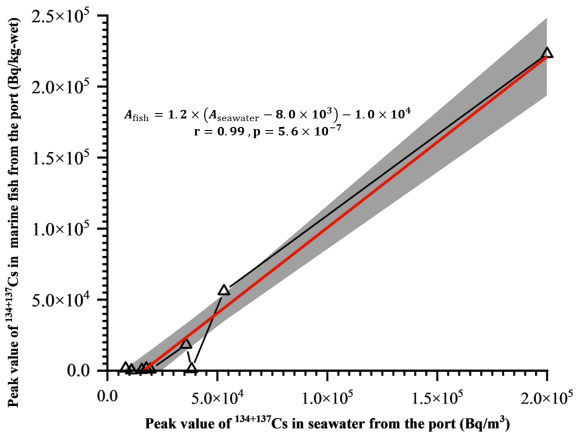

FIGURE 11
Positive relationship between the corresponding peak of $^{134+137}$Cs activity in marine fish and seawater.

the scientific evaluation of the decommissioning of the FDNPP, and share lessons on the fate of Fukushima-derived radionuclides in the marine environment for the prediction and assessment of nuclear-contaminated water discharged into the ocean.

Data availability statement

The original contributions presented in the study are included in the article/supplementary material. Further inquiries can be directed to the corresponding author.

Author contributions

WL: Conceptualization, Data curation, Formal analysis, Funding acquisition, Investigation, Methodology, Project

administration, Resources, Software, Supervision, Validation, Visualization, Writing – original draft. YZ: Methodology, Software, Visualization, Writing – original draft. JD: Data curation, Formal analysis, Resources, Visualization, Writing – original draft. JX: Funding acquisition, Methodology, Resources, Software, Writing – original draft. FT: Methodology, Resources, Visualization, Writing – original draft.

Funding

The author(s) declare that financial support was received for the research, authorship, and/or publication of this article. This work was supported by the National Natural Science Foundation of China (42276044); the Natural Science Foundation of Guangxi Province (2021GXNSFAA220053), and the open fund of the State Key Laboratory of Satellite Ocean Environment Dynamics, Second Institute of Oceanography, MNR (QNHX2320).

Acknowledgments

The authors would like to thank TEPCO, METI, and the Japan Meteorological Agency for sharing data on the websites.

Conflict of interest

The authors declare that the research was conducted in the absence of any commercial or financial relationship that could be construed as a potential conflict of interest.

Publisher's note

References

Buesseler, K. O. (2020). Opening the floodgates at Fukushima. *Science* 369, 621–622. doi: 10.1126/science.abc1507

IAEA (2004). *Sediment Distribution Coefficients and Concentration Factors for Biota in the Marine Environment* (Vienna: IAEA).

Japan-Meteorological-Agency (2023) *Past Weather Data*. Available online at: https://www.data.jma.go.jp/gmd/risk/obsdl/index.php.

Kanda, J. (2013). Continuing ^{137}Cs release to the sea from the Fukushima Dai-ichi Nuclear Power Plant through 2012. *Biogeosciences* 10, 6107–6113. doi: 10.5194/bg-10-6107-2013

Lin, W., Chen, L., Yu, W., Ma, H., Zeng, Z., and Zeng, S. (2016). Radioactive source terms for the Fukushima Nuclear Accident. *Sci. China: Earth Sci.* 59, 214–222. doi: 10.1007/s11430-015-5112-8

Lin, W., Yu, K., Du, J., Lin, H., Yu, W., and Mo, M. (2021). Consequences of marine ecological environment and our preparedness for Fukushima radioactive wastewater discharge into the ocean. *Chin. Sci. Bulletin* 66, 4500–4509. doi: 10.1360/TB-2021-0743

Liu, Y., Guo, X.-Q., Li, S.-W., Zhang, J.-M., and Hu, Z.-Z. (2022). Discharge of treated Fukushima nuclear accident contaminated water: macroscopic and microscopic simulations. *Natl. Sci. Rev.* 9, nwab209. doi: 10.1093/nsr/nwab209

Machida, M., Iwata, A., Yamada, S., Otosaka, S., Kobayashi, T., Funasaka, H., et al. (2023). Estimation of temporal variation of tritium inventory discharged from the port of Fukushima Dai-ichi Nuclear Power Plant:analysis of the temporal variation and comparison with released tritium inventories from Japan and world major nuclear facilities. *J. Nucl. Sci. Technol.* 60, 258–276. doi: 10.1080/00223131.2022.2093800

Machida, M., Yamada, S., Iwata, A., Otosaka, S., Kobayashi, T., Watababe, M., et al. (2020). Seven-year temporal variation of Caesium-137 discharge inventory from the port of Fukushima Daiichi Nuclear Power Plant: continuous monthly estimation of Caesium-137 discharge in the period from April 2011 to June 2018. *J. Nucl. Sci. Technol.* 57, 939–950. doi: 10.1080/00223131.2020.1740809

Ministry-of-Economy-Trade-and-Industry (2023a) *Monthly progress (January 26, 2023)*. Available online at: https://www.meti.go.jp/english/earthquake/nuclear/decommissioning/pdf/mp202301.pdf.

Ministry-of-Economy-Trade-and-Industry (2023b) *Progress Status Reports*. Available online at: https://www.meti.go.jp/english/earthquake/nuclear/decommissioning/progress_status.html.

Povinec, P. P., Hirose, K., Aoyama, M., and Tateda, Y. (2021). *Fukushima Accident: 10 Years After* (Amsterdam: Elsevier).

Song, J. H., Kim, T., and Yeon, J.-W. (2020). Radioactivity data analysis of ^{137}Cs in marine sediments near severely damaged Chernobyl and Fukushima nuclear power plants. *Nucl. Eng. Technol.* 52, 366–372. doi: 10.1016/j.net.2019.07.017

Tanaka, K., Nagao, S., Kitade, Y., Niki, M., Katsumata, T., Miyama, T., et al. (2022). Spread of Fukushima-derived radiocesium over the coastal ocean in response to typhoon-induced flooding in September 2011. *Limnol. Oceanogr.* 67, 1184–1193. doi: 10.1002/lno.12065

Tokyo-Electric-Power-Company (2011) *Impact on the environment of Fukushima Daiichi nuclear power plant*. Available online at: https://www.tepco.co.jp/nu/fukushima-np/f1/index2-j.html.

Tokyo-Electric-Power-Company (2013) *Nuclide analysis of fish and shellfish (including data in port)*. Available online at: https://www.tepco.co.jp/nu/fukushima-np/f1/smp/2013/images/fish_130327-j.pdf.

Tokyo-Electric-Power-Company (2018) *Analysis of radioactive substances around Fukushima Daiichi nuclear power plant*. Available online at: https://www.tepco.co.jp/nu/fukushima-np/f1/smp/indexold-j.html.

Tokyo-Electric-Power-Company (2023a) *Analytical results of fish and shellfish*. Available online at: https://www.tepco.co.jp/decommission/data/analysis/pdf_csv/2023/2q/fish01_230605-j.pdf.

Tokyo-Electric-Power-Company (2023b) *List of past analysis results archives*. Available online at: https://www.tepco.co.jp/decommission/data/analysis/archive/index-j.html.

Tsumune, D., Tsubono, T., Misumi, K., Tateda, Y., Toyoda, Y., Onda, Y., et al. (2020). Impacts of direct release and river discharge on oceanic ^{137}Cs derived from the Fukushima Dai-ichi Nuclear Power Plant accident. *J. Environ. Radioactivity*, 214–214. doi: 10.1016/j.jenvrad.2020.106173

Uchiyama, Y., Tokunaga, N., Aduma, K., Kamidaira, Y., Tsumune, D., Iwasaki, T., et al. (2022). A storm-induced flood and associated nearshore dispersal of the river-derived suspended ^{137}Cs. *Sci. Total Environ.* 816, 151573. doi: 10.1016/j.scitotenv.2021.151573

Wang, C., Cerrato, R. M., and Fisher, N. S. (2018). Temporal changes in ^{137}Cs concentrations in fish, sediments, and seawater off Fukushima Japan. *Environ. Sci. Technol.* 52, 13119–13126. doi: 10.1021/acs.est.8b03294

frontiers | Frontiers in Marine Science

TYPE Brief Research Report
PUBLISHED 24 May 2024
DOI 10.3389/fmars.2024.1361157

OPEN ACCESS

EDITED BY
Jingzhen Wang,
Beibu Gulf University, China

REVIEWED BY
Dinesh Kumar Sundarraj,
Central Salt & Marine Chemicals Research Institute (CSIR), India
Gang Zhai,
University of Chinese Academy of Sciences, China

*CORRESPONDENCE
Xiaomei Shang
shangxiaomei@tust.edu.cn
Jun Sun
phytoplankton@163.com

RECEIVED 25 December 2023
ACCEPTED 07 May 2024
PUBLISHED 24 May 2024

CITATION
Shang X, Yang Y, Zan Y, Sun Z, Lu Z and Sun J (2024) Effects of temperature on the growth, total lipid content and fatty acid composition of *Skeletonema dohrnii*. *Front. Mar. Sci.* 11:1361157. doi: 10.3389/fmars.2024.1361157

Effects of temperature on the growth, total lipid content and fatty acid composition of *Skeletonema dohrnii*

Xiaomei Shang[1*], Yaning Yang[1], Yongling Zan[1], Zhenwei Sun[1], Zhengyi Lu[2] and Jun Sun[1,3*]

[1]Research Centre for Indian Ocean Ecosystem, Tianjin University of Science and Technology, Tianjin, China, [2]Research and Development Center, Tianjin Chenhui Modern Technology Group Co., Ltd., Tianjin, China, [3]College of Marine Science and Technology, China University of Geosciences, Wuhan, Hubei, China

The potential of diatoms as aquatic bait, attribute to their abundance in highly unsaturated fatty acids, has been extensively studied. Temperature plays a crucial role in the synthesis of these fatty acids. This study specifically investigated the impact of temperature on the growth, total lipid content, and fatty acid composition of *Skeletonema dohrnii*, a planktonic diatom commonly associated with red tides and water blooms in China. The aim is to evaluate its suitability as an aquatic bait and provide insights for large-scale factory farming. Results indicated that the highest biomass and maximum growth rate occurred at 28°C, with no significant deviation from the control group at 25°C. At 28°C and 15°C, there was a significant increase in the total lipid content and the total fatty acid content, with a more pronounced effect at 15°C. At 28°C, EPA and DHA content measured at 0.97 ± 0.01 mg.DW.L^{-1} and 0.264 ± 0.01 mg.DW.L^{-1} respectively, surpass those at 15°C due to lower biomass. Conversely, at 15°C, substantial synthesis of long-chain polyunsaturated fatty acids, with EPA constituting up to 32.24 ± 0.24% of the total fatty acids, is observed. Modulating the temperature could optimize the utilization of *S. dohrnii* as an aquatic feed source. These findings underscore the potential of *S. dohrnii* as a high-quality aquafeed and lay the groundwork for its success in ocean warming scenarios.

KEYWORDS

***Skeletonema dohrnii*, unsaturated fatty acids, temperature, aquafeed, ocean warming**

Introduction

Diatoms, a class of photosynthetic autotrophic unicellular microalgae eukaryotes, are widely distributed in the ocean, fresh water and wet soil. As the main group of phytoplankton, diatoms contribute to approximately 20% of global primary production and nearly 40% of marine primary production (Field et al., 1998). They play an important

role in the material and energy circulation within marine ecosystem, forming the foundation of the marine nutrient network (Falkowski et al., 1998; Armbrust, 2009; Sepúlveda and Cantarero, 2022). Diatoms are rich in polyunsaturated fatty acids (PUFAs), including eicosapentaenoic acid (EPA), docosapentaenoic acid (DHA), myristic acid, palmitic acid, and palmitoleic acid. These compounds have been associated with protective effects against cardiovascular disease, the promotion of healthy vision, and assistance in the prevention of psychiatric disorders (Yi et al., 2017; Marella and Tiwari, 2020). The presence of PUFAs, particularly EPA, renders diatoms a valuable source of nutrition for marine mussels, crustacean larvae, and fish larvae (Reitan et al., 1997; Renaud et al., 2002; Mishra and Tiwari, 2021). Not only can this synthesis effectively reduce production costs (Valenzuela-Espinoza et al., 1999), but the cultivation of marine diatoms for the replacement of fishmeal and fish oil made from harvesting of wild-caught fish, promote ecological sustainability (Sarker, 2023).

The metabolism of diatom fatty acids is influenced by various factors, including temperature, light, nutrients, and pH. Notably, temperature is an important one, compared to other factors, it exerts a substantial impact on the physiological processes of algae due to its involvement in numerous metabolic processes, enzymatic, and photosynthetic processes, directly influencing the synthesis and transformation of diatom fatty acids (Davison, 1991; Duarte, 2007; Converti et al., 2009; Boyd et al., 2013; Sepúlveda and Cantarero, 2022). Lower temperatures have been observed to prompt *Phaeodactylum tricornutum* and *Skeletonema menzelli* to synthesize and accumulate higher levels of essential fatty acids (EFAs) and PUFAs (Jiang and Gao, 2004; Gao et al., 2014). Additionally, *Nitzschia frustulum*, in colder conditions, has shown increased synthesis and storage of unsaturated fatty acids (USFAs), aiding in maintaining cellular membrane fluidity and permeability (Harwood, 1988; Renaud et al., 1995). Conversely, elevated temperatures have been noted to diminish the content of EFAs and DHA in *Chaetoceros* sp. while increasing the amount of saturated fatty acids (SFAs) (Renaud et al., 2002). This transition from USFAs to SFAs is believed to aid in preserving the fluidity and stability of the cell membrane (Quinn, 1981; Murata and Los, 1997; Sepúlveda and Cantarero, 2022). Maia et al. (2022) found that *Skeletonema costatum* shows greater temperature tolerance compared to *P. tricornutum*, likely due to *S. costatum*'s capacity to accumulate more USFAs and proteins when exposed to higher temperatures. Various species of microalgae exhibit distinct responses in their fatty acid profiles to changes in temperature. Hence, identifying the optimal temperature for PUFAs accumulation is crucial for reducing production costs.

The present research explores *Skeletonema dohrnii*, a member of the *Skeletonema* genus, among the most prevalent marine planktonic diatoms in the temperate zones of the World Ocean (Shevchenko et al., 2019). *S. dohrnii* often contributes to the occurrence of red tides or water blooms in China, which can exert a significant and detrimental impact on the environment (Gu et al., 2012). Its rapid growth, robust reproductive capacity, and ability to thrive make it an ideal subject for study, development, and exploitation. Currently, there is a scarcity of research on *S. dohrnii*, with the predominant focus of studies concentrated on its ecological and physiological characteristics, while only a minority delve into its potential applications (Yamada et al., 2010; Ogura et al., 2018; Thangaraj et al., 2019; Thangaraj and Sun, 2020). Marine diatoms are often thriving under adverse marine environmental conditions (Kooistra et al., 2007; Bowler et al., 2010; Thangaraj et al., 2019). Studies have indicated that diatoms have a range of adaptive mechanisms in response to seawater warming and ocean acidification, including the adjustment of saturated fatty acid ratios to mitigate adverse effects (Jin and Agustí, 2018; Thangaraj and Sun, 2020). As such, marine diatoms possess the potential to adapt to climate change. Exploring changes in their fatty acid content and composition in response to temperature, as alongside the investigation of the nutritional value, development, and utilization of *S. dohrnii*, could provide insight into its lipid accumulation rate. This, in turn, could serve as a foundation for fish feed and biodiesel production, supporting the sustainable development of marine resources.

Materials and methods

Experimental materials

The marine diatom *S. dohrnii*, was isolated from the Yellow Sea and cultivated in the laboratory using the f/2 medium (25°C 90–120 μmol photons $m^{-2}{\cdot}s^{-1}$, with 12:12 light-dark cycle).

Culture conditions

Artificial seawater media (ASW) supplemented with a silicate stock solution (28.40 $g{\cdot}L^{-1}$) was utilized in this experiment (Sunda et al., 2005). After being cultured and adapted in ASW, *S. dohrnii* was subjected to three different temperatures: 15°C (the low-temperature group), 25°C (the control group), and 28°C (the high-temperature group), for a single expansion culture. The initial cell concentration was set at $1{\times}10^5$ cell/mL. The cells were collected in the stationary growth phase, with triplicate samples established within each temperature group (n=3).

Growth rate analysis

Throughout the period from inoculation to collection, the algal solution was gently agitated and blended daily. Subsequently, 100 μl of the solution was carefully transferred to a cell counting plate using a pipette and examined under a microscope. The cell density of the sample was determined by calculating the average of the three counts (unit: cells/mL).

The specific growth rate was calculated using the following formula:

$$K = (\ln N_t - \ln N_{t-1})/t$$

Where N_t represents the number of cells after t days of cultivation, and t denotes the duration of the culture, N_{t-1} is the cell concentration on the day_{t-1}.

Lipid content measurement

Once the algal cells completed their exponential growth phase, the liquid was collected via centrifugation (4000r/min, 4°C). The resulting freeze-dried algal powder was then stored at -20°C, and the total lipid was determined following the guidelines of GB 5009.6. To initiate the process, 500 mg of the algal powder was weighed into a Maoshi bottle, and 4 mL of water along with 5 mL of 2M HCl were added. The mixture was then heated in a water bath at 75°C for 50 min. After cooling, 5 mL of ethanol was gradually introduced and mixed, after which 25 mL of ether was added. The bottle was shaken and allowed to settle for 30 min. The upper organic layer was carefully poured out, and the extraction process was repeated thrice. The resulting extract was gathered into a conical flask of constant weight, and the solvent was evaporated in a water bath. The remaining material was dried in an oven at 100°C for 1 h, cooled for 30 min, and then weighed. The obtained test data was presented as the mean ± standard deviation. The statistical software SPSS 26.0 was used for data analysis, while Excel 2019 and SPSS 26.0 were utilized for chart creation.

Fatty acid profile

Weigh 30 mg of freeze-dried algae powder and combine it with 10 mL of 4M HCl, then place the mixture in a boiling water bath for 10 min. Immediately afterwards, transfer it to a -20°C refrigerator for 15 min. Upon removal from the refrigerator, add 10 mL of chloroform and 5 mL of methanol, allowing the solution to rest at room temperature for 2 h. The lower chloroform phase is then collected via centrifugation and dried with nitrogen to obtain the total lipid. For further analysis, introduce 1 mL of n-hexane and 200 μL of potassium hydroxide-methanol solution. Vigorously shake the solution for 30 seconds and let it settle for layering. Transfer the upper n-hexane phase to a sample bottle for analysis. The percentage content of each fatty acid was determined using a gas chromatograph (GC-2014, Shimadzu Manufacturing Institute) following the internal standard method outlined in GB 5009.168.

Additionally, the area normalization method was employed to calculate the percentage content of each fatty acid. This method involves summing the peak areas of all components, which collectively represent 100% of the total peak area, and then calculating the percentage of each individual peak area relative to the total peak area. The calculation formula utilized was as follows:

$$C_i\,\% = (m_i/m) \times 100\,\% = f_i' A_i/(\sum fi' A_i) \times 100\,\%$$

where C_i% represents the percentage content of the measured component i. f_i' is the relative mass correction factor of the measured component i. A_i denotes the peak area of the measured component i. m is the mass of the measured sample. And m_i represents the mass of the tested component i.

Results

Growth rate and the biomass

The growth of *S. dohrnii* under cultivation at three different temperatures was measured and is visually in Figure 1. All inoculated *S. dohrnii* samples exhibited growth, with the shortest growth cycle occurring at the highest temperature, spanning a period of 3 days. The maximum growth rate was observed to be the lowest at 15°C, with a value of 0.62 ± 0.09 ($p<0.005$), which was significantly different from the other two temperatures. Additionally, the maximum death rate was recorded at 15°C, with a value of -0.35 ± 0.03, which was statistically different from the rated observed at the other temperatures (Table 1). However, the highest growth rates were observed at 28°C (0.89 ± 0.02), followed by 25°C (0.8 ± 0.01). The results of the experiment indicated that the highest cell density of *S. dohrnii* was 6.5×10^6 cells/mL achieved at 25°C, while density at 28°C and 15°C were 6.35×10^6 cells/mL and 5.80×10^6 cells/mL, respectively. Likewise, the cultures initiated with a biomass concentration of 0.006 ± 0.001 g DW L^{-1}, and eventually reached their maximum concentrations at 0.046 ± 0.002 (15°C), 0.120± 0.001 (25°C), and 0.122 ± 0.001 (28°C) g DW L^{-1} for *S. dohrnii*, respectively. Notably, there was no significant difference ($p<0.05$) observed between the biomass at 25°C and 28°C (Table 1).

The total lipid and fatty acid profile of *S. dohrnii* at different temperatures.

In the three experimental groups, temperature exhibited a significant impact on the total lipid content of the algae. As the temperature increased, there was a corresponding decrease in the total lipid content of the algae. The highest total lipid content was observed at 15°C (39.23 ± 0.32 mg/g), followed by the high-temperature group at 28°C (37.43 ± 0.31 mg/g), and the lowest content was in the control group at 25°C (30.97 ± 0.06 mg/g). These variations between the groups were statistically significant ($p<0.05$)

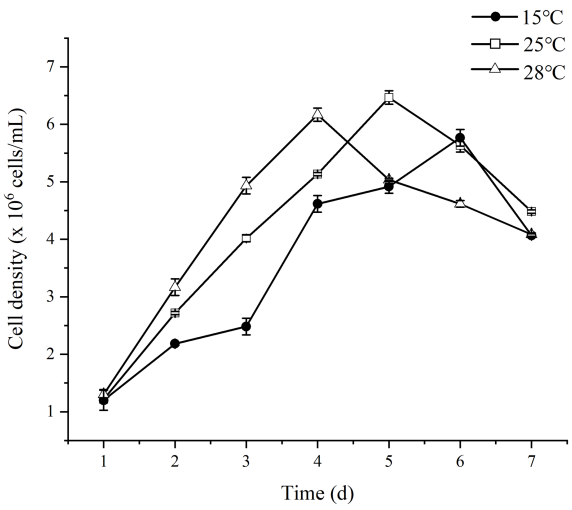

FIGURE 1
The growth curve of *S. dohrnii* under three temperature conditions.

TABLE 1 Specific growth rate, biomass and total lipid content of *S. dohrnii* under three temperature conditions.

Samples	Day 1	Day 2	Day 3	Day 4	Day 5	Day 6	Initial biomass/g DW L^{-1}	Final biomass/g DW L^{-1}	Total lipid content
15°C	0.61 ± 0.15^{a}	0.13 ± 0.07^{a}	0.62 ± 0.09^{b}	0.06 ± 0.05^{b}	0.16 ± 0.05^{b}	0.35 ± 0.03^{a}	0.006± 0.001	0.046 ± 0.002^{a}	39.23 ± 0.32^{c}
25°C	0.8 ± 0.01^{b}	0.39 ± 0.03^{b}	0.25 ± 0.01^{a}	0.23 ± 0.02c 0.02^{c}	0.14 ± 0.04^{a}	0.23 ± 0.01^{b}		0.120 ± 0.001^{b}	30.97 ± 0.06^{a}
28°C	0.89 ± 0.02^{b}	0.44 ± 0.08^{b}	0.22 ± 0.01^{a}	0.2 ± 0.02^{a}	0.09 ± 0.01^{a}	0.12 ± 0.01^{c}		0.122 ± 0.001^{b}	37.9 ± 0.17^{b}

In the same column of data, superscripted with different lowercase letters, indicate significant differences between the various experimental groups ($p<0.05$). Superscripted with the same lowercase letter indicates a non-significant difference between the different experimental groups.

(Table 2). A total of 23 kinds of fatty acids were detected in this experiment, albeit some species were only detected at specific temperatures. About the fatty acids composition, the analysis revealed 11 types of SFAs, 12 types of USFAs, 5 types of monounsaturated fatty acids (MUFAs), and 7 types of polyunsaturated fatty acids (PUFAs).

The fatty acid composition of *S. dohrnii* primarily consists of C14:0, C18:1:ω9, and C20:5:ω3, collectively representing nearly 60% of the total fatty acid (TFA) content. In order to facilitate comparisons of fatty acid compositions, the measured data have been converted here to percentage occupancy. Given its proximity to the natural habitat temperature of *S. dohrnii*, the fatty acid content at 25°C was utilized as a reference point. Notably, C14:0 and C20:5:ω3 exhibited elevated concentrations, accounting for 23.45 ± 0.25% and 25.79 ± 0.11%, respectively, whereas C18 and C22 of USFAs displayed lower levels. These observed characteristics align with the typical profile of Bacillariophyta (Zhukova and Aizdaicher, 1995; Chen, 2012). For further details, please refer to Table 2.

In comparison to the control group (25°C), at 15°C, the USFAs content in *S. dohrnii* exhibited a significant increase from 10.21 ± 0.01 mg/g to 27.09 ± 0.10 mg/g, while the PUFAs content showed a significant increase from 5.9 ± 0.07 mg/g to 18.31 ± 0.19 mg/g. Among the PUFAs, EPA was the most predominant, ranging from 4.08 ± 0.01 mg/g to 12.03 ± 0.03 mg/g, followed by DHA at 0.89 ± 0.03 mg/g to 2.62 ± 0.19 mg/g. Conversely, with a rise in temperature compared to the control group, at 28°C, both USFAs and PUFAs, as well as EPA and DHA, exhibited increases in content, with values of 22.55 ± 0.2 mg/g, 11.36 ± 0.13 mg/g, 7.95 ± 0.01 mg/g, and 2.16 ± 0.03 mg/g respectively (Table 2). The TFA content varied across experimental conditions, with the control group displaying the lowest level (15.77 ± 0.01 mg/g) and the low-temperature group exhibiting the highest (36.99 ± 0.05 mg/g), followed by the high-temperature group (35.02 ± 0.17 mg/g). Fatty acid compositions shifted in response to temperature variations, as depicted in Figure 2. The percentages of PUFAs decreased with increasing temperatures, registering at 49.15 ± 0.04% at 15°C, 37.17 ± 0.09% at 25°C, and 30.59 ± 0.19% at 28°C. Similarly, the proportions of EPA declined with rising temperatures, measuring 32.24 ± 0.24% at 15°C, 25.79 ± 0.11% at 25°C, and 21.73 ± 0.12% at 28°C. Conversely, the proportions of SFAs and MUFAs exhibited an upward trend with elevated temperatures. SFAs increased from 26.59 ± 0.06% at 15°C to 35.64 ± 0.20% at 28°C, while MUFAs rose from 24.26 ± 0.10% at 15°C to 32.77 ± 0.09% at 28°C (Figure 2). DHA exhibited minimal changes, showing a decrease, albeit not statistically significant, between 25°C and 28°C (Figures 2B, C). However, the percentage of both EPA and DHA in the PUFAs increased significantly with temperature, but there was little change in the data (Figure 2).

The analysis of fatty acid carbon chain length revealed that short and medium-chain fatty acids predominantly constituted the SAFs, exhibiting consistent distribution across different temperatures. However, the distribution of long-chain fatty acids exhibited significant variability based on the temperature conditions. The long-chain fatty acid content in both SFA and MUFA was positively and significantly different from the temperature change. Specifically, at 28°C, the highest count of saturated fatty acid species (10) and very long-chain unsaturated fatty acid species (3) were observed, while at 15°C, the highest count of unsaturated fatty acid species (11) and very long-chain unsaturated fatty acid species (2) was identified. Moreover, the highest content of long-chain unsaturated fatty acids (LC-USAFs) was observed at 15°C, reaching up to 24 mg/g, whereas the highest content of long-chain saturated fatty acids (LC-SAFs) was recorded at 28°C, approximately 10 mg/g.

Discussion

The ability of *S. dohrnii* in ocean warming

The Intergovernmental Panel on Climate Change (IPCC, 2018) has projected that by the end of the century, global marine warming will lead to a temperature increase of 1–3°C in sea surface temperatures. This climatic shift is anticipated to trigger various impacts, including physiological alternations in marine phytoplankton, ocean stratification, a reduction in the depth of the upper mixed layer, and diminished nutrient supply to the upper layer of seawater. Consequently, these changes may result in nutrient limitation and a decline in primary productivity (Laufkötter et al., 2015; Jin and Agustí, 2018). Temperature has been identified as a major factor influencing the metabolic processes, enzymatic reactions, and photosynthesis of diatoms and other microalgae (Depauw et al., 2012; Bermudez et al., 2015; Dong et al., 2016; Liang et al., 2019; Thangaraj et al., 2020).

In this study, results showed that the highest biomass and maximum growth rate were observed at 28°C, with no statistically significant difference compared to the control group. Notably, at 28°

10.3389/fmars.2024.1361157

TABLE 2 Effects of temperature on fatty acid composition in *S. dohrnii*..

Types	15°C		25°C		28°C		Carbon Chain Lengths
	ISM(mg/g)	ANM(%)	ISM(mg/g)	ANM(%)	ISM(mg/g)	ANM(%)	
4:0	0.64 ± 0.03^{a}	0.59 ± 0.02^{a}	0.66 ± 0.03^{a}	1.45 ± 0.06^{c}	0.79 ± 0.04^{b}	0.83 ± 0.02^{b}	short
8:0	0.47 ± 0.02	1.07 ± 0.14^{a}	0.46 ± 0.01	2.51 ± 0.02^{b}	0.47 ± 0.01	1.2 ± 0.07^{a}	mid
12:0	0.16 ± 0.01^{a}	0.43 ± 0.05^{a}	0.14 ± 0.01^{a}	0.91 ± 0.03^{c}	0.2 ± 0.02^{b}	0.55 ± 0.03^{b}	mid
13:0	0.05 ± 0.02	0.12 ± 0.01	ND	ND	ND	ND	long
14:0	7.64 ± 0.02^{b}	20.47 ± 0.14^{a}	3.72 ± 0.07^{a}	23.45 ± 0.25^{b}	9.31 ± 0.12^{c}	26.82 ± 0.15^{c}	long
14:1:ω9	0.08 ± 0.01^{a}	0.21 ± 0.01^{a}	0.06 ± 0.01^{a}	0.37 ± 0.01^{c}	0.1 ± 0.03^{a}	0.28 ± 0.02^{b}	long
15:0	0.22 ± 0.01^{a}	0.6 ± 0.03^{a}	0.11 ± 0.01^{b}	0.66 ± 0.03^{a}	0.23 ± 0.02^{a}	0.66 ± 0.06^{a}	long
16:0	0.44 ± 0.02^{a}	2.49 ± 0.08^{a}	0.41 ± 0.01^{a}	5.45 ± 0.09^{c}	0.74 ± 0.04^{b}	4.42 ± 0.01^{b}	long
16:1:ω9	5.69 ± 0.15^{b}	15.63 ± 0.27^{a}	2.82 ± 0.03^{a}	18.21 ± 0.14^{b}	7.56 ± 0.03^{c}	22.01 ± 0.11^{c}	long
18:0	0.12 ± 0.02^{a}	0.33 ± 0.01^{a}	0.07 ± 0.01^{a}	0.45 ± 0.02^{b}	0.21 ± 0.04^{b}	0.60 ± 0.07^{c}	long
18:1:ω9	2.85 ± 0.03^{b}	7.93 ± 0.13^{a}	1.43 ± 0.02^{a}	9.37 ± 0.18^{b}	3.38 ± 0.04^{c}	10.04 ± 0.14^{c}	long
18:2:ω6	3.49 ± 0.02^{b}	9.85 ± 0.14^{c}	0.83 ± 0.02^{a}	5.48 ± 0.14^{b}	0.87 ± 0.04^{a}	2.57 ± 0.17^{a}	long
18:3:ω3	0.04 ± 0.02^{a}	0.11 ± 0.01^{a}	0.06 ± 0.02^{a}	0.38 ± 0.01^{a}	0.06 ± 0.02^{a}	0.16 ± 0.03^{b}	long
18:3:ω6	0.12 ± 0.02^{b}	0.34 ± 0.02^{a}	0.05 ± 0.01^{a}	0.31 ± 0.01^{b}	0.25 ± 0.04^{c}	0.75 ± 0.05^{a}	long
20:1	0.07 ± 0.01	0.19 ± 0.01	ND	ND	ND	ND	long
20:3:ω6	0.05 ± 0.02^{a}	0.12 ± 0.01^{a}	ND	ND	0.08 ± 0.01^{a}	0.22 ± 0.01^{b}	long
20:5:ω3	12.03 ± 0.03^{c}	32.24 ± 0.24^{c}	4.08 ± 0.01^{a}	25.79 ± 0.11^{a}	7.95 ± 0.01^{b}	21.73 ± 0.12^{b}	long
22:0	ND	ND	ND	ND	0.04 ± 0.02	0.13 ± 0.01	very long
22:1:ω9	0.11 ± 0.04^{a}	0.31 ± 0.01^{a}	ND	ND	0.15 ± 0.04^{a}	0.44 ± 0.02^{b}	very long
22:2	ND	ND	ND	ND	0.18 ± 0.02	0.52 ± 0.01	very long
22:6:ω3	2.62 ± 0.19^{c}	6.49 ± 0.13^{b}	0.89 ± 0.03^{a}	5.21 ± 0.09^{a}	2.16 ± 0.03^{b}	5.15 ± 0.12^{a}	very long
23:0	ND	ND	ND	ND	0.12 ± 0.01	0.35 ± 0.01	very long
24:0	0.16 ± 0.01^{a}	0.50 ± 0.01^{a}	ND	ND	0.18 ± 0.02^{a}	0.55 ± 0.02^{b}	very long
SFAs	9.89 ± 0.05^{b}	26.59 ± 0.06^{a}	5.56 ± 0.01^{a}	34.88 ± 0.04^{b}	12.29 ± 0.05^{c}	36.12 ± 0.18^{c}	NA
USFAs	27.09 ± 0.11^{c}	73.41 ± 0.06^{c}	10.21 ± 0.01^{a}	65.12 ± 0.04^{b}	22.55 ± 0.2^{b}	63.88 ± 0.18 ^{a}	NA
MUFAs	8.79 ± 0.08^{b}	24.26 ± 0.10^{a}	4.31 ± 0.05^{a}	27.96 ± 0.05^{b}	11.18 ± 0.08^{c}	32.77 ± 0.02^{c}	NA
PUFAs	18.31 ± 0.19^{c}	49.15 ± 0.04^{c}	5.9 ± 0.07^{a}	37.17 ± 0.09^{b}	11.36 ± 0.13^{b}	31.11 ± 0.2^{a}	NA
TFA	36.99 ± 0.05^{c}	NA	15.77 ± 0.01^{a}	NA	35.02 ± 0.17^{b}	NA	NA
Total lipid	39.23 ± 0.32^{c}	NA	30.97 ± 0.06^{a}	NA	37.9 ± 0.17^{b}	NA	NA

Differential comparison of the same type of data at different temperatures. Values are mean ± standard error of duplicate measurements.
Different lowercase letters labeled on the same row of data for the same fatty acid indicate significant differences between different experimental groups ($p<0.05$), and no shoulder label indicates no significant difference.
SFAs, Saturated Fatty Acids; USFAs, Unsaturated Fatty Acids; MUFAs, Mono Unsaturated Fatty Acids; PUFAs, Poly Unsaturated Fatty Acids; TFA, Total fatty acid.
ND, Not Detected; NA, Not applicable; ISM, Internal Standard Method; ANM, Area Normalization Method.

C, the TFA content (36.99 ± 0.05 mg/g), EPA content (7.95 ± 0.01 mg/g), and DHA content (2.16 ± 0.03 mg/g) were significantly higher than those recorded in the control group. Maia et al. (2022) found that *S. costatum* exhibited enhanced biomass and lipid production, particularly PUFAs, at elevated temperatures in comparison to *P. tricornutum*. This suggests that *S. costatum* may possess a higher degree of tolerance to temperature variations and adaptive capabilities in anticipation of future ocean warming. This suggests the potential adaptation of *S.dorhnii* to future ocean warming. Numerous prior studies have demonstrated the superiority of diatoms surviving in high temperature conditions. Research indicates that *S. dorhnii* has the potential to adapt to ocean warming by readjusting energy metabolism within cells to better suit to warmer waters (Cheng et al., 2022). Under stress conditions,

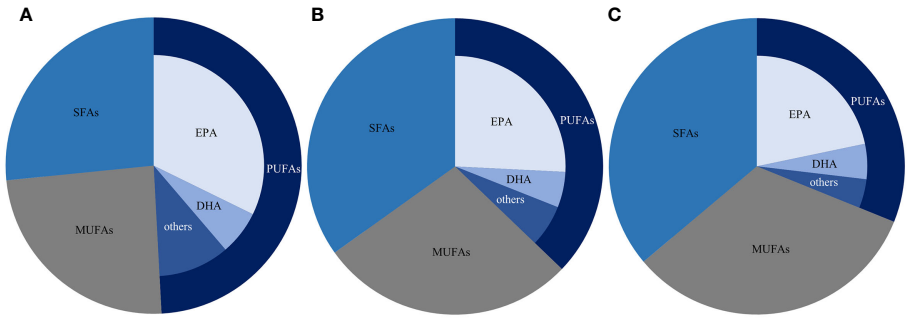

FIGURE 2
The proportion of the main fatty acids of *S. dohrnii* at 15°C **(A)**, 25°C **(B)** and 28°C **(C)** according to the area normalization method results.

S.dorhnii tends to synthesizes lipids, mainly in the form of TAGs, rather than serve as a carbon sink (Zulu et al., 2018). Proteomics analysis revealed that the lipid synthesis proteins in *S.dorhnii* were upregulated at high temperature (Thangaraj et al., 2020). Studies utilizing the transcriptomic approach have revealed that the preservation of protein processing machinery and membrane structure constitutes crucial short-term physiological mechanisms employed to counteract temperature variations. These mechanisms are identified as key components associated with the adaptation to different growth temperatures (Liang et al., 2019). Upon reaching the 700th generation, the lipid metabolism of *S.dorhnii* assumes prominence as a pivotal element in its sustained adaptation to ocean warming (Cheng et al., 2022). However, it is noteworthy that in the high-temperature environment, there was a notable increase in the proportion of SFAs and a concurrent decrease in the proportion of USFAs. The SAFs content of *S.dorhnii* was significant higher than that of the control group. A greater diversity and higher content of LC-SAFs were observed at 28°C and the content reached up to 10 mg/g. The increase in SFAs is believed to contribute to the maintenance of cell membrane fluidity and stability (Renaud et al., 2002; Sepúlveda and Cantarero, 2022). Moreover, elevated LC-SAFs can increase intracellular energy expenditure, reduce intracellular energy metabolism, and sustain healthy and normal metabolic activity (Giudetti et al., 2016).

In addition to alterations in fatty acid saturation under temperature stress conditions, diatoms may employ a rapid adaptation strategy to tackle higher temperatures (O'Donnell et al., 2019). This strategy involves adjusting the optimum temperature, enhancing the maximum specific growth rate, improving light-use efficiency, diminishing photosynthetic intensity, and achieving saturation in photosynthesis at an earlier stage (Jin and Agustí, 2018; Cheng et al., 2022). For example, *Chaetoceros tenuissimus* was observed to enhance its high-temperatures tolerance by modifying its optimum temperature, elevating its maximum specific growth rate, optimizing light-use efficiency, reducing photosynthetic intensity, and reaching saturation in photosynthesis earlier (Jin and Agustí, 2018). In our study, *S. dohrnii* was found to have a higher specific growth rate at 28°C, with a maximum biomass exceeding the optimum temperature. This suggests the likelihood of employing similar adaptive mechanisms to adapt to future ocean warming.

The potential of *S. dohrnii* as aquatic food

Microalgae play an important role in promoting the sustainable development of aquaculture feeds by reducing the pressure on fish stocks and fertile soils provoked by traditional feed production methods. At present, the aquatic species nourished by microalgae boast high survival rates and exceptional nutritional value (Sarker et al., 2016; Velasquez et al., 2016; Sales et al., 2021), driving the significant momentum behind the industrial-scale integration of microalgae in aquaculture feeds (Beal et al., 2018; Shah et al., 2018; Sarker et al., 2020).

The primary obstacle hindering the widespread application of microalgae as aquaculture feeds is the high production cost. To mitigate this, the selection of high-quality microalgae species and the implementation of large-scale production processes serve as effective means to reduce expenses. The selection of appropriate microalgae for aquafeed must consider various factors, such as cell size, cell wall thickness, digestibility, pigment content, and growth rate (Gladue and Maxey, 1994; Renaud et al., 2002). Among these factors, the growth rate of algae assumes particular importance in large-scale production of microalgae as aquaculture feeds. In our study, *S.dorhnii* exhibited rapid growth and reproduction, enabling the cultivation of numerous algal strains in a short period of time. Its substantial accumulation of fatty acids aligns well with the requisites for large-scale production, rendering it a good candidate for the development of aquafeeds.

In addition to the factors mentioned above, nutritional value is a crucial consideration, particularly for the fatty acids, especially PUFAs, play a vital role in the growth and development of aquaculture animals. Since the 1940s, over 100 fatty acids from microalgae have been identified and applied in the development and production of aquafeeds (Roy and Pal, 2015). *Spirulina platensis* is recognized as an important biological source of γ-linolenic acid, constituting 20%-30% of its fatty acid composition (Becker, 2003). Cyanobacteria typically contain 25–60% PUFA and exhibit richness in fatty acids such as linoleic acid (18:2) and linolenic acid (18:3), as well as EPA (20:5) and arachidonic acid (20:4) (Borowitzka and Borowitzka, 1988). Notably, the red alga *P. cruentum* stands out for its high arachidonic acid content, comprising roughly 36% of the TFA content, highlighting microalgae as a reliable source of n-3 fatty acids, a significant component of high-quality fish oils (Ahern

et al., 1983). These specific fatty acids are primary metabolites that accumulate in large quantities with cell growth, forming the basis for their industrial production. Studies have demonstrated that the intake of n-3 fatty acids by cultured animals can significantly reduce the risk of stress responses and chronic diseases (Zuo et al., 2012). *S. costatum* abundant in highly unsaturated fatty acids (HUFAs) (EPA and DHA, both n-3 fatty acids), essential amino acids, and other nutrients necessary for the growth and development of marine larvae, is widely used as an additive in aquaculture feeds (Herawati et al., 2014; Lestari et al., 2014; van Houcke et al., 2017). EPA play a crucial role in the growth and development of marine organisms, with diatoms, including *S. dohrnii*, particularly abundant in EPA compared to other marine microalgae (Ratnayake and Galli, 2009; Nodumo et al., 2018). The diatom *Odontella aurita* has been successfully cultured and marketed as a dietary supplement high in omega-3 fatty acids for several years. In cold environmental conditions, *O. aurita* contains 45% PUFAs and is rich in EPA, constituting up to 39% of its composition, similar to *S. dohrnii* (Pasquet et al., 2014). Under such conditions, biochemical processes are activated, stimulating the production of EPA and DHA. These fatty acids are synthesized through a series of desaturation and elongation reactions, as evidenced by previous studies on other diatoms and microalgae (Mimouni et al., 2003; Guihéneuf et al., 2013).

Furthermore, fish metabolize fatty acids with the highest efficiency in the order of PUFAs, followed by MUFAs and SAFs. As the chain length of MUFAs and SAFs increases, their absorption efficiency decreases (Xu et al., 2020). Our research revealed that *S. dohrnii* exhibited a substantial percentage of long-chain polyunsaturated fatty acids (LC-PUFAs, $>C_{18}$) at 49.15± 0.04% and a notable percentage of USFAs at 73.41± 0.06% in cold temperatures. Long-chain fatty acids were also lowest in both SFAs and MUFAs in cold temperatures. Despite variations in temperature conditions, the proportion of PUFAs remained consistently high, suggesting its suitability as fish bait, especially for marine species.

Nevertheless, sustaining controlled low temperatures for large-scale cultivation in factories proves financially burdensome. Additionally, at low temperatures, the biomass of algal cells experiences a significant reduction, negatively impacting the overall yield of algal lipids, particularly EPA and DHA. Our research indicated that temperature stress induces an elevation in total lipid content, especially TFA content, regardless of whether it is high or low temperature stress. This phenomenon occurs due to diatoms redirecting their carbon flux from polysaccharide chrysolaminarin (β-1,3-gluvan) utilization, a typical carbon sink under normal conditions (Kroth et al., 2008), toward lipid synthesis under stress conditions, storing them as TAG (Zulu et al., 2018). Our data indicated that under the culture conditions, EPA and DHA production in the low-temperature group amounted to 0.553 ± 0.01 $mg.DW.L^{-1}$ and 0.121 ± 0.01 $mg.DW.L^{-1}$, respectively. Conversely, in the high-temperature group, EPA content measured at 0.97 ± 0.01 $mg.DW.L^{-1}$ and DHA content at 0.264 ± 0.01 $mg.DW.L^{-1}$, both surpassing those in the low-temperature group. Moreover, water temperature significantly influences the normal reproduction and growth of bait organisms during high summer temperatures (Bao and You, 2004; Pasquet et al., 2014). Many aquatic seedling nursery processes experience the high-temperature period in summer, such as the seedlings of *Urechis unicinctus*. Consequently, the demand for live microalgae at this stage is high. However, the microalgae utilized struggle to survive under high-temperature and intense light conditions, leading to their decay. This results in an inadequate and untimely supply of microalgae, thereby causing potential problems in aquatic seeding production (Pasquet et al., 2014; Zhao et al., 2021). Hence, there's an urgent need to identify bait microalgae capable of stable growth at temperatures of 28°C and above, ensuring a reliable supply of microalgae during summer. Coupled with the aforementioned adaptive mechanism, it was found that *S.dorhnii* has the potential to adapt to high temperatures. With certain experimental conditions of stress, there may be a possibility to enhance the optimal temperature and tolerance without resorting gene editing. Through rapid evolutionary strategies, *S.dorhnii* might evolve into a source of high-temperature-tolerant aquatic microalgae during the summer period.

However, each of these feed microalgae has certain limitations (Chauton et al., 2015). At present, to enable large-scale commercial production of *S. dorhnii*, it is necessary to further enhance its fatty acid production capacity. A negative correlation between the optimal growth rate and lipid accumulation was observed at temperatures below the optimal range. To address this issue, a two-step culture method, in conjunction with the study of Roleda et al. (2013), can be employed.

Conclusions

Currently, the amount of lipids in *S. dohrnii* cultivated in the laboratory is not on par with that of other extensively produced aquatic microalgae. However, the increased proportion of EPA and DHA at lower temperatures suggests that temperature has a considerable influence on fatty acid concentration. Through additional exploration of various environmental factors, its potential as a source of aquatic microalgae could be further enhanced. In the future, the development of aquatic microalgae should involve considering the combination of different microalgae to maximize their individual benefits.

Data availability statement

The original contributions presented in the study are included in the article/supplementary material. Further inquiries can be directed to the corresponding authors.

Author contributions

XS: Writing – review & editing, Writing – original draft, Visualization, Supervision, Resources, Project administration, Methodology, Investigation, Conceptualization. YY: Writing – original draft, Investigation, Data curation. ZS: Writing – original draft, Investigation, Data curation. YZ: Writing – original draft, Investigation, Data curation. ZL: Writing – original draft,

Methodology, Investigation. JS: Supervision, Writing – review & editing, Resources, Conceptualization.

Funding

The author(s) declare financial support was received for the research, authorship, and/or publication of this article. This work was supported by the Natural Science Foundation of China (No. 42206087) and the National Key Research and Development Project of China (No. 2019YFC1407800).

Conflict of interest

Author ZL was employed by the company Tianjin Chenhui Modern Technology Group Co., Ltd.

The remaining authors declare that the research was conducted in the absence of any commercial or financial relationships that could be construed as a potential conflict of interest.

The author(s) declared that they were an editorial board member of Frontiers, at the time of submission. This had no impact on the peer review process and the final decision.

Publisher's note

References

Ahern, T. J., Katoh, S., and Sada, E. (1983). Arachidonic acid production by the red alga *Porphyridium cruentum*. *Biotechnol. Bioeng.* 25, 1057–1070. doi: 10.1002/bit.260250414

Armbrust, E. V. (2009). The life of diatoms in the world's oceans. *Nature* 459, 185–192. doi: 10.1038/nature08057

Bao, Y. B., and You, Z. J. (2004). Influences of several environmental factors on growth in marine shellfish larvae. *Fish. Sci.* 12, 39–41. doi: 10.16378/j.cnki.1003–1111.2004.12.012

Beal, C. M., Gerber, L. N., Thongrod, S., Phromkunthong, W., Kiron, V., Granados, J., et al. (2018). Marine microalgae commercial production improves sustainability of global fisheries and aquaculture. *Sci. Rep.* 8, 15064. doi: 10.1038/s41598–018-33504-w

Becker, E. W. (2003). "Microalgae in human and animal nutrition," in *Hand book of microalgal culture*. Ed. A. Richmond (Oxford, Blackwell), 312–351. doi: 10.1002/9780470995280.ch18

Bermudez, R., Feng, Y. Y., Roleda, M. Y., Tatters, A. O., Hutchins, D. A., Larsen, T., et al. (2015). Long-term conditioning to elevated pCO_2 and warming influences the fatty and amino acid composition of the diatom *Cylindrotheca fusiformis*. *PloS One* 10, e0123945. doi: 10.1371/journal.pone.0123945

Borowitzka, M. A., and Borowitzka, L. J. (1988). "Limits to growth and carotenogenesis in laboratory and large-scale outdoor cultures of *Dunaliella salina*," in *Algal Biotechnology*. Ed. T. Stadler (Elsevier Applied Science, Essex, UK), 371–381.

Bowler, C., Vardi, A., and Allen, A. E. (2010). Oceanographic and biogeochemical insights from diatom genomes. *Annu. Rev. Mar. Sci.* 2, 333–365. doi: 10.1146/annurev-marine-120308-081051

Boyd, P. W., Rynearson, T. A., Armstrong, E. A., Fu, F. X., Hayashi, K., Hu, Z. X., et al. (2013). Marine phytoplankton temperature versus growth responses from polar to tropical waters-Outcome of a scientific community-wide study. *PloS One* 8, e63091. doi: 10.1371/journal.pone.0063091

Chauton, M. S., Reitan, K. I., Norsker, N. H., Tveterås, R., and Kleivdal, H. T. (2015). A techno-economic analysis of industrial production of marine microalgae as a source of EPA and DHA-rich raw material for aquafeed: Research challenges and possibilities. *Aquaculture* 436, 95–103. doi: 10.1016/j.aquaculture.2014.10.038

Chen, Y. C. (2012). The biomass and total lipid content and composition of twelve species of marine diatoms cultured under various environments. *Food Chem.* 131, 211–219. doi: 10.1016/j.foodchem.2011.08.062

Cheng, L. M., Zhang, S. F., Xie, Z. X., Li, D. X., Lin, L., Wang, M. H., et al. (2022). Metabolic adaptation of a globally important diatom following 700 generations of selection under a warmer temperature. *Environ. Sci. Technol.* 56, 5247–5255. doi: 10.1021/acs.est.1c08584

Converti, A., Casazza, A. A., Ortiz, E. Y., Perego, P., and Del Borghi, M. (2009). Effect of temperature and nitrogen concentration on the growth and lipid content of *Nannochloropsis oculata* and *Chlorella vulgaris* for biodiesel production. *Chem. Eng. Process.: Process Intensification* 48, 1146–1151. doi: 10.1016/j.cep.2009.03.006

Davison, I. R. (1991). Environmental effects on algal photosynthesis: temperature. *J. Phycol.* 27, 2–8. doi: 10.1111/j.0022-3646.1991.00002.x

Depauw, F. A., Rogato, A., d'Alcalá, M. R., and Falciatore, A. (2012). Exploring the molecular basis of responses to light in marine diatoms. *J. Exp. Bot.* 63, 1575–1591. doi: 10.1093/jxb/ers005

Dong, H. P., Dong, Y. L., Cui, L., Balamurugan, S., Gao, J., Lu, S. H., et al. (2016). High light stress triggers distinct proteomic responses in the marine diatom *Thalassiosira pseudonana*. *BMC Genomics* 17, 994. doi: 10.1186/s12864-016-3335-5

Duarte, C. M. (2007). Marine ecology warms up to theory. *Trends Ecol. Evol.* 22, 331–333. doi: 10.1016/j.tree.2007.04.001

Falkowski, P. G., Barber, R. T., and Smetacek, V. (1998). Biogeochemical controls and feedbacks on ocean primary production. *Science* 281, 200–206. doi: 10.1126/science.281.5374.200

Field, C. B., Behrenfeld, M. J., James, T. R., and Falkowski, P. (1998). Primary production of the biosphere: Integrating terrestrial and oceanic components. *Science* 281, 237–240. doi: 10.1126/science.281.5374.237

Gao, X. Z., Jiang, X. M., and Ye, L. (2014). Effects of temperature, light intensity and salinity on the growth and fatty acid composition of *Skeletlnema munzelii* SM-1 and SM-2. *J. Biol.* 31, 64–70. doi: 10.3390/ijms17060817

Giudetti, A. M., Eleonora, S., Luisa, S., Gabriele, V. G., and Fabrizio, D. (2016). Nutritional and hormonal regulation of citrate and carnitine/acylcarnitine transporters: Two mitochondrial carriers involved in fatty acid metabolism. *International Journal of Molecular Sciences* 17 (6), 817. doi: 10.3390/ijms17060817

Gladue, R. M., and Maxey, J. E. (1994). Microalgal feeds for aquaculture. *J. Appl. Phycol.* 6, 131–141. doi: 10.1007/BF02186067

Gu, H., Zhang, X., Sun, J., and Luo, Z. (2012). Diversity and seasonal occurrence of *Skeletonema* (Bacillariophyta) species in Xiamen Harbour and surrounding seas, China. *Cryptogamie Algologie* 33, 245–263. doi: 10.7872/crya.v33.iss3.2012.245

Guihéneuf, F., Ulmann, L., Mimouni, V., and Tremblin, G. (2013). Use of radiolabeled substrates to determine the desaturase and elongase activities involved in eicosapentaenoic acid and docosahexaenoic acid biosynthesis in the marine microalga *Pavlova lutheri*. *Phytochemistry* 90, 43–49. doi: 10.1016/j.phytochem.2013.02.014

Harwood, J. L. (1988). Fatty acid metabolism. *Annu. Rev. Plant Physiol. Plant Mol. Biol.* 39, 101–138. doi: 10.1146/annurev.pp.39.060188.000533

Herawati, V. E., Hutabarat, J., and Radjasa, O. K. (2014). Nutritional Content of *Artemia* sp. Fed with *Chaetoceros calcitrans* and *Skeletonema costatum*. *HAYATI Journal of Biosciences*. 21, 4, 166–172. doi: 10.4308/hjb.21.4.166

IPCC (2018). *IPCC Special Report on Global warming of 1.5°C*. Eds. M. Allen, M. Babiker, Y. Chen, H. de Coninck, S. Connors, R. van Diemen, O. Dube, K. Ebi, F. Engelbrecht, M. Ferrat, J. Ford, P. Forster, S. Fuss, T. Guillén Bolaños, J. Harold, O. Hoegh-Guldberg, J. C. Hourcade, D. Huppmann and K. Zickfeld (Geneva: IPCC).

Jiang, H., and Gao, K. (2004). Effects of lowering temperature during culture on the production of polyunsaturated fatty acids in the marine diatom *Phaeodactylum tricornutum* (Bacillariophyceae). *J. Phycol.* 40, 651–654. doi: 10.1111/j.1529-8817.2004.03112.x

Jin, P., and Agustí, S. (2018). Fast adaptation of tropical diatoms to increased warming with trade-offs. *Sci. Rep.* 8, 17771. doi: 10.1038/s41598–018-36091-y

Kooistra, W., Gersonde, R., Medlin, I., and Mann, D. (2007). The origin and evolution of the diatoms: Their adaptation to a planktonic existence. *Evol. Primary Producers Sea*. 58 (11), 207–249. doi: 10.1016/B978-012370518-1/50012-6

Kroth, P. G., Chiovitti, A., Gruber, A., Martin-Jezequel, V., Mock, T., Parker, M. S., et al. (2008). A model for carbohydrate metabolism in the diatom *Phaeodactylum*

tricornutum deduced from comparative whole genome analysis. *PloS One* 3, e1426. doi: 10.1371/journal.pone.0001426

Laufkötter, C., Vogt, M., Gruber, N., Aita-Noguchi, M., Aumont, O., Bopp, L., et al. (2015). Drivers and uncertainties of future global marine primary production in marine ecosystem models. *Biogeosciences* 12, 6955–6984. doi: 10.5194/bg-12-6955-2015

Lestari, D. P., Ekawati, A. W., and Maftuch, M. (2014). Dried *Skeletonema costatum* in feed formulation for the growth of Vaname Shrimp (*Litopenaeus vannamei*). *J. Exp. Life Sci.* 4, 45–49. doi: 10.21776/ub.jels.2014.004.02.04

Liang, Y., Koester, J. A., Liefer, J. D., Irwin, A. J., and Finkel, Z. V. (2019). Molecular mechanisms of temperature acclimation and adaptation in marine diatoms. *ISME J.* 13, 2415–2425. doi: 10.1038/s41396-019-0441-9

Maia, I. B., Carneiro, M., Magina, T., Malcata, F. X., Otero, A., Navalho, J., et al. (2022). Diel biochemical and photosynthetic monitorization of *Skeletonema costatum* and *Phaeodactylum tricornutum* grown in outdoor pilot-scale flat panel photobioreactors. *J. Biotechnol.* 343, 110–119. doi: 10.1016/j.jbiotec.2021.11.008

Marella, T. K. , and Tiwari, A. (2020). Marine diatom *Thalassiosira weissflogii* based biorefinery for co-production of eicosapentaenoic acid and fucoxanthin. *Bioresour. Technol.* 307, 123245. doi: 10.1016/j.biortech.2020.123245

Mimouni, V., Ulmann, L., Tremblin, G., and Robert, J. M. (2003). Desaturation of linoleic acid in the marine diatom *Haslea ostrearia* Simonsen (Bacillariophyceae). *Cryptogamie Algol.* 24, 269–276.

Mishra, B., and Tiwari, A. (2021). Cultivation of *Anabena variabilis, Synechococcus elongatus, Spirulina platensis* for the production of C-Phycocyanin, C-Phycoerythrin and *Thalassiosira, Skeletonema, Chaetoceros* for fucoxanthin. *Syst. Microbiol. Biomanuf.* 1, 356–361. doi: 10.1007/s43393-020-00020-w

Murata, N., and Los, D. (1997). Membrane fluidity and temperature perception. *Plant Physiol.* 115, 875–879. doi: 10.1104/pp.115.3.875

Nodumo, N. Z., Krzysztof, Z., Katharina, V., and Ivo, F. (2018). Current trends to comprehend lipid metabolism in diatoms. *Prog. Lipid Res.* 70, 1–16. doi: 10.1016/j.plipres.2018.03.001

O'Donnell, D. R., Du, Z. Y., and Litchman, E. (2019). Experimental evolution of phytoplankton fatty acid thermal reaction norms. *Evol. Appl.* 12, 1201–1211. doi: 10.1111/eva.12798

Ogura, A., Akizuki, Y., Imoda, H., Mineta, K., Gojobori, T., and Nagai, S. (2018). Comparative genome and transcriptome analysis of diatom, *Skeletonema costatum*, reveals evolution of genes for harmful algal bloom. *BMC Genomics* 19, 765. doi: 10.1186/s12864-018-5144-5

Pasquet, V., Ulmann, L., Mimouni, V., Guihéneuf, F., Jacquette, B., Morant-Manceau, A., et al. (2014). Fatty acids profile and temperature in the cultured marine diatom *Odontella aurita*. *J. Appl. Phycol.* 26, 2265–2271. doi: 10.1007/s10811-014-0252-3

Quinn, P. J. (1981). The fluidity of cell membranes and its regulation. *Prog. Biophys. Mol. Biol.* 38, 1–104. doi: 10.1016/0079-6107(81)90011-0

Ratnayake, W. M. N., and Galli, C. (2009). Fat and fatty acid terminology, methods of analysis and fat digestion and metabolism: a background review paper. *Ann. Of Nutr. And Metab.* 55, 8–43. doi: 10.1159/000228994

Reitan, K. I., Rainuzzo, J. R., Øie, G., and Olsen, Y. (1997). A review of the nutritional effects of algae in marine fish larvae. *Aquaculture* 155, 207–221. doi: 10.1016/S0044-8486(97)00118-X

Renaud, S. M., Thinh, L. V., Lambrinidis, G., and Parry, D. L. (2002). Effect of temperature on growth, chemical composition and fatty acid composition of tropical Australian microalgae grown in batch cultures. *Aquaculture* 211, 195–214. doi: 10.1016/S0044-8486(01)00875-4

Renaud, S. M., Zhou, H. C., Parry, D. L., Thinh, L.-V., and Woo, K. C. (1995). Effect of temperature on the growth, total lipid content and fatty acid composition of recently isolated tropical microalgae *Isochrysis* sp., *Nitzschia closterium*, *Nitzschia paleacea*, and commercial species *Isochrysis* sp. (clone T.ISO). *J. Appl. Phycol.* 7, 595–602. doi: 10.1007/BF00003948

Roleda, M. Y., Slocombe, S. P., Leakey, R. J. G., Day, J. G., Bell, E. M., and Stanley, M. S. (2013). Effects of temperature and nutrient regimes on biomass and lipid production by six oleaginous microalgae in batch culture employing a two-phase cultivation strategy. *Bioresour. Technol.* 129, 439–449. doi: 10.1016/j.biortech.2012.11.043

Roy, S. S., and Pal, R. (2015). Microalgae in aquaculture: A review with special references to nutritional value and fish dietetics. *Proc. Zool. Soc.* 68, 1–8. doi: 10.1007/s12595-013-0089-9

Sales, R., Galafat, A., Vizcaíno, A. J., Sáez, M. I., Martínez, T. F., Cerón-García, M. C., et al. (2021). Effects of dietary use of two lipid extracts from the microalga *Nannochloropsis gaditana* (Lubián 1982) alone and in combination on growth and muscle composition in juvenile gilthead seabream, *Sparus aurata*. *Algal Res.* 53, 102–162. doi: 10.1016/j.algal.2020.102162

Sarker, P. K. (2023). Microorganisms in fish feeds, technological innovations, and key strategies for sustainable aquaculture. *Microorganisms* 11, 439. doi: 10.3390/microorganisms11020439

Sarker, P. K., Kapuscinski, A. R., Lanois, A. J., Livesey, E. D., Bernhard, K. P., and Coley, M. L. (2016). Towards sustainable aquafeeds: Complete substitution of fish oil with marine microalga *Schizochytrium* sp. improves growth and fatty acid deposition in Juvenile Nile Tilapia (*Oreochromis niloticus*). *PloS One* 11, e0156684. doi: 10.1371/journal.pone.0156684

Sarker, P. K., Kapuscinski, A. R., Vandenberg, G. W., Proulx, E., and Sitek, A. J. (2020). Towards sustainable and ocean-friendly aquafeeds: Evaluating a fish-free feed for rainbow trout (*Oncorhynchus mykiss*) using three marine microalgae species. *Elementa: Sci. Anthropocene* 8, 5. doi: 10.1525/elementa.404

Sepúlveda, J., and Cantarero, S. I. (2022). Phytoplankton response to a warming ocean. *Science* 376, 1378–1379. doi: 10.1126/science.abo5235

Shah, M. R., Lutzu, G. A., Alam, A., Sarker, P., Chowdhury, M. A. K., Parsaeimehr, A., et al. (2018). Microalgae in aquafeeds for a sustainable aquaculture industry. *J. Appl. Phycol.* 30, 197–213. doi: 10.1007/s10811-017-1234-z

Shevchenko, O. G., Ponomareva, A. A., Turanov, S., and Dutova, D. I. (2019). Morphological and genetic variability of *Skeletonema dohrnii* and *Skeletonema japonicum* (Bacillariophyta) from the northwestern Sea of Japan. *Phycologia*. 58 (1), 1–13. doi: 10.1080/00318884.2018.1517540

Sunda, W. G., Price, N. M., and Morel, F. M. (2005). Trace metal ion buffers and their use in culture studies. *Algal Culturing Techniques* 4, 35–63. doi: 10.1016/b978-012088426-1/50005-6

Thangaraj, S., Giordano, M., and Sun, J. (2020). Comparative proteomic analysis reveals new insights into the common and specific metabolic regulation of the diatom. *Front. Plant Sci.* 11, 578915. doi: 10.3389/fpls.2020.578915

Thangaraj, S., Shang, X. M., Sun, J., and Liu, H. J. (2019). Quantitative proteomic analysis reveals novel insights into intracellular silicate stress-responsive mechanisms in the diatom *Skeletonema dohrnii*. *Int. J. Mol. Sci.* 20, 2540. doi: 10.3390/ijms20102540

Thangaraj, S., and Sun, J. (2020). The biotechnological potential of the marine diatom *Skeletonema dohrnii* to the elevated temperature and pCO_2. *Mar. Drugs* 18, 259. doi: 10.3390/md18050259

Valenzuela-Espinoza, E., Millán-Núñez, R., and Núñez-Cebrero, F. (1999). Biomass production and nutrient uptake by Isochrysis aff. galbana (Clone T-ISO) cultured with a low cost alternative to the f/2 medium. *Aquacultural Engineering* 20 (3), 145–147. doi: 10.1016/S0144-8609(99)00011-4

van Houcke, J., Medina, I., Maehre, H. K., Cornet, J., Cardinal, M., Linssen, J., et al. (2017). The effect of algae diets (*Skeletonema costatum* and *Rhodomonas baltica*) on the biochemical composition and sensory characteristics of Pacific cupped oysters (*Crassostrea gigas*) during land-based refinement. *Food Res. Int.* 100, 151–160. doi: 10.1016/j.foodres.2017.06.041

Velasquez, S. F., Chan, M. A., Abisado, R. G., Traifalgar, R. F. M., Tayamen, M. M., Maliwat, G. C. F., et al. (2016). Dietary Spirulina (*Arthrospira platensis*) replacement enhances performance of Juvenile Nile tilapia (*Oreochromis niloticus*). *J. Appl. Phycol.* 28, 1023–1030. doi: 10.1007/s10811-015-0661-y

Xu, H. G., Giovanni, M. T., David, S. F., Liang, M. Q., Thomas, S. M., Artur, R., et al. (2020). Are fish what they eat? A fatty acid's perspective. *Prog. Lipid Res.* 80, 101064. doi: 10.1016/j.plipres.2020.101064

Yamada, M., Katsuki, E., Otsubo, M., Kawaguchi, M., Ichimi, K., Kaeriyama, H., et al. (2010).). Species diversity of the genus *Skeletonema* (Bacillariophyceae) in the industrial harbor Dokai Bay, Japan. *J. Oceanogr.* 66, 755–771. doi: 10.1007/s10872-010-0062-4

Yi, Z., Xu, M., Di, X., Brynjolfsson, S., and Fu, W. (2017). Exploring valuable lipids in diatoms. *Front. Mar. Sci.* 4. doi: 10.3389/fmars.2017.00017

Zhao, D. H., Zhao, L. D., You, H., Qin, S., Wang, Y. S., and Jiao, X. D. (2021). Breeding and feeding characteristics of high-temperature-resistant strains of *Isochrysis galbana*. *Oceanol Limnol Sin.* 52, 206–212. doi: 10.11693/hyhz20200300091

Zhukova, N. V., and Aizdaicher, N. A. (1995). Fatty acid composition of 15 species of marine microalgae. *Phytochemistry* 39, 351–356. doi: 10.1016/0031-9422(94)00913-E

Zulu, N. N., Zienkiewicz, K., Vollheyde, K., and Feussner, I. (2018). Current trends to comprehend lipid metabolism in diatoms. *Prog. Lipid Res.* 70, 1–16. doi: 10.1016/j.plipres.2018.03.001

Zuo, R., Ai, Q., Mai, K., Xu, W., Wang, J., Xu, H., et al. (2012). Effects of dietary n-3 highly unsaturated fatty acids on growth, nonspecific immunity, expression of some immune related genes and disease resistance of large yellow croaker (*Larmichthys crocea*) following natural infestation of parasites (*Cryptocaryon irritans*). *Fish Shellfish Immunol.* 32, 249–258. doi: 10.1016/j.fsi.2011.11.005

frontiers | Frontiers in Marine Science

TYPE Original Research
PUBLISHED 07 June 2024
DOI 10.3389/fmars.2024.1402528

OPEN ACCESS

EDITED BY
Jingzhen Wang,
Beibu Gulf University, China

REVIEWED BY
Daniele Brigolin,
Università Iuav di Venezia, Italy
Gorka Bidegain,
University of the Basque Country, Spain

*CORRESPONDENCE
Yang Liu
Yangliu315@ouc.edu.cn

RECEIVED 17 March 2024
ACCEPTED 27 May 2024
PUBLISHED 07 June 2024

CITATION
Li C, Liu Y, Yin Z, Si Z, Li Q and Saitoh S-I (2024) Evaluation of the Pacific oyster marine aquaculture suitability in Shandong, China based on GIS and remote sensing. *Front. Mar. Sci.* 11:1402528. doi: 10.3389/fmars.2024.1402528

Evaluation of the Pacific oyster marine aquaculture suitability in Shandong, China based on GIS and remote sensing

Chunlin Li[1], Yang Liu[1]*, Zixu Yin[1], Zhangqi Si[1], Qi Li[2] and Sei-Ichi Saitoh[3]

[1]Deep Sea and Polar Fisheries Research Center, Ocean University of China, Qingdao, China, [2]Key Laboratory of Mariculture, Ministry of Education, Ocean University of China, Qingdao, China, [3]Arctic Research Center, Hokkaido University, Sapporo, Japan

The Pacific oyster (*Crassostrea gigas*) is a marine aquaculture species with rapid production growth in recent years. China accounts for nearly 90% of global production by 2021, especially in Shandong province. Evaluating suitability is crucial for ensuring the sustainable growth of Pacific oyster marine aquaculture and achieving a blue transition. This study developed a suitability evaluation model for Pacific oyster marine aquaculture using a Geographic Information System (GIS), Maximum Entropy (MaxEnt) model, remote sensing, and reanalysis data. A literature review and Analytic Hierarchy Process (AHP) were used to establish an evaluation model encompassing water quality, hydrology, climate and meteorology, and socioeconomic factors. The results showed that within a 20 km range of the Shandong coast, 49% of the area was highly suitable, 51% was moderately suitable, and the overall annual high score proportion (HSP) fluctuated around 50%, with higher suitability observed in the spring and autumn. The inner bays of the coastal areas (Laizhou, Rongcheng, Jimo) exhibited high suitability (HSP over 80%); in contrast, the offshore areas (Changdao, Rushan) farther from the coast had lower suitability and showed significant monthly variations. The result was consistent with the spatial distribution and temporal variation of Shandong's existing Pacific oyster marine aquaculture areas. The study also found that El Niño significantly impacts Rongcheng, Rushan, and Jimo during summer. We predicted an overall increase of suitability in the Shandong offshore areas under future climate change scenarios, with a more significant increase of suitability in the north. El Niño-Southern Oscillation (ENSO) influenced the concentration of parameters such as chlorophyll-a (Chl-a) and total suspended sediment (TSS) in the coastal waters through its impact on precipitation (Pr), resulting in suitability fluctuations.

KEYWORDS

pacific oyster, marine raft aquaculture, suitability evaluation, GIS, remote sensing, ENSO, climate change

1 Introduction

The Pacific oyster (*Crassostrea gigas*) (Thunberg, 1793) in GBIF Secretariat (2023) has been extensively introduced and expanded for marine aquaculture worldwide due to its high commercial value (Barillé et al., 2020). Since the 1990s, it's production in China has steadily increased, accounting for nearly 90% of the global production by 2021, and reaching 5.8377 million tonnes (FAO, 2022), significantly higher than in other countries. Shandong province is China's leading producer of Pacific oysters, accounting for 75.20% of the national production in 2018. The primary marine aquaculture method is raft aquaculture (Yu et al., 2008; China Fishery Statistical Yearbook, 2023), characterized by continuous immersion in seawater, rapid growth, high yield, low cost, easy management, and not being restricted by seabed sediment, allowing for mobility, so it is widely applied (Zou et al., 2021).

The continuous increases in Pacific oyster marine aquaculture production have created economic and social benefits but have also caused severe environmental impacts. High-density and repetitive marine aquaculture reduce water exchange capabilities (Wang et al., 2018; Huang et al., 2023), leading to biological sedimentation and nutrient enrichment (Forrest et al., 2009), and reducing ecological carrying capacity (Gao et al., 2020; Brito et al., 2023). This, in turn decreases the sustainability and per-area yield. On the other hand, the growing marine aquaculture industry needs to develop new areas with the potential, which have suitable environmental and socioeconomic conditions. This is essential to ensure the growth potential of Pacific oyster and avoid conflicts with other planned uses and economic benefits (Barillé et al., 2020). Therefore, suitability evaluation is essential for assessing existing marine aquaculture areas and identifying potential areas for sustainable expansion of Pacific oyster marine aquaculture.

Satellite remote sensing provides unrestricted, long-time series data with a high spatial and temporal resolution, capturing continuous changes in marine environments, and was introduced into marine aquaculture research as early as 1987 (Liu, 2021). Numerical models and data assimilation provide reanalysis and forecast data for historical and future periods. Suitability evaluation models based on Geographic Information Systems (GIS) and the Analytic Hierarchy Process (AHP) are practical tools for evaluating suitable areas. After the 1990s, the application of remote sensing and GIS in marine aquaculture site selection and evaluation gradually increased (Bacher et al., 2003; Radiarta et al., 2008, Radiarta et al, 2011; Saitoh et al., 2011; Cho et al., 2012; Liu et al., 2013, Liu et al, 2014; Aura et al., 2016; Snyder et al., 2017; Liu et al., 2020a). The Maximum Entropy (MaxEnt) model is a species distribution model (SDM) based on the principle of maximum entropy, first proposed in 2006 (Phillips et al., 2006; Yang et al., 2023), predicting potential habitable zones for species based on known distribution data and related environmental factors (Wang et al., 2023; Zhang et al., 2023; Wang et al., 2024). Additionally, MaxEnt can incorporate future climate prediction data, such as bioclimatic factors, making it an effective tool for assessing future suitability changes under climate change impacts (Liu et al., 2024a, Liu et al., 2024b).

Marine aquaculture suitability is influenced by climate change, such as single bivalve marine aquaculture systems in shallow coastal waters, being particularly vulnerable to gradual climate changes like El Niño-Southern Oscillation (ENSO). Climate change could cause environmental and meteorological shifts, which may reduce or increase marine aquaculture areas' in different regions. Choosing areas less affected by climate change is more beneficial for the long-term development of marine aquaculture than vulnerable areas (Saitoh et al., 2011; Liu et al., 2013, Liu et al, 2014; Liu et al., 2020a). Moreover, the intensity and frequency of regional extreme events such as Marine Heatwaves (MHWs), extreme precipitation and droughts, storms, and storm surges have increased, result in more significant impacts (Beniston et al., 2007). Future climate change will also affect marine aquaculture in estuaries (Brito et al., 2023). For example, mass mortality events of Pacific oyster worldwide during summer may be caused by MHWs that promote the proliferation, growth, and pathogenicity of pathogens (Yang et al., 2021), weakening the immune response of Pacific oyster (Green et al., 2019). Global warming is expected to lead to more intense and frequent occurrences of MHWs (Frölicher et al., 2018). Therefore, considering climate factors affecting Pacific oyster marine aquaculture, accurately assessing climate change impacts, adapting to climate change through appropriate management, and setting climate factor indicators tailored to local conditions are increasingly emphasized (FAO, 2022).

This study aims to (1) construct a suitability evaluation model for Pacific oyster marine aquaculture in offshore areas of Shandong, summarizing the spatial and temporal characteristics of suitability; (2) explore the impact of climate events such as ENSO and future climate change on suitability, and investigate the mechanisms of climate change impact; (3) provide management recommendations for Pacific oyster marine aquaculture.

2 Materials and methods

2.1 Study area

Shandong is bordered by the Bohai Sea and the Yellow Sea (Figure 1). It boasts a coastline spanning 3,345 km and shallow sea areas within a depth of 20 m, covering 29,731 km^2. This area accounts for 37% of the total area of the Bohai Sea and the Yellow Sea (Peoples Government of Shandong Province, 2023), making it highly suitable for marine aquaculture and has the most production of Pacific oysters in the world. The rivers in Shandong particularly the Yellow River, transport significant amounts of freshwater and sediment to the Bohai Sea, affecting the salinity, nutrient, and sediment concentration near the estuary (Zheng et al., 2021).

The offshore areas of Shandong are primarily influenced by the north Shandong coastal current, which originated from the Bohai Sea and flows eastward to the Yellow Sea eastward. This current runs parallel to the northern coastline of the Shandong peninsula, turning southward along the eastern coast before

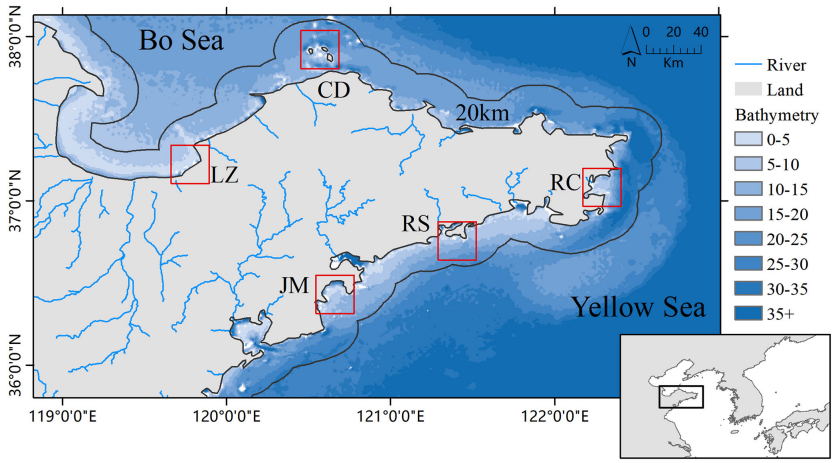

FIGURE 1
Study area. The 20 km line indicates the study area within 20 km of the Shandong coast as shown; Red box represents the existing main marine aquaculture areas for Pacific oyster, including Laizhou (LZ), Changdao (CD), Rongcheng Sanggou Bay (RC), Rushan (RS), and Jimo Aoshan bay (JM). The classify of blue color as in the legend indicates depth.

eventually moving southwestward along the southern coast of the Shandong peninsula. The north Shandong coastal current correlates well with wind speed (Zheng et al., 2021), becoming more pronounced in winter when northerly winds prevail (Zhang et al., 2018), causing sea level rise in LZ Bay (Li et al., 2015), and transporting large amounts of freshwater and sediment from the Yellow River eastward along the northern coast (Yang et al., 2011; Wang et al., 2020), resulting in low salinity and high turbidity in the coastal waters along the north coast of the Shandong Peninsula (Yang et al., 2011).

The climate of Shandong is controlled by the East Asian monsoon (Song et al., 2021). Winter winds are predominantly blow from the north while summer winds are predominantly southerly. This monsoonal climate is characterized by distinct seasons, higher summer temperatures with concentrated precipitation (60%–70%), with the temperature gradients increasing from the southeast coast to the northwest inland and precipitation patterns showing the opposite trend (Peoples Government of Shandong Province, 2023).

2.2 Data preprocessing

The environment, climate, meteorology, and socioeconomic data utilized in this study, along with their sources and resolutions, are listed in Table 1. To assess the spatiotemporal distribution of suitable areas for Pacific oyster marine aquaculture along the Shandong offshore, we acquired and processed monthly average data of factors from May 2011 to December 2022 and correlated these with climate events. The climate data used for future climate impact analysis, including its source, model, scenarios, time series, and resolution, are detailed in Table 1. Among them, 12 factors, including Chl-a, TSS, SST, DO, pH, SO, WW, Res, VO, WS, Tas, and Pr, have time series data from May 2011 to December 2022. Bathymetry, bioclimatic, distance to city, pier, and WWTPs lack time series data. Mean data will be used for both time series and climate scenarios.

The water quality factors considered in this study included chlorophyll-a (Chl-a), total suspended sediment (TSS), sea surface temperature (SST), dissolved oxygen concentration in seawater (DO), seawater pH reported on the total scale (pH), seawater salinity (SO). Chl-a and TSS data were obtained from the Geostationary Ocean Color Imager (GOCI) onboard the Korean geostationary orbit satellite. Their data were downloaded from the Korea Ocean Satellite Center (http://kosc.kiost.ac.kr/index.nm) with a resolution of 500 m for Level 1 data. The GOCI Data Processing System 2.0 (GDPS 2.0) software's Batch Process tool was used to calculate Chl-a and TSS bands. ENVI 5.3 software was used for geometric correction based on the official GLT files. After GOCI concluded its observation mission in March 2021, Chl-a and TSS data from April 2021 to December 2022 were obtained from the second Korean geostationary orbit satellite (GOCI-II). This study used Level 2 data with an initial resolution of 250 m. Monthly average data were computed using SeaDAS 8.0 software by selecting cloud-free data each month. SST data were sourced from the Moderate Resolution Imaging Spectroradiometer (MODIS) aboard NASA's AQUA sun-synchronous polar-orbiting satellite. Data were obtained from the Ocean Color website (https://oceancolor.gsfc.nasa.gov/) with a resolution of 1 km for Level 2 data. Daily data were filtered to minimize cloud cover impact, atmospheric data was corrected using the OCSSW tool in SeaDAS 8.0, and monthly averages were calculated using ArcGIS 10.7 with interpolation and other processing performed in SeaDAS. SO, DO, and pH were obtained from the E.U. Copernicus Marine Service Information (CMEMS) Marine Data Store (MDS).

Hydrological factors include bathymetry, water velocity (VO), and sea surface wind wave significant height (WW). Bathymetry data were sourced from the General Bathymetric Chart of the Oceans (GEBCO, https://www.gebco.net/), offering a global resolution of approximately

10.3389/fmars.2024.1402528

TABLE 1 Source and resolution of the data.

	Time series date		Mean date			
	May 2011—2020	2021—2022	History	2010–2040	2040–2070	2070–2100
Chl-a(mg/m^3)	COMS-GOCI L1B 500m	GK-2B-GOCI II L2 250m	History mean			
TSS(g/m^3)			History mean			
SST(°C)	MODIS-Aqua L2 1km		History mean	+0.6/+0.8	ORACLE 9km	
Bathymetry(m)	GEBCO 15”		History mean			
DO(mmol/m^3)	CMEMS 0.25°×0.25°		History mean			
pH			History mean			
SO(‰)	CMEMS 0.083°×0.083°		History mean		ORACLE v2.2 9km	
WW(m)	CMEMS 0.2°× 0.2°	CMEMS 0.083° × 0.083°	History mean			
VO(m/s)	CMEMS 0.083°×0.083°		History mean			
WS(m/s)	ECMWF 0.5°×0.5°		History mean			
Tas(°C)			History mean	+0.6/+0.8	+0.9/+1.5	+0.9/+3.5
Pr(mm)			History mean			
Bioclimatic	CHELSA Version 2.1 30’		CHELSA - 1981–2010 - 1km	CHELSA GFDL-ESM4 2011–2040 SSP126/585 1km	CHELSA GFDL-ESM4 2041–2070 SSP126/585 1km	CHELSA GFDL-ESM4 2071–2100 SSP126/585 1km
City	EULUC-China (Gong et al., 2020)		History mean			
Pier	POI		History mean			
WWTPs	HydroWASTE (Ehalt Macedo et al., 2022)		History mean			

15 arc seconds (500m). VO and WW were obtained from the CMEMS MDS. VO was calculated from the square root of the sum of the squares of the eastward and northward sea water velocities.

Meteorological data include wind speed at 10 m above the surface (WS), total precipitation (Pr), and 2-meter dewpoint temperature (Tas). They were sourced from the European Centre for Medium-Range Weather Forecasts’ ERA5 reanalysis monthly average data, these data were interpolated for missing values using MATLAB.

Climate data, the climate scenario data in 2010–2040 for SST and Tas are based on the projected temperature increases associated with the SSP1–2.6 and SSP5–8.5 mentioned in the sixth assessment reports of the Intergovernmental Panel on Climate Change (IPCC). The climate scenario data in 2040–2070, 2070–2100 for SST, Tas, and the future predictions for VO are sourced from the Biogeographic Oceanic and Regional Seas Environmental Predictive Model (Bio-ORACLE). Nineteen bioclimatic parameters (Karger et al., 2017) were derived from Climatologies at High resolution for the Earth’s Land Surface Areas (CHELSA), which offers high-resolution data (30 arc seconds, ~1 kilometer). We selected the GFDL-ESM4 model, the SSP1–2.6 and SSP5–8.5 scenarios in four periods: 1981–2010, 2011–2040, 2041–2070, and 2071–2100, these two scenarios can produce a more pronounced contrast to the suitability. The Oceanic Niño Index (ONI) and the Multivariate ENSO Index (MEI) (Wolter & Timlin, 2011) were used for climate events. ONI is available from NOAA’s Climate Prediction Center (https://origin.cpc.ncep.noaa.gov/products/analysis_monitoring/ensostuff/ONI_v5.php). The MEI can be obtained from NOAA’s Physical Sciences Laboratory (https://psl.noaa.gov/enso/mei/).

Socioeconomic data included the location of cities, piers, and wastewater treatment plants (WWTPs). Cities data were taken from global multi-temporal urban boundary data (Gong et al., 2020), which includes all global cities and surrounding settlements over 1 square kilometer, effectively capturing the contours of urban-rural edge areas. Pier data were extracted from coastal Points of Interest (POI) available in relevant map services. WWTP data came from the global database of HydroWASTE (Ehalt Macedo et al., 2022). Socioeconomic data on suitability distribution were obtained using the Euclidean Distance tool in ArcGIS 10.7.

All data were resampled to 500 m resolution using ArcGIS 10.7. Due to varying data sources, to ensure temporal continuity, 1000

random samples were generated within a 20 km range of the Shandong offshore using the ArcGIS10.7 Create Random Points tool to ensure temporal continuity. The relationship between datasets was quantified through linear fitting to ensure usability (Park et al., 2021) and consistency. Environmental (except Bathymetry) and meteorological data from May 2010 to December 2020 were statistically analyzed for the five Pacific oyster marine aquaculture areas and all offshore areas within 20 km of Shandong Peninsula to understand further the spatiotemporal variation characteristics of environmental and meteorological factors in Shandong.

2.3 Suitability distribution map and validation

Figure 2 illustrates the schematic diagram of the suitability evaluation model for Pacific oyster marine aquaculture, which primarily includes four categories of factors: water quality (Chl-a, SST, TSS, SO, pH, DO), hydrology (Bathymetry, VO, WW), climate and meteorology (WS, Tas, Pr, Bioclimatic), and socioeconomic factors (distance to city, pier, WWTPs). Each factor was assigned a score ranging from 1 to 8, with 1 representing the least suitable and 8 representing the most appropriate. The model employed the Analytic Hierarchy Process (AHP), a multi-criteria decision-making method proposed by American operations researcher Saaty in the early 1970s (Saaty, 1977), to determine the weights of each factor and each sub-model. The model utilizes ArcGIS 10.7 for Reclassify, Spatial Analyst, and Model Builder to enable batch processing of time series data, generating spatial distribution maps of suitability for Pacific oyster marine aquaculture. The ArcGIS raster calculator also calculated quarterly averages for all data from May 2011 to December 2022. A comparison was made between the highly suitable areas and the marine aquaculture areas identified through high-resolution satellite imagery (Wang et al., 2018; Liu et al., 2020b) to validate the accuracy of the model.

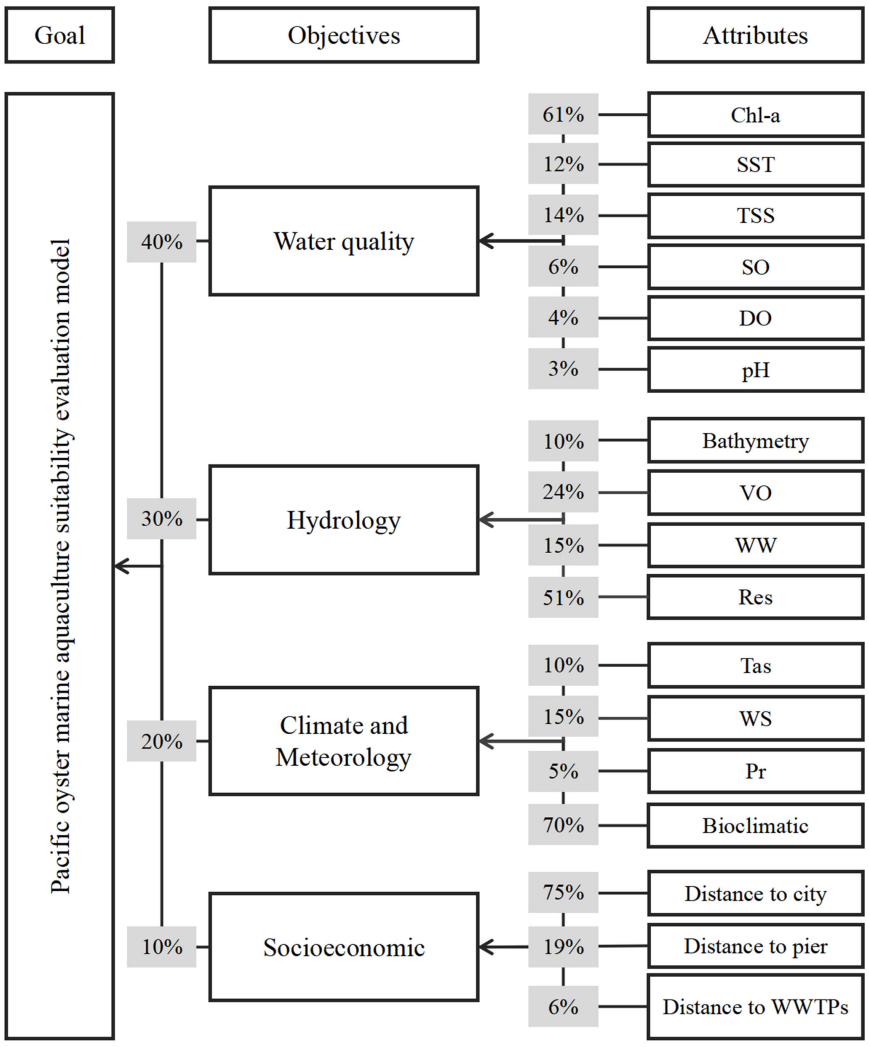

FIGURE 2
Suitability evaluation model of Pacific oyster marine aquaculture.

2.4 Pearson's correlation analysis

This study analyzed the impact of climate change on Pacific oyster marine aquaculture suitability from two aspects: the effects of climate events and the future climate change on suitability. Firstly, when investigating the influence of climate events such as El Niño on the suitability of Pacific oyster marine aquaculture, we compared the suitability of average years with El Niño (2015) and La Niña (2022) and utilized time series data from May 2011 to December 2022. We conducted Pearson correlation analysis and box plot analysis between time series data and the High Suitability Percentage (HSP), ONI, and MEI indices, with significance testing based on a significance level of 0.01 and 0.05 for t-tests. The causes of temporal and spatial variations in suitability were analyzed by combining existing research with correlation analysis results.

2.5 Prediction of future suitability based on MaxEnt

Mean data were used to investigate the impact of future climate change on suitability. Except for the predicted values and databases (SST, SO, Tas, Bioclimatic) shown in Table 1, all other data were based on the mean values from May 2011 to December 2022, including mean data, Bathymetry, Bioclimatic, distance to city, pier, WWTPs, as history and future periods date. Bioclimatic factors data were used with the MaxEnt model to predict suitable historical and future suitable zones. Pacific oyster distribution data were sourced from the Global Biodiversity Information Facility (GBIF) (GBIF, 2023). Due to insufficient data in the offshore area of Shandong, distribution data from the northwest Pacific region (117°E-146°E, 30°N-45°N) were used for suitable zone prediction, supplemented with *in-situ* oyster reef distribution area and wild Pacific oyster population sampling point data (Supplementary Table 1) from literature (Gu et al., 2005; Fang et al., 2007; Quan et al., 2012; Wang et al., 2014; Ran et al., 2018; Zhong et al., 2019; Li et al., 2020; Song et al., 2021; Zhang et al., 2021; Quan et al., 2022; Hong et al., 2023). ENMTools software was used to calculate spatial autocorrelation and exclude highly correlated (>0.8) features with a lower contribution, combining historical data for the MaxEnt model suitable zone prediction. The accuracy of the MaxEnt model was evaluated using the Area Under Curve (AUC) under the Receiver Operating Characteristic (ROC) Curve. The species' habitable probability obtained was graded to determine suitability distribution.

3 Result

3.1 Spatiotemporal distribution characteristics of time series factors in Shandong offshore

Figure 3A illustrated the changes in the monthly average and Figure 3B illustrated the quarterly spatial distribution of time series factors across different regions from May 2011 to December 2022. Chl-a and TSS exhibited similar spatial distribution patterns, with concentration gradually decreasing from the coast toward the open sea. In winter, the concentration of Chl-a was highest, while the lowest concentration was observed in summer. LZ had the highest Chl-a concentration, and CD had the lowest, yet all areas have Chl-a concentration above the 20 km average. In contrast, all areas had lower TSS concentrations than the 20 km average, except for JM, which had higher TSS concentrations in summer.

SST was highest in summer and lowest in winter, with minimal spatial variation and almost no inter-regional differences. LZ Bay experienced higher SST in spring, while the area near RC exhibited lower temperatures in summer. SO increased spatially from the coast toward the open sea, with LZ Bay exhibiting the lowest yearly SO but noticeable seasonal fluctuations, being higher in summer and lower in winter. The spatial and temporal pH variation was minimal, with slight differences among regions, and the entire Shandong offshore had a weakly alkaline pH. DO was higher in winter and spring but lower in summer and autumn, with LZ Bay having the highest winter DO concentration.

WW increased from the coast toward the open sea, with the lowest wave heights observed in summer. The CD region exhibited the most significant variation in WW, reflecting its location in the open sea. VO was more robust in winter and spring, with spatial differences in VO, which can identify the coastal currents in the Shandong offshore, and LZ had the lowest water flow across all years.

Pr and Tas followed similar seasonal patterns, with more rainfall in the south than in the north during spring and autumn, though regional differences were not pronounced, and CD had the least rainfall. WS showed minor spatial variation, with higher speed in summer and winter.

3.2 Pacific oyster marine aquaculture suitability evaluation model

Table 2 outlines the final evaluation model, with grading indicators determined based on existing research and the actual conditions of the Shandong offshore. This study set a high Chl-a concentration threshold detrimental to marine aquaculture at more than 5 mg/m^3 (Terauchi et al., 2014). However, the Chl-a concentration in the Shandong offshore did not exceed 3.17 mg/m^3. Therefore, in the grading indicators, the higher the Chl-a concentration, the higher the score. The grading indicators for TSS were based on the experimental levels: 0, 0.10, 0.25, and 0.5 g/L (Suedel et al., 2015a), with lower TSS concentrations receiving higher scores. SST in the Shandong offshore exhibited seasonal variations, with high summer temperatures causing mass mortalities of marine aquaculture oyster (Yang et al., 2021). The grading indicators for SST were based on the Arrhenius temperature of oyster (Van Der Veer et al., 2006). The grading indicators for SO were based on Wang et al (2023), with 25‰-35‰ representing the highest suitability, decreasing linearly outside this optimal range. The grading indicators for DO were based on the concentration needed for oyster reef restoration (Wang et al., 2023). The seawater pH in Shandong ranges from 7.9–8.2, showing minor

10.3389/fmars.2024.1402528

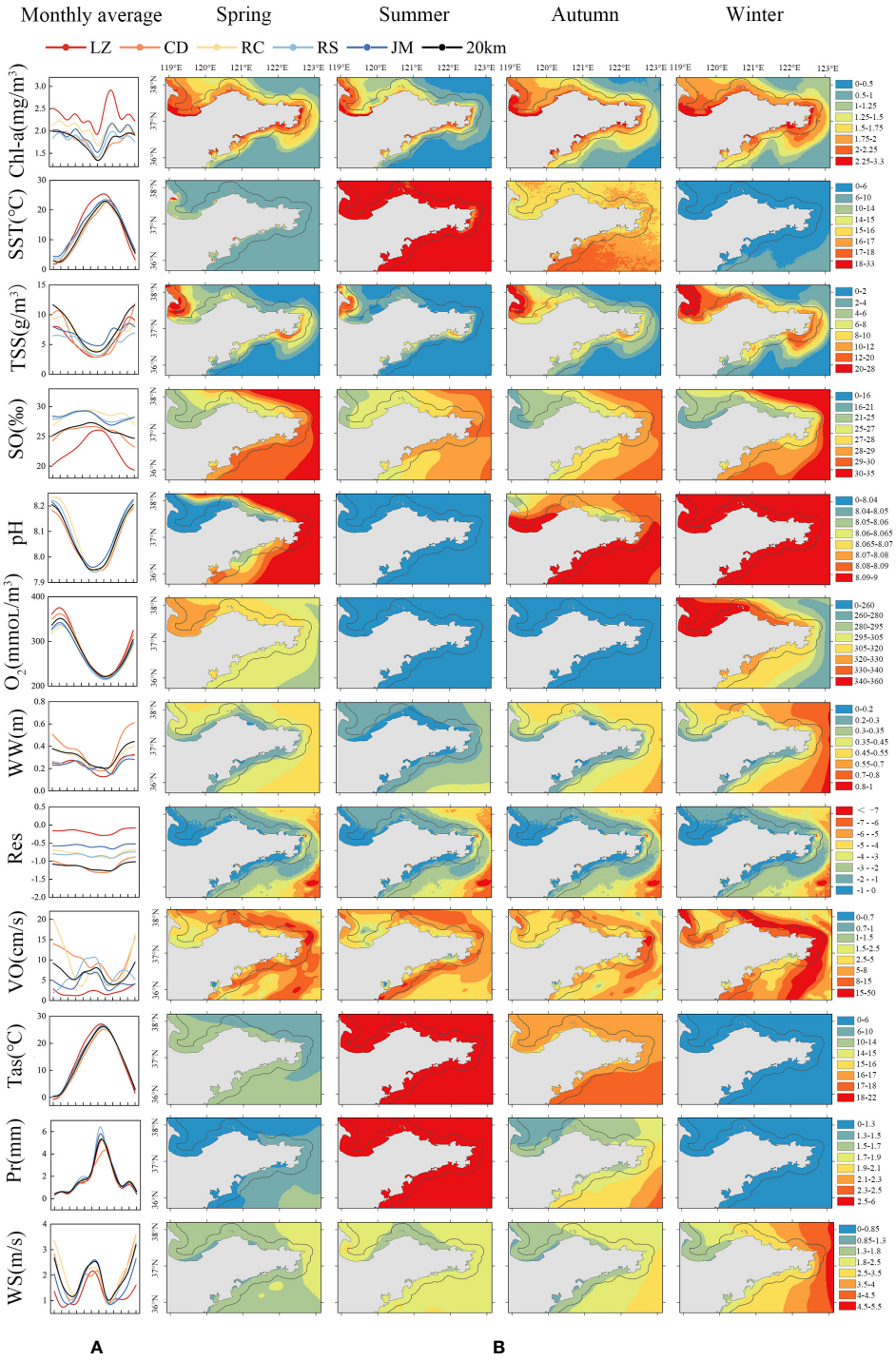

FIGURE 3
(A) Monthly average change of time series factors in Shandong offshore different areas from May 2011 to December 2022; **(B)** The quarterly change of spatial distribution for time series factors.

seasonal differences. The grading indicators were set that higher pH values indicate higher suitability.

As the depth increased from the coast toward the open sea in the Shandong offshore but did not overall exceed 20m, and VO did not exceed 20 cm/s (except in RC), the grading indicators were set that greater depth and water flow indicated higher suitability. The resuspension of seabed sediments caused by wind waves could also determine the best suitable area. For the resuspension effect, which had a critical depth (h < 10WW), we used WW-h/10 as a grading indicator. If the effects was harmful, it could not cause resuspension; if it was positive, it could cause resuspension and was considered a positive factor, providing more nutrients. However, waves could

TABLE 2 Each factor's weights and grading indicator.

Parameter		Suitability Score							
		1	2	3	4	5	6	7	8
Water quality 40%									
Chl-a(mg/m^3)	61%	0–0.2	0.2–0.4	0.4–0.6	0.6–0.8	0.8–1.0	1.0–1.2	1.2–1.4	>1.4
TSS(g/m^3)	14%	>8+	6–8	4–6	2–4	1–2	0.25–1	0.1–0.25	0.-0.1
SST(°C)	12%	0–0.5	0.5–2	2–4	4–7	7–10	10–13	13–16	16–21
		>32	29–32	27.25–29	25.75–27.25	24.5–25.75	23–24.5	21–23	
SO(‰)	6%	0–6	6–7.5	7.5–9	9–10.5	10.5–12	12–13.5	13.5–15	15–26
		>32	31–32	30–31	29–30	28–29	27–28	26–27	
DO(mmol/m^3)	4%	<264	264–270	270–276	276–282	282–288	288–294	294–300	>300
pH	3%	0–7	7–7.2	7.2–7.4	7.4–7.6	7.6–7.8	7.8–8	8–8.2	>8.2
Hydrology 30%									
Bathymetry(m)	10%	0–3	3–4	4–5	5–6	6–7	7–8	8–10	>10
Res	15%	<-7	-7 - -6	-6 - -5	-5 - -4	-4 - -3	-3 - -2	-2 - -1	-1 - 1
		>7	6 - 7	5 - 6	4 - 5	3 - 4	2 - 3	1 - 2	
WW(m)	51%	>0.7	0.6–0.7	0.5–0.6	0.4–0.5	0.3–0.4	0.2–0.3	0.1–0.2	0–0.1
VO(m/s)	24%	0–0.01	0.01–0.02	0.02–0.03	0.03–004	0.04–0.05	0.05–0.06	0.06–0.07	>0.07
Climate and Meteorology 20%									
WS(m/s)	15%	0–1	1–1.3	1.3–1.6	1.6–1.9	1.9–2.2	2.2–2.5	2.5–2.8	>2.8
Tas(°C)	10%	<-0.5	0.5–2	2–4	4–7	7–10	10–13	13–16	16–21
		>32	29–32	27.25–29	25.75–27.25	24.5–25.75	21–23	21–23	
Pr(mm)	5%	0	0–1	1–2	2–3	3–4	4–5	5–6	>6
Bioclimatic	70%	0–0.1	0.1–0.2	0.2–0.3	0.3–0.4	0.4–0.5	0.5–0.6	0.6–0.7	0.7–1
Socioeconomic 10%									
City(km)	75%	>18	16–18	14–16	12–14	10–12	8–10	6–8	0–6
Pier(km)	19%	>18	16–18	14–16	12–14	10–12	8–10	6–8	0–6
Waste(km)	6%	0–6	6–8	8–10	10–12	12–14	14–16	16–18	>18

negatively impact rafts, so a lower WW was considered better for suitability (Ogle et al., 1977; Goseberg et al., 2017).

WS was graded from less suitable to more suitable in an arithmetic sequence, as the average monthly WS in the Shandong offshore did not exceed 5 m/s, making its potential impact on marine aquaculture rafts relatively small. Tas had the same grading indicators as SST, based on the Arrhenius formula (Van Der Veer et al., 2006). Pr was graded from less suitable to more suitable in a linear relationship. After correlation analysis (Supplementary Figure 1) and contribution contrast (Supplementary Table 2), the bioclimatic factors finally selected include bio2 (mean diurnal range), bio5 (max temperature of the warmest month), bio8 (mean temperature of the wettest quarter), bio10 (mean temperature of the warmest quarter), bio14 (precipitation of the driest month), and bio16 (precipitation of the wettest quarter). The training and test set values for both historical and future periods were above 0.9 (Supplementary Figures 2, 6, 10, 14, 18, 22, 26), indicating good prediction results and high reliability. Response curves (Supplementary Figures 3, 7, 11, 15, 19, 23, 27), Variable contributions (Supplementary Tables 3, 4, 5, 6, 7, 8, 9) and jackknife test of variable importance (Supplementary Figures 4, 8, 12, 16, 20, 24, 28) of historical and future periods were in the Supplementary Material. The bioclimatic factors graded the habitability probability (Supplementary Figures 5, 9, 13, 17, 21, 25, 29) obtained from the MaxEnt model.

In practical production, factors related to oyster harvesting, such as storage, transportation, waste disposal, and maintaining a certain distance to piers equipped with specific equipment (marine aquaculture equipment and vessels), are necessary to ensure profitability; otherwise, costs become significantly higher (Liu et al., 2014). This is particularly challenging for individual farmers and small enterprises (Barillé et al., 2020). Proximity to

cities facilitates oyster transportation, processing, and sales. Our model incorporates socioeconomic factors that could quantify the specific impact of distance, such as distance to piers and cities. It also considers the negative impact of WWTPs, quantifying their impact on marine aquaculture activities using distance metrics. In socioeconomic factors, proximity to cities and piers indicated higher suitability, while proximity to WWTPs indicated lower suitability scores.

The weight value for each factor was obtained through a literature review and experts' opinions (Radiarta et al., 2008, Radiarta et al, 2011; Saitoh et al., 2011; Cho et al., 2012; Liu et al., 2013, 2014; Aura et al., 2016; Snyder et al., 2017; Barillé et al., 2020; Liu et al., 2020a; Jiang et al., 2022). Environmental factors such as SST, Chl-a, TSS, SO, DO, and Bathymetry were commonly considered. Socioeconomic factors, including distance to the city, piers, land-based facilities, and constraints like harbors, townships, industrial areas, and river mouths, were also considered in the evaluation model.

Compared to socioeconomic factors, environmental factors hold a higher weight. Among the environmental factors, water quality, such as SST, Chl-a, and TSS, carries a significant weight of 40%. Chl-a concentration reflects the biomass and productivity of phytoplankton in seawater and can indicate food availability (Xing et al., 2017). Furthermore, it has been found to have a significant positive correlation with oyster growth (Mizuta et al., 2012). Oysters tend to increase their feeding activity to a maximum level and stabilize, increasing Chl-a concentration within a specific range (Tenore and Dunstan, 1973). TSS can negatively impact oyster pumping and clearance rates (Loosanoff and Tommers, 1948; Suedel et al., 2015). SST is a crucial parameter influencing biological processes, and high summer temperatures can lead to mass mortality in oyster marine aquaculture (Yang et al., 2021). While Pacific oyster are euryhaline species, SO does not significantly affect their growth (Nell and Holliday, 1988). However, increased freshwater influx can result in rapid, short-term salinity reduction, limiting oyster growth (Swam et al., 2022). In the Shandong offshore area, the maximum SO does not exceed 30‰, and the LZ Bay exhibits the lowest SO due to extensive river inputs, necessitating consideration of SO variations. DO in coastal ecosystems is experiencing more significant fluctuations than other environmental variables, and seasonal hypoxia events are rising (Diaz, 2001). Considering the decrease in DO with increasing marine aquaculture density, this factor needs consideration, albeit with a lower weight (Brito et al., 2023). pH reduction can impede the growth of early life stages of oyster (Ko et al., 2014). The pH value of seawater in Shandong ranges from 7.9 to 8.2, with minimal seasonal variation, warranting a lower weight.

Hydrological factors are also crucial in influencing the growth and marine aquaculture of Pacific oyster, and they hold a weight of 30% in this model, relatively lower than water quality factors. Suspended particles influenced by WS and WW, such as Chl-a and TSS, exhibit good temporal consistency with the mass concentration and diffusion intensity. Wind and waves play a significant role in the spatial and temporal distribution and diffusion of suspended particles, including Chl-a and TSS (Liu and Wang, 2019). Hence, the weight assigned to Res is relatively higher. Deeper waters contribute to higher VO (10–20 cm/s), resulting in faster water renewal and more favorable nutrient conditions. These conditions affect the feeding physiology of oyster, leading to higher growth rates (Lee et al., 2017). Offshore wind and wave conditions, persistent wave action, and strong ocean currents can impact marine aquaculture facilities (Ogle et al., 1977).

Meteorological factors such as WS, Pr, and Tas are less commonly considered in suitability site selection studies for oyster marine aquaculture. These climate and meteorological factors do not directly impact marine aquaculture and carry a lower weight of 20%. However, they exhibit strong correlations with environmental factors. For example, Tas is related to SST, and the Res is caused by wind and waves, leading to changes in TSS concentration. Pr affects river flow rates, influencing factors such as SO and river nutrient inputs, which can impact Pacific oyster marine aquaculture.

Furthermore, meteorological factors directly reflect variations in these factors that can characterize climate changes and extreme weather events. Due to the lack of relevant data, this study considers fewer socioeconomic factors, weighing only 10%. Among the socioeconomic factors, city areas and piers with established infrastructure often carry a higher weight.

3.3 Quarterly variation in the spatial distribution of each sub-model and the final suitability scores

The quarterly variations in the spatial distribution of suitability for each sub-model in the Shandong offshore are shown in Figure 4. The results indicated that water quality and hydrology suitability in the Shandong offshore are suitable, with scores of 6 or above within the range. Water quality suitability decreases in the summer, while hydrological conditions are best in winter and spring. Compared to other areas, the water quality and hydrological conditions in LZ were relatively poorer. Climate suitability in Shandong is relatively low, exhibiting higher suitability only near the coast, which may be attributed to the limited availability of distribution data for wild Pacific oyster in the Shandong offshore.

Averaging 140 suitability distribution maps from May 2011 to December 2022, we obtained the final spatial suitability distribution (Figure 5A). The suitability scores were categorized into three levels: high suitability (scores of 6–8), medium suitability (scores of 4, 5), and low suitability (scores of 1–3). The HSP was 48% in 20 km, with all areas except CD (19%) having higher HSP than the overall 20 km level, including LZ (100%), RC (92%), RS (72%), and JM (100%). High scores in LZ all being score of 6.

The suitability distribution in RC Sanggou Bay (Figure 5B) was compared with high-resolution satellite imagery and the offshore marine aquaculture database obtained by Liu et al (Liu et al., 2020b) (Figure 5D). This database is based on Landsat 8 remote sensing images and object-oriented NDWI and edge feature extraction (Wang et al., 2018), along with manual interpretation methods, providing the spatial distribution of marine aquaculture within a 100 km range of China's offshore areas. The red areas in Figure 5C

10.3389/fmars.2024.1402528

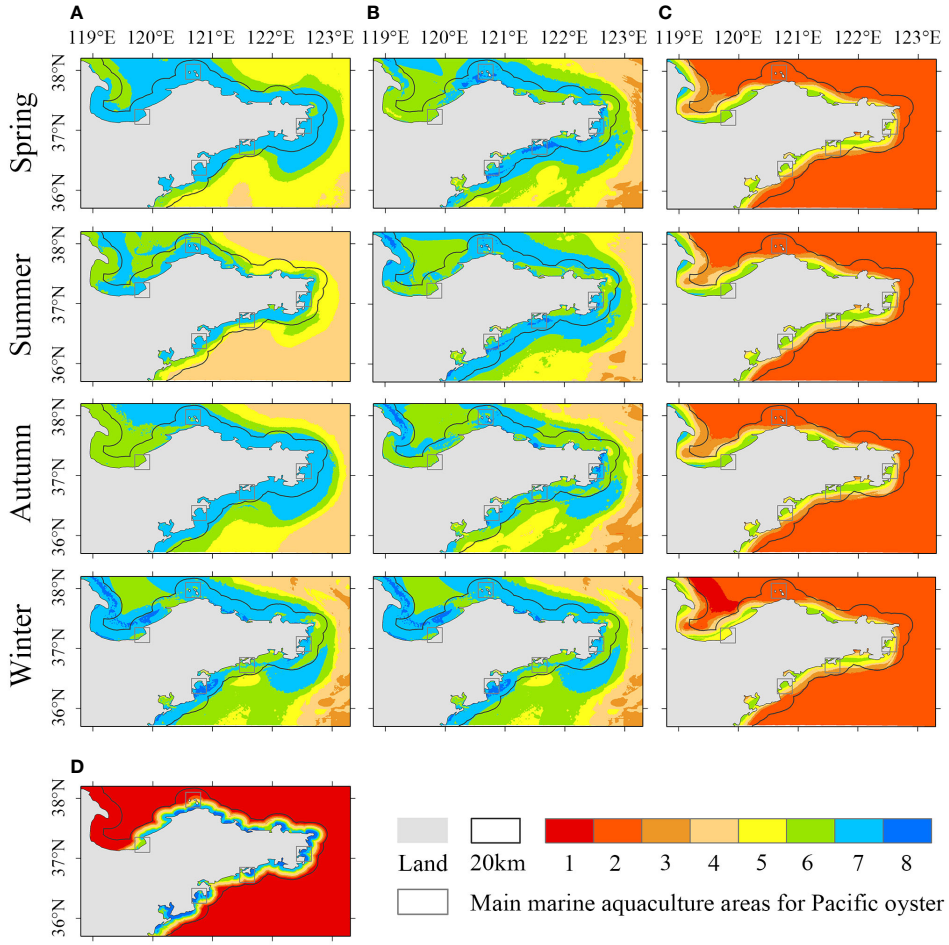

FIGURE 4
Quarterly variation of the spatial distribution of the suitability of each sub-model in Shandong coastal area: **(A)** Water quality; **(B)** Hydrology; **(C)** Climate and Meteorology; **(D)** Socioeconomic.

represented actual offshore marine aquaculture areas. In RC, the high suitability areas in spring, summer, and autumn matched the locations of rafts in this database, proving the accuracy of the evaluation model.

3.4 Monthly change in the spatial distribution of Pacific oyster marine aquaculture suitability

The monthly average change in the HSP (Figure 6B) showed that LZ (85.1%—100%), RC (87.16%—100%), and JM (80.39%—100%) maintained high suitability throughout the year (above 80%). The CD was more suitable in spring (March-May) but was lower than 20 km in other seasons. RS had lower suitability in summer (June-August), consistent with actual conditions, with minimal seasonal variation and HSP above 80% in other seasons. CD and RS exhibited more considerable monthly variation in suitability. Overall, the offshore areas within 20 km of Shandong had higher suitability in spring and autumn, with the annual HSP fluctuating around 50%. Spatially, the northern part of Shandong had higher suitability (Figure 6A).

3.5 Impact of ENSO on Pacific oyster marine aquaculture suitability

The time series of HSP from May 2011 to December 2022 (Figure 7A) indicated that summer (June-August) was the most susceptible to climate events. Comparing the spatial distribution of suitability in July of average years with El Niño and La Niña years (Figure 7B), the results showed a general decrease in suitability during El Niño years and an increase during La Niña years. LZ and CD were less affected by climate events. In contrast, RC, RS, and JM were more susceptible to climate events in summer, with a noticeable decrease in suitability (scores of 7) during El Niño years, and high HSP (scores 6–8) area expanded within the 20 km range during La Niña periods. The increase in suitability during La Niña could be related to positive anomalies of Chl-a forced by winds (Herrera-Cervantes et al., 2020).

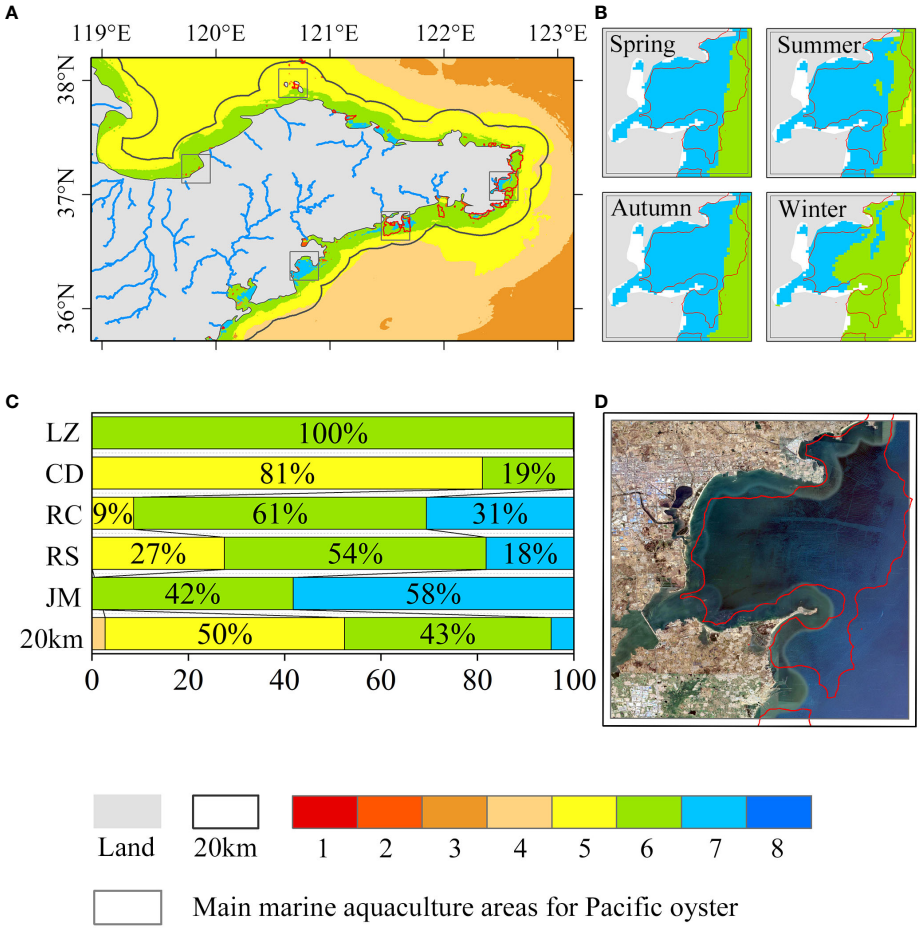

FIGURE 5
(A) Spatial distribution of final suitability; **(B)** Quarterly change of suitability spatial distribution in RC Sanggou Bay and comparison with the actual aquaculture area of offshore aquaculture database; **(C)** Proportion of suitability scores in each region; **(D)** High-resolution satellite imagery and the offshore marine aquaculture database (red area) obtained by Liu et al (Wang et al., 2018; Liu et al., 2020a).

3.6 Impact of future climate change on Pacific oyster marine aquaculture suitability

Figure 8 showed that under the SSP1–2.6 scenario, overall suitability in the Shandong offshore gradually increases in all future periods compared to the historical period. Under the SSP5–8.5 scenario, suitability initially increases and then decreases. However, the HSP (scores of 6–8) remains higher than the historical average, with a sharp decline in the proportion of the score of 7.

Our research indicated that future climate change impacts would increase suitability in the northern offshore of Shandong. Importantly, high suitability had remained stable at 100% in LZ, primarily with a score of 6. Furthermore, a suitability score of 7 increased under the SSP1–2.6 scenario and maintained the highest in the near term under the SSP5–8.5 scenario, later being surpassed by RC and RS in 2041–2070. This stability and high suitability would provide some reassurance in the face of potential climate change impacts.

4 Discussion

4.1 Development of the suitability evaluation model

The suitability evaluation model for Pacific oyster marine aquaculture develop in this study is applicable for assessing operations in the Shandong offshore area and can be adapted to suit the specific conditions of other regions as well. However, it is essential to note that there is still scope for further development of this model. Due to data limitations, this study considered a limited number of socioeconomic factors. When conducting suitability assessments, it is essential to take into account areas where marine aquaculture is prohibited or conflicts with existing activities, such as protected areas, net fishing, touristic traffic, commercial traffic, etc (Brigolin et al., 2017; Barillé et al., 2020; Porporato et al., 2020). Additionally, it is necessary to consider the infrastructure that can be integrated with marine aquaculture activities, such as offshore wind farms (Buck et al., 2008; Benassai et al., 2014; Di Tullio et al., 2018) and oil drilling platforms (Ogle

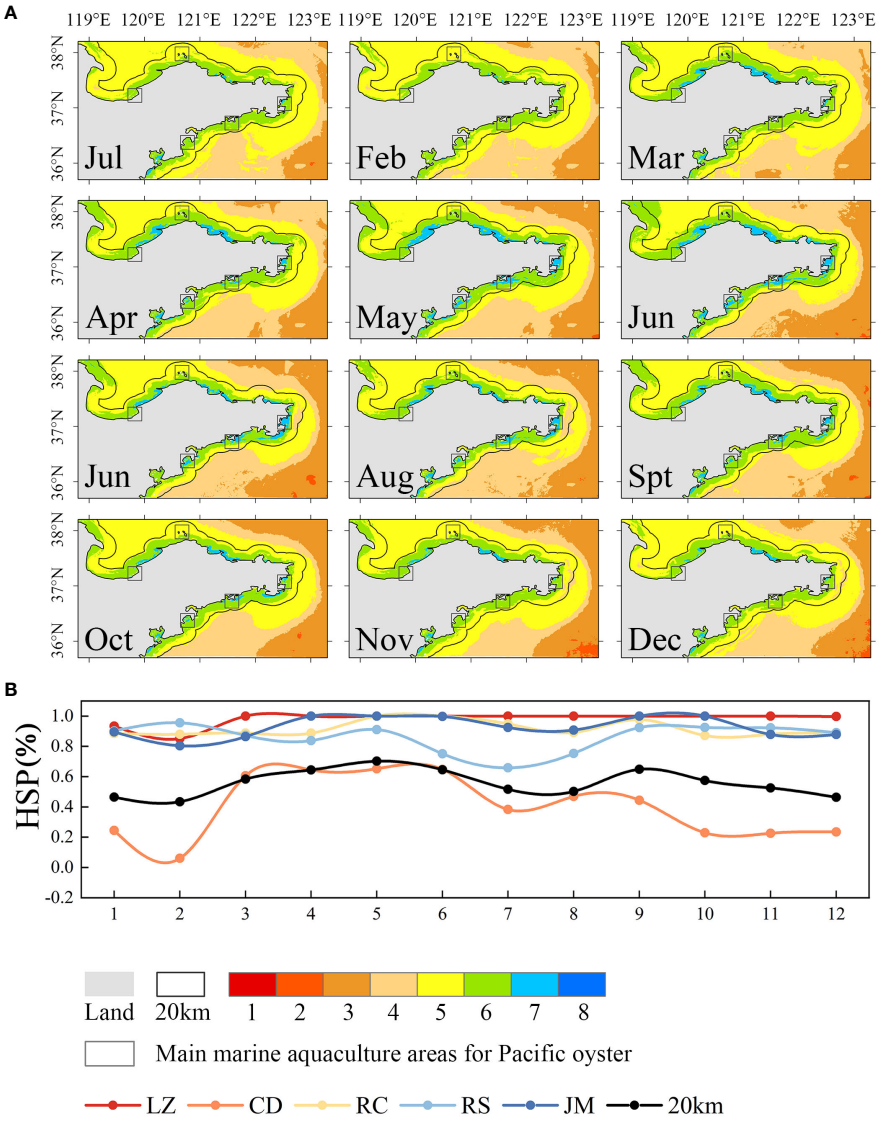

FIGURE 6
(A) Monthly change of the spatial distribution of suitability; **(B)** Monthly change of the HSP.

et al., 1977), which has been piloted and studied worldwide and may serve as potential areas for Pacific oyster marine aquaculture.

The MaxEnt model used in this study has demonstrated superior predictive accuracy compared to other species' geographic distribution models (Phillips et al., 2006; Wang et al., 2007). It has shown promising results even dealing with limited species distribution data (Hernandez et al., 2006), addressing the challenge of predicting species distributions with small sample sizes in marine environments. The application of MaxEnt in marine studies has witnessed rapid development (Hu et al., 2021; Hughes and King, 2024; Yang et al., 2024; Yati et al., 2024). In this study, due to the scarcity of wild Pacific oyster distribution data in the Shandong offshore area, we utilized available data (Supplementary Table 1) from the entire northwest Pacific region (117°E-146°E, 30° N-45°N) for prediction. However, this approach may lead to an expanded study scope and imbalanced species distribution data, potentially affecting the accuracy of the predictions (Soley-Guardia et al., 2024). Obtaining more species distribution data in future research will enhance the accuracy of MaxEnt predictions. Additionally, utilizing surrogate species with easily accessible data, can be employed to predict suitable habitats for species with insufficient survey data (Barata et al., 2024).

4.2 Correlation analysis of time series factors and suitability causes

Pearson correlation analysis of the time series data for each factor (Figure 9) explored their interactions and impact on suitability, categorizing the Pearson correlation coefficients into five levels: very strong (0.8–1.0), strong (0.6–0.8), moderate (0.4–0.6), weak (0.2–0.4), and very weak (0–0.2), and analyzed the correlation between HSP, ONI, and MEI with time series factor.

10.3389/fmars.2024.1402528

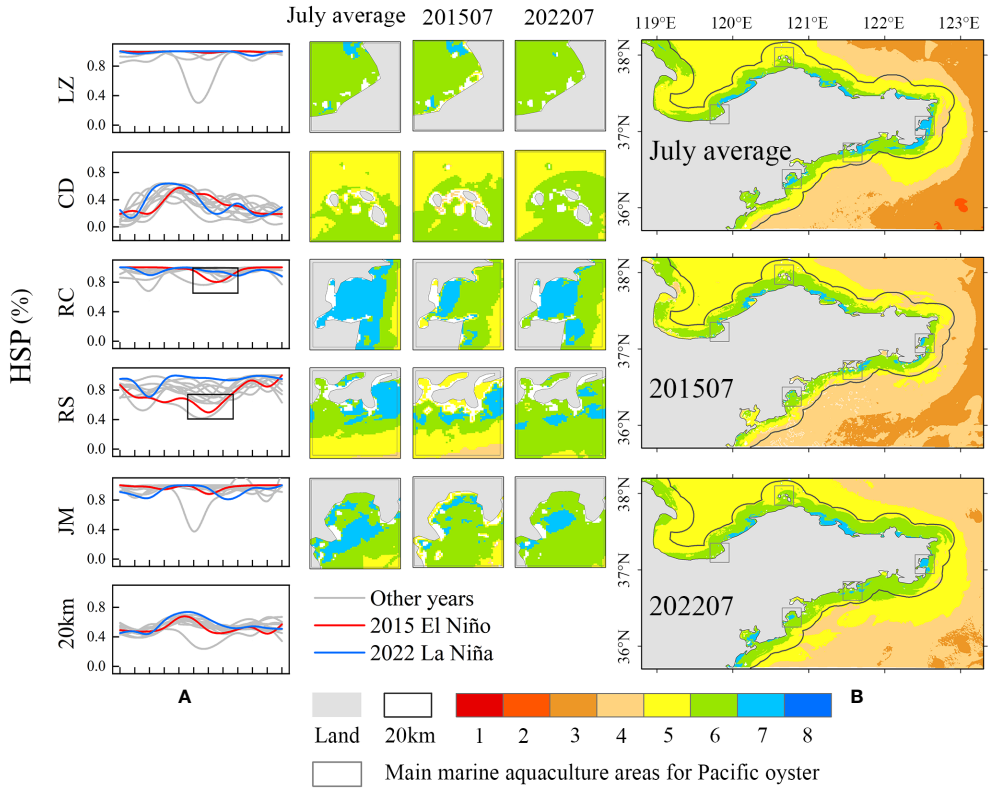

FIGURE 7
(A) The annual comparison of the HSP in each region, the red line represents the El Niño year, the blue line represents the La Nina year, the gray line indicates the other years; **(B)** The July average of each region, the comparison of the suitability spatial distribution of July in El Niño year (2015) and La Nina year (2022).

According to Pearson's correlation analysis, HSP is moderately positively correlated with Chl-a, TSS, and pH, weakly negatively correlated with WW, Res, WS, and SO, weakly positively correlated with Tas, and very weakly correlated with SST. The result indicated that suitability was mainly affected by Chl-a, TSS, and pH.

Although the analysis showed no direct correlation between HSP and climate indices, research indicated that climate events could impact suitability through factors like SST, wind speed (Liu et al., 2014), Pr, and Chl-a (Liu et al., 2014; Liu et al., 2020a). In this study, the MEI index was weakly negatively correlated with SO and Pr, only weakly negatively correlated with Pr in LZ. The ONI index was weakly negatively correlated with SO and showed a weaker negative correlation with Pr. The MEI index had a stronger correlation with each factor than the ONI index. It could serve as a better standard for determining whether suitability was affected by climate events.

Based on the above correlation analysis, the ENSO could cause more extreme changes in Pr. ENSO typically matures in winter and effects on subsequent summer precipitation in eastern China (Liu, 2021; Liu et al., 2024c). The difference between the suitability of Shandong marine aquaculture in El Niño and La Niña years (Figure 6B) reflects the asymmetry of their effects on precipitation (Liu et al., 2024c). Compared with La Niña, El Niño had a more noticeable impact on precipitation in Shandong (Guo et al., 2017).

Pr was weakly or more associated with all water quality factors except SO. The study showed that the increase in precipitation would increase the dissolved inorganic nitrogen and inorganic phosphorus of semi-enclosed bay seawater through the way of atmospheric settlement and runoff input, thereby causing an increase in Chl-a (Han et al., 2023; Xiao et al., 2024) and TSS (Meng et al., 2022; Ma et al., 2024), the Pr negatively associated with Chl-a and TSS concentration, which may result from more summer precipitation diluting Chl-a and TSS in seawater.

Additionally, the increase in freshwater flow caused by precipitation may lead to a rapid decrease in seawater salinity in the short term (Swam et al., 2022); precipitation changes may further lead to other factors affecting the suitability. For example, the correlation between Pr and water quality factors in LZ was small, and the suitability was mainly affected by the Chl-a concentration. The Chl-a concentration remained high and changed less in a year, which was less affected by ENSO and had high stability.

4.3 Outlier changes of time series factors under the influence of ENSO

According to the correlation analysis, Figure 10 showed a boxplot analysis of time series factors and the HSP The graph visually showed the distribution of outliers of time series factors; among them, SST, DO, Res, and pH, Tas had no outliers. SO, WW,

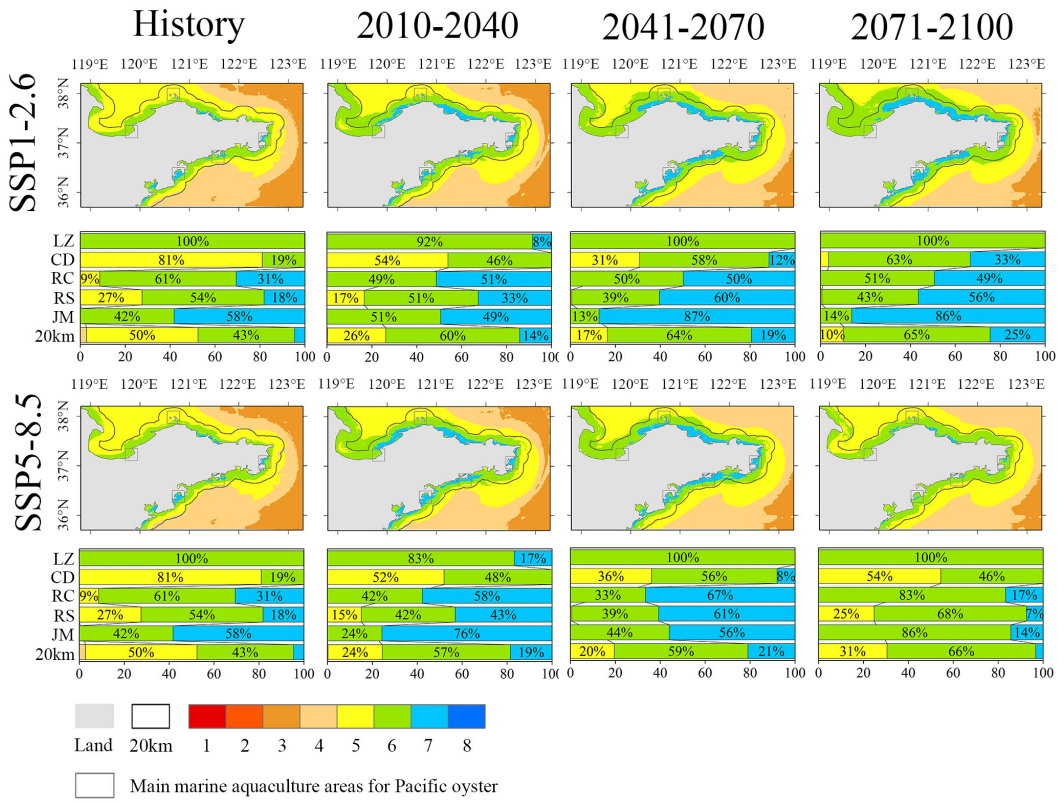

FIGURE 8
Percentage difference in the spatial distribution of suitability in the historical period between the SSP1–2.6 and the SSP5–8.5 scenario.

VO, and WS had fewer outliers and differences across regions, and ENSO was less likely to cause outlier changes by larger spatiotemporal scales. Chl-a, TSS, and Pr had more outliers in all regions, and they strongly correlate with the HSP and the climate index. This suggested that the appearance of outliers may be due to ENSO, Chl-a had many low values, TSS had many high values, Pr had many high values, and HSP declining more, which was consistent with the above correlation.

El Niño was classified based on the Oceanic Niño Index (ONI) values: weak (+0.5°C to +0.9°C), moderate (+1.0°C to +1.8°C), and high (greater than +1.8°C), represented by shades of red from light to deep. La Niña classifications were similarly based on ONI values: weak (-0.5°C to -0.9°C), moderate (-1.0°C to -1.8°C), and high (less than -1.8°C), represented by shades of blue from light to deep in Figure 11.

Combining the correlation analysis and the boxplot analysis, we calculated the difference of Chl-a, TSS, Pr, and HSP between the monthly average from May 2011 to December 2022 to contrast the occurrence of outliers with the occurrence ENSO. We observed that the abnormal increase in Pr generally occurred in the summer of the second year following the La Niña event (Wang et al., 2000) in 2011, 2012, 2017, 2020, and 2022. However, Pr did not increase significantly during El Niño events. During the development period of El Niño, Pr decreased in East Asia, whereas Pr increased during the decline period of El Niño (Cao et al., 2017).

Chl-a consistently showed low values in the summer, It had declined in the summer following La Niña events in 2011, 2012, 2018, and 2021, consistent with Pr being affected by climate events. In addition, El Niño also had an impact on Chl-a. During the strong El Niño year of 2015, RS and JM showed low values, with an overall decline in December 2018. The reduction in Chl-a concentration during that period may be due to the resuspension caused by wind and waves (Liu and Wang, 2019) rather than precipitation; During the strong El Niño of 2015, East Asian summer winds weakened (Liren et al., 1997), result in weak resuspension and thus low Chl-a concentration, these two factor have weakly positively correlation.

TSS exhibited outliers during the autumn and winter seasons of the ENSO events, for example, an unusual increase in LZ in 2011 and in different areas in 2016, 2020, and 2022. The mature phase of ENSO typically occurs during the northern winter and is accompanied by the weaker-than-average winter winds along the East Asian coast (Liren et al., 1997). Consequently, the weakened resuspension did not result in an increased TSS concentration, and the Pr did not decrease significantly during this time. Although there was no correlation between the SST and the climate index in this study, SST in the Shandong offshore was strongly negatively associated with TSS and had a moderate negative correlation with Chl-a. The results indicated that the changes of SST will also affect the concentration of Chl-a and TSS, but the specific mechanism still requires further study. We found a sizeable abnormal decrease in Chl-a concentration in the summer of 2014, which led to the reduction of HSP, this phenomenon may be due to data processing and still needs further research.

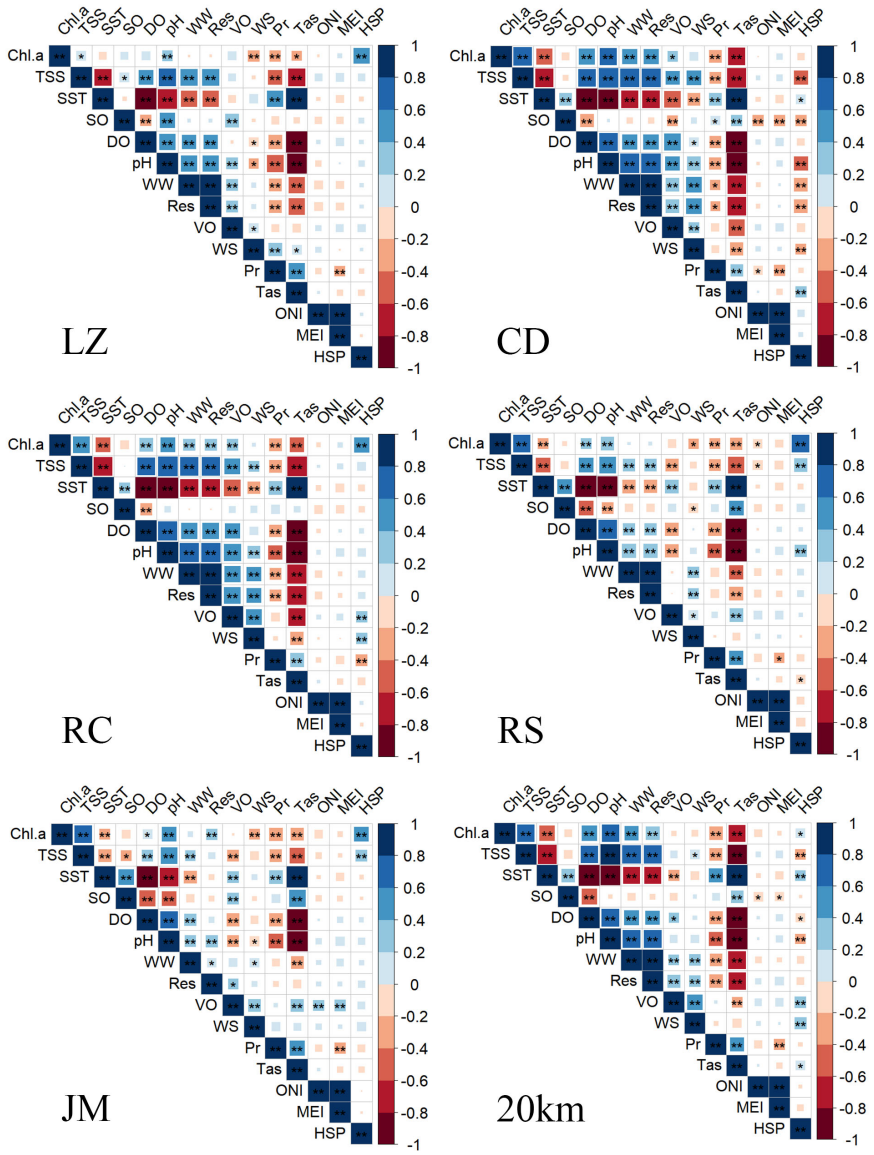

FIGURE 9
Pearson correlation analysis of time series factors and ONI, MEI, HSP in each regions. * Correlation is significant at the 0.05 level. ** Correlation is significant at the 0.01 level.

4.4 Management suggestions for Pacific oyster marine aquaculture development

Due to the favorable water quality and hydrological conditions, the Shandong offshore maintained a high suitability in approximately 50% of the region throughout the year. LZ, RC, and JM exhibit exceptionally high suitability (over 80%), making them ideal for developing Pacific oyster marine aquaculture. It was recommended to increase the aquaculture scale in high-suitability areas (LZ, RC, and JM) while reducing it in low-suitability areas (CD, RS) to avoid issues such as the declining sustainability of existing marine aquaculture environments (Forrest et al., 2009; Wang et al., 2018; Gao et al., 2020; Brito et al., 2023; Huang et al., 2023). Simultaneously, it is crucial to closely monitoring factors related to suitability, such as Chl-a, TSS, and pH. Furthermore, based on the results of a suitability evaluation and monthly variations, it was possible to relocate aquaculture operations across multiple marine regions. For instance, Pacific oyster marine aquaculture could be conducted in CD during spring, while RS can be avoided during summer.

The existing RC, RS, and JM marine aquaculture areas are susceptible to ENSO. Therefore, during the summer following El Niño and La Niña events, it is necessary to monitor abnormal weather conditions, especially abnormal rainfall, and develop appropriate response measures, such as reducing the density and scale of Pacific oyster marine aquaculture. Moreover, in JM and RC, which have high suitability but are susceptible to climate events, Pacific oyster could be integrated into an Integrated Multi-Trophic Aquaculture (IMTA) system (Shpigel and Blaylock, 1991; Jiang et al., 2013). This approach could enhance the carrying capacity and

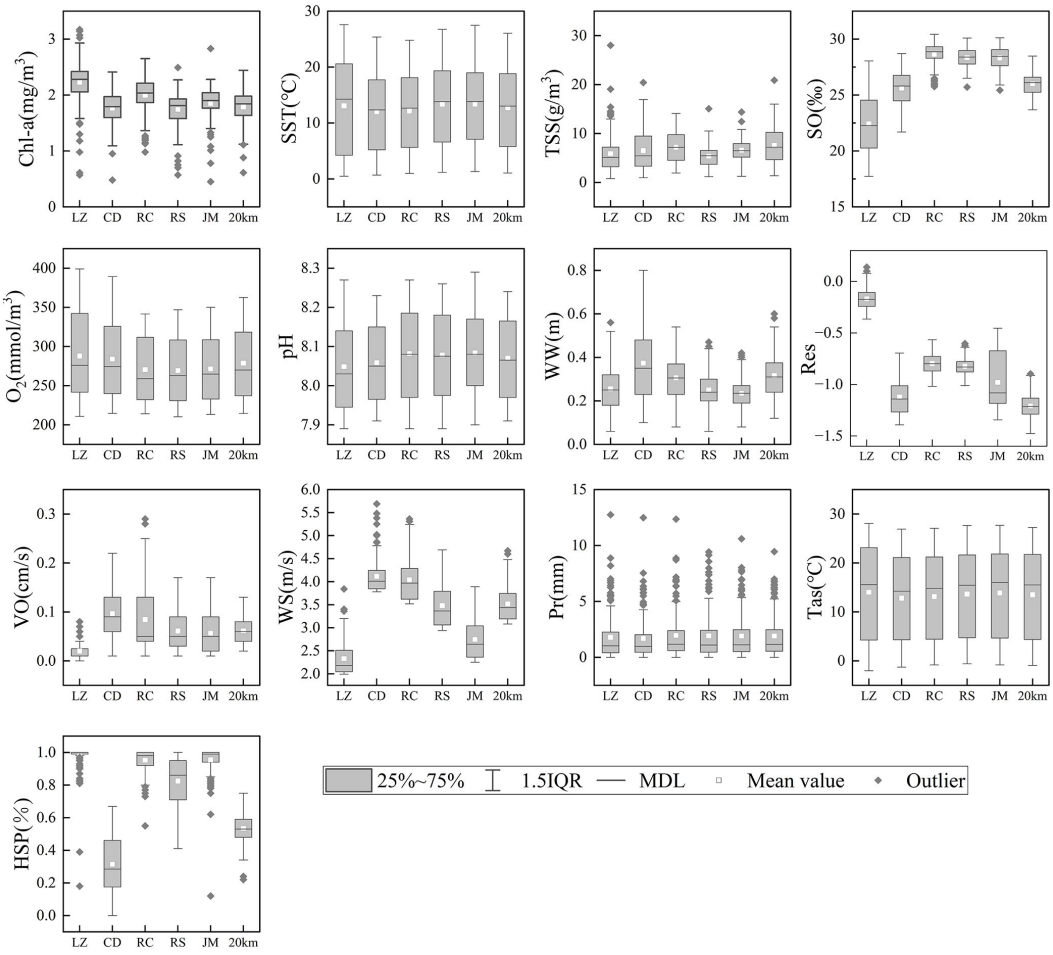

FIGURE 10
Boxplot of the time series factors and the HSP from May 2011 to December 2022.

stability of the marine aquaculture ecosystem while also adapting to climate change (Ahmed and Glaser, 2016) and ensuring system sustainability (Khanjani et al., 2022).

Future climate change may increase the suitability in open sea, providing opportunities for the Pacific oyster marine aquaculture. Specifically, the spring in CD exhibits higher suitability, with hydrological conditions similar to those in winter (Figure 4B), which may contribute to higher growth rates (Lee et al., 2021). In the future, marine aquaculture in open sea areas with increased suitability could help mitigate the impacts of climate change on bivalve aquaculture systems (Walker et al., 2006; Froehlich et al., 2018). One of the challenges open sea areas faces is their susceptibility to meteorological conditions, which can impact marine aquaculture infrastructure. Pacific oyster's marine aquaculture can be integrated with future offshore structures and platforms, such as offshore wind farms (Buck et al., 2008; Benassai et al., 2014; Di Tullio et al., 2018) and oil drilling platforms (Ogle et al., 1977). These developments have created new opportunities for Pacific oyster marine aquaculture. Some research is underway to explore integrating physical and biological conditions for the site selection of these co-located systems.

Furthermore, from 2070 to 2100 under the SSP5–8.5 scenario, except for LZ, the suitability for aquaculture significantly decreased, indicating that suitability did not exhibit a continuous upward trend and necessitates ongoing assessment. LZ maintained a stable suitability throughout the ENSO and future climate change scenarios, making it suitable for long-term marine aquaculture of Pacific oyster.

5 Conclusion

This study employed the Analytic Hierarchy Process (AHP) in conjunction with Geographic Information Systems (GIS) and the Maximum Entropy Model (MaxEnt) to construct an evaluation model for assessing the suitability of Pacific oyster marine aquaculture. The model incorporated various factors, including water quality (Chl-a, TSS, SST, SO, DO, pH), hydrology (bathymetry, VO, WW), climate and meteorology (WS, Pr, Tas, Bioclimatic), and socioeconomic factors (distance to city, pier, WWTPs). The resulting suitability distribution map revealed that 49% of the area was highly suitable (scores of 6–8), while 51% was moderately suitable (scores of 4–5), with higher suitability observed during the spring and autumn seasons. In the offshore areas, the inner bays (LZ, RC, JM) exhibited exceptionally high suitability

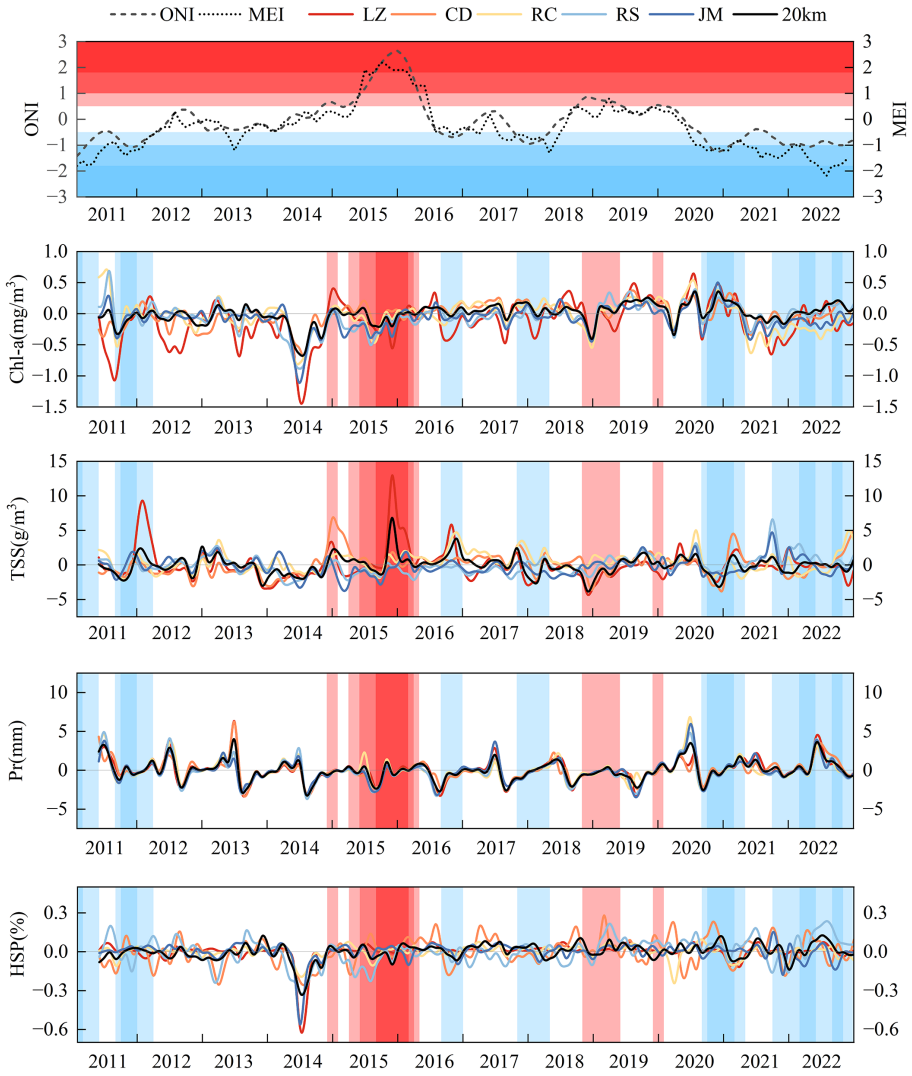

FIGURE 11
Time series of Chl-a, TSS, Pr, and HSP in different regions between May 2011 and December 2022.

(over 80%), while the open sea (CD, RS) farther from the coast showed lower suitability with noticeable monthly variations. The spatial and temporal distribution of suitability aligned with the actual Pacific oyster marine aquaculture areas in the coastal waters of Shandong Province, and the high suitability regions correspond to the actual distribution areas of marine aquaculture rafts, validating the accuracy of the evaluation model.

This study revealed that El Niño-Southern Oscillation (ENSO) decreases suitability during the summer in the southern part of Shandong, including RC, RS, and JM. Correlation analysis indicated that Chl-a, TSS, and pH are the primary factors influencing the suitability of marine aquaculture in the coastal waters of Shandong Province, while Pr and SO exhibit strong correlations with climate indices. ENSO affected Pr in Shandong, subsequently influencing water quality factors such as Chl-a and TSS offshore and altering the suitability of Pacific oyster marine aquaculture. Overall, the suitability for Pacific oyster marine aquaculture in the Shandong offshore is projected to increase with future climate change, but the increase is more pronounced in the northern regions. Finally, considering the temporal and spatial variations in the suitability of Pacific oyster marine aquaculture in Shandong offshore and their susceptibility to climate influences, management recommendations were proposed for current and future Pacific oyster marine aquaculture development.

Data availability statement

The original contributions presented in the study are included in the article/Supplementary Material. Further inquiries can be directed to the corresponding author.

Author contributions

CL: Data curation, Formal analysis, Validation, Visualization, Methodology, Writing – original draft. YL: Conceptualization, Data

curation, Supervision, Funding acquisition, Validation, Investigation, Visualization, Methodology, Project administration, Writing – review & editing. ZY: Data curation, Writing – review & editing. ZS: Data curation, Writing – review & editing. LQ: Writing – review & editing. S-IS: Writing – review & editing, Methodology.

Funding

The author(s) declare financial support was received for the research, authorship, and/or publication of this article. This work was financially supported by the Natural Science Foundation of China (No. 41976210).

Conflict of interest

The authors declare that the research was conducted in the absence of any commercial or financial relationships that could be construed as a potential conflict of interest.

The author(s) declared that they were an editorial board member of Frontiers, at the time of submission. This had no impact on the peer review process and the final decision.

Publisher's note

Supplementary material

The Supplementary Material for this article can be found online at: https://www.frontiersin.org/articles/10.3389/fmars.2024.1402528/full#supplementary-material

References

Ahmed, N., and Glaser, M. (2016). Can "Integrated Multi-Trophic Aquaculture (IMTA)" adapt to climate change in coastal Bangladesh? *Ocean Coast. Manage.* 132, 120–131. doi: 10.1016/j.ocecoaman.2016.08.017

Aura, C. M., Saitoh, S.-I., Liu, Y., Hirawake, T., Baba, K., and Yoshida, T. (2016). Implications of marine environment change on Japanese scallop (Mizuhopecten yessoensis) aquaculture suitability: a comparative study in Funka and Mutsu Bays, Japan. *Aquaculture Res.* 47, 2164–2182. doi: 10.1111/are.12670

Bacher, C., Grant, J., Hawkins, A. J. S., Fang, J., Zhu, M., and Besnard, M. (2003). Modelling the effect of food depletion on scallop growth in Sungo Bay (China). *Aquat. Living Resour.* 16, 10–24. doi: 10.1016/S0990–7440(03)00003–2

Barata, I. M., Uhlig, V. M., Cortês, L. G., Fath, F., and Griffiths, R. A. (2024). Overcoming the lack of distribution data for range-restricted habitat specialist frogs. *Austral Ecol.* 49, e13522. doi: 10.1111/aec.13522

Barillé, L., Le Bris, A., Goulletquer, P., Thomas, Y., Glize, P., Kane, F., et al. (2020). Biological, socio-economic, and administrative opportunities and challenges to moving aquaculture offshore for small French oyster-farming companies. *Aquaculture* 521, 735045. doi: 10.1016/j.aquaculture.2020.735045

Benassai, G., Mariani, P., Stenberg, C., and Christoffersen, M. (2014). A Sustainability Index of potential co-location of offshore wind farms and open water aquaculture. *Ocean Coast. Manage.* 95, 213–218. doi: 10.1016/j.ocecoaman.2014.04.007

Beniston, M., Stephenson, D. B., Christensen, O. B., Ferro, C. A. T., Frei, C., Goyette, S., et al. (2007). Future extreme events in European climate: an exploration of regional climate model projections. *Climatic Change* 81, 71–95. doi: 10.1007/s10584–006-9226-z

Brigolin, D., Porporato, E. M. D., Prioli, G., and Pastres, R. (2017). Making space for shellfish farming along the Adriatic coast. *ICES J. Mar. Sci.* 74, 1540–1551. doi: 10.1093/icesjms/fsx018

Brito, A. C., Pereira, H., Picado, A., Cruz, J., Cereja, R., Biguino, B., et al. (2023). Increased oyster aquaculture in the Sado Estuary (Portugal): How to ensure ecosystem sustainability? *Sci. Total Environ.* 855, 158898. doi: 10.1016/j.scitotenv.2022.158898

Buck, B. H., Krause, G., Michler-Cieluch, T., Brenner, M., Buchholz, C. M., Busch, J. A., et al. (2008). Meeting the quest for spatial efficiency: progress and prospects of extensive aquaculture within offshore wind farms. *Helgol Mar. Res.* 62, 269–281. doi: 10.1007/s10152–008-0115-x

Cao, Q., Hao, Z., Yuan, F., Su, Z., Berndtsson, R., Hao, J., et al. (2017). Impact of ENSO regimes on developing- and decaying-phase precipitation during rainy season in China. *Hydrology Earth System Sci.* 21, 5415–5426. doi: 10.5194/hess-21–5415-2017

China Fishery Statistical Yearbook (2023). *Bureau of fisheries* (Beijing: Chinese Ministry of Agriculture).

Cho, Y., Lee, W.-C., Hong, S., Kim, H.-C., and Kim, J. B. (2012). GIS-based suitable site selection using habitat suitability index for oyster farms in Geoje-Hansan Bay, Korea. *Ocean Coast. Manage.* 56, 10–16. doi: 10.1016/j.ocecoaman.2011.10.009

Crassostrea gigas (Thunberg, 1793) in GBIF Secretariat (2023) *GBIF backbone taxonomy*. Available online at: https://doi.org/10.15468/39omei (Accessed May 5, 2024).

Di Tullio, G. R., Mariani, P., Benassai, G., Di Luccio, D., and Grieco, L. (2018). Sustainable use of marine resources through offshore wind and mussel farm co-location. *Ecol. Model.* 367, 34–41. doi: 10.1016/j.ecolmodel.2017.10.012

Diaz, R. J. (2001). Overview of hypoxia around the world. *J. Environ. Quality.* 30, 275–281. doi: 10.2134/jeq2001.302275x

Ehalt Macedo, H., Lehner, B., Nicell, J., Grill, G., Li, J., Limtong, A., et al. (2022). Distribution and characteristics of wastewater treatment plants within the global river network. *Earth System Sci. Data* 14, 559–577. doi: 10.5194/essd-14–559-2022

Fang, E., Li, W., and Yu, J. (2007). Sustainable use of live oyster reef in bohai gulf. *Modern Fishery Inf.* 11), 12–14. doi: 10.3969/j.issn.1004–8340.2007.11.003

FAO (2022). "The state of world fisheries and aquaculture 2022," in *Towards blue transformation* (FAO, Rome). doi: 10.4060/cc046len

Forrest, B. M., Keeley, N. B., Hopkins, G. A., Webb, S. C., and Clement, D. M. (2009). Bivalve aquaculture in estuaries: Review and synthesis of oyster cultivation effects. *Aquaculture* 298, 1–15. doi: 10.1016/j.aquaculture.2009.09.032

Froehlich, H. E., Gentry, R. R., and Halpern, B. S. (2018). Global change in marine aquaculture production potential under climate change. *Nat. Ecol. Evol.* 2, 1745–1750. doi: 10.1038/s41559–018-0669–1

Frölicher, T. L., Fischer, E. M., and Gruber, N. (2018). Marine heatwaves under global warming. *Nature* 560, 360–364. doi: 10.1038/s41586–018-0383–9

Gao, Y., Fang, J., Lin, F., Li, F., Li, W., Wang, X., et al. (2020). Simulation of oyster ecological carrying capacity in Sanggou Bay in the ecosystem context. *Aquacult Int.* 28, 2059–2079. doi: 10.1007/s10499–020-00576–3

Gong, P., Chen, B., Li, X., Liu, H., Wang, J., Bai, Y., et al. (2020). Mapping essential urban land use categories in China (EULUC-China): preliminary results for 2018. *Sci. Bull.* 65, 182–187. doi: 10.1016/j.scib.2019.12.007

Goseberg, N., Chambers, M. D., Heasman, K., Fredriksson, D., Fredheim, A., and Schlurmann, T. (2017). ""Technological approaches to longline- and cage-based aquaculture in open ocean environments,"," in *Aquaculture perspective of multi-use sites in the open ocean*. Eds. B. H. Buck and R. Langan (Springer International Publishing, Cham), 71–95. doi: 10.1007/978–3-319–51159-7_3

Green, T. J., Siboni, N., King, W. L., Labbate, M., Seymour, J. R., and Raftos, D. (2019). Simulated marine heat wave alters abundance and structure of vibrio populations associated with the pacific oyster resulting in a mass mortality event. *Microb. Ecol.* 77, 736–747. doi: 10.1007/s00248–018-1242–9

Gu, Y., Qi, D., Ge, Y., Yu, R., and Zhang, R. (2005). Ecological evaluation and conservation of oyster reefs in Xiaomiaohong tidal channel in Jiangsu Coast. *Mar. Sci.* 03), 42–47. doi: 10.3969/j.issn.1000–3096.2005.03.010

Guo, F., Bi, W., Guo, F., and Wang, J. (2017). Interannual climate variabillity in shandong and its relationship with ENSO. *Oceanologia Limnologia Sin.* 48, 465–474. doi: 10.11693/hyhz20161100266

Han, H., Xiao, R., Gao, G., Yin, B., Liang, S., and lv, X. (2023). Influence of a heavy rainfall event on nutrients and phytoplankton dynamics in a well-mixed semi-enclosed bay. *J. Hydrology* 617, 128932. doi: 10.1016/j.jhydrol.2022.128932

Hernandez, P. A., Graham, C. H., Master, L. L., and Albert, D. L. (2006). The effect of sample size and species characteristics on performance of different species distribution modeling methods. *Ecography* 29, 773–785. doi: 10.1111/j.0906–7590.2006.04700.x

Herrera-Cervantes, H., Lluch-Cota, S. E., Cortés-Ramos, J., Farfán, L., and Morales-Aspeitia, R. (2020). Interannual variability of surface satellite-derived chlorophyll concentration in the bay of La Paz, Mexico, during 2003–2018 period: The ENSO signature. *Cont. Shelf Res.* 209, 104254. doi: 10.1016/j.csr.2020.104254

Hong, X., Cheng, J., Li, Q., Wu, S., Yan, J., and Shi, H. (2023). An experimental study on dissipating effect of double-layer oyster reefs in Binzhou coastal seawater. *Trans. Oceanology Limnology* 45, 106–111. doi: 10.13984/j.cnki.cn37–1141.2023.04.014

Hu, W., Zhang, D., Chen, B., Liu, X., Ye, X., Jiang, Q., et al. (2021). Mapping the seagrass conservation and restoration priorities: Coupling habitat suitability and anthropogenic pressures. *Ecol. Indicators.* 129, 107960. doi: 10.1016/j.ecolind.2021.107960

Huang, Y., Li, Z., Sun, C., Feng, Z., Li, J., Wei, D., et al. (2023). Using the roughness height and manning number in hydrodynamic model to estimate the impact of intensive oyster aquaculture by floating & fixed rafts on water exchange with an application in Qinzhou Bay, China. *Ecol. Model.* 476, 110230. doi: 10.1016/j.ecolmodel.2022.110230

Hughes, C., and King, J. W. (2024). Maximum entropy modelling to identify optimal locations for an IMTA system comprising Sparus aurata, Mytilus galloprovincialis and Ulva rigida on Europe's Atlantic coastline. *Aquat. Living Resour.* 37, 4. doi: 10.1051/alr/2024002

Jiang, B., Boss, E., Kiffney, T., Hesketh, G., Bourdin, G., Fan, D., et al. (2022). Oyster aquaculture site selection using high-resolution remote sensing: A case study in the gulf of maine, United States. *Front. Mar. Sci.* 9. doi: 10.3389/fmars.2022.802438

Jiang, Z., Wang, G., Fang, J., and Mao, Y. (2013). Growth and food sources of Pacific oyster Crassostrea gigas integrated culture with Sea bass Lateolabrax japonicus in Ailian Bay, China. *Aquacult Int.* 21, 45–52. doi: 10.1007/s10499–012-9531–7

Karger, D. N., Conrad, O., Böhner, J., Kawohl, T., Kreft, H., Soria-Auza, R. W., et al. (2017). Climatologies at high resolution for the earth's land surface areas. *Sci. Data.* 4, 170122. doi: 10.1038/sdata.2017.122

Khanjani, M. H., Zahedi, S., and Mohammadi, A. (2022). Integrated multitrophic aquaculture (IMTA) as an environmentally friendly system for sustainable aquaculture: functionality, species, and application of biofloc technology (BFT). *Environ. Sci. pollut. Res.* 29, 67513–67531. doi: 10.1007/s11356–022-22371–8

Ko, G. W. K., Dineshram, R., Campanati, C., Chan, V. B. S., Havenhand, J., and Thiyagarajan, V. (2014). Interactive effects of ocean acidification, elevated temperature, and reduced salinity on early-life stages of the pacific oyster. *Environ. Sci. Technol.* 48, 10079–10088. doi: 10.1021/es501611u

Lee, Y.-J., Kang, H. Y., Lee, W. C., and Kang, C.-K. (2017). Hydrodynamic effects on growth performance of the pacific oyster crassostrea gigas cultured in suspension in a temperate bay on the coast of korea. *Estuaries Coasts* 40, 1551–1565. doi: 10.1007/s12237–017-0252-z

Lee, J.-Y., Marotzke, J., Bala, G., Long, C., Corti, S., Dunne, J. P., et al. (2021)Future global climate: scenario-based projections and near-term informationin *Climate change 2021: the physical science basis. Contribution of working group I to the sixth assessment report of the intergovernmental panel on climate change* (Cambridge University Press, Cambridge).

Li, J., Shang, Z., Chen, Y., Tian, L., Jiang, X., Wang, F., et al. (2020). Research status and protection suggestions on oyster reef in Bohai Bay. *Geological survey Res.* 43, 317–333. doi: 10.3969/j.issn.1672–4135.2020.04.003

Li, Y., Wolanski, E., and Zhang, H. (2015). What processes control the net currents through shallow straits? A review with application to the Bohai Strait, China. *Estuarine Coast. Shelf Sci.* 158, 1–11. doi: 10.1016/j.ecss.2015.03.013

Liren, J., Sun, S., Arpe, K., and Bengtsson, L. (1997). Model study on the interannual variability of Asian winter monsoon and its influence. *Adv. Atmos. Sci.* 14, 1–22. doi: 10.1007/s00376–997-0039–4

Liu, Y. (2021). Application and progress of remote sensing technology in the suitability research of mariculture. *J. Fujian Polytechnic Normal Univ.* 39, 101–111.

Liu, Y., Hu, Z.-Z., Wu, R., Ding, Y., and Jha, B. (2024c). Evolution of ENSO-related seasonal precipitation anomalies in East Asia: A robustness revisit. *Int. J. Climatology* 44, 269–285. doi: 10.1002/joc.8327

Liu, B., Liu, Z., Chen, Y., Lu, R., Li, C., Ma, P., et al. (2024a). Potential distribution of Crassostrea sikamea (Amemiy) along coastal China under global climate change. *Global Ecol. Conserv.* 50, e02843. doi: 10.1016/j.gecco.2024.e02843

Liu, B., Liu, Z., Li, C., Yu, H., and Wang, H. (2024b). Geographical distribution and ecological niche dynamics of Crassostrea sikamea (Amemiy) in China's coastal regions under climate change. *Sci. Total Environ.* 920, 171061. doi: 10.1016/j.scitotenv.2024.171061

Liu, Y., Saitoh, S.-I., Radiarta, I. N., Igarashi, H., and Hirawake, T. (2014). Spatiotemporal variations in suitable areas for Japanese scallop aquaculture in the Dalian coastal area from 2003 to 2012. *Aquaculture* 422–423, 172–183. doi: 10.1016/j.aquaculture.2013.11.033

Liu, Y., Saitoh, S.-I., Radiarta, I. N., Isada, T., Hirawake, T., Mizuta, H., et al. (2013). Improvement of an aquaculture site-selection model for Japanese kelp (Saccharinajaponica) in southern Hokkaido, Japan: an application for the impacts of climate events. *ICES J. Mar. Sci.* 70, 1460–1470. doi: 10.1093/icesjms/fst108

Liu, Y., Tian, Y., Saitoh, S.-I., Alabia, I. D., and Mochizuki, K.-I. (2020a). Impact of climate Extremes on suitability dynamics for Japanese scallop aquaculture in shandong, China and funka bay, Japan. *Sustainability* 12, 833. doi: 10.3390/su12030833

Liu, L., and Wang, Z. (2019). Temporal and spatial distributions and formation mechanism of suspended sediment in the coastal area of the Shandong Peninsula. *Mar. Sci.* 43, 55–65. doi: 10.11759/hykx20190312004

Liu, Y., Wang, Z., Yang, X., Zhang, Y., Yang, F., Liu, B., et al. (2020b). Satellite-based monitoring and statistics for raft and cage aquaculture in China's offshore waters. *Int. J. Appl. Earth Observation Geoinformation* 91, 102118. doi: 10.1016/j.jag.2020.102118

Loosanoff, V. L., and Tommers, F. D. (1948). Effect of suspended silt and other substances on rate of feeding of oysters. *Science* 107, 69–70. doi: 10.1126/science.107.2768.69

Ma, Z., Zhao, Y., Zhao, W., Feng, J., Liu, Y., Tsou, J. Y., et al. (2024). Estimating Total Suspended Matter and Analyzing Influencing Factors in the Pearl River Estuary (China). *Journal of Marine Science and Engineering* 12, 167. doi: 10.3390/jmse12010167

Meng, L., Xing, Q., Gao, X., Ji, D., Qu, F., Wang, X., et al. (2022). Effects of an episodic storm-induced flooding event on the biogeochemistry of a shallow, highly turbid, semi-enclosed embayment (Laizhou bay, bohai sea). *Sustainability* 15, 563. doi: 10.3390/su15010563

Mizuta, D. D., Silveira, N., Fischer, C. E., and Lemos, D. (2012). Interannual variation in commercial oyster (Crassostrea gigas) farming in the sea (Florianópolis, Brazil, 27° 44′ S; 48°33′ W) in relation to temperature, chlorophyll a and associated oceanographic conditions. *Aquaculture* 366–367, 105–114. doi: 10.1016/j.aquaculture.2012.09.011

Nell, J. A., and Holliday, J. E. (1988). Effects of salinity on the growth and survival of Sydney rock oyster (Saccostrea commercialis) and Pacific oyster (Crassostrea gigas) larvae and spat. *Aquaculture* 68, 39–44. doi: 10.1016/0044–8486(88)90289-X

Ogle, J., Ray, S. M., and Wardle, W. J. (1977). The effect of depth on survival and growth of oysters in suspension culture from a petroleum platform off the texas coast. *GCR.* 6, 31–37. doi: 10.18785/grr.0601.04

Park, M.-S., Jung, H. C., Lee, S., Ahn, J.-H., Bae, S., and Choi, J.-K. (2021). The GOCI-II early mission ocean color products in comparison with the GOCI toward the continuity of chollian multi-satellite ocean color data. *Korean J. Remote Sens.* 37, 1281–1293. doi: 10.7780/kjrs.2021.37.5.2.6

Peoples Government of Shandong Province (2023) *Geographical resources*. Available online at: http://www.shandong.gov.cn/art/2024/2/18/art_98093_206404.html (Accessed March 14, 2024).

Phillips, S. J., Anderson, R. P., and Schapire, R. E. (2006). Maximum entropy modeling of species geographic distributions. *Ecol. Modelling.* 190, 231–259. doi: 10.1016/j.ecolmodel.2005.03.026

Porporato, E. M. D., Pastres, R., and Brigolin, D. (2020). Site suitability for finfish marine aquaculture in the central mediterranean sea. *Front. Mar. Sci.* 6. doi: 10.3389/fmars.2019.00772

Quan, W., An, C., Ma, C., Huang, H., Cheng, W., Wang, Y., et al. (2012). Biodiversity and community structure of benthic macroinvertebrates on the Xiaomiaohong oyster reef in Jiangsu province, China. *Oceanologia Limnologia Sinica.* 43, 992–1000. doi: 10.11693/hyhz201205017017

Quan, W., Zhang, Y., Qi, Z., Xu, M., Fan, R., Wang, T., et al. (2022). Distribution and ecological status of natural oyster reefs on the coast of Caofeidian-Leting,Tangshan, Hebei Province. *Acta Ecologica Sin.* 42, 1142–1152. doi: 10.5846/stxb202005101172

Radiarta, I. N., Saitoh, S.-I., and Miyazono, A. (2008). GIS-based multi-criteria evaluation models for identifying suitable sites for Japanese scallop (Mizuhopecten yessoensis) aquaculture in Funka Bay, southwestern Hokkaido, Japan. *Aquaculture* 284, 127–135. doi: 10.1016/j.aquaculture.2008.07.048

Radiarta, I. N., Saitoh, S.-I., and Yasui, H. (2011). Aquaculture site selection for Japanese kelp (Laminaria japonica) in southern Hokkaido, Japan, using satellite remote sensing and GIS-based models. *ICES J. Mar. Sci.* 68, 773–780. doi: 10.1093/icesjms/fsq163

Ran, W., Teng, J., Liu, Y., Wu, D., Hou, C., Wang, Q., et al. (2018). Microplastic ingestion characteristics in the Pacific oysters collected from the intertidal zone of the Bohai Rim. *Mar. Sci. Bull.* 37, 583–590. doi: 10.11840/j.issn.1001–6392.2018.05.012

Saaty, T. L. (1977). A scaling method for priorities in hierarchical structures. *Journal of Mathematical Psychology* 15, 234–281. doi: 10.1016/0022-2496(77)90033-5

Saitoh, S.-I., Mugo, R., Radiarta, I. N., Asaga, S., Takahashi, F., Hirawake, T., et al. (2011). Some operational uses of satellite remote sensing and marine GIS for sustainable fisheries and aquaculture. *ICES J. Mar. Sci.* 68, 687–695. doi: 10.1093/icesjms/fsq190

Shpigel, M., and Blaylock, R. A. (1991). The Pacific oyster, Crassostrea gigas, as a biological filter for a marine fish aquaculture pond. *Aquaculture* 92, 187–197. doi: 10.1016/0044–8486(91)90020–8

Snyder, J., Boss, E., Weatherbee, R., Thomas, A. C., Brady, D., and Newell, C. (2017). Oyster aquaculture site selection using landsat 8-derived sea surface temperature, turbidity, and chlorophyll a. *Front. Mar. Sci.* 4. doi: 10.3389/fmars.2017.00190

Soley-Guardia, M., Alvarado-Serrano, D. F., and Anderson, R. P. (2024). Top ten hazards to avoid when modeling species distributions: a didactic guide of assumptions, problems, and recommendations. *Ecography* 2024, e06852. doi: 10.1111/ecog.06852

Song, X., Gu, Y., Zhai, F., Li, P., Liu, P., Liu, Z., et al. (2021). Climatology and seasonal variability of satellite-derived chlorophyll a around the Shandong Peninsula. *J. Ocean. Limnol.* 39, 1222–1244. doi: 10.1007/s00343–020-0249–5

Suedel, B. C., Clarke, J. U., Wilkens, J., Lutz, C. H., and Clarke, D. G. (2015). The effects of a simulated suspended sediment plume on eastern oyster (Crassostrea virginica) survival, growth, and condition. *Estuaries Coasts* 38, 578–589. doi: 10.1007/s12237–014-9835–0

Swam, L. M., Couvillion, B., Callam, B., La Peyre, J. F., and La Peyre, M. K. (2022). Defining oyster resource zones across coastal Louisiana for restoration and aquaculture. *Ocean Coast. Manage.* 225, 106178. doi: 10.1016/j.ocecoaman.2022.106178

Tenore, K. R., and Dunstan, W. M. (1973). Comparison of feeding and biodeposition of three bivalves at different food levels. *Mar. Biol.* 21, 190–195. doi: 10.1007/BF00355249

Terauchi, G., Tsujimoto, R., Ishizaka, J., and Nakata, H. (2014). Preliminary assessment of eutrophication by remotely sensed chlorophyll-a in Toyama Bay, the Sea of Japan. *J. Oceanogr.* 70, 175–184. doi: 10.1007/s10872–014-0222-z

Van Der Veer, H. W., Cardoso, J. F. M. F., and van der Meer, J. (2006). The estimation of DEB parameters for various Northeast Atlantic bivalve species. *J. Sea Res.* 56, 107–124. doi: 10.1016/j.seares.2006.03.005

Walker, B., Salt, D., and Reid, W. (2006). Resilience thinking: sustaining ecosystems and people in A changing world. Bibliovault OAI repository, the university of chicago press.

Wang, B., Cao, L., Micheli, F., Naylor, R. L., and Fringer, O. B. (2018). The effects of intensive aquaculture on nutrient residence time and transport in a coastal embayment. *Environ. Fluid Mech.* 18, 1321–1349. doi: 10.1007/s10652–018-9595–7

Wang, C., Liu, Z., Harris, C. K., Wu, X., Wang, H., Bian, C., et al. (2020). The impact of winter storms on sediment transport through a narrow strait, bohai, China. *JGR Oceans.* 125 (6), e2020JC016069. doi: 10.1029/2020JC016069

Wang, Z., Ma, Q., Liang, S., Liu, Y.-A., Liu, L., Huang, C., et al. (2024). Study on the distribution and habitat suitability of seagrass in the Northern Chinese Seas. *Front. Mar.* 10. doi: 10.3389/fmars.2023.1297137

Wang, T., Wang, Q., Shang, X., Wang, Y., and Song, W. (2014). The water quality environment analysis of the National special Marine reserve in Tianjin Dashentang oyster reef. *Fishery Modernization* 41, 47–50. doi: 10.3969/j.issn.1007–9580.2014.06.010

Wang, B., Wu, R., and Fu, X. (2000). Pacific–east asian teleconnection: how does ENSO affect east asian climate? *J. Climate* 13, 1517–1536. doi: 10.1175/1520–0442(2000)013<1517:PEATHD>2.0.CO;2

Wang, Y., Xie, B., Wan, F., Xiao, Q., and Dai, L. (2007). Application of ROC curve analysis in evaluating the performance of alien species' potential distribution models. *Biodiversity Sci.* 15, 365. doi: 10.1360/biodiv.060280

Wang, Z., Yang, X., Liu, Y., and Lu, C. (2018). Extraction of coastal raft cultivation area with heterogeneous water background by thresholding object-based visually salient NDVI from high spatial resolution imagery. *Remote Sens. Lett.* 9, 839–846. doi: 10.1080/2150704x.2018.1468103

Wang, X., Zhang, J., Zhong, Y., Liu, Y., and Wu, W. (2023). GIS-based spatial suitability assessment for pacific oyster Crassostrea gigas reef restoration: A case study of Laizhou Bay, China. *Mar. pollut. Bull.* 186, 114416. doi: 10.1016/j.marpolbul.2022.114416

Wolter, K., and Timlin, M. S. (2011). El Niño/Southern Oscillation behaviour since 1871 as diagnosed in an extended multivariate ENSO index (MEI.ext): EL NIÑO/SOUTHERN OSCILLATION BEHAVIOUR SINCE 1871. *Int. J. Climatol.* 31, 1074–1087. doi: 10.1002/joc.2336

Xiao, R., Gao, G., Yang, D., Su, Y., Ding, Y., Bi, R., et al. (2024). The impact of extreme precipitation on physical and biogeochemical processes regarding with nutrient dynamics in a semi-closed bay. *Sci. Total Environ.* 906, 167599. doi: 10.1016/j.scitotenv.2023.167599

Xing, X., Claustre, H., Boss, E., Roesler, C., Organelli, E., Poteau, A., et al. (2017). Correction of profiles of *in-situ* chlorophyll fluorometry for the contribution of fluorescence originating from non-algal matter. *Limnology Oceanography: Methods* 15, 80–93. doi: 10.1002/lom3.10144

Yang, Z., Chen, W., Wang, X., Liu, B., Dong, J., and Deng, Y. (2024). Suitable habitat of the scad fish (Decanters spp.) in Northern South China Sea predicted by MaxEnt model. *Regional Stud. Mar. Sci.* 69, 103315. doi: 10.1016/j.rsma.2023.103315

Yang, J., Dong, M., Zhong, Y., and Xu, Q. (2023). Application of maximum entropy model in the prediction of marine biological suitable areas. *J. Appl. Oceanography* 42, 698–707. doi: 10.3969/J.ISSN.2095–4972.20220801001

Yang, Z., Ji, Y., Bi, N., Lei, K., and Wang, H. (2011). Sediment transport off the Huanghe (Yellow River) delta and in the adjacent Bohai Sea in winter and seasonal comparison. *Estuarine Coast. Shelf Sci.* 93, 173–181. doi: 10.1016/j.ecss.2010.06.005

Yang, B., Zhai, S., Li, X., Tian, J., Li, Q., Shan, H., et al. (2021). Identification of Vibrio alginolyticus as a causative pathogen associated with mass summer mortality of the Pacific Oyster (Crassostrea gigas) in China. *Aquaculture* 535, 736363. doi: 10.1016/j.aquaculture.2021.736363

Yati, E., Sadiyah, L., Satria, F., Alabia, I. D., Sulma, S., Prayogo, T., et al. (2024). Spatial distribution models for the four commercial tuna in the sea of maritime continent using multi-sensor remote sensing and maximum entropy. *Mar. Environ. Res.* 198, 106540. doi: 10.1016/j.marenvres.2024.106540

Yu, R., Li, Q., and Kong, L. (2008). Current situation of Pacific oyster seedling cultivation and breeding in northern China. *Sci. Fish Farming* 6, 3–5. doi: 10.14184/j.cnki.issn1004–843x.2008.06.002

Zhang, X., Fan, C., Huo, Z., Ma, P., Li, Y., Li, J., et al. (2021). A comparative analysis of shell traits among different populations of Crassostrea gigas. *Periodical Ocean Uinversity China* 51, 1–9. doi: 10.16441/j.cnki.hdxb.20200305

Zhang, Z., Qiao, F., Guo, J., and Guo, B. (2018). Seasonal changes and driving forces of inflow and outflow through the Bohai Strait. *Continental Shelf Res.* 154, 1–8. doi: 10.1016/j.csr.2017.12.012

Zhang, M., Shi, W., Gui, F., Zeng, X., Xu, K., and Zhang, S. (2023). Study of suitable habitats for Sepiella maindroni in Zhoushan sea areas based on MaxEnt model. *South China Fisheries Sci.* 19, 22–31. doi: 10.12131/20230080

Zheng, X., Zhang, H., Li, Y., Zou, T., Liu, X., and Xing, Q. (2021). The features and mechanisms of the North Shandong Coastal Current: a case study in 2014. *J. Oceanogr.* 77, 631–646. doi: 10.1007/s10872–021-00597–3

Zhong, J., Li, Q., and Wang, T. (2019). Comparison of feeding and metabolism between black-shell strain and wild population of the Pacific oyster (Crassostrea gigas). *J. Fisheries China* 43, 1038–1047. doi: 10.11964/jfc.20180411248

Zou, Y., Liu, G., Zhang, T., Song, A., Li, Q., and Guo, W. (2021). Main aquaculture mode of Pacific oyster in China. *Sci. Fish Farming* 11, 63–64. doi: 10.14184/j.cnki.issn1004–843x.2021.11.034

frontiers | Frontiers in Marine Science

TYPE Original Research
PUBLISHED 26 July 2024
DOI 10.3389/fmars.2024.1379571

OPEN ACCESS

EDITED BY
Tangtian He,
Hong Kong Polytechnic University,
Hong Kong SAR, China

REVIEWED BY
Alfonso Olaya Abril,
University of Cordoba, Spain
Biao Wu,
Chinese Academy of Fishery Sciences (CAFS), China

*CORRESPONDENCE
Qing-Zhi Wang
wqzlm@126.com

†These authors have contributed equally to this work

RECEIVED 31 January 2024
ACCEPTED 12 July 2024
PUBLISHED 26 July 2024

CITATION
Gao J, Xie X, Liu X-F, Bai Y-A, Yang M, Teng W-M, Liu H-J and Wang Q-Z (2024) Efficacy of calcein as a chemical marker of *Potamocorbula laevis*. *Front. Mar. Sci.* 11:1379571. doi: 10.3389/fmars.2024.1379571

Efficacy of calcein as a chemical marker of *Potamocorbula laevis*

Jin Gao[1,2†], Xi Xie[1,2,3†], Xiang-Feng Liu[1,3], Yong-An Bai[4], Miao Yang[5], Wei-Ming Teng[1,3], Hai-Jiao Liu[6] and Qing-Zhi Wang[1,2,3*]

[1]Dalian Key Laboratory of Genetic Resources for Marine Shellfish, Key Laboratory of Protection and Utilization of Aquatic Germplasm Resource, Ministry of Agriculture and Rural Affairs, Liaoning Ocean and Fisheries Science Research Institute, Dalian, China, [2]College of Fisheries and Life Science, Dalian Ocean University, Dalian, China, [3]Dalian Jinshiwan Laboratory, Dalian, China, [4]Panjin Guanghe Crab Industry Co., LTD, Panjin, China, [5]Key Laboratory of Plant Biotechnology of Liaoning Province, School of Life Sciences, Liaoning Normal University, Dalian, China, [6]Dalian Changhai-Yide Aquatic Products Co., LTD, Dalian, China

Introduction: Calcein was used to develop a shell marking method for *Potamocorbula laevis*.

Methods: The suitable conditions for marking were investigated, including marking concentration, immersion time, and water temperature. The impacts and feasibility of the marking method were assessed based on the survival rate of *P. laevis*, the success rate of fluorescence marking, marking quality, and alterations in activities of antioxidant enzymes in the digestive gland of the experimental bivalves. Two concentrations of calcein (20 and 50 mg/L) were used and the immersion time included 1 and 2 h, respectively. The experiment was performed in two rounds, with water temperatures of 12.84 ± 0.09 and 24.18 ± 0.04 °C, respectively.

Results and discussion: The results indicated that calcein did not significantly impact the survival of *P. laevis* after 7 d of recovery. The catalase activity and malondialdehyde content in low temperature-marked *P. laevis* showed significant decreases, and the relative abundances of certain fatty acids also exhibited significant changes within 2 h post exposure to 20 mg/L of calcein. However, these indicators returned to normal levels within 7 d. The marking impact of calcein was proportional to the calcein concentration and immersion time. Higher temperature generated a negative impact on the marking effect of 20 mg/L of calcein, while no obvious impacts were observed for 50 mg/L of calcein. The marking success rates and the recapture rates of *P. laevis* for *in situ* tests in the two experimental groups were both 100% and 4.44 ± 1.29% after one month. Also, the recapture marking rates and the marking good rates of the recaptured individuals were both 100%. There were no significant differences between these parameters for 50 and 75 mg/L of calcein. Given the cost and safety of labeling, a strategy in terms of an immersion in 50 mg/L of calcein for 2 h could be considered as an effective *in situ* labeling scheme for *P. laevis*. In conclusion, calcein can be employed as a marking method for *P. laevis*. These findings could be potentially beneficial for development of *in situ* labeling technology, proliferation as well as release of shellfish in tidal flats and resource conservation.

KEYWORDS

Potamocorbula laevis, calcein, marking conditions, antioxidant capacity, fatty acid

1 Introduction

P. laevis belongs to the Bivalvia class, Myida order, and Corbulidae family. It is a eurythermal benthic bivalve commonly inhabiting the intertidal zone or shallow waters of the subtidal zone. It is a primary benthic species throughout many estuarine areas in East Asia (Sun et al., 2013; Chen et al., 2017). It is small and has an elongated oval or nearly triangular shape. The shell is hard, with the left valve being smaller than the enlarged right valve. The shell surface is smooth and lacks ribs, and the adult shell length is approximately 1.5 ~ 2.5 cm. *P. laevis* is rich in proteins, low in fat, and abundant in minerals. The meat of this bivalve is consumed by humans and can also serve as high-quality bait for shrimp, crabs, or fish (Liu and She, 2003; Liu, 2022). Recently, the natural resources of *P. laevis* have significantly declined due to overharvesting and environmental pollution. The ecological value (Zhou et al., 2017), nutritional value (Liu, 2022), reproductive habits (Liu and She, 2003), and responses to environmental factors (Li et al., 2015; Ning et al., 2016; Teng et al., 2018) of this bivalve have garnered significant attention. However, there is currently limited research regarding the population dynamics and dispersal patterns of this bivalve in its natural habitat.

Marking technology is a widespread method in shellfish proliferation and release. It can reflect the growth and population variability of shellfish based on changes in external traits, recapture position, quantity, and time before and after biomarker observation. Among these markers, chemical fluorescence labeling is predominantly employed for shellfish owing to its high labeling efficiency, high success rate, and high retention rate (Sugiura and Kikuya, 2017; Gancel et al., 2019; Mahé et al., 2021). The principle of chemical labeling relies on the complexation of fluorescent dyes with biological tissues to generate fluorescent markers visible under a specific wavelength light source.

Calcein is a calcium ion fluorescent indicator with an excitation wavelength of 495 nm and an emission wavelength of 515 nm (Xia and Li, 2015). Although direct contact with calcein may cause skin, respiratory, and eye irritation to humans, calcein typically binds to cells or biomolecules through internal or surface staining methods when labeling biological samples, and it has been shown to generate no significant toxicity to humans. Currently, there have not been detailed reports on the bioaccumulation and biodegradation of calcein in natural environments. The half-life of calcein in aquatic environments has been found to vary depending on environmental conditions, ranging from hours to days (Keller et al., 2004). The U.S. Federal Drug Administration approved a new veterinary drug research application (INADA) for calcein in 2011, allowing calcein to be used in edible animal feeding activities. The hypotoxic calcein has been used as a release marker for *Crassostrea virginica* (Spires et al., 2022), *Perna Canacillus* (Fitzpatrick et al., 2013), *Argopecten irradians* (Moran and Marko, 2005) and other aquatic organisms, such as fish, echinoderms (Zhao et al., 2011), etc (Supplementary Table S1). The available concentration range of calcein in bivalve mollusks generally varies between 25 - 600 mg/L, e.g., 25 - 250 mg/L for Ostreidae, 40 - 200 mg/L for Pteriidae, 50 - 600 mg/L for Pectinidae, and 200 - 300 mg/L for Arcidae, etc (Supplementary Table S2). However, it is worth noting that, the safety of calcein remains to be relative, and if the labeling concentration or exposure time of calcein is much higher or longer, certain adverse impacts appear to occur on clams or other labeling organisms. The growth of shellfish seems to be limited and the resulting death might even occur. Hence, the application of appropriate calcein labeling on *P. laevis* or other clams is potentially prospecting in large-scale stocking, and the food safety risks are likely within deemed safety range, to certain extent.

Organisms are able to clear large amounts of reactive oxygen species produced by exogenous factors through their antioxidant system, reducing oxidative damage. Antioxidant enzymes are an important component of this system, and their activity can reflect the extent of damage to the organism (Duan et al., 2016). Fatty acids are able to participate in various biochemical pathways such as energy supply, biological membrane formation, and signaling molecules, and are pivotal for maintaining normal body function (Lee et al., 2018). In addition, the fatty acids are very sensitive to pollutants and environmental changes, and often used as a bioindicator in response to external stressors in marine bivalves (Gonçalves et al., 2016). Thus, the fatty acids deserved to be focused on to evaluate the labeling effects of calcein on the clams in this work.

Geligang is a sandbank between the Liaohe River and the Shuangtaizi River in the northern part of the Liaodong Bay, China. The area is about 10,000 hm^2, with an average altitude of –2 m. Its water quality is characterized by high turbidity, low transparency, and serious eutrophication. Approximately 80% of the beach surface is dry for about 3 h per day on average. The beach surface is flat, the surface water flow is turbulent, and there is a long freezing period in winter. It is rich in *Mactra veneriformis*, *P. laevis*, *Solen grandis* and other economic shellfish. In this study, the clam *P. laevis* from Geligang was focused on to investigate the appropriate marking conditions of the fluorescent dye calcein for both laboratory and *in situ* labeling. The antioxidant capacities as well as the fatty acid profiles served as biochemical indicators to explore the feasibility of chemical labeling and the optimal conditions of calcein on *P. laevis*. These results could be potentially beneficial for recovery and utilization of the clam *P. laevis*.

2 Materials and methods

2.1 Materials

P. laevis was collected in April and July 2023, respectively, at Geligang, Liaodong Bay, China. The collected samples were transported back to the laboratory by express cold chain and temporarily maintained in a polyvinyl chloride tank with fine sand until the survival rate remained stable, and half of seawater was exchanged every day. Three commercial microalgal powders for two green algae, i.e., *Dunaliella salina* and *Chlorella vulgaris*, and one blue-green alga, i.e., *Spirulina* sp., were mixed in a mass ratio of 2:3:5, and the feeding proportion of algae was equivalent to 1% of the soft tissue mass of the bivalves.

The stock solution of calcein was prepared using distilled water, and stored in a light-protected container. To avoid discrepancies

between experimental and theoretical concentrations, the calcein stock solutions used in the experiments were prepared within 24 h before use to prevent precipitation due to prolonged storage. During preparation, a small amount of $NaHCO_3$ was added to adjust the pH, and stirring continued until calcein completely dissolved. Therefore, the actual concentrations used in the experiments remained relatively consistent with the theoretical concentrations. The stock concentration was set at 1 g/L. The stock solution was diluted into 20 and 50 mg/L using seawater, respectively.

2.2 Experiment 1: low temperature labeling

The ambient seawater temperature was maintained at 12.84 ± 0.09°C. The experimental tests (Figure 1) included Group A (control, 0 mg/L), Group B (low concentration, 20 mg/L, 1 h), Group C (low concentration, 20 mg/L, 2 h), and Group D (high concentration, 50 mg/L, 2 h). Each group had 3 replicates with 30 P. *laevis* per replicate. The shell length, shell width, and wet weight of the tested clams were 22.45 ± 1.04 mm, 14.76 ± 0.75 mm, and 1.87 ± 0.27 g, respectively. The labeling process is carried out in an opaque foam box. The individuals were immersed into 10 L of seawater with 7.06 ± 0.08 mg/L of dissolved oxygen and 33.14 ± 0.06 of salinity during the marking process. The stocking density was 9 ind./L, and the clams were fasting throughout the marking process. Following the immersion, the residual calcein on the surface of the bivalve's shell was gently rinsed using fresh seawater. Then the clams were transferred to a 0.16 m^3 transparent glass tank covered with approximately 5 cm thick of sea sand that was filtered through 30~50 mesh for 7 d.

Nearly 70% of the cultured seawater was exchanged at regular intervals every day during acclimation. The clams were fed with algal powder in a mixed mass ratio of *D. salina*: *C. vulgaris* = 1:1, and the feeding proportion was 1% of the soft tissue mass of the clams. The seawater was aerated for 24 h prior to labeling. The temperature, dissolved oxygen, salinity and pH value of seawater were 12.80 ± 0.03°C, 7.54 ± 0.07 mg/L, 32.95 ± 0.03, and 7.96 ± 0.10 during the recovery culture, respectively.

2.3 Experiment 2: high temperature labeling

The ambient seawater temperature during labeling was 24.18 ± 0.04°C. The experimental tests concluded one more Group E (high concentration, 50 mg/L, 1 h) in relative to Experiment 1. The shell length, shell width, and wet weight of *P. laevis* were 21.16 ± 1.55 mm, 13.83 ± 1.08 mm, and 1.45 ± 0.39 g, respectively. The dissolved oxygen and salinity were 6.26 ± 0.16 mg/L and 30.87 ± 0.55, and the stocking density was also 9 ind./L during labeling. The temperature, dissolved oxygen, salinity and pH value of seawater were 24.32 ± 0.24°C, 6.14 ± 0.16 mg/L, 31.40 ± 0.41, and 8.10 ± 0.05 during the recovery culture, respectively.

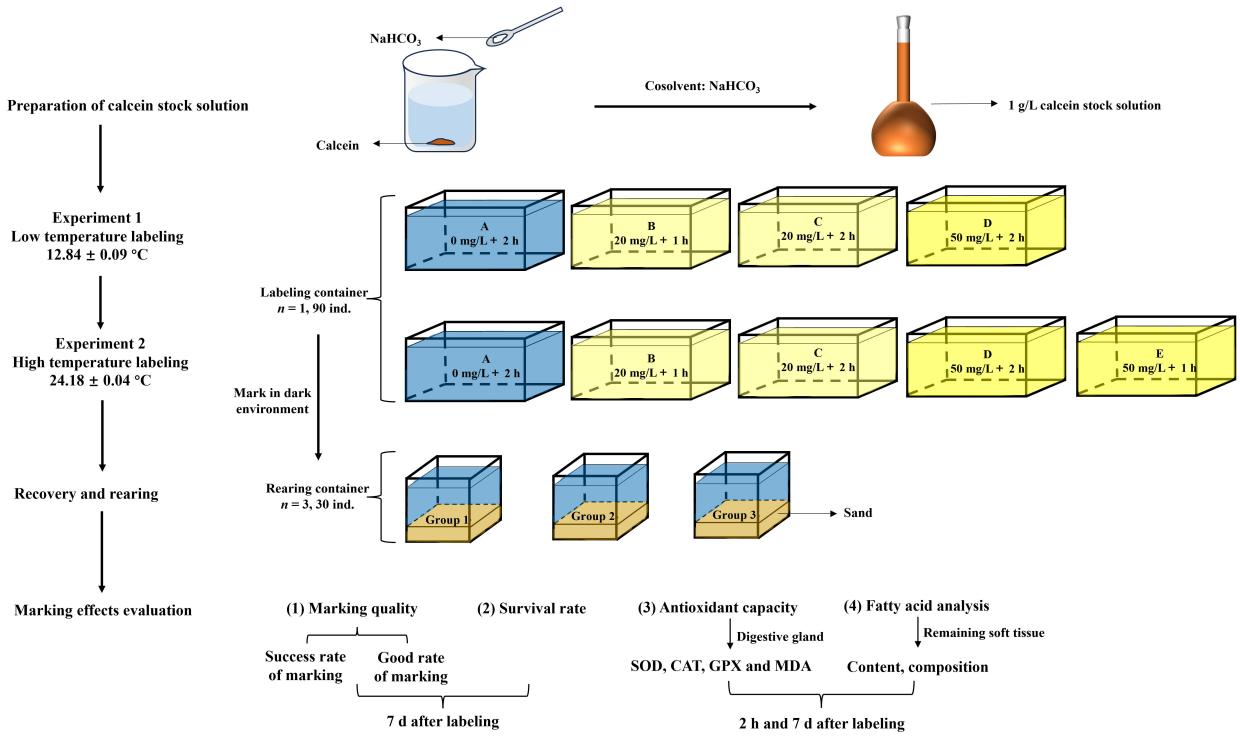

FIGURE 1
Experiment design for labeling of *P. laevis*.

2.4 Experiment 3: *in situ* labeling

The *in situ* labeling experiment took place at Geligang in the Liaodong Bay, China. The calcein concentrations included 0, 50 and 75 mg/L and the immersion time was 2 h. Three parallel sampling sites were set for each calcein concentration. There were thirty individuals of *P. laevis* at each sampling site, and the native specimens were collected from Geligang, with a shell length of 24.42 ± 1.09 mm. Water temperature was 25.76 ± 0.08°C. The labeling process was performed within sealed light-free containers to avoid quenching of calcerin and the seawater volume was 20 L.

Seven sites with a distance of about 50 m were selected in Geligang tidal flat (40°N, 121°E). During the ebb tide, the *in situ* device was installed (Figures 2A, B), and the labeled *P. laevis* were transferred to the *in situ* device. After a month, the labeled individuals at each site were recaptured, and the recapture rate, the labeling rate of recaptured individuals, and the good labeling rate were then evaluated.

2.5 Grade evaluation of marking effects

After 7 d of marking, all the remaining smooth-shell clams were dissected, and the soft segments were removed. The shells were cleaned and dried at 50°C. Fluorescent markings on the shells were observed using a fluorescence flashlight (Luyor-3280LB) at 480 ~ 490 nm. The quality of fluorescent marking was assessed using Grade 0 ~ 5 (Table 1). Grade 0, 1, 2 and 3 indicated that the marking was not visible, blurry, clearly marking, and brightly marking under the fluorescence flashlight, respectively. Grade 4 and 5 indicated that the marking was visible, and clearly marking under the transmitted light, respectively (Lü et al., 2014). Markings with a quality of no less than Grade 2 were considered acceptable. The success rate of marking and the rate of good markings (Grade 2 or higher) were separately calculated for each experimental group.

2.6 Sample treatments

Samples were obtained after 2 h following labeling and 7 d following temporary culture. Five individuals of *P. laevis* were randomly selected from each replicate. The digestive glands and soft tissues were dissected on ice and stored at –80°C. The digestive glands were used to determine the antioxidant enzymes activities and MDA content. The soft tissues were lyophilized and grounded into powder filtered through an 80-mesh sieve. The fine powder was then used to perform fatty acid analysis.

2.7 Antioxidant capacity determination

The antioxidant indexes in labeled *P. laevis* were determined by superoxide dismutase (SOD) assay kit, CAT assay kit, and glutathione peroxidase (GPX) assay kit from Nanjing Jiancheng Biological Co., Ltd. (Nanjing, China), and the MDA and total protein amounts were assessed using assay kits from Servicebio (Nanjing, China), respectively.

2.8 Fatty acid analysis

The fatty acids in labeled *P. laevis* was analyzed using the modified one-step acid-catalyzed esterification method (Liu et al., 2015). The accurately weighed powder (50 ~ 100 mg) were added to a 10-mL round-bottom flask followed by addition of 5 mL 2% H_2SO_4 in methanol. After complete ultra-sonication, the mixture was heated at 70°C for 1 h. The hexane-extracted fatty acid methyl esters (FAMEs) were quantified using a Bruker GC 456 equipped with FID and a DB-23 column (30 m length × 320 μm inner diameter × 0.25 μm thickness, Agilent Technologies, USA). C19:0-ME were used as internal standards for quantification of FAMEs.

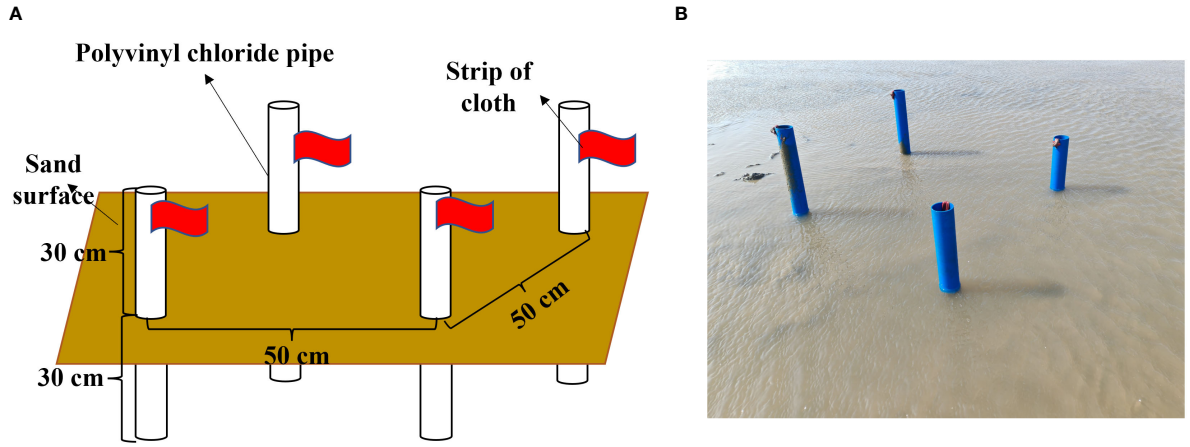

FIGURE 2
In situ labeled experimental model diagram and field device. **(A)** *In situ* device design diagram; **(B)** *In situ* device image.

10.3389/fmars.2024.1379571

TABLE 1 Evaluation criteria for marking grade.

Grade	Rating criteria
0	The labeling is not visible under fluorescence irradiation
1	Blurred labeling under fluorescent irradiation
2	Clearly labeled under fluorescence irradiation
3	Bright labeling under fluorescence irradiation
4	Mark visible under transmitted light
5	Marking clear under transmitted light

The fluorescent flashlight at 480 ~ 490 nm was used.

The injection volume was 1 μL and the carrier gas was nitrogen with purity of 99%. The split ratio was 30:1. Column temperature was programmed from 130 to 170°C increasing at 10°C/min, then to 210°C at 2.5°C/min and held at 210°C for 3 min. The running time was 23 min. The temperatures of the front inlet and front detector were both 270°C. The formula for calculating the relative (P_i) and absolute (M_i) content of each fatty acid were as follows.

$$P_i = A_i/\sum A_i \times 100\,\% \quad (1)$$

$$M_i = (A_i/A_s \times M_s)/M_a \quad (2)$$

Where A_i and ΣA_i in Equations 1, 2 indicated the peak area of the individual fatty acid and that of the total fatty acids, respectively. A_s, M_s and M_a in Equation 2 indicated the peak area of the internal standard, the addition mass of internal standard, and the amount of the added sample.

2.9 Statistical analysis

The data were statistically analyzed by SPSS 26.0 and denoted as average ± standard deviation (SD, n = 3). Statistical significance of the difference was determined by one-way analysis of variance Tukey's honestly significant difference (HSD) test with the significance level of 0.05.

3 Results

3.1 Mortality

There were no significant differences in the survival rates of calcein-labeled *P. laevis* for both Experiment 1 and 2 after 7 d of recovery. The survival rates of individuals in Experiment 1 were 86 ~ 90%, and that in Experiment 2 were 83 ~ 86% (Figures 3A, B). The labeling scheme used in this study had no significantly negative impact on the short-term survival of *P. laevis*.

3.2 Oxidation resistance

The activities of SOD and GPX presented no notable differences between distinct groups in low (Figures 4A, C) and high (Figures 5A, C) temperatures labeling, after 2 h or 7 d of labeling. In addition, a majority of CAT activities and MDA contents in distinct groups showed no significant differences among different treatments (Figures 4B, D, 5B, D). In particular, the CAT activities in Groups B and C (20 mg/L, low-concentration of calcein) of Experiment 1 (low temperature labeling) were found to prominently decline by 95% and 71% relative to the control Group A following 2 h of labeling, respectively. The MDA content in Group B following 2 h of labeling was notably lower by 28% than that in Group A of Experiment 1 (low temperature labeling, Figure 4).

3.3 Effect of calcein on fatty acid profiles of *P. laevis*

In *P. laevis*, 28 species of fatty acids were detected, including 6 saturated fatty acids (SFA), 7 monounsaturated fatty acids (MUFA), and 15 polyunsaturated fatty acids (PUFA, Supplementary Tables S3, S4). The main fatty acids in *P. laevis* included C16:0, C20:5n3, and C22:6n3, while the minor fatty

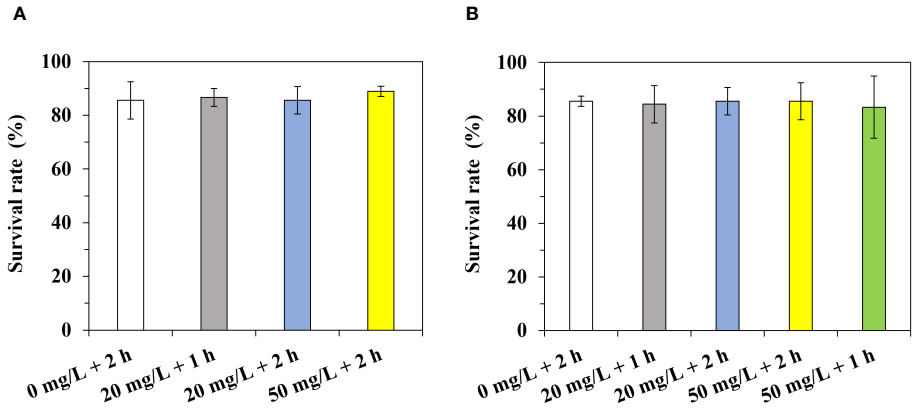

FIGURE 3
Survival rates of *P. laevis* during the marking period. **(A)** Experiment 1. **(B)** Experiment 2. Values are means of three biological replicates ± SD (n = 3).

10.3389/fmars.2024.1379571

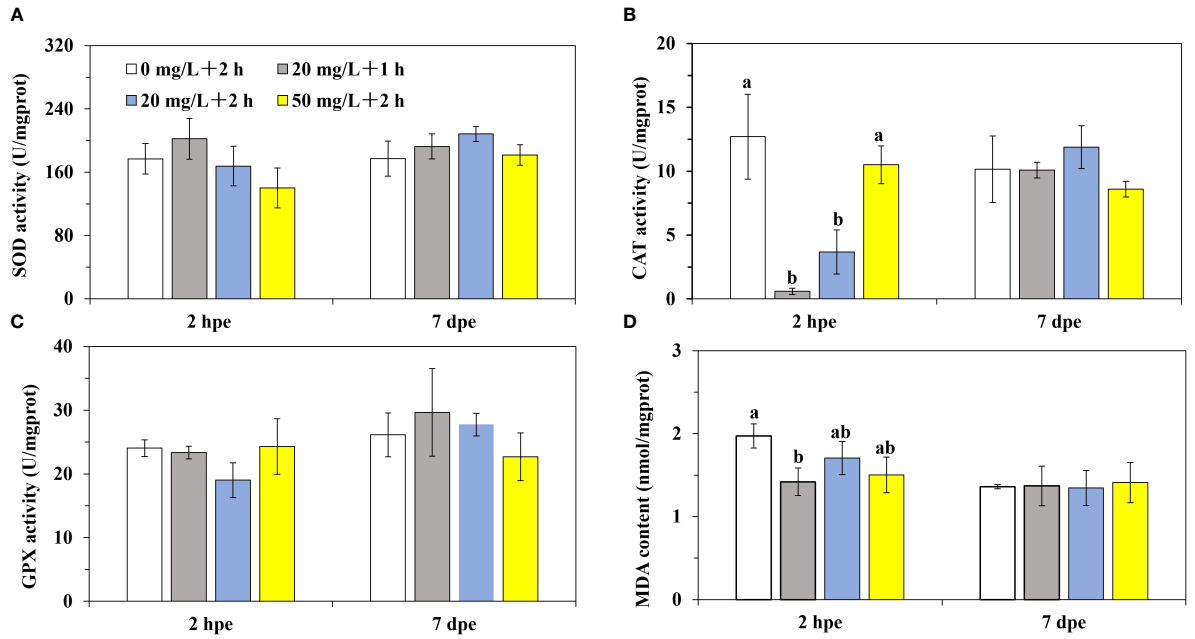

FIGURE 4
The antioxidant capacity of *P. laevis* in Experiment 1. **(A)** Experiment 1, 2 h post exposure (2 hpe). **(B)** Experiment 1, 7 d post exposure (7 hpe). **(C)** Experiment 2, 2 h post exposure. **(D)** Experiment 2, 7 d post exposure. Values are means of three biological replicates ± SD (n = 3). The a and b indicated significant difference between the treatment groups (*P< 0.05). SOD, CAT, GPX, and MDA indicated superoxide dismutase, catalase, glutathione peroxidase, and malondialdehyde, respectively.

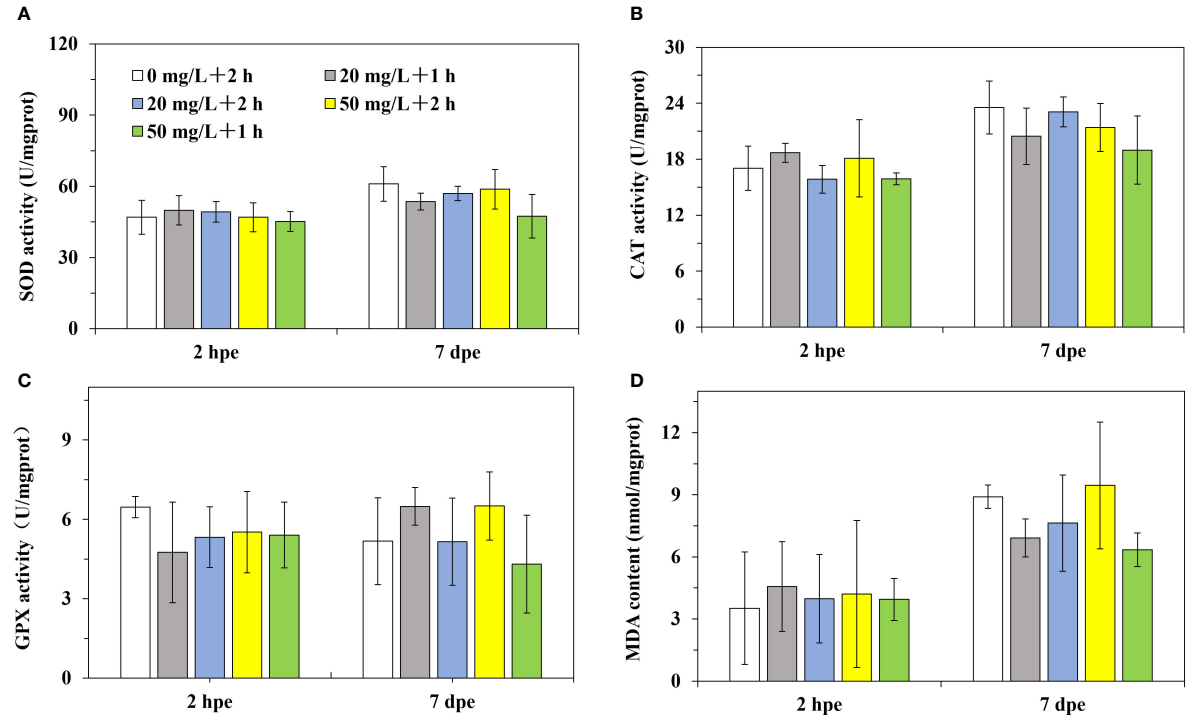

FIGURE 5
The antioxidant capacity of *P. laevis* in Experiment 2. **(A)** Experiment 1, 2 h post exposure (2 hpe). **(B)** Experiment 1, 7 d post exposure (7 hpe). **(C)** Experiment 2, 2 h post exposure. **(D)** Experiment 2, 7 d post exposure. Values are means of three biological replicates ± SD (n = 3). SOD, CAT, GPX, and MDA indicated superoxide dismutase, catalase, glutathione peroxidase, and malondialdehyde, respectively.

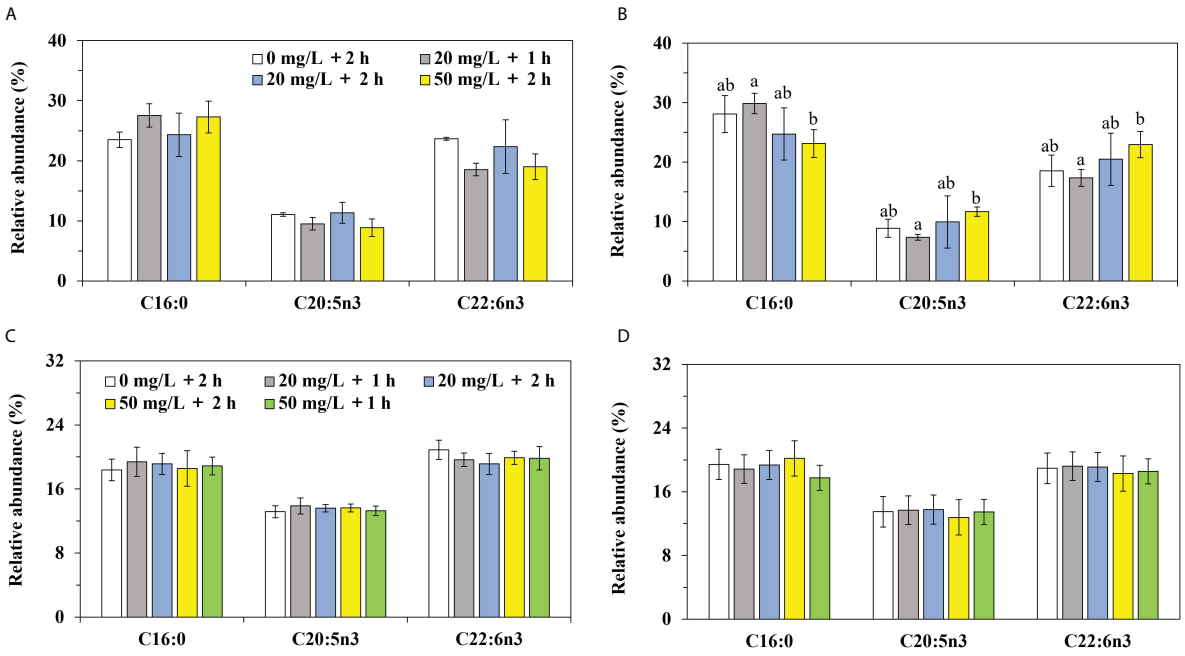

FIGURE 6
The relative abundances of the major fatty acids in *P. laevis*. **(A)** Experiment 1, 2 h post exposure (2 hpe). **(B)** Experiment 1, 7 d post exposure (7 hpe). **(C)** Experiment 2, 2 h post exposure. **(D)** Experiment 2, 7 d post exposure. Values are means of three biological replicates ± SD (*n* = 3). The major fatty acids referred to C16:0, C20:5n3 and C22:6n3. The relative abundance of the individual fatty acid was more than 10% and the total relative abundances of the three fatty acids in *P. laevis* were more than 50%. The a and b indicated significant difference between the treatment groups (*P< 0.05).

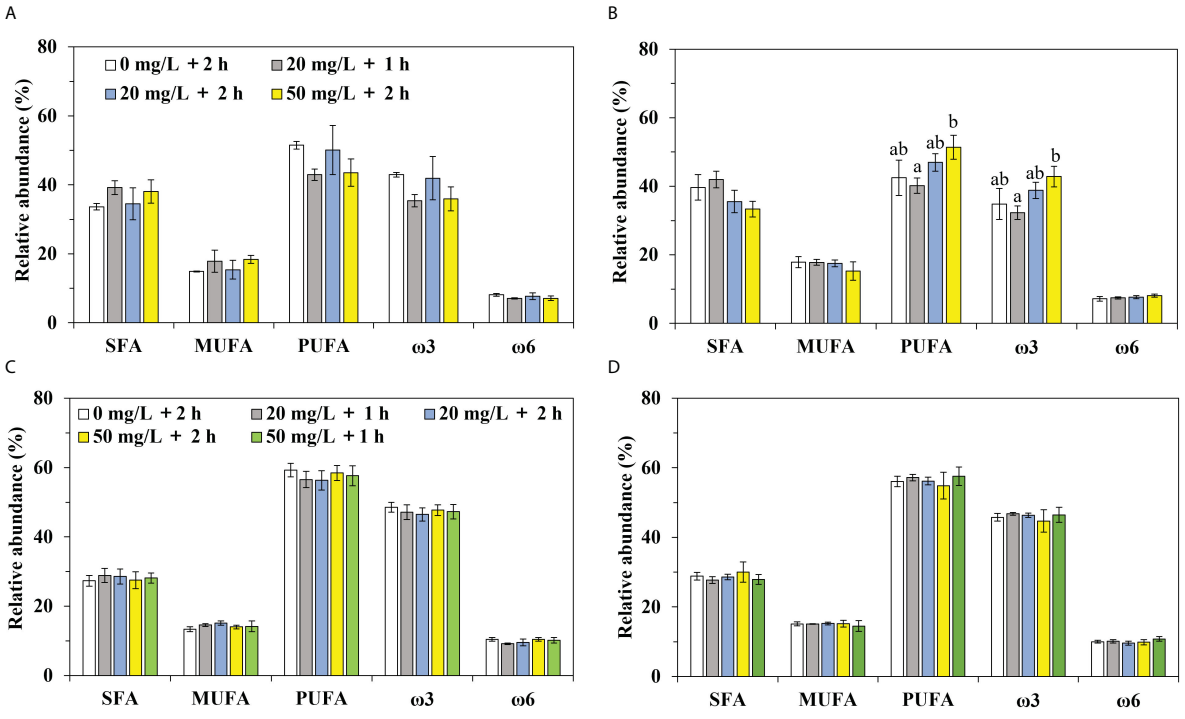

FIGURE 7
The relative abundances of fatty acids with distinct saturation degrees in *P. laevis*. **(A)** Experiment 1, 2 h post exposure (2 hpe). **(B)** Experiment 1, 7 d post exposure (7 hpe). **(C)** Experiment 2, 2 h post exposure. **(D)** Experiment 2, 7 d post exposure. Values are means of three biological replicates ± SD (*n* = 3). The a and b indicated significant difference between the treatment groups (*P< 0.05). SFA, MUFA, PUFA indicated saturated, monounsaturated, and polyunsaturated fatty acids, respectively. ω3 referred to C16:4n3, C18:3n3, C18:4n3, C20:3n3, C20:4n3, C20:5n3, C22:5n3, and C22:6n3. ω6 referred to C16:2n6, C18:2n6, C20:2n6, C20:3n6, C20:4n6, and C22:4n6.

10.3389/fmars.2024.1379571

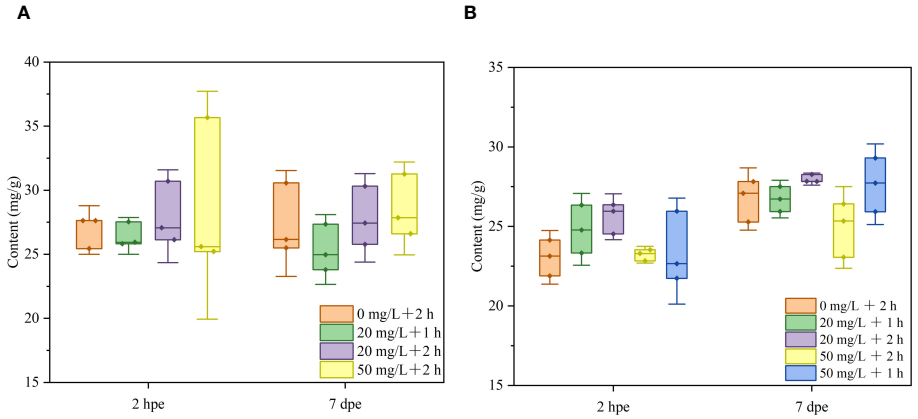

FIGURE 8
The total fatty acid contents of *P. laevis* under distinct labeling regimes. **(A)** Experiment 1. **(B)** Experiment 2. Values are means of three biological replicates ± SD (n = 3).

acids included C16:1n7 and C16:4n3 (Figures 6A–D). The relative abundances of the fatty acids with distinct saturation degrees were ranked as SFA< MUFA< PUFA, and the proportion of ω3 fatty acids was found to be much higher than that of ω6 fatty acids (Figures 7A–D). In both Experiment 1 and 2, there were almost no significant changes in the relative levels of the main fatty acids in calcein-labled *P. laevis* after 2 h and 7 d of labeling (Figures 6, 7). Additionally, all groups maintained relatively stable contents in the total fatty acid (Figures 8A, B). In conclusion, the labeling scheme used in this study does not have a significantly negative impact on the fatty acids of *P. laevis*.

TABLE 2 Marking quality of calcein for Experiments 1 and 2.

Experiment	Treatment group	Marking scheme	Rate of success (%)	Good rate (%)
Experiment 1	A	0 mg/L + 2 h	/	/
	B	20 mg/L + 1 h	93.33 ^{a}	36.67 ± 3.34 ^{a}
	C	20 mg/L + 2 h	100 ^{a}	56.67 ± 6.67 ^{c}
	D	50 mg/L + 2 h	100 ^{a}	71.11 ± 1.92 ^{d}
Experiment 2	a	0 mg/L + 2 h	/	/
	b	20 mg/L + 1 h	82.22 ± 7.70 ^{b}	16.67 ± 3.34 ^{b}
	c	20 mg/L + 2 h	95.56 ± 1.93 ^{a}	16.67 ± 5.77 ^{b}
	d	50 mg/L + 2 h	100 ^{a}	70.00 ± 5.77 ^{cd}
	e	50 mg/L + 1 h	100 ^{a}	42.22 ± 5.09 ^{a}

Values are means of three biological replicates ± SD (n = 3). Values in the same column that did not share the same superscripts are significantly different (*P< 0.05; one-way ANOVA).

3.4 Evaluation of laboratory marking effect of calcein on *P. laevis*

All the *P. laevis* individuals in Experiment 1 exhibited 100% marking success rates, except for Group B with a success rate of 93% (Table 2). Moreover, there were significant differences in the marking rate with an intensity level of 2 or higher among the groups. Group D had a significantly higher marking rate than Group C (*P< 0.05), while Group C had a significantly higher marking rate than Group B (*P< 0.05). In Experiment 2, the success rates of marking in all other groups exceeded 95% except for that in Group B. There were no significant differences in the marking rates between the low-concentration groups, but they were all significantly lower than the high-concentration groups. Among the high-concentration groups, Group C had a significantly higher labeling rate with a soaking time of 2 h, compared to Group E with a soaking time of 1 h. Under the same soaking scheme, the marking quality in Experiment 2 experienced varying degrees of decrease.

3.5 Evaluation of *in situ* marking effect of calcein on *P. laevis*

The marking success rates and the recapture rates of *P. laevis* for *in situ* tests in the two experimental groups were both 100% and 4.44 ± 1.29% after one month (Table 3; Supplementary Table S5). Also, the recapture marking rates and the marking good rates of the recaptured individuals were both 100%. There were no significant differences between these parameters for 50 and 75 mg/L of calcein (Table 3). Given the cost and safety of labeling, a strategy in terms of an immersion in 50 mg/L of calcein for 2 h could be considered as an effective *in situ* labeling scheme for *P. laevis*.

4 Discussion

The mortality rate directly reflects the impact of fluorescent labeling on the organisms, indicating the feasibility of the proposed

TABLE 3 Evaluation of *in situ* labeling effect of calcein on *P. laevis*.

Group	Marking success rate (%)	Recapture rate (%)	Recapture marking rate (%)	Marking good rate (%)
0 mg/L + 2 h	—	0	—	—
50 mg/L + 2 h	100	4.44 ± 1.29	100	100
75 mg/L + 2 h	100	4.44 ± 1.29	100	100

Marking success rate refers to the labeling rate after calcein staining. Recapture rate is the percentage of individuals recaptured a month later. Recapture marking rate is the proportion of fluorescence signal in recaptured individuals. Marking good rate is the proportion of signal above level 2 in the recaptured individuals with fluorescence signal. Values are means of three biological replicates ± SD (n = 3).

labeling scheme. When the dye concentration or labeling time is too high, it can result in death or growth inhibition on the labeled organisms. In Experiment 1, 4 h post exposure of labeling, acute deaths occurred in all experimental groups except for the control, but there were no significant differences between groups (Supplementary Table S6). In both rounds of experiments, there were no significant differences in the survival rates between the experimental and control groups following 7 d of labeling. This indicates that the calcein concentrations and immersion time employed in the experiment did not have a significantly negative impact on the short-term survival of *P. laevis*. In fact, several studies have demonstrated that calcein does not have a significant negative effect on the growth and survival of bivalves under suitable conditions (Zhou et al., 2017; Mahé et al., 2021; Spires and North, 2022), and it may even enhance the growth and survival of certain shellfish (Moran and Marko, 2005; Spires and North, 2022; Spires et al., 2022).

When exposed to stress, organisms generate a large amount of reactive oxygen species (ROS) in the body. Once produced in excess, ROS can result in lipid peroxidation in tissues and be harmful to the organism. The antioxidant system is important for defense against the detrimental effects of ROS, including SOD, CAT, and GPX. These antioxidants can effectively respond to exogenous substances impacting the body (Cao et al., 2012; Duan et al., 2016). ROS primarily include superoxide anion (O_2^-), hydroxyl radical (OH•), and non-radical hydrogen peroxide (H_2O_2) (Schieber and Chandel, 2014). SOD can convert superoxide anions (O_2^-) into H_2O_2 and O_2 through dismutation, and the generated H_2O_2 is then converted into non-toxic H_2O and O_2 by CAT (Arockiaraj et al., 2012). GPX has a similar function to CAT, as it is able to eliminate H_2O_2 and lipid hydroperoxides in the body, inhibit lipid peroxidation, and prevent oxidative damage to cell membranes and tissues (Hiramatsu et al., 1992). MDA, in contrast, is a product generated from lipid peroxidation caused by free radicals induced by oxidative stress in the body. It can react with cellular proteins, DNA, and other components, resulting in cell damage. The MDA content in tissues can indirectly reflect the extent of cellular damage (Zhang et al., 2016).

In Experiment 1, the CAT activity across all experimental groups decreased within 2 h of labeling. As the concentration of calcein or immersion time decreased, CAT activity gradually decreased (Figure 4B). The reduction in CAT activity may be attributed to two factors. Firstly, the organism's stress response could lead to the generation of a large amount of H_2O_2, consuming CAT. Secondly, immersion in calcein may reduce or inhibit the defense capacity of the organism's antioxidant system, preventing the timely replenishment of CAT following consumption. Moreover, CAT activity in the digestive gland of smooth river blue mussels decreased when immersed in 20 mg/L of calcein. However, as the concentration of calcein increased, its activity also increased. This may be explained by the "toxicant hormesis effect", wherein CAT activity is inhibited at low concentrations and stimulated at high concentrations. This observation is consistent with the observation in Meretrix meretrix under Cu^{2+} stress (Tian et al., 2022). Similar phenomena have also been observed in Chlamys farreri (Wand et al., 2008) and Mytilus edulis (Zhang et al., 2004). In this study, SOD and GPX activities in the visceral mass of *P. laevis* were not significantly impacted by the concentration of calcein or the immersion time (Figures 4A, C). This suggested that the labeling conditions employed in the experiment resulted in limited stress on *P. laevis* and did not perturb the organism's antioxidant balance, resulting in minimal impact that can be overcome within a short period of time. Similar findings have been reported in low-concentration tetracycline hydrochloride labeled Danio rerio and *Oreochromis niloticus* (Oruc and Uner, 2001). Following 2 h of labeling, the MDA content in Group A significantly decreased compared to the control group (Figure 4D). This may be due to the production of ROS as a stress response, leading to the consumption of a large amount of CAT to eliminate ROS and limit the peroxidation level in the organism, causing a decrease in MDA content.

In contrast to Experiment 1, there were no significant changes in the activities of SOD, CAT, GPX, and MDA levels in all experimental groups in Experiment 2 after marking. The reason for this phenomenon may be related to the water temperature. *P. laevis* belongs to eurythermal and euryhaline bivalves, capable of surviving at temperatures as low as -4°C, but growth is nearly halted below 10° C and accelerated above 20°C (Sun, 1988). The water temperature in Experiment 2 was around 24°C, within the optimal range for *P. laevis*. The appropriate water temperature may have enhanced the ability of *P. laevis* to resist external stress, while the water temperature in Experiment 1 was around 13°C, which could have compromised the stress resistance of *P. laevis* due to lower temperatures.

The fatty acids in *P. laevis* were also influenced by the experimental water temperature, showing a similar pattern of changes to antioxidant capacity. In Experiment 1, significant differences in some fatty acids between Groups A and B were observed initially after marking, but they returned to normal levels after 7 d. Moreover, the magnitude of change in Experiment 1 was much greater than that in Experiment 2. However, it is worth noting that both Experiment 1 and 2 showed cases where there were no significant differences in fatty acids among the experimental groups initially after marking, but significant changes occurred after 7 days. This suggested that the fatty acids of *P. laevis* could respond to the stress caused by calcein, but this response exhibited delayed manifestation and required some time to become evident. Overall, the composition and content of fatty acids in *P. laevis* were indeed unaffected by fluorescent labeling. It was implicated that the

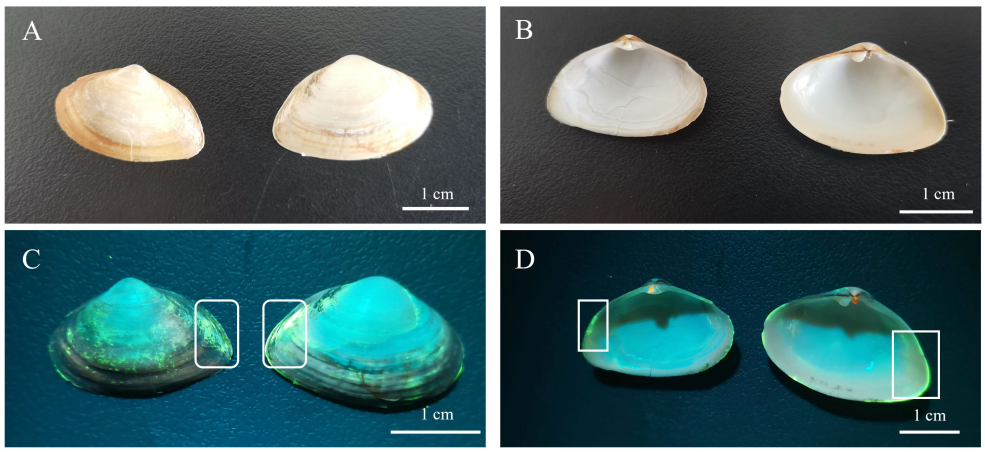

FIGURE 9
Fluorescent labeling of calcein on *P. laevis*. **(A)** Shell profiles of *P. laevis* under natural light. **(B)** Inner shell view of *P. laevis* under natural light. **(C)** Shell view of *P. laevis* irradiated using a Luyor−3280LB fluorescent flashlight. The white frame highlighted the presence of calcein. **(D)** Inner shell view of *P. laevis* irradiated using a Luyor−3280LB fluorescent flashlight. The white frame highlighted the presence of calcein.

labeling scheme used in this study appeared to cause no prominent stress on *P. laevis*, hinting on the safety of this labeling scheme, to certain extent. As the fatty acids in shellfish can change in response to environmental stress, the potential fatty acids biomarkers might exist in clams in adaption to fluorescent labeling. If the concentration or immersion time of calcein is further increased, it is expected to disclose the related fatty acids biomarkers responsive to fluorescent labeling in *P. laevis*, which deserves further exploration in our future work.

The concentration of dye and the labeling time significantly impacted the fluorescence labeling effect. The success rate and quality of labeling were augmented with increased concentration and incubation time. It was found that the concentration of calcein was the main factor affecting the labeling effect on *P. laevis*, and the soaking time took second place based on the batch labeling tests. When the calcein concentration reached ≥ 50 mg/L, the clams could be largely labeled with high quality in a short time. Moreover, if the soaking time of calcein extended, the labeling quality of *P. laevis* could also be further improved. When the labeling concentration was 50 mg/L or higher, the success rate of labeling reliably reached 100%. Under identical conditions, the high-concentration group consistently exhibited a significant advantage in labeling success rate compared to the low-concentration group. The experimental group immersed for 2 h had a higher labeling success rate than those immersed for 1 h (Table 2). The previous studies revealed that the labeling quality of calcein on *Haliotis rubra* (Chick, 2010), *Perna canaliculus* (Fitzpatrick et al., 2013) and *Anadara broughtonii* (Zhou et al., 2017) got enhanced with the increase of concentration and immersion time (Supplementary Table S7). The case for *P. laevis* in this work was also in line with these previous studies. In addition, a supplementary experiment at an ambient water temperature of 13.40°C (Experiment 1: 12.84 ± 0.09°C) was also conducted (Supplementary Methods). The results showed that the labeling success rates for 50 mg/L of calcein for 1 h and 2 h were both 100%, and the labeling good rate of 50 mg/L + 1 h was 43.33 ± 3.34%, which was significantly lower than that of 50 mg/L + 2 h (67.78 ± 5.09%) (Supplementary Table S8). As we speculated, the low temperature did not improve the labeling quality of 50 mg/L + 1 h. Following successful labeling, calcein will generate a blue-green fluorescent mark visible under blue light (480 ~ 490 nm) on the surface of the shell as well as the growth edge of the shell (Figures 9A–D). Differently from calcein-labeled *Mactra veneriformis*, the fluorescent markers on *M. veneriformis* were mainly concentrated on the outer surface of the shell (unpublished data), and the markers at the growth

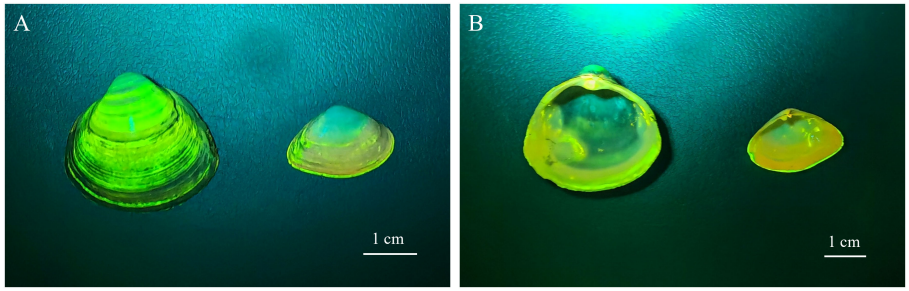

FIGURE 10
Labeling effect of calcein on *P. laevis* and *M. veneriformis*. **(A)** Shell view of *P. laevis* and *M. veneriformis* irradiated using a Luyor−3280LB fluorescent flashlight. **(B)** Inner shell view of *P. laevis* and *M. veneriformis* irradiated using a Luyor−3280LB fluorescent flashlight.

edge were more discrete, while in *P. laevis*, the clear fluorescent markers were more at the growth edge (Figures 10A, B). This phenomenon may be related to the differences in shellfish body size, growth rate and shell microstructure.

Temperature can impact calcein labeling, and higher temperatures have a negative impact on low-concentration calcein labeling. In Experiment 1, the labeling water temperature was 12.84 ± 0.09°C, while in Experiment 2, the labeling water temperature was 24.18 ± 0.04°C. When the labeling concentration was 20 mg/L, the success rate of labeling in Experiment 2 was reduced, and the high-quality labeling rate was significantly lower than in Experiment 1 ($^*P< 0.05$) over the same period. However, the effect of temperature increase on the high-concentration group was not significant (Table 2).

To our knowledge, the labeling method, especially chemical labeling, is characteristic in terms of species specificity, developmental stages and living habits of the labeled organism. The form, concentration, labeling time and labeling species of chemical dyes greatly affect the effect of chemical labeling. *P. laevis* is not only one of the main shellfish in the Geligang of Liaodong Bay, but also one of the main benthic species in many estuarine waters of East Asia. The edible clam can also be used as a high-quality feed for shrimp, crab or fish. In recent years, its natural resources have greatly declined due to large-scale harvesting and environmental pollution. However, the chemical labeling approach for the clam *P. laevis* has not been elucidated. In addition, fatty acids serve as the crucial components of lipids, and are vital for formation and permeability of cell membranes, resulting in their great sensitivity to multiple stressors and environmental alterations (Gonçalves et al., 2016). This trait has made fatty acids become the protruding biomarkers to indicate altered environmental changes. It is appropriate and innovative to take fatty acids as the evaluation factor in the labeling method of *P. laevis*. On the other hand, the *in situ* labeling tests combined with the laboratory experiments are applicable for resource stocking, conservation and assessment of the economic clams, to certain extent. In this study, the main complexation site of calcein was the calcified shell structure of *P. laevis*. This part is generally not ingested by predators, and it can further reduce the degree of calcein enrichment in organisms. Moreover, calcein is easily quenched under light. These factors suggested that calcein might be a relatively safe chemical dye with insignificant environmental impacts. Overall, the innovation of the methodology in our work lies in the establishment of chemical labeling method for the unreported clams *P. laevis* at distinct temperatures, the innovative evaluation of the sensitive biomarker fatty acids of clams, as well as the retests of *in situ* labeling experiments for *P. laevis*.

5 Conclusion

The calcein used in this study had a significant marking effect on *P. laevis*, and it did not cause any noticeably negative impacts. The most stable and bright marking effect was achieved by soaking the clams in 50 mg/L of calcein for 2 h. Although high temperature (24.18 ± 0.04°C) resulted in reduced marking effectiveness at 20 mg/L of calcein, the significantly marking effects were still observed when the soaking time was 2 h under low-temperature conditions (12.84 ± 0.09°C). Although this may induce certain oxidative stress on the clams, the stress extent was returned to normal levels within 7 d. Considering the marking cost, both options have practical value: (1) Water temperature at 13°C, soaking in 20 ~ 50 mg/L of calcein for 2 h; (2) Water temperature at 24°C, soaking in 50 mg/L of calcein for 2 h.

Data availability statement

The data that support the findings of this study are available from the corresponding author upon reasonable request. Requests to access these datasets should be directed to Q-ZW, wqzlm@126.com.

Ethics statement

The manuscript presents research on animals that do not require ethical approval for their study.

Author contributions

JG: Writing – review & editing, Writing – original draft, Investigation, Data curation. XX: Writing – review & editing, Methodology, Data curation, Conceptualization. X-FL: Writing – original draft, Investigation. Y-AB: Writing – original draft, Resources. MY: Writing – review & editing, Data curation. W-MT: Writing – original draft, Investigation. H-JL: Writing – original draft, Investigation. Q-ZW: Writing – review & editing, Supervision, Resources, Funding acquisition, Conceptualization.

Funding

The author(s) declare financial support was received for the research, authorship, and/or publication of this article. This work was supported by Ocean Economic Development Grants of Liaoning Province (202222), National Key Research and Development Program of China (2022YFD2400305), China Scholarship Council, Science and Technology Foundation of Dalian (2021YF16SN015, 2021JB11SN035), a grant from Dalian Key Laboratory of Genetic Resources for Marine Shellfish, Foundation of Liaoning Academy of Agricultural Sciences (2022DD268339), Ocean and Fisheries Research Grants of Liaoning Province (201826, 201818) and Modern Agro-industry Technology Research System of China (CARS-49).

Conflict of interest

Author Y-AB was employed by the company Panjin Guanghe Crab Industry Co., LTD. Author H-JL was employed by the company Dalian Changhai-Yide Aquatic Products Co., LTD.

The remaining authors declare that the research was conducted in the absence of any commercial or financial relationships that could be construed as a potential conflict of interest.

Publisher's note

All claims expressed in this article are solely those of the authors and do not necessarily represent those of their affiliated organizations, or those of the publisher, the editors and the reviewers. Any product that may be evaluated in this article, or claim that may be made by its manufacturer, is not guaranteed or endorsed by the publisher.

Supplementary material

The Supplementary Material for this article can be found online at: https://www.frontiersin.org/articles/10.3389/fmars.2024.1379571/full#supplementary-material

References

Arockiaraj, J., Easwvaran, S., Vanaraja, P., Singh, A., Othman, R. Y., and Bhassu, S. (2012). Molecular cloning, characterization and gene expression of an antioxidant enzyme catalase (MrCat) from *Macrobrachium rosenbergii*. *Fish Shellf. Immunol.* 32, 670–682. doi: 10.1016/j.fsi.2015.12.018

Cao, L., Huang, W., Shan, X., Ye, Z., and Dou, S. (2012). Tissue-specific accumulation of cadmium and its effects on antioxidative responses in Japanese flounder juveniles. *Environ. Toxicol. Pharmacol.* 33, 16–25. doi: 10.1016/j.fsi.2015.12.018

Chen, W. Q., Wang, W. X., and Tan, Q. G. (2017). Revealing the complex effects of salinity on copper toxicity in an estuarine clam *Potamocorbula laevis* with a toxicokinetic-toxicodynamic model. *Environ. pollut.* 222, 323–330. doi: 10.1016/j.envpol.2016.12.033

Chick, R. C. (2010). Batch-tagging blacklip abalone (*Haliotis rubra*) for identification of hatchery-reared individuals on natural coastal reefs in New South Wales, Australia. *J. Shellf. Res.* 29, 209–215. doi: 10.2983/035.029.0117

Duan, Y., Zhang, J., Dong, H., Wang, Y., Liu, Q., and Li, H. (2016). Effect of desiccation and resubmersion on the oxidative stress response of the kuruma shrimp *Marsupenaeus japonicus*. *Fish Shellf. Immunol.* 49, 91–99. doi: 10.1016/j.fsi.2015.12.018

Fitzpatrick, M. P., Jeffs, A. G., and Dunphy, B. J. (2013). Efficacy of calcein as a chemical marker of green-lipped mussel (*Perna canaliculus*) larvae and its potential use for tracking larval dispersal. *Aquacult. Res.* 44, 345–353. doi: 10.1111/are.2013.44.issue-3

Gancel, H. N., Carmichael, R. H., Park, K., Krause, J. W., and Rikard, S. (2019). Field mark-recapture of calcein-stained larval oysters (*Crassostrea virginica*) in a freshwater-dominated estuary. *Estuaries Coasts.* 42, 1558–1569. doi: 10.1007/s12237-019-00582-6

Gonçalves, A. M. M., Mesquita, A. F., Verdelhos, T., Coutinho, J. A. P., Marques, J. C., and Gonçalves, F. (2016). Fatty acids' profiles as indicators of stress induced by of a common herbicide on two marine bivalves species: *Cerastoderma edule* (Linnaeus 1758) and *Scrobicularia plana* (da Costa 1778). *Ecol. Indic.* 63, 209–218. doi: 10.1016/j.ecolind.2016.03.044

Hiramatsu, M., Edamatsu, R., and Mori, A. (1992). Free radicals, lipid peroxidation, SOD activity, neurotransmitters and choline acetyltransferase activity in the aged rat brain. *EXS* 62, 213–218. doi: 10.1007/978-3-0348-7460-1_21

Keller, A., Mohamed, A., Dröse, S., Brandt, U., Fleming, I., and Brandes, R. (2004). Analysis of dichlorodihydrofluorescein and dihydrocalcein as probes for the detection of intracellular reactive oxygen species. *Free Radical Res.* 38, 1257–1267. doi: 10.1080/10715760400022145

Lee, M. C., Park, J. C., and Lee, J. S. (2018). Effects of environmental stressors on lipid metabolism in aquatic invertebrates. *Aquat. Toxicol.* 200, 83–92. doi: 10.1016/j.aquatox.2018.04.016

Li, R., Ding, J., Shen, Y., Chang, Y., and Li, Z. (2015). Analysis and fitted of the experimental data about the enzyme activity response of the clam *Potamocorbula laevis* to water temperature change above freezing. *Mar. Environ. Sci.* 34, 706–712. doi: 10.13634/j.cnki.mes.2015.05.011

Liu, J. (2022). Analysis and evaluation of nutrient composition of Potamocorbula laevis North. *Chin. Fish.* 41, 6–11. doi: 10.3969/j.issn.1674-2419.2022.01.002

Liu, J., Liu, Y., Wang, H., and Xue, S. (2015). Direct transesterification of fresh microalgal cells. Bioresource Technology. *Bioresour. Technol.* 176, 284–287. doi: 10.1016/j.biortech.2014.10.094

Liu, J., and She, J. (2003). Reprodutctive behaviour of *potamocorbula laevis* (Hinds). *Fish. Sci.* 22, 12–13. doi: 10.16378/j.cnki.1003-1111.2003.05.003

Lü, H., Zhang, X., Xi, D., and Gao, T. (2014). Use of calcein and alizarin red S for immersion marking of black rockfish *Sebastes schlegelii* juveniles. *Chin. J. Oceanol. Limnol.* 32, 88–98. doi: 10.1007/s00343-014-3022-9

Mahé, K., Bellamy, E., D'Amico, F., and Caill-Milly, N. (2021). *In situ* fast marking study of manila clams (*Ruditapes philippinarum*). *Int. J. Fish. Aquat. Stud.* 9, 47–51. doi: 10.22271/fish.2021.v9.i1a.2387

Moran, A. L., and Marko, P. B. (2005). A simple technique for physical marking of larvae of marine bivalves. *J. Shellf. Res.* 24, 567–571. doi: 10.2983/0730-8000(2005)24[567:ASTFPM]2.0.CO;2

Ning, J., Chang, Y., Liu, W., Song, J., and Shi, M. (2016). Stress responses of clam *Potamocorbula laevis* to sharp decrease in temperature. *Fish. Sci.* 35, 117–122. doi: 10.16378/j.cnki.1003-1111.2016.02.004

Oruc, E. O., and Uner, N. (2001). Combined effects of 2, 4-D and azinphosmethyl on antioxidant enzymes and lipid peroxidation in liver of *Oreochromis niloticus*. *Comp. Biochem. Phys. C.* 127, 291–296. doi: 10.1016/S0742-8413(00)00159-6

Schieber, M., and Chandel, N. S. (2014). ROS function in redox signaling and oxidative stress. *Curr. Biol.* 24, R453–R462. doi: 10.1016/j.cub.2014.03.034

Spires, J. E., Dungan, C. F., and North, E. W. (2022). Marking the shells of pediveliger eastern oysters *Crassostrea virginica*, with a calcein fluorochrome dye. *J. Shellf. Res.* 40, 479–487. doi: 10.2983/035.040.0304

Spires, J. E., and North, E. W. (2022). Marking the shells of juvenile and adult eastern oysters, *Crassostrea virginica*, with the fluorochrome dye calcein and measuring growth and mortality after marking. *J. Molluscan Stud.* 88, eyac00. doi: 10.1093/mollus/eyac004

Sugiura, D., and Kikuya, N. (2017). Validation of the age estimation method using the shell section of the manila clam *Ruditapes philippinarum* in Mutsu Bay, northern Japan. *Aquacult. Sci.* 65, 193–202. doi: 10.11233/aquaculturesci.65.193

Sun, J. T. (1988). Preliminary study on the population dynamics of the clam *Potamocorbula laevis* (Hinds). *Trans. Oceanol. Limnol.* 10, 62–68. doi: 10.13984/j.cnki.cn37-1141.1988.04010

Sun, C., Liu, Z. H., Yang, A. G., Zhou, L. Q., Wu, B., Yang, J. K., et al. (2013). Genetic diversity of mitochondrial COI gene in three wild populations of *Potamocorbula laevis*. *Hunan Agric. Sci.* 07, 4–7. doi: 10.16498/j.cnki.hnnykx.2013.07.037

Teng, W. M., Gao, S. L., Liu, X., Yan, H. W., Xie, X., Li, X. D., et al. (2018). Effects of salinity on filtration and ingestion rates of surf clam *Mactra veneriformis* and clam *Potamocorbula laevis* in Liaodong Bay. *Fish. Sci.* 37, 622–627. doi: 10.16378/j.cnki.1003-1111.2018.05.007

Tian, Z., Zhang, Z. D., Chen, A. H., Wu, Y. P., Chen, S. H., Zhang, Y., et al. (2022). Effect of Cu^{2+}on antioxidant capacity of red shell color breeding line and natural population of hard clam *Meretrix meretrix*. *Fish. Sci.* 41, 62–68. doi: 10.16378/j.cnki.1003-1111.20145

Wand, F., Zhao, Y., Lu, J., and Liu, C. (2008). Effect of Cu^{2+} on the antioxidant enzyme of scallop *Chlamys farreri's* viscera. *Fish. Sci.* 27, 622–624. doi: 10.16378/j.cnki.1003-1111.2008.12.004

Xia, Y. Q., and Li, W. B. (2015). Study of calcein fluorescence properties. *Guangdong Chem. Industry* 42, 29–30. doi: 10.3969/j.issn.1007-1865.2015.07.014

Zhang, S., Sun, Y., Song, Y., and Yu, Z. (2004). Kinrtic features of four heavy metals bioaccumulation of mussel *Mytilus edulis*. *Oceanol. Limnol. Sin. (in Chinese).* 05, 438–445. doi: 10.3321/j.issn:0029-814X.2004.05.007

Zhang, Q., Wu, X., Zheng, J., and Sun, M. (2016). Progress of researches on methods for determination of malondialdehyde in biological samples. *Phys. Test. Chem. Anal.* 52, 979–985. doi: 10.11973/lhjy-hx201608026

Zhao, P., Yang, H. S., Wang, X. Y., Lin, C. G., and Li, X. P. (2011). Marking sea cucumber *Apostichopus japonicus* with calcein and its effects on antioxidant system. *J. Fish. China* 35, 372–378. doi: 10.3724/SP.J.1231

Zhou, S., Zhang, X., Li, W., Li, L., and Cai, X. (2017). Experimental evaluation of fluorescent (alizarin red S and calcein) and clip-tag markers for stock assessment of ark shell, *Anadara broughtonii*. *Chin. J. Oceanol. Limnol.* 35, 265–274. doi: 10.1007/s00343-016-5137-7

Frontiers in Marine Science

Explores ocean-based solutions for emerging global challenges

The third most-cited marine and freshwater biology journal, advancing our understanding of marine systems and addressing global challenges including overfishing, pollution, and climate change.

Discover the latest Research Topics

See more →

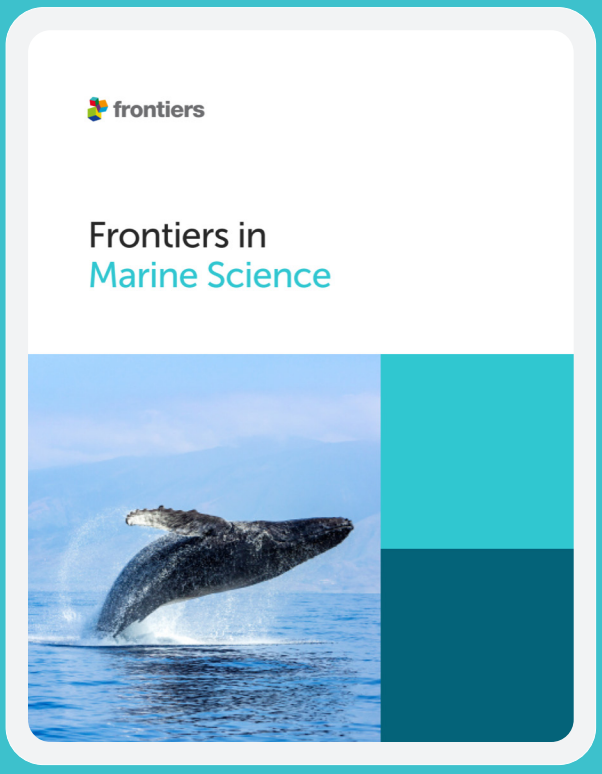

Frontiers

Avenue du Tribunal-Fédéral 34
1005 Lausanne, Switzerland
frontiersin.org

Contact us

+41 (0)21 510 17 00
frontiersin.org/about/contact